Strategies in Size Exclusion Chromatography

EDITED BY

Martin Potschka and

Paul L. Dubin

ACS Symposium Series 635

Downloaded by 217.66.152.32 on October 8, 2012 | http://pubs.acs.org
Publication Date: May 30, 1996 | doi: 10.1021/bk-1996-0635.fw001

Strategies in Size Exclusion Chromatography

In Strategies in Size Exclusion Chromatography; Potschka, M., et al.;
ACS Symposium Series; American Chemical Society: Washington, DC, 1996.

Downloaded by 217.66.152.32 on October 8, 2012 | http://pubs.acs.org
Publication Date: May 30, 1996 | doi: 10.1021/bk-1996-0635.fw001

In Strategies in Size Exclusion Chromatography; Potschka, M., et al.;
ACS Symposium Series; American Chemical Society: Washington, DC, 1996.

ACS SYMPOSIUM SERIES **635**

Strategies in Size Exclusion Chromatography

Martin Potschka, EDITOR
Scientific Consultant

Paul L. Dubin, EDITOR
Indiana University-Purdue University

Developed from a symposium sponsored
by the Division of Polymer Chemistry, Inc.,
and the Division of Analytical Chemistry
at the 209th National Meeting
of the American Chemical Society,
Anaheim, California,
April 2–6, 1995

American Chemical Society, Washington, DC

Downloaded by 217.66.152.32 on October 8, 2012 | http://pubs.acs.org
Publication Date: May 30, 1996 | doi: 10.1021/bk-1996-0635.fw001

QD 272 .C444S77 1996 Copy 1

Strategies in size-exclusion chromatography

Downloaded by 217.66.152.32 on October 8, 2012 | http://pubs.acs.org
Publication Date: May 30, 1996 | doi: 10.1021/bk-1996-0635.fw001

Library of Congress Cataloging-in-Publication Data

Strategies in size exclusion chromatography / Martin Potschka, editor, Paul L. Dubin, editor.

p. cm.—(ACS symposium series, ISSN 0097–6156; 635)

"Developed from a symposium sponsored by the Division of Polymer Chemistry and the Division of Analytical Chemistry, at the 209th National Meeting of the American Chemical Society, Anaheim, California, April 2–6, 1995."

Includes bibliographical references and indexes.

ISBN 0–8412–3414–0

1. Gel permeation chromatography—Congresses.

I. Potschka, Martin, 1955– . II. Dubin, Paul. III. American Chemical Society. Division of Polymer Chemistry. IV. American Chemical Society. Division of Analytical Chemistry. V. American Chemical Society. Meeting (209th: 1995: Anaheim, Calif.) VI. Series.

QD272.C444S77 1996
543′.0892—dc20 96–13254
CIP

This book is printed on acid-free, recycled paper.

Copyright © 1996

American Chemical Society

All Rights Reserved. The appearance of the code at the bottom of the first page of each chapter in this volume indicates the copyright owner's consent that reprographic copies of the chapter may be made for personal or internal use or for the personal or internal use of specific clients. This consent is given on the condition, however, that the copier pay the stated per-copy fee through the Copyright Clearance Center, Inc., 222 Rosewood Drive, Danvers, MA 01923, for copying beyond that permitted by Sections 107 or 108 of the U.S. Copyright Law. This consent does not extend to copying or transmission by any means—graphic or electronic—for any other purpose, such as for general distribution, for advertising or promotional purposes, for creating a new collective work, for resale, or for information storage and retrieval systems. The copying fee for each chapter is indicated in the code at the bottom of the first page of the chapter.

The citation of trade names and/or names of manufacturers in this publication is not to be construed as an endorsement or as approval by ACS of the commercial products or services referenced herein; nor should the mere reference herein to any drawing, specification, chemical process, or other data be regarded as a license or as a conveyance of any right or permission to the holder, reader, or any other person or corporation, to manufacture, reproduce, use, or sell any patented invention or copyrighted work that may in any way be related thereto. Registered names, trademarks, etc., used in this publication, even without specific indication thereof, are not to be considered unprotected by law.

PRINTED IN THE UNITED STATES OF AMERICA

American Chemical Society
Library
1155 16th St., N. W.
Washington, D. C. 20036

Downloaded by 217.66.152.32 on October 8, 2012 | http://pubs.acs.org
Publication Date: May 30, 1996 | doi: 10.1021/bk-1996-0635.fw001

Advisory Board

ACS Symposium Series

Robert J. Alaimo
Procter & Gamble Pharmaceuticals

Mark Arnold
University of Iowa

David Baker
University of Tennessee

Arindam Bose
Pfizer Central Research

Robert F. Brady, Jr.
Naval Research Laboratory

Mary E. Castellion
ChemEdit Company

Margaret A. Cavanaugh
National Science Foundation

Arthur B. Ellis
University of Wisconsin at Madison

Gunda I. Georg
University of Kansas

Madeleine M. Joullie
University of Pennsylvania

Lawrence P. Klemann
Nabisco Foods Group

Douglas R. Lloyd
The University of Texas at Austin

Cynthia A. Maryanoff
R. W. Johnson Pharmaceutical
Research Institute

Roger A. Minear
University of Illinois
at Urbana–Champaign

Omkaram Nalamasu
AT&T Bell Laboratories

Vincent Pecoraro
University of Michigan

George W. Roberts
North Carolina State University

John R. Shapley
University of Illinois
at Urbana–Champaign

Douglas A. Smith
Concurrent Technologies Corporation

L. Somasundaram
DuPont

Michael D. Taylor
Parke-Davis Pharmaceutical Research

William C. Walker
DuPont

Peter Willett
University of Sheffield (England)

In Strategies in Size Exclusion Chromatography; Potschka, M., et al.;
ACS Symposium Series; American Chemical Society: Washington, DC, 1996.

Downloaded by 217.66.152.32 on October 8, 2012 | http://pubs.acs.org
Publication Date: May 30, 1996 | doi: 10.1021/bk-1996-0635.fw001

Foreword

THE ACS SYMPOSIUM SERIES was first published in 1974 to provide a mechanism for publishing symposia quickly in book form. The purpose of this series is to publish comprehensive books developed from symposia, which are usually "snapshots in time" of the current research being done on a topic, plus some review material on the topic. For this reason, it is necessary that the papers be published as quickly as possible.

Before a symposium-based book is put under contract, the proposed table of contents is reviewed for appropriateness to the topic and for comprehensiveness of the collection. Some papers are excluded at this point, and others are added to round out the scope of the volume. In addition, a draft of each paper is peer-reviewed prior to final acceptance or rejection. This anonymous review process is supervised by the organizer(s) of the symposium, who become the editor(s) of the book. The authors then revise their papers according to the recommendations of both the reviewers and the editors, prepare camera-ready copy, and submit the final papers to the editors, who check that all necessary revisions have been made.

As a rule, only original research papers and original review papers are included in the volumes. Verbatim reproductions of previously published papers are not accepted.

ACS BOOKS DEPARTMENT

Preface

THIS BOOK INTEGRATES THREE DIFFERENT PERSPECTIVES on size exclusion chromatography (SEC): detector-focused approaches, chromatography-focused approaches, and synthesis and characterization of porous packings. The symposium that engendered this book, "Cross-evaluation of Strategies in Size Exclusion Chromatography," was similarly developed to represent the three main themes in modern SEC. The goal of this book is to present these co-existing themes and to reveal their merits to practitioner and researcher.

In the first approach, SEC per se comprises one component of an analytical system, the purpose of which is to separate the sample prior to spectroscopic or hydrodynamic characterization. This approach is not much concerned with the separation mechanism. In the second approach, the objective being pursued in SEC is a clear definition of "size" and the concomitant answers to basic questions about the separation process. The chemical and structural nature of the stationary phase is the focus of the third approach, in which one seeks to optimize chromatograhpic efficiency, steric selectivity, and the chemical surface properties of the packing.

Current and potential workers in the field of SEC have varied backgrounds and interests. Some need to carry out one particular measurement with maximum accuracy and reliability, and they might confront technological problems, such as the need to operate with exotic solvents at high temperature. Others, dealing with branched or chemically heterogeneous polymers, may seek more sophisticated information on polymer structure. For some, particularly in the biological realm, SEC may be a "sizing" technique used to observe, for example, protein aggregation. Finally, some readers would like to explore novel applications of SEC as a tool, for example, in studying the surface structure of porous materials. We have intentionally chosen, in this book, a broad range of problems so that readers may find some unexpected insights along with anticipated information.

An analysis of literature citations on the subject of SEC is informative. First, it shows how nomenclature served to fragment and distort the field, inasmuch as the terminology "gel filtration," "gel permeation," and "molecular sieving" divided a uniform phenomenon into the bailiwicks of biochemists and polymer chemists, and furthermore propagated misunderstandings of the fundamental nature of the chromatographic process.

Downloaded by 217.66.152.32 on October 8, 2012 | http://pubs.acs.org
Publication Date: May 30, 1996 | doi: 10.1021/bk-1996-0635.pr001

In Strategies in Size Exclusion Chromatography; Potschka, M., et al.;
ACS Symposium Series; American Chemical Society: Washington, DC, 1996.

Downloaded by 217.66.152.32 on October 8, 2012 | http://pubs.acs.org
Publication Date: May 30, 1996 | doi: 10.1021/bk-1996-0635.pr001

Second, the number of articles with size exclusion chromatography (SEC) in the title is diminishing, but the number that contain references to it is increasing. This development might seem an indication of the maturity of the field, but, as noted, we can now identify areas of significant activity. For example, technology is currently focused on the use of multiple detectors. In addition to the classical refractive index and UV detectors, we now see viscometric, light-scattering (both static and dynamic), and infrared detectors coupled to SEC. The application of these detector systems to biopolymeric conjugates or to the analysis and characterization of complex synthetic polymers—heterogeneous with respect to branching, composition, or both—is still a subject of vigorous investigation.

In addition to this technology-driven exploration, a long-term effort to resolve fundamental issues is still underway. A rather remarkable fact is that no one is completely sure what "size" means in the context of SEC. Generally, one could define this "size" as the dimension of a hard sphere that has the same migration velocity as the macromolecule in question. But there is no a priori reason to assume that this is either the viscosity radius or the Stokes radius, although both convenience and phenomenology have persuaded many workers to adopt this position. The problem arises from several sources: the paucity of such "ideal" spherical solutes, the complexity of modeling permeation in real porous media, and the difficulty of ensuring the absence of solute-stationary phase interactions. Even a fundamental (and possibly simplistic) question—what do apparently successful treatments of SEC as an equilibrium phenomenon imply about the dynamic nature of the process?—still lacks a definitive answer.

From the point of view of fundamental theory, macromolecule-stationary phase interactions represent a serious complication. Yet, appropriate manipulation of either coulombic or nonelectrostatic solute-packing interactions leads to some useful separation strategies. Two cases in point are the separation of proteins by "mixed-mode ion-exchange SEC" and "critical-condition chromatography" of polymers. Thus, the role of solvent in SEC is the subject of continued study. This work is represented in the chapters by Soria et al., Hunkeler et al., Belenkii et al., Mori and Oosaki, and Meehan et al.

The relationship of SEC to other phenomena is gaining increased recognition. Close parallels may be drawn between the permeation of macromolecules in porous stationary phases, through porous membranes, or in biological matrices. SEC should be viewed in the context of other characterization methods that also involve hydrodynamics. Hoagland makes such comparisons between SEC, hydrodynamic chromatography, and gel electrophoresis, and Sarkanen explores the relationship between SEC and ultracentrifugation. Macromolecular permeation is also the foundation of the inverse chromatography method described by Jeřábek.

The goal of a fundamental understanding of the separation process, with the expectation that this will lead to the measurement of a well-defined and significant quantity, a molecular dimension, from SEC alone is the approach implicit in the papers by Busnel et al., Potschka, and Hoagland. The application of multiple detection, as portrayed in the studies by Radke and Müller, Reed, Meehan et al., and Vilenchik et al., is being explored for the characterization of macromolecules more complex than nonionic linear polymers. At the same time, efforts are being directed to solve problems specific to certain classes of macromolecules, such as polysaccharides (Huber and Praznik and Striegel and Timpa), and proteins (le Maire et al.).

Acknowledgments

Our goal was to present a wide range of perspectives, and we were pleased to have strong participation from abroad, including Sweden, Germany, Russia, France, Spain, and England. This would not have been possible without financial assistance from the sponsoring organizations. Travel assistance for overseas speakers was provided by the ACS Division of Analytical Chemistry, and the Division of Polymer Chemistry, Inc., and the following corporate sponsors: Lab Connections, Polymer Laboratories, Precision Detectors, Viscotek, and Wyatt Technologies.

MARTIN POTSCHKA
Porzellangasse 19/2/9
A–1090 Vienna
Austria

PAUL L. DUBIN
Department of Chemistry
Indiana University–Purdue University
Indianapolis, IN 46202

February 23, 1996

Downloaded by 217.66.152.32 on October 8, 2012 | http://pubs.acs.org
Publication Date: May 30, 1996 | doi: 10.1021/bk-1996-0635.pr001

Chapter 1

Molecular Weights of Copolymers Obtained by Gel Permeation Chromatography–Light Scattering

Wolfgang Radke and Axel H. E. Müller

Institut für Physikalische Chemie, Universität Mainz, Welderweg 15, D–55099 Mainz, Germany

Downloaded by 217.66.152.32 on October 8, 2012 | http://pubs.acs.org
Publication Date: May 30, 1996 | doi: 10.1021/bk-1996-0635.ch001

The true number-average molecular weight, M_n, of copolymers is obtained by GPC coupled with a light scattering detector even if the composition and therefore the refractive index increment varies with elution volume, provided slices taken are monodisperse with respect to molecular weight and composition. In contrast, only an apparent weight-average molecular weight, M_w^{app}, can be obtained by the conventional GPC-light scattering combination, even for a perfect chromatographic resolution.

Gel permeation chromatography (GPC) has become a powerful method for the determination of the molecular weight distribution (MWD) of polymers. For homopolymers the column set can be calibrated with standards of narrow MWD or by using universal calibration *(1)* if the Mark-Houwink parameters for the polymer under investigation in the eluent are known. The lack of suitable standards for column calibration has been overcome by the use of molecular weight-sensitive detectors, such as on-line viscosity or light-scattering detectors *(2-7)*.

For copolymers a multi-detector approach *(8)* has been used as an approximate method which involves the use of at least one concentration detector for each component. From the ratios of the signals of the various detectors the composition in each slice is calculated and the molecular weight in this slice is determined as the weighted average of the molecular weights obtained from the calibration curves for the homopolymers. This method, although simple, has serious disadvantages: it needs calibration of the detectors and of the column set for each homopolymer (or, for universal calibration the Mark-Houwink constants must be known in the GPC eluent). Moreover, the hydrodynamic volume of the copolymer does not necessarily depend on composition in a linear way.

0097–6156/96/0635–0002$15.00/0

The use of a light-scattering detector for copolymers is complicated by the fact that for chemically non-homogeneous copolymers the composition of the eluted molecules will vary as a function of elution volume, even if the slices are monodisperse. This leads to a change in the refractive index increment with elution volume and therefore introduces errors in the determination of the copolymer concentration, if a refractive index detector is used for the determination of the concentration. The same is true for the absorption coefficient in UV detection.

The most rigorous method to overcome these problems would be a two-dimensional separation according to both molecular weight and chemical composition *(9-13)*. Such systems have become commercially available *(14)*. The individual fractions would have to be analyzed in terms of composition using the multi-detector approach. Knowing the concentrations of the individual components, the total copolymer concentration and the refractive index increments could be calculated for each GPC slice. Using these informations, correct molecular weight distributions could be obtained by on-line light scattering or viscometry. Obviously, this method, although probably the most correct one, involves a lot of labor.

Goldwasser *(15)* and Rudin *(16)* proposed a method for the determination of M_n of copolymers using exclusively an on-line viscosity detector together with a universal calibration curve, which overcomes the problem of compositional drift. The application of GPC-light scattering (GPC-LS) to copolymers has yet not reached much attention. It will be shown, that under certain conditions this method provides the true number-average molecular weight of copolymers without the use of two-dimensional methods.

Theory

We assume the GPC slices to be monodisperse in composition as well as in molecular weight. Since the concentrations in (GPC-LS) are low, the true molecular weight, M_i, in the i-th GPC slice of constant volume ΔV which is assumed to be monodisperse with respect to composition and molecular weight, is obtained from the equation:

$$M_i = \frac{R_i(\Theta = 0)}{K_i \cdot c_i} \tag{1}$$

Here, $R(\Theta = 0)$ is the Raleigh ratio extrapolated to the angle $\Theta = 0$, c is the weight concentration and the optical constant K is defined as

$$K_i = \frac{2\pi \cdot n_0^2}{\lambda_0^4 \cdot N_A} \nu_i^2$$

where $\nu = dn/dc$ is the refractive index increment, λ_0 is the wavelength of the incident beam in vacuum and n_0 is the refractive index of the solvent at λ_0.

The signal S of the refractive index detector which is conventionally used as a concentration detector in GPC-LS experiments, is proportional to the product of refractive index increment and weight concentration, $c_i = m_i/\Delta V$,

Downloaded by 217.66.152.32 on October 8, 2012 | http://pubs.acs.org
Publication Date: May 30, 1996 | doi: 10.1021/bk-1996-0635.ch001

$$S_i = k_{RI} \cdot \Delta n = k_{RI} \cdot c_i \cdot \nu_i \quad \text{or} \quad c_i = \frac{S_i}{k_{RI} \cdot \nu_i} \tag{2}$$

where k_{RI} is the absolute response factor of the instrument and m_i is the polymer mass within the slice of constant volume ΔV.

Using the definition of the number-average molecular weight and eq. 1 we obtain:

$$M_n = \frac{\sum c_i}{\sum \frac{c_i}{M_i}} = \frac{m_{inj} / \Delta V}{\sum \frac{K_i \cdot c_i^2}{R_i(\Theta = 0)}} \tag{3}$$

where m_{inj} is the total polymer mass injected.
Combination with eq. 2 renders

$$M_n = \frac{k_{RI}^2 \cdot m_{inj} / \Delta V}{\sum \frac{K_i \cdot S_i^2}{\nu_i^2 \cdot R_i(\Theta = 0)}} \tag{4}$$

However, K_i is not a constant but depends on the copolymer composition in the particular slice, due to the dependence on ν_i. Thus, it is convenient to define the true constant $K' = K_i/\nu_i^2$. Doing so the refractive index increments cancel out and we finally obtain

$$M_n = \frac{k_{RI}^2 \cdot m_{inj.} / K' \cdot \Delta V}{\sum \frac{S_i^2}{R_i(\Theta = 0)}} \tag{5}$$

In this equation the right hand side consists of known constants in the numerator and measurable quantities in the denominator only. Thus, according to eq. 5 the true number-average molecular weight of the copolymer can be obtained without explicit knowledge of the refractive index increment, when the absolute calibration constant of the refractive index detector has been determined.

For other moments of the molecular weight distribution the situation is different. For the weight-average molecular weight the same approach leads to

$$M_w = \frac{\sum c_i \cdot M_i}{\sum c_i} = \frac{\sum \frac{R_i(\Theta = 0)}{\nu_i^2}}{K' \cdot m_{inj.} / \Delta V} \tag{6}$$

Since the refractive index increments of the individual fractions, ν_i, enter into this equation, it is not possible to determine the true weight-average molecular weight of the copolymer by GPC-LS unless the refractive index increments of all fractions are determined. When using the average refractive index increment of the whole sample, $\bar{\nu} = \sum w_i \nu_i$, we can obtain an apparent weight-average molecular weight

Downloaded by 217.66.152.32 on October 8, 2012 | http://pubs.acs.org
Publication Date: May 30, 1996 | doi: 10.1021/bk-1996-0635.ch001

$$M_w^{app} = \frac{\sum c_i^{app} \cdot M_i^{app}}{\sum c_i^{app}} = \frac{\sum \frac{c_i^{app} \cdot R_i(\Theta = 0)}{K' \cdot \bar{\nu}^2 \cdot c_i^{app}}}{\sum c_i^{app}} = \frac{\sum R_i(\Theta = 0)}{m_{inj} \cdot K' \cdot \bar{\nu}^2 \Delta V} \tag{7}$$

where c_i^{app} is an apparent concentration calculated according to eq. 2 using $\bar{\nu}$. The apparent molecular weight calculated according to eq. 7 is identical to the one obtained by a conventional batch measurement*(17)* as is easily shown by introducing eq. 1 into eq. 7.

Results and Discussion

In order to test the usefulness of the method, mixtures of poly(methyl methacrylate) and polystyrene with narrow molecular weight distribution were prepared. These mixtures represent the limiting case of a "copolymer with infinite chemical heterogeneity". In contrast to real copolymers, the molecular weight averages of the mixtures can be easily calculated from composition and molecular weights of the individual homopolymers. The experimental number- and weight-average molecular weights of the mixtures were determined by GPC-LS and compared to the calculated ones (Radke, W.; Simon, P.F.W.; Müller, A.H.E., submitted to *Macromolecules*)

As predicted, the M_w values determined experimentally strongly deviate from the true weight-average molecular weights. They are close to the expected apparent molecular weights calculated using the average refractive index increments, the composition and molecular weights of the components. In contrast to this observation, the calculated number-average molecular weights and those obtained by GPC-LS differ by less that ±10 %, showing the correctness of eq. 5, and indicating that the polydispersity of the slices with respect to both molecular weight and chemical composition can be neglected. This seems to indicate, that at least in our mixtures, the method is also not very sensitive towards the chemical heterogeneity in the GPC slices.

Although it is shown that the requirement of monodisperse slices is of minor importance is in our investigation, it should be kept in consideration. Copolymers which sufficiently meet the requirement will probably be copolymers synthesized by "living" polymerization, since these polymers only show chemical heterogeneity of second order (i.e. compositional changes along the polymer chain).

Conclusions

It has been shown that the true number-average molecular weight, M_n, of copolymers is obtained by GPC coupled with a light scattering detector even if the composition and therefore the refractive index increment varies with elution volume. Although the slices taken should be monodisperse with respect to molecular weight and composition this effect does not lead to significant deviations in the result.

It should be stressed again at this point, that the determination of molecular weights of copolymers by light scattering is a problem due to the two-dimensional distribution function of the polymer. Even if we would be able to determine the composi-

Downloaded by 217.66.152.32 on October 8, 2012 | http://pubs.acs.org
Publication Date: May 30, 1996 | doi: 10.1021/bk-1996-0635.ch001

tion and therefore the refractive index increments of the individual slices, the determination of the molecular weights would not be correct, unless the slices are truly monodisperse. Therefore the use of a two dimensional chromatographic system, not the implementation of further detectors, will be the method of choice to overcome this problem.

As shown by Goldwasser *(15)* and Rudin *(16)*, GPC-viscometry yields true M_n values for copolymers, even if the slices are heterogeneous. Their method relies on the validity of universal calibration for the copolymer under investigation whereas this requirement is not necessary for GPC-LS, i.e. separation according to size exclusion is not even required. In contrast, GPC-LS (in principle) requires monodisperse slices. Thus, both methods depend on different requirements, and can be used to cross-check the results when using GPC equipped with both light scattering and viscometric detection.

Downloaded by 217.66.152.32 on October 8, 2012 | http://pubs.acs.org
Publication Date: May 30, 1996 | doi: 10.1021/bk-1996-0635.ch001

Literature Cited

1) Benoît, H.; Grubisic, Z.; Rempp, P.; Decker, D.; Zilliox, J.G. *J. Chem. Phys.* **1966**, *63*, 1507
2) Ouano, A.C. *J. Polym. Sci. Part A-1* **1972**, *10*, 2169
3) Haney, M.A. *J. Appl. Polym. Sci.* **1985**, *30*, 3023, 3037
4) Haney, M.A. *American Laboratory* **1985**, 41, 116
5) Yau, W.W. *Chemtracts, Macromol. Chem.* **1990**, 1, 1
6) Jackson, C.; Barth, H.G.; Yau, W.W. *Proceedings, Waters Intl. GPC Symposium* **1991**
7) Wyatt, P.J. *Anal. Chim. Acta* **1993**, *272*, 1
8) Johann, C.; Kilz, P. *Abstracts, 1st Intl. Conf. on Molar Mass Characterization*, Bradford UK **1989**
9) Glöckner, G.; Koningsfeld, R. *Makromol. Chem., Rapid Commun.* **1983**, *4*, 529
10) Glöckner, G. *Pure Appl. Chem.* **1983**, *55*, 1553
11) Glöckner, G. *Makromol. Chem., Macromol. Symp.* **1992**, *61*, 239
12) Kilz, P.; Krüger, R.P.; Much, H.; Schulz, G. Prepr., *Am. Chem. Soc., Polym. Mater. Sci. Eng. Div.* **1993**, *69*, 114
13) Kilz, P.; Krüger, R.-P.; Much, H.; Schulz, G. in: *"Polymer Characterization"*; T. Provder, Ed., ACS Advances in Chemistry Series, p. 247 (1995)
14) Kilz, P. *Labor-Praxis* **1992**, *16*, 628
15) Goldwasser, J.M. *Proceedings, Intl. GPC Symposium, Newton, Mass.* **1989**, 150
16) Sanayei, R.A.; Suddaby, K.G.; Rudin, A. *Makromol. Chem.* **1993**, *194*, 1953
17) Huglin, M.B. *"Light Scattering from Polymer Solutions"*, Academic Press, London and New York 1972

Downloaded by UNIV OF GUELPH LIBRARY on October 10, 2012 | http://pubs.acs.org
Publication Date: May 30, 1996 | doi: 10.1021/bk-1996-0635.ch002

Chapter 2

Coupled Multiangle Light-Scattering and Viscosimetric Detectors for Size Exclusion Chromatography with Application to Polyelectrolyte Characterization

Wayne F. Reed

Department of Physics, Tulane University, New Orleans, LA 70118

Theoretical and technical aspects of coupled multi-angle light scattering (MALLS), refractometric and viscosimetric detectors for SEC applications are considered. Absolute mass, radius of gyration and reduced viscosity distributions are obtained in this configuration, and an example application is made to characterizing water soluble polyelectrolytes. This characterization also includes illustrations of polymer form factors, interparticle structure factors, the failure of 'universal calibration', and a comparison of low angle light scattering (LALLS) and MALLS. Finally, a summary of sources of systematic and random errors is given, with estimates of the effects of each source on the characterization parameters.

Polydispersity has long been the bane of macromolecular characterization. Different techniques applied to unfractionated 'batches' of polymer, such as static and dynamic light scattering, osmotic pressure and viscometry, all yield different averages over the mass distribution for the quantities they measure. The averages are often difficult to interpret and compare to each other, and contain no direct information about the width, shape, or peculiarities of the mass distribution.

It is hence desirable that fractionation techniques, such as size exclusion chromatography (SEC), be able to provide an absolute determination of the mass distribution, from which all the mass moments can be computed, and, simultaneously, be able to measure as many useful , associated, mass-dependent properties, X(M) as possible. These latter properties may include the root mean square radius of gyration R_g ($\equiv \langle S^2\rangle^{1/2}$, where $\langle S^2\rangle$ is the mean square radius of gyration), intrinsic viscosity $[\eta]$, diffusion coefficient, specific conductivity, etc. Over the past fifty years a large body of theoretical and empirical knowledge has been built up concerning the physical relationship between polymer structure, dimensions, interactions and hydrodynamics, as revealed by such properties. Many

0097–6156/96/0635–0007$17.00/0

of the theories are formulated in terms of mass scaling laws, which is precisely what coupled detectors in the SEC context permits measurement of. For example, Rg(M) and [η](M) often follow scaling relations of the form

$$R_g = AM^{\gamma} \tag{1a}$$

and

$$[\eta] = BM^{\beta} \tag{1b}$$

[η] is actually proportional to hydrodynamic volume V_H divided by M, so that when V_H is proportional to R_g^3,

$$\beta = 3\gamma - 1 \tag{2}$$

For the purposes of determining the relationship among different polymer properties, both for testing and developing theories and for practical purposes, the greater the polydispersity of the polymer sample, the wider the window of opportunity for characterization.

This chapter deals with coupled multi-angle light scattering (MALLS), viscosimetric, and refractometric (RI) detectors. These allow for absolute determination of the mass distribution C(M), (in this chapter, C(M)dM denotes the concentration, in g/cm^3, of polymer in a given solution with mass between M and M+dM), the root mean square radius of gyration distribution Rg(M), and something close to the intrinsic viscosity distribution [η](M). Basic principles of the MALLS and viscosimetric detectors are briefly discussed, specific characterization examples are given, sources of error are pointed out, and associated expressions for error estimates are given. While this detector scheme is presented within the context of SEC, it should be readily adaptable to systems using other fractionation methods, such as Field Flow Fractionation (1) and Capillary Hydrodynamic Fractionation (2).

Polyelectrolytes, electrically charged polymers, are used as a specific application of SEC with combined detectors in this work. While a fairly satisfactory state of understanding has been reached for neutral polymers in organic solvents, many problems associated with understanding polyelectrolytes, both naturally occurring and synthetic, remain unresolved.

Instrument considerations

Viscometer. Single capillary (3) and hydraulic Wheatstone bridge (4) capillary viscometers are commonly used as SEC detectors. Both assume that SEC flow in the cylindrical capillaries is viscous and laminar, and obeys Poiseuille's equation:

$$\eta = \frac{\pi R^4 \Delta P}{8LQ} \tag{3}$$

where η is the total solution viscosity in Poise (g/cm-s), ΔP=the pressure drop (in dynes/cm^2) across the capillary of radius R and length L, through which liquid flows at a volume flow rate Q (in cm^3/s). Normally, a differential pressure transducer(s) is used to give a voltage output signal proportional to ΔP. In turn, η is proportional to this voltage.

Downloaded by UNIV OF GUELPH LIBRARY on October 10, 2012 | http://pubs.acs.org
Publication Date: May 30, 1996 | doi: 10.1021/bk-1996-0635.ch002

Downloaded by UNIV OF GUELPH LIBRARY on October 10, 2012 | http://pubs.acs.org
Publication Date: May 30, 1996 | doi: 10.1021/bk-1996-0635.ch002

One is normally first interested in the reduced viscosity η_r of the polymer itself, which is related to the measured, total solution viscosity η by

$$\eta_r = \frac{\eta - \eta_s}{\eta_s c} \tag{4}$$

where η_s is the viscosity of the pure solvent, and c is the polymer concentration. Ultimately, one normally wishes to know the intrinsic viscosity of the polymer $[\eta]$, for which most polymer viscosity models are made. This is obtained from extrapolation of η_r to zero polymer concentration, c=0, and to zero shear rate by

$$[\eta] = \lim_{\substack{c \to 0 \\ \dot{\gamma} \to 0}} \eta_r \tag{5}$$

where $\dot{\gamma}$, the shear rate, is given for laminar, parabolic flow in a capillary by

$$\dot{\gamma} = \frac{dv(r)}{dr} = \frac{-4Qr}{\pi R^4} \tag{6}$$

where r is the distance from the center of the capillary. The negative sign indicates that the fluid velocity v(r) is zero at the capillary wall (maximum shear surface) and maximum at the center. The shear rate averaged over the cross section of the capillary is

$$\dot{\gamma}_{ave} = \frac{8Q}{3\pi R^3} \tag{7}$$

For typical SEC conditions of Q= 1 mL/min ($0.0167\text{cm}^3/\text{s}$) and R = 0.02cm , the average shear rate is $\dot{\gamma}_{ave} \sim 1800\ \text{s}^{-1}$. Shear rates may be even higher in other parts of the SEC system, such as in the columns. Such shear rates are actually quite high, well above the region where many polymers show non-Newtonian behavior, such as shear-thinning (5,6). Fortunately, such effects usually decrease significantly with polymer concentration, and SEC measurements are typically performed at very low c. Nonetheless, attention should be paid to the shear rate when using these viscosity detectors.

An advantage of the single capillary detector, besides its simplicity and low cost, is that no calibration factors are needed to compute the reduced viscosity η_r. It suffices to measure the baseline voltage V_{base}, then η_r at elution volume v is related to the voltage at that volume $V_v(v)$, by

$$\eta_r(v) = \frac{\eta - \eta_s}{\eta_s c} = \frac{V_v(v) - V_{v,base}}{V_{v,base}\, c} \tag{8}$$

The main advantage of the 'hydraulic Wheatstone' Bridge viscometer is that it can smooth out pressure pulses from poorly damped pumps, as well as small thermal fluctuations. It requires, however, two absolutely calibrated (i.e. Pascals/volt) pressure transducers. Attention should be given to the long term stability of the calibration factors. We are currently making a detailed, simultaneous comparison of single capillary and bridge capillary detectors on our SEC system at

Tulane (7), which is similar to the one at the CERMAV in Grenoble, described below.

Light scattering principles. Static light scattering has long been a standard tool for absolute characterization of polymer molecular weights. The celebrated Zimm equation (8) relates the absolute, angular dependent excess Rayleigh scattering ratio I(q), of a solution of scattering particles to the particles' weight averaged molecular weight M_w, second virial coefficient A_2, and scattering form factor P(q), via

$$\frac{Kc}{I(q)} = \frac{1}{M_w P(q)} + 2A_2 c \tag{9}$$

where K is an optical constant, given for vertically polarized incident light as

$$K = \frac{4\pi^2 n^2 (dn/dc)^2}{N_A \lambda^4} \tag{10}$$

where n is the index of refraction of the solvent, dn/dc is the differential refractive index of the polymer in the solvent, λ is the vacuum wavelength of the incident light, and N_A is Avogadro's number. The scattering wave vector q, is given by

$$q = \left(\frac{4\pi n}{\lambda}\right)\sin(\theta/2) \tag{11}$$

where θ is the scattering angle. I(q) represents the fraction of incident intensity scattered per unit solid angle (steradian) at q, per cm of pathlength in the scattering solution. I(q) is an 'excess' quantity, in that it represents, at a given q, the total scattering from the solution minus the pure solvent scattering background. In static light scattering the scattering volume (i.e. the portion of the illuminated volume allowed to reach a given photodetector, using lenses, apertures, or any other means of optical field definition), is made large enough that intensity fluctuations due to particle diffusion are negligible compared to the total scattering; i.e. the detector should subtend many coherence areas. In contrast, dynamic light scattering (9) measures and autocorrelates the intensity fluctuations, so that a minimum number of coherence areas are subtended by the detector. In this sense, static and dynamic light scattering are antagonistic towards each other in terms of the amount of illuminated sample volume they should sample.

When the particles are small enough that $q^2 \langle S^2 \rangle \ll 1$, then P(q) converges to the same limiting form for all particle shapes (spheres, rods, random coils, wormlike chains, etc.), and yields

$$\frac{Kc}{I(q)} = \frac{1}{M_w}\left(1 + \frac{q^2 \langle S^2 \rangle_z}{3}\right) + 2A_2 c \tag{12}$$

Traditionally, in 'batch' (unfractionated) mode, I(q) is determined for a family of concentrations, from which M_w, A_2, and $\langle S^2 \rangle_z$ are subsequently determined ($\langle S^2 \rangle_z$ is the z-average mean square radius of gyration). In SEC, c at

Downloaded by UNIV OF GUELPH LIBRARY on October 10, 2012 | http://pubs.acs.org
Publication Date: May 30, 1996 | doi: 10.1021/bk-1996-0635.ch002

Downloaded by UNIV OF GUELPH LIBRARY on October 10, 2012 | http://pubs.acs.org
Publication Date: May 30, 1996 | doi: 10.1021/bk-1996-0635.ch002

each elution slice is usually so low, that the extrapolation to c=0 can be considered obtained, although it is generally better to introduce A_2 into the computation for M_w and $<S^2>_z$ to account for finite concentrations, especially when polyelectrolytes at low ionic strengths are involved. A_2 must be known or determined independently, in a 'batch' light scattering experiment, for example. In principle, A_2 is a function of M, but often the variation is small enough, that a single value from a batch determination is adequate. For example, for an ideal random coil A_2 should vary as $M^{-0.2}$ (10). Errors arising from A_2 effects are discussed below.

It should also be pointed out that there are finite shear rates in a MALLS scattering flow cell. For a capillary type, such as in the Wyatt Dawn-F system, for example, the average shear rate can be computed from eq. 7 with R being replaced by the flow cell radius R_{cell}. This R is typically far greater than that for the capillary viscometer, giving much lower shear rates in the Dawn-F flow cell than in the viscometer; e.g. the Dawn flow cell has R_{cell}=0.063cm, giving an average shear rate of about 57 s^{-1} for a flow rate of 1 mL/minute. The laser beam in the cell actually samples an even lower average shear rate than this. The sampled shear rate (Ignoring corrections due to integrating over a Gaussian or other laser beam profile. A Gaussian profile would lead to an even lower sampled average shear rate.), is given by

$$\dot{\gamma}_{ave} = \frac{8QR_{laser}}{3\pi R^4_{cell}} = \dot{\gamma}_{ave,cell}\left(\frac{R_{laser}}{R_{cell}}\right) \qquad (13)$$

The stock laser beam diameter in the Dawn system is about 0.4mm, so that the average shear rate is about 18 s^{-1}.

Normalization of multiple photodetectors. When multiple, fixed angle photodetectors are used, each one generally has a different response when exposed to the same scattered intensity, and each detector may detect light from different size scattering volumes. Normalization refers to the procedure whereby the response of each detector is scaled to the response of a single detector in the group (often the 90° detector is chosen as the reference detector). As long as a scattering sample is homogeneous throughout its illuminated volume, it is not necessary that each photodetector be sampling the same amount of volume, (nor the same volume corrected by $\sin\theta$, as has been traditionally required for single detectors on movable rotary stages). The only requirement to make the normalization procedure valid, is that all the photodetectors be working within their linear response range.

A normalization solution is one which scatters isotropically (a 'Rayleigh scatterer'); that is, one which has no angular dependence in its scattered light. This will occur for particles whose characteristic size (e.g. diameter) d is such that $d<<\lambda$. For λ=632nm light from a Helium-Neon laser, particles such as low molecular weight dextrans or polyethylene oxides, (e.g. M~15,000), and sodium dodecyl sulfate micelles, are reasonable choices for aqueous solutions.

If cylindrical, upright sample cells are used, then there is no change in θ along the line of sight through the interfaces from the scattering volume to the detectors, no matter what the index of refraction of the solvent in the sample cell, so that a pure solvent, such as toluene, may be used for normalization, as well as

Downloaded by UNIV OF GUELPH LIBRARY on October 10, 2012 | http://pubs.acs.org
Publication Date: May 30, 1996 | doi: 10.1021/bk-1996-0635.ch002

calibration. For geometries where refraction at one or more interfaces yields a difference in scattering angle between light traveling in the solvent and that passing through any of the interfaces intervening between the illuminated volume and the detector (e.g. the longitudinal cylindrical cell in the Wyatt Dawn F, where the cylinder and laser beam axes are parallel), it becomes necessary to use a normalization solution in the same solvent as the sample to be measured. Unfortunately, for aqueous SEC applications, water cannot be used, because its scattering is too weak for reliable measurement.

As mentioned, aqueous normalization solutions can include low molecular weight dextran, polyethylene oxide, and small neutral or zwitterionic micelles, etc. When possible, concentrations should be high enough that the excess scattering signal is well above the pure solvent level, and amounts to a significant percentage of the full scale voltage of each detector.

Once the normalization solvent is chosen, the normalization coefficients are computed as follows:

$$N(q)=\frac{V_n(q_r)-V_s(q_r)}{V_n(q)-V_s(q)} \tag{14}$$

where $V_n(q_r)$ is the scattering voltage from the normalization solution at the scattering vector q_r that corresponds to the reference angle θ_r, $V_s(q_r)$ is the scattering voltage at q_r from the pure solvent the normalization solution is made in, and $V_n(q)$ and $V_s(q)$ are the normalization solution and pure solvent scattering voltages, respectively, at angle θ. In the case of the upright sample cells, where a pure solvent could be used as the normalization solution, $V_s(q_r)$ and $V_s(q)$ refer to the photodetector dark counts (i.e. the voltage measured from a photodetector when no light is incident on it), at the reference angle θ_r and the angle θ, respectively.

It is pointed out that this procedure automatically subtracts out ***constant*** stray light in the system. Constant stray light results from 'glare' off of slightly misaligned or optically 'dirty' windows, imperfections in spatial filtering of the incident laser beam, etc.; it is virtually impossible to totally eliminate stray light, and it is most pronounced at very low and very high scattering angles. In general, large, 'batch' scattering cells exhibit less glare than the small volume flow cells used for SEC. Schmidt (11) has proposed using the ratio of reference solvent (e.g. toluene) scattering with the SEC cell to that of a batch cell as a measure of how well stray light is minimized in the more optically difficult SEC situation. While this ratio is valuable for batch and flow cells of identical geometry, it cannot be used to compare flow and batch cells of different geometry (e.g. upright cylindrical batch cell and a longitudinal flow cell, such as for the Wyatt Dawn F).

As long as the glare remains constant, the normalization, calibration and computational procedures are valid. Care should be taken, however, to reduce stray light to a minimum, by proper sample cell and laser beam alignment and optical cleanliness, and by frequent checks that no additional stray light has built up.

Calibration. Calibration is needed to relate the voltages due to the scattered light to the corresponding, absolute Rayleigh ratio. This requires that a reference scatterer be used, whose absolute Rayleigh ratio I_a, is known. Toluene is

Downloaded by UNIV OF GUELPH LIBRARY on October 10, 2012 | http://pubs.acs.org
Publication Date: May 30, 1996 | doi: 10.1021/bk-1996-0635.ch002

a convenient standard, whose Rayleigh ratio at T=25°C has been measured to be $I_a = 0.00001408\text{cm}^{-1}$ for λ=632nm, and 0.0000396cm^{-1} at λ=488nm. The Absolute Rayleigh ratio I(q) for a scattering voltage V(q) is then given by

$$I(q)=\frac{V(q)-V_s(q)}{V_a(q_r)-V_d(q_r)}N(q)I_aF \tag{15}$$

where $V_a(q_r)$ and $V_d(q_r)$ are the scattering voltages of the calibration reference solvent and the dark voltage, respectively, at the reference angle θ_r. Again, this procedure automatically eliminates, by subtraction, the effects of any constant stray light at θ.

F in the above equation is an optical constant which accounts for two effects: First of all, there is a reflection loss at each interface, and, secondly, because of refraction effects in two dimensions at the sample cell interface, the luminosity of the sample volume will appear smaller for solvents of higher index of refraction. Hence, if samples are measured in solvents different from that of the absolute calibration solvent, a correction for this effect must be made, which depends both on the cell geometry, and the solvents used. This effect has long been recognized (12,13). In the Wyatt Dawn F longitudinal, cylindrical flow cell, it essentially amounts to the ratio of the index of refraction of the sample pure solvent to that of the reference solvent (14).

Minimum measurable mean square radius of gyration $<S^2>_{min}$. It is worthwhile to estimate the minimum mean square radius of gyration $<S^2>_{min}$, which can be measured by a MALLS detector. This estimate addresses the limit set by the actual signal and noise levels of the photodetectors/associated electronics and signal variations of the scattered photon field, and does not include fitting, normalization, glare, scattering impurities or other errors.

$<S^2>_{min}$ depends on the concentration of the scatterer as well as the noise level and resolution of the detectors. If $\sin^2(\theta_{max}/2) \sim 1$, then it is easy to show that $<S^2>_{min}$ is approximated by

$$\langle S^2\rangle_{\min} \approx \left(\frac{3}{q^2{}_{\min}}\right)\left(\frac{\mathrm{N}\delta V}{V(q_{\min})}\right) \tag{16}$$

where ΔV=NδV is the measured voltage difference between scattering at high and low angles (where $\sin^2(\theta_{min}/2)$ is taken as approximately 0) normalized to that at q_{max}, and N is the number of minimum measurable voltages δV, in ΔV. The minimum measurable voltage δV, can be taken as the standard deviation of the voltage fluctuations. The standard deviation squared for the voltage from detector x, V_x , is termed $\sigma^2{}_{V_x}$ and can be computed from a series of m voltage measurements, following the standard definition;

$$\sigma^2{}_{V_x}=\frac{1}{(m-1)}\sum_{i=1}^{m}\left(V_{x,i}-\bar{V}_x\right)^2 \tag{17}$$

Downloaded by UNIV OF GUELPH LIBRARY on October 10, 2012 | http://pubs.acs.org
Publication Date: May 30, 1996 | doi: 10.1021/bk-1996-0635.ch002

where $\bar{V}_x$ is the average voltage of the m measurements from detector x, and $V_{x,i}$ is the voltage of the i^th^ measurement. If $\sigma^2_{V_x}$ is determined from the baseline voltages in an SEC run, then $V_{x,i}$ is the voltage of the i^th^ elution point. It should be pointed out that the origin of δV is actually quite complicated, and embodies noise sources from Poisson fluctuations in the scattered photon field, particle fluctuations in the scattering volume, quantum efficiency of the photodetector, and Gaussian and non-Gaussian noise in the electronics. Highly asymmetric noise from 'dust' and other impurity particles which give a long tail towards the high end of the voltage distribution may also be present, but is not assumed to be part of δV. As such, δV may depend on $\bar{V}_x$ itself, and, in principle, δV should be determined at the voltage level $V(q_{max})$ in eq. 16.

The error estimate is $2\delta V/V(q_{max})$, taking into account errors from the high and low detectors, and assuming the δV of each is the same. For small errors, the error in $Rg=\langle S^2\rangle_{min}^{1/2}$ goes as 1/N. For example, the system at the CERMAV had δV =0.001V for a typical detector. Then, for $V(q_{max}) = 1.0$ V, ($q_{max}=2.64 \times 10^5 cm^{-1}$), R_g=100 A +/- 4.3%, and 60A+/- 12%.

It is clear from equation 16 that the higher the scattering voltage $V(q_{max})$, the smaller the $\langle S^2\rangle_{min}$ that can be resolved. The error level, however, will depend on the details of how δV varies with $V(q_{max})$.

Minimum measurable mass M, by MALLS. Actually, one cannot state the minimum mass M_{min} which is measurable by MALLS, since the minimum detectable intensities depend on all the factors in equation 9. As in the case in the preceding section, the following estimates concern only errors arising from detector signal to noise ratio and scattered field fluctuations. Assume that for minimum measurements the particles will often be quite small and dilute, so that $P(q)\approx 1$ and $A_2c \ll 1$. Then, using equations 12 and 15 (with F~1 in the latter), yields, for a typical detector at any angle;

$$KMc \cong I = \frac{\Delta V I_a}{(V_a - V_d)} \tag{18}$$

Here $\Delta V=V_p-V_s$, where V_p is the voltage of the detector measuring the solution with polymer, and V_s is the voltage measuring pure solvent, I_a is the Rayleigh ratio of the calibration solvent (e.g. toluene), V_a is the voltage of the detector measuring the calibration solvent, and V_d is the dark count of the detector. As in the preceding section ΔV can be expressed in terms of the number of minimum measurable voltages N, as $\Delta V=N\delta V$. Eq. 18 suggests that the sensitivity S, of a detector can be defined in terms of volts per unit Rayleigh ratio, that is,

$$S \equiv \frac{V_a - V_d}{I_a} \tag{19}$$

The minimum value of the product KMc which can be measured is $(KMc)_{min}$, and can be expressed as,

$$(KMc)_{\min} = \frac{\Delta V}{S} \pm \frac{\delta V}{\Delta V} \tag{20}$$

For example, a typical detector in the CERMAV system had $\delta V \sim 0.001V$, for $V_p \sim 1V$, and $V_a - V_d \sim 1.30V$ for toluene at 25°C and for $\lambda = 632nm$. Such a detector thus has a sensitivity of $S = 9.2 \times 10^4$ (volts per unit Rayleigh ratio). For an accuracy of 10%, N must be 10, so that the minimum measurable KMc at this level of accuracy is around 1.1×10^{-6}. For a typical water soluble polymer, dn/dc is around 0.15, so that $K = 1.64 \times 10^{-7}$ and so $Mc = 0.65$ at the 10% error level. Hence, to measure a polymer of M=10,000 to 10%, the minimum concentration would be 6.5×10^{-5} g/cm^3. At the same concentration as this, a polymer of mass 5,000 could be measured to ±20%. Care must be taken, however, not to overload the columns by using excessively high injection concentrations. A rough rule is that the injection concentration should be below the overlap concentration of the polymer c^* for the given eluant conditions, where $c^* \sim M/(4\pi Rg^3 N_A/3)$.

In this context, where $P(q) \sim 1$, averaging multiple detectors will give a more accurate representation of the true mass of the polymer in a given slice, from the point of view of detector limited noise. Hence, from detector limited errors, making a single SEC injection with a MALLS system of, say, 15 light scattering detectors is equivalent to making 15 separate, identical SEC injections into a single angle detector, providing anomalous scattering, such as from 'dust', is not present.

The preceding considerations on minimum measurable Rg and M apply equally to static light scattering in both SEC and 'batch' modes.

Refractometer. RI detectors in the SEC usually use split sample cells in which one half of the sample cell contains the reference solvent, and the flowing sample passes through the other half. A common detection scheme involves passing a laser beam through the cell, which suffers a slight deflection proportional to the index of refraction difference between the liquids in the two halves of the cell. A balanced, split detection diode, which gives a null signal when the liquid in each half of the cell is identical, gives a measurable imbalance signal proportional to this difference. These detectors are usually quite sensitive and can easily measure differences in index of refraction as low as $\Delta n = 5 \times 10^{-7}$. Such RI detectors often come pre-calibrated and give their calibration factor CF in terms of Δn/volt. For uncalibrated instruments, or aging pre-calibrated ones, it is recommendable to check the calibration periodically; e.g. by injecting saline solutions of known Δn through the flow cell. The Polymer Handbook, (15) for example, gives extensive calibration information for different salts in aqueous solution. For aqueous solutions of NaCl at T=25°c and $\lambda = 632nm$,

$$\Delta n = 1.766 \times 10^{-3}[\text{NaCl}] \tag{21}$$

where [NaCl] is measured in grams of NaCl per 100 grams of water.

In order to compute the weight averaged mass of each elution slice i, termed M_i, it is necessary to know the concentration of the slice c_i, as well as the

Downloaded by UNIV OF GUELPH LIBRARY on October 10, 2012 | http://pubs.acs.org
Publication Date: May 30, 1996 | doi: 10.1021/bk-1996-0635.ch002

Downloaded by UNIV OF GUELPH LIBRARY on October 10, 2012 | http://pubs.acs.org
Publication Date: May 30, 1996 | doi: 10.1021/bk-1996-0635.ch002

scattered intensity at each detector q, $I_i(q)$. c_i can be computed two different ways: The absolute calibration factor CF, of the RI can be used;

$$c_i = \frac{\Delta V_{RI,i} CF}{(dn/dc)} \tag{22}$$

where $\Delta V_{RI,i}$ is the baseline subtracted RI voltage at the i^{th} elution slice. As long as one is confident of the values of CF and dn/dc, this method is preferable to the second method of *assuming* that all the injected material elutes completely through the SEC system (i.e. that $M_{eluted} = C_0 V_{inj}$, where V_{inj} is the injection loop volume and C_0 is the injected concentration) and summing the RI signal over the whole elution peak, with Δv_j the elution volume increment of the j^{th} point, and taking

$$c_i = \frac{C_0 V_{inj} \Delta V_{RI,i}}{\sum_j \Delta V_{RI,j} \Delta v_j} \tag{23}$$

(The error in eq. 10 in ref. 30 is noted here). The problem with this latter method is that, at least in aqueous SEC, there is often adsorption of material in the column, so that it cannot be assumed that all the material passes through. In fact, if the CF and dn/dc values are known, the fraction of material eluting through the columns is simply the sum over all i elution slices of $c_i \Delta v_i$, with c_i given by equation 22, divided by the total injected mass $C_0 V_{inj}$.

Instrumentation used. Data were collected from an SEC system at the CERMAV/CNRS in Grenoble, and consisted of a Waters 150c gel permeation chromatograph containing the injector and RI. A single capillary fitted with T-junctions leading to a differential pressure transducer, was used for the viscometer. A Hewlett Packard series 1050 pump gave smooth operation with no pulsing in the viscometer input, whereas the stock pump of the Waters 150c gave a high level of pulsation. Originally the system was equipped with a Chromatix CMX 100 low angle light scattering detector (LALLS), and the system in that configuration was described earlier (16). A Wyatt Dawn F (MALLS) (17) was installed along with the other detectors. The SEC flow went from the columns to the viscometer, to the LALLS, to the MALLS, and finally to the refractometer. After a comparison between the LALLS and MALLS was made, the LALLS was removed in subsequent work.

Fifteen angles from the MALLS and the RI signal were captured on the 16 single input lines to the DT2801-A analog-to-digital (A/D) converter in the bus of an IBM compatible microcomputer. The DT2801-A has 12 bits of resolution. A second A/D board, a DT2808/5716, with 16 bit resolution and 8 differential inputs, was installed in the microcomputer and assigned to Direct Memory Access (DMA) channel #3. This board captured the full viscometer output signal, as well as the nulled output (i.e. with the solvent baseline viscosity voltage subtracted), and the LALLS signal. Thus, a total of 19 signals were captured and analyzed. The author wrote software to simultaneously collect, and subsequently analyze, data from the coupled instruments.

Interdetector dead volumes are critically important factors in accurately analyzing the data, as discussed below, and were roughly assessed to be 0.088mL

Downloaded by UNIV OF GUELPH LIBRARY on October 10, 2012 | http://pubs.acs.org
Publication Date: May 30, 1996 | doi: 10.1021/bk-1996-0635.ch002

between the viscometer and the LALLS, 0.105mL between the LALLS and MALLS, and 0.230mL between the MALLS and RI detectors.

Materials. Highly purified bacterial sodium hyaluronate was obtained from both Sigma Chemical Co. and other industrial sources. Dialyzed sodium polystyrene sulfonate (NaPSS) was obtained from Pressure Chemical Co. Proteoglycan subunits were a gift from Dr. Anna Plaas at Shriners Childrens' Hospital (Tampa, Florida).

The SEC eluants were aqueous solutions of NH_4NO_3 at varying ionic strengths. The pH of the eluant was unadjusted, and was around 6.0. All the polyelectrolytes used were fully ionized (at least to the 'counterion condensation limit') in these eluants.

The SEC columns were Shodex OHpak SB-804HQ and OHpak SB-805HQ (from JM Science, Buffalo, NY), connected in series. The column packing material was poly(hydroxymethyl methacrylate) gel.

Results

Typical Data. Figure 1a shows typical raw, unsmoothed data for scattering at $\theta = 90^o$, the RI and single capillary viscometer data. Data were always clean enough, even at the low angles, that no type of smoothing was necessary. The sample was sodium hyaluronate (HA), partially degraded by HCl, eluted in a low ionic strength solution; 0.005M NH_4NO_3. At this fairly low ionic strength, A_2=0.016 cm^3-mole/g^2 (18), quite a large value compared to about 0.003 at high Cs, making its inclusion in the computation based on equation 9 important. The value of dn/dc was taken as 0.155. The flow rate was 1 mL/min, the injected volume of the 2 mg/mL stock solution was 0.2mL, and the detectors were sampled every two seconds.

Figure 1b shows the resulting distributions for C(M), Rg(M) and η(M), respectively. Table I gives the corresponding mass, Rg and viscosity averages and exponents, with estimates of errors from the different sources discussed below. The value of γ is consistent with high electrostatic excluded volume in the HA polyelectrolyte chain (18), and the value of β is consistent with equation 2.

As a preliminary test of the system against 'known standards', various fractions of NaPSS were measured. The manufacturer's value of dn/dc=0.189 (based on multiple independent tests from outside laboratories) was used. The results are shown in Table II. The measured M_w for the nominal M_w= 35,000 and 200,000 were basically exact, and showed very low polydispersity, whereas the nominal M_w=780,000 material was seen to be significantly degraded, with measurable polydispersity.

Comparison of MALLS and LALLS. LALLS detectors make the assumption that $q^2<S^2>$ is nearly zero in equation 12, so that the mass can be computed directly from the value of the low angle intensity. Since the low angle of the Chromatix CMX 100 subtends 5.1^o to 6.1^o, this assumption will be good to within 5%, for particles with Rg=170nm. In this case, the mass distribution C(M) resulting from extrapolation of MALLS data to q=0 and that from the LALLS data should agree.

Figure 2a gives an example of the MALLS/LALLS C(M), taken on the same

Downloaded by UNIV OF GUELPH LIBRARY on October 10, 2012 | http://pubs.acs.org
Publication Date: May 30, 1996 | doi: 10.1021/bk-1996-0635.ch002

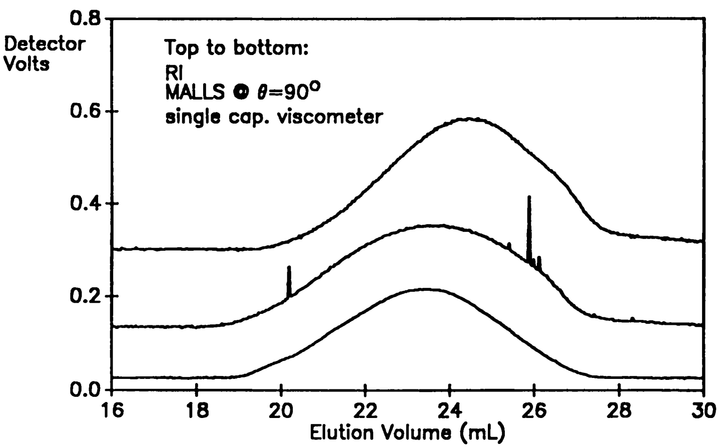

Figure 1a. Typical raw voltage signals from the RI, MALLS (only the $\theta=90^{\circ}$ signal is shown), and baseline-subtracted single capillary viscometer. The sample was partially degraded sodium hyaluronate in low ionic strength eluant (5mM NH_4NO_3). Flow rate was 1 mL/min, and 2 mg/mL were injected into a 0.2mL injection loop.

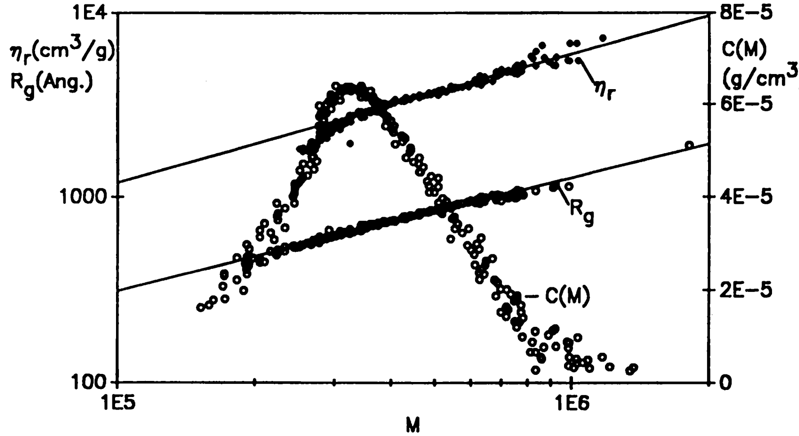

Figure 1b Analysis of data from fig. 1a in terms of C(M), Rg(M) and $\eta_r(M)$. Table I gives the numerical values of the corresponding moments and exponents, and the error bars for each parameter.

In Strategies in Size Exclusion Chromatography; Potschka, M., et al.;
ACS Symposium Series; American Chemical Society: Washington, DC, 1996.

Downloaded by UNIV OF GUELPH LIBRARY on October 10, 2012 | http://pubs.acs.org
Publication Date: May 30, 1996 | doi: 10.1021/bk-1996-0635.ch002

Table I SEC characterization of partially degraded HA. Eluant was 0.1M NH_4NO_3. Injection concentration was 2.0 mg/ml in an injection volume of 0.2mL

	M_n kDal	M_w kDal	M_z kDal.	$R_{g,w}$(Ang.)	γ	$\eta_{r,w}$	β
Best value	339.8	392.8	486.9	710	0.603	2572	0.828
Source of Error				Errors in %			
Random noise/fitting	0.9	1.8	13.1	1.7	1.0	0.1	1.6
$\delta\tau_1$(0.15±0.05 mL)	-	-	-	-	-	-	7.8
$\delta\tau_2$(0.105±0.08 mL)	2.0	-	1.4	0.6	6.8	-	-
A_2 (0.016±0.002)	6.2	7.4	10.5	4.3	0.6	-	1.1
dn/dc,(0.155± 0.008cm^3/g)	5.2	5.2	5.2	-	-	5.2	-
RI cal.fact., CF	3.0	3.0	3.0	-	-	3.0	-
Total error in %	8.9	10.0	17.9	4.7	6.9	6.0	8.0

Table II. Molecular weight results for NaPSS 'standards' (Pressure Chemical Co.). Manufacturer lists $M_w/M_n \leq 1.10$.

Nominal M_w	M_n	M_w	M_z
35,000	33,700 ± 900	35,170 ± 750	36,900 ± 1,200
200,000	199,300 ± 1,700	200,200 ± 1,600	201,100 ± 1,800
780,000	464,500 ± 20,100	567,500 ± 15,800	659,100 ± 15,400

Downloaded by UNIV OF GUELPH LIBRARY on October 10, 2012 | http://pubs.acs.org
Publication Date: May 30, 1996 | doi: 10.1021/bk-1996-0635.ch002

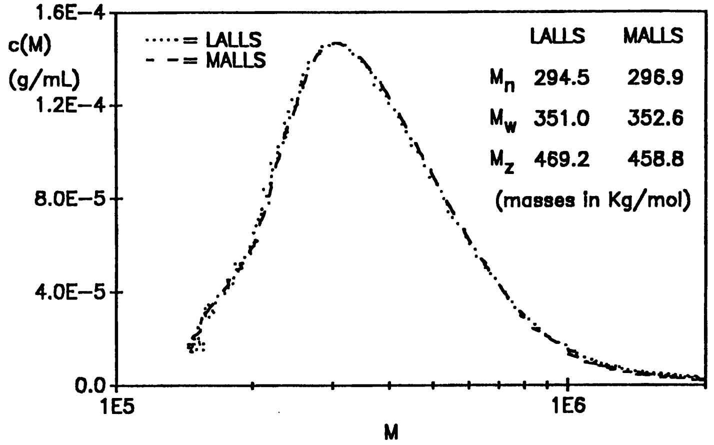

Figure 2a Comparison of LALLS and MALLS for partially hydrolyzed hyaluronate at [NH_4NO_3]=0.1M. The results are virtually identical. (Printed with permission from ref. 30)

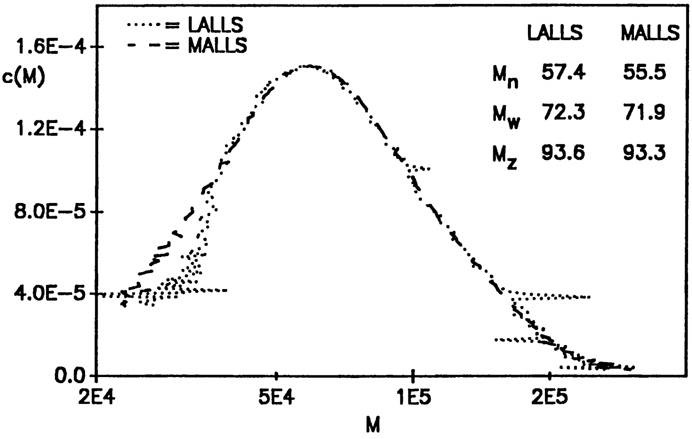

Figure 2b Further comparison of LALLS and MALLS for lower mass HA. Again, agreement is good, but problems with 'scattering spikes' in LALLS are more evident. (Printed with permission from ref. 30)

injected sample, when the LALLS and MALLS were connected in series. The general agreement of the C(M) shapes, and corresponding moments are excellent. Because the MALLS can measure multiple angles over a wide range, however, it has the advantages of sampling scattering at higher angles, which are less prone to scattering from 'dust' and other optical impurities, and also averages out anomalous fluctuations and noise by providing data from many angles. Figure 2b shows the comparison for more highly degraded, smaller mass HA than in figure 1a. The agreement between the MALLS/LALLS is again quite good, but with weaker scattering signals the problems of 'dust spikes' in the LALLS spectrum are more apparent, but are absent in the MALLS spectrum.

Further advantages of the MALLS are that it provides Rg(M) information, as well as possible detailed information on the form of the molecule from P(θ). Figure 3 shows Kc/I vs. q^2 for a renatured xanthan (heated to 80°C then cooled), indicating a wormlike chain conformation (19) with mass around 2.5×10^6. The inset is a representation of qI/Kc, from whose plateau the mass per unit contour length of the polymer M/l can be determined according to (20)

$$\frac{qI}{Kc} = \pi \frac{M}{l} \tag{24}$$

The ratio of the peak height to plateau allows an estimation of the number of Kuhn segment lengths in the polymer using a procedure by Schmidt et al (21). For the xanthan of figure 3, there are about 6 Kuhn lengths, of length L_k about 188nm, and the xanthan has a contour length of around 1130nm.

A further advantage of the multi-angular P(q) data is to obtain possible information on interparticle correlation (see section "Liquid-like Correlations..." and figure 7, below).

From these data and considerations it is clear that MALLS is the method of choice for static light scattering detection in the SEC environment. Furthermore, the price of diode photodetectors is low enough, and the complete automation and powerful data storage and processing afforded by inexpensive microcomputers are so compelling, that MALLS detectors should be outfitted with as many angles as possible. For utterly routine determinations of substances of low enough molecular weights and dimensions that the $q^2\langle S^2\rangle \ll 1$ criterion is always fulfilled, a small number of detectors may nonetheless be adequate. For larger particles whose P(θ) reveal important structural information, and/or whose interactions give significant interparticle structure information S(q), a large number of angles is desirable.

Application to polyelectrolytes

Ionic strength effects on elution behavior of polyelectrolytes.

The effects of ionic strength on both columns and elution behavior have been dealt with by various authors (22,23).

Figure 4 shows how strongly the elution profile of a highly charged polyelectrolyte, NaPSS of M=35,000 g/mole, is affected by changes in ionic strength; expansion of the molecule and the repulsive interaction of its more extended ionic atmosphere with the gel pores at low ionic strength (5mM), causes it

Downloaded by UNIV OF GUELPH LIBRARY on October 10, 2012 | http://pubs.acs.org
Publication Date: May 30, 1996 | doi: 10.1021/bk-1996-0635.ch002

Downloaded by UNIV OF GUELPH LIBRARY on October 10, 2012 | http://pubs.acs.org
Publication Date: May 30, 1996 | doi: 10.1021/bk-1996-0635.ch002

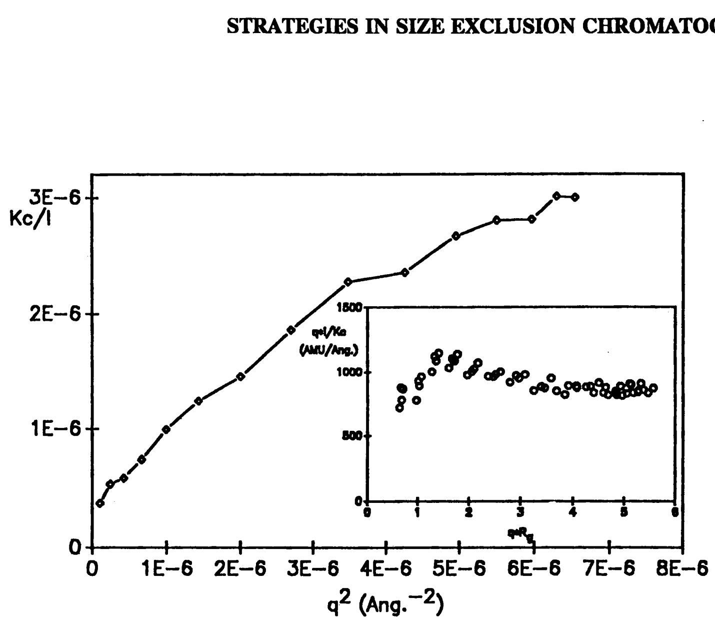

Figure 3. Kc/I vs. q^2 for renatured xanthan fractionated by SEC, showing wormlike chain form factor. Xanthan concentration is 4.2 x 10^{-6} g/mL. Inset shows qI/Kc, whose plateau at high q yields the mass per length of the xanthan M/L, via. equation 24. (Adapted from ref. 19)

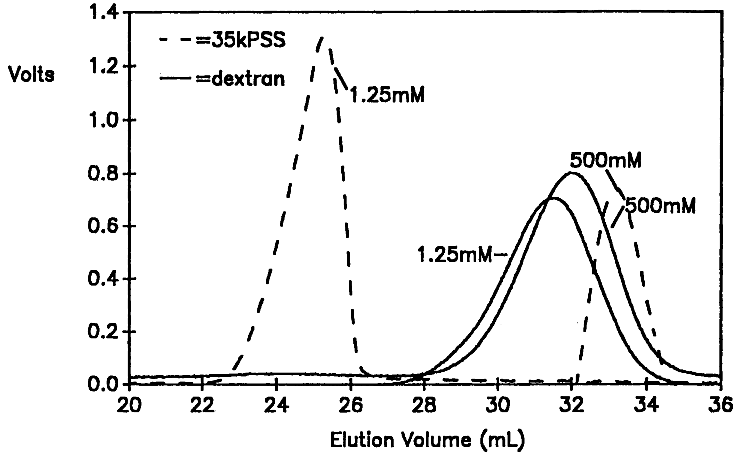

Figure 4. Effect of ionic strength on elution profiles of two small polymers. 35k NaPSS, a strong polyelectrolyte is highly affected by the change in ionic strength, whereas neutral dextran of similar mass, suffers a much smaller effect.

Downloaded by UNIV OF GUELPH LIBRARY on October 10, 2012 | http://pubs.acs.org
Publication Date: May 30, 1996 | doi: 10.1021/bk-1996-0635.ch002

to act as an effectively larger molecule and elute at lower volumes. Electrostatically neutral dextran of similar mass, in contrast, shows only a minor change in elution profile with changing ionic strength.

Although the shifts in elution profiles for polyelectrolytes with changing ionic strength are irrelevant as far as data evaluation is concerned, since absolute parameter determinations using MALLS are independent of the mode of separation, it is nonetheless instructive to see how such changes can radically affect the 'universal calibration' (24) procedure in the case of polyelectrolytes. It is recalled that this method involves plotting $[\eta]M$ vs. elution volume to produce a single curve for all polymers of 'similar architecture' (e.g. random coils). $[\eta]M$ is proportional to the hydrodynamic volume of the polymer, which means that a single curve vs. elution volume will be produced as long as the SEC column truly separates polymers according to hydrodynamic volume. While this mechanism may often apply for neutral polymers in organic solvents (25), it frequently fails for aqueous solutions of polyelectrolytes (26-30). Figure 5a shows how much this can fail when different polyelectrolytes at different ionic strengths are used. Actually $[\eta]$ is replaced by η_r in $[\eta]M$, since it is η_r which is measured by SEC. The failure of 'universal calibration' in contexts such as figure 5a is thought to be due to non-size exclusion effects being involved in the separation, such as specific sorption and electrostatic effects.

Whereas figure 5a shows that separation in the polyelectrolyte context does not take place according to hydrodynamic volume, figure 5b shows Rg vs. elution volume, illustrating the fact that the separation is also not taking place according to Rg; i.e. molecules of widely varying Rg can elute at the same elution volume.

Determination of polyelectrolyte dimensions as a function of ionic strength. Decreasing the ionic strength of a solution of semi-flexible polyelectrolytes leads to an increase in the dimensions a polyelectrolyte coil, as the like charges on the chain repel each other. A full rodlike form is not easily reached, however, since the all-trans form needed for the coil to become rodlike is the lowest entropy state of all the coil conformations. Hence, there is a balance between the tendency for the coil to expand due to electrostatic repulsion, and for it to remain highly random due to entropy. Several theories exist to quantify the dimensions of polyelectrolyte chains, which involve two main ideas; the local stiffening of the chain due to the charge, embodied in the 'electrostatic persistence length' concept (EPL) (31,32), and the long range effect of the electrostatic repulsion preventing distant monomers along the chain getting too close to each other, embodied in the electrostatic excluded volume (EEV) concept (33,34). Combinations of these theories, with no adjustable parameters, have enjoyed reasonable success in describing polyelectrolyte dimensions and second virial coefficients (A_2) for moderate ionic strengths (i.e. roughly 1mM to 1M) (18,35-39).

Static light scattering has been a useful means of determining polyelectrolyte dimensions and interactions, especially since extremely low concentrations (less than 10^{-5}g/cm^3), below the overlap concentration c^* can be used. While neutrons and x-rays allow direct determinations of the local stiffness of polymers, such experiments typically require at least one thousand times more concentration (>10^{-2}g/cm^3), well above c*, in order to be performed (40). Dynamic light scattering of

Downloaded by UNIV OF GUELPH LIBRARY on October 10, 2012 | http://pubs.acs.org
Publication Date: May 30, 1996 | doi: 10.1021/bk-1996-0635.ch002

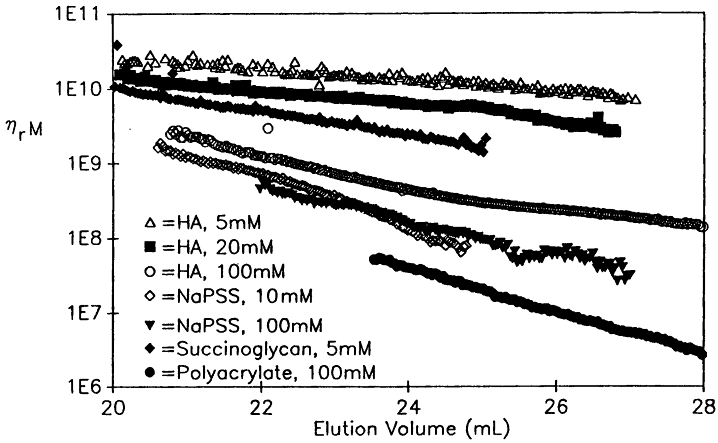

Figure 5a Failure of universal calibration for various polyelectrolytes at different ionic strength. (Printed with permission from ref. 30)

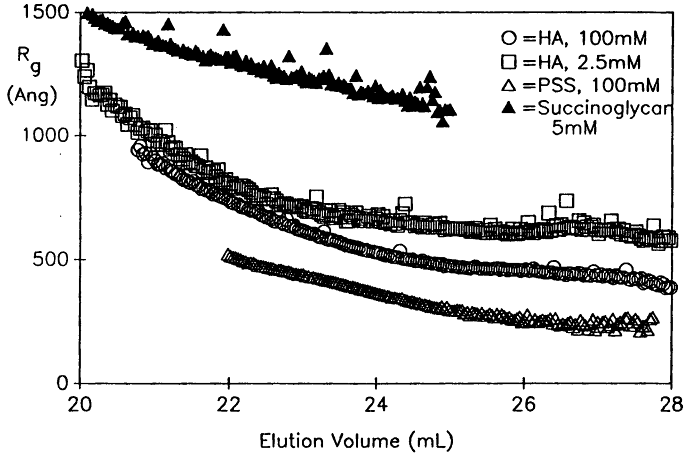

Figure 5b Separation in the columns also does not take place according to R_g. (Printed with permission, from ref. 30)

polyelectrolytes under changing ionic strength has been shown to be insensitive to changes in coil dimensions for several linear polyelectrolytes (18,35,38).

Since SEC with the MALLS and RI requires no calibration, eluting with different ionic strengths is a valuable means of studying changes in polyelectrolyte dimensions and viscosity. Figure 6, taken from ref. 36, shows the same HA as in figures 1a,b and 2a, eluted at different ionic strengths. The calculated grid is from the combined EPL and EEV theories, with no adjustable parameters. The experimental points fall virtually on top of the computations, indicating the adequacy of the calculations for the range of ionic strengths studied.

Unfortunately, there is no adequate theory for polyelectrolyte viscosity, which accounts for excluded volume effects. A first approach, with no excluded volume corrections, however, is found in ref. 41. Usually, that theory seems to overestimate the viscosity (42).

Downloaded by UNIV OF GUELPH LIBRARY on October 10, 2012 | http://pubs.acs.org
Publication Date: May 30, 1996 | doi: 10.1021/bk-1996-0635.ch002

Liquid-like correlations of polyelectrolytes under shear flow. The light scattered from very dilute, salt-free polyelectrolyte 'batch' solutions often manifests a broad angular peak (39,43-45). Figure 7 shows the angular scattering envelopes under SEC flow (adapted from ref. 46) for proteoglycan subunits (aggrecan), which consist of a protein backbone to which many highly charged poly- and oligosaccharide chains are attached. The proteoglycan mass is about 1.5 million. The fact that the peaks continue to exist even under the high shear flow conditions in the SEC suggest that dynamic, liquid-like correlations are the origin of the effect, not any type of clustering or long range order. On the same figure, the normal, monotonically decreasing I(q) from elution with a moderate ionic strength is also shown. The peaks are lost, in fact, when the salt concentration is on the order of the concentration of charged monomers.

Error analysis

Systematic errors. These include errors in the physical parameters dn/dc and A_2, and in the RI calibration constants, the factor F in equation 14, interdetector dead volumes, diffusion broadening effects, and anisotropic normalization. Most of these errors have been treated at length in ref. 30, and are only summarized here. Diffusion broadening has been treated elsewhere (47,48)

Interdetector dead volume errors. This seemingly lowly source of error actually has very deleterious effects on the data evaluation from the coupled detectors. Let $\delta\tau_1$ be the *error* in the dead volume determination between the viscometer and the MALLS and $\delta\tau_2$ be that between the MALLS and the RI. Let M_n', M_w', and M_z' be the erroneous values of the number, weight and z-averaged masses respectively, due to the dead volume error. Then, to first order, considering that $\delta\tau_1$ and $\delta\tau_2$ much smaller than the width of the elution peak, it has been shown that to first order (30),

Downloaded by UNIV OF GUELPH LIBRARY on October 10, 2012 | http://pubs.acs.org
Publication Date: May 30, 1996 | doi: 10.1021/bk-1996-0635.ch002

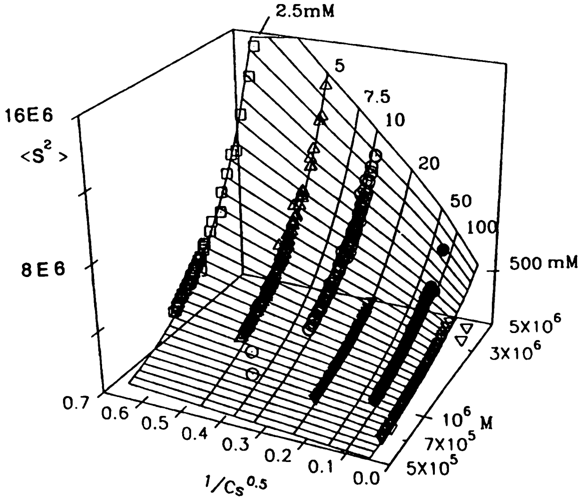

Figure 6. SEC of hyaluronate at different ionic strengths. $\langle S\rangle^2$ is the vertical axis, vs. mass M, and $1/\sqrt{C_S}$. The grid is the calculation of $\langle S^2\rangle$, with no adjustable parameters, using combined EPL and EEV theories. (Printed from ref. 36).

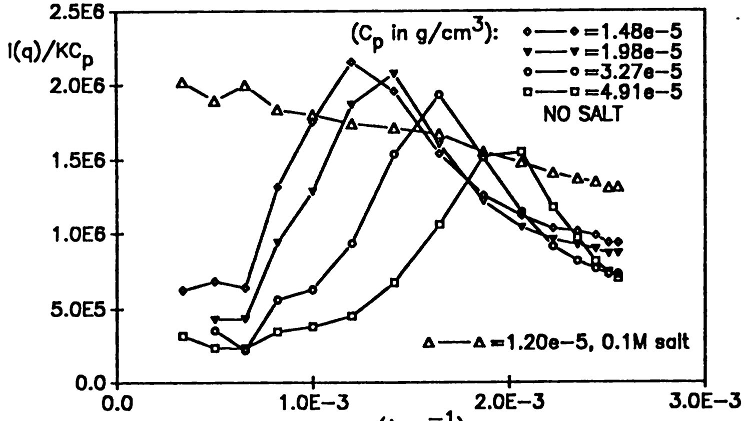

Figure 7. I/Kc vs. q for proteoglycan subunits. The peaks are obtained when elution is with pure water, and are presumably due to dynamic, liquid-like correlations between the highly charged proteoglycans in the shear flow. When salt is added (monotonically decreasing line), the peak disappears. (Adapted from ref. 46).

$$M_n' = M_n\left(1 - 2\delta\tau_2 \frac{\sum \dot{c}_i / M_i}{\sum c_i / M_i}\right) \tag{25a}$$

where $\dot{c}_i \equiv \left.\frac{\partial c}{\partial v}\right)_i$ is the derivative of the RI signal with respect to the elution volume, evaluated at the i^{th} elution slice.

Fortunately, to first order there is no dead volume effect on M_w, so that

$$M_w' \cong M_w \tag{25b}$$

M_z' is affected according to

$$M_z' \cong M_z - \delta\tau_2 \frac{\sum M_i^2 \dot{c}_i}{\sum M_i c_i} \tag{25c}$$

Figure 8a shows the effects on M_n', M_w', and M_z' due to errors in $\delta\tau_2$, using the same HA as in the other figures. It is seen that M_n' and M_z' are affected in opposite ways, and hence the polydispersity indices M_z/M_w and M_w/M_n are overestimated by negative values of $\delta\tau_2$, and underestimated by positive values.

To first order, the effect of $\delta\tau_2$ on $<S^2>$ is negligible at each elution slice, that is

$$<S^2>_i' \cong <S^2>_i \tag{26}$$

Hence, the n-, w- and z-averages of $<S^2>$ are also only negligibly affected by $\delta\tau_2$.

The effect of $\delta\tau_2$ on the exponent γ in equation 1a is quite alarming. In fact, an error in $\delta\tau_2$ should cause a plot of $\log(<S^2>)$ vs. logM to be non-linear, with an instantaneous slope γ' given by

$$\gamma'_i \cong \gamma\left(1 - \frac{\dot{c}_i\, \delta\tau_2}{c_i}\right) \tag{27}$$

This equation suggests that, in principle, the true γ can be found to a good approximation, despite dead volume error, from the slope of the $\log(<S^2>)$ vs. logM curve, at the point(s) where $\dot{c}_i = 0$, that is, at the peaks of the concentration elution profile c(v). Figure 8b shows γ' from forced linear fits for different values of $\delta\tau_2$.

For a log-normal polymer mass distribution of the form

$$c(\mathrm{v}) = c_o \exp\left[-\alpha(\mathrm{v} - \mathrm{v}_o)^2\right] \tag{28}$$

where $1/\sqrt{\alpha}$ is the width of the distribution, the erroneous γ are given by

$$\gamma' \cong \gamma\left[1 + 2\alpha(\mathrm{v} - \mathrm{v}_o)\delta\tau_2\right] \tag{29}$$

This shows that the narrower the polymer mass distribution, the greater the error in γ for a given $\delta\tau_2$.

The viscosity exponent β in equation 1b depends, in principle, on both dead

Downloaded by UNIV OF GUELPH LIBRARY on October 10, 2012 | http://pubs.acs.org
Publication Date: May 30, 1996 | doi: 10.1021/bk-1996-0635.ch002

Downloaded by UNIV OF GUELPH LIBRARY on October 10, 2012 | http://pubs.acs.org
Publication Date: May 30, 1996 | doi: 10.1021/bk-1996-0635.ch002

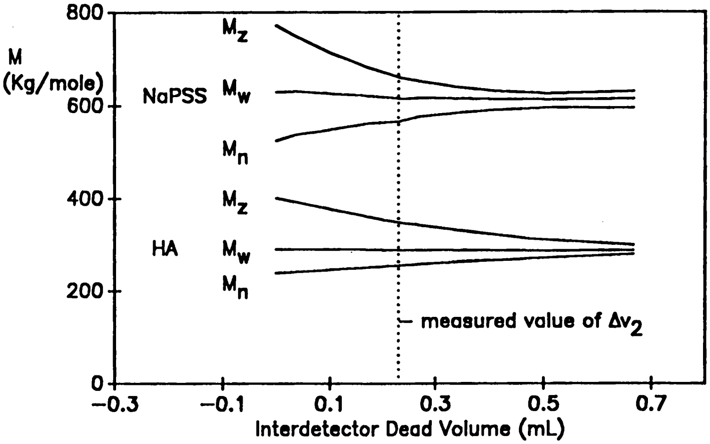

Figure 8a Dead volume effect on Mn, Mw, Mz. For HA of figure 1a, except at 0.1M NH_4NO_3 elution. (Adapted with permission from ref. 30)

Downloaded by UNIV OF GUELPH LIBRARY on October 10, 2012 | http://pubs.acs.org
Publication Date: May 30, 1996 | doi: 10.1021/bk-1996-0635.ch002

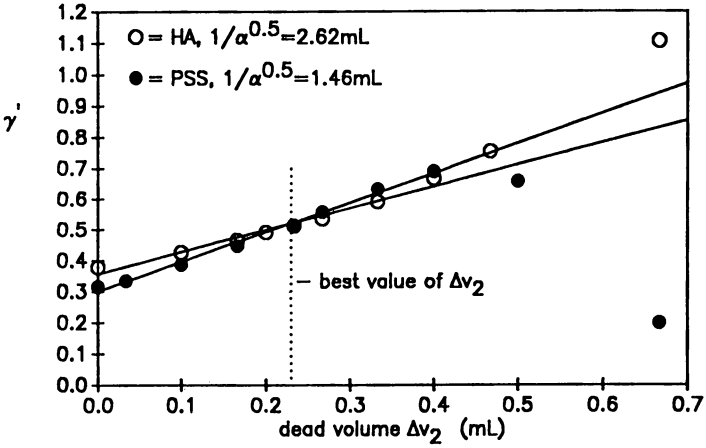

Figure 8b. Dead volume effects on Rg exponent γ in equation 1a. Same HA and conditions as figure 8a. (Printed with permission from ref. 30)

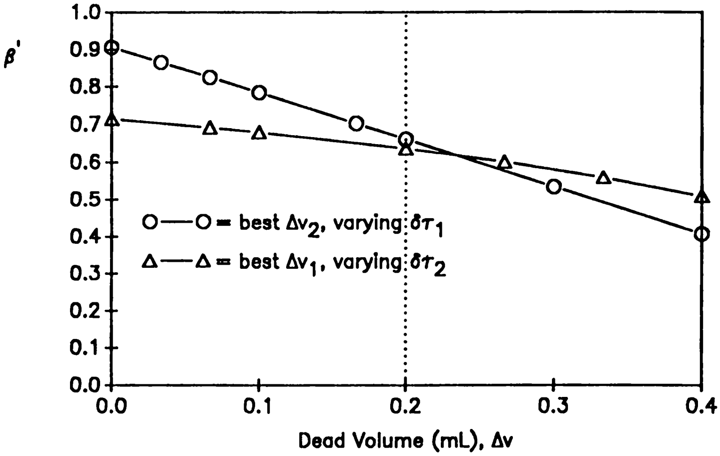

Figure 8c. Dead volume effects on viscosity exponent β in equation 1b. Same HA and conditions as figure 8a. (Printed with permission from ref. 30)

volume errors $\delta\tau_1$ and $\delta\tau_2$. Carrying out the analysis, however, reveals that, to first order,

$$\beta' \cong \beta\left(1+\frac{\dot{c}_i}{c_i}\delta\tau_1\right) \tag{30}$$

Figure 8c shows β' as a function of $\delta\tau_1$ and $\delta\tau_2$, showing the dependence on $\delta\tau_2$ is much slighter than on $\delta\tau_2$. Furthermore, it turns out that to all orders, there are no dead volume effects on the weight averaged viscosity η_w, that is

$$\eta_w' = \eta_w \tag{31}$$

Errors due to A_2. Values of A_2 normally need to be determined in a separate experiment (e.g. a 'batch' static light scattering measurement). In the following, A_2' is the erroneous value of A_2, and A_2 is assumed to be independent of M. Naturally, the effects of A_2 increase with the concentration of material injected into the SEC system.

The n- and w- averages of mass are affected according to

$$M_n' \cong M_n\left[1+2(A_2'-A_2)\frac{\sum c_i^2}{\sum c_i / M_i}\right] \tag{32}$$

and

$$M_w' \cong M_w + 2(A_2'-A_2)\frac{\sum M_i^2 c_i^2}{\sum c_i} \tag{33}$$

To first order, there is no effect on γ from using an erroneous value of A_2. The value of the w-averaged $<S^2>$, however, is systematically affected according to

$$<S^2>_w' \cong <S^2>_w + 2(A_2'-A_2)\frac{\sum <S^2>_i M_i c_i^2}{\sum c_i} \tag{34}$$

(The error in the denominator of the second term in eqs. 55 and 58 in ref. 30 for M_w' and $<S^2>_w'$ are noted here).

Finally, η_w is independent of errors in A_2 to all orders, whereas small errors in A_2 will have a slight effect on β.

Details on errors due to 'fossilized' normalization errors and non-isotropic normalization can be found in ref. 30, whereas effects due to interdetector diffusion broadening, theories employed for light scattering interpretation, and flow effects of viscometry measurements can be found in refs. 49 and 50, respectively.

Random errors. The main source of random errors is the random noise in each SEC detector, and long-term detector drift, which may be 'systematic' for a given run, but varies randomly from run to run.

Downloaded by UNIV OF GUELPH LIBRARY on October 10, 2012 | http://pubs.acs.org
Publication Date: May 30, 1996 | doi: 10.1021/bk-1996-0635.ch002

Downloaded by UNIV OF GUELPH LIBRARY on October 10, 2012 | http://pubs.acs.org
Publication Date: May 30, 1996 | doi: 10.1021/bk-1996-0635.ch002

The noise level in each detector is most simply characterized by the standard deviation of the baseline voltage. The standard deviation squared for the voltage from detector x is given by equation 16. In fits and calculations involving voltages from detector x, weighting factors of $1/\sigma^2_{V_x}$ can optionally be used, according to the procedures of Bevington (51), for example. Ref. 30 provides a compendium of expressions for estimating the errors in the mass, radius of gyration and viscosity averages, as well as on the exponents γ and β, based on these computed values of $\sigma^2_{V_x}$.

Drift in the detector baselines can lead to severe distortions in all of the distributions C(M), Rg(M) and η_r(M), and the corresponding moments and exponents. Examples of such distortions are given in ref. 30. The best means of avoiding this effect is obviously to use well stabilized detectors before beginning SEC runs. Data analysis programs often offer a linear correction to wandering baselines. While this latter method is no substitute for truly stable instruments, it is often a reasonable approximate solution, and better than using no correction at all.

Table I gives the errors associated with the various parameters for the data and distributions from figures 1a,b. Since most of the errors are completely independent of each other, it is assumed they add in quadrature in determining the total error bar on each quantity. Interestingly, in this example the single largest error in most of the parameters is the value of A_2, a systematic error independent of the SEC apparatus. Being a strong, semi-flexible polyelectrolyte, the value of A_2 is strongly dependent on Cs (18, 35-39). At Cs= 5 mM, A_2=0.016±0.002, which is quite high compared to the value at high Cs of about 0.003. Except for the effect on M_z, the random fitting errors from the raw data are quite small compared to the systematic errors. It is noted that the viscosity and Rg exponents β and γ, respectively, fall clearly within the relationship of equation 2.

Conclusions

The use of coupled MALLS, RI and viscosimetric detectors to SEC systems affords a comprehensive, practical characterization of polymers in terms of absolute mass distributions, static polymer dimensions and reduced viscosity. Furthermore, such characterizations allow current polymer theories to be tested. An example of the application to polyelectrolyte characterization shows the expected, strong effect of ionic strength on polyelectrolyte dimensions and viscosity.

No type of 'universal' calibration (which can fail dramatically in many instances) nor other column-based calibration is needed when MALLS and RI detectors are present. A number of sources of error, however, must be accounted for when analyzing data from the coupled detectors. Interdetector dead volume effects can be particularly pernicious, especially as concerns the scaling relations between Rg, η_r and M.

SEC with coupled RI, MALLS and viscometric detectors can be usefully applied to the practical characterization of polyelectrolytes, including their behavior as a function of ionic strength. At high enough ionic strengths (often about 0.1M salt), polyelectrolyte behavior can resemble that of neutral polymers. Large, water soluble polymers can also be characterized, but attention must then be paid both to whether they are truly separating on a given column, or merely coming out in the exclusion volume, and to the form of P(q) used in eq. 9.

Symbols Used

RI= refractive index detector
MALLS= multi-angle laser light scattering
LALLS= low angle laser light scattering
SEC= size exclusion chromatography
M= molecular mass
M_n= number averaged molecular mass
M_w= weight averaged molecular mass
M_z= z-averaged molecular mass
M_n', M_w', M_z' = erroneous mass averages
$<S^2>$= mean square radius of gyration
R_g=$<S^2>^{1/2}$= root mean square radius of gyration
A_2= second virial coefficient (cm^3-mole/g^2)
V_H= polymer hydrodynamic volume
c= polymer concentration (g/cm^3)
η= total solution viscosity (Poise)
η_r= reduced viscosity (cm^3/g)
[η]=intrinsic viscosity (cm^3/g)
I(q)= excess Rayleigh scattering ratio from polymer (cm^{-1})
P(q)= polymer form factor
$q=(4\pi n/\lambda)\sin(\theta/2)$=scattering vector ($cm^{-1}$)
n= solvent index of refraction
θ= scattering detection angle
λ= vacuum wavelength of incident light source
dn/dc= incremental refractive index for a polymer/solvent system
N_A= Avogadro's number
Q= volume flow rate (cm^3/s)

$\dot{\gamma}$= shear rate (s^{-1})
C_s= concentration of added salt
CF= refractive index detector calibration factor (Δn/volt)
N(q)= normalization factor for photodetector at scattering vector q
q_r= q of photodiode used for normalizing the other photodiodes
$V_n(q)$=voltage of photodetector at q due to scattering from normalization solution
$V_s(q)$=voltage of detector at q due to scatt. from pure solvent of polymer solution
$V_d(q)$= dark voltage (i.e. no scattering signal) of detector at q
$V_a(q_r)$=voltage at q_r due to scattering from calibration solvent (e.g. toluene)
V_v= voltage from the viscosity detector
$\delta\tau_1$= *error* in dead volume determination between viscometer and MALLS
$\delta\tau_2$= *error* in dead volume determination between MALLS and RI detector
EPL= electrostatic persistence length
EEV= electrostatic excluded volume

Downloaded by UNIV OF GUELPH LIBRARY on October 10, 2012 | http://pubs.acs.org
Publication Date: May 30, 1996 | doi: 10.1021/bk-1996-0635.ch002

NaPSS= sodium polystyrene sulfonate
HA= sodium hyaluronate

Acknowledgments

The author acknowledges support from NSF MCB 9116605, Elf Aquitaine Corp. and the Academie des Sciences (France). Many conversations with Marguerite Rinaudo are likewise acknowledged.

Literature Cited

1. Provder, T. *Particle Size Distribution II*, **1991**, ACS Symposium Series 472
2. Dos Ramos, J.G.; Silebi, C.A. *J. Colloid & Int. Sci.*, **1990**, 135, *1*, 165
3. Lecacheux, D.; Lesec, J.; Quivoron, C. *J. App. Polym. Sci.*, **1982**, *27*, 4867
4. Haney, M.A. *J. App. Polym. Sci.*, **1985**, *30*, 3023
5. Bo, S.; Milas, M.; Rinaudo, M. *Int. J. Biol. Macromole.*, **1987**, *9*, 153
6. Campana, S.; Andrade, C.; Milas, M.; Rinaudo, M. *Int. J. Biol. Macromole.*, **1990**, *12*, 379
7. Norwood, D.P.; Reed, W.F. in preparation
8. Zimm, B.H. *J. Chem. Phys.*, **1948**, *1093*, 1099
9. Berne, B.J.; Pecora, R. *Dynamic Light Scattering*, **1976**, John Wiley and Sons
10. de Gennes, P.-G. *Scaling Concepts in Polymer Physics*, **1979**, Cornell University
11. Schmidt, M. presentation at the SEC symposium, ACS meeting 4/95, Anaheim, California
12. Doty, P.M.; Zimm, B.H.; Mark, H. *J. Chem. Phys.*, **1945**, *13*, 159
13. Ahad, E.; Jennings, B.R. *J. Phys. D: Appl. Phys.*, **1970**, *3*, 1059
14. Short, D.W. *Wyatt Technical Notes*, **1991**, Wyatt Technology Corp., Sta. Barbara, Cal.
15. Brandrup, J.; Immergut, E.H., Eds. *Polymer Handbook, 3rd ed.*, **1989**, John Wiley & Sons
16. Tinland, B.; Mazet, J.; Rinaudo, M. *Makromol. Chemie Rapid Comm.*, **1988**, *9*, 69
17. Wyatt, P.J. *Analitica Chim. Acta*, **1993**, *272*, 1
18. Ghosh, S.; Li, X.; Reed, C.E.; Reed, W.F. *Biopolym.*, **1990**, *30*, 1101
19. Milas, M.; Reed, W.F.; Printz, S., *Intl. J. Biol. Macromole*, in press
20. Coviello, T.; Kajiwara, K.; Burchard, W.; Dentini, M.; Crescenzi, V. *Macromole.*, **1986**, *19*, 2826
21. Schmidt, M.; Paradossa, G.; Burchard, W. *Makromole. Chem. Rapid Comm.*, **1985**, *6*, 767
22. Rinaudo, M.; Tinland, B. *J. Appl. Polym. Sci.*, **1991**, *48*, 19
23. Dubin, P.L.; Larter, R.M.; Wu, C.J.; Kaplan, J.I. *J. Phys. Chem.*, **1990**, *94*, 7243
24. Benoit, H.; Grubisic, C.; Rempp, P.; Decker, D.; Zilliox, J.G. *J. Chim. Phys. Phys.-Chim. Biol.*, **1966**, *63*, 1506

Downloaded by UNIV OF GUELPH LIBRARY on October 10, 2012 | http://pubs.acs.org
Publication Date: May 30, 1996 | doi: 10.1021/bk-1996-0635.ch002

25. Grubisic, Z.; Rempp, P.; Benoit, H. *J. Polym. Sci., Polym. Lett. Ed.*, **1967**, *5*, 753
26. Dubin, P.L.; Edwards, S.L.; Mehta, M.S. *J. Chromatogr.*, **1993**, *635*, 51
27. Bahary, W.S.; Jilani, M. *J. Appl. Polym. Sci.*, **1993**, *43*, 1531
28. Dubin, P.L.; Principi, J.M. *Macromole.*, **1989**, *22*, 1891
29. Dubin, P.L. *Sep. Purif. Methods*, **1981**, *10*, 287
30. Reed W.F. *Macromole. Chem. and Phys.*, **1995**, *196*, 1539
31. Odijk, T. *J. Polym. Sci. Phys. Ed.*, **1977**, *15*, 477
32. Skolnick, J.; Fixman, M. *Macromole.*, **1977**, *10* , 9444
33. Odijk, T.; Houwaart, A.C. *J. Polym. Sci. Phys. Ed.*, **1978**, *16*, 627
34. Fixman, M.; Skolnick, J. *Macromole.*, **1978**, *11*, 8638
35. Reed, W.F.; Ghosh, S.; Medjhadi, G.; Francois, J. *Macromole.*, **1991**, *24*, 6189
36. Reed, W.F. *Macroion Characterization*, **1994**, Ed. K. Schmitz, Ch. 10, ACS series 548
37. Reed, C.E.; Reed W.F. *J. Chem. Phys.*, **1991**, *94*, 8479
38. Peitzsch, R.M.; Burt, M.J.; Reed, W.F. *Macromole.*, **1992**, *25*, 806
39. Li, X.; Reed, W.F. *J. Chem. Phys.*, **1991**, *94*, 4568
40. Higgins, J.S.; Benoit, H. *Polymers and Neutron Scattering*, **1994**, Clarendon Press, Oxford
41. Yamakawa, H.; Fujii, M. *Macromole.*, **1974**, *7*, 128
42. Fouissac, E.; Milas, M.; Rinaudo, M.; Borsali., R. *Macromole.*, **1992**, *25*, 5613
43. Drifford, M.; Dalbiez, J.P. *J. Phys. Chem.*, **1984**, *88*, 5368
44. Wang, L.; Bloomfield, V. *Macromole.*, **1991**, *24*, 5791
45. Morfin, I.; Reed, W.F.; Rinaudo, M.; Borsali, R. *J. de Physique (France)*, **1994**, *4*, 1001
46. Reed, W.F. *J. Chem. Phys.*, **1994**, *100*, 7825
47. Van Dijk, J.A.P.P.; Varkevisser; F.A., Smit, J.A.M., *J. Polym. Sci., Part B: Polym. Phys.*, **1987**, *25*, 149
48. Balke, S.T.; Hamielec, B.P.; LeClair, S.C.; Pearce, S.C., *Ind. Eng. Chem. Prod. Res. Dev.*, **1969**, *8*, 54
49. Jeng, L.; Balke, S.T., *J. App. Polym. Sci.*, in press
50. Lesec, J.; Quiveron, *Analysis*, **1976**, *4*, 399
51. Bevington, P.R. *Data Reduction and Error Analysis for the Physical Sciences*, **1969**, McGraw Hill, N.Y.

Downloaded by UNIV OF GUELPH LIBRARY on October 10, 2012 | http://pubs.acs.org
Publication Date: May 30, 1996 | doi: 10.1021/bk-1996-0635.ch002

Chapter 3

Gel Chromatography as an Analytical Tool for Characterization of Size and Molecular Mass of Proteins

M. le Maire[1], A. Ghazi[2], and J. V. Møller[3]

[1]Section de Biophysique des Proteines et des Membranes, Département de Biologie Cellulaire et Moléculaire, CEA et Centre National de la Recherche Scientifique, Unité de Recherche Associée 1290, CE Saclay F–91191 Gif, France
[2]Laboratoire des Biomembranes, Unité de Recherche Associée 1116, Bât. 433, Université Paris-Sud, F–91405 Orsay, France
[3]Department of Biophysics, University of Aarhus, Ole Worms Allé 185, DK–8000 Aarhus C, Denmark

Although experience with watersoluble, globular proteins supports Stokes radius as an appropriate size parameter, governing elution position, for both classical and HPLC gel columns, extrapolation of this concept to other kinds of conformation and substances requires caution. Current evidence suggests the viscosity based Stokes radius as the best suited size parameter for many flexible macromolecules (guanidinium HCl denatured proteins, dextrans), whereas many detergent micelles and detergent solubilized membrane proteins elute somewhat earlier, and elongated (e.g. myosin) or SDS denatured proteins elute later, than indicated by their hydrodynamic behaviour. The review includes a discussion of the use of globular proteins of known size to characterize gel pore size distribution.

The purpose of this review is to briefly consider the scope of gel chromatography, or size exclusion chromatography (SEC), in the determination of sizes and molecular masses of proteins. This kind of separation is performed either as classical type chromatography, using gels such as Sepharose (agarose), Sephacryl (allyl-dextran crosslinked with N,N-methylene bisacrylamide) and Superose, or by HPLC with the aid of matrices capable of withstanding high pressures such as silica based TSK SW- or polyacrylamide based TSK PW columns. We first briefly review the theoretical foundation for use of the technique in the estimation of molecular mass and size of watersoluble, globular proteins. We then proceed to consider the use of the technique to analyze other kinds of proteins (elongated or fibrous type proteins, detergent-solubilized membrane proteins) and the effect of a disordered conformation (SDS- or GuHCl denaturation). Finally, we consider the use of globular proteins in the characterization of the pore characteristics of the gels.

0097–6156/96/0635–0036$15.00/0

Basic theory and application to watersoluble, globular proteins

In gel chromatography it is assumed that there is an absence of interaction between the macromolecules and the gel. This may appear as an idealized assumption, given the high density of hydrophilic, charged, and hydrophobic amino acid side chains on the surface of the proteins. However, from a large number of experimental observations on the elution of watersoluble proteins performed with the kind of chromatographic gels mentioned above, enthalpic interactions appear to be modest, so that the passage of the macromolecule can be described by processeses which include (i) convectional passage along the interstices, surrounding the gel particles, and (ii) delays caused by the diffusional entrance into size-discriminating pores in the gel particles. However, it should be noted that, especially for HPLC gels, convectional passage probably also occurs through large pores in the gel network *(1)*. For large macromolecules, incapable of entering the size-discriminating gel pores, the elution volume defines the void volume, V_0, of the column, while small molecules, having free access to all pores, define V_t, the total solution volume of the column. Macromolecules of intermediate size, which have partial access to the pores, elute at a position, V_e, located somewhere in between V_0 and V_t. Provided that the column is run under equilibrium conditions, a partition coefficient, K_D, independent of column dimension, defines the elution position of the macromolecule according to

$$K_D = \frac{V_e - V_o}{V_t - V_o} \qquad (1)$$

The value of K_D is dependent on the pore characteristics of the gel in addition to the size and shape of the macromolecule. To obtain a good separation of molecules of widely different dimensions a dispersion of pore sizes is required, although some degree of separation, due to geometric constraints, can be obtained even if pores are of uniform dimensions (cf. the last Section and Figure 6). Compared to many other polymers, most watersoluble proteins in their native state are distinguished by being folded in compact conformations with a globular shape which make them good probes for estimating the size of the gel pores. These properties are also the basis for the popular use of estimating molecular mass of proteins from K_D measurements, on the basis of a calibration curve obtained with a number of protein standards. However, the shortcomings of such a procedure can be appreciated from Figure 1, which shows that among a total of 15 selected watersoluble, globular proteins, covering a wide range of molecular sizes, three proteins (bovine serum albumin, tyrosyl-tRNA synthetase, and ferritin) fall outside a common calibration curve. Among these ferritin, as discussed below, presents a particular problem, due to the presence of iron in a variable amount. However, the other two proteins can be obtained in a homogenous state with a negligeable content of non-protein compounds. If we regard these as "test" proteins, we would from the calibration curve estimate molecular masses of 113 and 214 kDa, to be compared with documented values of 67 kDa and 94 kDa, respectively *(2)*.

What is the reason for these deviations? To analyze the situation it is necessary to enquire into the hydrodynamic properties of the proteins. The size of a hydrodynamic particle, P, can be expressed in terms of its Stokes radius (R_s)

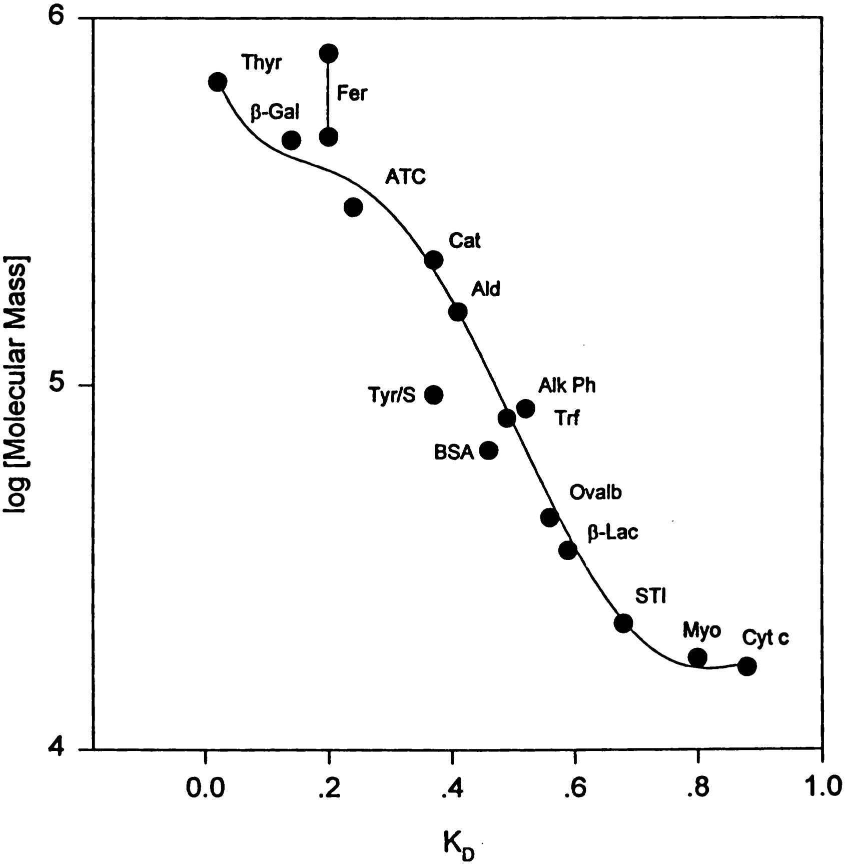

Figure 1. Calibration curve for watersoluble proteins on a TSK 3000SW column (7.5 x 300 mm). The eluant and equilibration media contained 200 mM sodium acetate, 10 mM imidazol, 30 mM Hepes, 0.1 mM $CaCl_2$, pH 7.0, and 0.5 mg/ml $C_{12}E_8$. Flow rate was 0.5 ml/min. Abbreviations: Thyr, thyroglobulin; β-Gal, β-galactosidase; Fer, ferritin; ATC, aspartate transcarbamylase; Cat, catalase; Ald, aldolase; Tyr/S, tyrosyl-tRNA synthetase; Alk Ph, alkaline phosphatase; Trf, transferrin; BSA, bovine serum albumin; Ovalb, ovalbumin; β-Lac, β-lactoglobulin; STI, soybean trypsin inhibitor; Myo, myoglobin; Cyt *c*, cytochrome *c*. The calibration curve for the watersoluble proteins is represented as the logarithm of the molecular mass as a function of the K_D. The fit was obtained with a polynomial of degree 5 but note that the points for ferritin, tyrosyl - tRNA synthase and BSA have not been included in this calculation.

(Reproduced with permission from reference 2. Copyright 1986 Academic Press, Inc.)

which is defined as the radius of a sphere that would have the same frictional coefficient as the particle under consideration. R_s can be calculated from f_p according to Stokes law

$$f_p = RT/ND_p = 6\pi\eta_o R_s \tag{2}$$

where D_p is the diffusion coefficient, η_o is the viscosity of the solution, and R,T,N have their usual meaning. The frictional coefficient can be obtained from the sedimentation rate of the particle in an analytical ultracentrifuge or by measurements of the diffusion coeffient. In a hydrodynamic experiment, such as a determination of the sedimentation velocity in a centrifuge, proteins carry with them during their movement a certain amount of solvent, in addition to what is bound to the polar groups and in crevices *(3)*. Furthermore, proteins are never perfectly spherical. As a result they behave as spheres with a somewhat larger radius than calculated from their protein mass and density. Typically, globular proteins have $R_s/R_{min} = f/f_{min}$ of around 1.2. But sometimes, as the result of an asymmetric shape, the ratio is higher, and this turns out to be the case for serum albumin and tyrosine synthetase for which values of f/f_{min} of 1.35 *(3)* and 1.48 *(2)*, respectively, are quoted. If instead of molecular mass we plot Stokes radius as a function of K_D, all of the 13 standard proteins fall on a smooth curve (Fig. 2). Thus, the deviations from the calibration curve observed in Figure 1 are in accordance with the gel chromatographic principle that in these experiments we measure molecular dimensions rather than molecular mass. This is a point which needs to be stressed in view of the popular use of gel chromatography for estimation of molecular mass of proteins.

To ensure sound estimations of molecular mass it is necessary to combine chromatographic data with an independent measurement of the hydrodynamic properties. Frequently this entails a determination of the sedimentation coefficient "s" (for a discussion of how this can be performed without the use of an expensive analytical ultracentrifuge, see e.g. Siegel and Monty *(4)* and Minton *(5)*. From the Svedberg equation ($M_p = RTs/(1-\bar{v}\rho)D_p$) and Eq (2) the following expression for the buoyant molecular mass ($M_p(1-\bar{v}\rho)$) is obtained

$$M_p(1-\bar{v}\rho) = 6\pi\eta_o R_s Ns \tag{3}$$

where $\bar{v}$ is the partial specific volume of the particle and ρ is the density of the solution. A very careful analysis of a large number of proteins supports the use of this relation, originally suggested by Siegel and Monty *(4)*, leading to an improvement of molecular mass estimations, as compared to data obtained by gel chromatography alone *(6)*.

To perform calibration of a column it is necessary to choose carefully the proteins to serve as standards. Several lists are available in the literature (see for instance Refs *2, 7-9)*. Problems that are often encountered comprise the tendency of proteins for reversible/ irreversible aggregation and the presence of impurities which

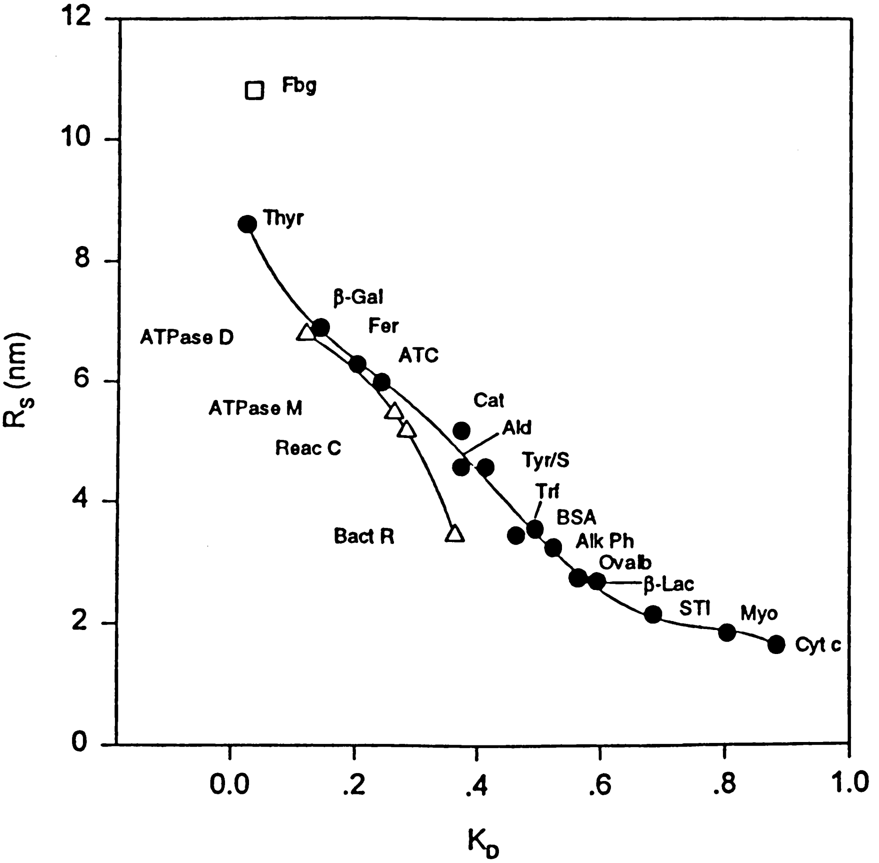

Figure 2. Calibration curves for watersoluble proteins and detergent-solubilized membrane proteins on a TSK 3000SW column (7.5 x 300 mm), using the frictional coefficient based Stokes radius as a size parameter instead of molecular mass. The eluant and equilibration media contained 200 mM sodium acetate, 10 mM imidazol, 30 mM Hepes, 0.1 mM $CaCl_2$, pH 7.0, and 0.5 mg/ml $C_{12}E_8$. Flow rate was 0.5 ml/min. The membrane proteins are indicated by open symbols (Δ). Abbreviations, as in Figure 1, and: Fbg, fibrinogen; ATPase D, Ca^{2+} ATPase dimer; ATPase M, Ca^{2+} ATPase monomer; Reac C, reaction center; Bact R, bacteriorhodopsin. The calibration curve for the watersoluble proteins is based on the same data as in Figure 1 and was obtained with a polynomial degree of 5; note that in this representation *all* the 13 proteins, is included in the calibration curve. However, fibrinogen, (shown with a different symbol (□)), which is very asymmetrical (*3*), is excluded. Among the detergent solubilized membrane proteins, bacteriorhodopsin, which binds a large amount of $C_{12}E_8$ (2 g/ g protein), also shows a large deviation from the calibration curve.

(Reproduced with permission from reference 2. Copyright 1986 Academic Press, Inc.)

can result in broad, ill-defined peaks. With some elution media, especially of low ionic strength and high pH, basic proteins like cytochrome c and ribonuclease interact with the column material, precluding their use as standards *(10)*. Ferritin is a special case: Commercial preparations are generally heterogeneous with respect to M_r because of a variable iron content which, however, does not appreciably affect Stokes radius (Refs *2* and *10*, see also Figure 2). If used as a standard it is therefore reasonable to assign to ferritin a molecular mass, corresponding to that of apoferritin. Finally, very elongated, fibre type proteins like fibrinogen, tropomyosin, or myosin should not be used for calibration, since the elution of these molecules is anomalous and with shapes that are difficult, or impossible, to characterize by one size parameter only.

The use of gel chromatography for characterization of randomly coiled and elongated polymers

As an alternative to ultracentrifugation and diffusion, one can calculate a viscosity based Stokes radius, R_η, on the basis of intrinsic viscosity, $[\eta]$, and molecular mass by use of Einstein's relation

$$[\eta] = \frac{10\pi N}{3M_p} \cdot R_\eta^3 \tag{4}$$

In the case of watersoluble, globular proteins no systematic difference has been found between R_s and R_η *(8)*. For randomly coiled polymers R_η exceeds R_s, theoretically by about 15 % *(11)*. For rodshaped molecules R_η is also larger than R_s, typically by 10-25 % *(12)*. But for SDS-denatured proteins with an asymmetric, but essentially unknown (pearl necklace?) conformation *(13)*, we found no systematic difference between R_s and R_η in a plot relating these parameters and molecular masses *(14)*. Values of R_η for proteins can be found in Refs *8, 9, 15-17*; for an updated summary see Nave et al. *(18)*. It has been pointed out that the elution position of proteins is better correlated with the viscosity-based Stokes radius than with R_s, as calculated from the frictional coefficient. Therefore, the use of R_η, rather than R_s, has been recommended as a way to obtain universal calibration of columns, regardless of conformational class *(9)*. We have tested this proposal by comparing the elution position of GuHCl (guanidinium hydrochloride) and SDS denatured peptides with that of watersoluble, globular proteins in their native state. As can be seen from Figure 3 there is good agreement between the elution of GuHCl-denatured and watersoluble, compact proteins. By contrast, the elution of the large SDS-protein complexes follows a different curve, being characterized by a relatively large R_η for the same elution volume. The data on GuHCl denatured and native proteins are in agreement with data reported by others *(8, 15)*, and by Nave et al. *(18)* for TSK 6000 PW, but not for Superose 6 columns. Horiike et al. *(8)* also showed that the agreement is less satisfactory if a frictional coefficient based Stokes radius is used. The deviating elution of SDS-protein complexes found by us agrees with previous observations by Nozaki et al.

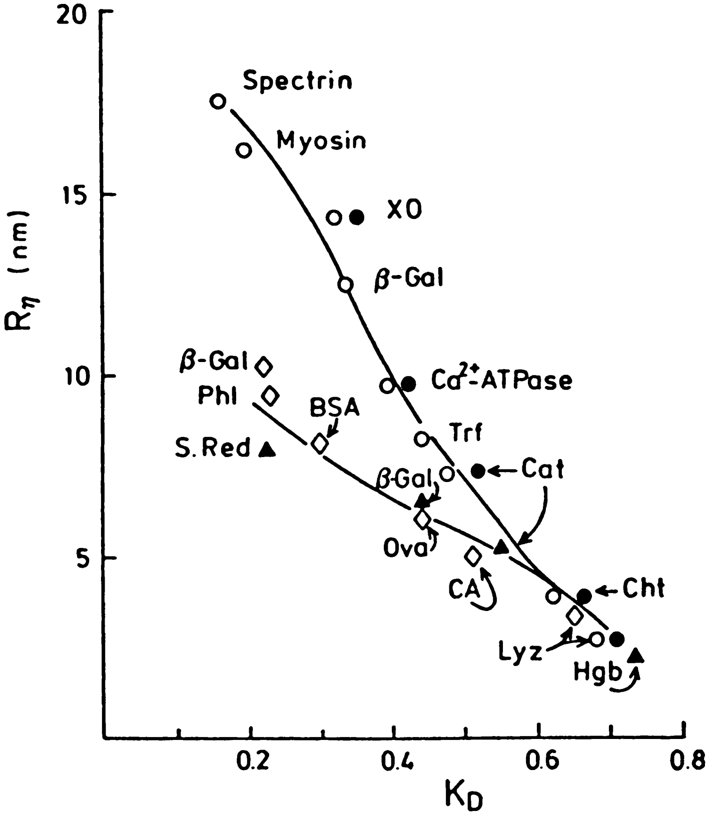

Figure 3. Relation between viscosity-based Stokes radii (R_η) and partition coefficient (K_D) on a Sepharose 4B column for watersoluble, globular proteins (▲), protein-SDS complexes (○, ●), and proteins denatured in 6 M GuHCl in their reduced and carboxymethylated state (◇): For watersoluble, globular proteins chromatography was performed in a medium containing 10 mM 3-[tris(hydroxymethyl)methylamino]-1-propanesulfonic acid (pH 8.0) and 100 mM KCl. For protein-SDS complexes chromatography was performed in 3.4 mM SDS and either 0.01 (○) or 0.033 M phosphate (●) buffer. XO, xanthine oxidase; Phl, phosphorylase; S. Red, sulfite reductase; CA, carbonic anhydrase; Cht, chymotrypsinogen; Lyz, Lysozyme; Hgb, hemoglobin. (Reproduced with permission from Ref. *19*. Copyright 1989 Academic Press, Inc.).

(7) who attributed the retarded elution to end-on insertion of the rod-like complexes into the gel pores. Supporting evidence for this idea comes from studies on the elution of native proteins with an elongated shape like fibrinogen and myosin which also elute later than expected from their Stokes radius *(2, 7, 10, 19)*. Furthermore, the elution position may be affected by the flexibility of these large, elongated molecules. In this respect it is of interest that the structure of SDS solubilized complexes of large protein has been described in terms of a necklace model in which a small number of spherical micelles is dispersed around the unfolded polypeptide chain (see for example (*20*)).

Similar results as for Sepharose 4B were obtained for the elution of SDS-protein complexes and native proteins from 3000 SW silica gel columns. In this case the elution of proteins with a small R_η appeared somewhat ahead of their native counterparts. But for large SDS-protein complexes the calibration curve was steep and rose above the calibration for native proteins in agreement with the data shown in Figure 3. Chikazumi and Ohta *(15)* also reported data that did not conform to a universal type plot, despite that they found lower values of R_η for SDS-denatured proteins than previously obtained *(21)*. This contrasts with Potschka *(9)* who also for elongated molecules reported satisfactory agreement between the elution of various types of macromolecules and their viscosity based Stokes radius. However, as mentioned above considerable uncertainty attends measurements of molecular radii of elongated, large macromolecules, and part of the discrepancy can probably also be attributed to experimental uncertainness in the assignment of Stokes radii (these were in part redetermined by Potschka *(9)* who generally obtained values lower than those previously reported).

Concerning the effect of conformation on elution it is also of interest to compare the elution behaviour of proteins with that of flexible polymer chains. Early observations had indicated to us that dextran and polyethylene glycol fractions elute ahead of water-soluble, globular proteins when plotted as a function of the frictional coefficient-based Stokes radius *(22)*. Figure 4 shows that when R_η is used as a measure of molecular size instead of R_s, satisfactory agreement is observed between the elution position of the dextran fractions and the water-soluble, globular proteins. However, the polyethylene glycol fractions still elute ahead of the proteins when plotted in this way. In comparison to dextrans, polyethylene glycol has been found to have a considerably more expanded structure which probably is the underlying reason for this deviation *(22)*.

Micelles of polyethylene glycol detergents also behave by gel chromatography as having a larger size than indicated by their viscosity properties. These kind of detergents are often used to solubilize integral membrane proteins in a native-like state *(19)*. For many protein-detergent complexes an anomaly in their gel chromatography behaviour was earlier described which resulted in a too early elution, relative to their Stokes radii *(2, 10)*. The anomaly is demonstrated in Figure 2 for bacteriorhodopsin, solubilized by $C_{12}E_8$ and applied to a TSK 3000 SW column. As can be seen this membrane protein with a relatively low molecular mass (M_r 27 kDa), elutes earlier than the watersoluble standards of similar R_s, whereas membrane proteins of higher molecular mass (photosynthetic reaction centre, M_r 90

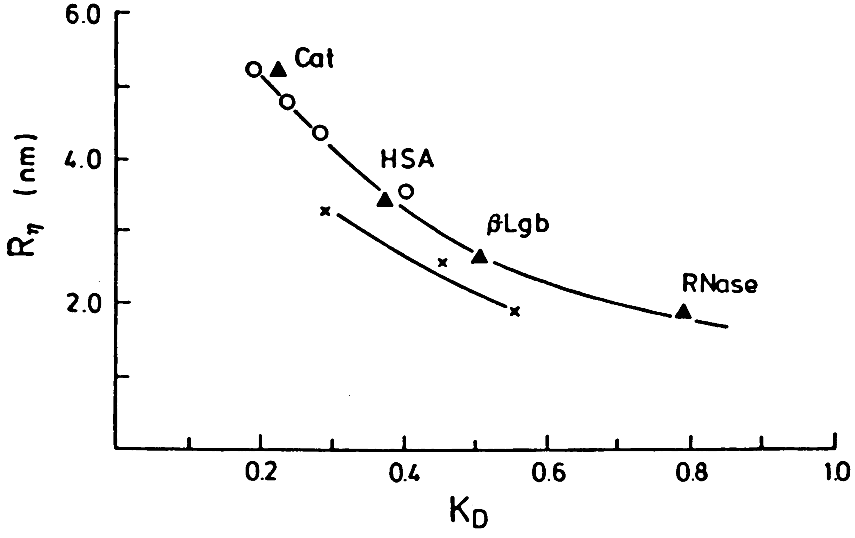

Figure 4. Relation between viscosity-based Stokes radius (R_η) and partition coefficient (K_D) on a Sephadex G-200 column for dextran fractions (o), polyethylene glycol fractions (x), and watersoluble, globular proteins (▲). Narrow dextran fractions were characterized by average molecular weights of 22,500, 33,500, 40,400, and 47,900 (Ref. *22*). Polyethylene glycol fractions were PEG 4000, 6000, and 10,000. The polymer fractions were eluted with 0.15 M NaCl, HSA, human serum albumin. (Reproduced with permission from Ref. *19*. Copyright 1989 Academic Press, Inc.).

kDa; Serca ATPase, M_r 110 kDa) elute closer to the calibration curve. Similar observations were made by the use of other column materials. However, for TSK 4000PW column the membrane proteins are retarded probably due to slight binding to the column materials *(2)*. In this connection it is worth mentioning that monomer detergent binds to TSK SW columns and Superose so that it is necessary to saturate the column with detergent before using it for separation of membrane proteins *(23)*. From the data of Fig 2 a misleadingly high value of R_s for bacteriorhodopsin is obtained by comparison with the calibration curve (5.3 nm, compared to a Stokes radius of 3.5 nm as measured by hydrodynamic analysis). This difference is too large to be accounted for by the use of R_s instead of R_η in the graph. Probably the anomalous behavior is due to a high detergent binding of this membrane protein (2 g/g protein, Ref. *23*), a circumstance which would make the gel chromatographic behaviour of this protein-detergent complex similar to that of polyethylene glycol micelles. In comparison to bacteriorhodopsin, detergent binding by the other membrane proteins is lower (about 0.5-0.8 g $C_{12}E_8$/g protein) which may result in a less pronounced detergent effect on the elution of these membrane proteins.

From the data presented above it seems fair to conclude that R_η probably is a better parameter than R_s with which to compare the size of different kinds of macromolecules. But as pointed out by Chikazumi and Ohta *(15)*, "the universal calibration procedure for proteins and polypeptide presents some serious problems that needs to be solved". The inherent ambiguity in defining the molecular radius of macromolecules such as random coils and long rods, which in their conformation deviate very much from a compact, spherical shape, represents an obstacle to universal calibration of gel columns. The characterization of such molecules is probably best carried out by the combined use of many hydrodynamic techniques.

Calibration plots and calibration curves

As discussed above determination of R_s of an unknown protein by gel chromatography requires a proper calibration of the column with proteins of known Stokes radii. On the assumption of a Gaussian distribution of pore sizes around a mean value a linear relationship between R_s and $\mathrm{erf}^{-1}(1 - K_D)$ was previously predicted by Ackers *(24, 25)*, where $\mathrm{erf}^{-1}(x)$ is the inverse function of the Gaussian probability integral. Due to the simplification that a linear plot provides, this procedure has been widely used for column calibration of proteins. However, we have shown that the derivation by Ackers is not strictly valid and that for any gel in common use the relationship between R_s and $\mathrm{erf}^{-1}(1 - K_D)$ is found to be non-linear *(26)*. This is in particular evident, when a large number of native proteins, covering a wide range of Stokes radii, is used to calibrate both classical gels and HPLC columns *(2, 10)*. The same problems are encountered when other mathematical models of size distribution which are supposed to result in linear relationships are used *(27)*. It should be stressed that a procedure which assumes approximate linearity in a given representation, and therefore makes use of few standards for calibration, may lead to gross errors in the determination of R_s for some proteins. Thus, we believe it is better to avoid any *a priori* assumption on the properties of the gel and,

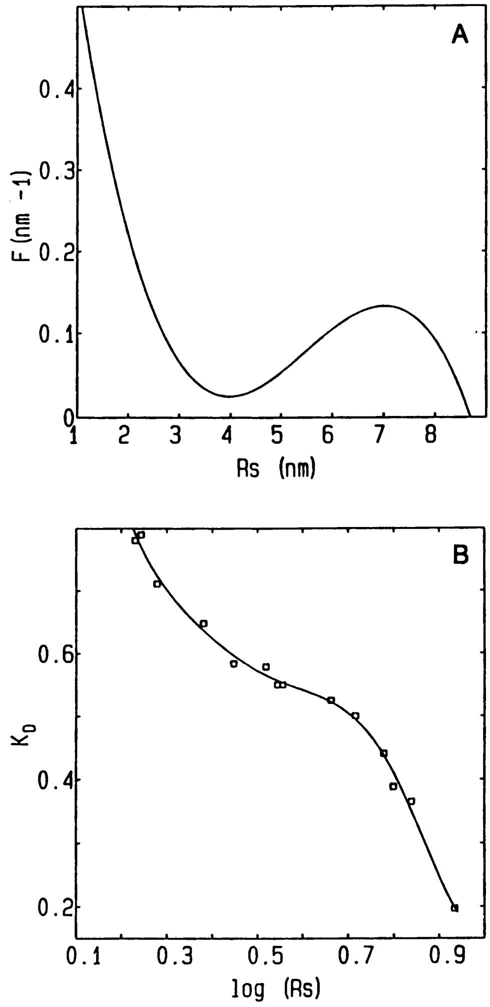

Figure 5.

5A. F for Sepharose 6B-CL, obtained as the derivative (multiplied by −1) of the polynomial of K_D as a function of R_s, suggesting the existence of two sets of pore sizes.

(Reproduced with permission from reference 26. Copyright 1987 Biochemical Society and Portland Press.)

5B. K_D of native proteins plotted against the logarithm of Stokes radius (R_s) for Sepharose 6B-CL. A semilogarithmic representation was chosen for the sake of comparison with theoretical calibration curves (cf. Figure 6). The points refer to data reported by le Maire et al. *(10)*, except that ferritin was added. Proteins may be identified on the basis of their R_s values (see the legend to Figure 1 in Ref. *10*, closed circles). The continuous line is the fit obtained with a polynomial of degree 5.

therefore, we have suggested to rely on a direct plot of R_S versus K_D obtained by the use of a large number of carefully chosen standards, covering the range of interest *(26)*. With the advent of fast flowing columns calibration this is not a time consuming procedure.

Nevertheless, a better understanding of the underlying mechanisms of SEC could provide better representations and be of help in improving the design of new columns. We have attempted to get some insight into the physical reality behind gel chromatography on the basis of an analysis of calibration curves of columns used in biochemical research *(26)*. For the analysis of such curves let us define the function Fl(a), such that Fl(a)da = dVp is the increase in volume penetrable by solute molecules when their radius decreases from a to (a-da).

Then $V_p = \int_a^\infty \mathrm{Fl}(a)\,da$, or:

$$K_D(a) = \int_a^\infty F(a)\,da = 1 - \int_0^a F(a)\,da \qquad (5)$$

where: $\int_0^a F(a)\,da = \int_0^a \mathrm{Fl}(a)\,da \Big/ \int_0^\infty \mathrm{Fl}(a)\,da$ (normalization). In a simple model where the pore volume, is freely accessible to the solute for pores having a diameter larger than that of the solute, Fl(a)da represents the volume of pores with radius between a and (a + da). Taking the first derivative of Eq(5) yields: $dK_D/da = -F(a)$ or, replacing the pore radius by Stokes radius,

$$dK_D/dR_S = -F(R_S). \qquad (6)$$

For a given column, the calibration curve obtained by the experimental determination of K_D for proteins of known Stokes radius is used to obtain $F(R_S)$. The experimental data can then be fitted to a polynomial which is formally differentiated to yield $F(R_S)$. By the use of carefully prepared calibration curves we obtained for both classical gel columns as well as HPLC columns a bimodal distribution of $F(R_S)$, most pronounced for classical gels (see the example of Sepharose 6B-CL shown in Figure 5A). The appearance of the curves suggested that these columns are best described by the superimposition of two distribution of pore sizes centered on different mean values *(26)*. A bimodal distribution is also reflected by the presence of a shoulder or plateau region which can be observed in the middle of the calibration curves, either in a direct representation or in a log representation (K_D as a function of log (R_S), see Figure 5B). The same conclusions have also been drawn by Harlan et al. *(28)* for several types of gels, including Superose. These authors have recently used this result as the basis for a calibration method, following a reverse procedure. Assuming F(a) to be the superimposition of two Gaussian distributions with means a1, a2, and standard deviations b1, b2, and with a relative weight of each Gaussian f, they fit the data to the equation $K_D = 1 - \int_0^{R_S} F(a)\,da$. This procedure provides a nice fitting of the experimental points by five parameters which is applicable to gels used in both classical and HPLC chromatography. Concerning this procedure it is worth noting that whereas a simple fit of the data to a polynomial usually yields a meaningless curve outside the extreme calibration points, this will probably not be the case for the fit used by Harlan et al. *(28)*.

The explicit meaning attributed here to F1(a) is probably an oversimplification of reality. As discussed in particular by Hagel *(29)*, it fails to take into account geometric constraints on the distribution of solute between pore and surrounding medium. Take for instance the case of a spherical solute of radius A penetrating a cylindrical pore of radius a and length ℓ. The pore volume accessible to the center of the molecule is reduced to a cylinder of radius (a-A) with volume $\pi (a-A)^2 \ell$. In such a pore the ratio of volume which can be occupied by the macromolecule to the pore volume is $\pi (a - A)^2 \ell / \pi a^2 \ell$. Consequently K_D is now given by:

$$K_D = \int_a^\infty \left[(a-A)^2/a^2\right] F(a)\,da = \int_a^\infty (1-A/a)^2 F(a)\,da \tag{7}$$

The correction factor $(1 - A/a)^2$ will of course be different (and more difficult to calculate) if the molecule is not spherical (if it is a rod for instance). In the case of spherical solutes, Knox and Scott *(30)* showed that differentiation of Eq 7 three times yields:

$$F(a) = -a^2/2\,(d^3 K_D/da^3) \tag{8}$$

Thus F(a) can be obtained from an experimental determination of K_D as a function of A. Using calibration curves of porous silica gel obtained with polystyrene samples, Hagel *(29)* obtained by this method a single distribution of pore sizes. We found this method (i.e. the use of Eq 8) difficult to apply to calibration curves obtained with proteins for two reasons. Firstly, Eq 8 is based on the assumption of spherical particles, which is certainly not valid for several of the proteins used as standards. Secondly, as noted by Hagel *(29)*, the use of Eq 8 requires a smooth expression of K_D as a function of R_s. Even the moderate scatter of the data which is inevitable in a calibration curve obtained with proteins, will have an enormous impact on the third derivative of a polynominal expression, and in many cases result in incoherent results. As indicated by Hagel *(29)*, this problem can be circumvented by use of a log-logistic function if the curve to be fitted is sigmoid. However, as mentioned above, the calibration curves obtained with proteins as standards are not sigmoid. Rather they show a characteristic shoulder in the middle of the curve (Figure 5A), a behaviour which is precisely to be expected from a bimodal distribution of pore sizes, as shown theoretically by Yau et al. *(31)* and as can be seen from curve c) in Figure 6 (data given by Hagel (*29*)).

Assuming that globular proteins are adequate as probes of pore size we therefore conclude that the properties of many gels in common use is best described as occurring through two distinct populations of pore sizes the exact properties of which are still subject to both theoretical and experimental investigation. It should be noted that among other methods commonly used to measure experimentally gel pore

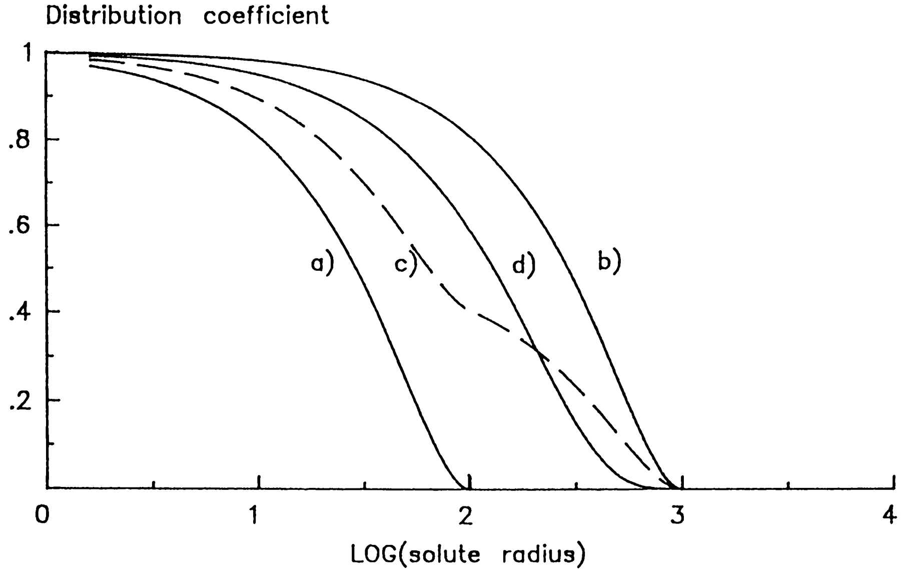

Figure 6. Theoretical calibration curves: a) and b) single pore size distribution with a = 100 Å and 1000 Å, respectively; c) mixture of supports with a = 100 Å and a = 1000 Å; d) multiple pore size support with $\bar{a}$ = 500 Å and σ = 200 Å. (Reproduced with permission from Ref. (*29*) Copyright 1988 Elsevier Science Publishers).

size (by electron microscopy, N_2-adsorption, or mercury porosimetry, cf. the review by Hagel (*29*)), there are, to our knowledge, few indications of a set of very small pore sizes in the SEC columns (i.e. pores of less than 2 nm, see Figure 5A). However, the resolution by electron microsopy (which usually also involves coating with heavy metal) is probably too low for visualization of such pores. It is of interest that evidence for the presence of small pores (0.4 - 0.6 nm) was obtained by N_2 adsorption at an early date in some kinds of silica gel (*32*). Furthermore, optical analysis and microscopic examination indicate heterogeneity of agarose gels, resulting from micro regions with a high concentration of agarose polysaccharide which may correspond to the set of smaller pores (*33*).

Fractal Model. In a different approach the use of a fractal, and possibly more realistic model of pore properties, has been suggested (*34*). Grain or pores in porous media may have a smooth or corrugated surface. When the irregularity of the surface increases, the fractal dimension of the surface (D_f) increases from 2 towards 3: D_f = 2 corresponds to a smooth surface, while values close to 3 correspond to a highly disordered surface. When, by a suitable choice of the eluent or of surface treatment, the macromolecular solutes are not attracted by the walls of the porous fractal, they are repelled from the solid surface by a size exclusion effect because of their finite size. A depletion layer of size R_s surrounds the fractal. This effect is precisely the basis of size exclusion chromatography. The application of fractal theory leads to the following equation.

$$\ln R_S = \ln L + [\ln(1 - K_D)] / (3 - D_f) \qquad (9)$$

Where L is the maximum radius of the largest pores of the packing material. We have tested this expression by use of our experimental data. For the classical gels which are in fact of heterogeneous structure this relationship is not verified, but in the case of HPLC gels, a straight line was obtained when *ln* R_s is plotted as a function of *ln* $(1-K_D)$. Thus, these gels can indeed be characterized by a fractal dimension D_f and a maximum radius of the pores *(35)*. Such values vary between 2.1-2.6 for D_f and between 87 and 209 Å for L in various TSK gels (*35*).

Acknowledgement

This work has been supported by the CNRS and the CEA, the Danish Medical Research Council, the Aarhus University Research Foundation, and the Danish Biomembrane Centre. We are grateful to Pierre Falson for his help in preparing the figures.

Literature cited

1. Potschka, M. *J. Chromatogr.* **1993**, *648*, 41-69.
2. le Maire, M.; Aggerbeck, L.P.; Monteilhet, C.; Andersen, J.P.; Møller, J.V. Anal. Biochem. **1986**, *154*, 525-535.
3. Tanford, C. *Physical Chemistry of Macromolecules*; Wiley, New York, N.Y., **1961**; pp 317-412.
4. Siegel, L.M.; Monty, K.J. *Biochim. Biophys. Acta* **1966**, *112*, 346-362.
5. Minton, A.P. *Anal. Biochem.* **1989**, *176*, 209-216.
6. Cabré, F.; Canela, E.I.; Canela, M.A. *J. Chromatogr.* **1989**, *472*, 347-356.
7. Nozaki, Y.; Schechter, N.M.; Reynolds, J.A.; Tanford, C. *Biochemistry* **1976**, *15*, 3884-3890.
8. Horiike, K.; Tojo, H.; Yamano, T.; Nozaki, M. *J. Biochem.* **1983**, *93*, 99-106.
9. Potschka, M. *Anal. Biochem.* **1987**, *162*, 47-64.
10. le Maire, M.; Rivas, E.; Møller, J.V. *Anal. Biochem.* **1980**, *106*, 12-21.
11. Mandelkern, L.; Flory, P.J. *J. Chem. Phys.* **1952**, *20*, 212-214.
12. Tanford, C.; Nozaki, Y.; Reynolds, J.A.; Makino, S. *Biochemistry* **1974**, *13*, 2369-2376.
13. Jones, M.N. *Chemical Society Reviews* **1992**, *21*, 128-136.
14. Deschamps, S.; Viel, A.; Garrigos, M.; Denis, H.; le Maire, M. *J. Biol. Chem.* **1992**, *267*, 13799-13802.
15. Chikazumi, N.; Ohta, T.J. *J. Liq. Chromatogr.* **1991**, *14*, 403-425.
16. Fish, W.W.; Reynolds, J.A.; Tanford, C. *J. Biol. Chem.* **1970**, *245*, 5166-5168.
17. Fish, W.W. *Methods Membr. Biol.*, **1975**, *4*, 189-276.
18. Nave, R.; Weber, K.; Potschka, M. *J. Chromatogr.* **1993**, *654*, 229-246.
19. le Maire, M.; Viel, A.; Møller, J.V. *Anal. Biochem.* **1989**, *177*, 50-56.
20. Sams6, M; Daban, J.-R.; Hansen, S.; Jones, G.R. *Eur. J. Biochem* **1995**, *232*, 818-824.

21. Reynolds, J.A.; Tanford C. *J. Biol. Chem.* **1970**, *245*, 5161-5165.
22. Jørgensen, K.E.; Møller, J.V. *Amer. J. Physiol.* **1979**, *236*, F103-F111.
23. Møller, J.V.; le Maire, M. *J. Biol. Chem* **1993**, *268*, 18659-18672.
24. Ackers, G.K. *J. Biol. Chem.* **1967**, *242*, 3237-3238.
25. Ackers, G.K. *Adv. Protein Chem.* **1970**, *24*, 343-446.
26. le Maire, M.; Ghazi, A.; Møller, J.V.; Aggerbeck, L.P. *Biochem. J.* **1987**, *243*, 399-404.
27. le Maire, M.; Chabaud, R.; Hervé, G. *Laboratory guide to Biochemistry, Enzymology and Protein Physical Chemistry: a study of aspartate transcarbamylase.* Plenum Publishing Corporation, New York, N.Y., **1991**, pp *74-79*.
28. Harlan, J.E.; Picot, D.; Loll, P.J.; Garavito; R.M. *Anal. Biochem.* **1995**, *224*, 557-563.
29. Hagel, L. In: *Aqueous Size-Exclusion Chromatography;* Dubin, P.L., Ed.; Elsevier Science Publishers B.V., Amsterdam, The Netherlands, **1988**, pp 119-155.
30. Knox, J.H.; Scott, H.P. *J. Chromatogr.* **1984**, *316*, 311-322.
31. Yau, W.W.; Ginnard, C.R.; Kirkland, J.J. *J. Chromatogr.* **1978**, *149*, 465-487.
32. Mikhail, R.S.H.; Brunauer, S.; Bodir, E.E. *J. Coll. Interf. Sci.* **1968**, *26*, 54-61.
33. Pines, E.; Prines, W. *Macromolecules* **1973**, *6*, 888-895.
34. Brochard, F.; Ghazi, M.; le Maire, M.; Martin, M. *Chromatographia* **1989**, *27*, 257-263.
35. le Maire, M.; Ghazi, A.; Martin, M.; Brochard, F. *J. Biochem.* **1989**, *106*, 814-817.

Chapter 4

Modeling of Size Exclusion Chromatography by Monte Carlo Simulation

Jean-Pierre Busnel, Christophe Degoulet, and Jean-François Tassin

Laboratoire de Physico-Chimie Macromoleculaire, Université du Maine, Unité de Recherche Associée 509, BP 535, 72017 Le Mans Cedex, France

By using Monte Carlo simulation, polymer chains of various flexibility and thickness can be constructed inside pores of various geometries. This allows to evaluate the corresponding steric partition coefficient K and the chromatographic radius R_C defined as the radius of the rigid sphere with the same K value. When comparing with R_η defined as the radius of the sphere with the same product $[\eta]$.M, R_C/R_η is clearly different from 1, and is not strictly independent of the flexibility and the relative thickness of the macromolecule. However, this ratio is generally almost stable and experimentally, for flexible polymers, the so-called universal calibration (UC) is often found to work well despite the lack of academic evidence.

Size exclusion chromatography (SEC) is now the current denomination for the chromatographic process first introduced by Moore (*1*) as Gel Permeation Chromatography (GPC). SEC has rapidly become a powerful tool for characterising the molar mass distribution of polymers. Recent technological improvements have made this technique even more attractive. Unfortunately this method relies on calibration using standards and does not yield the absolute molar masses as soon as the studied macromolecule is different from the one used in the calibration. Universal calibration (*2*) is an elegant solution to that problem as is simply relates each macromolecule size (i.e. each elution volume) to a product $[\eta]$M. Although the on-line viscosity measurements (*3-5*) raise experimental problems (*6,7*) especially with high performance column sets, intrinsic viscosity ($[\eta]$) measurements can nowadays be reliably (*8,9*) performed.

0097–6156/96/0635–0052$15.00/0

It has been claimed by many authors (first by Benoît (*10*)) that experimentally the UC is valid whatever the chemical nature and the structure of the polymer (*11*). However from a theoretical point of view the situation is different. Casassa (*12*)and Giddings (*13*) assume that the elution process is governed by the equilibrium distribution of the solute between the mobile phase and the stagnant phase inside pores. The equilibrium is characterised by the distribution coefficient, K, defined as the ratio between the concentration inside the pores to the concentration outside the pores. Using statistical mechanics, they have calculated K for random flight linear and branched chains as well as for rods, confined in pores with simple geometries. Casassa showed that UC is valid for any linear or branched macromolecule containing a large number of statistical segments. The results of Giddings lead to different distribution coefficients for a thin rod and for a flexible chain with the same viscometric radius. These idealised theoretical calculations indicate that UC can be applied to polymers of different architecture, but that rigidity might be a limiting factor.

The aim of this paper is to study the influence of the flexibility of linear chains through a Monte Carlo simulation of the size exclusion phenomenon .

Definition of Different Sizes of a Macromolecule

A single macromolecule has a complex temporal and spatial distribution of conformations and only average dimensions can be calculated or measured. A special mention is given to the radius of gyration which corresponds to a clear geometric definition. The simplest way to compare sizes as measured by different experimental techniques is by defining the corresponding size as the radius of a rigid sphere which has the same measured property as the macromolecule. The following sizes can be defined :

- The **Stokes radius** R_s obtained from measurements of the translational diffusion coefficient:

$$R_s = \frac{kT}{6\pi\eta_0 D_t} \quad (1)$$

where k, T, η_o and D_t are the Boltzman constant, the absolute temperature, the solvent viscosity and the translational diffusion coefficient.

- The **viscometric radius** R_η obtained from mass and intrinsic viscosity measurements:

$$R_\eta = \left[\frac{3[\eta]M}{10\pi N_a}\right]^{1/3} \quad (2)$$

where N_a is the Avogadro number.

- The **chromatographic radius** R_c obtained from SEC (R_c is the radius of the sphere that would have the same elution volume in a pure SEC experiment).

Using these definitions, UC applies if the relation between R_η and R_c doesn't depend on the nature of the sample (linear or branched, flexible or rigid). For linear chains, a good estimate of R_η can be obtained from theoretical work of Yamakawa et al. (*14*). R_c values have been calculated using a computer simulation in a wide range of realistic situations, especially for chains of variable stiffness ranging from freely rotating segments to rigid rods.

Principle of Simulation

In a large variety of real situations SEC experiments appear as pure equilibrium chromatographic processes. Recent measurements in our laboratory show that there is no significant elution volume shift (less than 0.05%) when changing flow rate from 0.5 to 1 $cm^3.min^{-1}$ for monodisperse standards analysed on classical columns either in THF or in water (Polystyrene standards in THF in the MW range 2.10^4 to 2.10^6 $g.mol^{-1}$ on columns PL GEL, mixed bead, particle diameter 10 µm ; in water 0.1 M ammonium acetate, Pullulan standards in the MW range 2.10^4 to 10^6 on TSK PW5000, particle diameter 10 µm). So the key parameter for SEC is the partition coefficient K related to the elution volume : $V_e=V_o+KV_p$, where V_e is the solute elution volume, V_o the void volume and V_p the pore volume of the column. For a rigid sphere of radius R_c, K is simply the volume fraction of the pores accessible to the centre of mass and for a number of pore geometries, there is a simple relation between R_c and K :

- For a cylindrical pore of circular section with radius R_p or of square section with side $2R_p$:

$$K = (1 - R_c/R_p)^2 \tag{3}$$

- For a spherical pore with radius R_p or a cubic pore with side $2R_p$:

$$K = (1 - R_c/R_p)^3 \tag{4}$$

In the general case, K is best defined as the equilibrium constant for solute exchange from intrapore volume to bulk solvent as proposed by Casassa :

$$\text{Solute in bulk solvent} \quad \rightleftarrows \quad \text{Solute inside pore}$$

$$K = \frac{[S]_p}{[S]_b}$$

K has been calculated as follows :

For a given pore geometry, a macromolecule is created by randomly choosing a starting point inside the pore volume. Then segments are successively placed using a random walk taking into account conformational constraints. If a segment reaches a pore wall the macromolecule doesn't exist inside the pore. After a large number of trials, $[S]_b$ is proportional to the number of trials and $[S]_p$ is proportional to the number of successful trials. Therefore, K appears as the value of the fraction of successful trials, for a large number of trials.

Chain geometry. We have studied freely rotating chains (Figure 1) defined by :

- The number of segments N.
- The length l and the diameter d of each segment
- A fixed value of α
- A value of β at random between 0 and 2π.

For highly flexible chains α = π/2 and N varies from 100 to 10^4. For worm-like chains N=100 and a varies from π/2 to 0. To take into account the effect of segment thickness it is sufficient to note that a thin molecule of chromatographic radius R_c in a pore of linear dimension R_p corresponds to a thick molecule (segment diameter d) with a chromatographic radius R_c+ d/2 in a pore of size R_p +

d/2. Mean values of the radius of gyration are obtained directly after simulation, as the position of each segment is explicitly known.

Pore Geometry. Observations by electron microscopy have been performed on various column packings : Controlled Porous glass (*15-18*) , Methacrylates gels (*19*), hydrophilic TSKPW gels (*20*), Styrene-Divinylbenzene gels (*21*). These packings are found to consist of beads obtained by partial fusion of small irregular particles. This produces very deep, tortuous channels whose cross sections are irregular but never with highly thin protuberances or sharp angles. To take into account the geometry encountered along a given pore, a reasonable model would be a combination of long cylinders with circular or square sections and of more compact closed volumes (spheres or cubes) and these four pore geometrical models were tested. Linear calibration curves are obtained by mixing several pore sizes, moreover due to the complex real geometry, each pore size corresponds to a distribution of sizes. So the elution volume for a given molecule in real situation is governed by the combination of different K values in different pore sizes and pore volumes and only an apparent K value is observed. For this reason we have tested situations with a unique pore size, for K values between 0.1 and 0.9, and in many cases it seems sufficient to check the situation for the central value K=0.5.

Comparison with Theoretical Results

The validity of the simulation procedure can be tested by comparison with explicit analytical results, available in limiting cases. The radius of gyration obtained by simulation using a pore of infinite size can be compared with theoretical values (*22*). For a chain with N freely jointed segments with length l , R_g is given by:

$$\left\langle R_g^2 \right\rangle = \frac{N(N+2)l^2}{6(N+1)} \tag{5}$$

Small values of N allow accurate checking of the uniformity of orientation randomness. After generation of 5.10^4 chains, deviation with theory was less than 0.1%. For a chain with a large number of freely rotating segments :

$$\left\langle R_g^2 \right\rangle = \frac{N(N+2)l^2}{6(N+1)} \frac{1+\cos\alpha}{1-\cos\alpha} \tag{6}$$

Using values of N from 100 to 500 and a from 0.2 to π/2, deviation with theory is less than 0.1% after generation of more than 10^5 chains. Pure helices are indeed obtained when β is fixed.

Concerning theoretical values of the partition coefficient in simple pores, two special cases have been investigated in the literature. Casassa (*12*) predicted for random coils containing large numbers of segments in cylindrical pores :

$$K = 4\sum_{i=1}^{\infty} \frac{1}{a_i^2} e^{\frac{-a_i^2 N l^2}{6R_p^2}} \tag{7}$$

Here α_i is root of $J_0(\beta) = 0$ and J_0 is a Bessel function of first kind and order 0. In the case of rigid rods in cylindrical pores Giddings (*13*) has derived expressions for K which are combinations of elliptical integrals depending only on l/R_p. Taking fixed values of the segment length (l=1 in both cases), the molecular size to pore

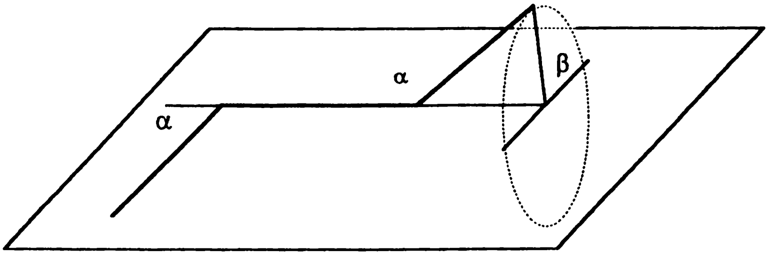

Figure 1. Schematic representation of a part of freely rotating chain.

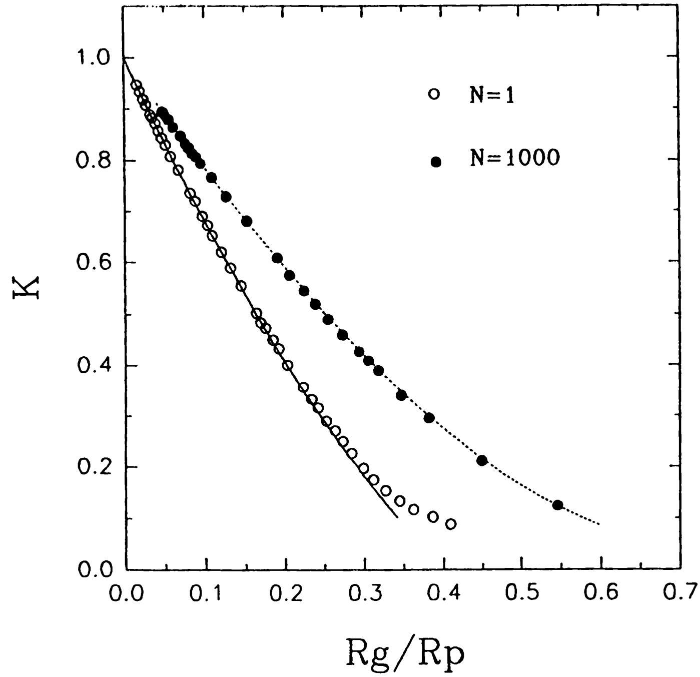

Figure 2. Partition coefficient K as a function of the ratio of the radius of gyration to the pore radius (R_g/R_p) for two values of the segment number N. The results of Casassa and Tagami (*12*) (dashed line) andGiddings et al. (*13*) (solid line) are included.

size ratio was varied. Figure 2 shows that there is close agreement between simulation and theory in these two limiting cases ; N=1 i.e. rigid rod and N=1000 i.e. flexible coil.

The limiting value K=1 is reached as the pore becomes infinitely large compared with the chain. Geometrical details have no influence and the problem is reduced to the estimation of the depletion layer. For a polymer solution near a non interacting wall there is a zone where the segment concentration C(x) increases from 0 for x=0 to C_{bulk} for $x=\infty$. The depletion layer D is defined by :

$$D = \frac{1}{C_{bulk}} \int_0^{\infty} C(x).dx \qquad (8)$$

For a population of rigid spheres the depletion layer is simply the radius of the sphere and therefore when K -> 1 , R_c -> D. For any kind of macromolecule, Cassasa (*23*) established that D=X/2, X being the mean projection of the unconfined molecule on an axis.
For a thin rigid rod one obtains D=L/4 and $R_c/R_g=0.86$.

For a Gaussian chain $D = \frac{1}{2}\left(\frac{8Nl^2}{3\pi}\right)^{1/2}$ and $R_c/R_g = 1.13$.

Simulation of these two situations with K=0.98 recovers these values within 0.5%.

In this study, the size of the test population is always chosen such that the error is less than 1%. It depends mainly on the number of segments, the angle between segments, and the value of the partition coefficient. Figure 3 illustrates a representative case for a chain with 100 segments of length 1 and with $\alpha=\pi/2$, in a cylindrical pore of radius 15. A good balance between time of simulation (which is roughly proportional to N) and accuracy can be obtained with 5.10^4 chains.

Results and Discussion

Influence of pore geometry. To study the influence of pore geometry on the chromatographic radius we have plotted the dimensionless ratio R_c/R_g versus K in different situations (Figure 4 and Figure 5).

For chains and for rods R_c/R_g depends on pore geometry and K values. For rods the variations are more pronounced and the ratio is strikingly unstable for low K values. Clearly the chromatographic radius is not an intrinsic property of the molecule and there is a coupling between the shape of pore and that of the molecule. This coupling is more important for rods and for low K values. So SEC cannot give absolute sizes. Nevertheless for rods (rejecting low K values), R_c/R_g is around 1±0.15 and for chains R_c/R_g is around 1.1±0.1.

Influence of flexibility. As it appears that the ratio R_c/R_g is different for coils and rigid rods for the same pore geometry it is interesting to study more precisely the intermediate situations. To characterise the overall chain flexibility a useful parameter is P, the ratio between contour length and persistence length.

As shown in Figure 6 small values of P give rod-like shapes (P<10), high values of P give coils (P>100) and there is a gradual transition for intermediate P values.

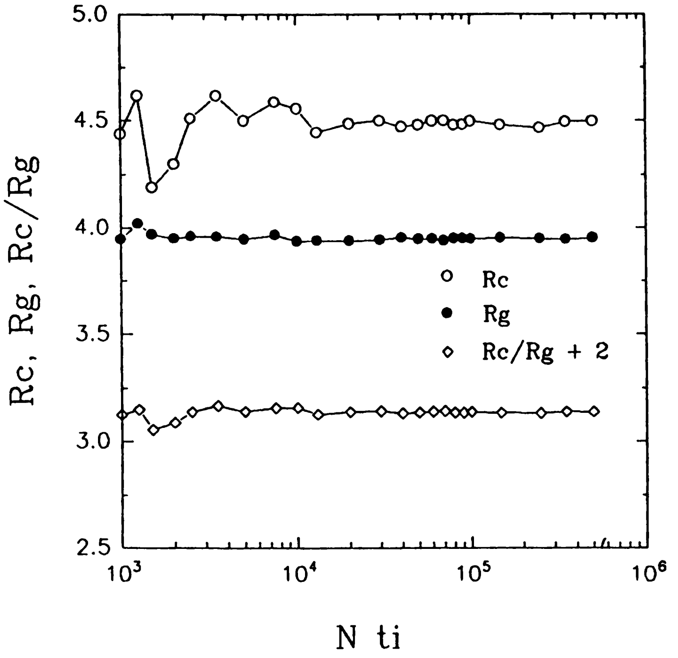

Figure 3. Chromatographic radius R_c, radius of gyration R_g and ratio R_c/R_g as a function of Nt, the number of generated chains (simulations with 100 segments of length l=1, and angle $\alpha=\pi/2$ in a cylindrical pore of radius $R_p=15$).

In Strategies in Size Exclusion Chromatography; Potschka, M., et al.;
ACS Symposium Series; American Chemical Society: Washington, DC, 1996.

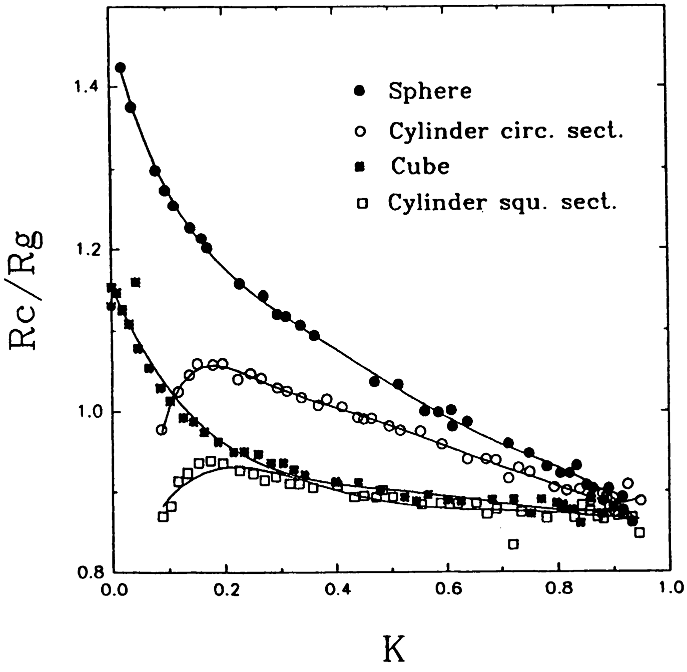

Figure 4. Ratio of the chromatographic radius R_c to the radius of gyration R_g as a function of the partition coefficient K for rods in pores of various geometries. Curves are obtained with length of rod l=1 and various pore sizes R_p.

In Strategies in Size Exclusion Chromatography; Potschka, M., et al.;
ACS Symposium Series; American Chemical Society: Washington, DC, 1996.

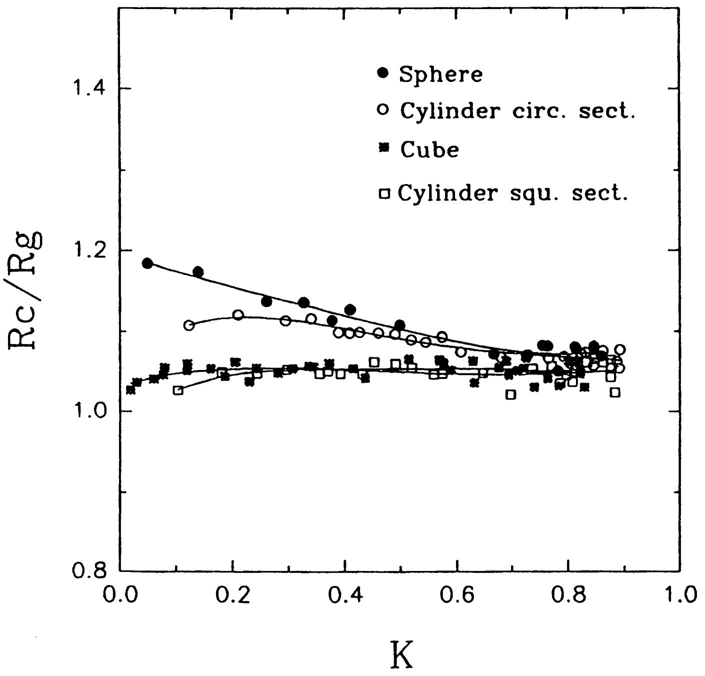

Figure 5. Ratio of the chromatographic radius to the radius of gyration as a function of the partition coefficient K for chains with N=100 segments in pores of various geometries. Curves are obtained with length of segment l=1 and various pore sizes R_p.

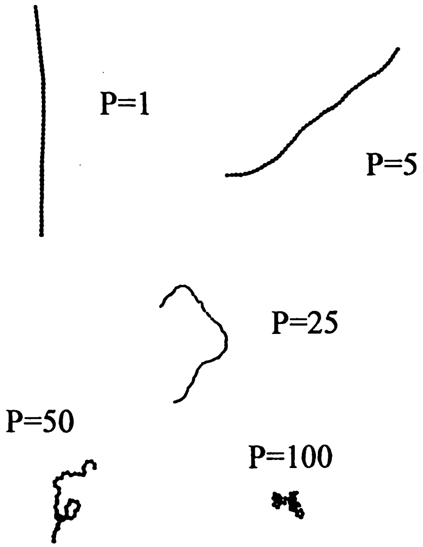

Figure 6. Shape of freely rotating chains as a function of flexibility parameter P.

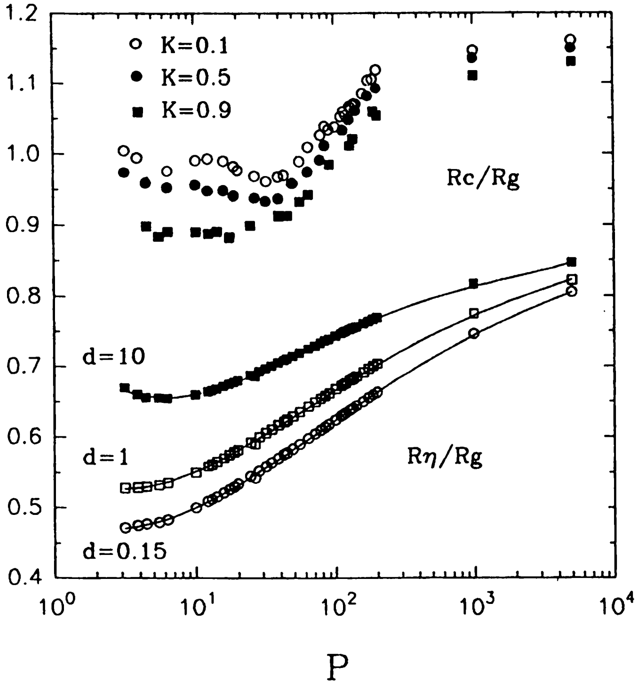

Figure 7. Top : Ratio of the chromatographic radius to the radius of gyration as a function of the flexibility parameter P for a cylindrical pore geometry. Results are plotted for three values of K .

Bottom : Ratio of the viscometric radius to the radius of gyration as a function of the flexibility parameter P. Curves are obtained from theoretical work of Yamakawa (*14*), using persistence length q=100 and three values of diameter d.

For freely rotating chains and large N values, persistence length is half the value of the Kuhn segment length and P is expressed as a function of N and α :

$$P = 2N\left(\frac{1-\cos\alpha}{1+\cos\alpha}\right)^{1/2} \qquad (9)$$

On average similar shapes are observed when generating by simulations molecules with the same P value from different sets of N and α values, so P appears as an efficient parameter defining the overall flexibility.

Dependence of R_c/R_g values with P is plotted on Figure 7. The curve is shifted when K varies and similar curves are obtained for other pore geometries. The ratio is almost stable for rod-like shapes, then gradually increases during the transition from rod-like to coil shapes, and a stable value is again reached for large P values.

Effect of segment thickness is only significant for very short chains (with N values less than 100) and is not reported here.

For flexible chains, persistence length is on the same order of magnitude than monomer length. So when analysing real flexible polymers, even with moderate molecular weight, we are generally concerned by high P values corresponding to a stable R_c/R_g ratio.

Dependence of R_η/R_g values with P is also plotted on the Figure 7. For worm-like chains with low d/q values R_η is obtained from the theoretical work of Yamakawa (*14*). Here the thickness of the segment has an important role. For thick chains the change of R_η/R_g when P varies is less pronounced. For highly flexible chains d/q becomes too large to allow direct use of Yamakawa calculations, but the tendency is to observe a stable ratio R_η/R_g for high P values.

Comparing the two sets of curves we can discuss qualitatively what happens to the ratio R_c/R_η. Clearly in most cases there is a partial compensation between the variation of R_c and R_η and this ratio remains relatively stable.

Highly flexible polymers correspond to a plateau zone with no P dependence, in consequence Universal Calibration applies well.

In the other cases the compensation is often efficient but the change in R_c/R_g ratio is not strictly correlated with the change in R_η/R_g ratio.

In order to illustrate more precisely the consequence for U.C. in real situations we have studied the ratio R_c/R_η for Schizophyllan, DNA and Pullulan (Figure 8). The situation for a flexible polymer like Pullulan is represented by a stable value R_c/R_η=1.35. For DNA which is a relatively thick stiff chain R_c/R_η exhibits a complex variation. Roughly it changes from 1.55 down to about 1.4 for increasing R_c values. For Schizophyllan, which is a very stiff chain relatively thin (*24*), the situation is extreme, and in this case the deviation from Universal Calibration is very important.

This example indicates clearly that UC does not strictly apply for these polymers as for the same R_c the values of R_η are not strictly the same. Nevertheless variations are important only for low MW and for high MW the three polymers tend to have the same ratio R_c/R_η.

Experimentally similar behaviour has been reported by Dubin (*25*) who compared the "Universal Calibration" plots of Pullulans, DNA and Schizophyllan. On these plots same apparent K values means same R_c, and lower value of $[\eta]$M means higher R_c/R_η ratio. In these experiments, globular proteins have same R_c/R_η

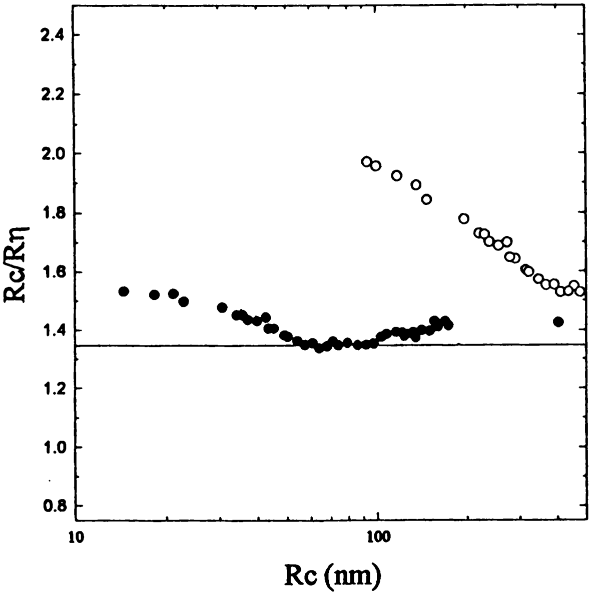

Figure 8. Ratio of the chromatographic radius R_c to the viscometric radius R_η as a function of the chromatographic radius R_c or the molecular weight MW. The points corresponding to DNA (●) and Schizophyllan (O) are obtained by combination of R_c/R_g derived from simulations and R_η/R_g from theoretical work of Yamakawa (*14*), using chain parameters of DNA (persistence length q=55 nm and diameter d=2.4 nm) and Schizophyllan (q=125 and d=2.6 nm) Results are plotted for K=0.5. The solid line represents the situation of the Pullulan (see text).

ratio than Pullulan. Our interpretation is that R_η represents the real hydrated radius of the protein, but R_c is much higher than this hydrated radius, due to electrostatic repulsion distance. Similar arguments have been presented by Potschka (*26*).

Conclusion

Monte carlo simulation of freely rotating chains allows detailed evaluation of the chromatographic radius of macromolecules with various flexibility. The chromatographic radius has not an intrinsic value since there is a shape-shape coupling between pores and macromolecules. Nevertheless the ratio R_c/R_g is increasing from 1.0 for rod-like shapes to 1.1 for coiled molecules. For highly flexible molecules this ratio becomes stable and this situation corresponds to synthetic polymers with M_W higher than 10000.

For stiff chains Yamakawa calculations allow us to estimate the viscometric radius. The R_η/R_g ratio is also increasing from rod-like to coiled species, the exact transition depending strongly on the chain thickness. For ideal, highly flexible chains this ratio has been estimated theoretically (*27, 28, 29*) and is about 0.87.

So, it appears clearly that the chromatographic radius is significantly higher than the viscometric radius, the R_c/R_η ratio being around 1.35.

It is necessary to admit that the origin of these two radii are physically very different. For viscosimetric radius each point is weighted with a non draining central part and an external zone in which draining effects become stronger and stronger, making the equivalent sphere smaller than the external dimension of the molecule. For chromatographic radius, each point in the external zone participates fully to the definition of the equivalent sphere and this explains why the ratio R_c/R_η is much higher than 1.

As R_c/R_g and R_η/R_g both increase when flexibility increases, it appears that the ratio R_c/R_η is generally almost stable, except in extreme situations, thereby confirming the practical efficiency of Universal Calibration. Nevertheless, it also indicates that there is no academic evidence for this rule.

Literature Cited

1 Moore, J. C. J. Polym. Sci. 1964, *A2*, 835

2 Benoit, H.; Grubizic, Z.; Rempp, P.; Dekker, D.; Zilliox, J. G.; *J. Chim. Phys.* 1966, *63*, 1507

3 Ouano, A. C. *J. Polym. Sci.* 1972, A-1, *10*, 2169

4 Yau, W. W.; Abbott, S. D.; Smith, G. A.; Keating, M. Y. In *"Detection and data analysis in Size Exclusion Chromatography"*, Provder, T., Ed. ACS SYMPOSIUM SERIES vol 352 1987, p80.

5 Brower, L.; Trowbridge, D.; Kim, D.; Mukherjee, P.; Seeger, R.; McIntyre, D. In *"Detection and data analysis in Size Exclusion Chromatography"*, Provder, T., Ed. ACS SYMPOSIUM SERIES vol 352 1987, p155.

6 Styring, M. G.; Armonas, J. E.; Hamielec, A.E. In *"Detection and data analysis in Size Exclusion Chromatography"*, Provder, T., Ed. ACS SYMPOSIUM SERIES vol 352 1987, p104.

7 Haney, M. A. ; Armonas, J. E.; Rosen, L. In *"Detection and data analysis in Size Exclusion Chromatography"*, Provder, T., Ed. ACS SYMPOSIUM SERIES vol 352 1987, p119.

8 Orvoen, J. B.; Busnel, J. P. *Spectra* 1985, *13*, 27

9 Lesec, J.; Millecant, M.; Havard, T. *12eme Colloque national C.E.S*, Lyon, 1991.

10 Grubizic, Z.; Rempp; P., Benoit, H. *J. Polym. Sci.* 1967, *B5*, 753

11 Potschka, M. *Anal. Biochem.* 1987, *162*, 47

12 Casassa, E.F.;Tagami, Y. *Macromolecules* 1969, *2*, 15

13 Giddings, J.C.; Kucera, E.; Russell, C.P.; Myers, M.N. *J.Phys.Chem* 1968, *72*, 4397

14 Yamakawa, H.; Fujii, M. *Macromolecules* 1974, *7*, 128

15 Hagel, L. In *Aqueous size exclusion chromatography*, Dubin, P. L. , Ed Elsevier. Amsterdam, 1988 p119.

16 Haller, W. *Nature* 1965, *206*, 693

17 Kirkland, J. J. *J. Chromatogr.* 1976, *125*, 231

18 Van Kreveld, M. E.; Van den Hoed, N. *J. Chromatogr.* 1973, *83*, 111

19 Mikes, O.; Strop, D.; Coupek, J. *J. Chromatogr.* 1978, *153*, 23

20 Kato, Y.; Kitamura , T.; Hashimoto, T. *J. Chromatogr.* 1985, *333*, 93

21 Meehan, E. Polymer Lab. *Personnal Communication.* 1993

22 Kramers, H.A *J.Chem.Phys* 1946, *14*, 415

23 Casassa, E. F. *Macromolecules* 1984, *17*, 601

24 Carriere, C. J.; Amis, E.; Schag, J. L.; Ferry, J. D. *Macromolecules* 1985, *18*, 2019

25 Dubin, P. J.; Principi, J. M. *Macromolecules.* 1989, *22*, 1891

26 Potschka, M. *Macromolecules.* 1991, *24*, 5023

27 Flory, P. J. *Principles of polymer chemistry*, Cornell University Press, Ithaca, New York, 1953 p611.

28 Pyun, C. W.; Fixmann, M. J. Chem. Phys. 1965, *42*, 3838.

29 Casassa, E. F. *Macromolecules.* 1976, *9*, 182

Chapter 5

A Soft-Body Theory of Size Exclusion Chromatography

Martin Potschka

Porzellangasse 19/2/9, A–1090 Vienna, Austria

Evidence that retention and dispersion are governed by different shape criteria makes a hydrodynamic transport mechanism of retention unlikely. This encourages us to propose a process of thermodynamic partitioning between a mobile and other phase(s). Here, retention is the probability finding a molecule within the stagnant volume of the pores or adsorbed at their surface. Earlier concepts of size assumed effectively hard-core non-interacting bodies whereas in reality all molecular forces have finite extensions that overlap with the force fields of other objects. While this concern is secondary for chain-polymers, for which proper statistical configurations are crucial, this distinction becomes essential for all compact bodies and interfaces. Fundamentally, size represents a distance average over the energy of interaction, which itself depends on the medium and therefore can be purposefully manipulated, e.g. varying ionic strength helps to identify the force-fields of polyelectrolytes and ultimately illuminates the chromatographic process mechanism itself. It is already clear that a theory of forces works well for SEC, corresponding to a 'Universal Calibration' different from earlier propositions.

The soft-body Model of Size Exclusion Chromatography

In the past retention in size exclusion chromatography (SEC) has been explained by two mutually exclusive models, namely by transport mechanisms or as an equilibrium process. Periodic arguments for an equilibrium process are based on the observation that retention normally is flow rate independent. The argument is insufficient, however, as Casassa (*1*) pointed out that even a transport mechanism would be independent of flow rate. On the other hand, overall transport rate through the column is too fast to permit complete equilibration of all of its pores. In support of this notion was quoted, that specially manufactured beads with a porous shell but a non-porous kernel did not improve dispersion (*2*). A strong argument against a transport determined mechanism of retention comes from studies of asymmetric solutes (*3*). In this

0097–6156/96/0635–0067$15.25/0

study different effects of asymmetry were found for retention and dispersion. The principle factor of retention seems to be an excluded-volume effect different from the consequences that the presence of walls has on the rate of migration for objects in similar sized cavities.

The notion of Ogston (*4*) that SEC is a 'virial coefficient amplifier' thus seems to be correct in principle, except for the fact that he underestimated the importance of higher order virial coefficients (simultaneous contact of solute with more than one matrix element) (*5*). Also the particular excluded-volume functions are hard-body models and may not properly represent the actual matrix morphology. Virial expansion does not appear to be a meaningful device to pursue.

In the excluded-volume model of SEC, retention is related to the volume which is accessible within the pores (or a homogeneous portion thereof). The contour of accessible volume is described by the center of an object rolling over the surface of the pores. Therefore, larger objects will have a smaller accessible volume and elute first. Traditionally this has been viewed as a geometric problem where two surfaces limit the extension of bodies in an all-or-none fashion. This geometric view, of course, is only a special case of the more general thermodynamic point of view, namely, that the dimensions of a body are defined by a discontinuous potential. In the submicron-world such potentials are not to be found. Rather, energetic fields of various kinds extend often far into the space which surrounds a kernel that might still be called a body proper. These soft interactions have to be taken into account when asking for the *probable* space that a body occupies within a cavity. (It might seem perplexing at first that extension is not a fixed property for any isolated body, however, measuring extension always depends operationally on the interaction with some other entity, be it another object in spatial contact or electromagnetic waves.) Because soft interactions are always present, it becomes misleading to use the label 'non-ideal' for all interactions other than hypothetic rectangular all-or-none potentials. This critique can be put into thermodynamic terms: Traditionally, ideal SEC has been defined as a purely entropic volume-related process whereas ideal 'other chromatography' was considered an enthalpy driven surface phenomenon lacking any volumetric contributions. But with repulsive forces one observes strong enthalpic contributions, yet a purely volume-related process (see below). I therefore argue for a reconsideration of the term 'non-ideal SEC'. All the oddities of so-called premature elution of anions at low ionic strength follow strictly and comprehensively from the indicated model.

Because electrostatic interactions are rather well modeled and modifiable by ionic strength variation they are an ideal paradigm for the argument in general. The fact that the subsequent discussion will focus on polyelectrolytes should not make one forget, that the issue is broader with Van-der-Waals attraction omnipresent. In absence of counteracting repulsive potentials solutes always adsorb to the chromatographic matrix and the premises of SEC are not even met (besides electrostatic one needs to mention solvation forces, since the miscibility energies in ternary mixtures are generally not zero).

The soft-body model of SEC thus is general. For any particular analysis some simplifying modeling assumptions are in order. Whereas pores clearly are not cylinders, such a model is frequently applied for its simplicity. At an empirical level one might model the true experimental calibration curve of a chromatographic column with some kind of pore size distribution, say cylinders of different width. The second major restriction at the level of quantitative analysis concerns the shape of solutes. For non-centrosymmetric objects the computation of (soft) contact hyperplanes becomes a tedious average of rotational configurations; for lack of analytical solutions one usually applies

Monte Carlo techniques. The initial restriction to centrosymmetrical objects, however, can be approximated on the experimental level by the choice of globular proteins as solutes. For computational amenities I shall thus limit the following quantitative considerations to such dense spherical objects with quasi-smeared surface charges that permeate cylinders. The extension to distributions of cylinders of different radii is straightforward, but omitted below.

The Model for electrostatic Forces

We write for the retention volume V (in ml)

$$V = V_{\text{void}} + (V_{\text{total}} - V_{\text{void}})\,K \tag{1}$$

with K the partition coefficient

$$K = \frac{[\text{solute}]_{\text{pores}}}{[\text{solute}]_{\text{bulk}}} \tag{2}$$

of solute concentration inside the pores to solute concentration in bulk solution. For SEC K ideally ranges from 0 to 1. For a hard-core sphere of radius R within a cylinder of radius R_{max}, presenting a non-interacting wall, we have

$$K = \left\{1 - \frac{R}{R_{\text{max}}}\right\}^2 \tag{3}$$

This, of course, is only a special case of integrating the probability to find the object at radial position r (in the interval $0 < r < R_{\text{max}}$); the probability is unity for $r < R_{\text{max}} - R$ and zero elsewhere. In the general case the probability is expressed by $\exp(-\Delta G(R_{\text{max}} - R - r)/kT)$ where $\Delta G(x)$ is the energy of interaction between solute and pore wall. The details of the electrostatic model are outlined in Appendix A and B. From eq. (B.1) together with eq. (B.6) and (A.13) we get

$$K = \frac{1}{R_{\text{max}}^2} \int_0^{R_{\text{max}} - R} 2r\, e^{-[4\pi\,\psi_1\,\kappa^{-1}\sigma\, R\left(\frac{R_{\text{max}}}{R_{\text{max}} - R - r}\right)^{(1/2)} \exp(-\kappa(R_{\text{max}} - R - r))]}\, \mathrm{d}r \tag{4}$$

with σ the surface charge density of the cylinder pore, κ^{-1} the Debye-Hückel length (defined in eq. (A.2)) and ψ_1 the pseudo-surface-potential of the sphere. The relationship of ψ_1 to the net charge Q is defined in eq. (A.11), respectively (A.12).

The integral in eq. (4) apparently has no closed analytical expression (see Appendix C). Intuitively one expects – for charge repulsion – a function with the following form

$$K = \left\{1 - \frac{R_{\text{sec}}}{R_{\text{max}}}\right\}^2 = \left\{1 - \frac{\left[R + \kappa^{-1}\dfrac{\mathrm{d}R_{\text{sec}}}{\mathrm{d}\kappa^{-1}} + \theta_i\right]}{R_{\text{max}}}\right\}^2 \tag{5}$$

because experimentally one obtains approximately linear dependencies of the apparent elution radius R_{sec} on Debye-Hückel length. θ_i adjusts the intercept, which is different from the radius R itself. Typical experimental data are shown in Fig. 1. This linearity was first reported in 1988 for proteins (*6*) and has since been confirmed with DNA and latex (*7*,*8*).

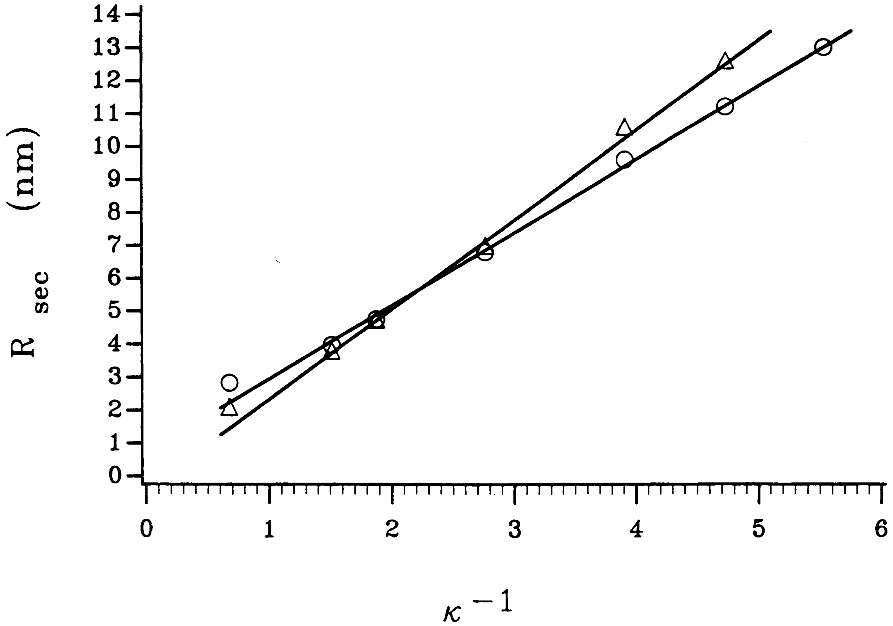

Figure 1. Effective molecular radius for chromatographic retention as a function of Debye-Hückel length in the case of charge repulsion. Superose-12, flow rate 0.5ml/min, room temperature. Eluent: Tris/HCl plus NaCl of varying ionic strength at *pH* 8.0. Retention radii R_{sec} were obtained by matching the elution volume to the known viscosity radii of some dozen calibration substances (see ref. (*5*)) at high ionic strength. This type of calibration is a zero order approximation only, given that the true R_{sec} values are consistently different from R_η (see text). Ovalbumin, slope $dR_{sec} / d\kappa^{-1} = 2.22$ (o); calmodulin, slope $dR_{sec} / d\kappa^{-1} = 2.72$ (Δ) .

A representative theoretical simulation of charge repulsion, eq. (4) plotted in terms of R_{sec}, is shown in Fig. 2. On the scale of this plot a similar more exact equation based on eq. (B.2),(B.3),(B.4) is virtually indistinguishable from the curve for eq. (4). This proves the validity of the simplifications made to arrive at eq. (B.6) (*7*). The specific form of eq. (4) makes use of eq. (B.6) instead.

The Poisson-Boltzmann equation can be solved for differing boundary conditions, either constant potential or constant charge, and it is not always clear which case is better to represent an experimental situation. Fig. 3 gives the comparison between eq. (4), which is based on eq. (B.6) and a similar equation based on eq. (B.10). It turns out that the constant charge case (eq. (B.10)) is more linear over the experimental range of interest – as shown in the case of small pore sizes (Fig. 3) –, but the distinction has little bearing on larger pore sizes, as expected. Experimentally, the decisive region, close to the void volume V_{void}, i.e. close to R_{max}, is difficult to measure reproducibly.

For charge attraction eq. (4) remains valid, but the functional appearance radically changes. This case is illustrated in Fig. 4 and demonstrates the need for gradient elution (as opposed to isocratic elution for charge repulsion). A similar equation presumably also applies to ion-exchange chromatography proper (which differs only in having higher matrix charges) except that eq. (A.13) needs to be replaced by eq. (A.14) and that at small distances repulsive forces have to be included. Furthermore it may not be permissible to ignore Van-der-Waals forces. The case of charge attraction will not be analyzed further.

The mean-field Approximation

To approximate the integral of eq. (4), one may start with a mean-field equivalence of the planar case (see Appendix C). Rather than integrating over all radial positions r, we assume that we can represent the distribution by a rectangular potential centered at the mean-field position, i.e. at the distance $x = R_{max} + R - r$ at which $\Delta G = \frac{1}{2} kT$. The situation is illustrated in Fig. 5. Solving eq. (B.1) with $f = 1$ for x one obtains

$$x \sim \ln(8\pi) + \ln(\psi_1 R) + \ln(\kappa^{-1}\sigma) \tag{6}$$

Eq. (6) is a fair model of the planar case for large R_{max} . This is also borne out by analytical solutions to the integral in Appendix C. Similarily one may solve the cylinder case with eq. (B.1) and f expressed by eq. (B.6). The additional minor terms, however, produce a worse agreement than eq. (6) with the integral solution eq. (4). According to the mean-field hypothesis we thus have

$$R_{sec} = R + \kappa^{-1} x \tag{7}$$

Comparison of eq. (7) with the exact solution of the integral in eq. (4) is shown in Figs. 2 and 3 and at once reveals the shortcomings for the cylinder case, namely a completely wrong intercept and failure to yield the proper dependence on pore size R_{max}. However, eq. (6) recovers – in the linearized domain of ψ_1 – useful limit laws about the logarithmic proportionality of the slopes on charge ($\mathrm{d}R_{sec} / \mathrm{d}\kappa^{-1} \propto \ln Q$, $\mathrm{d}R_{sec} / \mathrm{d}\kappa^{-1} \propto \ln \sigma$).

Inspecting the numerical results of eq. (4), we see that charge effects directly depend on pore size as well. To a first approximation

$$\frac{\mathrm{d}R_{sec}}{\mathrm{d}\kappa^{-1}} \propto \frac{\ln(\ln(R_{max}))}{\ln(2\pi)} \quad [\ln Q + \ln \sigma] \tag{8}$$

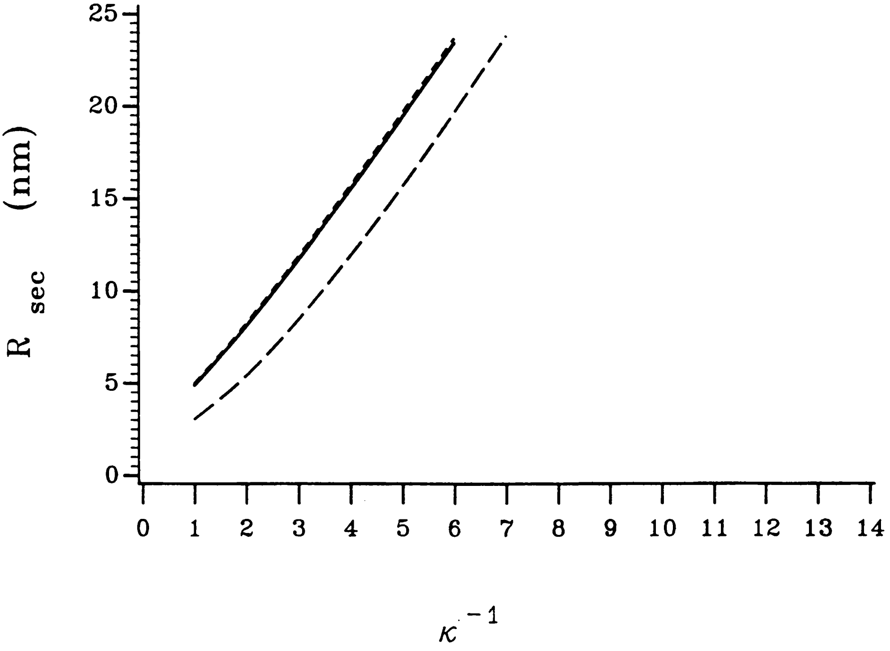

Figure 2. Theoretical simulation of the retention of charged spheres in cylindrical pores. Case of charge repulsion. Pore radius $R_{max} = 100$nm, sphere radius $R = 3$nm, polyelectrolyte net charge $Q = -12$, cylinder surface charge density $\sigma = -0.02\text{nm}^{-2}$. Solution of the integral in eq. (4), which makes use of eq. (B.6), (——); the exact integral solution using eq. (B.2) instead (···); mean-field approximation eq. (7) based on eq. (6) (– – –).

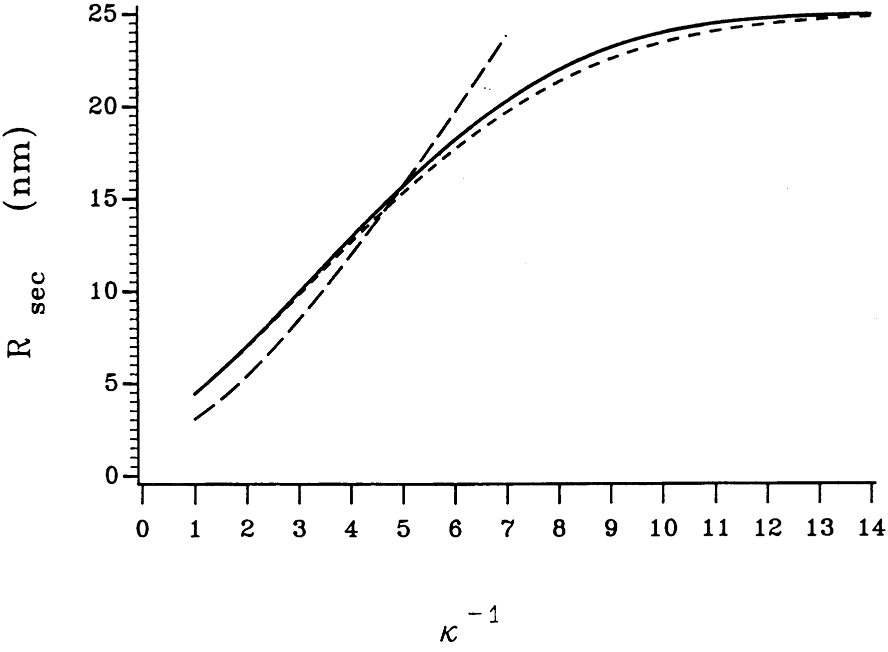

Figure 3. Theoretical simulation of the retention of charged spheres in cylindrical pores. Case of charge repulsion. Pore radius $R_{max} = 25$nm, sphere radius $R = 3$nm, polyelectrolyte net charge $Q = -12$, cylinder surface charge density $\sigma = -0.02\text{nm}^{-2}$. Solution of the integral in eq. (4) , i.e. the constant potential boundary condition eq. (B.6), (···); a similar integral based on the constant charge boundary condition eq. (B.10) instead (——); mean-field approximation eq. (7) based on eq. (6) (– – –). Note that the correct integrals asymptotically approach the maximum pore size R_{max}, i.e. the void volume V_{void}.

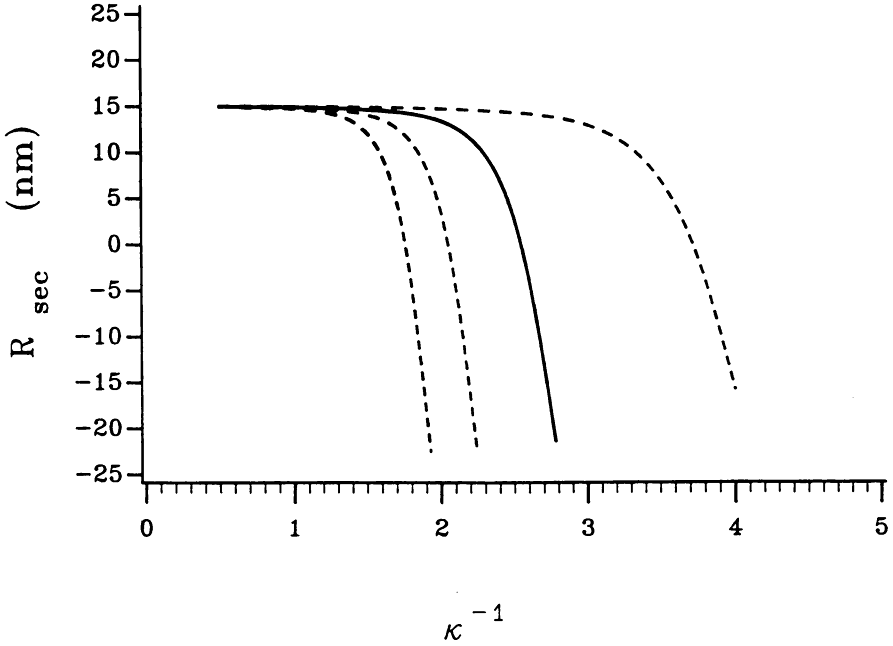

Figure 4. Theoretical simulation of the retention of charged spheres in cylindrical pores. Case of charge attraction. Pore radius $R_{max} = 25$nm, sphere radius $R = 15$nm, cylinder surface charge density $\sigma = -0.01$nm^{-2}. Solution of the integral in eq. (4). Polyelectrolyte net charge from right to left $Q = +1$ (···); $Q = +2$ (——); $Q = +3$ (···); $Q = +4$ (···). The ordinate units correspond to a range of $K = 2 - 0$.

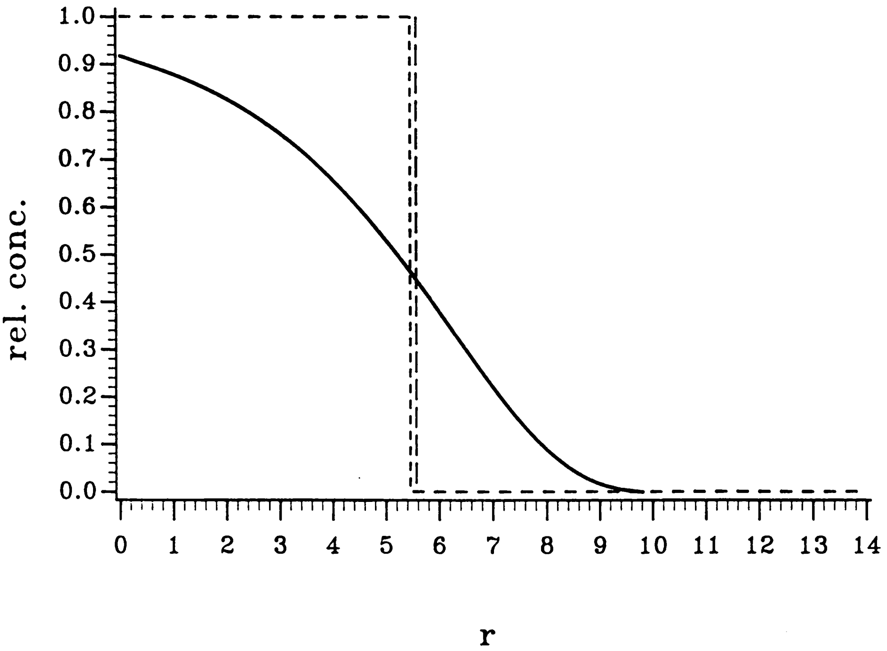

Figure 5. Sketch of the probability of finding the solute at a particular radial position *r*. The argument of the integral in eq. (4) was calculated with $R_{max} = 14\text{nm}$, $Q = -12$, $\sigma = -0.02\text{nm}^{-2}$, $R = 3\text{nm}$, $\kappa^{-1} = 3\text{nm}$ (——). The mean field approximation of this case, eq. (7), (— — —) fails to coincide with the exact volume - centroid position of the depletion layer at $R_{max} - R_{sec}$ (···).

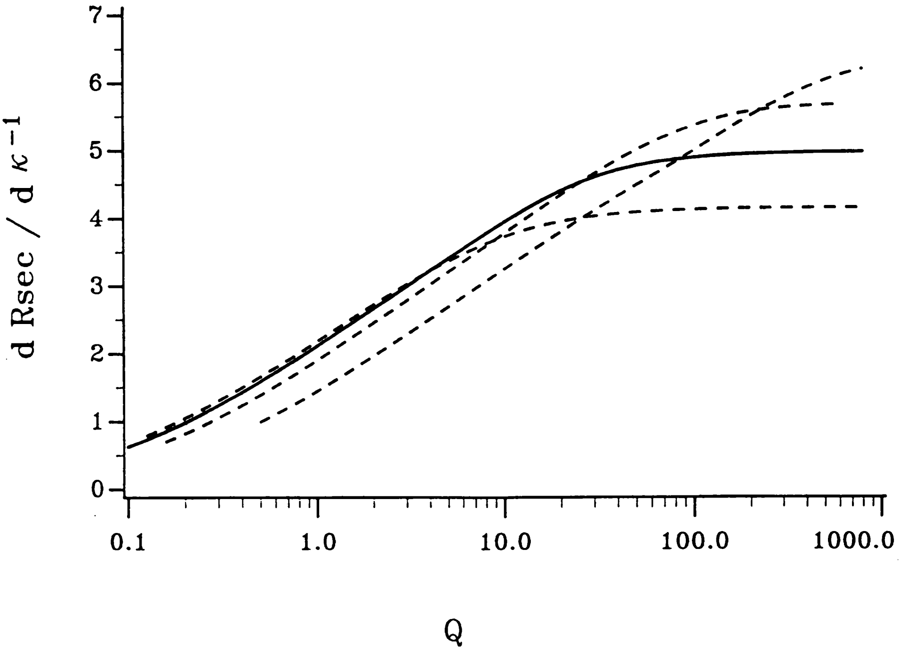

Figure 6. Linear range of integral solution (eq. (4)) as a function of net charge Q. A linear least squares fit to the integral solution for R_{sec} was performed in a variable interval $[1, \kappa_{max}^{-1}]$ adjusted to maximize the correlation coefficient (always > 0.99). Parameters $R_{max} = 100$nm, $\sigma = 0.02$nm^{-2}, increasing values of R from left to right: $R = 3$nm(——), $R = 1, 9, 27$nm (···). The onset of the plateau region of saturated charge is at about a scaled net-charge density $Q/4\pi R \sim 0.9$nm^{-1}.

(see Fig. 6). Scaling the R dependency is messy. Fig. 6 also shows that the function breaks into two regimes. At low charge the mentioned log-linear dependency is observed. At high net charge densities $Q/4\pi R \gtrsim 0.9\text{nm}^{-1}$ the slopes $dR_{sec} / d\kappa^{-1}$ reach a maximum plateau whose magnitude itself increases with R . This sharp transition from the linearized domain to the saturated range is a feature of eq. (A.4).

Non-spherical Solutes

I shall now compare the experimental results of two proteins, investigated on Superose-12, with the theoretical simulations in order to address possible extensions of theory to non-spherical objects.

Ovalbumin is a comparatively spherical, phosphorylated glycoprotein. The net charge at pH 8.0 is $Q = -16\pm2$ if titration data (*9*) are adjusted to the more widely accepted $pI = 4.7$. At pH 8.0, Q is independent of ionic strength. The diffusional Stokes radius $R_s = 2.96\text{nm}$ is based on critically selected sedimentation coefficients (*10,11*) together with a sequence molecular weight of 44310, which includes the carbohydrate content, plus two phosphate groups (*12*), and a partial specific volume of 0.748ml g^{-1}. Formerly a value of 2.83nm was used (*5*). Scaled net-charge densities of $Q/4\pi R \sim -0.4\text{nm}^{-1}$ are quite typical of many acidic proteins and of the same order of magnitude as the critical range of 0.9nm^{-1} (see Fig. 6). Presumably, few natural biopolymers exceed this critical amount of net charge, and only the linearized domain of ψ_1 is ultimately relevant.

Fig. 7 shows theoretical together with the experimentally determined slopes from Fig. 1. The matrix surface charge density was adjusted to $\sigma = -0.02\text{nm}^{-2}$ ($-0.033\mu\text{mol m}^{-2}$, -0.0032 C m^{-2}) in order to match the simulation to the experimental value of ovalbumin. The value is realistic given that the more highly charged CPG rigid porous glass gives about $\sigma = -0.04\text{nm}^{-2}$ at pH 5.0 (*13*). Based on a rough estimate of surface area S from retention data in the limit of $K \rightarrow 1$ (*14*)

$$V = V_{\text{total}} - R_{\text{sec}} S \tag{9}$$

we obtain for Superose-12 a surface area of $75\text{m}^2/\text{ml-bed}$ and thus $\sigma = -2.5\mu\text{mol/ml-bed}$ at pH 8.0. This corresponds well to an ionic capacity of $-4.5\mu\text{mol/ml-bed}$ at pH 12 for the same material based on a method described by Korpela (*15*) (L. Hagel, pers. comm.). Dubin's group (*16*) report somewhat larger values.

Calmodulin is a remarkably asymmetric calcium binding protein. Its axial ratio, approximately 5 (*17*), is significant in terms of surface area, yet too small to show an apprechiable difference between R_η and R_s. Binding of up to 4 calcium ions induces a conformational change that is substantial in terms of tertiary structure, but minor in terms of diffusional Stokes radii, $R_s = 2.14\text{nm}$ without Ca^{++} and $R_s = 2.09\text{nm}$ with Ca^{++} at physiological ionic strength (*18*). The Ca-free molecules undergo a continuous "conformational" change with decreasing ionic strength similar to charged coil-polymers. The viscosity radii are $R_\eta = 2.15\text{nm}$ at $I = 206\text{mM}$, $R_\eta = 2.31\text{nm}$ at $I = 106\text{mM}$ and $R_\eta = 3.0\text{nm}$ at $I = 6\text{mM}$ based on intrinsic viscosity (*19*). This polymer swelling needs to be taken into account when analyzing electrostatic effects. According to the sequence (*18*) the net charge at pH 8.0 should be approximately $Q = -16$ with Ca^{++} and $Q = -24$ without. Calmodulin was injected in Ca-bound form into a calcium free eluent.

Because of its high asymmetry, the true surface charge density of the calcium free form of calmodulin is only $Q/4\pi R^2 = -0.1\text{nm}^{-2}$ whereas the hy-

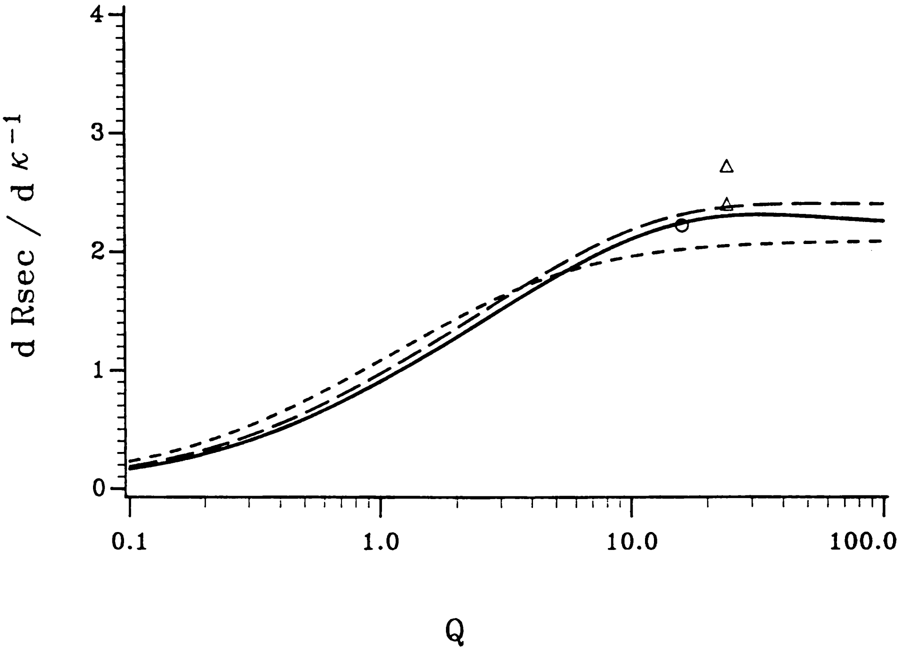

Figure 7. Linear least-squares fit to the integral solution (eq. (4)) in the interval $\kappa^{-1} = [2, 4]$ as a function of net charge Q. Only points with correlation coefficients > 0.99 are shown. Parameters of simulation were chosen to match the conditions in Fig. 1: $R_{max} = 14$nm , $\sigma = -0.02\text{nm}^{-2}$, and with $R = 2.96$nm(——) , $R = 2.14$nm (– – –), $R = 0.5$nm(···). Experimental values of ovalbumin (net charge $Q = -16$) (o) and calmodulin (net charge $Q = -24$) (Δ) from Fig. 1 and calmodulin corrected slope according to text (▲).

pothetical value based on the equivalent-volume Stokes-sphere is $Q/4\pi R^2 = -0.4\text{nm}^{-2}$. Apparently this is not a problem, however. The principal factor of discrepancy appears to be polyelectrolyte expansion. After correcting the slope $dR_{sec} / d\kappa^{-1} = 2.72$ for the concomitant change of viscosity radius, a slope of 2.4 is obtained, which fits well with theory. We may conclude, that SEC is a promising device to measure charge, both for unknown solutes and for unknown porous materials alike.

Universal Calibration of SEC

Since the seminal theoretical work of Giddings et al. (*20*) and Casassa (*21*) a fundamental contradiction has persisted in the field of chromatography. Experimentally, *Universal Calibration* in terms of viscosity radii works well in most, albeit not all cases (*5,7,22*), whereas theoretically it should not be so. The principle points are well summarized by Casassa (*23*).

We define the viscosity radius R_η

$$R_\eta = \left(\frac{3}{10\pi N_L} \right)^{1/3} ([\eta]M)^{1/3} \tag{10}$$

The mean linear extension R_L is half the maximum linear extension averaged over all orientations and conformations. For ideal random chains the mean end-to-end distance is equal to $2R_L$ (*24*). Note that frequently one finds the notation $\bar{X} = 2R_L$. There are a variety of synonyms for $\bar{X}$, e.g. average maximum linear extension, mean external length L-measure, mean maximal size, mean maximal projection, mean molecular projection, mean projection onto an axis, extent, span (see ref. (*25*)). It should not be confused with $\bar{Q} = 2R_Q$, the mean maximal cross-section, which some have used for universal calibration (*26,27*). The mean linear extension is the theoretically decisive parameter for the depletion layer as long as the non-interacting wall borders a semi-infinite solution. We then have $R_{sec} = R_L$. Whenever, in a real pore, the concentration at $r = 0$ becomes different from bulk, viz. for $K \rightarrow 0$, additional effects determine R_{sec} which then becomes dependent on pore size and geometry (*23,28*). For coiled polymers these additional effects are least pronounced and R_L is generally a good approximation of R_{sec}. We have

$$\text{linear coiled polymers: } R_L = \left(\frac{8}{\pi^{3/2}\Phi} \right)^{1/3} ([\eta]M)^{1/3} = 1.32\, R_\eta \tag{11}$$

The exact numerical value depends somewhat on the choice taken for the constant Φ (*23*). For spheres the geometric radius R is related to the diffusional Stokes radius R_s and viscosity radius R_η

$$\text{spheres: } R_L = R_\eta = R_s = R \tag{12}$$

Casassa also gives values for rods (eq. 14 in ref. (*23*)), for which antecedent numerical details might need some adjustment (*5*). Degoulet gives values for intermediate flexibilities and finite dimensions of the chains (*28*). Here we shall concern ourselves with comparing spheres and coils only.

How did the experimental evidence on *Universal Calibration* emerge? All experimental evidence concerning co-elution of spheres with other geometric shapes has relied on globular proteins (*7*), i.e. has involved polyelectrolytes, or – as some would call it – charged spheres. In doing this it was always assumed that at high ionic strength, all specific polyelectrolyte effects vanish and the relevant radius is simply the geometric one. Fig. 8 shows that this

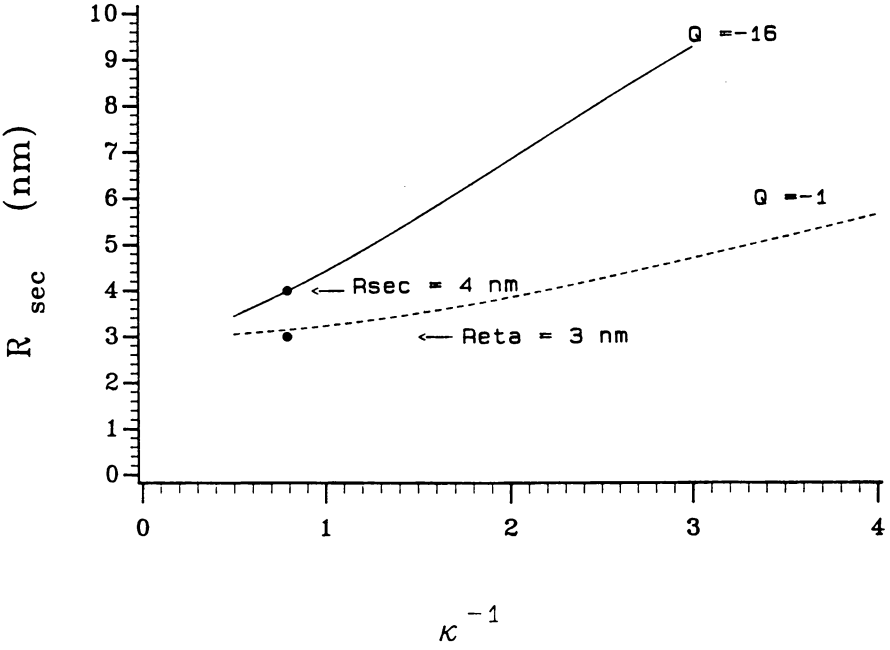

Figure 8. Theoretical simulation of the retention of charged spheres in cylindrical pores. Pore radii $R_{max} = 14$nm, polyelectrolyte net charge $Q = -16$(——) and $Q = -1$(···), cylinder surface charge density $\sigma = -0.02\text{nm}^{-2}$, sphere radius $R = 3$nm. The position $R = R_\eta$ and R_{sec} are shown for $I = 160$mM(●). The figure illustrates that the elution position R_{sec} of polyelectrolytes remain larger than expected on the basis of Stokes or viscosity radius, even at high ionic strength.

presumption is invalid. Even at $I = 160\text{mM}$ ionic strength a typical charged sphere elutes with a soft radius about 30% larger than its geometric size ($R_{sec} = 4\text{nm}$ vs. $R_\eta = 3\text{nm}$ in Fig. 8). Thus at high ionic strength for

charged spheres: $R_{sec} \sim 1.3R$ (13)

whereas for non-electrolyte

coiled polymers: $R_{sec} \sim 1.3R_\eta \sim R_L$ (14)

This coincidence seems to reconcile experimental evidence (erroneously attributed to R_η congruence) with theoretical predictions. It illustrates the fundamental consequences that a theory of charge effects has for a theory of SEC itself.

An example for this assertion is shown in Fig. 9. Two charge-mutants of the same protein, one being weakly positive charged ($Q \sim +1$) and one negatively ($Q \sim -1$) at the *pH* of measurement, are studied as a function of ionic strength. Rather than transforming the data into plots like Fig.1 the raw elution data are shown. In the case of the positively charged myoglobin species the matrix acts as a weak cation-exchange column, as expected. Because the involved amounts of charge are low, convergence is expected according to Fig. 8, yet this is not reached at 0.2M ionic strength.

Clearly the extent of extra size $R_{sec} - R$ varies with net charge also at high ionic strength (see Fig. 8). It will thus contribute a systematic error to the scatter of column calibration points, if these are performed in terms of core radius $R_s = R_\eta$, which is what has been done up to now.

Fig. 8 also shows that we cannot generally get rid of this extra size in practical SEC experiments. Only for conditions well over 1M salt might we expect to squeeze the repulsive electrostatic layer to negligibility. It is well known that under such conditions adsorption commences, a condition called hydrophobic interaction chromatography, for the very reason that repulsive forces finally are overcome.

There is another, more intriguing (and perhaps more speculative) thought. It is well known that at least large polyelectrolytes exhibit additional forces called hydration (solvation) forces that amount to 1-2nm decay length (*29,30*). Thus the true difference between R_{sec} and R may well be larger at high ionic strength than suggested by electrostatic considerations alone. With chromatographic operations further improved, SEC could become a technique to measure these more subtle kinds of force-fields relevant in structure - function relationships.

Originally *Universal Calibration* meant calibration in terms of viscosity volume $[\eta]\, M$, respectively viscosity radius R_η. As I do not know how to make the term *Universal Calibration* more general than Universal, I propose to call *Universal Calibration* any attempt at a unified picture of elution. The hierarchy of conditions relevant to such a novel theory would be: 1st) soft-body potentials because walls are always interacting; 2nd) proper statistical configurations; none of which actually scales with R_η. Yet by fortuitous coincidence, R_η will remain a useful and practical first guess at interpreting unknown data.

It is already clear that a theory of forces works well for SEC, limited only by the fact that translation of detailed chemical anatomy into physical net forces becomes operationally intractable at very fine resolution.

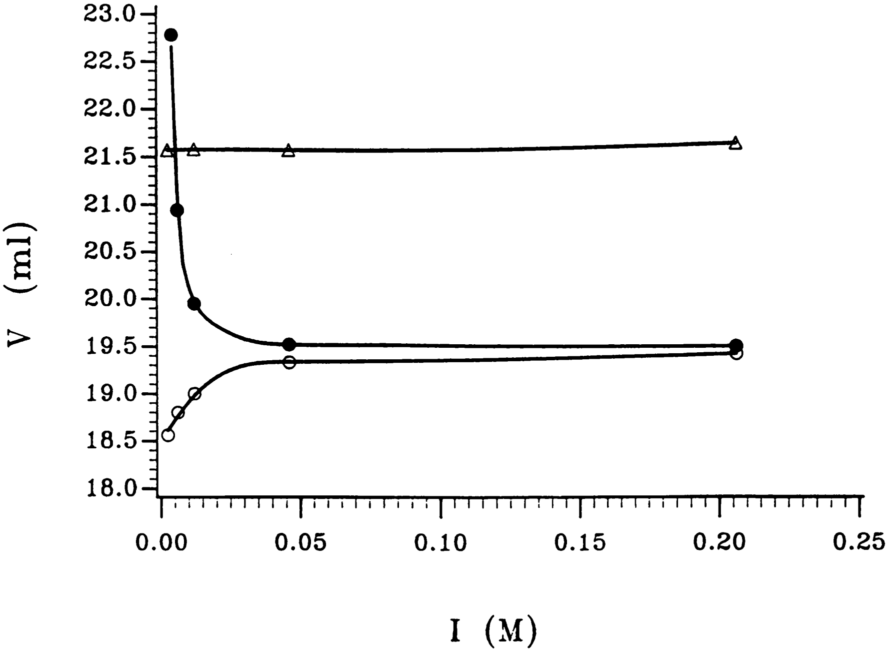

Figure 9. Variation of SEC retention volume as a function of ionic strength. TSK5000PW column 3, which has an exceptionally low residual negative surface charge density. Eluent: Tris/HCl plus varying amounts of NaCl at *pH* 8.0 , flow rate 0.42ml/min, room temperature. Horse myoglobin ($pI = 7.3$) is anionic at this *pH* (o), sperm whale myoglobin ($pI = 8.2$) is cationic at this *pH* (●), vitamin B_{12} is neutral and not affected by ionic strength (Δ). Its constant elution serves to indicate the degree of constancy in flow rate that was achieved in this experiment.

Conclusions

The elution of polyelectrolytes with its specific charge-related effects has been taken as model paradigm for a new conceptual approach to size exclusion chromatography. It was shown that soft-body potentials are crucial in defining universal elution characteristics.

Appendix A: The Relationship between Surface Charge and Potential

The best analytical approximations for the solution of the one-dimensional Poisson-Boltzmann equation are those of Ohshima et al. (*31*). Model I yields the surface charge density (their equations 10 and 47)

$$\frac{Qe}{4\pi R^2} = [\frac{\varepsilon_r \varepsilon_o kT}{e}]\, 2\kappa \sinh(y/2)\, \{1 + \frac{2\kappa R + 1}{\kappa^2 R^2 \cosh^2(y/4)}\}^{1/2} \qquad (A.1)$$

with Q the net charge at the surface of a sphere with radius R , y the true surface potential, κ the Debye-Hückel constant

$$\kappa^2 = \frac{2e^2 N_L}{\varepsilon_r \varepsilon_o kT}\, I \qquad (A.2)$$

(there is an extra factor 10^{-15} in eq. (A.2) to yield κ^{-1} in units of nm), ε_r the dielectric constant (80 for water at room temperature 293K), ε_o the vacuum permeability ($8.85 \cdot 10^{-12} CV^{-1}m^{-1}$), e the elementary charge ($1.60 \cdot 10^{-19}C$), k the Boltzmann constant ($1.38 \cdot 10^{-23} JK^{-1}$), T absolute temperature, I the ionic strength, and N_L Avogradro's number ($6.02 \cdot 10^{23} mol^{-1}$). Without the square-root term eq. (A.1) is identical to the original result of Gouy for flat plates (*32*).

Model II yields (their equations 10 and 24)

$$\frac{Qe}{4\pi R^2} = [\frac{\varepsilon_r \varepsilon_o kT}{e}]\, 2\kappa \sinh(y/2)\, \{1 + \frac{2}{\kappa R \cosh^2(y/4)} + \frac{8 \ln(\cosh(y/4))}{\kappa^2 R^2 \sinh^2(y/2)}\}^{1/2} \qquad (A.3)$$

Since the potentials always converge to an exponential decay at large distance one may model this relative to a pseudo-surface-potential ψ (their equation 52)

$$\psi = 8\tanh(y/4) \left[1 + \{1 - \frac{2\kappa R + 1}{(\kappa R + 1)^2} \tanh^2(y/4)\}^{1/2} \right]^{-1} \qquad (A.4)$$

The important feature of eq. (A.4) is that the pseudo-surface-potential ψ reaches a plateau for large amounts of charge whereas in theory the true surface potential rises unlimitedly. As a practical consequence different amounts of high surface charge density become indistinguishable when probed at medium to large distance.

To solve for ψ one first applies elementary transformations such as

$$\sinh(2z) = \frac{2\tanh(z)}{1 - \tanh^2(z)} \qquad (A.5)$$

$$\cosh^{-2}(z) = 1 - \tanh^2(z) \qquad (A.6)$$

In the Debye-Hückel limit ($y \rightarrow 0$) one obtains a dimensionless potential in simple form

$$p = [\frac{e^2}{4\pi\varepsilon_r\varepsilon_o kT}] \frac{Q}{R(1 + \kappa R)} \tag{A.7}$$

The general solution is then obtained by expansion of eq. (A.1) and (A.4)

$$p = \frac{4(4 - E\psi^2)\psi}{(4 + E\psi^2)^2 - \psi^2} (1 - \delta) \tag{A.8}$$

with

$$E = \frac{2\kappa R + 1}{16(\kappa R + 1)^2} \tag{A.9}$$

where δ measures approximately the discrepancy of eq. (A.3) relative to the principal result of eq. (A.1)

$$\delta < (\kappa R + 1)^{-1}(2\kappa R + 1)^{-1} [1 - \frac{\psi}{3} + ...] \tag{A.10}$$

Thus

$$\psi_1 = \frac{[8 + p^2 + 4(4 + p^2 - 16Ep^2)^{1/2}]^{1/2}}{2Ep} - [\frac{1}{4E^2} - \frac{4}{E} + \frac{1}{E^2p^2}]^{1/2} - \frac{1}{Ep} \tag{A.11}$$

and for $p \rightarrow 0$

$$\psi_1 = p - [\frac{1 - 12E}{16}]p^3 + [\frac{1}{128} - \frac{13E}{64} + \frac{11E^2}{8}]p^5 - O[p^7] \tag{A.12}$$

The surface charge density of a flat wall ($R \rightarrow \infty$) is

$$s = [\frac{e^2}{\varepsilon_r\varepsilon_o kT}] \kappa^{-1} \sigma \tag{A.13}$$

$$\psi_2 = \frac{4(4 + s^2)^{1/2} - 8}{s} \tag{A.14}$$

and for $s \rightarrow 0$

$$\psi_2 = s - \frac{s^3}{16} + \frac{s^5}{128} - O[s^7] \tag{A.15}$$

Appendix B: Potential Energy of a Sphere within a Cylinder

A solution of the mixed-coordinate, linearized Poisson-Boltzmann equation has been given by Smith and Deen (*33*). For practical purposes the mirror charge effects are negligible and further simplifications can be made (*7*). The free energy of interaction, by nature enthalpic rather than entropic, is

$$\frac{\Delta G_e(x)}{kT} = [4\pi\frac{\varepsilon_r\varepsilon_o kT}{e^2}] \psi_1 \psi_2 Rf e^{-\kappa x} \tag{B.1}$$

where ψ_1 is the apparent electric surface potential of a sphere and ψ_2 that of a plane wall representing the cylinder cavity (defined in Appendix A), R is the sphere radius, $R_{\max}$ the radius of the cylinder, κ the Debye-Hückel constant, k is the Boltzmann constant, T absolute temperature, x the distance between the two surfaces (of sphere and cylinder). For constant surface potential f is a function of the specific geometry (*7*)

$$f = \frac{\mathrm{I}_o(\kappa[R_{\max} - R - x])\,\mathrm{e}^{-(\kappa[R_{\max} - R - x])}}{\mathrm{I}_o(\kappa R_{\max})\,\mathrm{e}^{-(\kappa R_{\max})}\ \mathscr{H}} \tag{B.2}$$

$$\mathscr{H} = \{1 - \mathrm{e}^{-2\kappa x}\,\mathrm{g}(\kappa[R_{\max} - R - x]\,,\,\kappa R_{\max}\,,\,-1)\ \mathrm{e}^{-\kappa R}(\mathrm{e}^{\kappa R} - \mathrm{e}^{-\kappa R})\} \tag{B.3}$$

$$\mathrm{g}(z,a,i) = \frac{e^{2(a-z)}}{a}\ \mathrm{I}_o(z) \sum_{t=0}^{\infty} \frac{(\frac{z}{a})^t\,(2t)!}{2^{3t}\,(t!)^2}\ \mathrm{I}_t(z)\ [a\,\mathrm{K}_{t+1}(2a) + \frac{i}{4}\,\mathrm{K}_t(2a)] \tag{B.4}$$

where I_t and K_t are the modified Bessel functions of the first and second kind respectively. Because typically $\mathscr{H} \simeq 1$ and

$$I_o(z) = \frac{\mathrm{e}^z}{\sqrt{2\pi z}}\ \{1 + \frac{1}{8z} + \ldots\} \tag{B.5}$$

eq. (B.2) simplifies to (*7*)

$$f = \sqrt{\frac{R_{\max}}{R_{\max} - R - x}} \tag{B.6}$$

At constant charge, one obtains by analogy (from eq. 29 of ref. (*33*) together with eq. (A.7) and (A.13))

$$f' = \frac{\mathrm{I}_o(\kappa[R_{\max} - R - x])\,\mathrm{e}^{-(\kappa[R_{\max} - R - x])}}{\mathrm{I}_1(\kappa R_{\max})\,\mathrm{e}^{-(\kappa R_{\max})}\ \mathscr{H}'} \tag{B.7}$$

$$\mathscr{H}' = \{1 - \mathrm{e}^{-2\kappa x}\,\mathrm{g}(\kappa[R_{\max} - R - x]\,,\,\kappa R_{\max}\,,\,+3)\ \mathrm{e}^{-\kappa R}(\mathrm{e}^{\kappa R} - \mathrm{e}^{-\kappa R})\ \ell(\kappa R)\,\} \tag{B.8}$$

$$\ell(A) = \frac{A}{1 + A}\{\frac{1}{\tanh(A)} - \frac{1}{A}\} \ < 1 \tag{B.9}$$

and simplified (*34*)

$$f' = \sqrt{\frac{R_{\max}}{R_{\max} - R - x}}\ \{1 + \frac{1}{2\kappa R_{\max}} + \frac{3}{8(\kappa R_{\max})^2} + \frac{3}{8(\kappa R_{\max})^3} + \ldots\} \tag{B.10}$$

Note that for large $\kappa R_{\max}$: $f' \rightarrow f$.

Using the appropriate non-linear surface potentials (eq. (A.11) and (A.14)) the applicability of eq. (B.1) is extended. For support electrolytes other than type 1-1 further terms need to be considered.

Appendix C: Solution to a Class of Integrals relevant in Chromatography of Polyelectrolytes

Equations of the type $\int x\mathrm{e}^{-b\mathrm{e}^x}\,\mathrm{d}x$ cannot be solved in closed form. To make matters comprehensible we further restrict the following discussion to a constant b independent of x. This corresponds to the assumption $f = 1$ instead of eq. (B.6) and belongs to the case of spheres against planar walls. A number of studies in fact have applied this planar model to chromatography (*35-37*).

This model bears crucial mathematical simplifications compared to eq. (4).

Based on the relations

$$e^{-be^{+ax}} = 1 + \sum_{n=1}^{\infty} (-1)^n \frac{b^n e^{+nax}}{n!} \tag{C.1}$$

$$\int x e^{-e^{+hx}} \mathrm{d}x = \frac{e^{+hx}}{h^2} (hx - 1) \tag{C.2}$$

we can solve

$$\begin{aligned} y = \int_0^c 2x e^{-be^{-\kappa(c-x)}} \mathrm{d}x &= \left\{ x^2 + 2\kappa^{-2} \sum_{n=1}^{\infty} (-1)^n \frac{b^n e^{-n\kappa(c-x)}}{n^2\ n!} (n\kappa x - 1) \right\} \Bigg|_0^c \\ &= c^2 + 2\kappa^{-1} c \left[\sum_{n=1}^{\infty} (-1)^n \frac{b^n}{n\ n!} + \kappa^{-1} c^{-1} \sum_{n=1}^{\infty} (-1)^n \frac{b^n (e^{-n\kappa c} - 1)}{n^2\ n!} \right] \end{aligned} \tag{C.3}$$

where b has the meaning $b = 4\pi\psi_1\psi_2 R$ and $c = R_{\mathrm{max}} - R$.

To find a term for R_{sec} we need to determine $y^{1/2}$ by series expansion

$$y^{1/2} = c + \kappa^{-1}[..] - \frac{1}{2}\kappa^{-2}c^{-1}[..]^2 + \frac{1}{2}\kappa^{-3}c^{-2}[..]^3 - \frac{5}{8}\kappa^{-4}c^{-3}[..]^4 + \ldots \tag{C.4}$$

Using the relationship

$$\sum_{n=1}^{\infty} (-1)^n \frac{b^n}{n\ n!} = -\ln(|b|) - \gamma - \int_{+b}^{\infty} \frac{e^{-t}}{t} \mathrm{d}t \tag{C.5}$$

with Euler's constant $\gamma = 0.577216$ and substituting for c we thus obtain

$$\begin{aligned} R_{\mathrm{sec}} = R_{\mathrm{max}} - y^{1/2} &= R + \kappa^{-1}\{\ln(b) + \gamma\} - \ + \kappa^{-1} \left\{ \int_{+b}^{\infty} \frac{e^{-t}}{t} \mathrm{d}t \right\} \\ &- \frac{\kappa^{-2}}{R_{\mathrm{max}} - R} \left\{ \sum_{n=1}^{\infty} (-1)^n \frac{b^n (e^{-n\kappa(R_{\mathrm{max}} - R)} - 1)}{n^2 . n!} \right\} \\ &- \frac{\kappa^{-2}}{R_{\mathrm{max}} - R} \left\{ \ln(b) + \gamma + \int_{+b}^{\infty} \frac{e^{-t}}{t} \mathrm{d}t \right\}^2 + \ldots \end{aligned} \tag{C.6}$$

The convergence of this series is poor once $\kappa^{-1} \rightarrow (R_{\mathrm{max}} - r)$; whereas the leading term increases indefinitely, the true R_{sec} asymptotically approaches R_{max}.

This derivation recovers the principal feature of the mean field approximation, viz.

$$R_{\mathrm{sec}} = R + \kappa^{-1} \ln(2b) \tag{C.7}$$

except for the fact that Euler's constant is $e^{\gamma} = 1.78$ rather than 2. The integral term in eq. (C.6) is a minor correction for $b > 2$. The limit for $b \rightarrow 0$ however is

$$R_{\text{sec}} = R + \kappa^{-1} b \qquad (C.8)$$

i.e. a limiting slope of zero rather than $-\infty$ as in eq. (C.7).

Literature Cited

(1) Casassa, E. F. *J. Phys. Chem.* **1971,** *75,* 3929.
(2) Huber, J. F. K. *GIT Fachzeitschrift für das Laboratorium* **1995,** *39,* 125.
(3) Potschka, M. *J. Chromatogr.* **1993,** *648,* 41.
(4) Ogston, A. G. *J. Phys. Chem.* **1970,** *74,* 668.
(5) Potschka, M. *Anal. Biochem.* **1987,** *162,* 47.
(6) Potschka, M. *J. Chromatogr.* **1988,** *441,* 239.
(7) Potschka, M. *Macromolecules* **1991,** *24,* 5023.
(8) Potschka, M. *J. Chromatogr.* **1991,** *587,* 276.
(9) Cannan, R. K.; Kibrick, A.; Palmer, A. H. *Ann. N. Y. Acad. Sci.* **1941,** *41,* 243.
(10) Miller, G. L.; Bolder, R. H. *Arch. Biochem. Biophys.* **1952,** *36,* 249.
(11) Taylor, J. F. *Arch. Biochem. Biophys.* **1952,** *36,* 357.
(12) Nave, R.; Weber, K.; Potschka, M. *J. Chromatogr.* **1993,** *654,* 229.
(13) Dubin, P. L.; Speck, C. M.; Kaplan, J. I. *Anal. Chem.* **1988,** *60,* 895.
(14) Gorbunov, A. A.; Solovyova, L. Y.; Pasechnik, V. A. *J. Chromatogr.* **1988,** *448,* 307.
(15) Korpela, T.K. *J. Chromatogr.* **1982,** *242,* 33.
(16) Cai, C.-H.; Romano, V. A.; Dubin, P. L. *J. Chromatogr.* **1995,** *693,* 251.
(17) Heidorn, D. B.; Trewhella, J. *Biochemistry* **1988,** *27,* 909.
(18) Klee, C. B.; Crouch, T. H.; Richman, P. G. *Ann. Rev. Biochem.* **1980,** *49,* 489.
(19) Steiner, R. F.; Lambooy, P. K.; Sternberg, H. *Arch. Biochem. Biophys.* **1983,** *222,* 158.
(20) Giddings, J. C.; Kucera, E.; Russell, C. P.; Myers, M. N. *J. Phys. Chem.* **1968,** *78,* 4397.
(21) Casassa, E. F. *J. Polymer Sci. B* **1967,** *5,* 773.
(22) Dubin, P. L.; Principi, J. M. *Macromolecules* **1989, 22** ,1891.
(23) Casassa, E. F. *Macromolecules* **1976,** *9,* 182.
(24) Kuhn, H. *Helvetica Chimica Acta* **1948,** *31,* 1677.
(25) Casassa, E. F. *Macromolecules* **1984,** *17,* 601.
(26) Van Kreveld, M. E.; Van den Hoed, N. *J. Chromatogr.* **1973,** *83,* 111.
(27) Knox, J. H.; Ritchie, H. J. *J. Chromatogr.* **1987,** *387,* 65.
(28) Degoulet, C.; Busnel, J.-P.; Tassin, J.-F. *Polymer* **1994,** *35,* 1957.
(29) Israelachvili, J. N. *Intermolecular and Surface Forces* ; Academic Press: London, 1985.
(30) Parsegian, V. A.; Rand, R. P.; Rau, D. C. In *Physics of Complex and Supermolecular Fluids* ; Safran, S. A.; Clark, N. A., Eds.; Wiley: New York, 1987; p.115ff.
(31) Ohshima, H.; Healy, T. W.; White, L. R. *J. Colloid Interface Sci.* **1982,** *90,* 17.
(32) Verway, E. J. W.; Overbeek, J. T. G. *Theory of the Stability of Lyophobic Colloids* ; Elsevier: Amsterdam, 1948.
(33) Smith, F. G.; Deen, W. M. *J. Colloid Interface Sci.* **1983,** *91,* 571.
(34) Abramowitz, M.; Stegun, I. A. *Handbook of mathematical functions* ; Dover: New York, 1973; §9.7.
(35) Prieve, D. C.; Hoysan, P. M. *J. Colloid Interface Sci.* **1978,** *64,* 201.
(36) Silebi, C. A.; Mc Hugh, A. J. *Am. Inst. Chem. Eng. J.* **1978,** *24,* 204.
(37) Malone, D. M.; Anderson, J. L. *Chem. Eng. Sci.* **1978,** *33,* 1429.

Chapter 6

Influence of Net Protein Charge and Stationary Phase Charge on Protein Retention in Size Exclusion Chromatography

Vincent A. Romano, Tony Ebeyer, and Paul L. Dubin[1]

Department of Chemistry, Indiana University–Purdue University, Indianapolis, IN 46202

Protein retention on Superose 12 was studied at an ionic strength of 42 mM over a wide pH (3.3 to 10.6). A chromatographic parameter, Q, which contains the electrostatic contribution to protein retention was defined. The relation of Q with the product of protein and packing charge densities was studied with the goal of providing a method for prediction of protein retention in mixed mode SEC-IEC. Protein charge heterogeneity effects were taken into account. The results indicate the general validity of the approach and suggest further refinements.

Electrostatic interactions between proteins and various charged surfaces have been studied for many years [*1,2,3*]. These interactions play an important role in such diverse phenomena as protein binding within cell membranes [*4*], the formation of protein-polyelectrolyte complexes [*5,6,7*], and retention in protein chromatography [*8,9,10*]. Coulombic forces between proteins and packing materials govern the mobility of proteins in ion-exchange chromatography (IEC) columns and contribute significantly, along with size and hydrophobic effects, to retention in non-ideal size-exclusion chromatography (SEC). This is because most SEC columns carry a slight negative charge over a wide range of pH due to the presence of carboxylate or silanol groups and can therefore be thought of as weak cation exchangers. Since proteins may bear either a net positive or negative charge, electrostatic forces will affect the retention of the protein on the column leading to delayed retention at low pH ("attraction" or "adsorption") and early elution at high pH ("repulsion" or "exclusion").

---

[1] Corresponding author

0097–6156/96/0635–0088$15.00/0

Theories for adsorptive protein retention in IEC encompass stoichiometric displacement models [*10,11*] and electrostatic models [*9*]. The stoichiometric model of Kopaciewicz *et al.* [*10*] proposed visualizes a small, well-defined set of charged residues on the protein (charge patch) which displace a complementary set of small ions from charged groups on the packing. On the basis of this model Kopaciewicz *et al.* predicted a double logarithmic dependence of the capacity factor, k', with the inverse ionic strength, (1/I). It was also reported that the protein "patch" charge density could be calculated from the slope of this log k' vs. log 1/I plot. On the other hand, Ståhlberg *et al.* [*9*] proposed a non-stoichiometric model which treats the interaction between the protein and the column packing as an electrostatic interaction between two charged surfaces separated by a buffered salt solution. In this electrostatic model, the protein charges are smeared over the surface of a sphere, half of which interacts with the column, so that protein charge heterogeneity is neglected. On the basis of this model, Ståhlberg *et al.* predicted a linear dependence of ln k' on $1/\sqrt{I}$. Consequently, either the protein or packing charge density could also be calculated from the slope of the k' versus $1/\sqrt{I}$ plot. Recently, these two models were tested using protein chromatography data in which an SEC column (Superose 12) operated as a weak cation exchanger [*8*]. The data were in good agreement with the electrostatic model of Ståhlberg *et al.* with respect to both the form of the dependence of k' on I and the calculated value of packing charge density.

Electrostatic interactions between proteins and charged surfaces have also been considered computationally. Haggerty and Lenhoff [*12*] have shown an excellent correlation between the mean surface potential of proteins (calculated using the DelPhi electrostatics program) and their retention time on cation exchangers. Yoon and Lenhoff [2] found that the electrostatic interaction energy was dependent upon the orientation of the protein with respect to the charged surface as well as the separation distance between the two surfaces. Even when the net charge of the protein was opposite to that of the surface, a repulsive interaction was observed at certain orientations. Roush *et al.* (using the UHBD electrostatics program) [*3*] carried out similar calculations of electrostatic interaction energies between a protein and a simulated anion exchange as a function of orientation, separation distance, and ionic strength. In the latter two studies [2,*3*], a preferred orientation was found. This implies the existence of a localized area of charge that controls the retention of the protein, in contradistinction to the model proposed by Ståhlberg *et al.*

In this paper, we consider the effects of both protein and packing charge density on protein retention using a Superose 12 column as a weak cation exchanger. More specifically we have tested the correlation that is given between chromatographic retention and the product of these two charge densities. Such a correlation could provide a method for the prediction of chromatographic retention from non-chromatographic data.

TABLE I. CHARACTERISTICS OF PROTEINS USED IN THIS STUDY

Protein[a]	Source	MW	pI	R_S[b] (nm)	R_η[c] (nm)
Ribonuclease (L-6876)	Bovine Pancreas	13700	9.0	1.8	1.9
Lysozyme (R-5503)	Hen Egg White	14000	11.0	1.9	2.0
Myoglobin (M-0380)	Horse Skeletal Muscle	18800	7.3	1.9	2.1
Ovalbumin (A-5503)	Chicken Egg	45000	4.6	2.8	2.8
Hemoglobin (H-4632)	Horse	64650	7.0	3.2	---

[a] Sigma lot numbers given in parentheses.

[b] Stokes radius, from reference (13).

[c] Viscosity radius, from reference (13).

TABLE II. CHARACTERISTICS OF PULLULAN STANDARDS

Grade	M_wx10^{-3}(a)	M_w/M_n[a]	[η], (cm^3/g)	R_S[b], (nm)	R_h[c], (nm)
P-1600	1660	1.19	306[d]	---	43.2
P-400	380	1.12	115.5	17.6	19.1
P-200	186	1.13	70.4	12.8	12.8
P-100	100	1.10	45.9	8.8	9.0
P-50	48	1.09	28.6	6.1	6.0
P-20	23.7	1.07	18.1	4.0	4.1
P-10	12.2	1.06	11.9	3.0	2.9
P-5	5.8	1.07	7.9	2.1	1.9

[a] From manufacturer (Showa Denko K.K.), in water at 25° C.

[b] From reference (13), in pH 7.0, 0.3M phosphate buffer, via diffusion coefficient by quasielastic light scattering (QELS).

[c] Calculated using $R_\eta = \left\{\frac{3[\eta]M}{10\pi N_A}\right\}^{\frac{1}{3}}$.

[d] From reference (13), by extrapolation from other data in this column using $[\eta] = 0.021 \times M_w^{0.67}$.

Experimental

Materials. Table I lists protein characteristics, including source, molecular weight, isoelectric point (pI), Stokes radius (R_S), and viscosity radius (R_h). Pullulan samples (Shodex Standard P-82 lot # 20101) from Showa Denko K.K. are described in Table II. All buffers and salts were reagent grade from Sigma, Fisher or Aldrich. The raw Superose 12 column material used for titration was a gift from L. Hagel of Pharmacia.

Methods

Size-exclusion chromatography. A Superose 12 HR 10/30 (Pharmacia) column (12% cross-linked agarose medium) with a typical plate number of 40000 m^{-1} was used throughout the study. A Rheodyne 0.2 mm filter was used to protect the column, and a 2 μm frit was placed in-line between the column and a Rheodyne injector (Cotati, CA) equipped with a 100 μL injection loop. A Gilson UV detector (254 nm) in series with a Millipore-Waters differential refractometer R401 was coupled to a Kipp & Zonen two-channel recorder. A Milton-Roy miniPump (Riviera Beach, FL) was set to deliver a flow-rate of typically 0.52 ml/min. The flow rate was obtained by weighing eluant collected over a timed period, and was measured at the beginning and end of each day's experiments; it was found to be constant within 1%. The buffer pH and ionic strength were confirmed with an Orion pH/millivolt meter 811 and a YSI Conductivity Bridge (model 31) respectively.

The samples (proteins and pullulans) were dissolved in the buffer solution by the following procedure: after preliminary mixing with a Vortex Genie (Fisher Scientific), complete dissolution was carried out with a shaker (Thermolyne Speci-mix, Sybron) or a tumbler (Labquake). Samples were filtered (0.45 mm Gelman) prior to injection. K_{SEC} was calculated with V_0 determined from pullulan P-1600 (MW=1.66 x 10^6) and V_t determined from D_2O. Typical values for V_0 and V_t were 20.44 ± 0.04 ml and 7.10 ± 0.08 ml respectively. Every run was accompanied by at least one measurement with P-1600 and D_2O on the same day.

Superose 12 pH titration. In order to protonate all carboxylate groups on the surface of the gel, about 5g of Superose 12 column material was acid-washed thoroughly for more than three hours by tumbling in excess 0.5N HCl. The excess acid was removed by washing with water at least 30 times until the pH of the top layer became constant (pH=5.11). The water was then removed by freeze drying.

Approximately 500 mg of dried gel was suspended in 10.00g of NaCl solution (5mM and 42mM), then degassed by N_2 for 10 minutes. A layer of N_2 was maintained on the liquid surface throughout the titration process. The gel was titrated with a 0.2 ml microburet (Gilmont) with 0.10N NaOH from the initial pH value to

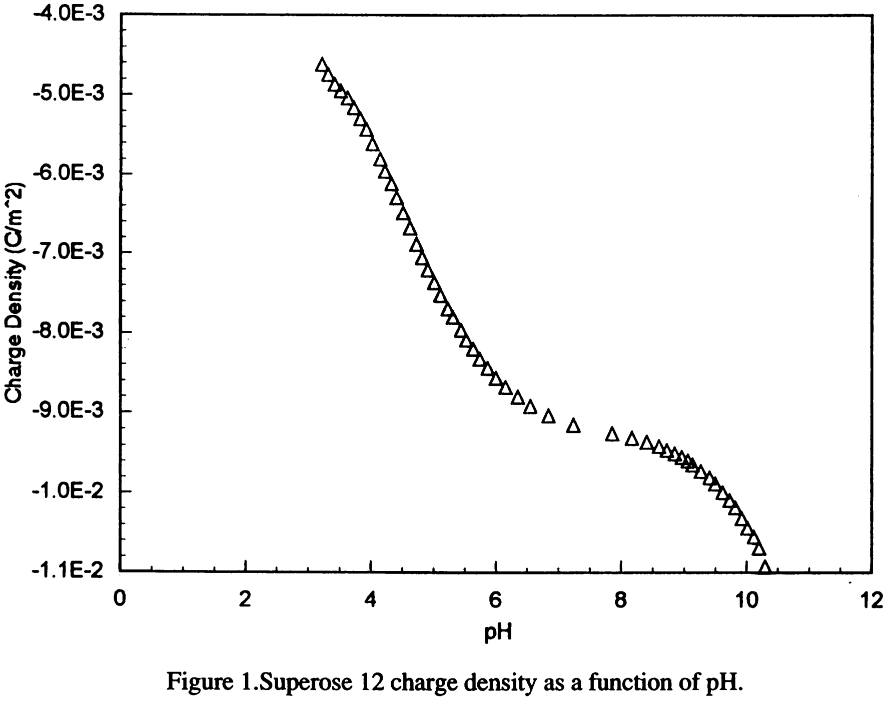

Figure 1. Superose 12 charge density as a function of pH.

pH 10 using an Orion Model 811 microprocessor pH/millivolt meter and a Cole Parmer glass body combination electrode (Model H-05990-40) calibrated with pH 4 and pH 7 buffer standards (Fisher Scientific). The same amount (by weight) of NaCl solution was used for blank titrations: an acid blank titrated with 0.103N HCl (calibrated against 0.10N NaOH) and a base blank with 0.10N NaOH. The acid blank is used to determine the number of protons that dissociate initially when the fully protonated Superose 12 is suspended in the salt solution and the base blank is used to determine the number of free protons in the salt solution.

Calculation of Protein Patch Charge Density. Structures for the five proteins were imported to Quanta from the Brookhaven Protein Databank as follows: 2dhb (hemoglobin), 8rat (ribonuclease), 1ymb (myoglobin), 1hel (lysozyme), and 1ova (ovalbumin). Solvent molecules were removed. UHBD calculations were carried out on all of the proteins with residue charges set to what they should be at each of the 5 pH values used above. Dipole moments were obtained from these calculations and the vectors were displayed along with the protein structures. A graphical slab with a thickness of a Debye length (14.84 Å at I = 42mM) was used to select a set of residues from the surface of the protein. The slab was oriented in a manner such that the dipole vector was orthogonal to the plane of the slab. The surface area of these residues was then calculated using the Molecular Surface utility of Quanta. The patch charge density was then calculated by summing up the net charge contained in the selected residues.

Results and Discussion.

Calculation of Superose 12 surface charge density (s_S). Using methods described previously [*8*], the column surface charge density, σ_S (C/m^2), was calculated by:

$$\sigma_s = \frac{\left[M_b\left(V_s - V_b\right) + M_a V_a\right] \cdot N_A \cdot e}{m_s \cdot 310} \qquad (1)$$

where M_b is the molarity (mol/L) of the NaOH used in the titration, M_a is the molarity (mol/L) of the acid used in the acid blank titration, V_S is the volume (ml) of NaOH consumed in the sample titration, V_b is the volume (ml) of NaOH consumed in the blank titration, V_a is the volume (ml) of acid consumed in the blank, N_A is Avogadro's number (molecules/mol), e is the electronic charge (Coulombs/molecule), m_s is the mass (g) of Superose 12 used in the titration, and 310 is the Superose 12 pore area per gram (m^2/g) [*8*]. Figure 1 shows the plot of Superose 12 charge density versus pH.

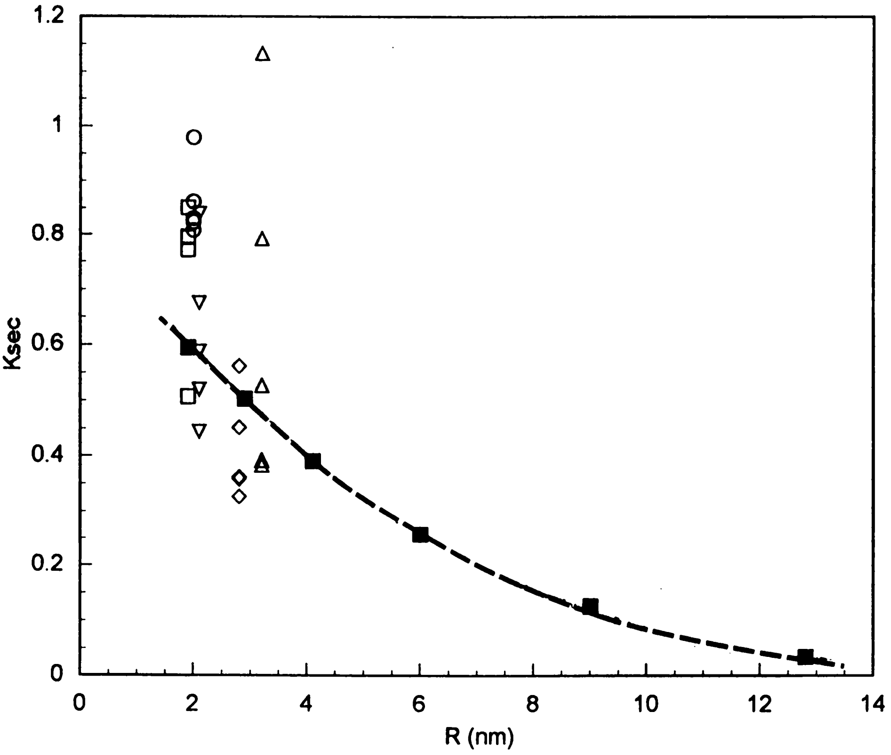

Figure 2. Dependence of K_{SEC} on radius for ovalbumin (◇), hemoglobin (△), myoglobin (▽), ribonuclease (□), and lysozyme (O). The curve indicates the "ideal calibration curve" generated by pullulans (■).

SEC on Superose 12. Figure 2 shows the dependence of K_{SEC} on solute radius for pullulans in pH 7.0 and I = 42mM phosphate buffer. These solutes which are non-ionic polysaccharides are used to construct what is known as an "ideal calibration curve" since there retention is dependent only upon steric effects [13]. K_{SEC} values for proteins are given in Table III and are shown by filled symbols in Figure 2. From Figure 2, the K_{SEC} values for the proteins all deviated significantly from the "ideal calibration curve". Positive deviations indicate electrostatic attraction between the charged protein and the weakly anionic Superose 12 and likewise, negative deviations indicate an electrostatic repulsion.

In order to examine these electrostatic phenomena, a parameter which isolates the electrostatic contribution to retention in SEC must be derived. Under the assumption that only steric effects and electrostatic effects contribute to retention, the Gibbs free energy of retention is given by:

$$\Delta G_{SEC} = \Delta G_{el} + \Delta G_i \qquad (2)$$

where ΔG_{el} is the electrostatic contribution to retention and ΔG_i is the steric contribution. It then follows that:

$$\Delta G_{SEC} = -RT\ln K_{SEC} \qquad (3a)$$
$$\Delta G_{el} = -RT\ln K_{el} \qquad (3b)$$
$$\Delta G_i = -RT\ln K_i \qquad (3c)$$

where K_{SEC} is the chromatographic partition coefficient, K_{el} is the equilibrium coefficient for the electrostatic contribution to the free energy, and K_i is the K_{SEC} obtained from the "ideal calibration curve" at the same radius as that of the solute of interest. By substitution of equations 3a-3c into equation 2, we get:

$$-RT\ln K_{SEC} = -RT\ln K_{el} - RT\ln K_i \qquad (4).$$

By rearrangement, equation. 4 reduces to:

$$-\ln K_{el} = \ln K_i - \ln K_{SEC} \qquad (5).$$

Now the parameter Q is defined as:

$$Q = -\ln K_{el} = \ln\left(K_i/K_{SEC}\right) \qquad (6).$$

A negative value of Q indicates attraction and a positive value indicates repulsion. In principle, there are no upper or lower limits to Q: for large repulsion, Q approaches infinity as K_{sec} approaches zero. For strong attraction, Q becomes a large negative number. In the attractive case, Q is somewhat analogous to the capacity factor, inasmuch as the retention time is being compared to that of a non-retained compound, although, in this case, we specify that the reference compound must have the same size as the protein of interest. Table IV shows Q values for the proteins at various pH and I = 42mM.

Relation of Q with Protein and Packing Charge Densities. Previous experiments have shown that retention in IEC correlates well with mean protein surface potential [*12*] (which is a function of net protein charge). Ståhlberg *et al.* [*9*] also proposed a model for IEC in which protein retention is given as a function of both the protein and packing charge densities. However, attempts to rationalize our data by plotting both the Gibb's Free Energy, according to ref. 9, and Q versus pH were not successful. Therefore, as a zeroth order approximation we propose that the retention depends on the simple product of the protein charge density, σ_p and packing charge density, σ_s. Figures 3a-e show plots of $\sigma_p*\sigma_s$ and Q (arbitrarily scaled) versus pH. An excellent correlation between these two functions is seen for ovalbumin (Figure 3a). Hemoglobin, myoglobin, and ribonuclease (Figures 3b-d) show progressive deviation from this prediction, while the correlation for lysozyme (Figure 3e) is poor. Figure 4 shows Q versus $\sigma_p*\sigma_s$ for all proteins and all pH's of this study. The imperfect correlation suggests a need to refine this simple approach; nevertheless, a clear trend with a variation of ca. ±0.2 in Q is observed.

Charge heterogeneity is a reasonable source for deviations from the predictions made above. Kopaciewicz *et al.* [*10*] have stated that retention in fact depends uniquely on some small well-defined set of charges ("charge patch") and both Yoon and Lenhoff [*2*] and Roush *et al.* [*3*] found that the electrostatic energy between proteins and packing surfaces depends on geometric orientaion. However, the concept of the "charge patch" remains fundamentally undefined. We may postulate that the "charge patch" is the area on the protein (sphere) that is within a Debye length (κ^{-1}) of the packing surface when the protein is just in contact with the packing and is oriented with its dipole (m) pointing toward the packing (See Figure 5). Charge densities for these patches, σ_p^{eff}, were calculated using Quanta and UHBD software, as mentioned in the introduction, and plotted against the chromatographic parameter Q (Figure 6). The data for the neutral and acidic proteins (filled symbols) clearly show an improved correlation. For the basic proteins, on the other hand, the correlation at low pH (attractive regime) is poor. An interesting feature of this plot is the break point between the attraction (Q < 0) and repulsion (Q > 0) data. This indicates that the function which describes retention is not identical for atraction and repulsion.

With appropriate refinements, this method might be useful for predicting protein retention in mixed mode SEC-IEC. One possible refinement involves the

TABLE III - K_{SEC} VALUES AT VARIOUS pH AND I = 42 mM

pH	3.27	5.04	6.99	9.0	10.6
Ovalbumin	0.56	0.45	0.36	0.36	0.33
Ribonuclease	0.85	0.79	0.79	0.77	0.50
Hemoglobin	1.13[a]	0.79	0.52	0.39	0.38
Myoglobin	0.84	0.67	0.58	0.52	0.44
Lysozyme	0.98	0.86	0.83	0.82	0.81

[a] This value was obtained at pH = 3.5.

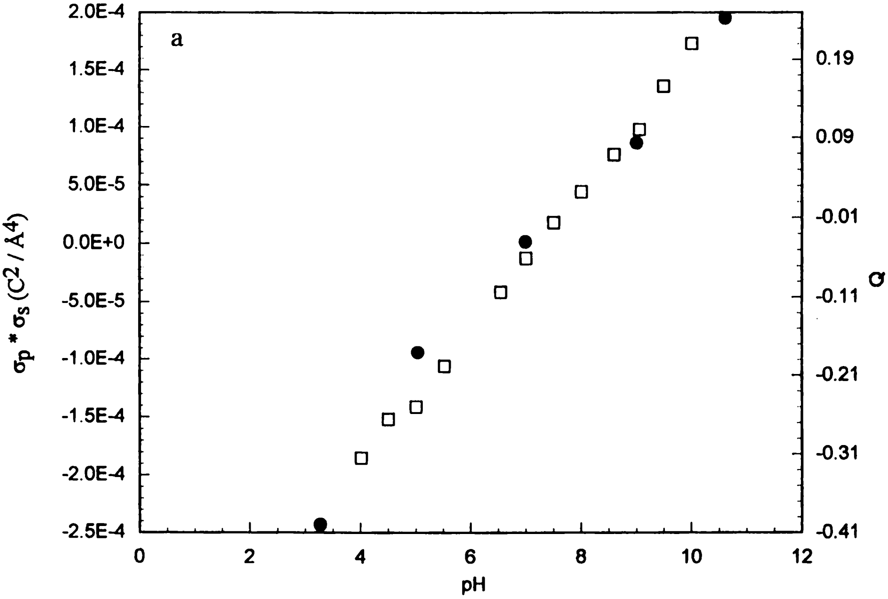

Figure 3. Electrostatic retention parameter Q (●) and the product of protein and packing charge densities (□) versus pH for (a) ovalbumin, (b) hemoglobin, (c) myoglobin, (d) ribonuclease, (e) lysozyme.

Continued on next page

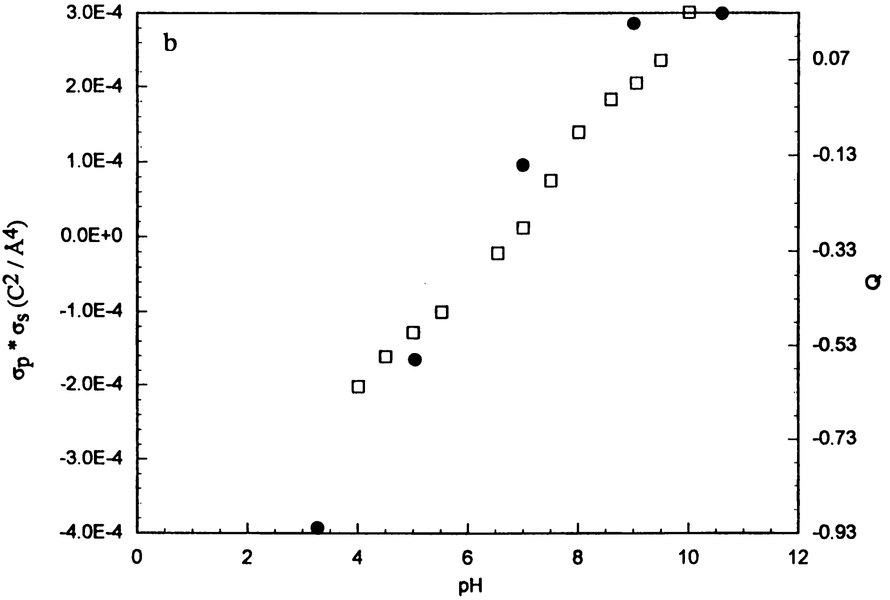

Figure 3b. *Continued*

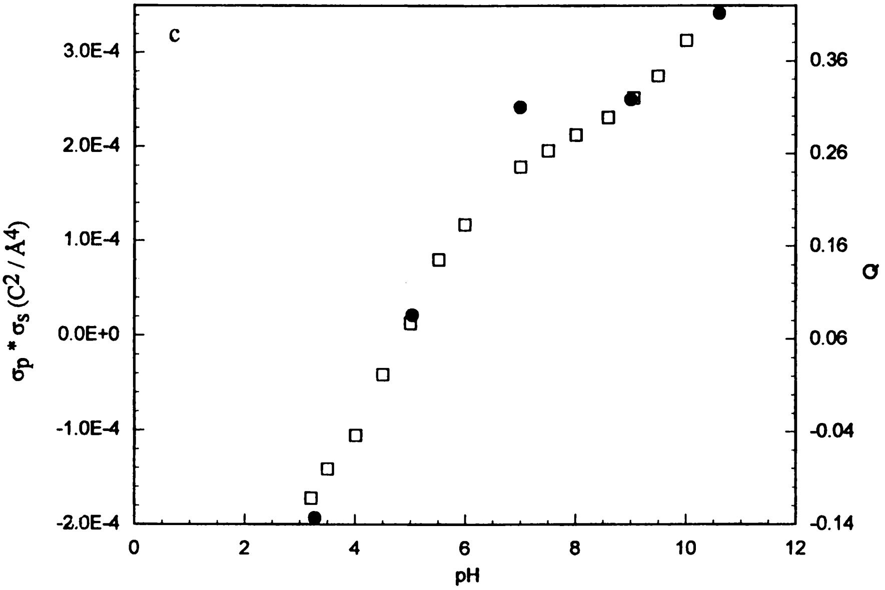

Figure 3c. *Continued*

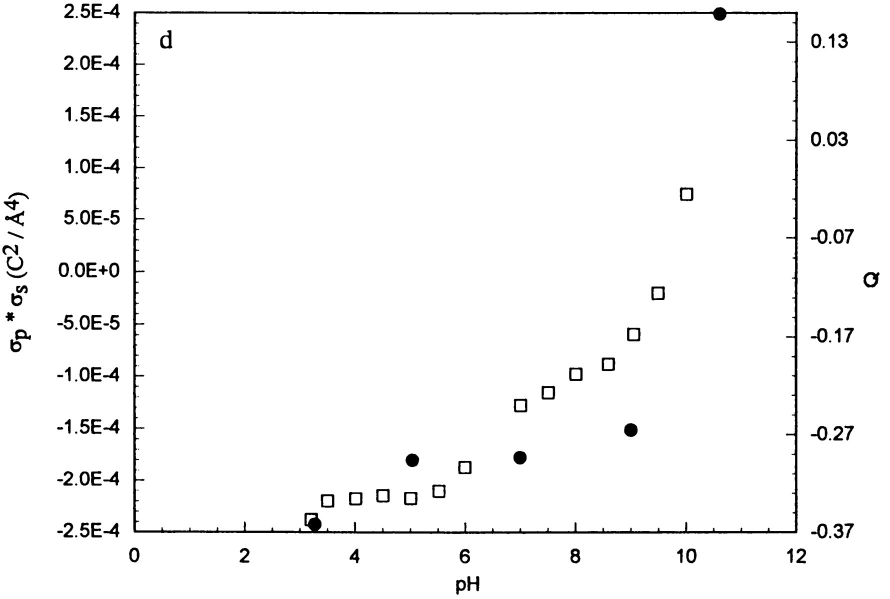

Figure 3d. *Continued*

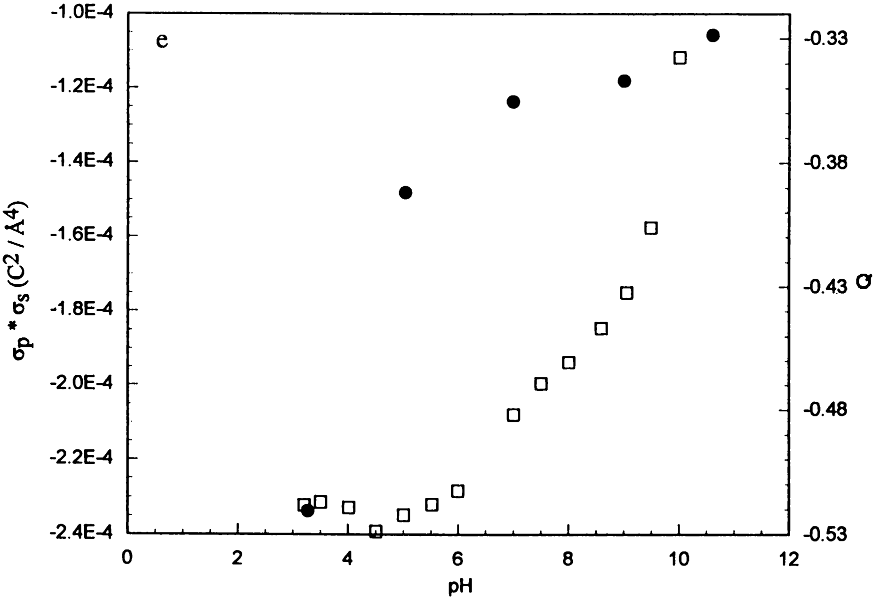

Figure 3e. *Continued*

TABLE IV - Q VALUES AT VARIOUS pH AND I = 42mM

pH	3.27	5.04	6.99	9.0	10.6
Ovalbumin	-0.13	0.08	0.31	0.32	0.41
Ribonuclease	-0.36	-0.30	-0.29	-0.27	0.16
Hemoglobin	-0.92	-0.56	-0.15	0.15	0.17
Myoglobin	-0.40	-0.18	-0.04	0.08	0.24
Lysozym	-0.52	-0.39	-0.36	-0.35	-0.33

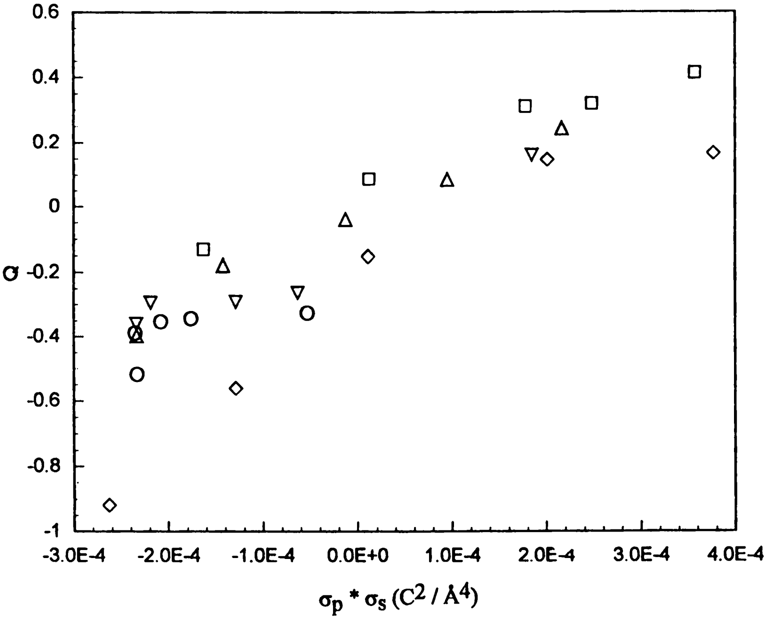

Figure 4. Relation of Q and the product of protein and Superose 12 charge densities for ovalbumin (□), hemoglobin (◇), myoglobin (△), ribonuclease (▽), and lysozyme (○) .

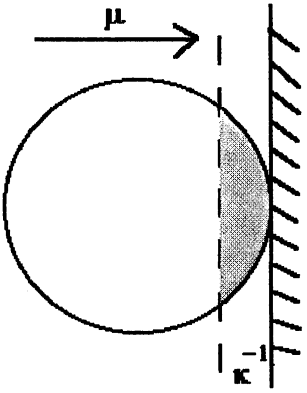

Figure 5. Illustration of protein charge patch definition. The protein is shown as a sphere in contact with the packing surface. The charge patch is defined by all residues on the surface of the protein within one Debye length of the packing surface and is shown by the shaded area.

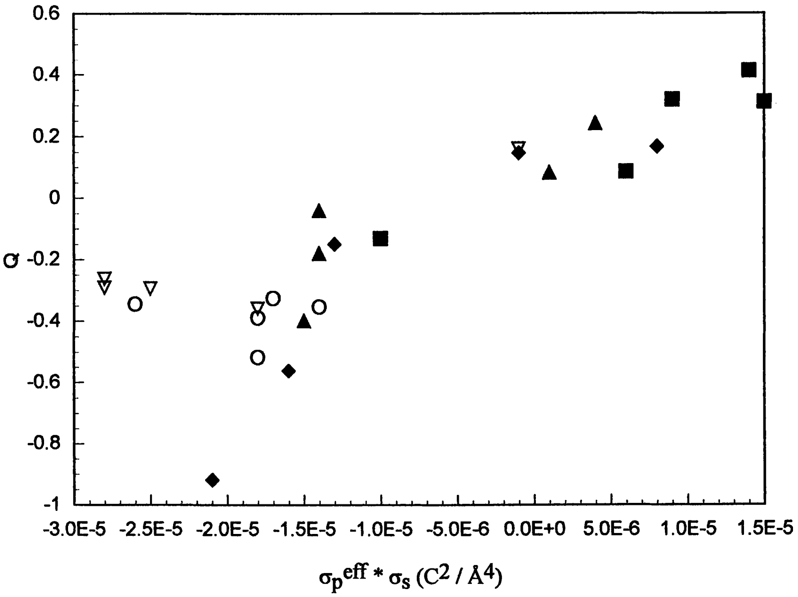

Figure 6. Relation of Q and the product of protein patch and Superose 12 charge densities for ovalbumin (■), hemoglobin (◆), myoglobin (▲), ribonuclease (▽), and lysozyme (○).

procedure for defining the charge patch. Instead of using the dipole moment to determine the location of the patch, calculations similar to those of Haggerty and Lenhoff [*12*] and Roush *et al.* [*3*] could be used to determine the preferred orientation of the protein with respect to the packing. To evaluate the success of this approach, further experimental work should include a greater number of proteins.

Conclusion.

Protein retention in mixed mode SEC-IEC must depend on some function of the protein and packing charge densities. We found some correlation between the product of these two charge densities ($\sigma_p{*}\sigma_s$) and the chromatographic parameter Q. A refined model using patch charge densities, σ_p^{eff}, instead of the global protein charge density, σ_p, showed improved correlation for the acidic proteins but not for basic proteins.

Acknowledgment.

This work was supported by NSF grant No. CHE 9505953. We thank Dr. Lars Hagel for the Superose column and raw Superose material. We also thank Daniel Robertson of the Facility for Computational Molecular and Biomolecular Science at Indiana University - Purdue University for his assistance with the computer calculations.

References.

1. Warshel, A.; S. Russel, S. *Quart. Rev. of Biophys.* **1984**, *17*, , 283.
2. Yoon, B.; A. Lenhoff, A. *J. Phys. Chem.* **1992**, *96*, 3130.
3. Roush, D.; Gill, D.; Wilson, R. *Biophys. J.*, **1994**, *66*, 1.
4. Honig, B.; Hubbell, W.; Flewelling, R.*Ann. Rev. Biophys. Biophys. Chem.*, **1986**, *15*, 163.
5. Dubin, P.L.; Gao, J.; Mattison, K. *Sep. Purif. Methods*. **1994**, *23*, 1.
6. Xia, J.; Dubin, P.L.; Kim, Y.; Muhoberac, B.B.; Klimkowski, V. *J. Phys. Chem.* **1993**, *97*, 4528.
7. Kokufuta, E.; Takahashi, K. *Polymer* **1990**, *31*, 1177.
8. Cai, C.; Romano, V.; Dubin, P.L. *J. Chromatogr.* **1995**, *693*, 251.
9. Ståhlberg, J.; Jönsson, B.; Horvåth, Cs. *Anal. Chem.* **1991**, *63*, 1867.
10. Kopaciewicz, W.; Rounds, M.A.; Fausnaugh, J.; Regnier, F.E.*J. Chromatogr.* **1984**, *283*, 37.
11. Boardman, N.K.; Partridge, S.M., *Biochem. J.* **1955**, *59*, 543.
12. Haggerty, L.; Lenhoff, A.*J. Phys. Chem.***1991**, *95*, 1472.
13. Dubin, P.L.; Edwards, S.L.; Mehta, M.S.; Tomalia, D. *J. Chromatogr.* **1993**, *635*, 51.

Chapter 7

Modeling of Stationary Phase in Size Exclusion Chromatography with Binary Eluents

V. Soria, A. Campos, J. E. Figueruelo, C. Gómez, I. Porcar, and R. Garcia

Department de Quimica Fisica and Institut de Ciència dels Materials, Universitat de València, E–46100 Burjassot, València, Spain

Distribution coefficients for polystyrene obtained from size-exclusion liquid chromatography experiments on a silica-based packing in benzene-methanol binary eluent, have served to test the validity of those theoretically predicted. For this purpose, we use the Flory-Huggins lattice theory for the thermodynamic description of the polystyrene behaviour in mixed solvents as eluent, including the preferential solvation effect. Moreover, an structural description of the stationary phase is performed through a binary-layered-phase model for methanol adsorption on the pore wall, involving a self-association process. Diverse alternative ways to evaluate the distribution coefficients are detailed in-depth and the results discussed.

Multicomponent eluents are often used in Liquid Chromatography (LC) under isocratic conditions in both organic and aqueous environments (*1,2*). The inherent advantage of using these eluents is to change gradually some properties such as eluent strength, viscosity, solubility respect to the solute, to decrease the boiling point for volatile single eluents, polarity, etc. In the case of size-exclusion chromatography (SEC) of polymers, two applications of the multicomponent eluents deserve to be mentioned. The first one refers to a new mode of SEC, called Critical SEC often used to separate polymers of the same molar mass but different functionality, end-groups or topology (linear, branched, comb) (*3-5*). These critical conditions are created with specific multicomponent eluents often formed by a non-solvent/solvent mixture at a given composition and temperature. However, the exact mechanism of the polymer retention under critical conditions is not clear yet. The second advantage of using this kind of eluents concerns the possibility to perform transient stationary phases by chemisorption of one or more components of the eluent on the active centres of the gel packing. Focusing our attention in a binary eluent formed by a solvent/non-solvent for the polymer, the stationary phase can be enriched or depleted in one of the components respect to the original composition of the mobile phase. This feature has been investigated in-depth many years ago from a

0097–6156/96/0635–0103$16.00/0

experimental viewpoint in both organic and aqueous media (*6-9*). However, up to date, a lack on the theoretical interpretation still remains. In this way, it has been experimentally evidenced that the polymer elution profiles shift toward lower or higher elution volumes by comparison with the elution of the same polymer in a single good solvent as eluent. This behaviour has been quantified by changes in the partition coefficient, K_p, which represents the solute partition between stationary and mobile phases. Values of K_p lower than unity mean that the polymer concentration (expressed in the usual weight/volume dimension) is larger in the free exterior volume respect to the interior of the pore. On the contrary, K_p values larger than unity denote the opposite behaviour.

Although significant progress has been made on the understanding of this fact, mainly from the experimental side, a general model has not been achieved yet. Much less work has been done on the description of the microscopic phase entrapped in the pores of the packing material, mainly if one of the components of the eluent specifically interacts with the active centres of the gel. In this regard, some contributions dealing with chromatographic modes other than SEC in multicomponent eluents have been published (*10-12*). Thus, Jaroniec and Martire (*13*) reported a description of solute retention in LC with mixed eluents involving non-specific solute-solvent and solvent-solvent interactions in both mobile and surface phases, as well as association equilibria in these phases. The surface (stationary) phase composition is expressed in terms of the volume fraction and of the activity coefficients of the components. Most recently, Boehm and Martire (*14*) have reported a statistical thermodynamic treatment based on the Bethe-Guggenheim quasi-chemical approach to predict solute distribution between a binary solvent mobile phase and a stationary phase consisting of a monolayer of solvent molecules sorbed on a chemically homogeneous planar support surface.

On the other hand, the use of multicomponent mixtures as mobile phases leads to the formation of extra peaks often called "system peaks", as a consequence of a thermodynamic phenomenon resulting from the perturbation of the chemical equilibrium (*2,15*). At the onset of this perturbation of equilibrium, the chromatographic system (stationary and mobile phases) begin to relax towards a new state of equilibrium by transferring mobile phase components, in addition to solute, between the two phases. In the field of polymers solved in a binary solvent mixture, preferential solvation generally occurs. At a molecular level, better solvation of the polymer by one of the solvents renders the solvent composition within the chain coils, different from that outside. SEC has been used for quantitative evaluation of the preferential solvation by analysis of an extra peak termed in this context as "vacant peak". An in-depth explanation of this methodology has been reported in the past (*16-19*).

In a previous report (*20*), we have studied polymer retention in SEC with mixed eluents on silica-based gel packings. The distribution coefficient of the polymer between mobile and stationary phases was evaluated on the framework of the Flory-Huggins (FH) lattice theory, including the preferential solvation of the polymer by one of the eluent components. In order to improve our previous proposal, we present here an extension of this thermodynamic treatment including more elaborated models for the stationary phase. As it will be explained throughout the text, the exact knowledge of the domains forming the stationary phase will be of paramount importance and a way to reach this purpose will be detailed in-depth.

A mixed model is developed here to account for the solute retention mechanisms represented by the partition coefficient, K_p, which denotes the solute transfer between the two chromatographic phases. The solute distribution is described by the conventional FH formalism often used to deal with the liquid-liquid phase equilibrium in polymer solutions (*21,22*). For the evaluation of the surface (stationary) phase composition, we have substantiated the theory of association equilibria (*23,24*) for a binary mixture when one component (the polar) can undergo self-association. The predictions of the present analysis are compared with experimental data on distribution coefficients obtained from SEC experiments for a set of narrow polystyrenes (PS) eluted on Lichrospher packing using Benzene-Methanol (80/20, v/v) binary mixture as eluent. The system used in the current investigation is well suited for basic studies on elution mechanisms in SEC since most of the non-chromatographic parameters, such as polymer-solvent and solvent-solvent interaction parameters, have been independently evaluated. In addition, the preferential solvation of PS in this mixture has been obtained from SEC measurements (*17*) being this phenomenon optionally introduced in our approach.

Experimental

Chemical and Reagents. Two sets of polystyrene samples with narrow molecular weight distributions were supplied by Waters Assoc. (Milford, Mass. USA) and by CRM (Strasbourg, France), respectively. The first set corresponds to W-2700, W-240, W-130, W-27, W-9 and W-2.9, and the second one to F-314, F-136, F-24.5 and F-20.5. In both cases the numbers of the codes denote the weight average molar mass of the polymer sample in kg.mol^{-1}. The reagents used, benzene (Bz) and methanol (MeOH) were of analytical reagent grade, distilled twice before use. The silica used for the adsorbent and for chromatographic packing was Lichrospher Si-100, Si-300 and Si-500 (Merck, Darmstad, Germany).

Column Preparation. Three stainless steel tubes of 30x0.78 cm. i.d. were packed with Lichrospher Si-100, Si-300 and Si-500. The packing of the chromatographic columns used here were carried out by the slurry technique. An adequate amount of gel was heated at 50 °C and dried under vacuum for 24 h. Next, the gel was dispersed in methanol and before packing the slurry was degassed and stirred by ultrasonic vibration to prevent possible particle aggregation and sedimentation. The mixture was introduced in a conventional slurry reservoir, connected with the column to be packed and the pump using n-hexane as displacing liquid.

Chromatographic Measurements. A Waters Assoc. (Milford, Mass. USA) liquid chromatographic equipment has been used a description of which has been reported elsewhere (*25*). A set of three columns packed with 4.45 g (Si-100), 4.39 g (Si-300) and 4.89 g (Si-500) were used in all experiments. Single eluent such as benzene or binary ones Bz-MeOH (80/20, v/v) have been used, following degassing and filtration in all instances through regenerated cellulose 0.45 μm pore diameter filters from Micro Filtration Systems (Dublin, CA, USA).

Adsorption Isotherms. In order to evaluate the volume fraction of the adsorbed component in the stationary phase, static experiments of Bz-MeOH binary mixtures in presence of Lichrospher were conducted. The adsorption experiments have been performed as follows: a fixed amount of dry Lichrospher (approx. 1 g.) was transferred to a 10 mL flask and then mixed with 4 mL of Bz-MeOH at a fixed composition. The mixture in the glass flask was mechanically shaken in a water bath attached with a shaker for 24 h to determine the adsorption isotherms. After this period of incubation, long enough to reach an equilibrium, the supernatant was carefully withdrawn and the composition analysed. To this end, a calibration of refractive index against the composition of each liquid mixture was obtained in absence of gel. These reference mixtures were prepared in a graduate pycnometer, previously calibrated, to calculate the correction due to the excess volume. The adsorbed amounts of MeOH were determined from the difference of the concentrations between the dosage and the supernatant.

General Considerations

Let us consider a set of polystyrene (PS) standards of different molecular weight as solute (component 3) chromatographed in the eluent benzene-methanol (Bz-MeOH, 80/20, v/v) considered as components 1+2, which behave as a good solvent and a non-solvent, respectively. The solvent (1) -solvent (2) and solvent (1 or 2)-solute interactions in the mobile (m) and stationary (s) phases will be described in terms of g_{ij}-functions in the framework of the Flory-Huggins lattice model of polymer solutions. Specific interactions between component 2, methanol, and the active centres of the silanol groups on the Lichrospher gel will be located in the stationary phase only. Preferential interaction of the MeOH will change slightly the eluent composition near to the pore wall with respect to the original eluent composition. On the other hand, the PS can undergo preferential solvation by one of the components of the binary eluent (*17,25*). In this case, the composition of the liquid mixture near and far from the PS coil will also be slightly different. Both phenomena, preferential interaction and preferential solvation caused by the silanol groups and the PS, respectively, are included in this report. To this end, we have introduced the conventional notation often used in thermodynamics of polymers in mixed solvents systems to account for the composition of diverse domains in the multicomponent solution (*26*). Thus, $\phi_{i\alpha}$ (i=1,2,3; α=m,s) refers to the volume fraction of the component i in the phase α. Hereafter subscript 1 denotes the apolar (inner) component, subscript 2 refers to the minority or polar component and 3 refers to a monodisperse polymer sample. When a polymer sample is dissolved in a mixture of two single liquids, as in the present case, one can introduce the two microphase approximation consisting of a microphase or domain far away from the polymer coil (free of polymer) where the composition of the two liquids can be expressed as $\phi^{\circ}_{i\alpha}$ (i=1,2; α=m,s) i.e. the volume fraction referred to the binary mixed solvents. Obviously, both $\sum_{i=1}^{3}\phi_{i\alpha}=1$ and $\sum_{i=1}^{2}\phi^{\circ}_{i\alpha}=1$ must be fulfilled. In absence of polymer, the binary liquid mixture composition will be expressed by $\phi_{i0,\alpha}$ (i=1,2; α=m,s), the volume fraction of the component i in the binary phase, being $\sum_{i=1}^{2}\phi_{i0,\alpha}=1$ also fulfilled. The volume fraction of the solvent mixture in the domain of the polymer coil will be denoted by $u_{i\alpha}$ (i=1,2; α=m,s) being $\sum u_{i\alpha}=1$. For the phase α, the parameters $\phi_{i\alpha}$ and $u_{i\alpha}$ can be easily correlated through $u_{i\alpha}=\phi_{i\alpha}/(1-\phi_{3\alpha})$.

In a previous paper (*20*) we considered the stationary phase as an isotropic phase meaning that the composition is the same near or far of the pore wall.

However, when the eluent is constituted by an inner (apolar) and an active (polar) components, the above scheme is not valid and more complex models of mobile phase must be implemented. Here, it has been assumed that the active centres of the gel, mainly consisting on free silanol groups, interact with the polar component via hydrogen bonding forming a monolayer of solvent molecules. Thus, we show in Figure 1 a pictorial representation of the mobile and stationary phases in SEC of binary eluents. The conventional stationary phase confined to the pores of the gel packing, will be considered as a binary-layered-phase made up by an inlet region (zone III) which is formed by a monolayer of component 2, methanol in this case, chemically adsorbed on the silica gel surface. Next, zone II represents an outlet region, in contact with the mobile phase, formed by self-associated methanol and a Bz (1)-MeOH (2) mixture. Lastly, zone I refers to the mobile phase placed outside of the pores and formed by Bz (1)-MeOH (2) mixture of the same composition as the eluent. We consider that the polymer partition takes place between zone I (m-phase) and zone II (s-phase). According to this picture, the PS is fully excluded from zone III since the polymer is not soluble in pure methanol.

In order to clearly distinguish between the composition of the aforementioned inlet and outlet layers of the stationary phase, it is necessary to introduce a new parameter ν_i which denotes the volume fraction of the component i (i=1,2) "adsorbed" upon the pore surface. In the absence of polymer, the amount of i per mL of quasistationary phase can be expressed as $\nu_i + (1-\nu_i)\phi_{i0,s}$. When the polymer is included in this phase, the amount of the component i can be expressed as follows: $u'_{is} = \nu_i + (1-\nu_i)u_{is}$, where $\phi_{is} = u'_{is}(1-\phi_{3s}) = [\nu_i + (1-\nu_i)u_{is}](1-\phi_{3s})$. It is well known that when an analytical chromatographic column is used, as the one considered here, the feed sample (about 50 μL) is so small compared to the column volume of about 10 mL, that the elution can be considered to take place at infinite polymer dilution. Moreover, if the preferential solvation of the polymer by one of the two liquids is disregarded, then $u_{is} \approx \phi^{\circ}_{is}$, and the above expression can be transformed into:

$$\phi_{is} = [\nu_i + (1-\nu_i)\phi^{\circ}_{is}](1-\phi_{3s}) \qquad (1)$$

We notice that the ν_i evaluation is crucial and an attempt is made here to offer an adequate and quantitative description of the multilayer composition of the stationary phase in SEC with binary solvents on active gel packings. Thus, ϕ_{is} evaluation demands to elucidate previously the entity of the right hand side of equation 1 which is often difficult and requires new rational assumptions. From a phenomenological viewpoint, this entity can be defined as:

$$[\nu_i + (1-\nu_i)\phi^{\circ}_{is}] = \frac{\text{cm}^3\text{ of i in zone III} + \text{cm}^3\text{ of i in zone II}}{\text{cm}^3\text{ of stationary phase}} = \frac{\text{cm}^3\text{ of i in zone III} + \text{cm}^3\text{ of i in zone II}}{\text{cm}^3\text{ total pore volume}} \qquad (2)$$

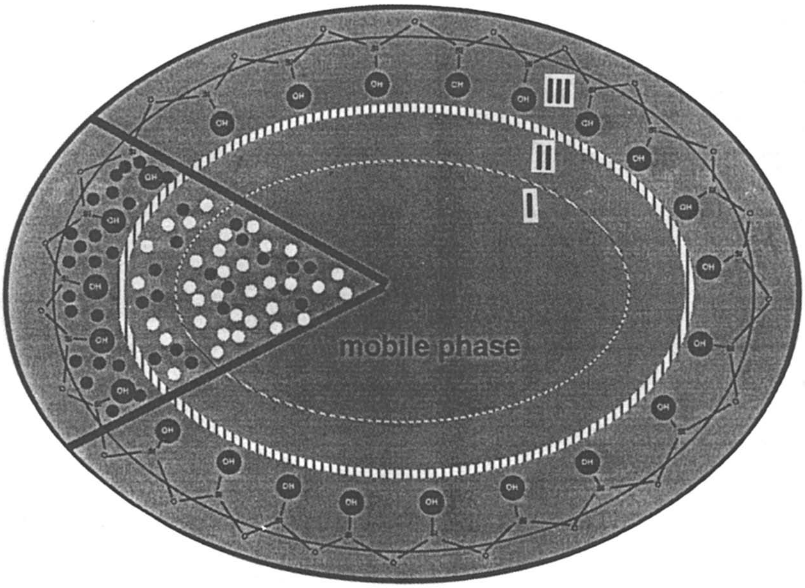

Figure 1. Pictorial representation of a binary-layered stationary phase (zones II and III) and mobile phase (zone I). Methanol (filled) and benzene (empty) symbols.

Note that in liquid chromatographic experiments when a macromolecular solute is eluted according to a pure size-exclusion mechanism, the volume of the stationary phase agree fully with the total pore volume of the gel packing.

Moreover, when the polymer is preferentially solvated by one of the components of the binary liquid mixture, a new notation dealing with this feature must be included. The preferential solvation parameter is commonly defined as $\lambda = \Delta\phi^{\circ}_{i\alpha}/c_{3\alpha}$, being $\Delta\phi^{\circ}_{i\alpha}$ the excess of volume fraction of solvent i in ternary microphases with regard to that of bulk solvent per polymer concentration unit in phase α, $c_{3\alpha}$. Therefore, when the λ parameter is included, the new solvent composition, $\phi^{\lambda}_{i\alpha}$, is given by:

$$\begin{aligned}\phi^{\lambda}_{i\alpha} &= (1-\phi_{3\alpha})u^{\lambda}_{i\alpha} = (1-\phi_{3\alpha})\left(\phi^{\circ}_{i\alpha} \pm \Delta\phi^{\circ}_{i\alpha}\right) = \\ &= \phi_{i\alpha} \pm (1-\phi_{3\alpha})\Delta\phi^{\circ}_{i\alpha}\end{aligned} \qquad (3)$$

where $u^{\lambda}_{i\alpha} = \phi^{\circ}_{i\alpha} \pm \Delta\phi^{\circ}_{i\alpha}$.

Solute Distribution Between Chromatographic Phases

The Flory-Huggins equation for the Gibbs free energy of mixing, ΔG, can be written as:

$$\frac{\Delta G}{RT} = \left(\frac{\Delta G}{RT}\right)_{comb} + \left(\frac{\Delta G}{RT}\right)_{res} \qquad (4)$$

where the subscripts *comb* and *res* stand for combinatorial and residual contributions to ΔG. When a ternary mixture is formed by two single liquids and a polymer, the above contributions are defined as follows (*22*):

$$\left(\frac{\Delta G}{RT}\right)_{comb} = n_1 \ln\phi_1 + n_2 \ln\phi_2 + n_3 \ln\phi_3 \qquad (5)$$

and

$$\left(\frac{\Delta G}{RT}\right)_{res} = n_1\phi_2 g_{12} + n_1\phi_3 g_{13} + n_2\phi_3 g_{23} + n_1\phi_2\phi_3 g_T \qquad (6)$$

g_{ij} being Koningsveld-type functions (*27*) accounting for the nearest neighbour-neighbour interchange interaction energies between the components i and j. g_T is a fit parameter including other than two-body interactions as well as the non-combinatorial contribution to the entropy of mixing. $\phi_i(= n_i/\Sigma n_i)$ represents the volume fraction of the component i in the incompressible ternary mixture and n_i the number of solvent molecules or segments of the macromolecule. For simplicity, we will consider the component 3 as a monodisperse polymer sample, often represented by a narrow polymer standard.

The chemical potential of the component 3, the polymer, can be easily obtained upon differentiation of equation 4 with respect to n_3:

$$\frac{\Delta\mu_3}{RT} = \frac{1}{RT}\left(\frac{\partial \Delta G}{\partial n_3}\right)_{T,p,n_1,n_2} = \left(\frac{\Delta\mu_3}{RT}\right)_{comb} + \left(\frac{\Delta\mu_3}{RT}\right)_{res} \qquad (7)$$

where

$$\left(\frac{\Delta\mu_3}{RT}\right)_{comb} = -\phi_1 - \frac{V_1}{V_2}\phi_2 + \frac{V_1}{V_3}\left(\ln\phi_3 + 1 - \phi_3\right) \qquad (8)$$

and

$$\begin{aligned}\left(\frac{\Delta\mu_3}{RT}\right)_{res} &= -\phi_1\phi_2 g_{12} + \phi_1\left(1-\phi_3\right)g_{13} + \frac{\phi_1\phi_3}{1-\phi_3}\frac{dg_{13}}{d\phi_3} + \\ &\frac{V_1}{V_2}\phi_2\left(1-\phi_3\right)g_{23} + \frac{V_1}{V_2}\frac{\phi_2\phi_3}{(1-\phi_3)}\frac{dg_{23}}{d\phi_3} + \\ &\phi_1\phi_2\left(1-2\phi_3\right)g_T + \frac{\phi_1\phi_2\phi_3}{1-\phi_3}\frac{\partial g_T}{\partial\phi_3}\end{aligned} \qquad (9)$$

In general, for a LC process the polymer can be transferred from the m-phase to the s-phase according to partition models (*28-33*). For low molecular weight solutes, this transfer may occur through distribution of single solute molecules and a 1:1 solute-solvent complexes between both phases (*13*). For high molecular weight solutes, such as polymers and other assemblies, it is often assumed that the solute transfer or distribution between both phases concerns exclusively to the polymer.

For equilibrium partitioning of the polymer between both chromatographic phases at a given temperature, the solute chemical potential must be equivalent. Thus, $\mu_{3s} = \mu_{3m}$ and hence from equation 9 is obtained:

$$\begin{aligned}&-\phi_{1s} - \frac{V_1}{V_2}\phi_{2s} + \frac{V_1}{V_3}\left(\ln\phi_{3s} + 1 - \phi_{3s}\right) - \\ &\phi_{1s}\phi_{2s}g_{12} + \phi_{1s}\left(1-\phi_{3s}\right)g_{13} + \frac{\phi_{1s}\phi_{3s}}{1-\phi_{3s}}\frac{dg_{13}}{d\phi_3} + \\ &\frac{V_1}{V_2}\phi_{2s}\left(1-\phi_{3s}\right)g_{23} + \frac{V_1}{V_2}\frac{\phi_{2s}\phi_{3s}}{(1-\phi_{3s})}\frac{dg_{23}}{d\phi_3} + \\ &\phi_{1s}\phi_{2s}\left(1-2\phi_{3s}\right)g_T + \frac{\phi_{1s}\phi_{2s}\phi_{3s}}{1-\phi_{3s}}\frac{\partial g_T}{\partial\phi_3} =\end{aligned}$$

$$-\phi_{1m} - \frac{V_1}{V_2}\phi_{2m} + \frac{V_1}{V_3}\left(\ln\phi_{3m} + 1 - \phi_{3m}\right) -$$

$$\phi_{1m}\phi_{2m}g_{12} + \phi_{1m}\left(1 - \phi_{3m}\right)g_{13} + \frac{\phi_{1m}\phi_{3m}}{1 - \phi_{3m}}\frac{dg_{13}}{d\phi_3} +$$

$$\frac{V_1}{V_2}\phi_{2m}\left(1 - \phi_{3m}\right)g_{23} + \frac{V_1}{V_2}\frac{\phi_{2m}\phi_{3m}}{(1 - \phi_{3m})}\frac{dg_{23}}{d\phi_3} +$$

$$\phi_{1m}\phi_{2m}\left(1 - 2\phi_{3m}\right)g_T + \frac{\phi_{1m}\phi_{2m}\phi_{3m}}{1 - \phi_{3m}}\frac{\partial g_T}{\partial\phi_3} \qquad (10)$$

where V_i (i=1,2,3) refers to the molar volume of the component i. The practical use of equation 10 requires clarification of the known parameters as well as the unknown ones. In our context, we consider as input parameters the g-type functionalities as well as other minor parameters such as the molar volumes of the components. The main features of g_{ij} and g_T functions as well as their derivatives have been previously determined and their meaning widely discussed (see Table 1 from ref. 20). The volume fractions $\phi_{i\alpha}$ are the magnitudes to be evaluated. The ϕ_{im} values can be easily obtained from the eluent composition as well as from the injected polymer concentration. On the contrary, the ϕ_{is} evaluation is a difficult task since requires to perform models dealing with the composition of solvent layers adsorbed onto the pore. In the next sections we present the steps needed to carry out this purpose.

Evaluation of the Total Pore Volume

For the evaluation of the total pore volume, V_p, in equation 2, two geometrical shapes for the pore can be assumed. Thus, for a spherical pore shape:

$$\overline{V}_p = V_{p,exp}\left(\langle r\rangle / r\right)^3 \qquad (11)$$

and for cylindrical pores:

$$\overline{V}_p = V_{p,exp}\left(\langle r\rangle / r\right)^2 \frac{H}{h} \qquad (12)$$

where $\overline{V}_p$ stands for the average pore value; $V_{p,exp}$ for the experimental pore volume, $\langle r\rangle$ is an average pore radius, r the experimental pore radius, $h = \langle r\rangle + r$ and $H = 2\langle r\rangle$, respectively.

The $V_{p,exp}$ values can be easily obtained from data of the elution volume of two standards falling within the linear region of the universal calibration plot log $M[\eta]$ vs. V_R. Thus, from the relationship $K_{SEC} = (V_R - V_0)/V_{p,exp}$, the $V_{p,exp}$ value can be extracted. A value of $V_{p,exp}$=17.83 mL has been obtained for the PS standards in Bz-MeOH eluent on Lichrospher as gel packing.

Evaluation of the Average Pore Radius. The average pore radius, $\langle r \rangle$, has been calculated from data of the manufacturer for this gel. Thus, we have defined a weight average pore radius, $\langle r_w \rangle$, as follows:

$$\langle r_w \rangle = \frac{\sum w_i r_i}{\sum w_i} \tag{13}$$

w_i being the mass of gel of pore radius r_i. Recalling that the columns used here were formed by 4.45 g of Lichrospher of 50 Å (Si-100), 4.39 g of 150 Å (Si-300) and 4.89 g of 250 Å (Si-500), we obtain:

$$\langle r_w \rangle = \frac{4.45 \times 50 + 4.39 \times 150 + 4.89 \times 250}{13.73} = 153.2 \text{ Å} \tag{14}$$

In addition, a number average pore radius can also be defined by assuming an homogeneous distribution of the number of pores of a certain size. Thus, one pore of 250 Å will be equivalent to 1.66 pores of 150 Å and to 5 pores of 50 Å, respectively, so that:

$$\langle r_n \rangle = \frac{\sum n_i r_i}{\sum n_i} = \frac{5 \times 50 + 1.66 \times 150 + 1 \times 250}{7.66} = 97.9 \text{ Å} \tag{15}$$

Evaluation of the Experimental Pore Radius. Two procedures have been used, the first one being based on the Dawkins and Hemming equation (*34,35*):

$$\ln(V_R - V_0) = -\frac{R}{r_1} + \ln\frac{2K_p}{r_1} \tag{16}$$

where R is the hydrodynamic radius of the macromolecule, r_1 the experimental pore radius of the gel and the remaining parameters do have the conventional meaning. R can be obtained from the Einstein equation:

$$R = \left(\frac{30 \times 10^{24} M[\eta]}{\pi N_A}\right)^{1/3} \tag{17}$$

where N_A is Avogadro's number, $[\eta]$ the intrinsic viscosity of the polymer in dL.g^{-1} and R in Å. According to equation 16, a plot of $\ln(V_R - V_0)$ *vs.* R, will give a straight line, from which r_1 is obtained from the slope.

A second way is based on the insertion into equation 17 of the $M[\eta]$ values of the middle of the "plateau" extracted from the conventional universal calibration plot. The pore radius obtained with this last procedure is denoted by r_2. A more in-depth discussion about both methods has been reported in the past (*6*). Summarising, the values found for r_1 and r_2 were 63.21 Å and 48.20 Å, respectively.

At this point, we can use equations 11 and 12 to obtain the $\overline{V}_p$ values by combining both $\langle r_w \rangle$ or $\langle r_n \rangle$ with r_1 or r_2 values, taking into account the pore geometry for each combination, as it can be seen in Table I.

Table I
$\overline{V}_p$ Data (in cm^3) from Equations 11 and 12 for Lichrospher

Pore radii combination	Spherical	Cylindrical
$\langle r_n \rangle$-r_1	66.26	51.99
$\langle r_n \rangle$-r_2	149.44	98.60
$\langle r_w \rangle$-r_1	253.89	148.90
$\langle r_w \rangle$-r_2	574.80	275.08

Association Equilibria

The next step deals with the evaluation of the amount of methanol chemiadsorbed on Lichrospher, closely related to the numerator of equation 2. For this purpose, we shall use the theory of association equilibria (*23,24*) based on the view of association complexes formed by hydrogen bonding between primary molecules being in mutual thermodynamic equilibrium. Let us first to apply this theory to the binary system formed by inert/polar components such as the referred Bz-MeOH (80/20, v/v) mixture in the presence of gel. This silica-based gel posseses active centres most of them coming from the silanol groups located at the gel surface. The adsorption of methanol on the pore wall can be regarded as a polymerisation reaction in chemical equilibrium. Thus, in a first step a molecule of methanol is bound to a silanol group according to:

$$\equiv SiOH + CH_3OH \rightarrow \equiv SiOH{-}{-}{-}{-}OHCH_3$$

and in a second step the self-association of methanol can lead to chain-like complexes of any length. In general, the chain reaction mechanism proposed can be represented by:

$$S + MeOH \xrightarrow{\eta} S - MeOH$$

$$S - MeOH + MeOH \xrightarrow{\delta} S - (MeOH)_2$$

$$S - (MeOH)_2 + MeOH \xrightarrow{\delta} S - (MeOH)_3$$

....

$$S - (MeOH)_{i-1} + MeOH \xrightarrow{\delta} S - (MeOH)_i$$

where S and MeOH denote the silanol group and the methanol molecule, respectively. The equilibrium constants, assuming the hypothesis of equal reactivity, are η for the direct bond of the first methanol molecule to the silanol group, and δ for the self-association process. This mechanism can be condensed as follows:

$$S + i\ MeOH \xleftrightarrow{K} S - (MeOH)_i$$

K being the overall equilibrium constant, given by:

$$K = \eta\delta^{i-1} = \frac{[S - (MeOH)_i]}{[MeOH]^i[S]} \qquad (18)$$

Although it has been proved by ^{29}Si-NMR that silica surface consists of various kinds of silanols and siloxanes (*36*), we have considered here, for simplicity, only silanols as active centres for strong adsorption whereas the siloxane sites are usually regarded as hydrophobic centres. In addition, silanol groups can exist in single, geminal or vicinal forms but for the sake of simplicity we will assume an unique single form for these groups. Up to date, controversy exists about the reactivity of different kinds of silanol groups. Mauss and Engelhardt (*37*) have shown by FTIR measurements that molecules with basic properties are adsorbed preferentially on acidic isolated silanols, whereas solutes with hydroxyl groups, such as the methanol considered here, are able to interact with vicinal hydrogen-bonded silanols being adsorbed on these sites. In contrast, Snyder and Ward (*38*) states the opposite, i.e. that vicinal hydrogen-bonded silanols form the so-called "reactive" silanols which are more reactive than single isolated silanols. For a discussion in-depth on this issue see refs. 36 and 39.

Structural Description of the Stationary Phase

Next we present two models of the methanol adsorption based on the above depicted mechanism:

Model A

By making assumptions about the distance between two vicinal reactive hydroxyl groups, represented by the oxygen atoms (d_{O-O}), it is feasible to perform a model for the methanol adsorbed on the gel. Thus, under static conditions, and assuming d_{O-O} = 9.3 Å, which corresponds to 4.6 hydroxyl/100 Å^2 very close to the value of 4.56 hydroxyl/100 Å^2 reported for the randomly dehydrated β-crystobalite and calculated by a Monte Carlo method, three molecules of methanol hydrogen-bonded between them can be placed (see Figure 2a). This assumption is also consistent with the distance between oxygen atoms $d'_{O\text{-}O}$ = 2.4–2.8 Å reported for the hydrogen bonding (*38*). Though, even in the static state conditions assumed for the chromatographic separation, the driving forces causing flow can distort the uniformity of the chemiadsorbed methanol monolayer, as depicted in zone III from Figure 2b. This distortion can lead to long chain self-associated methanol partially located in the so-called zone II, as illustrated in the same figure. Obviously, zone I refers to the mobile phase where no specific interactions of the eluent components with the silica surface take place.

Notice that region III from Figure 2 is exclusively formed by methanol molecules which behaves as a very poor solvent for the PS, rejecting the polymer chain from this space and causing a reduction on the available pore volume. This statement is supported by macroscopic evidence based on the deviations of the PS elution profiles toward lower elution volumes (*25*). This behaviour cannot be considered as a general trend in SEC of binary eluents. Thus, when the chemiadsorbed component of the binary eluent behaves as a good solvent for the polymer, as is the case for methyl ethyl ketone (MEK)-n-heptane mixtures (see Figure 2 from ref. 6), the PS exhibits a certain affinity for the MEK monolayer increasing its time of residence inside the pores and, consequently, the PS elution profiles will shift to the opposite direction. However, we do not consider it appropriate at this point to introduce new assumptions on the weak adsorption effects on SEC with binary eluents. In a following contribution we will deal with this other secondary effect, using a similar way as developed here.

In light of the above arguments, zone II will be considered as a true stationary phase. In this regard, in SEC experiments using this kind of binary eluents, the partitioning of the macromolecular solute will take place between zone I (mobile phase) and zone II (stationary phase), as it can be seen in Figure 2b.

Model B

This model is slightly different from the preceding one. Now, we have shortened the distance between two vicinal hydroxyls, exactly at $d_{O\text{-}O}$ = 7.55 Å corresponding to 7 active hydroxyl groups/100 Å^2 (see Figure 3a). The methanol molecules are also chemically adsorbed on the active hydroxyls via hydrogen bonding but cannot be bounded between them due to the steric hindrance. The same methanol distribution on the Lichrospher surface can be assumed under flow conditions, being the self-association process allowed only in the direction depicted in Figure 3b.

According to models A and B, under flow conditions, the maximum amount of methanol chemically adsorbed by weight of gel can be evaluated. Table II shows the results obtained with both models.

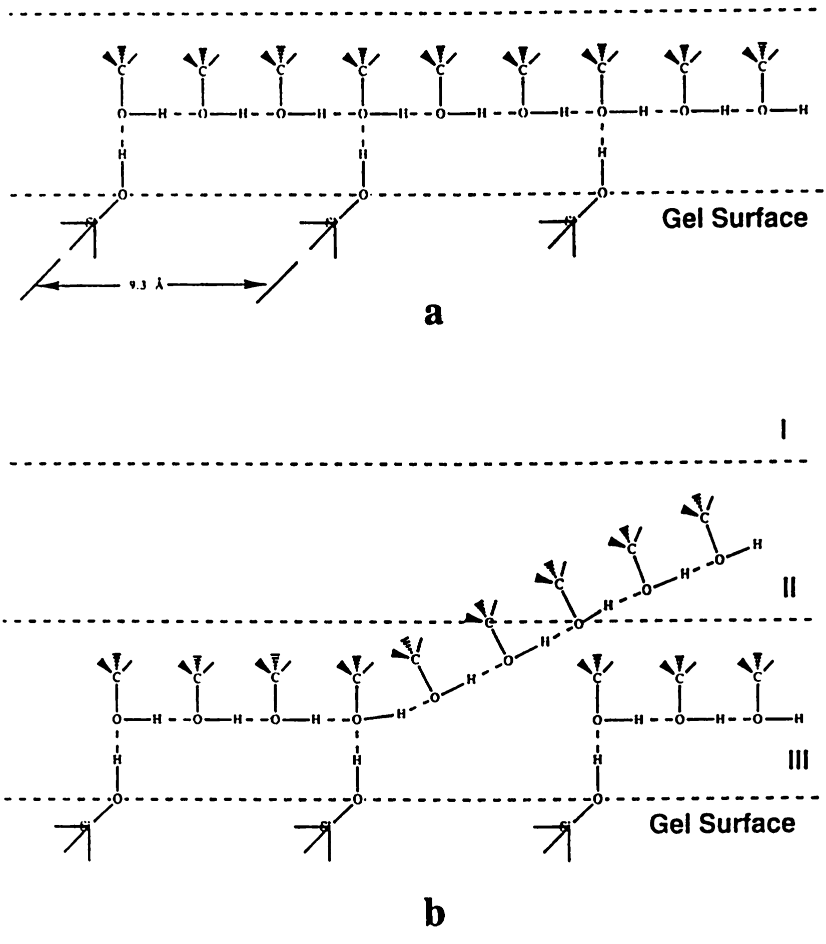
9.3 Å
Gel Surface
a
I
II
III
Gel Surface
b

Figure 2. Planar view of the adsorbed methanol on the Lichrospher under static (part a) and under flow (part b) conditions according to model A.

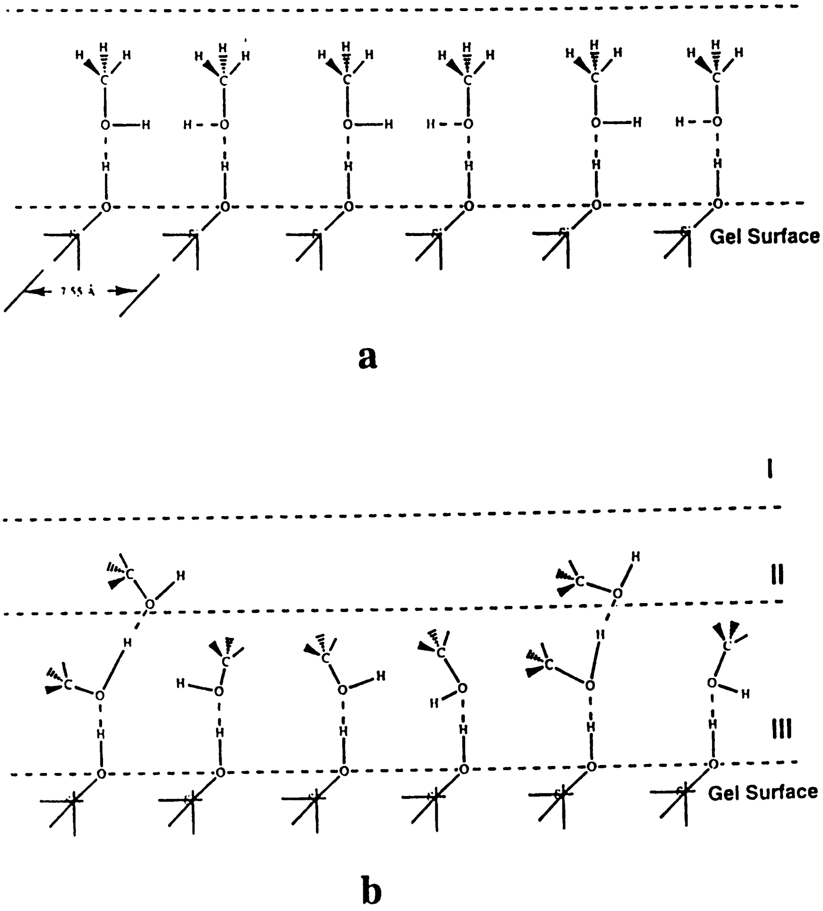
7.55 Å
Gel Surface
a
I
II
III
Gel Surface
b

Figure 3. Planar view of the adsorbed methanol on the Lichrospher under static (part a) and under flow (part b) conditions according to model B.

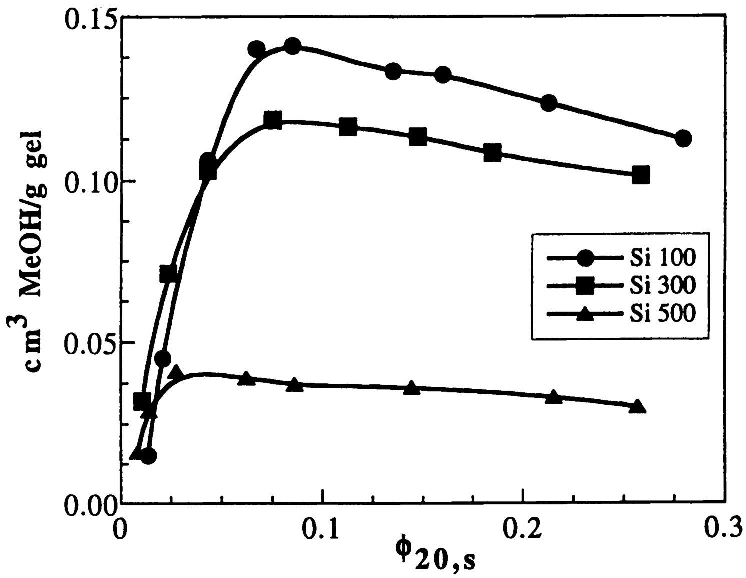

Figure 4. Equilibrium adsorption isotherms for benzene-methanol mixtures on Lichrospher with three different porosities.

TABLE II
Maximum Amount of Methanol (in cm^3/g gel) Adsorbed on the Lichrospher Surface

Lichrospher	Model A	Model B
Si-100	0.2317	0.118
Si-300	0.2317	0.118
Si-500	0.0463	0.024

Adsorption Isotherms

In order to test the validity of the assumptions made before to justify the spatial distribution of the methanol molecules across the pore wall, it is convenient to evaluate the mobile and stationary phase compositions in the region encompassed by the polymer molecules. In principle, the relation between the compositions of the eluent components in both phases can be obtained through the equilibrium adsorption isotherms.

Experimental data of methanol adsorption from the Bz-MeOH (80/20, v/v) mixture on Lichrospher with three different porosities can be seen in Figure 4. Initially, the isotherms rise steeply with the increase in the value of MeOH volume fraction in the Bz-MeOH mixture, and reach plateau regions. The amounts of saturated adsorption for MeOH in Si-100 and Si-300 are almost the same and much lower for the Si-500 gel packing. This trend is consistent with the specific surface data for this kind of gel, that is, 250 $m^2.g^{-1}$ for Si-100 and Si-300, and 50 $m^2.g^{-1}$ for Si-500. In all cases, the amount of MeOH corresponding to the assayed mixture fall into the plateau region, where the amount (in cm^3/g gel) of adsorbed MeOH remains nearly constant as the volume fraction of methanol increases. These data also reflect the stronger interaction of MeOH with silica surface arising from its more polar character and greater hydrogen bonding ability.

The comparison of data compiled in Table II with those experimental coming from adsorption isotherms (see Figure 4) reveals that data from model B agree well whereas large departures are observed when model A is used. This fact denotes that the assumptions introduced in model B become apparently more congruents.

Stationary Phase Composition

According to equation 2, the stationary phase composition can be evaluated from v_i data. Next, we present the method followed to obtain the values of this parameter as referred to the amount of methanol adsorbed within the pores under static conditions in absence of polymer. In the equilibrium constant for the associated-non associated methanol mixture detailed before (see equation 18), the values of η and δ have been taken from the literature (*40,24*), being 3 and 380, respectively. We have considered i=3, denoting that methanol can perform chains of trimers in both A and B models. Therefore, the overall constant will be:

$$K = \eta\delta^{3-1} = 3\times 380^2 = \frac{[S-(MeOH)_3]}{[MeOH]^3[S]} \tag{19}$$

For practical purposes, equation 19 can also be expressed as a function of experimental parameters or magnitudes previously evaluated, so:

$$K = \frac{Z\times\dfrac{1000}{V_p}v_{MeOH}}{\phi_{20,s}\times 1000 - \dfrac{Z\times 1000}{V_p}v_{MeOH}\,[S]} = 3\times 380^2 \tag{20}$$

Z being the amount of methanol adsorbed at saturation point on the gel (data listed in Table II); v_{MeOH} the specific volume of methanol (density/molar mass), $\phi_{20,s}$ the volume fraction of methanol in the s-phase from the adsorption isotherms, and $V_p = \overline{V}_p/3\times g$ gel, denoting the total pore volume for a given column per mass of gel. Then, from this equation, we obtain a value of $[S] = 5.60\times 10^{-9}$ which can be disregarded by comparison with the values of the remaining parameters.

In order to calculate the amount of adsorbed methanol in zone II, the s-phase, as illustrated in Figures 2 and 3, we assume the same value of K under static and flow conditions. The implementation of this assumption leads to:

$$\frac{\dfrac{Z}{V_p}v_{MeOH}}{\phi_{20,s} - \dfrac{Z}{V_p}v_{MeOH}} = \frac{\dfrac{Z+x}{V_p}v_{MeOH}}{\phi_{2s}^{o}\,v_{MeOH}} \tag{21}$$

Note that $[S]_{static}$ and $[S]_{flow}$ have been suppressed from the above expression because both should be approximately identical. The new parameter, x, represents the amount of methanol (in cm^3/g of gel) adsorbed in zone II which can be easily evaluated from equation 21. Recalling that the parameter of interest is the volume fraction ν_2 instead of x, the transformation can be directly made using $\nu_2 = x/V_p$. Table III shows the V_p data for each kind of gel according to the pore shape and pore radii combination. These data have been used to calculate the ν_2 parameter through equation 21 listed in Table IV for model A and in Table V for model B.

Next step deals with the evaluation of the polymer composition, ϕ_{3s}, in the stationary phase. For this end, these values have been computed from equation 10 for three different values of ϕ_{3m} and for a given PS sample inserting the g_{ij} and g_T parameters, as well as the volume fractions of the binary eluent in both mobile and stationary phases. However, the ϕ_{3s} evaluation is not a trivial task since the referred equation 10 contains this variable in an implicit form and it cannot be directly extracted.

TABLE III
Available Pore Volume, V_p, (in cm^3) for Lichrospher in Bz-MeOH (80/20, v/v) at 293 K

Pore shape	Pore radii combination	Si-100	Si-300	Si-500
S	$\langle r_w\rangle - r_1$	4.96	5.03	4.51
S	$\langle r_w\rangle - r_2$	11.19	11.34	10.18
S	$\langle r_n\rangle - r_1$	19.24	19.27	17.30
S	$\langle r_n\rangle - r_2$	43.05	43.64	39.18
C	$\langle r_w\rangle - r_1$	3.89	3.94	3.54
C	$\langle r_w\rangle - r_2$	7.38	7.48	6.72
C	$\langle r_n\rangle - r_1$	11.15	11.30	10.15
C	$\langle r_n\rangle - r_2$	20.60	20.88	18.75

S= spherical, C= cylindrical.

TABLE IV
Values of v_2 from Equation 21 According to the Model A for Lichrospher in Bz-MeOH (80/20, v/v) at 293 K

Pore shape	Pore radii combination	Si-100	Si-300	Si-500
S	$\langle r_w\rangle - r_1$	0.01142	0.00818	0.00071
S	$\langle r_w\rangle - r_2$	0.00193	0.00141	0.00013
S	$\langle r_n\rangle - r_1$	0.00062	0.00047	0.00005
S	$\langle r_n\rangle - r_2$	0.00012	0.00009	0.00001
C	$\langle r_w\rangle - r_1$	0.02009	0.01421	0.00117
C	$\langle r_w\rangle - r_2$	0.00470	0.00342	0.00031
C	$\langle r_n\rangle - r_1$	0.00194	0.00142	0.00014
C	$\langle r_n\rangle - r_2$	0.00054	0.00040	0.00004

S= spherical, C= cylindrical.

TABLE V

Values of ν_2 from Equation 21 According to the Model B for Lichrospher in Bz-MeOH (80/20, v/v) at 293 K

Pore shape	Pore radii combination	Si-100	Si-300	Si-500
S	$\langle r_w \rangle - r_1$	0.00333	0.00243	0.00023
S	$\langle r_w \rangle - r_2$	0.00061	0.00045	0.00004
S	$\langle r_n \rangle - r_1$	0.00020	0.00015	0.00001
S	$\langle r_n \rangle - r_2$	0.00004	0.00003	0.00000
C	$\langle r_w \rangle - r_1$	0.00561	0.00408	0.00037
C	$\langle r_w \rangle - r_2$	0.00144	0.00106	0.00010
C	$\langle r_n \rangle - r_1$	0.00061	0.00045	0.00004
C	$\langle r_n \rangle - r_2$	0.00017	0.00013	0.00001

A z-basic program has been implemented which briefly consists of calculating the right-hand side of equation 10 where all the parameters are known. Then, by an iterative process the program try different values of ϕ_{3s} and calculates the left-hand side of equation 10 until the convergence is reached. The program stops when the absolute difference between both sides of the expression is lower than 10^{-6}.

Alternatively, one can also consider the preferential solvation of one component of the eluent by the polymer. Then, equation 3 should be used to evaluate the mixed solvent composition in each chromatographic phase.

Distribution Coefficients

Experimental values of the distribution coefficient, K_p^E (see Table VI), have been directly obtained from data on retention volumes, V_R, considering an ideal reference system such as PS in benzene (*20*), according to:

$$\left[K_p^E\right]_{Bz-MeOH} = \left(V_R - V_0\right)_{Bz-MeOH}\left(V_R - V_0\right)_{Bz}^{-1} \qquad (22)$$

and assuming $[K_p]_{Bz} = 1$ for ideal SEC.

For equilibrium partitioning of the polymer between the chromatographic m- and s-phases, the theoretical distribution coefficient can be expressed as the ratio of the polymer concentration in both phases equivalent to the polymer volume fraction:

$$K_p^T = \frac{\phi_{3s}}{\phi_{3m}} \qquad (23)$$

TABLE VI
Experimental Distribution Coefficients, for Polystyrene in Bz-MeOH (80/20, v/v) binary eluent at 293 K

M_w (Kg mol^{-1})	K_p^E
2.9	0.883
9.0	0.858
20.5	0.827
24.5	0.821
37.1	0.767
50.0	0.774
100.0	0.686
130.0	0.613
136.0	0.638
240.0	0.639
314.0	0.628
450.0	0.390

It is evident that a great number of theoretical K_p^T data can be generated owing to the different assumptions and alternative ways of calculation as explained in-depth throughout the text. Briefly, we have considered two possible geometries for the pore shape, spherical and cylindrical (see equations 11 and 12); two average pore radii, $\langle r_w \rangle$ and $\langle r_n \rangle$ (equations 13 and 15); two experimental pore radii, r_1 and r_2 (equations 16 and 17); two structural models for the stationary phase (see Figures 2 and 3) and the inclusion or not of the preferential solvation parameter, $\phi_{1\alpha}^{\lambda}$. In addition, we have selected three arbitrary ϕ_{3m} values falling within the range of concentrations loaded in SEC experiments in order to obtain proper elution profiles. The ϕ_{3m} values used for computation of were: 1.3×10^{-4}, 3.24×10^{-5} and 4.5×10^{-6}. Note that the quantities related to the polymer volume fraction are very small because SEC experiments take place at very dilute concentration. However, the ratio ϕ_{3s}/ϕ_{3m} is often close to unity.

For the sake of simplicity, we believe it to be more convenient to show graphically instead of numerically the comparison between experimental and theoretical values of distribution coefficients, due to the high number of parameters and combinations handled. Thus, Figure 5 shows, as an example, plots of K_p^T against K_p^E obtained with model B for both geometries assayed, different radii combination and taking or not into account the preferential solvation parameter for a given value of $\phi_{3m}=1.3\times10^{-4}$. As it can be seen in this Figure, good agreement

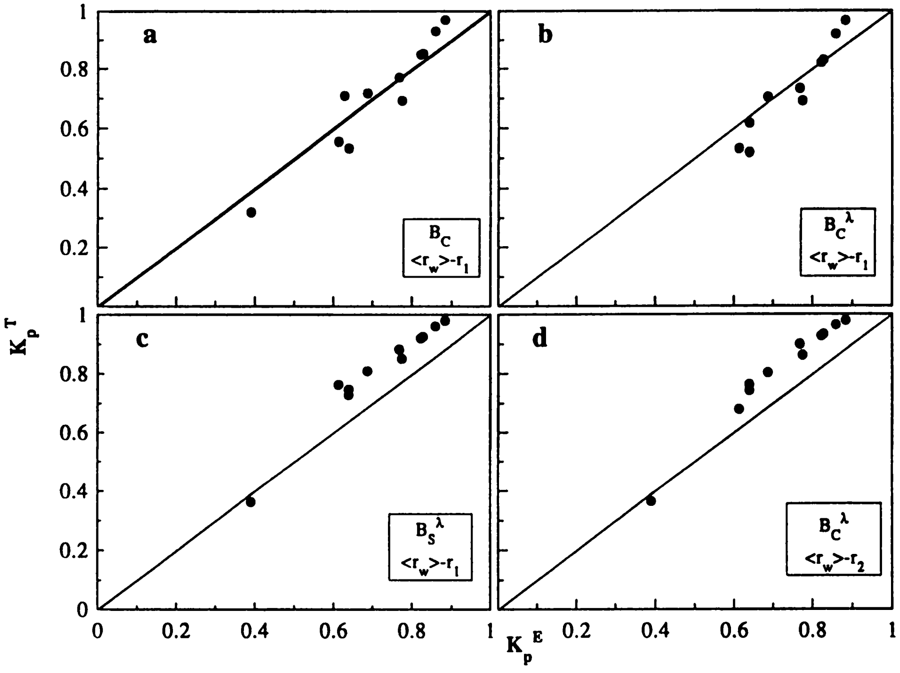

Figure 5Comparison between experimental and theoretical distribution coefficients for polystyrene in benzene-methanol (80/20, v/v) mixture as eluent. Acronysms depicted into the plots refers to the model, pore shape, pore radii combination and preferential solvation parameter selected.

between experimental and predicted values is obtained in all cases, with deviations lower than 15%. However, the best fit is reached when model B, cylindrical pore shape, $\langle r_w \rangle - r_l$ combination and including the preferential solvation contribution (part b), where the observed departures are lower than 10%. Nevertheless, a generalization of this conclusion must be regarded with caution since each particular ternary system requires to model properly the stationary phase.

Conclusion

A generalized view of the obtained results allow us to elucidate that when the exclusion secondary effect takes place, best predictions are obtained with an structural description of the stationary phase given by model B assuming a cylindrical pore shape, selecting a weight average pore radius and considering the influence of the preferential solvation. In addition, it can also be stated that values of ϕ_{3m} lower than 10^{-4} are not recommended since the predictions made do not seem to retain the molecular weight dependence on K_p.

Acknowledgments

This work was patially supported by Grant No. PB91-0808 from CICYT (Spain). One of the authors (I.P.) is also grateful to the Ministerio de Educación y Ciencia (Spain) for a long-term fellowship.

Literature Cited

1. Riedo, F.; Kováts, E. *J. Chromatogr.* **1982**, *239*, 1.
2. Riedo, F.; Kováts, E. In *Theoretical Advancement in Chromatography and Related Techniques*; Dondi, F.; Giochon, G., Eds.; NATO ASI Series; Kluwer: Dordrecht, 1992; pp. 211-226.
3. Gorshkov, A.V.; Much, H.; Becker, H.; Pasch, H.; Evreinov, V.V.; Entelis, S.G. *J. Chromatogr.* **1990**, *523*, 91.
4. Pasch, H.; Zammert, I. *J. Liq. Chromatogr.* **1994**, *14&15*, 3091.
5. Cools, P.J.C.H.; Van Herk, A.M.; German, A.L.; Staal, A.W. *J. Liq. Chromatogr.* **1994**, *14&15*, 3133.
6. Figueruelo, J.E.; Soria, V.; Campos, A. In *Liquid Chromatography of Polymers and Related Materials II*; Cazes, J.; Delamare, X., Eds.; Chromatographic Science Series; Marcel Dekker Inc.: New York, 1980, Vol. 13; pp. 49-71.
7. Mori, S. In *Steric Exclusion Liquid Chromatography of Polymers*; Janca, J., Ed.; Chromatographic Science Series; Marcel Dekker Inc.: New York, 1984, Vol. 25; pp. 161-211.
8. Dubin, P.L. In *Aqueous Size-Exclusion Chromatography*; Dubin, P.L., Ed.; Journal of Chromatography Library, Elsevier Science Publishers: Netherlands, 1988, Vol. 40; Chapter 3.
9. Balke, S.T. In *Modern Methods of Polymer Characterization*; Barth, H.G.; Mays, J.W., Eds.; Chemical Analysis; John Wiley & Sons: New York, 1991, Vol. 113; Chapter 1.
10. Jaroniec, M.; Martire, D.E.; Borowko, M. *Adv. Colloid Interface Sci.* **1985**, *22*, 177.

11. Boehm, R.E.; Martire, D.E.; Amstrong, D.W.; Bui, K.H. *Macromolecules* **1983**, *16*, 466.
12. Boehm, R.E.; Martire, D.E.; Amstrong, D.W.; Bui, K.H. *Macromolecules* **1984**, *17*, 400.
13. Jaroniec, M.; Martire, D.E. *J. Liq. Chromatogr.* **1987**, *10*, 541.
14. Boehm, R.E.; Martire, D.E. *J. Phys. Chem.* **1994**, *98*, 1317.
15. Knox, J.H.; Kaliszan, R. *J. Chromatogr.* **1985**, *349*, 211.
16. Berek, D.; Bleha, T.; Revna, Z. *J. Polym. Sci. Polym. Lett. Ed.* **1976**, *14*, 323.
17. Soria, V.; Campos, A.; Figueruelo, J.E. *An. Quim.* **1978**, *78*, 1026.
18. Quivoron, C. In *Steric Exclusion Liquid Chromatography of Polymers*; Janca, J., Ed.; Chromatographic Science Series; Marcel Dekker Inc.: New York, 1984, Vol. 25; Chapter 5.
19. Porcar, I.; Garcia, R.; Campos, A.; Soria, V. *J. Chromatogr. A* **1994**, *673*, 65.
20. Garcia, R.; Celda, B.; Soria, V.; Tejero, R.; Campos, A. *Polymer* **1990**, *31*, 1694.
21. Flory, P.J. *Principles of Polymer Chemistry*; Cornell University Press: Ithaca (NY), 1953, Chapter 5.
22. Munk, P. In *Modern Methods of Polymer Characterization*; Barth, H.G.; Mays, J.W., Eds.; Chemical Analysis; John Wiley & Sons: New York, 1991, Vol. 113; Chapter 5.
23. Prigogine, I.; Defay, R. *Chemical Thermodynamics*; Longmans Green & Co.: London, 1954, Chapter XXVI.
24. Pouchly, J.; Zivny, A. *Makromol. Chem.* **1985**, *186*, 37.
25. Campos, A.; Soria, V.; Figueruelo, J.E. *Makromol. Chem.* **1979**, *180*, 1961.
26. Campos, A.; Gavara, R.; Tejero, R.; Gómez, C.; Celda, B. *J. Polym. Sci. Polym. Phys. Ed.* **1989**, *27*, 1569.
27. Koningsveld, R.; Kleitjens, L.A.; Schoffeleers, H.M. *Pure Appl. Chem.* **1974**, *39*, 1.
28. Minton, A.P. *Biophys. Chem.* **1980**, *12*, 271.
29. Waldmann-Mayer, H. *J. Chromatogr.* **1985**, *350*, 1.
30. Maltsev, V.G.; Belenkii, B.G.; Zimina, T.M. *J. Chromatogr.* **1984**, *292*, 137.
31. Davidson, M.G.; Ulrich, W.S.; William, M.D. *Macromolecules* **1987**, *20*, 1141.
32. Giddings, J.C.; Kucera, E.; Rusell, C.P.; Myers, M.N. *J. Phys. Chem.* **1968**, *72*, 4397.
33. Cassasa, E.F.; Tagami, Y. *Macromolecules* **1969**, *2*, 14.
34. Dawkins, J.V.; Hemming, M. *Makromol. Chem.* **1975**, *176*, 1795.
35. Dawkins, J.V.; Hemming, M. *Makromol. Chem.* **1975**, *176*, 1815.
36. Nawrocki, J. *Chromatographia* **1991**, *31*, 177.
37. Mauss, H.; Engelhardt, H. *J. Chromatogr.* **1986**, *371*, 235.
38. Snyder, L.R.; Ward, J.W. *J. Phys. Chem.* **1966**, *70*, 3941.
39. Nawrocki, J. *Chromatographia* **1991**, *31*, 193.
40. Figueras, F.; Nohl, A.; Mourgues, L.; Trambouze, Y. *Trans. Faraday. Soc.* **1971**, *6*, 1155.

Chapter 8

Behavior of Macromolecules in Nonhomogeneous Hydrodynamic Fields: Degradation Mechanism of Macromolecules

E. V. Chubarova and V. V. Nesterov

Institute of Macromolecular Compounds, Russian Academy of Sciences,
Bolshoi pr. 31, 199004 Saint Petersburg, Russia

The mechanism of degradation of macromolecules in a non-homogeneous hydrodynamic field is proposed. It is based on the distortion of homogeneous concentration in the bulk of polymer solution because macromolecules undergo directed migration transverse to flow lines. As a result, a layer of high concentration is formed near the surface. Degradation depends on both the properties of the retarding surface and the rate of the flow which tends to tear off this layer. The entangled layer is formed by the macromolecules of such a size that under these experimental conditions they can reach the surface during the experimental time.

The behavior of solutions and/or melts of macromolecules in non-homogeneous hydrodynamic fields has been investigated for a long time. At present it attracts even greater attention because of its important practical aspects. It is necessary to elucidate the main features of polymer transport in porous media (chromatography, oil industry, etc.) and the concomitant changes in the structure and properties of macromolecules. Of particular interest is the problem of the possible degradation of macromolecules.

There are two fundamental theoretical papers on polymer degradation. Frenkel (*1*) has shown that in a stretching flow the macromolecule oriented along the flow is either degraded or reached stable deformation limit. The most probable break occurs in the chain center. Bueche (*2*) has considered the shear effect on the macromolecule placed in a viscous medium and has shown that degradation can proceed only as a result of chain entanglement of neighboring macromolecules, and the most probable place of degradation is a chain part near the center.

In experimental papers (see for example review(*3*)) in order to explain the results of degradation either the theory considered in

0097–6156/96/0635–0127$17.50/0

(*1*) for dilute solutions or that in (*2*) for concentrated solutions is usually applied. It is stated in these works that the degree of degradation increases with molecular weight (M) at a given shear stress and that it is this stress, i.e. the product of shear rate by solvent viscosity, that controls degradation. It was found that degradation occurs for macromolecules in solutions with concentrations ranging from 10^{-2} g/dl to those exceeding the critical chain overlap concentration c_c :

$$c_c = \frac{6}{\pi}\frac{M}{N_A} < s^2 >^{3/2} \tag{1}$$

where N_A is Avogadro's number and $< s^2 >^{1/2}$ is the mean-square end-to-end distance of a random coil (calculated from intrinsic viscosity). The concept of degradation of macromolecules in SEC is considered in greatest detail in Giddings' review (*4*). This author believes that the individual molecule is degraded because stretching caused by shear degradation takes place near the walls of the widest interparticle channels in which the highest shear rates are observed. Giddings provides the recommendations for decreasing degradation by using sorbents with minimum particle size and by decreasing the elution rate.

However, at present there are many facts which do not agree with the general concepts (*1-4*). Thus, when degradation was studied in dilute aqueous polyacrylamide (PAA) solutions ($M_w \approx 5 \cdot 10^6$ Da) in a Couette viscometer at high shear rates, low molecular weight degradation products consisting of 5-10 monomer units appeared (*5*). During turbulent flow in a capillary of poly(decyl methacrylate) of different concentrations it was also found that small fragments are formed (*6*). Subsequently it has been shown (*6-10*) that degradation decreases with increasing solution concentration and increases when solvent quality becomes inferior (*8,11,12*). This fact seems strange because with inferior solution quality the macromolecule tends to adopt the conformation of a non-draining compact coil (*13*). Additional effort is needed to transform it into trans-conformation which undergoes degradation to a greater extent (*14*). Moreover, it has been shown (*11*) in a model unit for dilute solutions ($c < 0.5\, c_c$) that the degradation of polystyrene (PS), poly(methyl methacrylate) (PMMA), and sodium polystyrene sulphonate occurs at a stretching force acting on the -C-C- bonds which is much lower than its theoretical critical value ($\approx 10^{-3}$dynes). In the same work the concept of chain self-entanglement increasing the probability of its degradation has been proposed . However, this concept contradicts theoretical calculations (*13*) which show that chain self-entanglement is energetically unfavourable. It has been shown (*15*) that in SEC the degree of degradation increases on sorbents with a smaller pore size and a smaller size of sorbent particles. It was also established that degradation is greater for more flexible chains. The authors of (*15*) assume that the macromolecules are degraded at the pore entrance where the self-entangled macromolecules "clutching" at a pore are subjected to the effect of the eluent flow passing the particle. According to the classical mechanism of SEC, the "clutching" of macromolecules can take place only in the case of the non-equilibrium of mass-transfer near the pore entrance. However, in chromatographic experiments in which the degradation of macromolecules was observed the equilibrium always takes place because the time of passing of the macromolecular zone near the porous particle considerably exceeds the relaxation time of macromolecules.

Hence, it may be concluded on the basis of this brief literature review that there is no single degradation mechanism that could be explain all experimental data.

Experimental

Three types of experiments were performed: on chromatographic columns, on membranes in flat cells, and during thermal field flow fractionation (TFFF).

In all cases degradation was studied for a PS sample with $M_w = 1.12 \cdot 10^7$ Da and $M_n = 7.64 \cdot 10^6$ Da. Narrow-disperse PS ("Polymer Laboratories", USA) in the M_p range from $8.3 \cdot 10^5$ Da to $12.25 \cdot 10^6$ Da were used as calibration standards (where $M_p = (M_w M_n)^{1/2}$). In all experiments the concentration of PS solutions and calibration standards did not exceed 0.03-0.05 g/dl.

Size-Exclusion Chromatography (SEC). Standard chromatographic columns 30 cm in length with 0.4 cm i.d. packed with macroporous glass particles (MPG) with a pore size of 400, 115, and 25 nm were used as well as non-porous quartz particles, spherical silica gels, and glass balls. THF or mixtures of methyl-ethyl ketone (MEK) with methanol (MeOH) were used as eluents. A spectrophotometric detector at a wavelength of 210 nm (for MEK:MeOH eluents) and a differential refractometer for SEC in THF were used.

Degradation experiments in SEC were carried out as follows. Not less then 25 solutes of the same PS investigated with an initial concentration of 0.03 g/dl were chromatographed under fixed experimental conditions (sorbent, eluent, and flow rate). The injection loop volume was 20 μl and the above numbers of injections were needed both to collect a sufficient amount of sample for rechromatography and to exclude the concentration factor. The eluates were collected at the outlet of the columns and concentrated to c ≈ 0.03 g/dl. Concentration procedure in mild conditions (temperature 40°C) did not result in degradation of macromolecules as was shown in blank experiment. Concentrated eluates were analyzed in the same two chromatographic columns with MPG 400 nm under the conditions excluding degradation (eluent - THF, flow rate 5.9 ml/h).

Experiments with Membranes. Macroporous glass membranes with different pore diameters and a non-porous teflon support were used. The membrane thickness was ≈100 μm, their external diameter was 25 mm, and porosity was 0.60-0.67. The membrane was placed in a standard teflon ultrafiltration cell in which the solution can be stirred with a magnetic stirrer. Stirring frequency was 400 rpm. At first PS solution was agitated in the cell over the membrane and the teflon film for one or two hours. After these time intervals the solutions were poured out, and the molecular weight distribution (MWD) of the PS sample was measured with the aid of SEC under non-degrading conditions. In the other experiment the PS solution

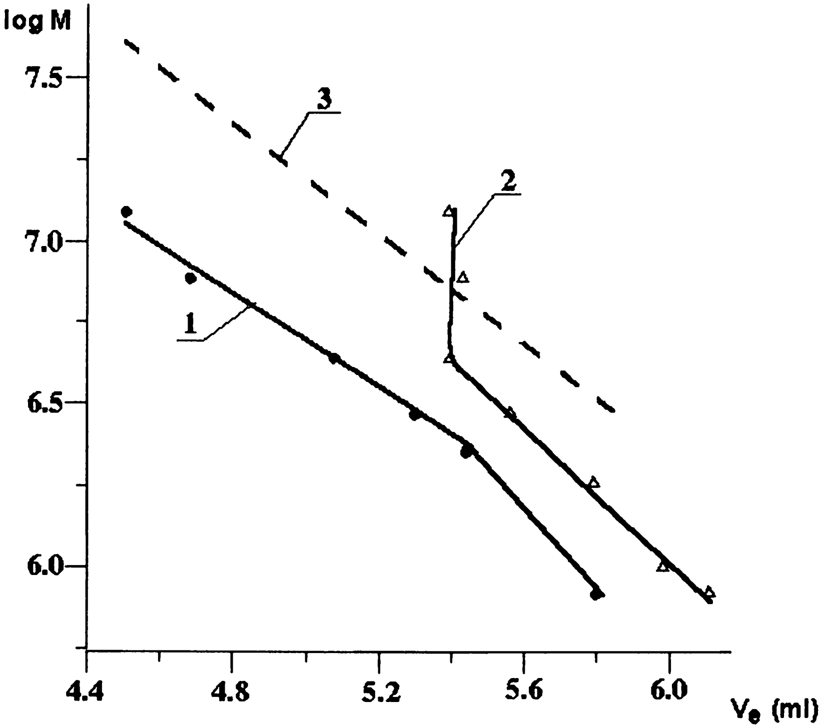

Figure 1. Calibration dependences for a system consisting of two columns packed with MPG with a pore diameter of 400 nm. (1) eluent - THF, (2) eluent - ME:MeOH 89.3:10.7 mixture, (3) - calculated calibration dependence for PS in eluent (2). The following values of constants in the Mark-Houwink equation were used: for PS in eluent (2) $a_\theta = 0.5$ and $K_\theta = 7.3 \cdot 10^{-2}$ dl/g, for PS in THF $a = 0.766$ and $K = 6.8 \cdot 10^{-3}$ dl/g. Flow rate 5.9 ml/h.

was ultrafiltrated at an exceed pressure of 0.5 and 1.0 atm. One half of the initial sample volume (8 ml) was filtered through membranes. In all cases the filtration time was less than 30 min. The MWD of filtrates and concentrates was determined by SEC under non-degrading conditions.

Thermal Field Flow Fractionation. For TFFF a unit similar to that described in ref. (*16*) was used: the channel height was 200 μm, the width was 1 cm, the channel was u-shaped and 50·2 cm in length. The fractograms were recorded with a photometer at a wavelength of 254 nm. The loop volume was 20 μl, and the eluent was THF. The temperatures of the cold and hot walls were $T_c = 10°C$ and $T_h = 20°C$. For detection reliability the working concentration c was 0.05 g/dl. In the experiments on degradation during TFFF the initial concentration of the PS sample was 0.5 g/dl. The MWD in the TFFF method were determined in the TFFF unit itself (TFFF column) at minimal elution rate and using a standard calibration procedure.

The degree of degradation in all experiments was determined from the degradation index I :

$$I = M_{no} / M_n - 1 \tag{2}$$

where M_{no} and M_n are the number-average M of the initial and degraded polymer.

Results and Discussion

SEC in Good and Poor Solvents. The calibration curve for two columns packed with MPG with a pore size of 400 nm (Figure 1, curve 1) was obtained in THF (good solvent) with the aid of narrow-disperse PS standards. This calibration has a linear part in the range of $2 \cdot 10^6$ Da$-12 \cdot 10^6$ Da. With the aid of this calibration dependence obtained at an elution rate of 5.9 ml/h the MWD and I of the initial PS and all eluates were calculated in SEC and membrane experiments.

Figure 2 shows degradation indices of a PS sample that passed through columns packed with MPG of 400 nm (Figure 2a), 115 nm (Figure 2b), and 25 nm (Figure 2c) pore sizes at different elution rates. Corrected rates were determined from the retention volume of o-dichlorobenzene internal standard. It is noteworthy that the dependence of I on elution rate is non-monotonic. It was detected that with increasing elution rate, hence, with increasing shear stress as well, the degree of degradation can sometimes decrease. For each sorbent some optimum rates exist at which I is close to 0. In particular, for MPG of 400 nm this first optimum rate is equal to 5.9 ml/h. At this rate the calibration dependence was obtained (curve 1, Figure 1). A similar character of the dependence of I on elution rate u is also observed under other conditions (*17*). The experimental results in (*17*) show the relationship between I and the shape and size of sorbent particles. In particular, at comparable rates degradation is less pronounced on balls than on particles of an irregular shape. Moreover, for each sorbent an optimum particle size probably exists.

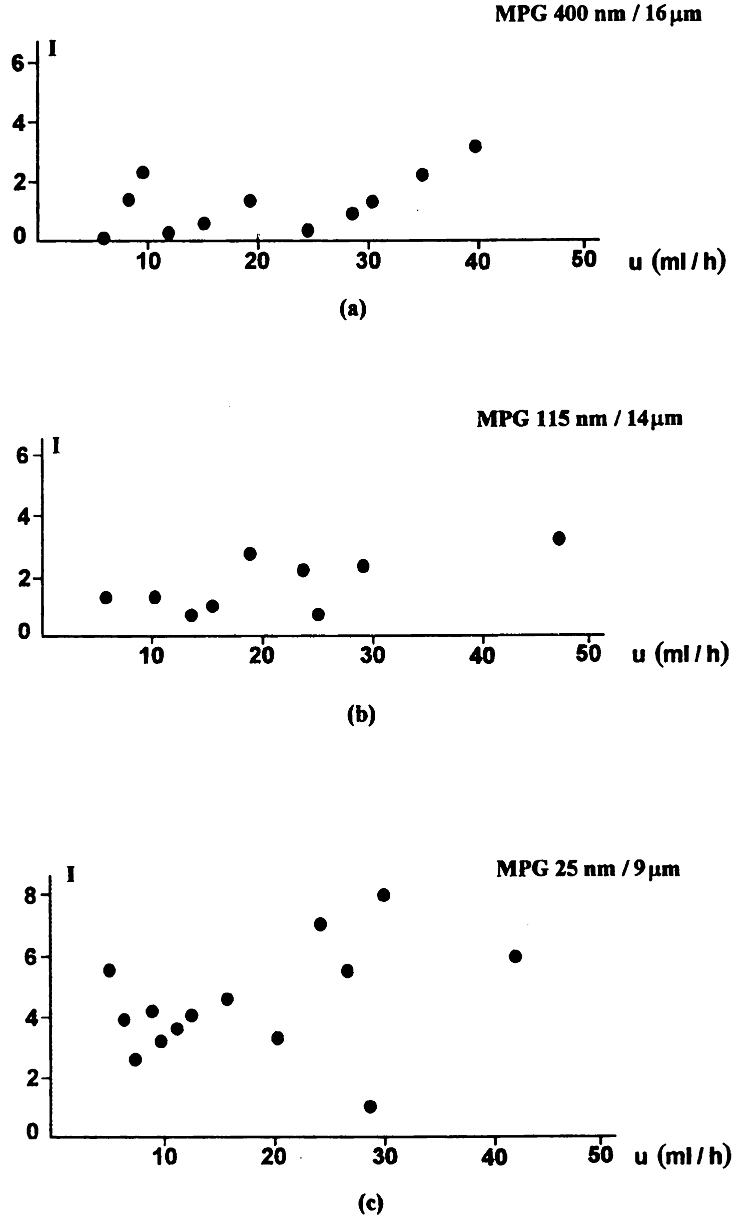

Figure 2. Degradation indices vs flow rate in SEC on MPG with different particle and pore sizes.

(Reproduced with permission from reference 17. Copyright 1990 Marcel Dekker, Inc.)

The indispensable criterion for "non-degradative" condition is the choice of the optimum rate at given pore and particle sizes. An nontrivial conclusion follows from Figure 2 that it is not possible to apply SEC for the determination of the MWD of polymers with ultrahigh M if the pores of sorbents are smaller than the size of the largest macromolecules of the sample (e.g. for PS with $M_w \approx 10^7$ the size of the macromolecule is about 200 nm (*4*)). Hence, for SEC of superhigh molecular weight polymers one cannot use any arbitrary column systems. Note that the results of PMMA degradation on a system of columns packed with MPG of 400 nm (*17*) show that at comparable elution rates u the degree of degradation I is lower for PMMA than for PS. This is probably due to lower thermodynamic chain flexibility of PMMA than that of PS (*15*).

Since the experiments on the determination of I are long (particularly at low u) and difficult, the question arises whether the experimental data are reproducible. After three months we performed a new checking series of chromatographic experiments on degradation of PS at some elution rates on a column with MPG of 400 nm and a column with MPG of 25 nm. Calculated degradation indices for previous (I_1) and checking (I_2) series were as follows. For columns with MPG of 400 nm at u=5.9 ml/h, I_1=0.025 and I_2=0.019; at u=14.4 ml/h, I_1=0.344 and I_2=0.421. For column with MPG 25 nm at u=28.7 ml/h, we have I_1=0.799 and I_2=0.812. Therefore, the errors in determining I are much less than the differences in I values measured at different rates u. An indirect confirmation of the reproducibility of results is the coincidence of optimum rates for PS and PMMA (i.e. the rates at which $I \approx 0$), although the time between these two series of experiments was more than six months (*17*).

Now let us consider the retention effect of macromolecules on the surface of sorbent particles. The assumption of the possible "retardation" of macromolecules has already been formulated in (*18*) and it has been shown that with increasing elution rate the retention volumes of the low molecular weight reference sample and PS on porous and non-porous sorbents increase. Moreover, the distribution coefficient slightly decreases In our experiments the retardation effect is most pronounced on non-porous balls and for those porous sorbents the pore size of which is smaller than the size of PS molecules. Figure 3a shows overlapping chromatograms of a mixture of PS and o-dichlorbenzene obtained at different u on a column packed with glass balls. It is clear that PS is eluted at a higher volume than that of the low molecular weight reference sample. Furthermore, the elution volumes of PS increase with u. Similar results are shown in Figure 3b for the spherical silica gel with a pore size of 30 nm (Si-300) and a particle size of 10 mm. In this case a part of the PS sample is eluted at a retention volume smaller than that of the low molecular weight reference sample and another part is eluted at a greater volume. With increasing rate an increasing part of the PS is "retarded" and at a relatively high rate all polymer is eluted with retention volume exceeding that of the low molecular weight reference sample.

In order to make sure that the PS molecules are actually retarded on the sorbent surface and are eluted at retention volumes exceeding the total elution volume, the following experiment was carried out. At a flow rate of 16 ml/h the PS

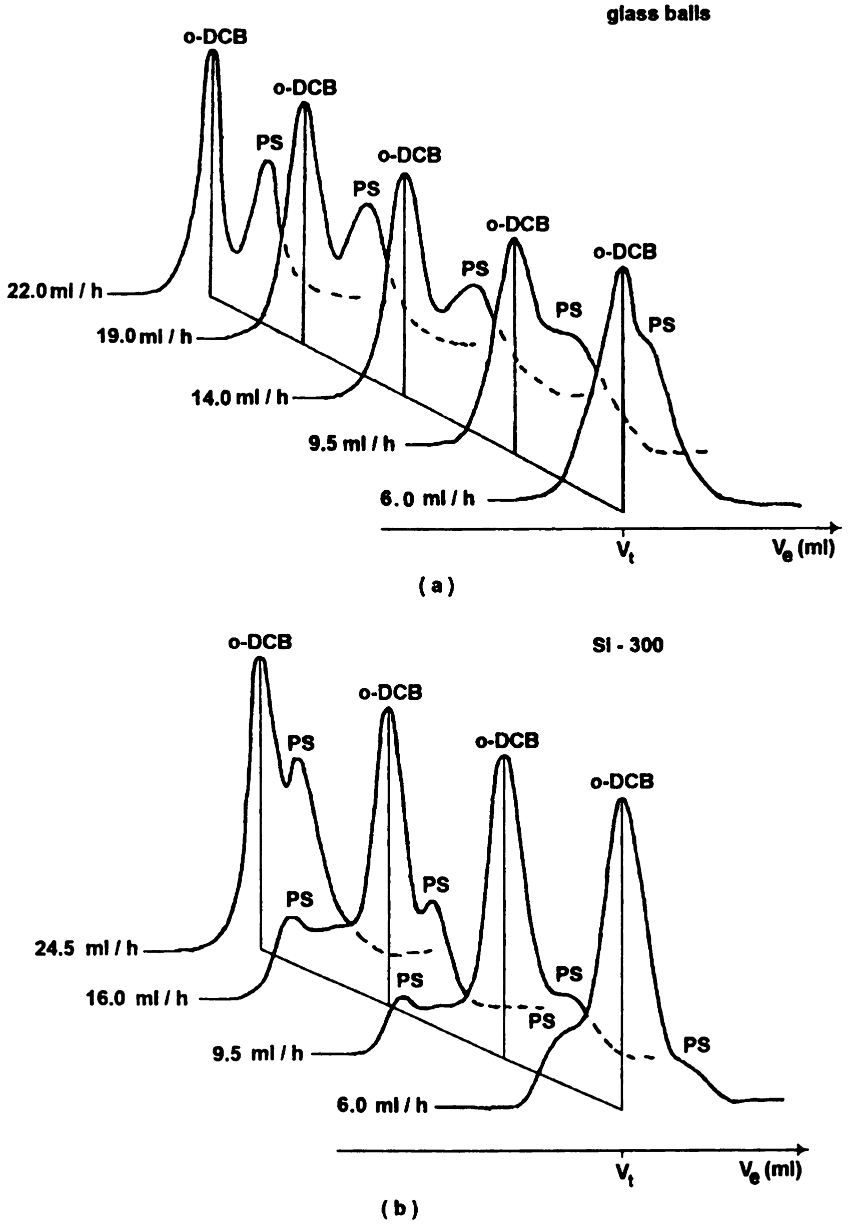

Figure 3. Overlapping chromatograms of a mixture of PS and o-dichlorobenzene, obtained for SEC on non-porous glass balls with a mean particle diameter (d_p) of 7.3 μm (a) and a spherical Si-300 silica gel with a pore diameter of 30 nm and an average particle diameter of 10 μm (b). V_t - the total elution volume.

(Reproduced with permission from reference 17. Copyright 1990 Marcel Dekker, Inc.)

samples at a concentration of 0.03 g/dl were injected 60 times in THF on a column with a Si-300 sorbent. In each injection fractions were collected as is shown in Figure 4a. Fraction I was eluted at the minimum retention volumes, in contrast, fraction III was eluted at the maximum retention volumes, and fraction II at intermediate volumes. The collected fractions were concentrated to the initial concentration (0.03 g/dl) and analyzed again on an analytical system of columns the calibration dependence of which is shown in Figure 1 (curve 1). The MWD of these fractions obtained with the aid of this calibration dependence are shown in Figure 4b, and the results of calculations of their average molecular weight characteristics are given in Table I.

Table I. Average M of fractions of a PS sample

Fraction	$M_w \cdot 10^{-6}$ Da	$M_n \cdot 10^{-6}$ Da	M_w / M_n
I	6.89	2.90	2.37
II	16.09	9.84	1.63
III	13.84	9.72	1.42

It follows from all these experimental data that when steric hindrance exists, the largest macromolecules are retarded to the greatest extent, and much smaller macromolecules (evidently, a part of macromolecules from the initial distribution, which have not been degraded, and fragments of degraded macromolecules) are eluted at smaller retention volumes.

For sorbents with pore sizes exceeding those of PS molecules the retardation effect with increasing rate has also been observed (*17*), but the inversion of the elution order of the low M (o-dichlorobenzene) component and the polymer was not observed. It should be noted that the retardation effect is more pronounced not only on sorbents with a smaller pore size but also on those with a smaller particle size (*17*).

The problem of the relationship between polymer degradation and the thermodynamic quality of the solvent has not yet been solved (*6,19-21*). Zimm (*22*) has studied this problem on model units. In particular, because of the ambiguous experimental data, he has suggested that degradation depends not only on the quality of the solvent but also on its viscosity. When we studied the effect of solvent quality on degradation in SEC, a good solvent (THF) and a solvent close to the θ-solvent for PS (the MEK:MeOH mixture) were used. For the θ-solvent (MEK:MeOH 88.7:11.3) the Mark-Houwink constants for PS; K_θ and a , are known (*19*): $K_\theta = 7.3 \cdot 10^{-2}$ dl/g and $a_\theta = 0.5$. In the MEK:MeOH 89.3:10.7 eluent (which is close to the θ-eluent) the experimental calibration dependence for two columns with MPG 400 nm (Figure 1, curve 2) was obtained. Moreover, with the aid of K_θ, a_θ, constants K and a for good solvent (THF) $K = 6.8 \cdot 10^{-3}$ dl/g and a=0.766 (*19*) and the relationship

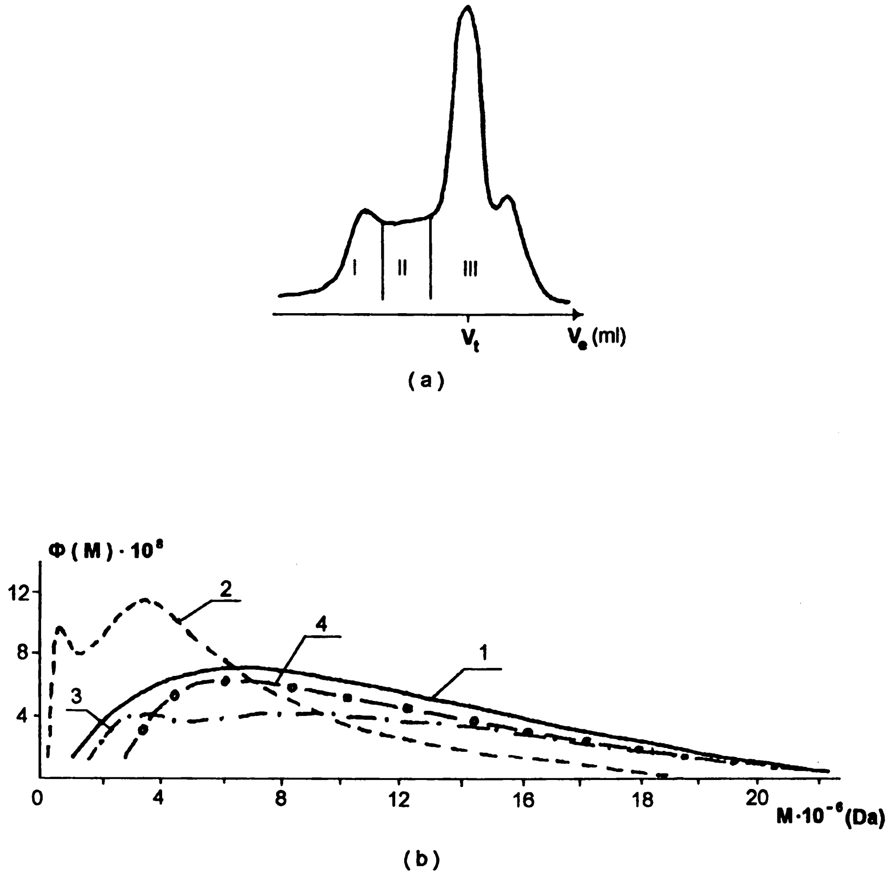

Figure 4. Chromatogram of a PS sample obtained on a Si-300 column at u=16 ml/h with fractions indicated (a). Overlapping MWD of fractions obtained under conditions corresponding to curve 1 in Figure 1: 1 - MWD of initial PS, 2 - MWD of fraction I, 3 - MWD of fraction II, 4 - MWD of fraction III (b). V_t - the total elution volume.

$$\log M_\theta = \frac{\log(K / K_\theta)}{a_\theta + 1} + \frac{a+1}{a_\theta + 1}\log M \qquad (3)$$

the hypothetical calibration dependence (Figure 1, curve 3) was calculated. Here $\log M_\theta$ and $\log M$ are related to the same elution volume for θ-solvent and good solvent (Figure 1, curve 1).

Figure 1 shows that experimental calibration in a poor solvent (curve 2) is displaced towards higher elution volumes in comparison with calibration in a good solvent (curve 1) but does not coincide with hypothetical calibration. The displacement towards higher elution volumes (for linear part of curve 2) can be explained by a decrease in the hydrodynamic size of the macromolecular coil in the poor solvent. Non-coincidence of curves 2 and 3 can be explained by incorrect values of Mark-Houwink constants which we used for the MEK:MeOH 89.3:10.7 eluent as if it were a θ-solvent (MEK:MeOH 88.7:11.3). However, the deviation from linearity of the calibration in the poor solvent in the range of $M > 4 \cdot 10^6$ Da cannot be explained by these reasons.

In order to elucidate this situation, the effect of the inferior eluent quality (obtained by adding MeOH to the MEK:MeOH mixture) on the separation of PS and THF was investigated. Figure 5 shows overlapping chromatograms of a PS sample and THF when the eluent quality became successively more and more inferior. It is clear that in this case resolution also becomes inferior, and very close to the θ-conditions (MEK:MeOH 88.9:11.1)the peaks of PS and THF virtually cannot be separated. It is clear that the reason for this is not a decrease in hydrodynamic dimensions of PS because even under θ-conditions the sizes of the molecules of THF and PS with $M_w = 10^7$ differ greatly.

Figure 6a shows overlapping chromatograms of a PS and THF mixture and an individual THF peak in an eluent of the most inferior thermodynamic quality (MEK:MeOH 88.9:11.1) at different elution rates. With increasing elution rate the separation of THF and PS seems to improve but a part of the polymer remains in the column, which can be clearly seen from a decrease in polymer peak contribution to the common (with THF) chromatogram. It is assumed that at a flow rate u = 5.8 ml/h the area under the PS+THF chromatogram corresponds to 100% yield, then at u = 9.3 ml/h the yield is 85%, at u = 18.7 ml/h it is 98% and at u = 69.6 ml/h it is 91%. In other words, polymer yield depends non-monotonically on the flow rate. During the experiment volume elution rates were measured directly, which made it possible to calculate exactly the retention volumes of PS and THF (Table II).For convenience elution volumes were calculated and compared according to the beginning of the appearance of the polymer peak V_b^{PS} and the THF peak V_b^{PS}. Table II shows that with increasing rate retention volumes decrease for PS and THF more or less to the same extent. The decrease in retention volumes of THF shows that a part of accessible pore volume is blocked by immobilized PS molecules. This blocking was irreversible: it was not possible to elute later the polymer from the columns even when a good solvent (THF) was pumped through them for a long time.

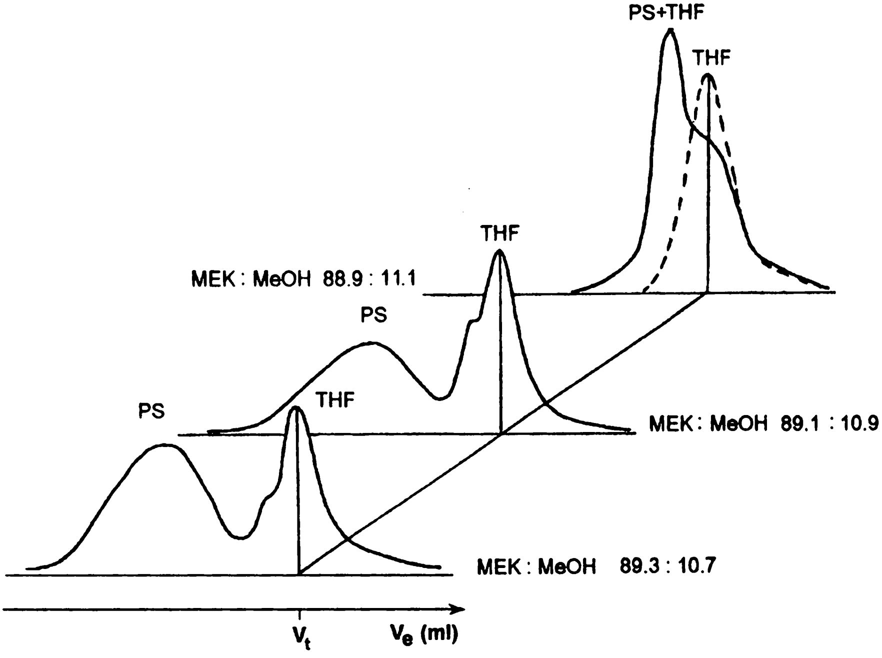

Figure 5. Retention volumes of PS and a low M reference solvent (THF) vs thermodynamic quality of the eluent. Two columns packed with MPG of 400 nm, flow rate 5.8 ml/h. V_t - the total elution volume.

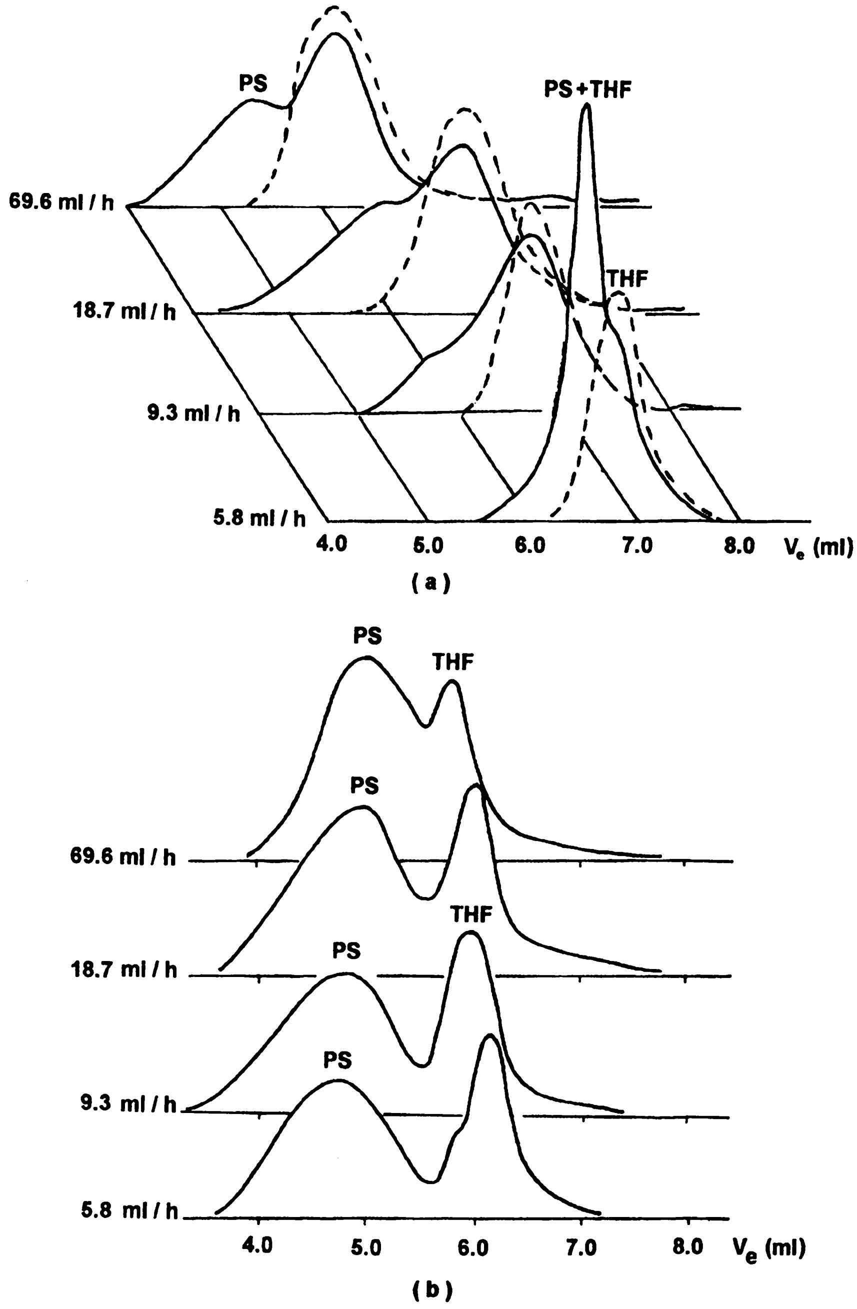

Figure 6. Chromatogram shape for a PS+THF mixture vs flow rate in (a) the eluent of the lowest quality MEK:MeOH 88.9:11.1 and (b) an eluent MEK:MeOH 89.3:10.7 . Two columns packed with MPG of 400 nm, sample concentration 0.03 g/dl. Broken line shows individual THF chromatography obtained under the same conditions.

Figure 6b shows overlapping PS chromatograms at different elution rates in a binary eluent of a better thermodynamic quality (MEK:MeOH 89.3:10.7) as compared to that in Figure 6a (MEK:MeOH 88.9:11.1). It is in this eluent that calibration dependence 2 in Figure 1 was obtained. Quantitative calculations of polymer yield carried out by analogy with Figure 6a show a similar picture, and the 120% polymer yield at a rate of 18.7 ml/h as compared to the assumed 100% yield at a minimum rate of 5.8 ml/h indicates that the polymer partly remains in columns at any elution rate. However, with improving solvent quality polymer yield increases. This fact is suggested by comparison of the areas under elution profiles at corresponding u in Figure 6a and Figure 6b. With increasing flow rate the transformation of the polymer part of the chromatogram in Figure 6b is mainly due to the displacement of the corresponding peak towards higher retention volumes.

Table II. Retention volumes of PS and THF in MEK:MeOH 88.9:11.1 vs elution rate on columns packed with MPG and glass balls

	u *ml/h*	V_b^{THF} *ml*	V_b^{PS} *ml*
MPG 400 nm	5.8	6.17	5.27
	9.3	5.93	4.88
	18.7	5.80	4.52
	37.1	5.59	4.38
	69.6	5.27	4.35
glass balls	3.8	1.45	1.34
	5.6	1.36	1.23
	9.2	1.35	1.20
	14.0	1.32	1.20
	18.5	1.29	1.18
	27.8	1.28	1.18
	36.8	1.25	1.18
	46.5	1.26	1.20

Similar experiments were also carried out on a column packed with glass balls in an eluent the quality of which is closest to that of the θ-solvent (MEK: MeOH 88.9:11.1). With increasing flow rate the separation of the THF and PS peaks decreases, but at all rates elution volumes of PS were smaller than those for THF. This is opposite to the situation observed in analogous experiments on the same columns in a good solvent (Figure 3a). The calculated values of retention volumes for PS and THF are also given in Table II. It is clear that with increasing rate retention volumes decrease, just as in the case of a porous sorbent. Moreover, they decrease almost to the same extent for PS and THF, which indicates that the polymer partly remains in the column.

The observed transformation of the polymer peak at different elution rates on different sorbents in a poor solvent can be due both to the retardation effect and to the degradation of some macromolecules. Degradation experiments in a poor solvent were performed according the scheme described above. It should be noted that the eluates obtained in poor solvent were concentrated and analyzed in THF on an analytical column system under conditions excluding degradation. Table III gives the corresponding degradation indices of some eluates calculated from the chromatograms. These indices obtained previously (Figure 2a) with THF are given for comparison. Table III shows that in chromatography on a porous sorbent in a θ-eluent PS-degradation is much higher than that in chromatography on non-porous balls. In THF the corresponding degradation values are comparable. Furthermore, in chromatography on a porous sorbent degradation is greater in a θ-eluent than in THF, whereas in chromatography on non-porous balls the opposite situation is observed.

Table III. Degradation indices of PS, obtained in chromatography in different eluents on columns packed with different sorbents at different elution rates

Sorbent	*u* *ml/h*	*Eluent*	*I*
MPG 400 nm	5.9	THF	0.02
	19.4	THF	1.30
	5.8	MEK:MeOH[a]	1.90
	18.7	MEK:MeOH	3.26
Glass balls	5.7	THF	0.32
	19.2	THF	1.47
	5.6	MEK:MeOH	0.24
	18.5	MEK:MeOH	0.66

[a] Composition of MEK:MeOH 88.9:11.1

Experiments with Membrane. In order to elucidate the details of degradation mechanism in SEC, model experiments were carried out by stirring PS solutions above the membranes with different pore sizes and a non-porous teflon support without excess pressure as well as by solution ultrafiltration at a low excess pressure.

Figure 7 shows the MWD of a PS sample obtained after stirring its solution above membranes with different pore sizes for two hours. It is clear that the MWD shape depends on membrane type. When the solvent is stirred above a membrane with a pore diameter of about 580 nm which is higher than the average size of the macromolecules (about 200 nm), the degree of degradation is highest. Both large fragments with $M \approx 5 \cdot 10^6$ and small fragments with $M \approx 2.5 \cdot 10^6$ and $M \leq 10^6$ (Figure 7, curve 2) are formed. When stirring is performed over a membrane with a pore diameter of about 110 nm, large fragments are not formed and the degree of degradation and the fraction of degraded macromolecules are much lower than in the former case (Figure 7, curve 3). For a teflon film (Figure 7, curve 4) the situation seems intermediate. It may be assumed that the defects on the surface of the film (the existence of which, just as a possible presence of through pores proven by measuring the mechanical and electrical film characteristics (*23*)) are of intermediate sizes with respect to membrane pores. Table IV lists degradation indices, average M, and polydispersities of the sample, which are calculated from MWD. It can be seen that for marked sample degradation considerable time (about 2h) is necessary.

Table IV. Calculated M characteristics and degradation indices of samples in membrane experiments without filtration

Sample	$M_w\cdot10^{-6}$ Da	$M_n\cdot10^{-6}$ Da	M_w/M_n	*Stirring time, h*	*Mean pore diameter, nm*	*I*
Initial PS	11.18	7.64	1.47			
After stirring above a teflon film	10.44	7.14	1.46	1	-	0.07
	8.54	6.04	1.42	2	-	0.27
After stirring above membranes	10.10	7.58	1.33	1	580	0.01
	7.72	4.19	1.84	2	580	0.82
	11.52	7.40	1.56	1	110	0.03
	10.99	6.89	1.60	2	110	0.11

The results of experiments on PS solution filtration through membranes with different pore sizes are given in Table V and Figure 8. It is clear that during filtration degradation increases with decreasing pore size, which is opposite to degradation effect occurring for stirring without filtration. For filtration through membranes with a pore diameter of 110 nm (smaller than the mean size of PS molecules) a large number of degraded macromolecules is observed both in the filtrate and in the concentrate (Table V). In this case some largest macromolecules were not degraded during filtration, which indicates that they can undergo deformation and pass through pores without degradation (Figure 8, curve 2). For membranes with a mean pore diameter of 580 nm, filtration does not lead to any degradation, although a considerable rate gradient exists: $0.7\cdot10^3\ s^{-1}$. In fact, in this case the MWD of the filtrate (Figure 8, curve 3) coincides with that of the initial PS. For membranes with a pore size of 238 nm, which is comparable to that of PS molequles, degradation indices have intermediate values (Table V).

Table V. Calculated molecular characteristics and degradation indices of samples in membrane experiments with filtration

Mean pore diameter, nm	*Pressure above the membrane, atm*	$M_w\cdot10^{-6}$ Da	$M_n\cdot10^{-6}$ Da	M_w/M_n	*I*	*Comments*
238	1.0	10.19	6.90	1.48	0.11	F[a]
238	1.0	9.31	5.94	1.57	0.29	C[b]
286	0.5	11.03	7.80	1.41	0.00	F
286	0.5	11.18	6.94	1.47	0.10	C
110	1.0	9.12	5.35	1.71	0.43	F
110	1.0	9.51	5.73	1.66	0.33	C

[a] Filtrate
[b] Concentrate

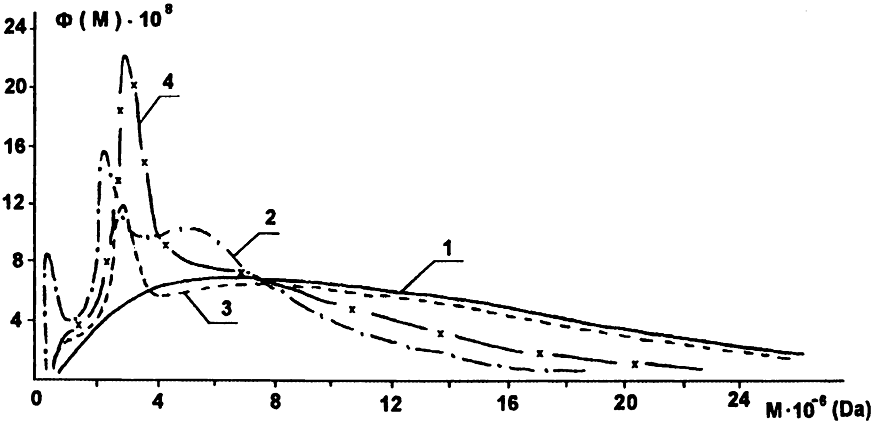

Figure 7. Comparative MWD of a PS sample, obtained after stirring for two hours above membranes with different pore sizes d. (1) - MWD of the initial PS, (2) - membrane d = 580 nm, (3) - membrane d = 110 nm, (4) - teflon film.

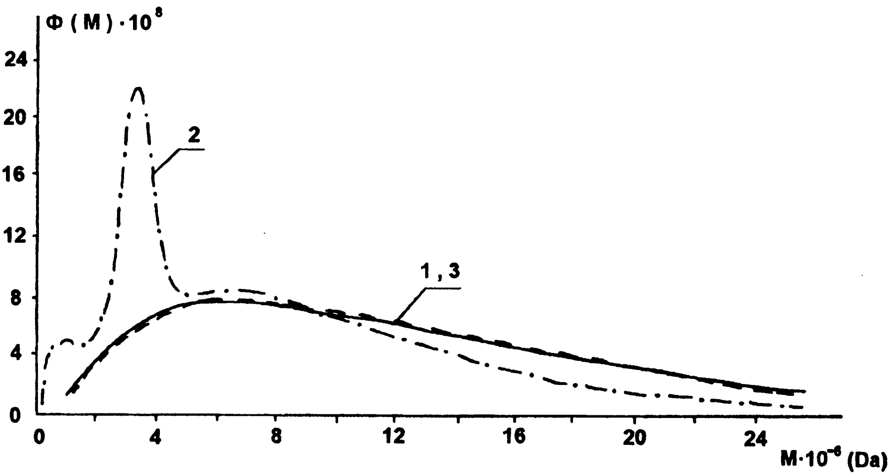

Figure 8. Comparative MWD of solution filtrates of a PS sample for membranes with different pore sizes. (1) - MWD of the initial PS, (2)- membrane d = 110 nm, (3) - membrane d = 286 nm.

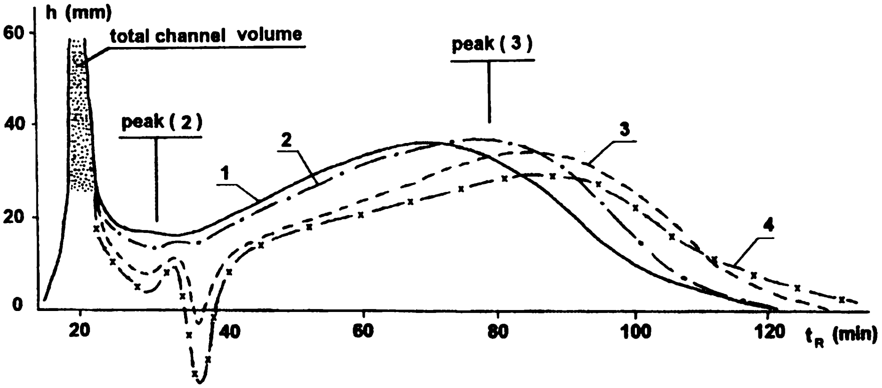

Figure 9. Overlapping fractograms of PS standard, $M_p=7.7\cdot10^6$ Da at different times of zone formation and v = 0.08 cm/s. (1)- τ = 0 min, (2)- τ = 2 min, (3)- τ = 10 min, (4)- τ = 20 min.

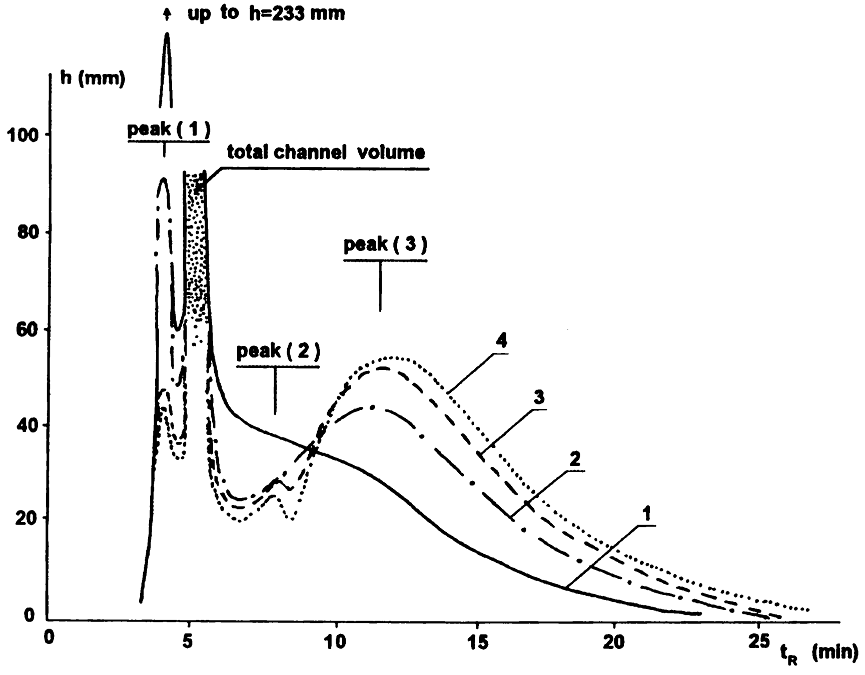

Figure 10. Overlapping fractograms of PS standards, $M_p=7.7\cdot10^6$ Da at different times of zone formation and v =0.4 cm/s. (1)- τ = 0 min,(2) - τ= 2 min, (3)- τ= 5 min, (4)- τ= 10 min.

Thermal Field Flow Fractionation. Finally, we have studied the behavior of a PS sample under TFFF conditions in connection with a unique possibility of applying this method to the determination of the MWD of synthetic polymer with $M > 2 \cdot 10^6$ Da (*24*). The experiments on TFFF may be regarded as a model for the behavior of macromolecules in the simpler variant of the shear field i.e. in flow with the Poiseuille profile of rate distribution between two parallel plates. The separation by the TFFF method (*16*) is based on the formation of a temperature gradient along the channel height. This gradient leads to non-selective thermal diffusion of macromolecules towards the cold wall (*25, 26*) and, hence, to their concentration at this wall. This separation is also based on the Brownian motion which results in the distribution of macromolecules along the channel height. As a result of the Poiseuille profile of flow rate distribution in the longitudinal direction, the smallest macromolecules will move in the channel at a higher rate, whereas the largest macromolecules will move at a minimum rate. At the moment when the zone leaves the channel, the macromolecules become distributed according to size. This distribution recorded by a concentration detector is called a fractogram. The minimum retention volume corresponds to the total volume of the TFFF channel (or TFFF column) determined from the retention volume of a low molecular weight substance (e.g. o-dichlorobenzene). The retention volume increases with the M of the corresponding fraction. It was found that for high molecular weight PS the minimum change in operating parameters (temperature of the cold, T_c, and hot, T_h, walls, linear elution rate v, and polymer concentration c) profoundly affects the shape of the fractograms and retention volumes. This has never been observed in the range of $M < 2 \cdot 10^6$ Da. The effect of operating parameters on the behavior of the superhigh molecular weight PS has been analyzed by us in detail (*27*) and has been confirmed by independent investigations (*28*).

It was shown in studying the effect of elution rate on elution volumes and the fractogram shapes at constant $T_h = 20°C$ and $T_c = 10°C$ for a PS standard with $M_p = 4.4 \cdot 10^6$ Da that with increasing v from 0.025 to 0.8 cm/s retention volumes decreased slightly but the fractogram shape did not change. For a PS standard with $M_p = 7.7 \cdot 10^6$ Da and higher and for the investigated PS sample the change in the rate from 0.04 cm/s to 0.8 cm/s leads to a change in the fractogram shape. Moreover, this change also depends on the time of zone formation near the cold wall τ, i.e. the time during which the eluent flow along the channel was stopped and the macromolecules were distributed along the channel height because of thermal diffusion and Brownian motion.

Overlapping fractograms of a PS standard with $M_p = 7.7 \cdot 10^6$ at different τ and elution rates of 0.08 and 0.4 cm/s are shown in Figures 9 and 10, respectively. It should be noted that at other rates from the same range of 0.04-0.8 cm/s the shape of the fractograms at different τ does not differ qualitatively from those shown in Figures 9, 10 for both the PS standard and the PS sample. Three peaks can be distinguished in Figure 10: (1) a polymer peak with a smaller retention volume than the total channel volume (the so-called "relaxation peak" (*29*)); (2) a peak

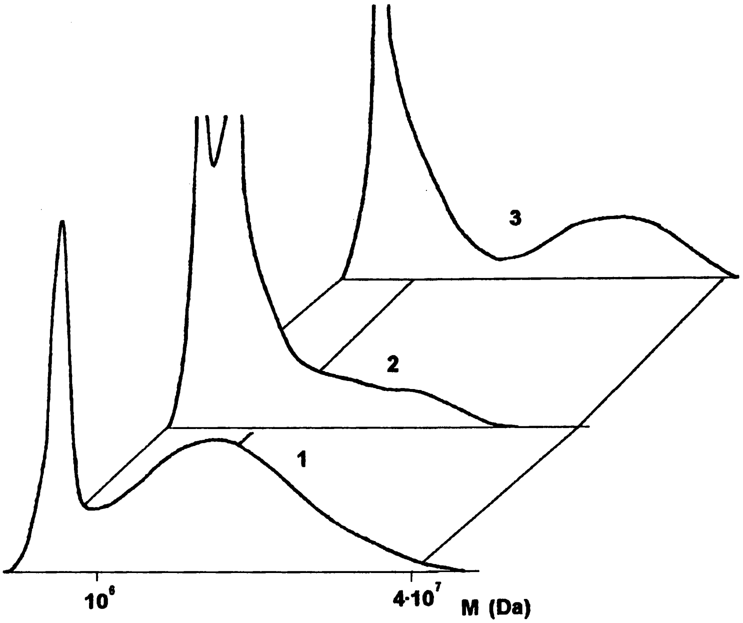

Figure 11. Combined fractograms of a PS sample at v=0.04 cm/s, τ = 0. (1)-initial fractogram, (2)- fractogram of an eluate obtained at v=0.04 cm/s, τ = 0, (3) fractogram of an eluate obtained at v=0.8 cm/s (τ = 10 min).

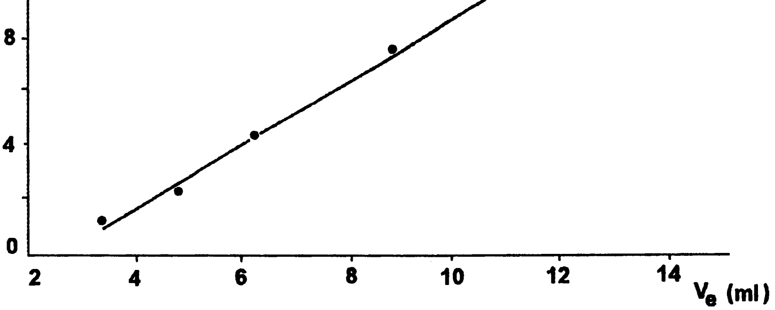

Figure 12. Calibration curve: peak value for narrow-disperse PS standards vs their retention volume at v=0.04 cm/s, τ = 0.

following the low molecular weight reference peak, and (3) the main polymer peak. At relatively low rates peak (1) can be absent at all τ values (Figure 9). In contrast, at relatively high rates and $\tau = 0$ only peak (1) is present, i.e. the whole sample is eluted at a retention volume smaller than the total channel volume. Our investigations have shown that the retention volumes of peak (1) and (2) remain constant at all rates and all τ. The retention volumes of polymer peak (3) increase with τ and decrease with increasing rate. Furthermore, the height of peak (1) increases with increasing rate and decreases with increasing τ.

In order to detect possible degradation during TFFF, the effect of flow rate v in the 0.04-0.8 cm/s range and zone formation time τ (at a constant temperature gradient $T_c = 10°C$, $T_h = 20°C$) were studied. At fixed v and τ the solution of PS sample with the concentration of 0.5 g/dl was injected and the eluate was collected at the outlet of the TFFF column and concentrated to c=0.05 g/dl. Then this concentrated eluate was analyzed on the TFFF column at the same temperature gradient, minimal flow rate (v=0.04 cm/s) and τ =0. These experimental conditions provided the possibility of obtaining linear calibration in the range of M $10^6 - 10^7$ Da and the absence of relaxation peaks. Figure 11 shows as an example three overlapping fractograms: (1) the primary fractogram of the PS sample at the minimal rate of 0.04 cm/s, $\tau = 0$; (2) the fractogram of the eluate obtained at v = 0.04 cm/s, $\tau = 0$; (3) the fractogram of the eluate obtained at v = 0.08 cm/s and τ = 10 min. All other eluate fractograms obtained by us at different v and τ, just as those shown in Figure 11, differ from the primary fractogram by the transformation of size distribution of macromolecules with increasing content of a fraction with M about 10^6 Da and less, which is absent in the primary fractogram. This situation indicates that polymer chains are degraded during fractionation.

In order to evaluate quantitatively the degree of degradation, the average M of PS were calculated from the fractograms of the eluates with the aid of a calibration dependence (Figure 12) obtained at the minimal rate of 0.04 cm/s ($\tau = 0$), i.e. with the use of primary fractograms of PS standards. The results of these calculations and also those of average M of the standards used and the PS sample from primary fractograms are given in Tables VI and VII.

These results provide only qualitative information because of the fact that partial degradation occurs even at minimal flow rate. Nevertheless comparative analysis is desirable.

The average M values given in Table VII and calculated with the fractograms of the eluates show that polymer chains undergo degradation, because only degradation can explain a decrease in the M_w and M_n and a increase in M_w/M_n as compared to the initial characteristics. Note that the calculated M values are even too high because fragments with $M < 10^6$ Da were not taken into account. The selectivity is absent in the range $M < 10^6$ Da and macromolecules with $M < 10^6$ Da are eluted with the total column volume (Figure 12). It is interesting that M does not decrease monotonically with increasing rate and, moreover, depends on τ. It is clear that with increasing elution rate degradation can also decrease as in the above chromatographic experiments. The data in Table VII show that degradation decreases with increasing τ at the same rates. The data calculated from fractograms also show higher average M for higher concentrations of the PS sample (Table VI).

Table VI. Average molecular characteristics calculated from initial fractograms of PS standards and of a PS sample

PS standards			
$M_p \cdot 10^{-6}$ Da	$M_w \cdot 10^{-6}$ Da	$M_n \cdot 10^{-6}$ Da	M_w / M_n
1.00	0.997	0.810	1.23
2.30	2.214	1.980	1.12
4.40	4.246	3.756	1.13
7.70	6.557	5.066	1.29
12.25	10.166	7.124	1.43
PS sample			
c *g/dl*	$M_w \cdot 10^{-6}$ Da	$M_n \cdot 10^{-6}$ Da	M_w / M_n
0.025	8.455	4.072	2.08
0.050	9.665	5.639	1.71

Table VII. Average molecular characteristics calculated from eluate fractograms of a PS sample obtained at different elution rates (v) and different times of zone formation (τ)

v *cm/s*	τ *min*	$M_w \cdot 10^{-6}$ Da	$M_n \cdot 10^{-6}$ Da	M_w / M_n
0.04	0	6.555	3.115	2.10
0.08	0	5.880	1.583	3.72
0.20	2	8.654	2.282	3.79
0.20	10	9.101	2.437	3.73
0.80	2	6.303	2.018	3.12
0.80	10	13.642	3.877	3.52

Physical Degradation Model . In order to explain all these complex and at first sight contradictory data, one should bear in mind the results of the works in which the behavior of macromolecules in non-homogeneous hydrodynamic fields of the Couette and Poiseuille types has been studied.

For both type of fields it has been shown in experiments and theoretically (*30-36*), that the concentration of macromolecules is redistributed as a result of their migration under the effect of shear transverse to the flow lines to the curvature center in the Couette field (in particular, to the internal rotating cylinder in the Couette viscometer) and to the capillary center in the Poiseuille field. The redistribution of polymer concentration due to circular and capillary flows should occur in streams through disperse media formed by both porous and non-porous particles as is supported by the results of a number of papers (*37-39*). In particular, it has been shown in the study of polymer solution flow through the porous packing of chromatographic columns (*39*) that polymer retention increases with increasing flow rate and decreases in the opposite case. Retention also increases with M. The effect of this change in retention was attributed by the authors of (*39*) to concentration redistribution of the macromolecules caused by the migration to the surface of sorbent particles in the eluent flow moving past a sorbent particle (circular flow). On the basis of the analyses of published theoretical and experimental works and our experimental data we attempt to formulate the degradation mechanism in SEC.

This mechanism is based on the distortion of the concentration homogeneity of the macromolecules inside the chromatographic column. This distortion is caused by the action of a non-homogeneous hydrodynamic field. In the flow moving past a sorbent particle (circular flow) the macromolecules migrate to its surface. If the pores size is sufficiently large, the macromolecules pass through them (*40-42*) without undergoing degradation. When steric hindrance exists (small pores), the macromolecules are concentrated near their surface forming an entangled matrix which is retained on this surface partially penetrating into the pores (*43*). Giddings (*4*) has pointed out that macromolecules can concentrate near the particle surface and has called this phenomenon the "polarizing effect". In this case the greater the concentration of macromolecules near the surface, the easier can entangled matrix penetrate into the pores to a large depth (*43*). Hence, with increasing steric hindrance the concentration near the surface of sorbent particles increases, the matrix penetrates into the particle to a greater depths, and the retention of the matrix on the surface increases and becomes even more pronounced when the through-pore flow exists. The flow moving past the particle tries to drag the matrix from its surface. Degradation can evidently proceed both at the outer boundary of the entangled layer because the free ends of macromolecules are entrained by the flow and at the inner boundary because the layer is torn off as a whole. After the entangled matrix is torn off from the surface, the macromolecules are disentangled at once. Subsequently, the migration and degradation process is repeated many times along the length of the packed layer until all the macromolecules capable of participating in this process under these condition are degraded. This mechanism explains the retardation effect and also the increasing degree of degradation with decreasing pore and particle size and increasing M. It becomes clear that the degree of degradation is in agreement with thermodynamic chain flexibility (*5*). In fact, the higher the flexibility, the easier it is for the macromolecules to become entangled, the smaller is the distance between the network junctions and, hence, the stronger the retardation effect (*43*). It is known that rigid macromolecules do not undergo degradation. Degradation mechanism in the most complex case, SEC, is schematically shown in Figure 13.

From the viewpoint of the proposed mechanism the results of polymer degradation in model units (Couette viscometer) can be regarded in a new way. It is claimed that in these units individual macromolecules are degraded by stretching in the shear flow (*4,5,7,8,12,22*). According to our mechanism, the macromolecules

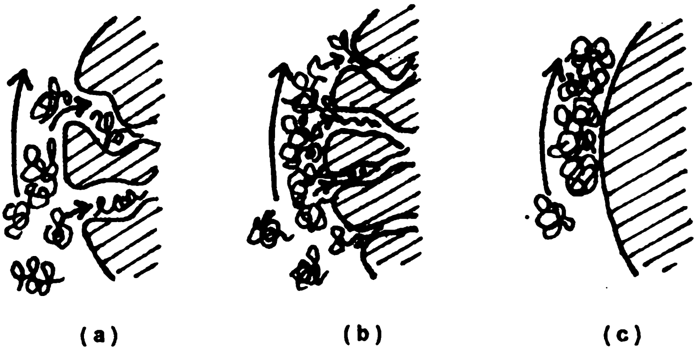

Figure 13. Scheme for the degradation mechanism of macromolecules on a sorbent with different pore sizes: (a)-pore size exceeding that of macromolecules, (b)-pore size smaller than that of macromolecules, and (c)- non-porous sorbent.

are not individually degraded but degradation occurs in the entangled layer which is formed as a result of their migration to the inner rotating cylinder. It is desirable to establish whether under given experimental conditions the macromolecules can pass the distance between two coaxial cylinders during the time necessary for establishing equilibrium in this degradation experiment in a Couette viscometer. According to (*30*), the average migration rate $\bar{v}$ of the non-draining coil transverse to flow lines in the Couette field is given by

$$\bar{v} = -0.00563\Omega^2 R_1 R_2 \frac{R_2^3 - R_1^3}{(R_2^2 - R_1^2)^3} \frac{\eta < s^2 >^{5/2}}{kT} \tag{4}$$

here Ω is the angular rotation velocity, R_1 and R_2 are the radii of the inner and outer cylinders, respectively, η is the solvent viscosity, $k = 1.38 \cdot 10^{-23}$ JK is the Boltzmann, constant, T is the temperature, $< s^2 >^{1/2}$ is the mean-square end-to-end distance $< s^2 >^{1/2} = (KM^{\alpha+1})^{1/3} \Phi^{-1/3}$, where K and α are constants in the Mark-Houwink equation, and $\Phi = 2.5 \cdot 10^{21}$ is the Flory constant.

In experiment with PS solutions with $M_\eta = 10.7 \cdot 10^6$ Da (*22*) the values of parameters in eq. (4) were: R_1=0.236cm, R_2=0.238cm, T=300 K, η=10^{-7} Ns/cm^2, and the shear rate $\gamma = 4.4 \cdot 10^6$ s^{-1}. The calculation gives $\bar{v} = -3.29 \cdot 10^{-2}$ cm/s and the mean migration time is $\bar{t} = 6.1 \cdot 10^{-2}$ s. The experimental time (rotation of the inner cylinder) was 1-2 s. In a similar way the values of $\bar{v}$ and $\bar{t}$ can be calculated for an experiment with aqueous solutions of polyacrylamides with $M_\eta = 5 \cdot 10^6$ (*5*) and $M_\eta = 4.6 \cdot 10^6$ (*12*) carried out during 60 s. The calculated values were $\bar{v} = -3.17 \cdot 10^{-4}$ cm/s, $\bar{t} = 8$ s and $\bar{v} = -4.3 \cdot 10^{-4}$ cm/s, $\bar{t} = 5.8$ s, respectively.

The calculations show that during experiment the macromolecules with a relatively high M can reach the surface of the inner cylinder and form the entangled matrix along its perimeter. Hence, the results of experiments on degradation in a Couette viscometer can be easily explained on the basis of the proposed mechanism. In fact, shear stress is the parameter determining the degree of degradation in these experiments, and it follows from eq. (4) that $\bar{v}$ is proportional to $\Omega^2\eta$. The existence of a critical M value under these experimental conditions follows from the dependence of $\bar{v}$ on $< s^2 >^{5/2}$ in eq. (4). With the aid of this mechanism it is easy to explain the decrease in degradation with increasing initial concentration. The higher the initial concentration, the greater the thickness of the layer near the surface. Therefore, the relative number of degraded macromolecules at the boundaries of this layer will be smaller for a thicker layer and, hence, for higher initial solution concentration. Degradation will naturally also depend on the properties of the retarding surface and will be higher if cylinders with rough surfaces are used (*22*).

According to our mechanism, degradation should depend on the density of the entangled layer. At low shear rates the layer is looser, the distance between the entanglement junctions is relatively large, and the chain can be broken near the center. At high shear rates a denser layer is formed during the same period, the inter-junctions distance decreases, which leads to the formation of small fragments during degradation. The layer density is also affected by solvent quality: at inferior quality the layer becomes dense, and the inter-junction distance decreases. However, for dilute solutions with inferior solvent quality the size of macromolecules decreases. Therefore, $\bar{v}$ also decreases and, hence, with a simultaneous change in shear rate and solvent quality degradation can change in different directions. Thus, it may be assumed that at low shear rates degradation can decrease when solvent quality becomes inferior. In the limiting case, when a solvent close to the θ-solvent is used, the concentration layer can become very dense and non-draining for the solvent, which can also lead to decreasing degradation.

Let us now consider the results of our experiments from the viewpoint of the degradation mechanism.

In the experiments on TFFF the formation of the entangled matrix near the cold wall is determined by the diffusion of macromolecules caused by temperature gradient along the channel height. The thickness and density of the entangled layer depend on experimental conditions (T, c, t,v). The concentration layer is fixed on the surface of the cold plate, and the longitudinal flow leads to the degradation of macromolecules at the boundaries of this layer. This layer is a macroscopic formation and, therefore, when transverse scratches were made on the cold wall, i.e. surface roughness increased, an increase in retention volumes of the fractograms was observed (*44*). Individual macromolecules would not be sensitive to these scratches. Being macroscopic, the concentration layer is not immobile but interacts with the flow. In addition to friction force holding it on the surface of the cold plate, it is subjected to a force that tends to displace it to the region of minimum deformation (to channel center) (*36*). The predominance of the latter force (e.g. owing to increasing elution rate) can lead to the tearing off of the entangled layer from the cold wall, chain disentanglement, and, correspondingly, to a decrease in degradation with increasing v observed in the experiment with the invariability of other operating parameters. The presence of relaxation peaks in the fractograms at relatively high elution rates is an evident confirmation of the fact that macromolecules migrate to the zero rate gradient (i.e. to the channel center), as has been pointed out first by Giddings (*45*).

The processes occurring in TFFF represent adequately the situation in chromatographic columns. Just as in TFFF, the non-monotonic character of the dependence of degradation indices on flow rate in SEC is due to two competing processes taking place in packing. This is the migration of macromolecules to particle surface (as a result of the curvature of the flow moving past this particle) and to zero flow rate gradient, i.e. to the center of interparticle channels (capillaries). The situation is complicated by the possible occurrence of the pore flow (*40-42*). Degradation may be absent either when the macromolecules pass through pores without forming concentration layer or when migration from particle surface prevails at relatively high flow rates. The latter is indirectly confirmed by calculations and rheological experiments (*46,47*).

Now the results of SEC in solvents of different thermodynamic qualities will be considered.

In an eluent of good thermodynamic quality the concentration layer can be draining for the solvent, which favors complete elution of the polymer from columns. If the pores are relatively large, the possibility of layer formation and, hence, of degradation also decreases. The presence of pores the size of which is comparable to that of the macromolecules and, particularly, of those with a smaller size, enhances degradation. On a non-porous surface the formation of the concentration layer leads to the retardation effect (Figure 4). However, the degrading effect of the retarding non-porous surface at comparable elution rates is always lower than that of the porous surface and, correspondingly, degradation is lower.

At inferior solvent quality the macromolecules acquire the shape of a dense coil, lose their ability to change conformations and tend to form associates (*13*). In this case also the concentration layer on the particle surface is partially degraded because it is influenced by the flow moving past the sorbent particles, by the degrading effect of the surface and also because of the possible pore - through flow. However, because of conformation hindrance the torn-off part of the layer is not disentangled and moves in the form of associates. This fact evidently demonstrate calibration dependence (Figure 1, curve 2).

Approaching the θ-conditions the layer on the surface of sorbent particles becomes non-draining, and as a result, in particular, some pores are plugged by the fragments of this layer (Figure 6) and, hence, the loss of the accessible volume for PS and for low M components is the same (Table II). Because of conformation hindrance the fragments of the destroyed layer should be of the sizes comparable to those of pores the diffusion in which has led to degradation. Therefore, in this solvent degradation should occur by analogy with that in a good solvent with the existence of steric hindrance. Hence, degradation on a porous sorbent in a poor solvent is greater than on non-porous balls and is greater than in a good solvent on the same porous sorbent (Table III).

When polymer solutions are stirred, inhomogeneous hydrodynamic fields are also formed, which should lead to concentration distribution. At present it is not possible to describe theoretically the distribution of shear rates in these fields. The results of degradation upon PS solution stirring above membranes with different pore sizes show that a high concentration layer is formed near the membrane surface. A special experiment on dye stirring for two hours with subsequent filtration at a low excess pressure showed (Figure 14) that the range of predominated concentration exists in the central part of the membrane (membrane is not uniformly colored in the photograph). Consequently, according to the mechanism proposed by us, steric hindrance for macromolecules at the pore entrances not only favors the formation of an entangled matrix but also increases the retarding properties of the surface at an excess pressure and decreases these properties when stirring occurs without filtration. In the former case this leads to increasing degradation indices with decreasing pore size, whereas in the latter case the decrease in the pore sizes leads to decreasing degradation indices (Table IV).

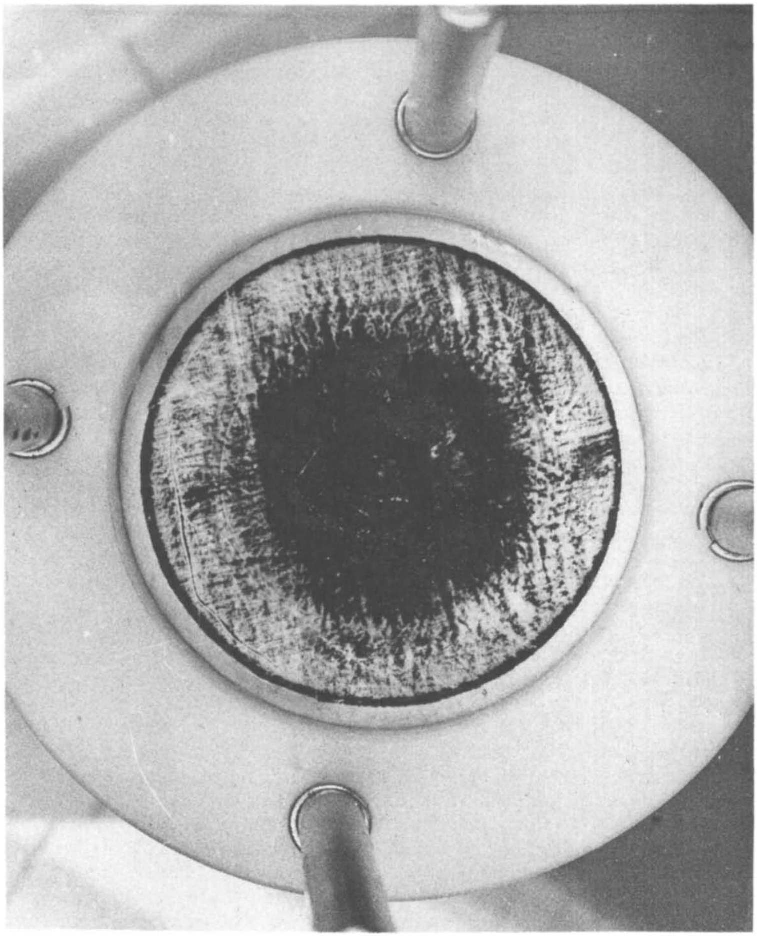

Figure 14. Membrane photograph after the dye suspension was stirred for 2h and then was filtered through it.

Conclusions

The mechanism of degradation of macromolecules in a non-homogeneous hydrodynamic field is proposed. It is based on the distortion of homogeneous concentration in the bulk of polymer solution because macromolecules undergo directed migration transverse to flow lines. As a result a layer of high concentration is formed near the surface, and phase transition (precipitation of polymer) can occur. Degradation depends on both the properties of the retarding surface and the rate of the flow which tends to tear off this layer. The entangled layer is formed by the macromolecules of such a size that under these experimental conditions they can reach the surface during the experimental time. The ability of macromolecules to be entangled depends on the chain thermodynamic flexibility and the critical entanglement length of this type of macromolecules, but we did not discuss in the article this problem in detail.

The proposed mechanism explains all the known results on degradation, the concentration, and rate dependences of the distribution coefficient in SEC, and some anomalous rheological effects (in particular, the decrease in viscosity of polymer solutions with increasing flow rate in narrow capillaries, which is evidently connected with migration of macromolecules to the capillary center). In other words this mechanism is universal and is an inherent part of the separation mechanism occurring during SEC.

Literature Cited.

1. Frenkel, J. *Acta Physicochimica*, U.R.S.S. **1944**, *vol*.19, p.51.
2. Bueche ,F. *J. Appl. Polym. Sci*.**1960**, *vol*.4, p.101.
3. Porter, R.S.; Casale A. *Polym. Eng. Sci*. **1985**, *vol*.25, p.129.
4. Giddings, J.C. *Advances in Chromatography*. **1982**, *vol*.20, p.217.
5. Abdel-Alim, A.H. Hamielec, A.E. *J.Appl. Polym. Sci*. **1973**, *vol*.17,. p.3769.
6. Muller, H.G.; Klein, J. *Makromol. Chem*., Rapid Commun. **1980**, *vol*.1, p.27.
7. Yu, J.F.S.; Zakin, J.L.; Patterson, G.K. *J. Appl. Polym. Sci*. **1979**, *vol*.23, p.2493.
8. Hunston, D.L.; Zakin, J.L. *Polym. Eng. Sci*. **1980**, *vol*.20, p.517.
9. Farinato, R.S.; Yen, W.S. *J. Appl. Polym. Sci*. **1987**, *vol*.33, p.2353.
10. Tabata, M.; Hosokava, Y.; Watanabe, O.; Sohma, J. *Polym. J*. **1986**, *vol*.18, p.699.
11. Merrill, E.W.; Leopairat, P. *Polym. Eng. Sci*. **1980**, *vol*.20, p.505.
12. Basedov, A.M.; Ebert, K.H.; Hunger, H. *Makromol. Chem*. **1979**, *vol*.180, p.411.
13. Graessly, W.W. *Advances in Polymer Sci*. **1974**, *vol*.16.
14. He, T. *Makromol. Chem*. **1987**, *vol*.188, p.2489.
15. McIntyre, D.; Shih, A.L.; Seeger, R.; MacArthur, A. *Size Exclusion Chromatography*, ACS Symposium Series, *vol*.245, p.227. American Chem. Soc., Washington, D.C. **1984**.
16. Giddings, J.C.; Martin, M.; Myers,M.N. *J. Chromatogr*. **1978**, *vol*.158, p.419.

17. Chubarova, E.V.; Nesterov, V.V. *J. Liquid Chromatogr.* **1990**, *vol*.13, p.1825.
18. Cheng, W.; Hollis, D. *J. Chromatogr.* **1987**, *vol*.40, p.9.
19. Soltes, L.; Berek, D.; Mikulasova, D. *Colloid and Polym. Sci.* **1980**, *vol*.258, p.702.
20. Nesterov, V.V.; Chubarova, E.V.; Belenkii, B.G. *Visokomolekularnye Soedinenia*. (Russia). **1984**, *vol*.26, p.864.
21. Nesterov, V.V.; Chubarova, E.V.; Belenkii, B.G. *Visomolekularnye Soedinenia*. (Russia). **1989**, *vol*.31, p.653.
22. Harrington, R.E.; Zimm, B.H. *J. Phys. Chemistry*. **1965**, *vol*.69, p.161.
23. Pugachev,A.K.; Rosliakov, R.A. In :*Processing of teflons*. L., Chimia (Russia). **1987**, p.47.
24. Gao, Y.S.; Caldwell, K.D.; Myers, M.N.; Giddings J.C. *Macromolecules*. **1985**, *vol*.18,p.1272.
25. Giddings, J.C.; Caldwell, K.D.; Myers, M.N. *Macromolecules*. **1976**, *vol*.9, p.106.
26. Bromhall, S.L.; Myers, M.N.; Caldwell, K.D.; Giddings, J.C. *J. Polym. Sci.*: Polym. Phys. Ed. **1985**, *vol*.23, p.2343.
27. Nesterov, V.V.; Chubarova, E.V. Conference, "*Chromatography of polymers and related materials*" .Czekoslovakia, Bratislava. **1991**, L16.
28. Janca, J.; Martin, M. *Chromatographia*. **1992**, *vol*.34, p.125.
29. Janca, J.; Chmelic, J.; Pribulova, D. *J. Liquid Chromatogr.* **1985**, *vol*.8, p.2343.
30. Shafer, R.H.; Laiken, N.; Zimm, B.H. *Biophys. Chem.* **1974**, *vol*.2, p.180.
31. Shafer, R.H. *Biophys. Chem.* **1974**, *vol*.2, p.185.
32. Dill, K.A. *Biophys. Chem.* **1974**, *vol*.10, p.327.
33. Aubert, J.H.; Tirrell, M. *J. Chem. Phys.* **1980**, *vol*.72, p.2694.
34. Sekhon, G.; Armstrong, R.C.; Jhon, M. *J. Polym. Sci.*: Polym. Phys. Ed. **1982**, *vol*.20, p.947.
35. Dill, K.A.; Zimm, B.H. *Nucleic Acids Research*. **1979**, *vol*.7, p.735.
36. Tirrell, M.; Malone, M.F. *J. Polym. Sci.*: Polym. Phys. Ed. **1977**, *vol*.15, p.1569.
37. Kozicki, W.; Hsu, C.J.; Tiu, C. *Chem. Eng. Sci.* **1967**, *vol*.22, p.487.
38. Barboza, M.; Rangel, C.; Mena, B. *J. Rheology*. **1979**, *vol*.23, p.281.
39. Aubert, J.H.; Tirrell, M. *Rheol. Acta*. **1980**, *vol*.19, p.452.
40. DiMarzio, E.A.; Guttman, C.M. *Macromolecules*. **1970**, *vol*.3, p.131.
41. Guttman, C.M.; DiMarzio, E.A. *Macromolecules*. **1970**, *vol*.3, p.681.
42. Afeyan, N.B.; Gordon, N.F.; Mazsaroff, I.; Varady, L.; Fulton, S.P.; Yang, Y.B.; Regnier, F.R. *J. Chromatogr.* **1990**, *vol*.519, p.1.
43. Daoudi, S.; Brochard, F. *Macromolecules*. **1978**, *vol*.11, p.751.
44. Giddings, J.C.; Smith, L.K.; Myers, M.N. *Sep. Sci. Technology*. **1978**, *vol*.13, p.367.
45. Giddings, J.C.; Li, S.; Williams, P.S.; Schimpf, M.E. *Makromol. Chem.*: Rapid commun. **1988**, *vol*.9, p.817.
46. Sheffield, R.E.; Metzner, A.B. *AIChE J.* **1976**, *vol*.22, p.736.
47. James, D.F.; McLaren, D.R. *J. Fluid Mech.* **1975**, *vol*.70, p.733.

Chapter 9

Intraparticle Convection in Chromatographic Permeable Packings

Alirio E. Rodrigues

Laboratory of Separation and Reaction Engineering, Faculdade de Engenharia, Universidade do Porto, 4099 Porto Codex, Portugal

Downloaded by UNIV OF GUELPH LIBRARY on October 8, 2012 | http://pubs.acs.org
Publication Date: May 30, 1996 | doi: 10.1021/bk-1996-0635.ch009

Permeable, "large-pore" materials are finding various applications in separation engineering as adsorbents, HPLC packings, and membranes. Intraparticle forced convection is a mass transport mechanism which, in addition to diffusive transport, can not be neglected in large-pore materials. The paper provides an historical retrospective of research work in intraparticle forced convection, stressing important and often forgotten contributions. The key concept to be retained is the "augmented" diffusivity by convection (Rodrigues *et al.*, 1982) which explains why the efficiency of adsorptive separation processes is improved when using large-pore supports. An extended Van Deemter equation has to be applied when calculating the HETP of chromatographic columns with flow-through particles. It is shown that the effect of forced convective flow in pores is to drive the separation performance between diffusion-controlled and equilibrium limits. Experimental results for protein separation by high pressure liquid chromatography in new packing media POROS Q/M and Q HYPER D are discussed.

"Large-pore" permeable materials are used in chemical engineering as adsorbents, HPLC packings, membranes, catalysts, building materials or supports for biomass growth and cell culture. Here we mean by "large-pores" those above 1000 Å. A review of materials and processes used in separation engineering applications is shown in Table 1. Examples in this table include polystyrene materials for HPLC like PL4000 with pore diameter of 4000 Å or POROS with pores of 7000 Å in diameter, BM329 (Rhone-Poulenc catalyst) with pores of 10000 Å or VERAX VX-100 beads with pores in the range of 20-40 μm.

The objectives of this review paper are:

i) to provide an historical retrospective of research work on intraparticle forced convection stressing important and often forgotten contributions;

ii) to discuss the concept of "augmented" diffusivity by convection and show how it explains the improved performance of separation processes;

iii) to stress that an extended Van Deemter equation is needed when calculating the performance (HETP) of chromatographic processes using large-pore materials;

0097–6156/96/0635–0157$15.00/0

In Strategies in Size Exclusion Chromatography; Potschka, M., et al.;
ACS Symposium Series; American Chemical Society: Washington, DC, 1996.

iv) to focus on recent areas of application of permeable packings in proteins separation and suggest avenues for future work.

Table 1. Applications of "large-pore" materials in chemical engineering

Materials	Processes	References
Catalysts /Supports		
α-alumina	Ethylene oxidation	*(1)*
Vanadium and phosphorus oxides (Rhone Poulenc BM329)	Butene oxidation to maleic anhydride	*(2)*
Mixture of iron and other oxides	Ammonia synthesis	*(3), (4)*
Ni/α-alumina	Steam-reforming	
Adsorbents		
Activated alumina (Selexsorb; Alcoa)	Removal of carbonyl disulfide from propylene	*(5)*
Diatomite (Johns Manville)	Chromatography	
HPLC packings		
Alumina (Unisphere, Biotage, USA)	Proteins separation	*(6)*
Polystyrene (PL4000, Polymer Laboratories, UK)	Proteins separation	*(7)*
Polystyrene (POROS, PerSeptive Biosystems, USA)	Proteins separation	*(8), (9)*
Silica gel (Daisogel SP 2705, Daiso Co)		
Hyper D (BioSepra, USA)	Proteins separation	*(10), (11), (12), (13)*
TSK- PW (Toso-Haas, Japan)	Proteins separation	*(44)*
Ceramic membranes		
Alumina (Ceraflo, Norton, UK)	Product concentration/ clarification	
Supports for mammalian cell culture		
Collagen particles (Verax VX100, Verax Corp, USA)	TPA from culture of Chinese hamster ovary cells	*(14), (15)*
Gelatin particles (Cultisphere-G; Percell Biolytica, Sweden)		
Supports for Biomass Growth		
Sintered glass (SIRAN, Schott Engineering, Germany)	Anaerobic digestion	*(16)*
Modified polyurethane (Bayer, Germany)	Anaerobic treatment of bleaching plant wastewater	*(17)*
Recycled glass (PORAVER, Dennert Poraver, Germany)	Cell immobilization for lactic acid production	*(18)*

Downloaded by UNIV OF GUELPH LIBRARY on October 8, 2012 | http://pubs.acs.org
Publication Date: May 30, 1996 | doi: 10.1021/bk-1996-0635.ch009

Historical Background

The need for large-pores for mass transport associated with diffusive (small) pores has been already recognized in the patent literature in relation with catalyst preparation for reaction engineering applications *(3,4)*. In "large-pore" materials intraparticle forced convection is a mechanism of mass transport which can not be neglected. Ahlborn Wheeler *(19)* claims that intraparticle convection will only be important for large-pores 10000 Å or high-pressure (100 atm) gas phase reactions. This remarkable paper provides order of magnitude analysis and the equation for intraparticle forced convection, diffusion and reaction in isothermal pellets at steady-state. His parameter **b** (after making the equation dimensionless) is really the intraparticle mass Peclet number λ which relates the intraparticle convective velocity and diffusion clearly defined later by Nir and Pismen *(20)*. Unfortunately, Wheeler did not solve the model equation and so he missed the point later recognized by Nir and Pismen, i.e., the enhancement of catalyst effectiveness by intraparticle forced convection in the intermediate range of Thiele modulus. The message to be learned here is that intuition, although important, is not enough.

Komiyama and Inoue *(21)* solved the problem of intraparticle convection, diffusion, and first order reaction in a finite cylinder parallel to flow; the parameter relating intraparticle convection and diffusion is called in that paper PeB. The theory was tested with an ion exchange reaction H^+/K^+ in a Dowex-50 ion exchange resin; spherical pellets of 11 mm in diameter were made by wrapping in nylon fabric resin beads of 1 mm diameter so intraparticle convection between the beads could be important. This important paper provides guidelines to estimate intraparticle convective velocity. Some experimental results were reported under reactive conditions *(22,23)*.

The effect of intraparticle forced convective flow (viscous flow or Poiseuille flow) due to a total pressure gradient was noticed when measuring effective diffusivities by chromatographic techniques *(2)*. The analysis of experimental results was first made with the conventional model ("simplified" model) which includes diffusion of tracer inside pores (in fact an "apparent" diffusivity lumping the "true" diffusivity and convection).The "apparent" effective diffusivity obtained was found to increase with the flowrate. The enhancement of diffusivity by convection was termed "augmented" diffusivity as explained by Rodrigues *et al.(2)*. For inert tracers a simple relation between the "apparent" effective diffusivity, the "true" effective diffusivity and the intraparticle mass Peclet number was presented.

The enhancement of the effective diffusivity by convection is the key to understand recent progress in improving adsorptive separation processes, e.g., high-pressure liquid chromatography by using large-pore (gigaporous in Horvath's nomenclature, *24*) packings for protein separations *(6-8,24-26)*. The classic Van Deemter analysis of column performance is based on the concept of height equivalent to a theoretical plate (HETP). The HETP versus superficial (eluent) velocity in HPLC is a straight line in most of the domain when conventional supports are used; however, the use of large-pores reduces HETP and the curve goes to a plateau as the velocity increases. As a consequence the column efficiency and the speed of separation are enhanced by intraparticle convection.

A literature survey on intraparticle forced convection in various fields of separation engineering is summarized in Table 2.

The Concept of "Augmented" Diffusivity by Convection.

There are three ways of eliminating or reducing mass transfer resistance inside particles (Figure 1): i) coating a nonporous support with an active species as it is done in pellicular packings but which have the disadvantage of low capacity; ii) reducing the

Downloaded by UNIV OF GUELPH LIBRARY on October 8, 2012 | http://pubs.acs.org
Publication Date: May 30, 1996 | doi: 10.1021/bk-1996-0635.ch009

Downloaded by UNIV OF GUELPH LIBRARY on October 8, 2012 | http://pubs.acs.org
Publication Date: May 30, 1996 | doi: 10.1021/bk-1996-0635.ch009

particle size so as to decrease the diffusion time constant; iii) increasing particle permeability by carefully providing large pores for transport connected to smaller diffusive pores.

New packing materials for chromatographic separation of proteins have been developed in the last decade and can be classified in several groups *(10):* a) homogeneous cross-linked polysaccharides, b) macroporous polymers based on synthetic polymers, c) tentacular sorbents and d) materials based on the concept of "soft gel in a rigid shell". The first group include particles such as agarose which have good capacity. The second group of packing is used in "perfusion chromatography" *(38-40)* whose high speed is possible because of the augmented diffusivity by intraparticle convection. Chromatographic media as POROS Q/M have "throughpores" with diameter of 6000-8000 Å and short diffusive pores of mean diameter 500-1000Å. This combination allows proteins to enter more readily into the diffusive pores. "Perfusion chromatography" allows better column efficiency and higher separation speed than with conventional packings.

The materials in the group c) are designed in such way that interaction between proteins to be separated and interactive groups is faster. Finally materials in group d) are developed in order to combine good sorption capacity of soft gels and rigidity of composite materials. Materials of this group are marketed under the name of Hyper D media (BioSepra, Villeneuve la Garenne, France).

The use of large-pore, permeable particles has been increasing recently in relation with proteins separation by high pressure liquid chromatography (HPLC). The key concept behind the improved performance of flow-through packings is that of *intraparticle diffusivity augmented by convection* inside transport pores as shown by Rodrigues *et al. (2)*. In fact, the augmented diffusivity $\tilde{D}_e$ is related with the effective diffusivity D_e by :

$$\tilde{D}_e = D_e \frac{1}{f(\lambda)} \qquad [1]$$

Table 2. Literature Survey on Intraparticle Forced Convection

Measurenment of effective diffusivities in large-pore materials		
Material	**Technique**	**References**
Rhone Poulenc BM329 catalyst	Chromatographic method	(2)
α-Alumina	Chromatographic method	(27)
α-Alumina	Diffusion-convection cell	(28), (29)
Separation Processes		
Process	**Application**	**References**
HPLC	Proteins separation	(7), (8), (24), (25), (30)
HPLC; gas/solid chromatography		(26), (31), (32), (33)
Pressure swing adsorption		(34)
Membrane chromatography	Proteins separation	(35)
Separation/Reaction Engineering		
Process	**Application**	**References**
Ceramic membrane reactors	Facilitated transport	(36), (37)

Downloaded by UNIV OF GUELPH LIBRARY on October 8, 2012 | http://pubs.acs.org
Publication Date: May 30, 1996 | doi: 10.1021/bk-1996-0635.ch009

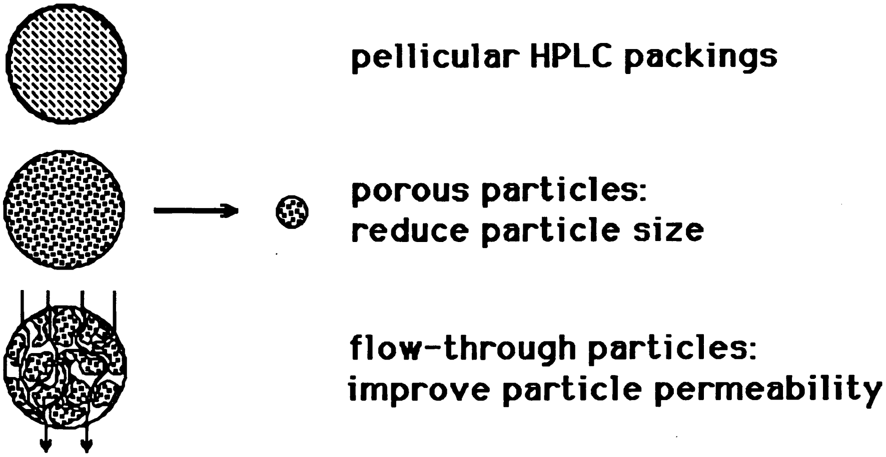

Figure 1. Different ways of reducing intraparticle mass transfer resistances.

where $f(\lambda) = \frac{3}{\lambda}\left(\frac{1}{\tanh\lambda} - \frac{1}{\lambda}\right)$.

The key parameter is the *intraparticle Peclet number* λ defined as the ratio between the time constant for pore diffusion $\tau_d = \varepsilon_p \ell^2/D_e$ and the time constant for intraparticle convection $\tau_c = \varepsilon_p \ell / v_o$, i.e., $\lambda = v_o \ell / D_e$ where ℓ is the half-thickness of the slab particle and v_o is the intraparticle convective velocity inside large-pores given by Darcy's law.

The enhancement of diffusivity by intraparticle convection is $1/f(\lambda)$. Equation (1) was derived on the basis of model equivalence between a complete model including mass transport inside pores by diffusion (D_e) and convection and a simpler model which lumped diffusion and convection in an "apparent" or "augmented" diffusivity $\tilde{D}_e$.

The transient mass balance for an inert or passive tracer in a large-pore support with slab geometry (half thickness ℓ) is then for the "lumped" model:

$$\tilde{D}_e \frac{\partial^2 c_p}{\partial z^2} = \varepsilon_p \frac{\partial c_p}{\partial t} \qquad [2]$$

However, when diffusion and convection are considered as independent processes, the mass balance for the "complete" model is:

$$D_e \frac{\partial^2 c_p}{\partial z^2} - v_o \frac{\partial c_p}{\partial z} = \varepsilon_p \frac{\partial c_p}{\partial t} \qquad [3]$$

where D_e is the effective diffusivity and v_o is the intraparticle convective velocity.

The particle transfer function, i.e., the ratio between the average concentration inside particle and the particle surface concentration in the Laplace domain, are for the "lumped" and "complete" model, respectively:

$$\tilde{g}_p(s) = \frac{\tanh\sqrt{\tilde{\tau}_d\, s}}{\sqrt{\tilde{\tau}_d\, s}} \qquad [4a]$$

and

$$g_p(s) = \frac{(e^{2r_2}-1)(e^{2r_1}-1)}{(e^{2r_2}-e^{2r_1})} \; \frac{\sqrt{\frac{\lambda^2}{4}+\tau_{d}s}}{\tau_{d}s} \qquad [4b]$$

where $r_1, r_2 = \frac{\lambda}{2} \pm \sqrt{\frac{\lambda^2}{4}+\tau_d s}$ and the "apparent" diffusion time constant $\tilde{\tau}_d = \varepsilon_p \ell^2 / \tilde{D}_e$. The equivalence between the "lumped" and "complete" models, leads to $\tilde{\tau}_d = \tau_d f(\lambda)$ or $\tilde{D}_e = D_e \frac{1}{f(\lambda)}$.

The key result is given by Eq(1); it was derived from the analysis of a chromatographic column with large-pore supports by Rodrigues *et al. (2)* and conveys the following message:

In large-pore supports the diffusivity is "augmented" by convection; the enhancement factor is 1/f(λ).

There are two limiting situations:

i) *diffusion-controlled case* - At low bed superficial velocities u_0, the intraparticle convective velocity v_0 is also small; therefore $f(\lambda)=1$ and so $\tilde{D}_e = D_e$.

ii) *convection-controlled case* - At high superficial velocities u_0, and therefore high v_0 and high λ, we get $f(\lambda)=3/\lambda$; the augmented diffusivity is then $\tilde{D}_e = D_e\lambda/3 = v_0\ell/3$ which depends only on the particle permeability, fluid viscosity and pressure drop across the particle.

Figure 2 shows the enhancement factor $1/f(\lambda)=\tilde{D}_e/D_e$ as a function of the intraparticle Peclet number λ. Carta *et al. (30, 41)* showed that Equation (1) is valid for spherical particles provided that the half thickness of the slab ℓ is replaced by $R_p/3$ where R_p is the radius of the sphere.

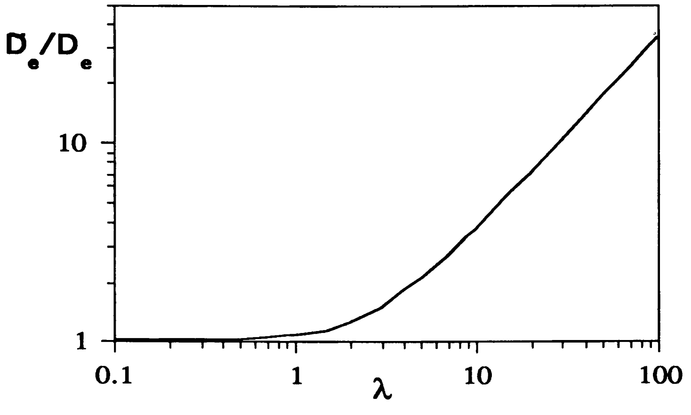

Figure 2. Enhancement factor $1/f(\lambda)= \tilde{D}_e/D_e$ as a function of λ.

Downloaded by UNIV OF GUELPH LIBRARY on October 8, 2012 | http://pubs.acs.org
Publication Date: May 30, 1996 | doi: 10.1021/bk-1996-0635.ch009

Downloaded by UNIV OF GUELPH LIBRARY on October 8, 2012 | http://pubs.acs.org
Publication Date: May 30, 1996 | doi: 10.1021/bk-1996-0635.ch009

Performance of Chromatographic Processes Using Permeable Particles.

In the following section we will discuss applications of the above concept in the area of protein separation by HPLC. The Van Deemter equation *(42)* for unretained species in conventional packings of sphere geometry can be written as :

$$\mathrm{HETP} = A + \frac{B}{u_o} + \frac{2}{15}\frac{\varepsilon_p(1-\varepsilon_b)b^2}{[\varepsilon_b+\varepsilon_p(1-\varepsilon_b)b]^2}\tau_d\, u_o \qquad [5]$$

where ε_p is the intraparticle porosity, ε_b is the bed porosity, $b=1+\{(1-\varepsilon_p)/\varepsilon_p\}m$ is the adsorption equilibrium parameter for a linear isotherm with slope *m* , and the time constant for diffusion is $\tau_d=\varepsilon_p R_p^2/D_e$. In a condensed form Van Deemter equation is

$$\mathrm{HETP} = A + B/u_o + Cu_o \qquad [6]$$

For large-pore packings since $\tilde{D}_e = D_e/\,f(\lambda)$ we have $\tilde{\tau}_d = \tau_d\, f(\lambda)$ and therefore the extended Van Deemter equation *(26)* is:

$$\mathrm{HETP} = A + \frac{B}{u_o} + \frac{2}{15}\frac{\varepsilon_p(1-\varepsilon_b)b^2}{[\varepsilon_b+\varepsilon_p(1-\varepsilon_b)b]^2}\tau_d\, f(\lambda)\, u_o \qquad [7]$$

or in a condensed form:

$$\mathrm{HETP} = A + \frac{B}{u_o} + C\, f(\lambda)\, u_o \qquad \textbf{Rodrigues equation} \qquad [8]$$

with $C=\frac{2}{15}\frac{\varepsilon_p(1-\varepsilon_b)b^2}{[\varepsilon_b+\varepsilon_p(1-\varepsilon_b)b]^2}\tau_d$.

The Van Deemter equation for conventional supports (dashed line) and Rodrigues equation for large-pore supports (full line) are shown in Figure 3 for a typical HPLC process.

At low velocities $f(\lambda)\approx 1$ and both equations lead to similar results. However, at high superficial velocities, $f(\lambda)\approx 3/\lambda$, and therefore the last term in Rodrigues equation becomes a *constant* since the intraparticle convective velocity v_o is proportional to the superficial velocity u_o. The ***HETP reaches a plateau which does not depend on the value of solute diffusivity but only on particle permeability and pressure gradient (convection-controlled limit).***

Two important features result from the use of large-pore, permeable packings:

i) improved column performance since HETP is reduced when compared with conventional packings (the C term in Van Deemter equation is reduced);

ii) the speed of separation can be increased (by increasing the superficial velocity) without loosing column efficiency.

Experimental results similar to the full line in Figure 3 have been reported in HPLC of proteins *(7,8,43)* and in size exclusion chromatography *(44,45)*.

Downloaded by UNIV OF GUELPH LIBRARY on October 8, 2012 | http://pubs.acs.org
Publication Date: May 30, 1996 | doi: 10.1021/bk-1996-0635.ch009

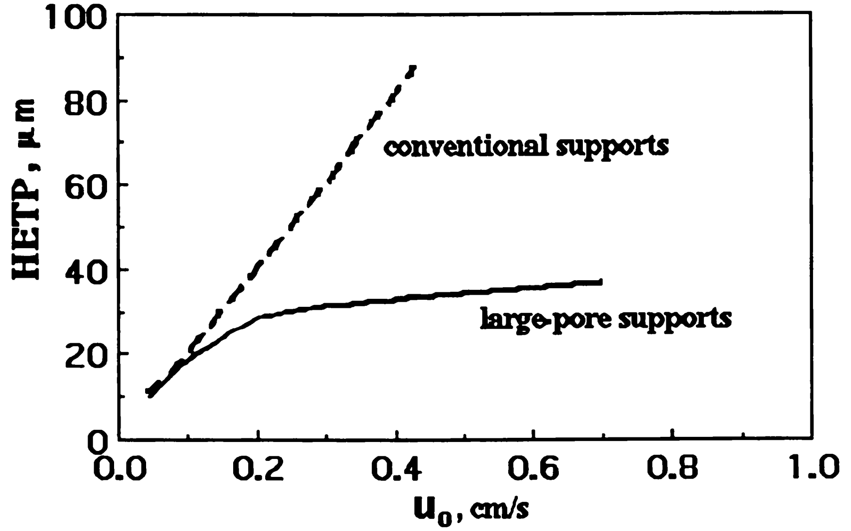

Figure 3. HETP versus u_0 (Van Deemter equation for conventional packings and Rodrigues equation for large-pore packings).

On the Importance of Adsorption/Desorption Kinetics.

The theoretical framework reviewed above allows complete calculations for linear perfusion chromatography. Protein separation by HPLC using large-pore packings is an area where the effect of intraparticle convective flow (of the order of 1% of the total flow through the bed) is sufficiently important to enhance the low diffusion coefficient for proteins ($\approx 5 \times 10^{-7}$ cm^2/s); therefore, intraparticle Peclet numbers λ of the order of 30 are easily obtained. The optimistic analysis of perfusion chromatography is sometimes confronted with the question: What happens if the kinetics of adsorption/desorption at the active sites of the packing is the controlling step? The problem was dealt with in my group, considering that the kinetics of adsorption/desorption is given by $\frac{\partial q_i'}{\partial t} = k_a c_i' - k_d q_i'$ where c_i' and q_i' are the species concentrations in the fluid phase inside pores and in adsorbed phase, respectively and k_a and k_d are the kinetic constants for adsorption and desorption *(46)*.

The extended Van Deemter equation *(46)*, accounting for axial dispersion, film mass transfer, intraparticle diffusion, intraparticle convection and kinetics of adsorption/desorption at the fluid/solid interface now becomes:

$$\text{HETP}= A +\frac{B}{u_0} +C\,\tau_d\{f(\lambda) + \frac{5}{Bi_m} + \frac{3(b-1)}{b^2\phi_d^2}\}u_0 \qquad [9]$$

Parameters accounting for film mass transfer are the Biot number $Bi_m = k_f R_p / D_e$ and the Thiele modulus ϕ_d based on the desorption kinetic constant with $\phi_d^2 = \tau_d k_d$. Figure 4 shows the effect of adsorption/desorption kinetics (ϕ_d) on the HETP versus u_0 curve. When the kinetics of adsorption/desorption is not infinitely fast, slower kinetics (lower ϕ_d) leads to higher HETP and so with a performance inferior to that obtained for infinitely fast kinetics. However, the performance of permeable packings is still better than that of conventional materials. In the extreme case of very slow adsorption/desorption kinetics the performances of both types of packings are very poor. One has to stress that intraparticle convection just enhances pore diffusivity but has no effect on the mechanism of adsorption/desorption.

The extension of the Van Deemter equation to the case of bidisperse adsorbents containing macropores and micropores has been made by Carta and Rodrigues *(41)*.

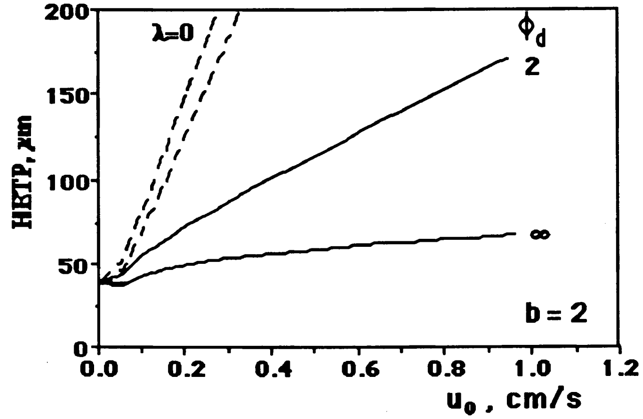

Figure 4. Influence of adsorption/desorption kinetics on HETP *vs.* u_0 curves (conventional supports : dashed lines; permeable packings: full lines).

Estimation of intraparticle velocity v_0

The calculation of the intraparticle Peclet number is the first step to assess the importance of convective flow in permeable particles. The difficulty here is to estimate the convective velocity v_o in pores. Kommiyama and Inoue *(21)* and Rodrigues *et al.* *(2)* estimated v_o based on the equality of pressure drops across the particle $\Delta p/d_p$ and across the bed $\Delta P/L$. In HPLC operation flow around the particles is in the laminar region (*Re* < *0.1*) and the same applies for the convective flow inside pores.

Since

$$\frac{\Delta P}{L} = \frac{\eta}{B_b} u_o \quad \text{and} \quad \frac{\Delta p}{d_p} = \frac{\eta}{B_p} v_o \qquad [10]$$

where B_b and B_p are bed and particle permeability, respectively, and η is the liquid viscosity we get

$$v_o = \frac{B_p}{B_b} u_o \qquad [11]$$

The fraction of flowrate entering the column which goes through the macropores by convection is $(1-\varepsilon)\ \frac{B_p}{B_b}$.

Downloaded by UNIV OF GUELPH LIBRARY on October 8, 2012 | http://pubs.acs.org
Publication Date: May 30, 1996 | doi: 10.1021/bk-1996-0635.ch009

As an example: for the Hyper D column (5mm x 10cm) with 35 μm particles at a flowrate of 8 ml/min or superficial velocity of 0.68 cm/s we get a bed pressure drop $\Delta P=7$ bar and so a pressure drop across the particle $\Delta p = 245$ Pa.

Protein Separation by Liquid Chromatography Using Permeable Particles (POROS Q/M and Q HYPER D)

Elution chromatography experiments under unretained conditions allow the understanding of mass transport mechanisms inside particles in the absence of extra effects related with protein adsorption. In this work studies are carried out in two anionic columns:

a) POROS^{TM} Q/M (Prot. nº PO11M526, Serial nº 030, Packing Batch Number 033) purchased from PerSeptive Biosystems, Cambridge MA, USA. POROS^{TM} Q consists of a polystyrene/divinylbenzene support coated with crosslinked polyethyleneimine and quaternized. The ionic groups are quaternary amino groups. This strong anion exchanger was obtained in a pre-packed column. It was equilibrated with the appropriate solvent before use. The dimensions of the POROS column were 4.6mm I.D. x 100mm L with a bed volume of 1.7ml packed with 20 μm diameter particles.

b) Q Hyper D cat nº 200227 Serial nº 32232 (UN 2196) from BioSepra Co., (Villeneuve la Garenne, France) with dimensions 5 mm (ID) x 100 mm (length) packed with 35 μm diameter particles.

All proteins reported in this study were purchased from Sigma (ST Louis, MO, USA). Three proteins were used: Myoglobin (Horse Skeletal Muscle, 95-100% of purity), Ovalbumin (Albumin, Chicken egg, 99% of purity) and Bovine Serum Albumin (BSA) (fraction V, 98-99% of purity).

The solvents used were TRIS-HCl 50mM, pH=8.6, mixed with NaCl 0.5M in HETP experiments. Temperature in all runs was 22 °C.

The chromatographic experiments were carried on a Gilson 715 HPLC system equipped with a Model 360 pump, a manual injector (with an injection loop of 20μl) and a Model 17UV (λ=280nm) detector. A computer system Gilson 715 HPLC software for data acquisition and a control system was used. Experiments with each protein were carried out at different flowrates up to 10 ml/min corresponding to superficial velocities up to 1 cm/s.

The diffusivities of proteins: Myoglobin, Ovalbumin and BSA in aqueous solution at 25 °C are given by Tyn and Gusek *(47)* and are respectively 16.1×10^{-7}, 6.4×10^{-7} and 1×10^{-7} cm^2/s.

Bed permeability. The measurement of the column pressure drop (ΔP) as a function of the bed superficial velocity u_o allows the calculation of bed permeability. In laminar flow, the pressure drop ΔP across a bed of length L packed with particle d_p is given by Darcy's law $\frac{\Delta P}{L} = \frac{\eta u_o}{B_b}$ where B_b is the bed permeability given by $B_b = \frac{\varepsilon_b^3 d_p^2}{150(1-\varepsilon_b)^2}$. Bed permeabilities B_b were obtained from the slope of the plot $\Delta P/L$ versus u_o and then the bed porosity ε_b was calculated.

Downloaded by UNIV OF GUELPH LIBRARY on October 8, 2012 | http://pubs.acs.org
Publication Date: May 30, 1996 | doi: 10.1021/bk-1996-0635.ch009

Downloaded by UNIV OF GUELPH LIBRARY on October 8, 2012 | http://pubs.acs.org
Publication Date: May 30, 1996 | doi: 10.1021/bk-1996-0635.ch009

For the POROS column (20 μm particles) the bed permeability is $B_b = 2.35 \times 10^{-9}$ cm^2/s and $\varepsilon_b = 0.34$; for the Hyper D column (35 μm particles) the bed permeability is $B_b = 1.02 \times 10^{-8}$ cm^2 and $\varepsilon_b = 0.37$.

Efficiency of chromatographic columns and HETP. Chromatographic peaks for the three proteins (BSA, Myoglobin and Ovalbumin) were obtained at various flowrates on POROS™ Q/M and Q Hyper D supports. The HETP as a function of superficial velocity has been calculated for each protein from the experimental peaks in elution chromatography by $HETP = \frac{\sigma^2 L}{\mu_1^2}$ where $\sigma^2 = \mu_2 - \mu_1^2$ is the peak variance, μ_1 is the first moment of the peak $\mu_1 = \frac{\int_0^\infty t\ c(t)\ dt}{\int_0^\infty c(t)\ dt}$, $\mu_2 = \frac{\int_0^\infty t^2\ c(t)\ dt}{\int_0^\infty c(t)\ dt}$ is the second moment and L is the column length. Figure 5 shows the experimentally measured reduced height equivalent to a theoretical plate ($h = HETP/d_p$) as a function of the bed superficial velocity. It can be seen that:

a) for the POROS column, the HETP increases linearly at low superficial velocity and then,at high superficial velocities, reaches a plateau;

b) for the HYPER D column the HETP is almost at a plateau, even at low u_o.

Analysis of HETP versus superficial velocity

The efficiency of chromatographic columns can be easily characterized by its height equivalent to a theoretical plate (HETP); for columns packed with permeable packings mass transport by convection equation (8) applies, i.e., $HETP = A + \frac{B}{u_o} + Cf(\lambda)u_o$. The A term accounts for eddy dispersion effects and becomes a constant at high superficial velocities, $A = 2d_p$; $B = 2\mathcal{D}_m$ and so the term B/u_o can be neglected in the case of proteins separation (at velocity $u_o = 1$ cm/s , B/u_o is around 10^{-7}cm). Film mass transfer resistance can also be neglected; film mass transfer coefficients estimated by available correlations *(48)* developed for purely diffusive media are conservative; in fact, in perfusive materials, intraparticle convection enhances film mass transfer, as shown by Lu *et al. (49)*.

The simplified equation for HETP is:

$$HETP \cong A + Cf(\lambda)u_o \qquad [12]$$

In the low velocity region where pore diffusion is the controlling mechanism of mass transfer, the slope of HETP *versus* u_o is:

$$C = \frac{dH}{du_o} = \frac{1}{30} \frac{\nu}{(1+\nu)^2} \frac{\varepsilon_p}{\varepsilon_b} \frac{d_p^2}{D_e} \qquad [13]$$

Downloaded by UNIV OF GUELPH LIBRARY on October 8, 2012 | http://pubs.acs.org
Publication Date: May 30, 1996 | doi: 10.1021/bk-1996-0635.ch009

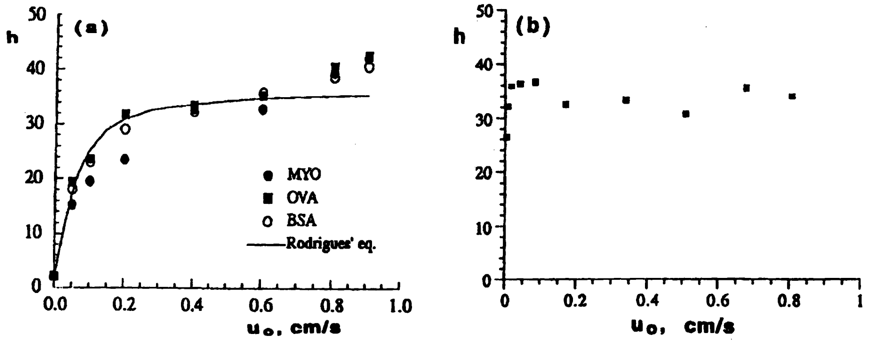

Figure 5. HETP versus superficial velocity for elution chromatography of proteins under unretained conditions: a) POROS Q/M ; b) Q HYPER D.

At high flowrates $f(\lambda) \approx \frac{3}{\lambda}$ and since $v_o \propto u_o$ we get

$$H_{plateau} = A + \frac{3}{5}\frac{\nu}{(1+\nu)^2}\frac{\varepsilon_p}{\varepsilon_b}\frac{B_b}{B_p}d_p \qquad [14]$$

where ν is $\frac{(1-\varepsilon_b)\varepsilon_p}{\varepsilon_b}$. When the particle structure (ε_p) is known these two equations provide measured values of D_e and B_p.

The straight line at low flowrates crosses the plateau at a critical point $A + Cu_{o,c} = H_{plateau}$ and then $u_{o,c} = \frac{18D_e}{d_p}\frac{B_b}{B_p}$. When the particle porosity ε_p is known equations (13) and (14) provide measured values of D_e and B_p. For POROS Q/M if we consider the value of $\varepsilon_p = 0.5$ found by Afeyan *et al.* *(25)*, we get $B_p=1.5 \times 10^{-11}$ cm^2 for an experimental "h plateau" of 36 (reduced HETP) and $D_e = 7 \times 10^{-8}$ cm^2/s .

For the Q HYPER D particles, the particle permeability was calculated from breakthrough experiments *(13)* as $B_p=8.9 \times 10^{-12}$ cm^2 and a particle porosity of $\varepsilon p = 0.13$ is estimated from the plateau. The effective diffusivity calculated from modeling of breakthrough curves is $D_e = 8.1 \times 10^{-9}$ cm^2/s. The experimental HETP versus u_o plot is almost a plateau indicating that gel diffusion should be the controlling factor at very low velocity and then paths are opened to allow intraparticle convection. This is supported by results under weakly retained conditions described below.

Frontal Chromatography Experiments

In frontal chromatography experiments a solution of protein with concentration c_o is continuously passed through the column under retained conditions (no salt in the feed). The concentration at the bed outlet as a function of time is the breakthrough curve from which the amount of protein retained in the adsorbent q_o^* is calculated by mass balance. Therefore a point of the adsorption equilibrium isotherm can be calculated from one experiment with a given feed concentration c_0. The adsorption equilibrium isotherm of BSA in POROS Q/M shown in Figure 6a follows Langmuir equation. Adsorption equilibrium isotherms of BSA on Q HYPER D , at various salt concentrations, are shown in Figure 6b. With no salt the isotherm is almost rectangular. With NaCl 0.3M the protein is weakly retained with linear isotherm.

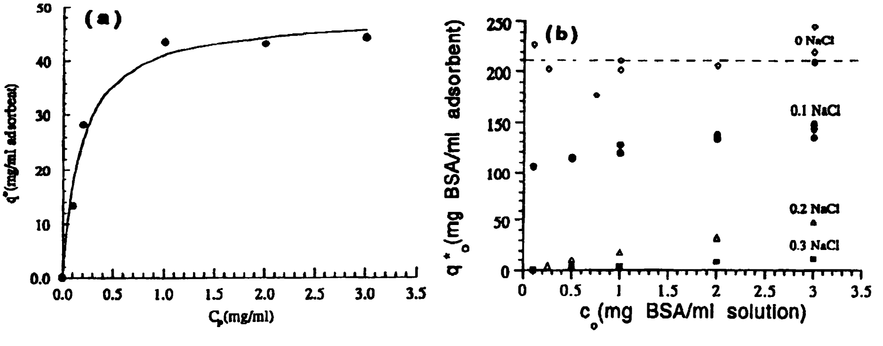

Figure 6. Adsorption equilibrium isotherms of BSA on POROS Q/M (a) and Q HYPER D (b)

Elution Chromatography of BSA on Q HYPER D Under Weakly Retained Conditions.

Elution experiments using BSA in a solution containing NaCl 0.3M were carried out; from the peaks HETP was calculated as a function of the superficial velocity. Results obtained in my laboratory *(13)* are shown in Figure 7. The theoretical line according Rodrigues equation reasonably fits the experimental results using the values of effective diffusivity and particle permeability reported above. Clearly , the tendency towards a plateau on HETP wouldn't be observed if intraparticle convection was not present. In this calculation linear adsorption equilibrium is taken into account.

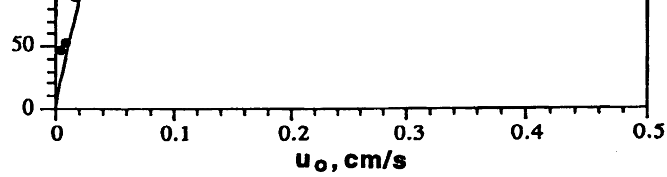

Figure 7. HETP versus superficial velocity for elution chromatography of BSA on Q HYPER D under weakly retained conditions.

Downloaded by UNIV OF GUELPH LIBRARY on October 8, 2012 | http://pubs.acs.org
Publication Date: May 30, 1996 | doi: 10.1021/bk-1996-0635.ch009

Downloaded by UNIV OF GUELPH LIBRARY on October 8, 2012 | http://pubs.acs.org
Publication Date: May 30, 1996 | doi: 10.1021/bk-1996-0635.ch009

Conclusions

In this review it is shown that the key concept behind the improved performance of large-pore, permeable chromatographic packings is the "augmented " diffusivity by convection. This concept has long been recognized in the reaction engineering area and explains how perfusion chromatography works . Experiments with new chromatographic media (POROS Q/M and Q HYPER D) show that intraparticle convection is an important mass transport mechanism in such materials.

Results obtained from elution chromatography experiments with POROS Q/M adsorbent show clearly the presence of a mass transfer intraparticle convection mechanism that enhances the mass transport performance of large-pore particles chromatographic supports. The reduced HETP vs superficial bed velocity plot, obtained for non-retained BSA, Myoglobin and Ovalbumin, allowed the calculation of a particle porosity $\varepsilon_p = 0.5$ from the plateau and an approximate effective diffusivity $D_e = 7 \times 10^{-8}$ cm^2/s from the initial slope.

Experimental results with Q HYPER D particles indicate that at very low flowrates gel diffusion is the control mechanism; as flowrate increases, pore diffusion becomes the main mass transfer process and at higher flowrates, the process is fully convection controlled. Otherwise no plateau could have been observed. From the plateau of the reduced HETP (Fig. 7), a particle porosity ε_p=0.13 is obtained; from the slope an effective diffusivity of D_e=8.1 x 10^{-9} cm^2/ s is extracted.

It is convenient to stress that intraparticle convection contributes to better mass transport in macropores. If the process is controlled by micropore diffusion , as in nitrogen production by pressure swing adsorption using carbon molecular sieves , or by chemical reaction as in various membrane processes , then intraparticle convection can do nothing to decrease those resistances. Applications in rapid pressure swing adsorption (RPSA), membrane chromatography, biofilm reactors with large-pore supports, reversal flow reactors, coupled separation/reaction are some examples of systems in which intraparticle convective flow should be considered.

Notation

Bi_m	mass Biot number , dimensionless
B_b	bed permeability, cm^2
B_p	particle permeability, cm^2
c_p	protein concentration in the pore fluid phase, mol/cm^3
c_o	feed concentration of protein in the external fluid phase, mol/cm^3
c	concentration in the fluid phase at the column outlet, mol/cm^3
d_p	particle diameter, cm
D_e	effective diffusivity, cm^2/s
$\tilde{D}_e$	augmented effective diffusivity, cm^2/s
$\mathcal{D}_m$	molecular diffusivity, cm^2/s
F	flowrate, cm^3/s
h	reduced HETP (HETP/d_p), dimensionless
H	height equivalent to a theoretical plate, cm
HETP	height equivalent to a theoretical plate, cm
k_f	mass transfer constant, cm/s
ℓ	half thickness of the slab, cm
L	bed length, cm
Δp	pressure drop across the particle, bar

ΔP	bed pressure drop, bar
q_o^*	adsorbed phase concentration in equilibrium with c_o, mg/ml adsorbent
R_p	particle radius, cm
t	time variable, s
u_o	bed superficial velocity, cm/s
$u_{o,c}$	critical velocity, cm/s
v_o	intraparticle convective velocity, cm/s
V	bed volume, ml
z	axial coordinate in the column, cm

Greek symbols

ε_b	bed porosity (interparticle volume/bed volume)
ε_p	intraparticle porosity (pore volume/particle volume)
λ	intraparticle Peclet number
η	fluid viscosity, g/cm. s
μ_1	1st order moment of the impulse response
ν	$(1-\varepsilon)\varepsilon_p/\varepsilon$
σ^2	variance
τ	space time, cm
τ_c	time constant for convection, s
τ_d	time constant for diffusion, s
$\tilde{\tau}_d$	"apparent" time constant for diffusion, s

Downloaded by UNIV OF GUELPH LIBRARY on October 8, 2012 | http://pubs.acs.org
Publication Date: May 30, 1996 | doi: 10.1021/bk-1996-0635.ch009

LITERATURE CITED

1 Cresswell, D. ; Orr, N. Measurement of Binary Gaseous Diffusion Coefficients Within Porous Catalysts" in *Residence Time Distribution Theory in Chemical Engineering*, ed.A.Petho and R.Noble,Verlag-Chemie, 1982.
2. Rodrigues, A.; Ahn, B. ; A.Zoulalian,*AIChEJ*. **1982**, *28*, 541-546.
3. Nielsen, A.; Bergh, S.; Troberg,B. US Patent 3,243,386, Mar 29, 1966.
4. Harbord, N. U.K.Patent 1484864, Sept 8., 1977.
5. Liu, P.T.K."Adsorption with Activated Alumina in Liquid Phase Applications", AIChE Meeting, New Orleans, 1988.
6. Carta, G., Personal Communication, University of Virginia, 1988.
7. Lloyd, L. ; Warner, F.*J.Chromatogr.*,**1990**, *512*, 365-376.
8. Afeyan, N.; Fulton, S.; Gordon,N.; Mazsaroff, I.;Varady, L. ; Regnier,F., *Bio/technology*, **1990**, *8*, 203-206.
9. Rodrigues, A. ; Chenou, C. ; Rendueles de la Vega, M., *The Chem Eng J, in press*.
10. Boschetti, E, *J Chromatogr.* A, **1994**, *658*, 207.
11. Horvath, J.; Boschetti, E.; Guerrier, L. ; Cooke, N., *J. of Chromatogr. A* **1994**, *679*, 11-22.
12. Rodrigues, A.; Loureiro, J.; Chenou, C.; Rendueles de la Vega, M., *J.Chromatogr. B* **1995**, *664*, 233-240.
13. Rendueles de la Vega, M.; Chenou, C.; Loureiro, J. ; Rodrigues, A., *J.Chromatogr A*., submitted.
14. Young, M.; Dean, R.*Bio/Technology* **1987**,*5* , 835-837.

15. Tung, A.; Sample, J.; Brown, T.; Ray, N.; Hayman, E. ; Runstadler, P., "TPA Production Through Mass Culturing Of Chinese Hamster Ovary Cells", Biopharm Manufacturing, February 1988.
16. Breitenbucher, K.;Siegl, M; Knupfer, A.; Radke, M., *Water Sci. Tech.*. **1990,** *22(1/2),* 25-32.
17. Pascik, L ., *Water Sci.Tech.*. **1990,** 22(1/2), 33-42.
18. Carrondo, M., Personal Communication, The New University of Lisbon, 1991.
19. Wheeler, A., *Adv. in Catalysis* **1951,** *3,* 250-337.
20. Nir, A.;.Pismen, L.,*Chem.Eng.Sci.*. **1977,** *32,* 35-41.
21. Komiyama, H.; Inoue,H. , *J.Chem.Eng. Japan* **1974,** *7(4),* 281-286.
22. Cogan, R., Pipko, G.; Nir, A. ,*Chem .Eng.Sci.*. **1982,** *37,* 147-151.
23. Cheng, S.; Zoulalian, A., *The Chem.EngJ.* **1989,***41,* 91-104.
24. Horvath, C., "Preparative HPLC", NATO ASI "Chromatographic and membrane processes in biotechnology", Azores(1990).
25. Afeyan,N.; Gordon, N.; Mazsaroff, I.; Varady, L.; Fulton, S.;Yang, Y.; Regnier, F.; *J. of Chromatogr.* **1990,** *519,* 1-29.
26. Rodrigues, A.; Lu, Z.; Loureiro, J., *Chem.Eng.Sci.*. **1991,***46(11),* 2765-2773.
27. Cheng, S.; Rodrigues, A.; Zoulalian, A.,"Diffusivity Measurements in Large Pore Catalysts by a Dynamic Chromatographic Technique", 9th Ibero-American Symp. on Catalysis, Lisbon(1984).
28. Cresswell, D. , *Applied Catalysis* **1985,***15,* 103-116.
29. Dogu, G.;Pekediz, A. ; Dogu, T., *AIChEJ.* **1989,** *35,* 1370-1375.
30. Carta, G.;Massaldi, H.;Gregory, M.; Kirwan, D.,*Separations Technology* **1992,** *2,* 62-72.
31. Rodrigues, A.; Lopes, J.; Dias, M.; Loureiro, J.; Lu, Z.; *J. of Chromatogr.* **1992,** *590,* 93.
32. Rodrigues, A.; *LC-GC* **1993,** *6,* 20.
33. Rodrigues, A.;Lu, Z.; Loureiro J.; Carta, G., *J. of Chromatogr. A* **1993,** *653,* 189.
34. Lu, Z.; Loureiro, J.; LeVan, D.; Rodrigues, A., *Ind.Eng.Chem.Res.* **1993,** *32,* 2740-2752.
35. Tennikova, T.; Svec, F., "Macroporous Membrane:New Stationary Phase for Chromatographic Separations in Any Scale", Proceedings PREP'92, Nancy 1992, pp353-358.
36. Chaara, M.; Noble, R.,*Sep.Sci. & Tech.* **1989,** *24,* 893-903.
37. Coelhoso, I.; Crespo, J. ; Rodrigues, A., "The effect of convective flow on the facilitated transport across a membrane", European Membrane Society Meeting, Paris, October 1992.
38. Afeyan,N.; Fulton,S. ; Regnier,F. , *J.Chromatogr.* **1991,** *544,* 267-279.
39. Afeyan, N.; Regnier, F.; Dean Jr, R., US Patent no. 5,019,270 May 28, 1991.
40. Afeyan, N.; Regnier, F.; Dean, Jr., R., US Patent no. 5,228,989 July 20, 1993.
41. Carta, G. ; Rodrigues, A., *Chem. Eng. Sci.* **1993,** *48(23),* 3927-3936.
42. Van Deemter, J.; Zuiderweg, F. ; Klinkenberg, A., *Chem.Eng.Sci.* **1956,** *5,* 271-289.
43. Frey, D.; Schwesnheim, E. ; Horvath, C., *Biotech. Prog.* **1993,** *9,* 273.
44. Potschka, M., *J. Chromatogr.* **1993,** *648,* 48.
45. Van Kreveld, M. ; Van den Hoed, N., *J. of Chromatogr.* **1978,** *149,* 71-91.
46. Rodrigues, A.; Ramos, A.; Loureiro, J., Dias, M.; Lu, Z.; *Chem. Eng. Sci.* **1992,** *47,* 4405.
47. Tyn, M.; Gusek, T., *Biotechnol. and Bioeng.* **1990,** *35,* 327.
48. Kataoka, T.; Yoshida, H.; Ueyama, K., *J. Chem. Eng. Japan* **1972,** *5,* 132.
49. Lu, Z.P.; Frey, D.; Rodrigues, A., *Ind. Eng. Chem. Res.* **1993,** *32,* 2159.

Downloaded by UNIV OF GUELPH LIBRARY on October 8, 2012 | http://pubs.acs.org
Publication Date: May 30, 1996 | doi: 10.1021/bk-1996-0635.ch009

Chapter 10

Unified Thermodynamic Model for Polymer Separations Produced by Size Exclusion Chromatography, Hydrodynamic Chromatography, and Gel Electrophoresis

David A. Hoagland

Department of Polymer Science and Engineering and Materials Research Science and Engineering Center, University of Massachusetts, Amherst, MA 01003

Polymer separations by size exclusion chromatography, hydrodynamic chromatography, and gel electrophoresis are discussed in the context of a single unifying principle, that of local equilibrium. The principle holds whenever migrating solute can fully equilibrate with the local environments of the separation matrix. Assuming enthalpic interactions between matrix and solute are minimized, each of these separation methods relies on spatial variation of solute confinement to produce partitioning according to molecular weight or size. Under local equilibrium, the fundamental operating parameter becomes confinement entropy, and with curved/irregular matrix interfaces, this entropy may not admit the definition of an "effective polymer radius" that can correlate the elution behavior of different species. The failure will be illustrated for several polymer and matrix models. The principle of local equilibrium is well-established for size exclusion chromatography and hydrodynamic chromatography, but the apparent absence of large scale matrix structure makes the principle's role less obvious for gel electrophoresis. Nonetheless, under a broad range of operating conditions, all three methods can be understood by one physical model.

Size exclusion chromatography (SEC), hydrodynamic chromatography (HDC), and gel electrophoresis (GE) all capitalize on the interaction of polymer solutes with porous supports to create polymer fractionations based on molecular weight or size (*1*-*5*). In fact, the parallels between the methods extend further. The pores of the support in each case are of molecular dimension, and the support/polymer enthalpic interaction, typically manifested as reversible or irreversible adsorption, is suppressed as much as possible. Differences between the methods are also obvious. Perhaps most importantly, GE can be applied only to charged polymers dissolved in high dielectric constant solvents, while SEC and HDC can be performed for essentially any polymer/solvent system that molecularly dissolves unaggregated polymer chains. Nearly as apparent is the reversal of migration patterns; large solutes move most rapidly through an SEC or HDC column, while in GE the order of elution is reversed, with large solutes moving most slowly. Nonetheless, theories for the methods possess many similarities, and investigators have frequently speculated that the methods separate polymers according to the same basic physical principles (*6*-*8*).

0097–6156/96/0635–0173$15.00/0

A frequent assumption has been that separations are based on molecular size, and that one size parameter can correlate separation across a group of polymers possessing different chain structure (*7,9-11*). For example, the elution behavior of a spherical molecule would "map" onto the same behavior for a rodlike molecule when data is presented in terms of an appropriately defined molecular radius. This assertion, underpinning the concept of "universal calibration", has never been fully justified and will be discussed extensively in the present contribution. Recent reptation theories clearly demonstrate that molecular size is not necessarily the controlling parameter for GE, but the finding applies only to this single technique and then only in the limit of high molecular weight and large chain flexibility. We will focus on the more common scenario, one in which a flexible polymeric solute is not strongly entangled in the porous separation matrix. A rigorous understanding of the fractionation mechanisms under these conditions is not just of theoretical importance but will play an increasingly important role as SEC, HDC, and GE are considered for synthetic polymer systems with no calibration standards available.

The interpretations given here for SEC and HDC are fairly standard, while that for GE is not. We consequently will devote a larger part of the theoretical discussion to GE, presenting SEC and HDC mainly to extract common physical principles. Our theoretical approach borrows heavily from the polymer partitioning models described by Laurent and Killander (*12*), Giddings et al. (*13*), Doi (*14*), Limbach et al. (*15*), Casassa et al. (*16-18*), and Ogston (*19*). In equal measure, the work borrows from the transport models developed by Altenberger and Tirrell (*20*), Maxwell (*21*), Koch and Brady (*22,23*), Brenner and Gaydos (*24,25*), and Muthukumar and Baumgartner (*26,27*). A recent contribution by Zimm and Lumpkin (*28*) closely guided our development of a quantitative entropic barriers model for GE. While focused on SEC, HDC, and GE as distinct entities, the present theory trivially encompasses potential hybrid technologies. For example, in one potential form of "electrochromatography", an electric field replaces the usual velocity field of an SEC experiment. Conventional separation technologies, inadvertently or not, may also produce mixed separations; SEC is often performed in the presence of the HDC mechanism, for example, and the entropic barriers transport described here for GE should play at least a minor role in SEC or HDC.

General Transport Theory

Mean Solute Velocity. When a constant driving force is applied in the z direction across a permeable separation matrix, dilute solute molecules introduced at axial position z=0 will migrate toward larger z with an average steady state velocity v. To relate this velocity to molecular level transport mechanisms, we consider a hypothetical case, one in which the solutes are injected at a constant rate, thereby yielding a uniform and steady solute stream for z>0. One can readily prove that a dilute pulse injection of solute at z=0 moves with the same mean velocity v; we choose to analyze the constant source case solely for its simplicity. The solute velocity can be expressed as a ratio of volume integrals involving the local solute concentration c(z,r) and local axial solute flux $J_z(z,r)$,

$$v = \frac{\int J_z(z,r)\, dz\, dr}{\int c(z,r)\, dz\, dr} \tag{1}$$

where r is a generalized radial position variable running orthogonal to z (in Cartesian coordinates, for example, dr = dx dy). For an inhomogeneous matrix, such as those typically employed in chromatography and electrophoresis, the integrals of eqn 1 must be evaluated over a sufficiently large volume to average out local variations in J(z,r) and C(z,r). The range of integration includes all space inside the selected volume, including regions occupied by matrix material.

Flux Equations. Further and more detailed calculations require the input of a constitutive relationship between $J_z(z,r)$ and c(z,r). A generalized version of Fick's law linearly sums flux contributions from diffusion, field-induced migration, and convection

$$J_z(z,r) = -D\frac{\partial c(z,r)}{\partial z} - \frac{Dc(z,r)}{kT}\frac{\partial \phi(z,r)}{\partial z} + v_z(z,r)c(z,r) \qquad (2)$$

Here, D is the solute diffusion coefficient within the matrix, $\phi(z,r)$ is the potential energy of solute, and $v_z(z,r)$ is the z-component of solvent velocity . The second term also contains the factor kT, the product of the Boltzmann constant and temperature. The radial solute flux obeys an analogous equation,

$$J_r(z,r) = J_r(r) = -D\frac{\partial c(z,r)}{\partial r} - \frac{Dc(z,r)}{kT}\frac{\partial \phi(z,r)}{\partial r} \qquad (3)$$

with the convection term deleted if, as is conventional, the transverse solvent flow is weak.

Expressions for the Solute Potential. When $\phi(z,r)$ includes the local variations of chemical potential arising from matrix inhomogeneity, and if D is equated to the free solution diffusion coefficient D_0, equations 2 and 3 embody the principle of local equilibrium. The assertion of thermodynamic control becomes obvious when one recognizes that the entire discrimination of dissimilar chemical species by the matrix can be traced to a single thermodynamic factor $\phi(z,r)$. We will show subsequently that equations 1-3, together with input of $\phi(z,r)$, provide a unified understanding of the separations obtained by SEC, HDC, and GE. Our arguments will parallel those employed to justify the standard equilibrium theory of liquid chromatography. More accurate models might also account for the medium's impact on solute transport, thus introducing an additional kinetic component. For example, a highly constraining pore structure will raise the solute hydrodynamic friction coefficient above that in bulk solvent, with the consequence that D is locally smaller than D_0. However, we believe that in most cases that the thermodynamic influence exerted through $\phi(z,r)$ is dominant.

If the matrix can be considered homogeneous at macroscopic length scales, $\phi(z,r)$ separates into applied and intrinsic components,

$$\phi(z,r) = \psi(z,r) + \Psi(z,r) \qquad (4)$$

where $\psi(z,r)$ represents the energy increase due to an externally applied potential, and $\Psi(z,r)$ accounts for the local variations in chemical potential associated with inhomogeneous matrix microstructure. When enthalpic interactions between matrix and solute can be ignored, the latter term incorporates only entropic effects. In most subsequent calculations we will assume that $\Psi(z,r)$ can be written

$$\Psi(z,r) = -T\Delta S_c(z,r) \qquad (5)$$

where $\Delta S_c(z,r)$ is the entropy penalty to confine a solute molecule in the pores of the matrix. The reference energy is generally taken as that for the unconfined solute in bulk solution, implying that confinement raises $\Psi(z,r)$ while reducing conformational entropy. If the externally applied field is modulated locally by matrix microstructure, there will be a coupling between $\psi(z,r)$ and $\Psi(z,r)$. For simplicity, these fluctuations in $\psi(z,r)$ will be disallowed in the present analysis, a reasonable approximation only in a dilute matrix structure. Fortunately, many experiments which impose an external potential also satisfy this matrix condition.

Size Exclusion Chromatography

Description. Size exclusion chromatography is performed in columns containing porous particles that can be either rigid or gel-like. For either case, one can identify two dominant microscopic length scales, the diameter of the particle d_p and the average intraparticle pore size l. With $d_p >> l$ and/or the pores dead-ended, solvent flow within particles is minimal or nonexistent. Nonetheless, polymer solutes can readily diffuse from the interstitial volume into the intraparticle pore space, and depending on the extent of their penetration, be hindered in overall migration through the column. This hindrance results from the large difference in fluid velocity between the two regions, intraparticle and interstitial. Typical values for d_p and l are 10 µm and 100 nm, respectively.

Modeling. To analyze solute velocity, we first recognize that the concentration c_o in the interstitial space is constant, a condition dependent on our placement of a steady solute source at z=0 and the lack of significant confinement effects across the interstitial region. Combined with the stipulation that no fluid motion occurs within particles, one deduces that the net radial and axial fluxes in the intraparticle pore space are identically zero for each value of r and z. Solving equations 3 and 4, we find the usual concentration mismatch between particle interior and exterior that defines the partition coefficient K_{SEC}

$$K_{SEC} = \frac{c_i}{c_o} = e^{\Delta S_c/k} \tag{6}$$

where c_i is the intraparticle solute concentration. To eliminate the r and z dependence of K_{SEC}, we have assumed that no external potential is applied and that a uniform pore dimension prevails throughout each particle and for all particles in the bed. Otherwise, K_{SEC} should be expressed by appropriate integrals over z and r.

Substituting equations 2 and 6 into equation 1, we obtain

$$v = \frac{\int v_z(r)\,dr}{K_{SEC}A_i + A_o} \tag{7}$$

where A_i are A_o are the cross-sectional areas associated with the intraparticle and interstitial pores spaces, respectively. The integral in the numerator can be recognized as the total flow rate through the matrix. For a pointlike solute without enthalpic interaction, all accessible locations in the interstitial and intraparticle pore spaces are thermodynamically equivalent and K_{SEC} equals unity. We denote the velocity of this pointlike solute as v_m. Equation 7 can then be rearranged to its standard textbook form

$$\frac{v}{v_m} = \frac{V_i + V_o}{K_{SEC}V_i + V_o} \tag{8}$$

after multiplying by the column length to transform A_i and A_o into the intraparticle and interstitial volumes, V_i and V_o, respectively.

Assertion of Equilibrium. The finite rate of solute permeation into packing particles might appear to place severe restrictions on the application of the equilibrium theory of SEC to real chromatography systems (*29,30*). A quick assessment of solute diffusion finds that a polymer transported past a single packing particle will not spend sufficient time in the particle's vicinity to sample all intraparticle pore space. In fact, a particle level Peclet number, $Pe = v_m d_p/D$, can be significantly greater than unity ($Pe \approx 300$ for nominal values $v_m=0.03$ cm/s, $d_p=10^{-3}$cm, and $D=10^{-7}$cm^2/s), revealing the dominance of interstitial convection over intraparticle diffusion. These factors suggest that the solute velocity might be regulated by the rate of intraparticle permeation and not by the extent of this permeation. Such reasoning, however, is misguided. A single polymer molecule migrating through a chromatography column, or even a pulse of these molecules, need not achieve equilibrium solute exchange at the length scale of a single particle or short column section for equation 8 to apply. Instead, equilibrium exchange must be established only prior to final elution from the column. The column length effecting equilibrium solvent exchange defines the Height Equivalent to a Theoretical Plate HETP (~ d_pPe), and the HETP is always orders of magnitude less than the column length L. In fact, a steady solute velocity can not be assured until the solute has migrated through a column section longer than HETP. We conclude that it is the dimensionless parameter $Pe(d_p/L)$, and not Pe, which must be small for equation 8 to apply. That the velocity from a steady solute source can be equated to the velocity from a pulse injection implicitly manifests the same result.

Hydrodynamic Chromatography

Description and Modeling. With nonporous packing particles of a size similar to those employed in SEC, solute partitioning in HDC is restricted to interstitial space. Chain confinement is consequently less severe than in SEC, being limited to near-surface regions. To simplify analysis, both radial velocity components and the z dependence of $\Delta S_c(z,r)$ are neglected (the former approximation is already implied in equation 3). These approximations eliminate the z dependence of c and yield a concentration profile conforming to equation 6. When this profile is substituted into equations 1 and 2, a standard governing equation for HDC is generated.

$$\frac{v}{v_m} = \frac{\int v_z(r)\, e^{\Delta S_c(r)/k}\, dr \int dr}{\int v_z(r)\, dr \int e^{\Delta S_c(r)/k}\, dr} \qquad (9)$$

Unlike SEC, the flow profile cannot be eliminated from the governing expression. Most theories assume that the interstitial space can be modeled as a capillary, and consequently, the flow profile is parabolic. (Remember that r has been defined as a generalized radial coordinate and cannot be equated to the radial variable R of a cylindrical coordinate system; if such a coordinate system is adopted for a tube geometry, then $dr=2\pi R dR$).

Gel Electrophoresis

Description. GE can be performed in many of the same media as SEC, although absence of the mechanical stress from an imposed flow permits broader use of "soft" gel matrices. During GE, a steady electric field of magnitude E drives solute outward from an injection site and into a bulk separation medium. Steady solute velocity v, or more fundamentally, solute mobility μ, characterizes the rate of field-driven transport. The mobility is obtained as the ratio v/E. At low applied fields, the only case to be analyzed here, μ attains an E independent plateau; this feature reveals that equilibrium structures of solute and matrix are not altered by the field. In analogy, flow rate independent elution at low pressure drop for SEC and HDC similarly implies that equilibrium structures of solute and matrix are not modified. The porous support in a GE experiment is monolithic, lacking interstitial space. Electrophoresis gels are selected and modified to the fullest extent possible to reduce enthalpic interactions between solute and support. As in SEC, a slight negative repulsion is common and acceptable, with origins in the residual matrix charge. The polymer concentration of an electrophoresis gel can range anywhere from 0.1% to 20%, with higher gel concentrations generally producing smaller and more uniform pores. Unlike SEC and HDC packings, GE media need not be reused, allowing pore size to be optimized for each experiment. These sizes range from one to several hundred nanometers.

Molecular Origins of the Separation. In absence of a support matrix, the free solution electrophoretic mobility μ_0 of a long chain molecule is independent of molecular weight M (*31,32*). To obtain such independence in the presence of an electrostatic force F_e linear in the number of chain segments N, the hydrodynamic drag F_h on a migrating chain must also be linear in N. Linearity of F_h can be traced to the cancellation by counterions of long range, field-induced hydrodynamic interactions between charged chain segments (an often cited alternative explanation for this linearity, relying on the intrinsic "free-draining" behavior of swollen polyelectrolytes, is incorrect; see refs. 33 and 34). The same cancellation occurs for chains enmeshed in a dilute gel, where F_e changes little from free solution and remains linear in N. We infer that a support matrix must effectively increase hydrodynamic drag to yield a molecular weight separation. As we will show, the increase of apparent drag arises most prominently from spatial fluctuations in $\Psi(z,r)$, not from coupled solute/matrix hydrodynamics or sliding friction. The key contribution of this article will be an explanation of GE using equations 1-5, the same equations that successfully explain SEC and HDC.

The partitioning of solute is obvious and critical for SEC and HDC, while for GE the partitioning is more subtle, principally because a monolithic gel has only one obvious length scale, the average pore size. How can a solute partition within a homogeneous space? The key to this paradox lies in the detailed microstructure of a polymer gel. At length scales comparable to a migrating polymer chain, real gels are highly irregular, possessing a broad but not random pore size distribution (*35-38*). Given sufficient time, a flexible solute can partition locally, between the relatively open and the relatively constricted matrix regions. Figure 1a shows a flexible chain enmeshed in an idealized random two-dimensional medium generated by the site percolation method. The volume fraction of the randomly placed square obstacles is 20%. Figure 1b shows a chain of comparable length placed inside a medium with regular structure. The matrix volume fraction is again 20%, and the average separation between obstacles is nearly the same as in the upper figure. Although the spatially averaged partition coefficients K_{SEC} for the two matrices are nearly identical, the heterogeneity of the more random structure strongly perturbs the flexible solute's localized thermodynamics, creating substantial concentration gradients. Similar thermodynamic considerations apply whenever a flexible or nonspherical Brownian solute is placed in an irregular space.

Modeling. A rigorous application of transport theory to the polymer and matrix of Figure 1a would appear difficult. To simplify, we first note that the $J_r(z,r)$ again averages to zero at each radial position, providing a cross-sectional concentration profile similar to that found in SEC and HDC,

$$c(z,r) = c_0(z)e^{\Delta S_c(z,r)/k} \tag{10}$$

where r and z dependencies have been made explicit. The unknown function $c_0(z)$ is evaluated by substituting equation 10 into equation 2 and then searching for a compatible solution for c(z,r). Such a solution can be written (*28*)

$$c(z,r) = e^{-\phi(z,r)/kT}\left\{ \int e^{\phi(z,r)/kT}[-J_z(z,r)/D]\, dz + c_1 \right\} \tag{11}$$

where constant c_1 can be assigned by requiring the average of c(z,r) remain finite. In an irregular but isotropic matrix, the term within braces becomes independent of r for integration over a large enough z interval. The potential $\phi(z,r)$ for an electrophoresis experiment decomposes into separate external and intrinsic components,

$$\phi(z,r) = -qEz - T\Delta S_c(z,r) \tag{12}$$

where the first term, proportional to solute charge q, represents the macroscopic potential arising from the applied field. The localized perturbations of E caused by the matrix have been neglected.

From the form of equation 11, the solute is seen to partition both in the radial and axial directions. While the latter partitioning has little role in either SEC or HDC, being ignored in standard molecular models of both, this partitioning provides the key to understanding GE under the local equilibrium hypothesis. One also notes that, while the axial solute flux J_z is constant everywhere, the solute concentration c(z,r) fluctuates strongly along the axial direction. These properties reflect the accumulation of chains in the less confining matrix zones, where the axial rate of solute motion proportionately increases to maintain constant flux. This behavior is reminiscent of a sequence of chemical reactions operating at steady state; along the reaction pathway, chemical intermediates accumulate to a finite, but variable extent depending on their thermodynamic stability. The depleted solute zones then have an analogy to the thermodynamically unstable transition states between individual sets of reactants and products.

Asserting that the local fluctuations in ΔS_c are uncorrelated with the globally applied steady electric field - an approximation rigorously valid only in a dilute gel - the integral of the equation 11 can be evaluated analytically and then substituted into the equation 1. After calculating the integration constant c_1, the two remaining integrals are readily performed over J_z and c(z,r). The result is a general expression for the electrophoretic velocity,

$$v = \frac{qED}{kT}\,\frac{1}{\langle e^{-\Delta S_c/k}\rangle \langle e^{\Delta S_c/k}\rangle} \tag{13}$$

where < >, the notation for an ensemble average, has replaced integrals effecting the z average; the averages are equivalent for an isotropic matrix. After normalizing v with the electrophoretic velocity in the absence of confinement,

$$\frac{v}{v_m} = \frac{1}{\langle e^{-\Delta S_c/k}\rangle \langle e^{\Delta S_c/k}\rangle} \tag{14}$$

a governing equation for GE analogous to those for SEC (equation 8) and HDC (equation 9) is finally obtained. Note that $v=v_m=qeD/kT$ when ΔS_c has no spatial variation. If enthalpic interactions between solute and matrix are present, an extended version of equation 14 can be rewritten with ΔS_c replaced by $-\Psi/T$.

Connections to Previous Theory. Equation 14 is essentially a new result, although there are weak connections between the ratio v/v_m and the "constrictive factor" calculated by Giddings and Boyack (*39,40*). The present derivation most closely follows a recent analysis by Zimm and Lumpkin (*28*), who presented a specialized form of equation 14 that assumes reptation as the mechanism of solute transport in the absence of confinement fluctuations. Under reptation, the variable v_m does not reflect free solution behavior as implied here. We do not believe that flexible chains "reptate" between regions of different confinement level, since matrix irregularities - such as those shown in figure 1a - usually occur at length scales comparable or smaller than the overall chain size. Zimm and Lumpkin assumed the opposite, that matrix structure is homogeneous at these length scales. Matrix fluctuations enter their analysis only at much greater length scales. Equation 13, however, admits the Zimm and Lumpkin result if D is assigned the reptation value. Reptation is a restricted mechanism of solute motion available only to flexible linear chain molecules, whereas equation 14 was derived without resorting to either a solute or matrix model, resulting in a wider range of applicability. In general, to correct for the potential impact of matrix structure on solute hydrodynamic friction, one can choose or calculate an appropriate expression for D and substitute this form into equation 13. Under the local equilibrium principle, D should be selected as D_0, the value in absence of a matrix.

Motion of a Pointlike Solute. To better understand equation 14, consider a matrix so dilute that the exponentials can be expanded for small values of their argument. Then, to second order,

$$\frac{v}{v_m} = \frac{1}{1+\langle(\Delta S_c/k)^2\rangle - \langle\Delta S_c/k\rangle^2+\ldots} \qquad (15)$$

an expression that highlights the role of spatial fluctuations, rather than mean thermodynamic properties, in attenuating solute transport. A good illustrative calculation is that for a non-interactive spherical solute. Although the local confinement entropy of such a solute is poorly defined, the replacement of ΔS_c by $\ln\langle\exp(-\Psi/T)\rangle$ is rigorous in this instance, and Ψ for a spherical solute possesses unambiguous physical meaning even at the local level: Ψ is infinite for center of mass locations inside the matrix material, or within one sphere radius of the matrix surface, and zero everywhere else. With these choices, v_m corresponds to the solute velocity in the absence of matrix, since Ψ equals zero in the reference thermodynamic state. Also note that Ψ follows a Poisson distribution in a hypothetical matrix imposing random obstacle locations. Combining these conclusions, and applying the relationship between the mean and variance of a Poisson distribution, a simplified version of equation 15 is quickly found

$$\frac{v}{v_m} = \frac{1}{1+\langle\Psi/kT\rangle} \qquad (16)$$

A Poisson distribution is not essential, as the same result applies to any dilute matrix with interactions sufficiently localized to write $\langle\exp(-\Psi/T)\rangle$ as $\exp\langle-\Psi/T\rangle$. The mean solute potential can be written in terms of the excluded volume fraction p, using the standard thermodynamic formula for a dilute system $\langle\Psi/kT\rangle = p$ and expanding for small values of p,

$$\frac{v}{v_m} = 1 - p \qquad (17)$$

For a pointlike solute, p is equal to the matrix volume fraction. Equation 17 has apparently not previously been presented in the form given here, although Altenberger and Tirrell (*20*) examined tracer diffusion in a similar environment and effectively derived the same expression. The formula can also be obtained from the classic Maxwell solution (*21*) for conduction in a composite medium if the applied field at the local level is constrained to be spatially uniform.

The electrophoretic motion of spherical solutes in low porosity gel matrices has often been described in terms of the Ogston model (*6,7,19*), a semiempirical approach that models the matrix as a random array of obstacles, usual rods, and then equates v/v_m to the solute's overall partition coefficient into this array,

$$\frac{v}{v_m} = K = \langle e^{-\Psi/kT} \rangle \tag{18}$$

As noted by both Morris (*8*) and Cobbs (*39*), there is no sound theoretical justification for this assignment of v/v_m. A comparison of equation 18 with equations 14 and 16 shows that the Ogston approach provides a reasonable approximation under the condition that $\langle \Psi/kT \rangle \ll 1$. Given the form of equation 16, $\langle \Psi/kT \rangle \ll 1$ corresponds to only a minor modification of v by the matrix; thus, we believe the Ogston model has little practical import, even for compact spherical solutes. A detailed examination of equation 14 shows that the Ogston model incorporates only the first factor in the denominator of this equation, albeit with different spatial averaging.

Motion of a Flexible Chain Solute. We and others have coined the term "entropic barriers transport" to describe both the electrophoretic and diffusive behaviors of a flexible polymer governed by matrix irregularity (*26,27,42,43*). Equation 14 is a general mathematical treatment for such transport if we identify the local entropy $\Delta S_c(z,r)$ with the configurational degrees of freedom possessed by a polymeric solute with center of mass position z and r. Local equilibrium is a necessary condition for the solute to sample fully its accessible degrees of freedom and thus to interpret configurational transport effects via a thermodynamic formalism. Entropic barriers transport is an activated process in which Brownian fluctuations drive solute across a spatially distributed energy surface; a specific configurational pathway for each barrier crossing is not assigned, or even needed, as all such pathways are randomly sampled. Discussions of activated transport in the presence of a potential field date back at least to the early 1940's (*44*).

Equation 15 is a considerable advance over our earlier, and more qualitative, discussions of entropic barriers transport (*42,43*). To place the equation into the context of polymer electrophoresis, we will analyze a second case, one based on the highly idealized matrix model shown in Figure 2. Here, a flexible chain is driven by an applied field down a periodic channel imposing alternating levels of confinement between two planar, parallel surfaces that locally define a slit geometry. Although this matrix is obviously not isotropic, one can demonstrate that the same formalism applies if the confinement entropy is analyzed as a cross-sectional average and the ensemble averages replaced by axial averages along the slit length. To further simplify, we stipulate that the alternating slit sections are much longer than the chain size, eliminating possible axial confinement effects for chains located near junctions. The ratio of chain size R to lateral dimension w thus dictates $\Delta S_c(z,r)$, which can adopt two discrete values, $\Delta S_c(1)$ and $\Delta S_c(2)$, for sections 1 and 2, respectively. We first assume that the alternating slit sections are of equal length. Applying equation 15, we find that the electrophoretic velocity follows

$$\frac{v}{v_m} = \frac{4}{[e^{-\Delta S_c(1)/k} + e^{-\Delta S_c(2)/k}][e^{\Delta S_c(1)/k} + e^{\Delta S_c(2)/k}]} \tag{19}$$

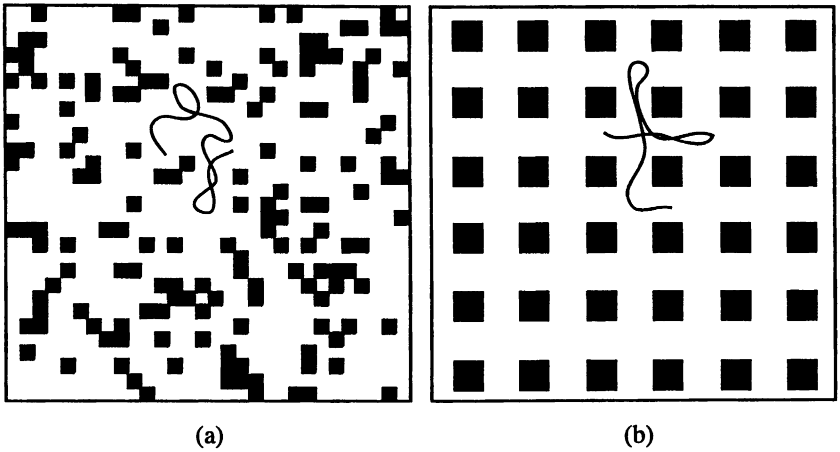

Figure 1. (a). A flexible polymer chain trapped in a random two-dimensional porous medium (volume fraction=0.2). The irregularity of the medium, coupled with the flexibility of the chain, will produce local fluctuations in chain concentration. To move macroscopically, the chain must traverse constricted zones under the action of Brownian motion. (b). A medium of the same volume fraction but more regular in microstructure. Here, the chain concentration is essentially uniform, and only weak energetic barriers must be surmounted for macroscopic chain motion.

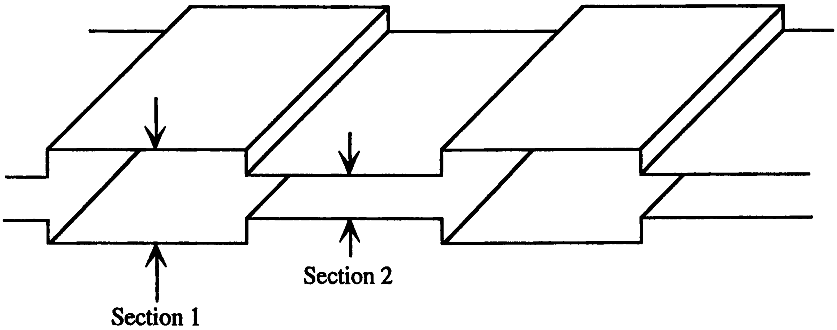

Figure 2. A periodically constricted channel that imposes entropic barriers on a flexible, translating polymer chain. The depth of the channel is infinite, but the lateral dimension w alternates between two discrete values. Lengths of sections 1 and 2 are both much greater than w.

$$\frac{v}{v_m} \sim e^{-\Delta S_c(1,2)/k}, \qquad \Delta S_c(1,2)/k \gg 1 \qquad (20)$$

where $\Delta S_c(1,2)$ is the difference in confinement entropy between section 1 and 2, i.e., $\Delta S_c(1,2) = \Delta S_c(1) - \Delta S_c(2)$. Equation 20 corresponds to the limiting case in which chain motion is controlled by a single slow step, chain diffusion or "hopping" from section 1 into section 2; we have discussed this case previously (*42*). Similar analyses show, that with all other geometric factors fixed, v is inversely proportional to the density of constricted zones in the periodic channel. Likewise, if the length of the narrow slit sections is a fraction F of the length of the wide sections, v is inversely proportional F. We prefer the idealized periodic slit geometry as a gel representation, since many exact values of ΔS_c are available for this environment; especially useful are the calculations by Laurent and Killander (*12*), Casassa and Tagami (*16*), and Giddings et al (*13*).

Calculations of Confinement Entropy

The models presented here for SEC, HDC, and GE predict that separations between dissimilar chemical species occur according to differences in ΔS_c. In practice, the experimentalist's objective is nearly always to separate homologous polymer chains according to molecular weight M or molecular size R. The relationship between ΔS_c and M or R thus becomes an important issue. Although the central role of ΔS_c has been recognized often in the SEC and HDC literature, experimental results continue to be interpreted using R as the fundamental operating parameter. For example, the "universal calibration" approach pioneered by Benoit (*45*) for SEC shows that the product of M and the intrinsic viscosity [η] successfully collapses elution data for a variety of different flexible polymer systems. For large M, hydrodynamic analyses show that [η]M is universally proportional to R^3; thus, when universal calibration holds, chains of different M but identical R are expected to elute at the same v. The situation in GE is less clear, with the Ogston model asserting that R is the key operating parameter and the reptation approach alternatively suggesting that M assumes this role. As shown by our own earlier experiments with star, circular, and linear polymers (*46*), a large parameter range exists in which neither concept properly accounts for v. Applying the fundamental statistical definition of entropy, we can write

$$\Delta S_c(z,r) = k \ln \frac{\Omega_i(z,r)}{\Omega_o} \qquad (21)$$

where $\Omega_i(z,r)$ is the number of accessible configurations for a solute stationed at center of mass position z and r, and Ω_o is the analogous number for the same solute in unconfined space. Once models for the solute and matrix are available, equation 21 poses a counting exercise. We are interested in determining which molecular property - M, R, or something else - best correlates the averages over $\Delta S_c(z,r)$ required in equations 6, 9 and 14. As there are many different ways to define R, this exercise might also provide guidance as to what molecular radius will be returned by a given method, if such a radius indeed exists.

Matrix Models. To address these questions, a matrix model must be adopted first. Practitioners of SEC have generally preferred what we will term "internal" pore models, those that place the solute inside a cavity. Examples are shown in Figure 3a. In contrast, analyses of GE are generally performed for "external" pore models, those that place the solute on the outside of an array of rigid impenetrable obstacles. Examples are displayed in Figure 3b. Others have alternatively employed the terms "predominantly concave" and "predominantly convex" in place of "internal" and "external" (*15*). The internal models generally establish no connectivity criterion, a reasonable simplification if axial transport pathways are unimportant and lateral partitioning is critical. We must only envisage that the cavity is part of a percolated network that eventually connects to interparticle space. For GE, on the other hand, the basic pore model must establish an axial pathway penetrating the entire network. HDC matrix models are most often based on an oriented capillary description, which can be viewed as a hybrid of the SEC and GE approaches. In cases where electron micrographs are available, the images are often more supportive of external pore models (*38,47-49*).

Chain Models. To understand their transport, polymer chains have often been modeled as rodlike, Gaussian, or spherical. In reality, few polymers adopt the latter conformation, although effective sphere models are extremely useful in correlating chain properties in unbounded solution. So-called Gaussian chains, for example, are far from spherical in an instantaneous snapshot, but after the orientational and configuration averaging intrinsic to bulk solution properties, a single size parameter can characterize the chains' spatial extent. Consequently, Gaussian chains obey many of the solution models derived for spherical particles, with an "effective" or "equivalent" radius proportional to the size of the chain's averaged spatial envelope. Upon confinement, however, Gaussian chains will not sample the same range of orientations and configurations, rendering an effective solution radius of dubious consequence. Nonetheless, many investigators have sought to define a single universal size parameter R_{eff} that can correlate elution data from different polymer systems. A strongly connected issue is the relevance of this R_{eff}, if it exists, across different separation methods. Do SEC, HDC, and GE separate polymers according to the same molecular property?

Failure of R_{eff}. Calculations of confinement entropy for rod-like, Gaussian chain, and spherical solutes have been performed for all of the matrix models in Figure 3, using methods described in a previous paper (*42*). With the external pore models, analytical calculations for Gaussian chains have been restricted to large obstacle spacing, a condition necessary to preclude simultaneous chain interaction with more than one obstacle. The confinement entropy in each case has been determined as a function of center of mass position, and where necessary, averages applied over this entropy as suggested in the governing equations for SEC, HDC, and GE. The absurd cases, such as the HDC of solutes in a spherical cavity, have been skipped.

The calculations show that, excepting a solute exposed to a single planar wall, the concept of R_{eff} fails. Figure 4 is a typical example. The figure shows the change in partition coefficient K_{SEC} for spheres, Gaussian chains, and rods, as solute size varies in a dilute array of cylinders at volume fraction ε. A random cylinder array is regarded by many investigators as the simplest realistic matrix model for a swollen gel. The figure explicitly plots the dimensionless coefficient V_d from the equation

$$K_{SEC} = 1 - V_d \varepsilon \qquad (22)$$

that applies in the low ε limit [an arithmetic error has been corrected from an earlier presentation (*42*) of the same graph]. The abscissa normalizes molecular size - radius S, radius of gyration R_g, or length H, respectively, for spheres, Gaussian chains, and rods - with cylinder radius a. Note that a simple linear redefinition of abscissa cannot map the different curves onto one another except when dimensionless solute size is small. In this limited region, cylinder surfaces are effectively planar, and the different curves indeed collapse when the usual linear mapping $R_{eff}=S=L/4=2R_g/4$ is applied However, in the more relevant range of large dimensionless solute size, any linear

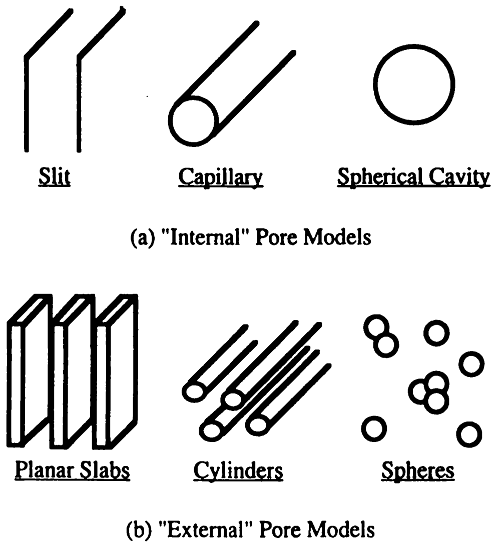
Slit
Capillary
Spherical Cavity
(a) "Internal" Pore Models
Planar Slabs
Cylinders
Spheres
(b) "External" Pore Models

Figure 3. Matrix models employed to study chain motion in SEC, HDC, and GE. The obstacles of external pore models are typically oriented and positioned less regularly than implied by the sketch.

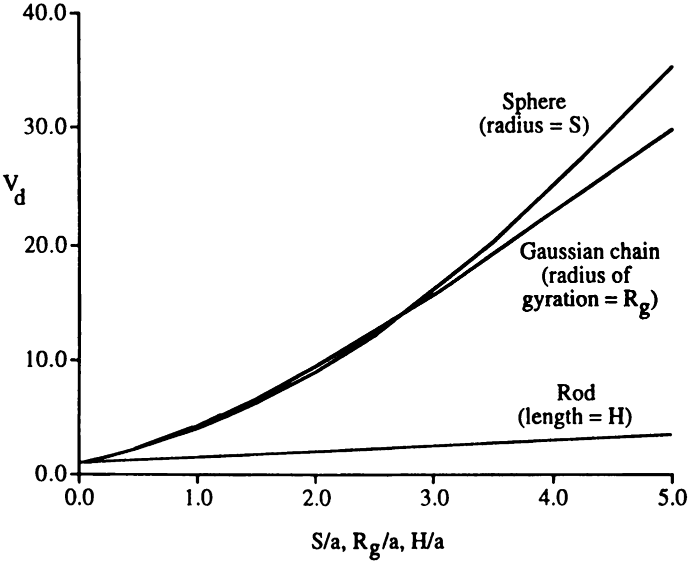

Figure 4. Exclusion parameter V_d as a function of dimensionless chain size for solutes modeled as spheres, Gaussian chains, and rods. Exclusion is from a dilute array of cylinders with radius a. The Gaussian chain curve crosses the sphere curve at an abscissa value near 2.8. Lower V_d implies less exclusion from the matrix.

mapping fails, precluding the definition of R_{eff}. The reason for the breakdown is obvious: in a curved confinement geometry, there is an extra length scale characterizing the radius of curvature of the matrix. In particular, Gaussian chains near cylinders are much less depleted than predicted by a sphere representation since the chains can adopt conformations that "wrap around" cylinders. This phenomenon, which has no manifestation in bulk solution properties, becomes more significant as chain size increases or as cylinder size decreases. For a gel matrix where cylinders represent gel fibrils, the ratio of chain to cylinder size will always much exceed unity, and in this geometric range, correlations by R_{eff} are the most problematical.

Under confinement more severe than permitted by equation 22, the difficulty with R_{eff} becomes even more immediate. If we consider the slit representation of figure 3, for example, we recognize that a Gaussian chain can always migrate, albeit at much reduced velocity under stronger confinement. A sphere larger than the narrowest slit section can not migrate at all. In fact, applying the channel model with the two slit widths comparable or smaller than the radius of gyration, both $\Delta S_c(1)$ and $\Delta S_c(2)$ become linear in M for a flexible chain solute (see ref. 50 for an explanation). From equation 20, we observe that the electrophoretic velocity will then decay as an exponential of M. In this limiting case, separation is an indirect function of free solution molecular size, at best, no matter what size parameter is chosen.

General Trends Discernible in Elution Behavior. Separations of flexible polymers by SEC, HDC, and GE fall broadly across a confinement spectrum. When pores are large and matrix curvature low, the elution velocity correlates well with the molecular size measured in unbounded solution. These are typical conditions for SEC and HDC, where the mean pore is an order of magnitude or more larger than the solute. In a gel matrix, on the other hand, pores are smaller and matrix curvature stronger, leading to a lessened role for molecular size. As confinement grows, i.e., with increasing chain length or gel concentration, the solute molecular weight begins to govern elution. These are typical conditions for GE. Ultimately, in a dense gel, kinetic effects overwhelm thermodynamic considerations and a flexible chain reptates (*51,52*), with the elution velocity controlled entirely by molecular weight.

In overview, enhanced confinement of flexible chains leads to a better discrimination according to chain length and an inevitable crossover from molecular size-based separation to molecular weight-based separation. For rigid but nonspherical solutes, similar molecular size-based separation occurs at low confinement, but at moderate to severe confinement, different pore structures will separate solutes according to different size parameters; there is no simple formula or trend able to correlate elution behavior. When confinement of a rigid solute is not too severe, the calculation schemes outlined by Giddings et al. (13), Doi (14) and Limbach et al. (15) provide a quantitative framework for predicting the partition coefficient, but only given that the solute and/or matrix structures are known *a priori*.

Constraints on the Thermodynamic Model

Three conditions lead to the failure of the principle of local equilibrium: (1) the axial length of the separation medium is too short for migrating chains to sample fully a representative range of local positions and chain conformations; (2) the applied field is large enough to alter the average chain conformation (or even the average matrix structure); and (3) the chain friction coefficient within the medium diverges from that in unbounded solution. The latter problem arises only in the context of GE, since the friction coefficient does not enter governing expressions for SEC or HDC. In GE, the dependence of chain friction on gel density can be ignored only when chain confinement is below a critical level. Unfortunately, this level cannot be predicted by any current theory. With long and flexible chains, failure of local equilibrium via this route accompanies the onset of chain motion by reptation, a transport mechanism impossible to frame in thermodynamic terms. For other solute types, hydrodynamic friction at high matrix density can only be assessed by calculating the friction for a representative set of local matrix geometries and then averaging (*53*).

Returning to the failure list, item 1 is trivial, as a good separation cannot be obtained for matrices possessing lengths comparable or less than HETP. The remaining condition creates the greatest concern for all three separation techniques. The symptom of failure by item 2 is field dependent elution. In HDC, for example, high flow rates can produce hydrodynamic stresses at pore convergences able to stretch, or even break, flexible chain molecules. In the absence of breakage, the result is an unexpected increase in v. Likewise, GE models for the separation of flexible polymers at high E must account for chain orientation and stretching, phenomena that also increase v. Although thermodynamic factors may continue to play a role when items 1-3 are operative, the governing equations given here must certainly be viewed with caution.

All of the equations presented in this chapter were derived while neglecting the local fluctuations in the applied field that arise from matrix inhomogeneity. Locally, field lines in a GE experiment are distorted in response to the mismatch of electrical properties between matrix material and mobile phase. We have also assumed that this material is rigid, a potentially unsuitable approximation for many common gel media. Depending on the geometry, physical properties, and concentration of matrix, any of these added complications could lead to quantitative errors of considerable magnitude.

Acknowledgments

The financial support of the University of Massachusetts Materials Research Science and Engineering Center (MRSEC) is gratefully acknowledged, as are the ideas and assistance of Evangelia Arvanitidou.

Literature Cited

1. Yau, W. W.; Kirkland, J. J.; Bly, D. D. *Modern Size-Exclusion Liquid Chromatography*; J. Wiley & Sons: New York, NY, 1979.
2 *Gel Electrophoresis of Proteins; a Practical Approach*; Rickwood, D., Hames. B. D.; Eds.; IRL Press: Washington DC, 1981.
3. Andrews, A. T. *Electrophoresis, Theory, Techniques, and Biochemical and Clinical Applications*, 2nd ed.; Clarendon Press: Oxford, UK, 1986.
4. Small, H.; Saunders, F. L.; Solc, J. *Adv. Coll. Int. Sci.* **1976**, *6*, 237-266.
5. McHugh, A. J. *CRC Critical Reviews in Analytical Chemistry* **1984**, *15*, 63-117.
6. Rodbard, D.; Chrambach, A. *Proc. Natl. Acad. Sci. USA* **1970**, *65*, 970-977.
7. Rodbard, D.; Chrambach, A. *Anal. Biochem.* **1972**, *40*, 95-134.
8. Morris, C. J. O. R.; Morris, P. *Biochem. J.* **1971**, *124*, 517-528.
9. Squire, P. G.; Magnus, A.; Himmel, M. E *J. Chrom.* **1982**, *242*, 255-266.
10. Potschka, M. *Anal. Biochem.* **1987**, *162*, 47-64.
11. Dubin, P. L.; Principi, J. M. *Macromolecules* **1989**, *22*, 1891-1896.
12. Laurent, T. C.; Killander, J. *J. Chrom.* **1964**, *14*, 317-330.
13. Giddings, J. C.; Kucera, E.; Russell, C. P.; Myers, M. N. *J. Phys. Chem.* **1968**, *72*, 4397-4407.
14. Doi, M. *Chem. Soc., London, Faraday Trans. II* **1975**, *71*, 1720-1729.
15. Limbach, K. W.; Nitsche, J. M.; Wei, J. *AIChE J.* **1989**, *35*, 42-51.
16. Casassa, E. F.; Tagami, Y. *Macromolecules* **1969**, *2*, 14-26.
17. Casassa, E. F. *J. Phys. Chem.* **1971**, *75*, 3929-3939.
18. Casassa, E. F. *Polym. Lett.* **1967**, *5*, 773-778.
19. Ogston, A. G. *Trans. Faraday Soc.* **1958**, *54*, 1754-1757.
20. Altenberger, A. R.; Tirrell, M. *J. Chem. Phys.* **1984**, *80*, 2208-2213.

21. Maxwell, J. C. *A Treatise on Electricity and Magnetism,* 3rd ed.; Clarendon Press: Oxford,UK, 1892; Vol. 1, pp 435-440.
22. Koch, D. L.; Brady, J. F. *J. Fluid Mech.* **1985**, *154*, 399-427.
23. Koch, D. L.; Brady, J. F. *AIChE J.* **1986,** *32*, 575-591.
24. Brenner, H.; Gaydos, L. J. *J. Coll. Int. Sci.* **1977**, *58*, 312-356.
25. Brenner, H. *Phil. Trans. Roy. Soc. London* **1980**, *A297*, 81-133.
26. Muthukumar, M.; Baumgartner, A. *Macromolecules* **1989**, *22*, 1937-1946.
27. Muthukumar, M.; Baumgartner, A. *Macromolecules* **1989**, *22*, 1941-1946.
28. Zimm, B. H.; Lumpkin, O. *Macromolecules* **1993**, *26*, 226-234.
29. Hermans, J. J. *J. Polym. Sci., Part A-2* **1968**, *6*, 1217-1226.
30. Aubert, J. H.; Tirrell, M. *J. Liq. Chrom.* **1983**, *6(S-2)*, 219-249.
31. Manning, G. S. *J. Phys. Chem.* **1981**, *85*, 1506-1515.
32. Olivera, B. M.; Baine, P.; Davidson, N. *Biopolymers* **1964**, *2*, 245-257.
33. VanderDrift, W. P. J. T.; deKeizer, A.; Overbeek *J. Coll. Int. Sci.* **1979**, *71*, 67-78.
34. Stigter, D. *J. Phys. Chem.* **1978**, *82*, 1417-1423.
35. Bastide, J.; Leibler, L. *Macromolecules* **1988**, *21*, 2647-2649.
36. Matsuo, E. S.; Orkisz, M.; Sun, S.-T.; Li, Y.; Tanaka, T. *Macromolecules* **1994**, *27*, 6791-6796.
37. Cohen, Y.; Ramon, O.; Kopelman, I. J.; Mizrahi, S. *J. Polym. Sci., Part B: Polym. Phys.* **1992**, *30*, 1055-1067.
38. Attwood, T. K.; Nelmes, B. J.; Sellen, D. B. *Biopolymers* **1988**, *27*, 201-212.
39. Giddings, J. C.; Boyack, J. R. *Anal. Chem.* **1964**, *36*, 1229-1233.
40. Giddings, J. C. Dynamics of Chromatography. Part 1. Principles and Theory; Marcel Dekker: New York, NY, 1965; pp 245-247.
41. Cobbs, G. *Biophys. J.* **1981,** *35*, 535-542.
42. Arvanitidou, E. S.; Hoagland, D. A.; Smisek, D. L. *Biopolymers* **1991**, *31*, 435-447.
43. Hoagland, D. A.; Muthukumar, M. *Macromolecules* **1992**, *25*, 6696-6698.
44. Chandrasekhar, S. *Rev. in Modern Physics* **1943**, *15*, 1-87.
45. Grubisic, Z.; Rempp, P.; Benoit, H. *J. Polym. Sci.* **1967**, *B5*, 753-759.
46. Smisek, D. L.; Hoagland, D. A. *Science* **1990**, *248*, 1221-1223.
47. Waki, S.; Harvey, J. D.; Bellamy, A. R. *Biopolymers* **1982**, *21*, 1909-1926.
48. Amsterdam, A.; Er-El, Z.; Shaltiel, S. *Arch. Biochem. and Biophys.* **1975**, *171*, 673-677.
49. Ruchel, R.; Brager, M. D. *Anal. Biochem.* **1975**, *68*, 415-428.
50. de Gennes, P.-G. *Scaling Concepts in Polymer Physics*; Cornell Univ. Press: Ithaca, NY, 1979; pp 46-51.
51. Lerman, S.; Fisch, H. L. *Biopolymers* **1982**, *21*, 995-997.
52. Lumpkin, O. J.; Dejardin, P.; Zimm, B. H. *Biopolymers* **1985**, *24*, 1573-1593.
53. Lumpkin, O. J. *J. Chem. Phys.* **1984**, *81*, 5201-5205.

Downloaded by UNIV OF GUELPH LIBRARY on October 8, 2012 | http://pubs.acs.org
Publication Date: May 30, 1996 | doi: 10.1021/bk-1996-0635.ch011

Chapter 11

Packings for Size Exclusion Chromatography: Preparation and Some Properties

D. Horák, J. Hradil, and M. J. Beneš

Institute of Macromolecular Chemistry, Academy of Sciences of the Czech Republic, Heyrovského sq. 2, 162 06 Prague 6, Czech Republic

Materials used as packings in size-exclusion chromatography can be divided into organic and inorganic ones. Organic packings include both synthetic and natural products. The preparation of these matrices, the mechanism of porous structure formation, depending on synthesis conditions, as well as the properties of packings, are reviewed.

Since the column is the heart of any chromatographic system, the choice of packing greatly affects the success of any analysis. The basic requirements for the packing material for size-exclusion chromatography (SEC) columns include chemical inertness and minimal adsorption of separated compounds so that the retention may be strictly based on hydrodynamic volume. Further requirements include high porosity which can be either permanent in macroporous resins, or swelling in low-crosslinked polymers. In addition to the chemical properties, the importance of physical properties such as the particle size must be stressed to achieve an adequate resolution of the packing. The particles should be spherical and uniform in size to minimize mass transfer limitations. Since the column separation efficiency increases with decreasing particle size, the size should be as small as possible, however, with good flow properties. High-speed, high-resolution chromatography also sets special requirements for geometrical and mechanical properties. They play a decisive role in the lifetime of the packing and the stability of the flow-rates through the column. It is therefore desirable that all the factors outlined above should be taken into account when choosing the packing. Generally, packings can be divided into universal and those that have a specific effect or "tailor-made" packings. A universal packing covers a broad molecular-weight distribution of the components of an unknown sample. Such preliminary assessment allows the subsequent choice of a resin that has the optimum properties for a given separation problem.

Chromatographical packings have been already systematically reviewed in many papers and monographs (*1-9*). The aim of article is to review the synthesis, morphology and other properties of packings which are important for SEC.

0097–6156/96/0635–0190$15.25/0

Types of SEC Packings

A classification according to the chemical nature of the matrix divides packing materials into several groups: packings based on both synthetic and natural organic polymers and packings based on inorganic materials.

Packings Based on Synthetic Organic Polymers

A basic contribution to the size-exclusion chromatography (SEC) with synthetic organic polymer-based packings was made by Moore in 1964 who prepared a series of styrene-divinylbenzene resins by using various precipitants and a suitable concentration of the crosslinking agent (*10*). Since then these resins have been extensively used as packings for SEC (*5*). Therefore the following discussion is mostly confined to styrene-divinylbenzene copolymers, but the same principles are applicable to other supports, such as methacrylic ester packings which are becoming increasingly popular. Other monomer systems for SEC include acrylamide (*11*), trimethylolpropane trimethacrylate (*12*), 4-methylstyrene crosslinked with 1,2-bis(*p*-vinylphenyl)ethane (*13*), glycidyl methacrylate crosslinked with divinylbenzene (*14*) or ethylene dimethacrylate (*15*), etc. A number of packing materials are available on the market: they are based on both hydrophobic and hydrophilic synthetic resins, usually with several pore and particle sizes and suitable for SEC of compounds with molecular weights from below 2×10^3 up to well over 10^7 (Table I). Recently, tentacle media, in which freely moving polymer chains are bound to the packing matrix by graft polymerization, have been developed by Merck. Due to the flexibility of polymer chains the tentacle media better fit the molecular structure of the analyzed compound and therefore they show better selectivity, higher capacity and higher separation speed compared with classical packings. Another modern approach to SEC recently marketed by Supelco uses templated beads. Template polymers were excellently reviewed by Wulff (*16*).

By far the most widely used technique to prepare the synthetic organic polymer-based chromatographical packings remains to be classical suspension polymerization. In a suspension polymerization, monomers (or their solution) are suspended as a discontinuous (organic) phase of droplets in a continuous phase and polymerized, typically by free-radical mechanism, resulting in regular spherical beads. The continuous phase is usually water, as most monomers are water-insoluble. Suspension stabilizers must be used to protect monomer droplets against coalescence. Water-soluble polymers, both natural (natural gums) or synthetic ones (poly(vinyl alcohol), poly(vinylpyrrolidone), or hydroxypropyl cellulose) are the dispersing agents most generally used. Sometimes surfactants (such as sodium dodecyl sulfate) are added. Inorganic stabilizers, e.g., tricalcium phosphate, magnesium hydroxide, calcium carbonate, bentonite, alumina, are also used. The main parameters which determine the behavior of polymer packings are bead size and mechanical properties, porosity and chemical stability.

There are two main classes of polymer packings - gel-type and macroporous resins.

Downloaded by UNIV OF GUELPH LIBRARY on October 8, 2012 | http://pubs.acs.org
Publication Date: May 30, 1996 | doi: 10.1021/bk-1996-0635.ch011

Table I. Commercial Synthetic Organic Polymer Packings for SEC

Product Name	*Matrix*	*Producer (Distributor)*
Bio-Beads S-X	ST/DVB	Bio-Rad, USA
Bio-Gel SEC	ST/DVB	Bio-Rad
Hamilton PRP	ST/DVB	Hamilton, Switzerland (Alltech, USA)
Nucleogel GPC	ST/DVB	Macherey-Nagel, Germany
PLgel	ST/DVB	Polymer Laboratories, USA (Alltech)
Progel-TSK H	ST/DVB	Supelco, USA
Shodex GPC	ST/DVB	Showa Denko, Japan (Alltech, Waters, USA)
Styragel	ST/DVB	Waters
TSK-Gel H	ST/DVB	TosoHaas, USA
Jordi GPC	DVB	Jordi (Alltech)
Bio-Gel P	acrylamide and *N,N'*-methylenebisacrylamide	Bio-Rad
Trisacryl GF	*N*-acryloyl-2-amino-2-hydroxymethyl-1,3-propanediol	Serva, Germany (Sigma, USA)
Progel-TSK PW	"ethylene glycol and methacrylate"	Supelco
TSK-GEL PW	"ethylene glycol and methacrylate"	TosoHaas
Toyopearl HW	"ethylene glycol and methacrylate"	TosoHaas (Supelco)
BiospherGM	GMA/EDMA	Labio, Czech Rep.
Fractogel	"methacrylate"	Merck, Germany
Separon	HEMA/EDMA	Tessek, Czech Rep.
Shodex OHpak SB-800HQ	"polyhydroxymethacrylate"	Showa Denko, Japan (Waters)
PL aquagel-OH	"polyhydroxyl"	Polymer Laboratories
Asahipak GF-HQ	poly(vinyl alcohol)	Showa Denko
Shodex OHpak Q-800	poly(vinyl alcohol)	Showa Denko (Waters)
Nucleogel GFC (aqua-OH)	"hydrophilic"	Macherey-Nagel

DVB - divinylbenzene, EDMA - ethylene dimethacrylate, GMA - glycidyl methacrylate, HEMA - 2-hydroxyethyl methacrylate (ethylene glycol methacrylate), ST - styrene

Downloaded by UNIV OF GUELPH LIBRARY on October 8, 2012 | http://pubs.acs.org
Publication Date: May 30, 1996 | doi: 10.1021/bk-1996-0635.ch011

Downloaded by UNIV OF GUELPH LIBRARY on October 8, 2012 | http://pubs.acs.org
Publication Date: May 30, 1996 | doi: 10.1021/bk-1996-0635.ch011

Gel-Type Resins. The gel-type resins are generally low crosslinked (1-5% of crosslinking agent) and appear translucent. They do not exhibit any measurable (permanent) porosity in the dry state but swell to varying degrees in organic solvents. They swell much more in a thermodynamically good solvent for the basic uncrosslinked polymer than in a thermodynamically poor solvent. Gel-type resins are often referred to as microporous, because the spaces between the crosslinks occupied by the swelling solvent are considered as small pores. Therefore the gel packings are suitable for SEC of low-molecular-weight compounds. The equilibrium degree of swelling attained is inversely proportional to the network density of the gel which also determines the working range of the gel; its decrease leads to an increase in the exclusion limit of the gel packing while at the same time reducing the mechanical strength of the particles, which is the limiting factor for the applicability of the packing. The drawback of insufficient resistance against volume changes is overcome in resins with permanent porosity which are used for SEC of high-molecular-weight compounds.

Macroporous Resins. The materials referred to as "macroporous" (or "macroreticular") resins, in contrast to the gel-type copolymers, contain a significant non-gel porosity in addition to the gel one, i.e., they are permanently porous in the dry state. Permanent (non-gel) porosity is characterized by the disappearance of transparency of the resin. The higher the porosity, the larger is the opacity. At sufficiently high concentrations of crosslinking agent the non-gel porosity is caused by the addition of an inert diluent to the monomers, which is removed from the final product. Any compound which roughly meets the three conditions, can be used as an inert diluent: it must be soluble or miscible with the monomers, does not react during the copolymerization, and at the end of polymerization can be easily removed from the resin obtained. It is obvious that not many compounds fulfil these conditions. According to their properties they cause either only the increase in the gel porosity or non-gel porosity is obtained. The non-gel porosity in reality are channels between agglomerates of microspheres of which the resin bead is composed.

Mechanism of Porous Structure Formation. The mechanism of the macroporous structure formation was described by Kun and Kunin for the copolymerization of styrene with divinylbenzene in the presence of non-solvating diluent as a process consisting of three stages (*17*). During the first stage, polymer microgels soluble in the monomer-diluent system are formed. As the monomers are converted into copolymer, the polymer chains become less and less swollen and then become entangled (intramolecularly crosslinked) by further progress of the polymerization. At the end of this stage, the nuclei (10-30 nm) are formed. Based on thermodynamic factors, the equation (1) for volume conversion α_c at which phase separation occurs was derived (*5*)

$$\ln(1 - \alpha_c v_3^{00}) + \alpha_c v_3^{00} + \chi_{13}(\alpha_c v_3^{00})^2 + (\nu / V_3)\bar{V}_1 \alpha_c v_3^{00}/2 = 0 \qquad (1)$$

where v_3^{00} is the volume fraction of monomers at the beginning of polymerization, $\chi_{1,3}$ is the Flory-Huggins interaction parameter, ν/V_3 is the effective degree of

Downloaded by UNIV OF GUELPH LIBRARY on October 8, 2012 | http://pubs.acs.org
Publication Date: May 30, 1996 | doi: 10.1021/bk-1996-0635.ch011

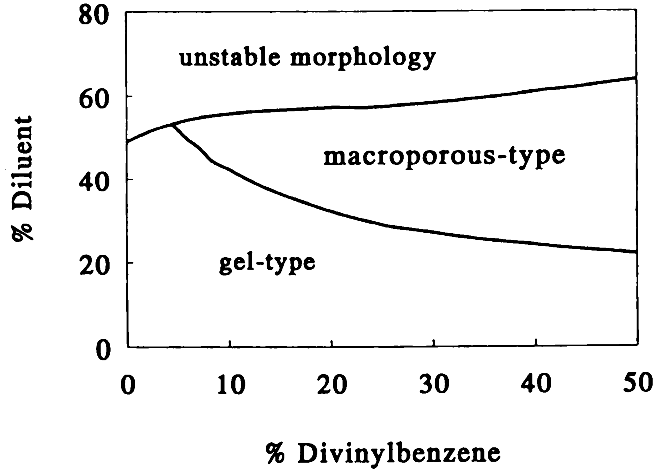

Figure 1. Products of styrene-divinylbenzene copolymerization in the presence of a non-solvating diluent.

Downloaded by UNIV OF GUELPH LIBRARY on October 8, 2012 | http://pubs.acs.org
Publication Date: May 30, 1996 | doi: 10.1021/bk-1996-0635.ch011

crosslinking and $\bar{V}_1$ is the molar volume of the diluent. Phase separation is promoted with increasing concentration of both the crosslinking agent and diluent. The phase separation of polymer and thus the size of pores are also closely related to the Flory-Huggins interaction parameter $\chi_{1,3}$. The lower the thermodynamic affinity of the diluent for the network (i.e., the higher the value of interaction parameter), the larger pores are produced due to easier phase separation (*5*). The polymer-diluent interaction parameter $\chi_{1,3}$ can be predicted by the knowledge of their solubility parameters (*18*). If the difference in the solubility parameter between a diluent and a formed copolymer is zero, miscibility is favored, i.e., the diluent is a good solvent which produces expanded network gel or small pores (*14*). If their difference is larger than 3 $(MPa)^{1/2}$, miscibility does not occur spontaneously so that the diluent separates from the polymer phase and acts as a precipitant of the copolymer; hence phase separation occurs during the polymerization process (*19*). The higher the difference between the solubility parameters of the diluent and of the copolymer, the lower the diluent solvating power - and the porosity of the resin increases (*20*). Some authors suggest that it is rather the dipolar and hydrogen-bond contributions to the solubility parameter which are responsible for pore structure (*21*). The above qualitative description of formation of heterogeneous networks during the crosslinking polymerization is simplified. In addition to thermodynamic factors, also kinetic factors play a certain role and larger pore diameters and narrower pore size distribution are obtained when the rate of polymerization is lower (*22*).

In the second stage of pore structure formation, the entanglements between the polymer chains increase and non-porous nuclei then aggregate into microspheres (100-200 nm). In the third stage, the microspheres aggregate forming particles more or less separated by large holes. Accordingly, the pores generated in this process can be classed into three groups of families: macropores, mesopores and micropores. The large pores (macropores, 50 nm - 1 μm) are interstices between agglomerates of microspheres. They are responsible for high pore volumes (up to 3 ml/g of dry matrix). The intermediate pores (mesopores, 2-50 nm) which account for moderate surface area (*ca.* 50 m^2/g) are the spaces between the microspheres that form these agglomerates. The smallest pores (micropores smaller than 2 nm) which are responsible for high surface area are formed by the voids between the nuclei that form the microspheres. In general, the size of agglomerates and macropores increase with the increase of the diluent and crosslinker proportion (*5*),(*23*). In a phase diagram with the amount of crosslinking agent as the abscissa and the amount of diluent as the ordinate (Figure 1), a macroporous domain may be defined, limited by two boundaries, where the three-level morphology mentioned above may be observed(*24*). Below the lower boundary (low crosslinking agent and low diluent contents), a gel-type material is obtained. Above the upper boundary (high diluent content) an unstable morphology consisting of separate microspheres is visible. Only large pores are present and the surface area is very modest (around 20 m^2/g) in this unstable region. The location of the boundaries is dependent on the nature of the diluent (*24*),(*25*).

An additional complication occurs in the copolymerization of styrene and divinylbenzene. Due to the different reactivity of vinyl groups in the divinylic monomer, pendant vinyl is created on polymer chains during the course of the copo-

Downloaded by UNIV OF GUELPH LIBRARY on October 8, 2012 | http://pubs.acs.org
Publication Date: May 30, 1996 | doi: 10.1021/bk-1996-0635.ch011

lymerization reaction (*26*). The pendant vinyl groups thus formed can then participate in cyclization, crosslinking, or multiple crosslinking reaction, or remain unreacted.

As it has been described (*5*),(*25*), the selection of a diluent added to the monomer phase is the main factor determining the porous structure of the obtained resins. Three main classes of diluent can be considered - solvents for the polymer formed, non-solvents for the polymer formed and finally polymers.

Solvating Diluent as a Porogen Agent. When a solvating diluent is used in a polymerization mixture, large amounts of both the diluent and the crosslinking agent are necessary to get a permanent porosity (*5*). In such conditions, a copolymer is obtained which is characterized by exclusion limit of molecular weight around 5×10^4, by a reduced swelling and by a certain, although limited, porosity in the dry state (pore volume around 0.5 ml/g). At the same time, high surface areas in excess of 500 m^2/g, with a narrow distribution of small pores (10 nm) are obtained (*25*). Microscopic examination of the morphology of a fractured bead shows large agglomerates of essentially one family of medium-sized nuclei (20-80 nm; Figure 2a). At low crosslinking agent and/or diluent content the final structure is only an expanded gel, since the chains are fully solvated during the polymerization and less shrinkage occurs than in the corresponding system in the absence of a solvating diluent (*5*).

Toluene, ethylbenzene, 1,2-dichloroethane, tetrachloromethane are typical solvating diluents for styrene-divinylbenzene resins.

Non-Solvating Diluent as a Porogen Agent. Non-solvating diluents for the copolymer chains are the most frequent porogens added to the monomer phase when macroporous resins are to be obtained (Figure 2b). When such diluents are used phase separation appears at considerably lower crosslinking agent content and lower dilutions than in the case of solvating diluents. Copolymers that have exclusion limits from 10^7 to 10^8 molecular-weight units are obtained and characterized by an internal surface area varying from 10 to 100 m^2/g, a large pore volume (0.6-3 ml/g), and a relatively large average pore diameter. The total pore volume and pore sizes of the resins are thus greater than for the similar resins prepared in the presence of solvating diluents (*27*). A higher degree of crosslinking shifts the pore distribution curves to smaller pore radius.

Aliphatic hydrocarbons such as isooctane or heptane, and organic alcohols such as 1- or 2-butanol, *tert*-amyl alcohol, decyl alcohol are typical examples of non-solvating diluents for styrene-divinylbenzene resins.

When mixtures of solvating and non-solvating diluents are used the resins show porous structures with intermediary characteristics regarding the resins prepared with pure diluents (*18*). The effects of synthesis conditions on the swelling properties are considerably more complex for resins obtained with diluent mixtures.

Polymer as a Porogen Agent. Macroporous resin can also be obtained when a polymer or a solution of polymer is used during the copolymerization (*5*),(*28*). The size of the microspheres and their aggregates and of pores of the macroporous resin prepared using polymer porogens is much larger (Figure 2c) than that of the

Downloaded by UNIV OF GUELPH LIBRARY on October 8, 2012 | http://pubs.acs.org
Publication Date: May 30, 1996 | doi: 10.1021/bk-1996-0635.ch011

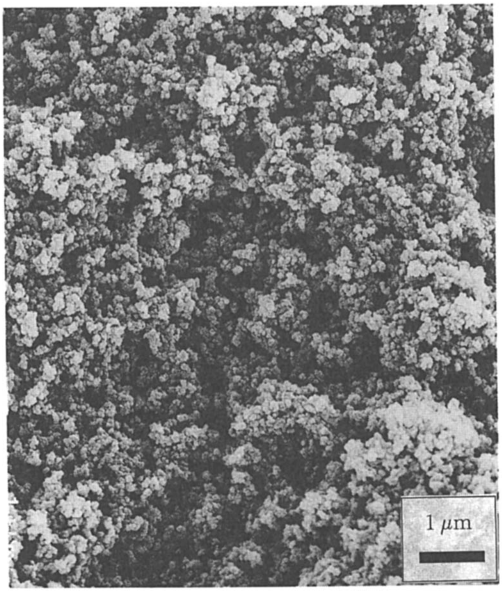

Figure 2. Scanning electron micrographs of macroporous glycidyl methacrylate-ethylene dimethacrylate resin prepared in the presence of (a) solvating diluent, (b) non-solvating diluent, (c) polymer. Reprinted with permission from ref.(*28*). Copyright 1993 Butterworth-Heineman journals, Elsevier Science Ltd.

Continued on next page

Downloaded by UNIV OF GUELPH LIBRARY on October 8, 2012 | http://pubs.acs.org
Publication Date: May 30, 1996 | doi: 10.1021/bk-1996-0635.ch011

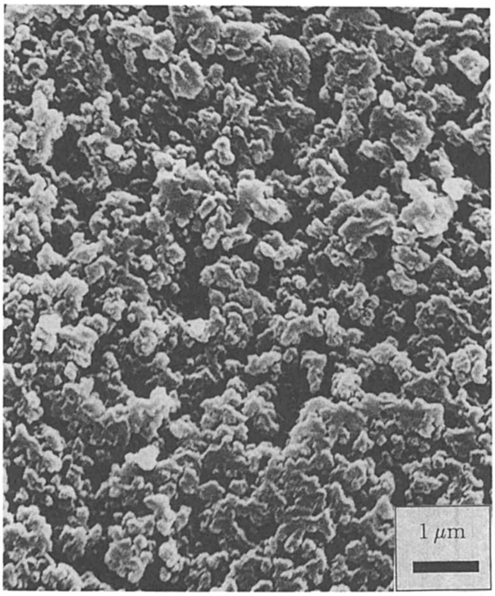

Figure 2b. *Continued*

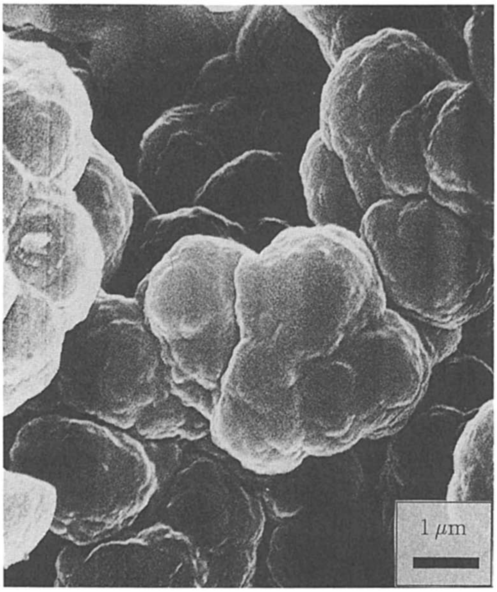

Figure 2c. *Continued*

conventional macroporous resins (Figure 2a,b). Addition of a polymer gives a resin characterized with a limited internal surface area smaller than 10 m^2/g, pore volume up to about 0.5 ml/g, and a large average pore diameter (in the micrometer range). The phase separation and thus the pore size distribution is influenced not only by the concentration of the polymer diluent but also by its molecular weight and its interaction parameter with the copolymer formed (*5*). A minimum concentration of the added polymer is necessary to obtain a permanently porous product. Then the porosity increases with increasing concentration of the polymer porogen. Low-molecular-weight polymer behaves as a low-molecular-weight solvating diluent (*5*). A polymer of high molecular weight (50,000 and more in the case of styrene-divinylbenzene resin when linear polystyrene is used as a diluent) behaves in this way only at low concentrations (up to 10 wt.%) (*5*). At higher concentrations phase separation occurs already at the beginning of crosslinking polymerization. As the molecular weight of linear polymer is increased, the average pore size becomes larger (*5*). The pore size distribution is dependent on the distribution of molecular weight of polymer diluent. It is narrowest for the linear polymer with the narrowest molecular weight distribution (*29*). Another factor which has an influence on the formation of permanent porosity is the concentrations of crosslinking agent.

Polystyrene is the most frequently used polymer diluent in styrene-divinylbenzene resins. Other polymers were used as well: poly(methyl methacrylate), poly(vinyl acetate), copolymer of maleic ester with vinyl acetate, etc.

An integral part of the production of macroporous resins is the removal of porogens by solvent extraction after polymerization. In contrast to the low-molecular-weight porogens, the polymer porogens are not so easy to remove from the final product. The complicated removal of polymer porogens became the main obstacle of their application in the preparation of macroporous resins.

Post-Crosslinked Resins. Post-crosslinked resins (so called macronetworks or also termed hypercrosslinked or isoporous polymers) are obtained by crosslinking linear polymers or swelled gel-type or macroporous resins using Friedel-Crafts alkylation or acylation. Typical crosslinking agents for polystyrene or low-crosslinked styrene-divinylbenzene copolymers include chloromethyl methyl (or ethyl) ether (*30*), (*31*), chloromethyl polyethers (*32*), *p*-xylylene dichloride (*33*),(*34*), α,α-dichloro-*p*-xylene (*35*), 4,4'-bis-(chloromethyl)biphenyl (*36*), dimethylformal (*36*), tris-(chloromethyl)mesitylene (*36*), 1,4-bis-(4-chloromethylphenyl)butane (*36*), sulfur halides (*37*), and tetrachloromethane (*38*). As the catalysts, tin(IV), iron(III) and titanium(IV) chlorides are used.

Post-crosslinked resins are characterized by high degree of swelling in thermodynamically good solvents, narrow distribution of small pores (*ca.* 2 nm) and high specific surface area (around 1,000 m^2/g). They also exhibit high thermal and mechanical stability. Commercially produced post-crosslinked resins such as Ambersorb 372 (Rohm and Haas), Purolite MN (Purolite) and Wofatit EP63 (Bayer AG) are used mainly as adsorbents and so far their application in SEC has been rather limited.

Downloaded by UNIV OF GUELPH LIBRARY on October 8, 2012 | http://pubs.acs.org
Publication Date: May 30, 1996 | doi: 10.1021/bk-1996-0635.ch011

Downloaded by UNIV OF GUELPH LIBRARY on October 8, 2012 | http://pubs.acs.org
Publication Date: May 30, 1996 | doi: 10.1021/bk-1996-0635.ch011

Control of Bead Size and Bead Size Distribution. Since the size and size distribution of the beads in the suspension polymerization is influenced by many factors, it is not easy to predict and control them. The choice of the suspension stabilizer and stirring are two most important factors (*39*). The suspension stabilizer or surfactant governs the interfacial tension between the continuous and discontinuous phase and determines thus bead size (*40*). Primarily, the stirring speed but also the design of the reactor and the stirrer control the shear distribution in various locations inside the reactor.

Suspension polymerization affords beads that have rather broad particle size distribution which cannot be used directly in chromatography. Good flow properties of the resin are the necessary condition for high-speed, high-resolution chromatography. In the case of polydisperse column packings, the flow-rate of eluent through the column is determined by the smallest particles, while its efficiency is controlled by the largest ones. While column efficiency increases as the bead size decreases, the column permeability decreases (*41*). To reduce the back pressure in the column and to increase its efficiency, i.e., to afford a narrow fraction of useful particles, careful and tedious size fractionation of the beads obtained by suspension polymerization has to be done. Although the fraction thus obtained has a reduced polydispersity, it is never strictly uniform, and the remainder is a waste. In the search for uniformly sized beads, Ugelstad developed a technique termed "activated multi-step swelling and polymerization" (*42*). In fact, this procedure is a suspension polymerization in which the size of the starting droplets is not determined by the stirring conditions but by the use of an aqueous dispersion of preformed swelled monosized seed particles. Monosized seed particles are prepared by emulsifier-free emulsion or dispersion polymerization. If these seeds contain a certain amount of low-molecular-weight, water-insoluble "swelling activator" (a typical activator for polystyrene seeds is 1-chlorodecane), a large increase in the diameter of seeds then occurs when swelled with monomer. This step is followed by a standard suspension polymerization, under the conditions that exclude coalescence of the enlarged particles. These recent technological developments make it possible to decrease the typically used particle size of SEC packings from 30-50 μm (such size range was available in the 1970s) (*43*), to 3, 5, or 10 μm.

Packings Based on Natural Organic Polymers

Materials based on synthetic polymers are known to show a rather hydrophobic character causing nonspecific interactions. They are operative not only in styrene-divinylbenzene resins but also in polymethacrylates which contain hydrophilic ester groups. Nonspecific interactions are highly undesirable especially in separation of biopolymers. Such effects are almost completely avoided in matrices from polysaccharides which are highly hydrophilic. Dextran, agarose and cellulose are the most versatile polysaccharide matrices for SEC applications. Porous matrices of regular spherical shape are usually prepared by gelation of a solution of an appropriate polysaccharide or its derivative dispersed in an immiscible medium. The sol-gel transition is induced by chemical reaction, e.g. elimination of groups responsible for solubility, or simply by lowering the temperature.

Downloaded by UNIV OF GUELPH LIBRARY on October 8, 2012 | http://pubs.acs.org
Publication Date: May 30, 1996 | doi: 10.1021/bk-1996-0635.ch011

Dextran. Dextran and its derivatives are the most important polysaccharides used as a matrix in SEC (*44*). Dextran is produced from saccharose by bacteria *Leucomonostoc mesenteroides* or by other microorganisms. Its chain is formed by D-glucose units connected predominantly with 1,6-glycosidic bond and to a lesser extent with 1,2-, 1,3- and 1,4-bonds. Crosslinking of alkaline aqueous dextran solution dispersed in an inert medium which is immiscible with water (e.g., toluene (*45*), (*46*), silicone oil (*47*)) occurs on addition of bifunctional alkylating agent (e.g., epichlorohydrin). Epichlorohydrin can be also used as a dispersion medium (*48*). Dispersion is stabilized, e.g., by poly(vinyl acetate) and tenside. Crosslinking density and thus the exclusion limit is controlled in a broad range by the molar ratio glucose units/epichlorohydrin/sodium hydroxide, by molecular weight and concentration of starting dextran, by the reaction time and temperature. Particle size is controlled by the stirring conditions. The most frequently used dextran matrix in SEC is still Sephadex, product of Pharmacia Biotech which is available in a range of different exclusion limits and with various particle size (Table II). Sephacryl is a porous crosslinked copolymer of allyldextran and *N,N'*-methylenebisacrylamide.

Agarose. Agarose is a linear polysaccharide from algae in which alternating units of D-glucose and 3,6-anhydro-L-galactose are connected by 1,4- and 1,3-glycosidic bonds. Acid sulfate and carboxylic groups present in the starting natural product are removed by hydrolysis and reduction. Agarose is soluble in water at moderate temperatures. Room temperature is sufficient for sol-gel transition. The material has rather poor mechanical and flowing properties. To improve these properties agarose is crosslinked with 2,3-dibromopropanol or epichlorohydrin (*49*),(*50*). Commercially available from Pharmacia is Sepharose 6B, 4B and 2B and its crosslinked analogs (Table II). High-crosslinked Superose has agarose matrix. Superdex is a composite matrix consisting of dextran covalently bonded to crosslinked agarose. It has excellent resolution and selectivity which are accompanied by chemical and physical stability.

Cellulose. Beaded porous cellulose is also used in SEC. Of practical importance are products obtained by thermal sol-gel transition or acid regeneration of viscose (cellulose xanthate) dispersed in an immiscible continuous phase. Cellulose xanthate groups are decomposed by heating to 80°C or by addition of an acid. As a result, cellulose is regenerated. Organic solvents (e.g., chlorobenzene (*51*), 1,2-dichloroethane (*52*), benzene (*53*),(*54*)) or an aqueous solution of a hydrophilic polymer (either ionogenic, e.g., sodium polyacrylate, or nonionogenic such as poly(ethylene oxide) (*55*)) are used as a continuous phase. Solutions of cellulose in the Schweizer reagent, cadoxen, Fe(II) tartrate (*54*) and Ca thiocyanate (*56*) are also used for preparation of beaded cellulose. The pore structure is influenced by the concentration and molecular weight of starting cellulose, by the rate of regeneration and by some additives. The product obtained is suitable for application at low or medium pressures. Their pressure properties can be improved by additional crosslinking with epichlorohydrin.

Downloaded by UNIV OF GUELPH LIBRARY on October 8, 2012 | http://pubs.acs.org
Publication Date: May 30, 1996 | doi: 10.1021/bk-1996-0635.ch011

Table II. Commercial Polysaccharide Materials for SEC

Product Name		*Fractionation Range, MW($\times 10^3$)*		*Producer*
		Globular Proteins	*Dextrans*	*(Distributor)*
Sephadex	G-10[a]	<0.7	<0.7	Pharmacia Bio,
	G-15[a]	<1.5	<1.5	Sweden
	G-25[b]	1-5	0.1-5	
	G-50[b]	1.5-30	0.5-10	
	G-75[c]	3-80 (70)	1-50	
	G-100[c]	4-150 (100)	1-100	
	G-150[c]	5-300 (150)	1-150	
	G-200[c]	5-600 (250)	1-200	
PDX	GF-25[d]	1-5		Polydex,
(dextran)	GF-50[d]	1.5-30		Canada
Sephacryl	S-100 HR[e]	1-100		Pharmacia Bio
	S-200 HR[e]	5-250	1-80	
	S-300 HR[e]	10-1,500	1-400	(Sigma, USA)
	S-400 HR[e]	20-8,000	10-2,000	(Supelco, USA)
	S-500 HR[e]		40-20,000	
	S-1000 HR[f]		5,000-100,000	
Sepharose	6B (6B-CL)[g]	10-4,000	10-1,000	Pharmacia Bio
	4B (4B-CL)[g]	60-20,000	30-5,000	
	2B (2B-CL)[h]	70-40,000	100-20,000	
Superdex	75[i]	3-70	0.5-30	Pharmacia Bio
	200[i]	10-600	1-100	
Superose	6 Prep grade[j]	5-5,000	-	Pharmacia Bio
	12 Prep grade[j]	1-300	-	
Beaded cellulose	90% porosity Perloza MT100[k]	10-1,000	-	Lovochemie, Czech Rep.
	93% porosity Perloza MT200[k]	100-3,000	-	(Sigma)
	95% porosity Perloza MT500[k]	2,000-5,000	-	

Particle size in the dry state: [a] 40-120 µm; [b] coarse: 100-300 µm, medium: 50-150µm, fine: 20-80 µm, superfine: 10-40 µm; [c] 40-120 µm, superfine: 10-40 µm; [d] 50-150 µm, 100-300 µm; particle size in water: [e] 25-75 µm; [f] 40-105 µm; [g] 45(40)-165 µm; [h] 60-200 µm; [i] 22-44 µm; [j] 20-40 µm; [k] (30-50 µm), 50-80 µm, 80-100 µm, 100-250 µm, 250-500 µm

Downloaded by UNIV OF GUELPH LIBRARY on October 8, 2012 | http://pubs.acs.org
Publication Date: May 30, 1996 | doi: 10.1021/bk-1996-0635.ch011

Porous polysaccharide materials (mainly agarose and cellulose, to a lesser extent also dextran) are often used for preparation of derivatives (e.g., ion-exchange and complexing). Polysaccharides are first activated by various methods which are followed by the immobilization of low- and high-molecular-weight ligands. Polysaccharide derivatives are intended for separation of biopolymers; in addition to SEC, also other chromatographic modes (ion-exchange, hydrophobic, immobilized metal affinity, affinity, etc.) are operative.

Packings Based on Inorganic Materials

Silica Gel. Silica gel which is a form of silica is probably the most widely used packing material in SEC (*57*). Its composition can be described by the formula $SiO_2.xH_2O$ (*58*). Silicas are classified on the basis of their crystal structure, surface composition and porosity. Unlike crystalline silicas (e.g., quartz, tridymite, cristobalite, stishovite, coesite), amorphous silica (e.g., opal, diatomaceous earth) has no regular structure and exhibits a higher degree of hydration than the crystalline one. Quartz glass and supercooled silica is considered as an intermediate between the crystalline and amorphous forms. Silica is available as a solution, sol, gel, xerogel, aerosol or precipitate. Hydroxy groups, which are responsible for the hydrophilic character of silica, are weakly acidic, having a pK of about 7.0. Solubility of silica is pH-dependent and dramatically increases above pH 9. Macroporous silica gel is an amorphous material which is produced by sol-gel transfer (*59*).

Preparation of Silica Gel and Formation of its Porous Structure. Many methods of producing silica particles have been described (*60*). Silica sols are made by acidifying concentrated sodium silicate solutions (the silicon dioxide to sodium oxide ratio 3.2) to pH 8-9. Silanol groups of the silicate oligomeric structures containing up to eight silicon atoms undergo complex condensation (*61*) according to the scheme

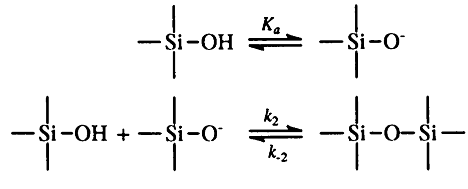

$$-\mathrm{Si{-}OH} \underset{}{\overset{K_a}{\rightleftharpoons}} -\mathrm{Si{-}O^-}$$

$$-\mathrm{Si{-}OH} + -\mathrm{Si{-}O^-} \underset{k_{-2}}{\overset{k_2}{\rightleftharpoons}} -\mathrm{Si{-}O{-}Si}-$$

On the surface of amorphous silicon dioxide, dissolved condensation products nucleate into colloid particles, 1-100 nm in size. This is called sol stage. The rate of nucleation reaction is proportional to the concentration of ionized silanol groups. Addition of salts accelerates nucleation and deposition of silicates. Silicate polymerization is sensitive to pH, ionic strength, dielectric constant of the solvent and temperature. The radius, *r*, of primary colloid particles is related to their solubility, *S*, by the Ostwald-Freundlich equation (2)

$$S = S_0 \exp\left(\frac{2\gamma_{SL} V_m}{\mathbf{R} T r}\right) \tag{2}$$

where S_0 is the solubility of a flat silica plate, γ_{SL} is the solid-liquid interfacial energy, V_m is the molar volume of the solid phase, **R** is the gas constant, and T is the temperature. The process of primary particle growth in which larger colloid particles grow at the expense of smaller ones (especially in strongly alkaline medium) is known as the Ostwald ripening. Low pH and high ionic strength promote the growth of smaller particles.

Silica polymerization can be also elucidated on the base- or acid-catalyzed hydrolysis of tetraalkoxy- or tetrachlorosilane in alcohol-water mixture, which is another widely used method for preparation of spherical silica gel particles (*62*). Reaction conditions dramatically influence the properties of the product. For example, acid-catalyzed hydrolysis of tetraethoxysilane at low water content results in a linear polymer. On the other hand, high water content favors the formation of highly crosslinked polymer. In the presence of ammonia, spherical colloid particles are obtained. Silica gel particles produced by acid-catalyzed hydrolysis of tetraethoxysilane or by acidification of sodium silicate exhibit ladder structure which arises by linear condensation of oligomers.

In the absence of stabilization, the dispersed primary colloid particles tend to aggregate. Four aggregation mechanisms are possible: gelation, coagulation, flocculation and coacervation. Mainly first two mechanisms are operative in the pore structure formation of silica gel. Gelation, i.e., interparticle aggregation with ultimate network formation, occurs if the concentration of silicon dioxide is sufficiently high (*ca.* 1 wt.%). As a result, a continuous silica gel structure is formed which appears to be uniform. Subsequent condensation within the gel causes shrinkage of the structure and release of water. This is called syneresis. If coagulation of the primary colloid particles occurs, densely-packed clumps (coagulate) are formed. Silica xerogel is obtained by heating the washed silica gel. This removes water and is accompanied by additional shrinkage of particles. Xerogel is macroporous and it usually contains 3-15 wt.% of water. This water is partly held within the silica bulk phase, partly adsorbed on the surface. It also comes from condensation of hydroxy groups on the surface. In its fully hydrated state silica gel contains 8-9 μmol hydroxy groups per sq.m. Silica gel can be further subjected to special thermal or hydrothermal treatment which changes its original porous structure, i.e. the shape of pores, their size and distribution. By heating silica at about 150-200°C under vacuum the adsorbed water is removed. When temperature is further increased, vicinal hydroxy groups react together, forming reactive siloxane groups. At about 600°C condensation of vicinal hydroxy groups is practically completed and condensation of isolated and geminal hydroxy groups follows. Sintering of xerogel at temperatures above 600°C leads to a decrease in porosity. This can be prevented if the pores are filled with sodium chloride. Silica gel annealed at 1100°C changes into a nonporous, crystalline, rather hydrophobic material.

To produce silica gel spherical particles, several micrometers in diameter, a silicate salt solution has to be dispersed as an emulsion in an organic liquid and the droplets are then gelled (*63*). Irregular porous glass particles are obtained from borosilicate glass which is heated at the melting temperature and etched with acidic or alkaline agents. These particles are characterized by relatively uniform pore size.

Downloaded by UNIV OF GUELPH LIBRARY on October 8, 2012 | http://pubs.acs.org
Publication Date: May 30, 1996 | doi: 10.1021/bk-1996-0635.ch011

As an example of commercially produced silica gel we mention two materials supplied by Supelco which possess comparable properties. The first material is Progel-TSK SW which is available with particle diameter 5 or 10 µm. The material with pore diameter 12.5 nm is suitable for separation of globular proteins with molecular weights 5×10^3-150×10^3. Progel-TSK SW containing 25 nm pores separates molecular weight 1×10^4-50×10^4 and Progel-TSK SW with pore diameter 45 nm separates molecular weights 2×10^4-$1{,}000\times10^4$. The second material is Supelcosil which is available with particle diameters 3 or 5 µm, pore diameter 10 or 30 nm, and pore volumes 0.6 or 0.5 ml/g. Silica gel with a mean pore diameter of 30 nm is suitable for SEC of high-molecular-weight compounds, whereas materials with 10 nm pores can only be used for separation of small molecules (*64*).

Downloaded by UNIV OF GUELPH LIBRARY on October 8, 2012 | http://pubs.acs.org
Publication Date: May 30, 1996 | doi: 10.1021/bk-1996-0635.ch011

Silica Gel Modifications. Although silica gel obtained by various techniques is macroporous, it is of limited value for SEC of biologically active compounds, when used without modification. The ionic character of silica gel causes that it behaves as a weak ion exchanger. Since the surface silanol groups on silica are responsible for the adsorption and denaturation of proteins and enzymes, they must be substantially eliminated. The most effective way of achieving this is chemical modification of surface silanol groups with organosilanes which introduce either nonpolar (e.g., alkylsilyl- and arylsilyl-), or polar groups (e.g., diol-, cyanoethyl-, chloropropyl- and aminopropyl-). In some cases, electrostatical bonding of positively charged ligands to silica gel anion exchange matrix is sufficient to eliminate the undesirable matrix effects. The modification often improves the chemical stability of silica gel (*58*). Other methods which are used to overcome the adsorption and denaturation of biologically active molecules on silica gel include grafting or coating silica with natural or synthetic polymers, e.g., dextran, glucose, poly(ethylene oxide), poly(vinylpyrrolidone) and polystyrene. In this case, epoxysilica is often used which is formed by the reaction of silica gel with (3-glycidyloxypropyl)trimethoxysilane (*65*). The advantage of dextran grafted to epoxysilica gel compared with low-molecular-weight ligands consists in steric shielding of residual silanols with grafted macromolecules (*66*). Dextran with positively charged 2-diethylaminoethyl functions immobilized on silica gel contributes to neutralization of the negative charges on silica gel surface, thus minimizing the nonspecific interactions (*67*),(*68*). Oligo(ethylene oxide)-modified silicas are prepared by the reaction of silanol groups with oligo(ethylene oxide) carrying trialkoxysilane (*69*), or coating silica gel with oligo(ethylene oxide) macromonomers which are then *in situ* polymerized (*70*) or by thermal immobilization of poly(ethylene oxide) (Carbowax 20M) on silica gel (*71*). *N*-vinylpyrrolidone is grafted to vinyltriethoxysilane- (*72*),(*73*) or 3-aminopropyltriethoxysilane-modified silica gel (*74*), or it is attached by radiation-, or peroxide-induced polymerization (*75*). This sorbent is supposed to possess higher stability and better hydrodynamic properties than Sepharose 4B or porous glass. To cover silica gel with polystyrene, it is reacted with a copolymer of styrene and vinylmethyldiethoxysilane (*76*). Another proposed modification procedure employs copolymerization of acrylamide with vinyl-polymerizable silane bonded to silica gel (*77*). Coupling of poly(*N*-isopropylacrylamide) with carboxyl end group to porous glass containing amino groups affords a temperature-responsive SEC packing (*78*).

Other Inorganic Packings. In addition to silica gel, packings for SEC can be also prepared on the basis of aluminium(III), titanium(IV), or zirconium(IV) oxides (*79*). Similarly to the case of silica, they behave as weak ion exchangers, and therefore it is necessary to deactivate them in order to eliminate undesirable effects. Alumina and zirconia are modified by covalent attachment of styrene-vinylsilane copolymer which can be subsequently crosslinked or polybutadiene and polychloromethylstyrene are adsorbed on alumina and then crosslinked (*80*).

Properties of Packings

Silica-based SEC packings have very rigid matrix backbones, which do not increase their volumes by swelling, and can be prepared with relatively uniform pore size. The advantage of good mechanical stability and efficiency is, however, accompanied by the drawback of low chemical stability at high pH and deterioration of the bonded phase, which ultimately results in uncovering of reactive silanol groups, thus spoiling the separation. On the other hand, synthetic macroporous resins usually possess a wide pore distribution which is an advantage for the characterization of the broad molecular wight distribution of polymer samples, but the selectivity is lower. Moreover, they can be used in a wide pH range and suit polar as well as non-polar solvents. Synthetic macroporous polymer packings are not only chemically stable but also resistant to the mechanical strains that prevail in a column and therefore, in contrast to the natural polymers, they permit elevated pressures and temperatures to be applied in the column. Increasing crosslinking improves the mechanical strength of the synthetic resins. On the other hand, their mechanical properties were observed to decrease with increasing volume of the diluent added to the monomers (*81*). Natural polymers, which are mostly soft, swell in solvents and have in some cases pores of nearly uniform size. Therefore their working range is limited. Moreover, their low-pressure stability precludes their use in high-performance SEC. The main advantage of natural polymer-based packings is the absence of non-specific interactions which is of utmost importance in separation of biopolymers. On the other hand, unlike silica or synthetic resins, polysaccharide packings do not resist microbial infection.

The porosity of the organic matrices is dependent also on the history of the resin before and during drying. Due to the flexibility of the network chains the pore structure varies with the type of solvent in which the resin is swollen before drying (*24*),(*82*),(*83*). The drying of the resin swollen in a thermodynamically good solvent leads to a partial or total collapse of macropores, depending on the degree of crosslinking (*82*). In low-crosslinked resin the surface area completely disappears when it is dried from a solvent which is a good swelling agent. The same situation occurs by heating the synthetic resin above the glass transition temperature. These effects are explained by the decrease in glass transition temperature of the resin due to the plasticizing effect of a thermodynamically good solvent (*22*). The pores reappear after the resins are swollen in a thermodynamically good solvent, followed

Downloaded by UNIV OF GUELPH LIBRARY on October 8, 2012 | http://pubs.acs.org
Publication Date: May 30, 1996 | doi: 10.1021/bk-1996-0635.ch011

Downloaded by UNIV OF GUELPH LIBRARY on October 8, 2012 | http://pubs.acs.org
Publication Date: May 30, 1996 | doi: 10.1021/bk-1996-0635.ch011

by replacing this solvent with a thermodynamically poor one and drying. Takeda calls them "shape-memory" pores (*22*). Such pores are observed mainly in resins prepared in the presence of solvating diluents.

Synthetic and inorganic SEC packings are most often characterized in the dry state using surface area measurements or mercury intrusion porosimetry. The two methods (mercury porosimetry and nitrogen adsorption) are complementary; each of them becomes increasingly uncertain as the pore size range approaches a limit: nitrogen adsorption at the upper end of the mesopore range and mercury porosimetry at the lower end. The adsorption analysis using nitrogen is suitable for the evaluation of pore diameters ranging from 2 to 20 nm, while mercury porosimetry is best suited for the mesopores and macropores, from above 20 nm to 1 μm. The combination of mercury porosimetry and nitrogen adsorption provides qualitative analysis of pore structure in the entire pore size range. Pore structure can be characterized also by other, although not very frequently available, methods, such as X-ray diffraction which does not perceive pores with the radius larger than 100 nm (*81*).

However, in most chromatographic applications the resin is used in the presence of solvent where it swells to a varying degree. In resins, which involve polymer phase and pores, the pores are filled by the solvent and the polymer phase may be swollen to a varying extent. Therefore, the dry porosity of resins does not necessarily correspond to the swollen-state porosity. Two main methods are known to determine the porous structure of macroporous resins swollen by a solvent: thermoporometry, which is based on the dependence of the pore size on the freezing point of a filling solvent (*84*), and inverse size-exclusion chromatography (*85*). Another method to measure the pore size distribution of swollen gels, so called mixed-solute exclusion, is introduced by Kuga (*86*). It employs size exclusion chromatography to determine the difference in probe solute concentration between the initial stock solution and the equilibrated solution surrounding the resin. Due to the difference between solute size and pore size, some of the solutes can migrate into the resin while others cannot.

Acknowledgments. Financial support by the grant No. 450101 of the Academy of Sciences of the Czech Republic is gratefully acknowledged.

Literature Cited

1. *Liquid Column Chromatography. A Survey of Modern Techniques and Applications;* Deyl, Z.; Macek, K.; Janák, J., Eds.; Elsevier: Amsterdam, 1975; Vol. 3.
2. *Laboratory Handbook of Chromatographic and Allied Methods;* Mikeš, O., Ed.; Wiley: Chichester, 1979.
3. *HPLC of Biological Macromolecules: Methods and Application;* Gooding, K.M.; Regnier, F.E., Eds.; Marcel Dekker: New York, 1990.
4. *Synthesis and Separations Using Functional Polymers;* Sherrington, D.C.; Hodge, P., Eds.; Wiley: Chichester, 1988.
5. Seidl, J.; Malinský, J.; Dušek, K.; Heitz, W. *Adv. Polym. Sci.* **1967,** *5,* 113.
6. Barth, H.G.; Boyes, B.E. *Anal. Chem.* **1992,** *64,* 428.

7. Barth, H.G.; Boyes, B.E.; Jackson, Ch. *Anal. Chem.* **1994,** *66,* 595.
8. Arshady, R. *J. Chromatogr.* **1991,** *586,* 181.
9. Arshady, R. *J. Chromatogr.* **1991,** *586,* 199.
10. Moore, J.C. *J. Polym. Sci.* **1964,** *A 2,* 835.
11. Walther, D.H.; Sin, G.H.; Blanch, H.W.; Prausnitz, J.M. *J. Macromol. Sci.-Phys.* **1994,** *B 33,* 267.
12. Rosenberg, J.E.; Flodin, P. *Macromolecules* **1986,** *19,* 1543.
13. Li, W.-H.; Stöver, H.D.H.; Hamielec, A.E. *J. Polym. Sci.* **1994,** *A 32,* 2029.
14. Kuroda, H.; Osawa, Z. *Eur. Polym. J.* **1995,** *31,* 57.
15. Horák, D.; Pelzbauer, Z.; Bleha, M.; Ilavský, M.; Švec, F.; Kálal, J. *J. Appl. Polym. Sci.* **1981,** *26,* 411.
16. Wulff, G. *Angew. Chem.* **1995,** *34,* 1812.
17. Kun, K.A.; Kunin, R. *J. Polym. Sci.* **1968,** *A-1 6,* 2689.
18. Poinescu, I.C.; Beldie, C. *Angew. Makromol. Chem.* **1988,** *164,* 45.
19. Rabelo, D.; Coutinho, F.M.B. *Polym. Bull.* **1994,** *33,* 479.
20. Rabelo, D.; Coutinho, F.M.B. *Macromol. Symp.* **1994,** *84,* 341.
21. Paine, A.J. *J. Polym. Sci.* **1990,** *A 28,* 2485.
22. Takeda, K.; Akiyama, M.; Yamamizu, T. *Angew. Makromol. Chem.* **1988,** *157,* 123.
23. Jacobelli, H.; Bartholin, M.; Guyot, A. *Angew. Makromol. Chem.* **1979,** *80,* 31.
24. Häupke, K.; Pientka, J. *J. Chromatogr.* **1974,** *102,* 117.
25. Sederel, W.L.; De Jong, G.J. *J. Appl. Polym. Sci.* **1973,** *17,* 2835.
26. Schwachula, G. *J. Polym. Sci.* **1975,** *C 53,* 107.
27. Millar, J.R.; Smith, D.G.; Kressman, T.R.E. *J. Chem. Soc.* **1965,** 304.
28. Horák, D.; Labský, J.; Pilař, J.; Bleha, M.; Pelzbauer, Z.; Švec, F. *Polymer* **1993**, 34, 3481.
29. Cheng, C.M.; Micale, F.J.; Vanderhoff, J.W.; El-Aasser, M.S. *J. Colloid Interface Sci.* **1992,** *150,* 549.
30. Davankov, V.A.; Rogozhin, S.V.; Tsyurupa, M.P. *US Pat. Appl.* **1971,** 3,729,457; *Chem. Abstr.* **1971,** *75,* 6,841.
31. Fiestel, L.; Schwachula, G.; Reuter, H.; Klinzman, H. *Ger. (East) Pat. Appl.* **1987,** 249,274; *Chem. Abstr.* **1988,** *109,* 55,918.
32. Crosby, G.A. *Synthesis* **1974,** 560.
33. Kraus, D.; Popov, G.; Schwachula, G. *Plast. Kautsch.* **1977,** *24,* 545.
34. Kraus, D.; Popov, G.; Schwachula, G.; Fiestel, L. *Ger. (East) Pat.* **1976,** 125,824.
35. Read, S.F. *Eur. Patent Appl.* **1980,** 7,792; *Chem. Abstr.* **1980,** *93,* 48,118.
36. Davankov, V.A.; Tsyurupa, M.P. *Reactive Polym.* **1990,** *13,* 27.
37. Sparow, J.T. *Tetrahedron Lett.* **1975,** 4637.
38. Hradil, J. *Czech Pat. Appl.* **1994,** PV 130-94.
39. Grulke, E.A. In *Encyclopedia of Polymer Science and Engineering;* Kroschwitz, J.I., Ed.; Wiley: New York, 1989, Vol. 16; pp 443-473.
40. Horák, D.; Pelzbauer, Z.; Švec, F.; Kálal, J. *J. Appl. Polym. Sci.* **1981,** *26,* 3205.
41. Deng, L.; Hu, X.; Wu, Q.; Meng, Q.; Li, Y.; Zhang, Y. *Sci. Sin. B*, **1982,** *25,* 905.

Downloaded by UNIV OF GUELPH LIBRARY on October 8, 2012 | http://pubs.acs.org
Publication Date: May 30, 1996 | doi: 10.1021/bk-1996-0635.ch011

42. Ugelstad, J.; Mørk, P.C.; Kaggerud, K.H.; Ellingsen, T.; Berge, A. *Adv. Colloid Interface Sci.* **1980,** *46,* 27.
43. Janák, J.; Čoupek, J.; Krejčí, M.; Mikeš, O.; Turková, J. In *Liquid Chromatography;* Deyl, Z; Macek, K.; Janák, J., Eds.; Elsevier: Amsterdam, 1975; pp 169-231.
44. Porath, J.; Flodin, P. *Nature* **1959,** *183,* 1657.
45. Pharmacia. *Brit. Pat.* **1964,** 97,4054; *Chem. Abstr.* **1965,** *62,* 4,175.
46. Peška, J.; Lenfeld, J.; Plichta, Z.; Beneš, M.; Švec, F.; Čoupek, J. *Czech. Pat.* **1986,** 249,368; *Chem. Abstr.* **1986,** *105,* 145,351.
47. Stojanovic, D.; Cvetkovic, D.; Pekic, B. *Hem. Ind. (Zagreb)* **1979,** *33,* 139.
48. Serumwerk Bernburg. *Brit. Pat.* **1967,** 1,087,964; *Chem. Abstr.* **1968,** *68,* 4,157.
49. Hjerten, S. *Biochim. Biophys. Acta* **1964,** *79,* 393.
50. Bengtson, S.; Philipson, L. *Biochim. Biophys. Acta* **1964,** *79,* 399.
51. Štamberg, J.; Peška, J.; Dautzenberg, H.; Philipp, B. In *Affinity Chromatography and Related Techniques*; Gribnau, T.C.J., Visser, J., Nivard, R.J.F., Eds.; Elsevier: Amsterdam, 1982; pp 131-141.
52. Chitumbo, K.; Brown, W. *J. Polym. Sci.* **1971,** *C 36,* 279.
53. Determann, H.; Meyer, N.; Wieland, T. *Nature* **1969,** *223,* 499.
54. Determann, H.; Rehner, H.; Wieland, T. *Makromol. Chem.* **1968,** *114,* 263.
55. Hara, M.; Okuma, S. *Japan Pat.* **1992,** 4,275,303; *Chem. Abstr.* **1993,** *118,* 61,809.
56. Kuga, S. *J. Chromatogr.* **1980,** *195,* 221.
57. Unger, K.K. *Porous Silica, its Properties and Use as Suport in Column Liquid Chromatography;* Elsevier: Amsterdam, 1979.
58. Unger, K.K. In *HPLC of Biological Macromolecules. Methods and Applications;* Gooding, K.M.; Regnier, F.E., Eds.; Marcel Dekker: New York, 1990; pp 3-24.
59. Brinker, C.J.; Scherrer, G.W. *Sol-Gel Science. The Physics and Chemistry of Sol-Gel Processing;* Academic Press: Boston, 1990; pp 97-233.
60. Johnson, D.W. Jr. *Ceram. Bull.* **1981,** *60,* 221.
61. Falcone J.S., Boyce S.D. In *Encyclopedia of Polymer Science and Engineering*; Kroschwitz, J.I., Ed.; Wiley: New York, 1989, Vol. 15; pp 178-204.
62. Unger, K.; Schick-Kalb, J.; Straube, B. *J. Colloid Polym. Sci.* **1975,** *253,* 658.
63. Matijević, E. In *Science of Ceramic Chemical Processing*; Hench, L.L.; Ulrich, D.R., Eds.; Wiley: New York, 1986; pp 463-481.
64. Tanaka, N.; Kimata, K.; Hosoya, K.; Araki, T.; Tsuchiya, H.; Hashizume, K. *J. High Resolut. Chromatogr.* **1991,** *14,* 40.
65. Herman, D.P.; Field, L.R; Abbott, S. *J. Chromatogr. Sci.* **1981,** *19,* 470.
66. Petro, M.; Gemeiner, P.; Berek, D. *J. Chromatogr.* **1994,** *A 665,* 37.
67. Zhou, F. L.; Muller, D.; Santarelli, X.; Jozefonvicz, J. *J. Chromatogr.* **1989,** *476,* 195.
68. Santarelli, X.; Zhou, F. L.; Muller, D.; Jozefonvicz, J. *Inst. Nat. Sante Rech. Med.* **1989,** *175,* 155.
69. Karger, B.L.; Miller, N.T.; Feibush, B.; Figueroa, A. *Eur. Pat. Appl.* **1985,** 160,988; *Chem. Abstr.* **1986,** *104,* 207,439.
70. Frere, Y.; Gramain, P. *Reactive Polym.* **1992,** *16,* 137.
71. Choma, I.; Dawidowicz, A.L. *J. Chromatogr.* **1993,** *641,* 211.

Downloaded by UNIV OF GUELPH LIBRARY on October 8, 2012 | http://pubs.acs.org
Publication Date: May 30, 1996 | doi: 10.1021/bk-1996-0635.ch011

72. Cohen, Y.; Eisenberg, P. *Polyelectrolyte Gels. ACS Symp. Ser.* **1992,** *480,* 254.
73. Cohen, Y.; Eisenberg, P.; Chaimberg, M.J. *J. Colloid Interface Sci.* **1992,** *152,* 597.
74. Ivanov, A.E.; Zigis, L.; Turchinskii, M.F.; Kopev, V.P.; Reshetov, P.D.; Zubov, V.P.; Kastrikina, L.N.; Lonskaya, N.I. *Mol. Genet., Mikrobiol. Virusol.* **1987,** *11,* 39.
75. Koehler, J. *Chromatographia* **1986,** *21,* 573.
76. Kurganov, A.; Kuzmenko, O.; Davankov, V.A.; Eray, B.; Unger, K.K.; Truedinger, U. *J. Chromatogr.* **1990,** *506,* 391.
77. Komiya, K.; Kato, Y. *Can. Pat.* **1987,** 1,293,083; *Chem. Abstr.* **1991,** *117,* 163,125.
78. Gewehr, M.; Nakamura, K.; Ise, N.; Kitano, H. *Makromol. Chem.* **1992,** *193,* 249.
79. Vilenchik, L.Z.; Ayotte, R.C.; Asrar, J.; Hardiman, C.J. *US Pat.* **1993,** 5,190,658; *Chem. Abstr.*, **1993,** *118,* 255,802.
80. Kurganov, A.; Davankov, V.A.; Isajeva, T.; Unger, K.; Eisenbeiss, F. *J. Chromatogr.* **1994,** *660,* 97.
81. Horák, D.; Švec, F.; Ilavský, M.; Bleha, M.; Baldrián, J.; Kálal, J. *Angew. Makromol. Chem.* **1981,** *95,* 117.
82. Okay, O. *Angew. Makromol. Chem.* **1988,** *157,* 15.
83. Jun, Y.; Rongan, X.; Juntan, Y. *J. Appl. Polym. Sci.* **1989,** *38,* 45.
84. Guyot, A. *Reactive Polym.* **1989,** *10,* 113.
85. Giddings, J.C.; Kucera, E.; Russels, Ch.P., Myers, N.M. *Phys. Chem.* **1968,** *72,* 4397.
86. Kuga, S. *J. Chromatogr.* **1981,** *206,* 449.

Downloaded by UNIV OF GUELPH LIBRARY on October 8, 2012 | http://pubs.acs.org
Publication Date: May 30, 1996 | doi: 10.1021/bk-1996-0635.ch011

Chapter 12

Inverse Steric Exclusion Chromatography as a Tool for Morphology Characterization

Karel Jeřábek

Institute of Chemical Process Fundamentals, Academy of Sciences of the Czech Republic, 165 02 Prague 6, Czech Republic

Inverse steric exclusion chromatography is used to investigate material used as the stationary phase in a chromatographic column under conditions that minimize specific (enthalpic) interactions. It is possible to obtain information about the pore volume distribution of the studied material by suitable mathematical treatment of the elution volumes of a series of standard solutes with known molecular size. The method is especially suitable for characterization of the morphology of swollen polymer materials, where it provides data impossible to obtain by conventional methods. Besides selection of suitable experimental conditions, the successful application also requires appropriate design of a simple geometrical model of the porous environment. In the description of morphology of swollen polymers it is advantageous to combine the Ogston model (pores as spaces between randomly oriented cylindrical bodies) as representative of a polymer gel with the conventional model of cylindrical pores for the description of macropores. The usefulness of this approach will be demonstrated with a number of examples.

Steric exclusion chromatography has a long history of application in the separation of investigated solutes according to molecular size by interaction with the pore system of the stationary phase of a calibrated chromatographic column. This chromatographic mode is operative when, due to a suitable choice of experimental conditions, all specific enthalpic interaction of the solutes with stationary phases are eliminated and the elution process is governed by entropic effects only. When this requirement is satisfied, it is possible to use the steric exclusion phenomena in the inverse mode. Inverse application of the steric exclusion chromatography, that is, characterization of the porous system of the column filling by measurement of the elution behavior of

0097–6156/96/0635–0211$15.00/0

standard solutes with known molecular size was independently proposed by Halász and Freeman (*1,2*). Halász's approach to the problem of how to transform the elution data into porosimetric information was very straightforward. From the point of view of the accessibility of pores to solute molecules of certain dimensions, he proposed two categories: totally accessible pores with diameters greater than the effective dimension of the solute and pores smaller than the effective dimensions of the solute molecule which are completely inaccessible. In this case, a cumulative pore distribution curve can be obtained by plotting the difference between elution volume of a standard solute and the dead volume V_O vs. the effective solute dimension. Using the effective dimensions of the standard solute molecules (a series of polystyrenes with narrow molecular weight), Halász found that by comparing the inverse steric exclusion chromatography (ISEC) data with the pore distribution determined by classical methods for various silicas and pore glasses, an effective molecular dimension for the application of his simplified concept has to be 2.5-times greater than the polymer coil diameter.

Inverse Steric Exclusion Chromatography - Theory

Halász's approach is a gross oversimplification of the exclusion phenomena. Partitioning of a solute molecule between the fluid phase and pore space continuously changes with changes of the solute molecular dimension even in a material with uniform pores. The elution volume V_e is given by equation 1, in which K is the equilibrium partition coefficient and V_p is the pore volume.

$$V_e = V_o + KV_p \qquad (1)$$

For uniform cylindrical pores and spherical solute molecules, the dependence of the partition coefficient K_c on pore diameter d_p and diameter of solute molecule d_m is described by equation 2:

$$K_c = [1-(d_m / d_p)]^2 \qquad (2)$$

The question how to expand the description of steric exclusion using equation 1 for a more realistic case of a stationary phase with non-uniform pore sizes was solved by Freeman (*2*) who proposed the application of expressions developed by Giddings et al. for the partition coefficient K in random polymer networks (*3*). Cassassa et al. (*4-6*) proposed a solution for various pore geometries based on the Brownian motion of a particle. Information on pores in the stationary phase can then be obtained from analysis of the dependence of K on the size of solute molecules. A numerical procedure seeking the smoothest non-negative distribution consistent with experimental distribution coefficient $K(d_m)$ was proposed by Prausnitz et al. (*7*). Vilenchik et al. (*8*) developed a computer program solving the problem for triangularly-shaped pore size distributions. One drawback of these approaches is their dependence on the pre-defined shape of the pore size distribution, which may differ from that of the investigated material. However, the main problem is the correct determination of K from experimental data for which it is necessary to know the value of the pore volume. Usually, V_p is determined from the elution volume of the smallest solute for which is declared K = 0. This could be an acceptable approximation for materials without meso- or micropores, but for the majority of materials, especially the swollen polymers, where ISEC can bring the most useful information, it is a too crude approximation.

Instead of an analytical solution based on expressions for K in random pore systems, a better alternative is to use a "numerical" approach, based on the supposition that the most important unknown quantity in equation (1) is the pore volume V_p (*9*). It uses simple equations for K in uniform pores of well-defined geometrical shape and the description of the fundamentally polydisperse morphology of the investigated materials is built as a sum of contributions of a discrete number of pore fractions, each consisting of simple pores of a single size only. V_e for a solute of the characteristic molecular dimension L in a porous system composed of n fractions is described by equation 3:

$$V_e = \sum_{i=1}^{i=n} K^i(L) V_p^i + V_0 \qquad (3)$$

The characteristic dimension of each fraction can be chosen in advance as a scale by which a real porous system will be described. The evaluation of investigated porous materials is then reduced to the determination of the volumes of individual pore fractions by a least square method which is minimized by the squared difference between experimental and computed values of V_e. ISEC data treatment based on the representation of a real morphology by the set of discrete pore fractions was also proposed by Knox and Ritchie(*10*), but their version includes the computation of K for each solute. Their treatment also contained a troublesome correction for the part of pore volume inaccessible even for the smallest solute.

The ability of ISEC to provide information on swollen materials makes it especially valuable for the characterization of functional polymers, as e.g. catalyst carriers or adsorbents. For these materials an indiscriminate application of experience gathered on their much more familiar inorganic counterparts would be misleading. Swelling of polymer carriers changes their porous texture and enables the penetration of molecules from the fluid phase into the interior of the polymer mass. In fact, the working phase in a majority of cases is the swollen polymer gel and not the surface of pore walls.

From the morphological point of view the polymer carriers are divided into two groups. The gel-type resins have no porosity in the dry state and their interior is accessible only after swelling in a liquid. Macroreticular (or macroporous) resins have a more complicated morphology. Beads of these resins can be imagined as clusters of polymer microparticles, featuring both swellable polymer mass and "true" pores which may remain open even in absence of a swelling (Figure 1). The model of cylindrical pores can be easily applied to the description of macropores (depicted in Figure 1 by the dashed lines). Characterization of the morphology of swollen polymer mass using the model of cylindrical pores can be successful from the mathematical point of view but the values of parameters (e.g. pore volume) may be unrealistic (*11*). A better model developed by Ogston (*12*), in which pores are defined by spaces between randomly oriented rigid rods, may be regarded as a better approximation of the three dimensional polymer network. An expression for the partition coefficient of spherical molecules in such a system, K_O, is given by equation 4:

$$K_O = \exp[-\pi C(d_s + d_c)^2 / 4] \quad (4)$$

This partition coefficient indicates which part of the total volume occupied by the porous system is accessible to spherical bodies having the diameter d_S. The diameter of randomly distributed rigid rods representing polymer chains is d_C; C is their concentration in length units per volume unit (nm^{-2}). It is important to remember that while in the model of cylindrical pores the distribution coefficient K_C indicates the relative accessibility of the pore volume alone , K_O in the Ogston model is related to the total volume of the porous system, i.e., to the sum of the volume of the free space and of that occupied by the skeleton.

Experimental

The requirements for interpretation of chromatographic data based only on steric effects in column packing for lipophilic polymers are satisfied with tetrahydrofuran as the mobile phase and n-alkanes and polystyrenes as standard solutes (*2*). ISEC investigation of hydrophilic polymers can be performed in 0.2 N aqueous sodium sulfate solution in heavy water with sugars and dextranes as standard solutes - the system proposed by Halász for investigation the swollen-state morphology of strongly acidic ion exchangers (*13*).

Investigated materials were ground and the fraction < 0.2 mm was separated by sieving, from which dust fractions were removed by decantation in water or tetrahydrofuran, depending on polymer type. Stainless steel columns (4.1 x 250 mm) were packed with a polymer suspension in the appropriate mobile phase. The efficiency of the resulting columns was sufficient if the individual solutes were injected independently. A conventional set-up consisting of a piston pump, Rheodyne 7125 injector and a refractometric detector was used for the chromatographic measurements. The detector signal was fed to a PC computer and the data sampling was synchronized with the mobile phase flow rate using a drop-counting probe. Elution volumes were determined on the base of the 1st statistical moments of the chromatographic peaks. This arrangement allowed to measure the elution volumes with a reproducibility of 0.01 cm^3.

Examples of ISEC applications

The most important field for ISEC is the investigation of polymer materials that are used as catalyst carriers or adsorbents. ISEC can provide information on their working, swollen-state morphology that is impossible to obtain by conventional porosimetric methods (mercury intrusion or nitrogen adsorption) which can work with the dry materials only. Knowledge of the swollen-state morphology of these materials is a great help in understanding relations between their structure and application properties. In the following part of this report a few cases of significant ISEC contribution in such studies will be presented.

Ion Exchanger Catalysts. Morphology of a wide series of ion exchanger catalysts ranging from low-crosslinked gel-type resin to high-crosslinked macroreticular types was characterized by ISEC and the information was successfully correlated with catalytic activity of the examined resins in the hydrolysis of sucrose (*14*) in aqueous solution. In the aqueous environment the active agent in the ion exchanger catalyst is the hydroxonium cation, more or less freely mobile in the vicinity of the anionic groups bonded to the polymer chains (*15*). The mechanism of the reaction is therefore very similar as that catalyzed by soluble acids. However, while for homogeneously catalyzed reactions the concentration of the reactant in free solutions is important, the rate of ion exchanger catalyzed reaction is determined by the reactant concentration inside the swollen gel cavities. In the absence of a specific affinity between the reactant molecules and the ion exchanger gel (which is the case for sucrose in water), the reactant concentration inside of the gel cavities is always lower than in the free solution, due to the steric exclusion depending on the local density of polymer chains and the size of the reactant molecules. The information about distribution of polymer chain density in the examined resin catalysts obtained by ISEC was used to express the relative decrease of the internal reactant concentration as a function of the reactant molecule size, $A_{rel.}(L)$. These data were correlated with activities of the ion exchangers in sucrose hydrolysis expressed also as relative values, $R_{rel.}$, related to the activity of p-toluenesulfonic acid as a soluble analog. Figure 2 shows the dependence of the squared differences between the relative catalytic activity $R_{rel.}$ and the ISEC-derived steric exclusion of the reactants $A_{rel.}(L)$ (squared correlation error) on the effective reactant size L. The best agreement between R_{rel} values of the hydrolysis of saccharose and the $A_{rel.}(L)$ derived from ISEC data was obtained for a limited range of L, close to the value used for saccharose as one of the standard solutes in ISEC. The correlation of R_{rel} and $A_{rel.}$ for the L corresponding to the lowest error is shown in Figure 3. It is an illustration how ISEC helped in this case to explain quantitatively the effects of heterogenization of a homogeneous catalyst on polymer support.

Accessibility of the Gel Phase in Macroporous Network Polymers. Macroporous network polymers are widely used as adsorbents or carriers of centers active as catalysts or reagents. They have a complicated texture created during their preparation by the influence of the addition of a co-solvent to the polymerization mixture. Accessibility of the polymer gel phase of styrene-type copolymers alternatively crosslinked by divinylbenzene or by diisopropenylbenzene and prepared in the presence of either toluene or acetonitrile as a porogen was investigated using the fluorescence probe and inverse steric exclusion chromatography (*16*). Polymers were prepared by bulk polymerization with a high content (about 50%) of the crosslinking agent, divinylbenzene (DVB) or diisopropenylbenzene (DIB). The porogenic agent was either Toluene, which swells this type of polymer network (polymers DVB-50-B-T and DIB-50-B-T), or acetonitrile, which is a precipitating solvent for such polymers (polymers DVB-50-B-A and DIB-50-B-A). All the polymers were laden with the Dansyl fluorescent probe. The utility of the Dansyl group as an environmental probe

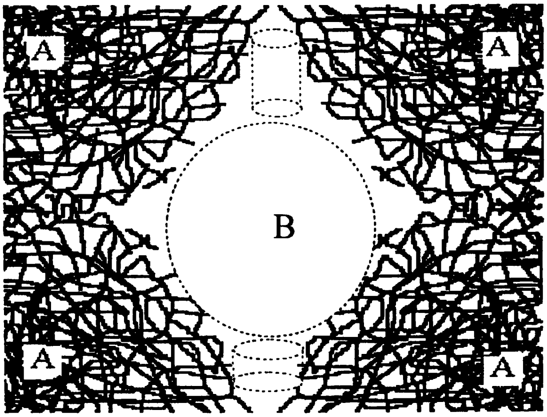

Figure 1. Element in the morphology of macroreticular resin. A - swollen polymer mass, B - real pore. Representation of the real pores as a set of cylindrical pores is depicted in dashed lines.

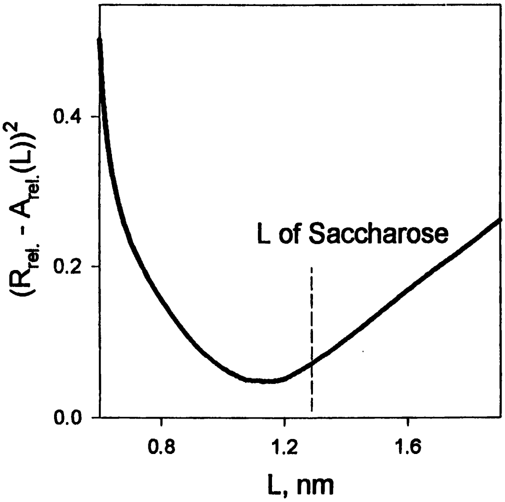

Figure 2. Dependence of the squared differences between the relative catalytic activity $R_{rel.}$ and the ISEC-derived steric exclusion of the reactants $A_{rel.}(L)$ on the effective reactant size L. (Reproduced with permission from ref. 14. Copyright 1990 John Wiley & Sons, Inc.)

originates from wavelength dependence of its fluorescence emission which varies as a function of the solvent microenvironment (*17*). Measurements of the solvatochromic shift of the Dansyl probe-laden polymers equilibrated in various solvents (hexane, toluene, tetrahydrofuran, dichloroethane, ethanol and methanol) showed penetration of the solvents into the polymer mass of all examined polymers except DVB-50-B-A, where the probe microenvironment in all the solvents was a collapsed polymer network inhibiting the solvent access.

In the ISEC evaluation of these macroreticular polymers all the pores with diameter > 10 nm were described using the model of cylindrical pores and the morphology of swollen polymer gel was depicted in terms of the Ogston model. Characteristic polymer chain concentrations C for individual fractions used for modeling the swollen polymer mass was chosen in the range $C = 0.1 - 2\ nm^{-2}$. The lower value corresponds to maximally swollen, effectively uncrosslinked polymer mass. A polymer fraction characterized by $C = 2\ nm^{-2}$ corresponds to a very dense polymer with a gel phase that is poorly accessible even for small solute molecules. The results are shown in Tables I and II.

Table I. Data on Macropores. Comparison of the ISEC data on swollen polymers with BET surface determined on dry samples

Polymer	Results of ISEC measurements		BET
	V_p (cm^3/g)	S_{cum} (m^2/g)	Surface Area (m^2/g)
DVB-50-B-T	0.10	16	455
DVB-50-B-A	1.27	76	79
DIB-50-B-T	0.03	0.8	0.6
DIB-50-B-A	2.10	98	54

(Reproduced with permission from ref. 16. Copyright 1992 John Wiley & Sons, Inc.)

A substantial difference was found in the gel structure of polymers prepared using either toluene or acetonitrile as porogen. Polymers prepared in the presence of acetonitrile have a well-developed macroporous structure with a substantial volume of pores wide enough that they cannot be described as part of swollen polymer gel phase (Table I). Particles of the polymers prepared with acetonitrile as the co-solvent probably consist largely of aggregated microspheres with voids between these microspheres forming the system macropores. Acetonitrile is a poor solvent for styrene-type polymers and it promotes the phase separation during polymerization process and formation of polymer microspheres. These microspheres consist of rather dense polymer gel which can swell to a very limited extend (Table II). Such structure of the gel phase is probably the consequence of substantial entanglement of polymer chains resulting from the lack of separation by co-solvent during their growth. This finding is consistent with the fluorescence studies of DVB-50-B-A, which revealed that the polymer's gel phase maintains a dry "solvent-free" like environment even in good solvents.

Polymers prepared in the presence of toluene have a negligible volume of pores which could be classified unambiguously as macropores. Practically all their porosity belongs to the domain of pore sizes which in the model of cylindrical pores would have diameter < 10 nm. To describe the structure of these polymers also as a cluster of solid polymer microspheres with pores formed by voids between them would require to imagine that the polymer microspheres formed in presence of toluene are smaller than microspheres formed in the presence of acetonitrile, e.i. that the phase separation occurred in the presence of the "good solvent" (toluene) at lower conversion of monomers than in the presence of the "poor solvent" (acetonitrile). This is not probable. More plausible is to imagine the pore system of polymers prepared in the presence of toluene in the terms of Ogston model, that is composed only from expanded polymer mass (Table II). This structure is a natural result of formation of the polymer in swollen state with the growing polymer chains solvated by toluene co-solvent. As shown in Table II, the polymer mass of samples prepared in the presence of toluene contains both a dense fraction of polymer mass (gel phase) similar to that observed in polymer prepared with acetonitrile and a more expanded, effectively less crosslinked fractions of polymer mass characterized by concentrations of polymer chains C in the range 0.1 to 0.8 nm^{-2} (Table II).

Table II. Gel-Type Porosity of Investigated Polymers

Polymer	Volumes of Swollen Polymer Fractions, V_g (cm^3/g)						
	C (nm^{-2}):	0.1	0.2	0.4	0.8	1.5	2.0
DVB-50-B-T		0.13	0.32	0.51	0.0	0.0	0.65
DVB-50-B-A		0.0	0.0	0.0	0.0	0.0	0.44
DIB-50-B-T		0.0	0.0	1.40	1.93	0.05	0.27
DIB-50-B-A		0.0	0.0	0.0	0.0	0.0	1.02

(Reproduced with permission from ref. 16. Copyright 1992 John Wiley & Sons, Inc.)

The different character of the gel phase produced during polymerization the presence of acetonitrile and toluene can be also documented by the comparison of surface areas computed from the data on macropores determined on solvent swollen polymers by ISEC and the BET surface areas measured on dry samples (Table I). In acetonitrile-modified polymers the surface area does not significantly change upon drying. In these materials, pores are liquid filled voids between polymer microspheres. The pore walls of these polymers are true interfaces between a polymer gel phase and a fluid phase. One can imagine that drying may deform this interface but does not substantially diminish its area - a process comparable with the formation of wrinkles on the skin of a dried fruit. On the other hand, in swollen toluene-modified polymers, the pores are in fact a part of the polymer gel phase and their stability during drying depends on the rigidity of polymer mass, i.e., to what extent is the swollen, expanded state fixed by crosslinks. The rigidity is indirectly proportional to the content unreacted double bonds. The residual content of unreacted double bonds in polymer DVB-50-B-T is much lower (9.8/%) than in the polymer DIB-50-B-T (25 %). Hence, a highly swollen gel phase observed the DIB polymer (fractions with C = 0.4 and 0.8 nm^{-2} in Table II) is poorly fixed by crosslinks and, subsequently, during drying it completely collapses. In the more highly crosslinked DVB polymer, upon drying a pore structure with considerable surface area is maintained (Table I).

Combined ESR-ISEC Approach to Molecular Accessibility of Swollen Gel Resins. Conceptually and experimentally quite independent techniques, electron spin resonance spectroscopy (ESR) and ISEC were combined for investigation of a number of microporous, fairly hydrophilic poly{N,N-dimethylacrylamide-methylenebisacrylamide} resins (*18*). For this study was prepared a series of polymers (resins M1 - M8) in which the cross-linking degree ranged from 1 to 8 %. The morphology of the investigated polymers in the swollen state is assumed to be composed of five discrete fractions of polymer mass, characterized by polymer chain density 0.1, 0.2, 0.5, 1.0 and 2.0 nm^{-2}, respectively. The pattern of volume distribution among the five fractions displayed by resins M1 - M8 swollen in water, as obtained from ISEC, is depicted in Figure 4.

The overall picture is very informative. Resins M8 and M6 appear to be dominated by high chain density (2 nm^{-2}) fractions, while resins M1 - M4 appear to be rather bidisperse materials. For ESR experiments each sample was analyzed after soaking the resin with a 10^{-4} M aqueous solution of the spin probe TEMPONE (2,2,6,6-tetramethyl-4-oxo-1-oxypiperidine). The ESR spectra of the aqueous solution of TEMPONE dispersed inside resins M1 - M8 reveal that TEMPONE, a molecule of substantial size (ca. 0.2 nm^3) easily gains access to the microporous domains in moderately cross-linked poly(dimethylacrylamide) matrices swollen in water. The probe rotates freely at room temperature inside the nanometer-sized cavities of these materials but the increasing rotational hindrance is experienced by TEMPONE in more highly cross-linked matrices reflects essentially a microviscosity phenomenon. The increase of viscosity is paralleled by an increase of polymer chain density, which, in turn, corresponds to a decrease of the size of the reticular cavities.

A physico-mathematical model was formulated resulting in a description of the relations between rotational correlation time τ of the spin probe inside the resin and the resin morphology. The ratio of τ to τ_0 (rotational correlation time τ of the spin probe to that in free solution) is for a resin of uniform chain concentration C given by equation 5

$$\tau / \tau_0 = \mathrm{A}^{\mathrm{C}} \tag{5}$$

where A is an adjustable parameter. For a resin composed of n fractions of various polymer chain concentrations it may be expected that the observable τ/τ_0 will be an weighed average taking into account the probe distribution (equation 6)

$$\tau / \tau_0 = \sum_{i=0}^{i=n} \left[\mathrm{K}_0^i \mathrm{V}^i \mathrm{A}^{\mathrm{C}_i} \Big/ \sum_{i=0}^{i=n} \left(\mathrm{K}_0^i \mathrm{V}^i \right) \right] \tag{6}$$

]

where K_0^i is the Ogston distribution coefficient of the probe in the i-th polymer fraction of volume V^i. Beside A, the other adjustable parameter is the molecular

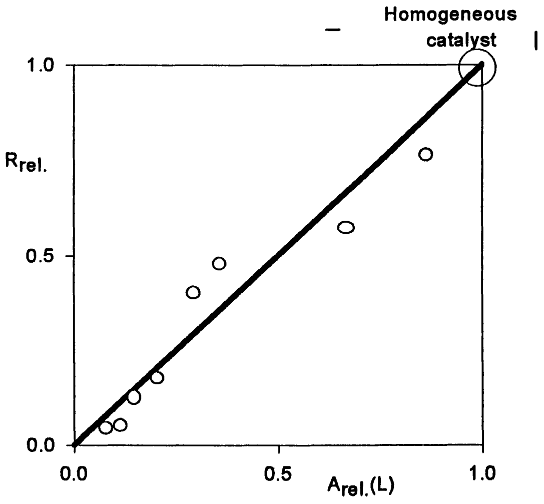

Figure 3. Correlation of the relative catalytic activity Rrel. and the ISEC-derived steric exclusion of the reactants Arel.(L) for the effective reactant size L corresponding to the minimum in Figure 2. (Reproduced with permission from ref. 14. Copyright 1990 John Wiley & Sons, Inc.)

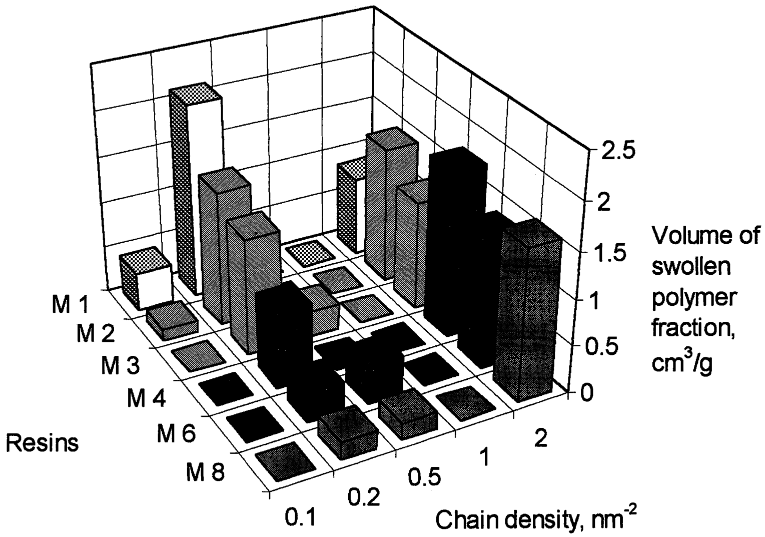

Figure 4. ISEC pattern displayed by resins M1 - M8 in water. (Reproduced with permission from ref. 18. Copyright 1995 ACS)

dimension of the probe d_m contained in K_0^1 (see equation 4). In contrast with A, the parameter d_m has a distinct physical meaning and its value should correspond to it. Figure 5 shows the dependence of the sum of squared differences of experimental and computed values of τ/τ_0 on the parameter d_m. Parameter A was optimized for each d_m separately. The best agreement of the experimental and computed values of τ/τ_0 was achieved for $d_m = 0.32$ nm. The same value of the molecular radius of TEMPONE was reported by Freed et al. (*19*). The excellent correlation of the value obtained as an adjustable parameter with its supposed physical meaning supports the reliability of the proposed physico-mathematical model based on the ISEC characterization of the swollen-state morphology of the investigated resins.

Simultaneous ISEC characterization of lipophilic and hydrophilic domains within one polymer. ISEC measurements generally require that the elution behavior of the solutes used for probing the pore space should be determined by steric effects only. To achieve this, it is important to use a mobile phase which is a very good swelling solvent for the investigated resin. Solvents which are "good" for the lipophilic polymers usually precipitate the hydrophilic polymers (and vice versa). Therefore, by alternate ISEC measurements in water and tetrahydrofuran, it is sometimes possible to characterize the morphology of polymers containing both the lipophilic and hydrophilic domains.

This approach will be demonstrated by analysis of properties of functional polymers prepared by copolymerization of p-styrenesulfonyl chloride (SSC) with divinylbenzene and styrene (*20*). Unhydrolyzed, these polymers are completely lipophilic. After hydrolysis, the hydrophilic domains containing the strongly acidic groups, if neutralized with metal cations, do not swell in organic solvents. Similarly, the lipophilic domains do not swell in an aqueous environment. The ISEC measurements of the unhydrolyzed polymers were performed in tetrahydrofuran. During characterization of the hydrolyzed polymers (in the Na^+ form) alternatively in water and tetrahydrofuran all the standard solutes were eluted in order of their molecular sizes and the values of their elution volumes did not suggest a presence of non-steric interactions with the investigated polymers. Two selected polymers whose composition is shown in Table III will be discussed.

Table III. Composition of the Polymerization Mixtures in Preparation of the Selected Polymers

Polymer	Monomer mixture composition, mol %			Added solvent*
.	SSC	Styrene + EVB	DVB	
A	89	5	6	Butanol
B	41	41	18	Butanol

*Solvents added to the polymerization mixture in the amount 2/3 of the weight of the monomers. (Adapted from ref. 20)

Figure 6 depicts the results of the ISEC investigation of polymer A. For this polymer before hydrolysis the ISEC measurement in THF shows bidisperse morphology with a substantial volume of polymer fraction characterized by high chain density with $C = 2\ \text{nm}^{-2}$ and a small volume of thinner fraction with $C = 0.5\ \text{nm}^{-2}$.

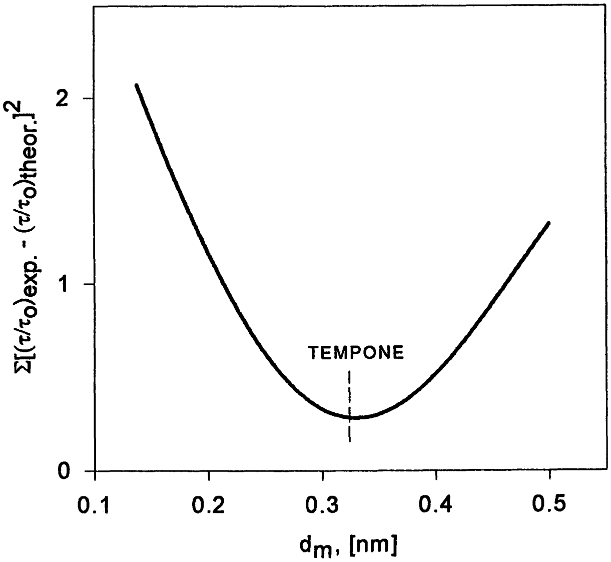

Figure 5 Dependence of squared errors of τ/τ_0 on d_m (the size of the spin probe) (Reproduced with permission from ref. 18. Copyright 1995 ACS)

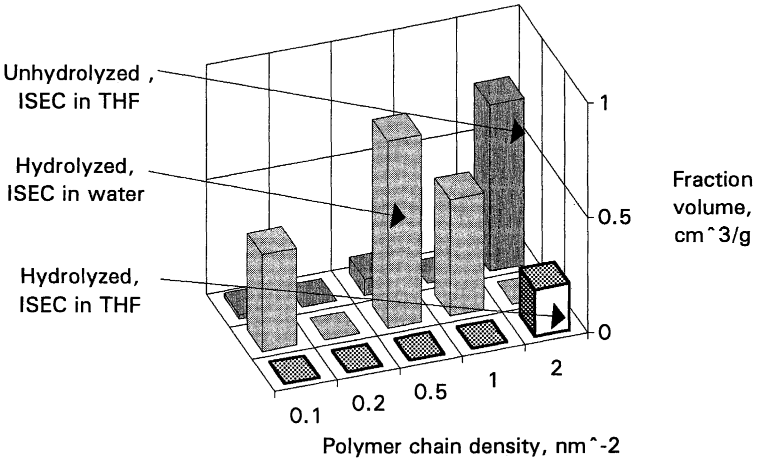

Figure 6. Comparison of the swollen-state morphologies of the polymer A before hydrolysis, from ISEC in THF and after hydrolysis, from ISEC in water and THF. (Reproduced with permission from ref. 20. Copyright 1995 ACS)

After hydrolysis by ISEC in water, a similar bidisperse morphology was detected, only more highly swollen. This is reflected in the shift towards lower polymer chain densities. The hydrolyzed polymer A in THF shows only a small volume of single fraction of poorly swollen, very dense polymer. This picture corresponds well with the composition of this sample that contains 89 mol. % SSC and hence, after hydrolysis, only a small part of the lipophilic polymer mass is swellable in THF.

The polymer B contains only 41 mol. % SSC and therefore in the hydrolyzed polymer the shares of the lipophilic and hydrophilic parts should be comparable. The results of the ISEC confirm it, as both in water and THF the hydrolyzed polymer shown substantial volumes of the swollen polymer mass (Figure 7).

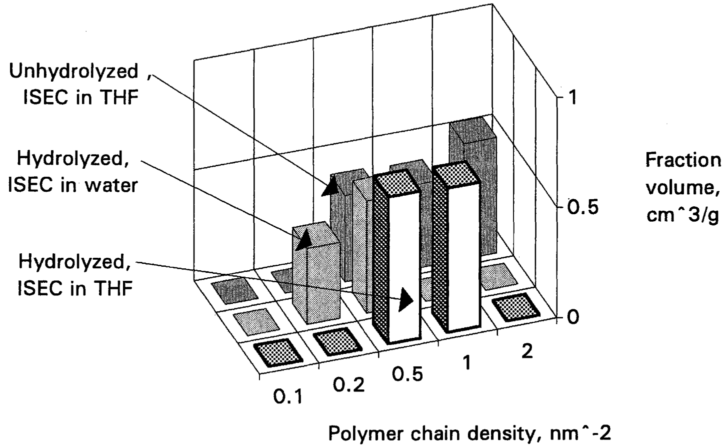

Figure 7. Comparison of the swollen-state morphologies of the polymer B before hydrolysis, from ISEC in THF and after hydrolysis, from ISEC in water and THF. (Reproduced with permission from ref. 20. Copyright 1995 ACS)

Observed separate swelling of the functionalized, hydrophilic and the unfunctionalized, lipophilic polymer mass would hardly be possible in a polymer composed from randomly alternating monomer units. This behavior is more compatible with a block copolymer morphology consisting of substantial lipophilic and hydrophilic domains. The creation of these separate domains could result from a possible phase separation of SSC-rich domains due to the strong mutual interaction of the functionalized monomer molecules or polymer segments.

Conclusions

During many years of practical use ISEC has proved to be a valuable tool for characterization of the morphology of a wide spectrum of various materials. As with any indirect porosimetric method, it depends on modeling the complicated natural morphology using a simple geometrical concept which makes it possible to define a clear relationship between the measured elution volumes and the structure of the materials studied. Experience with this model, which is based on a set of discrete pore fractions using either the cylindrical or Ogston model pore geometry, shows that this approach is a viable concept. It is simple enough to be easily applicable and yet sufficiently flexible to be used for the description of materials with complex morphology such as swollen macroreticular polymers. The credibility of the ISEC-derived information was confirmed by successful correlation with results from various independent methods.

Acknowledgements

Preparation of this review was supported by the Grant No. 104/94/0749 from the Grant Agency of the Czech Republic.

Literature Cited

1. Halász, I.; Martin, K. *Angew. Chem. Int. Ed.* **1978**, *17*, 901.
2. Freeman, D. H.; Poinescu, I. C. *Anal. Chem.* **1977**, *49*, 1183.
3. Giddings, J. C.; Kucera, E.; Russell, C. P., Myers, M. N. *J. Phys. Chem.* **1968**, *72*, 4397.
4. Cassassa, E. F. *J. Polym. Sci. Part B Polym. Phys.* **1967**, 5, 773.
5. Cassassa, E. F.; Tagami, Y. *Macromolecules* **1969**, *2*, 14.
6. Cassassa, E. F. *Macromolecules* **1969**, *2*, 14.
7. Kremer, M..; Pothmann, E.; Rössler, T.; Baker, J.; Yee, A.; Blanch, H; Prausnitz, J. M. *Macromolecules* **1969**, *2*, 14.
8. Vilenchik, L. Z.; Asrar, J.; Ayote, R. C.; Ternorutsky, L.; Hardiman, C. J. *J. Chromatogr.* **1993**, *648*, 9.
9. Jeřábek, K. *Anal. Chem.* **1976**, 9, 182.
10. Knox, J. H.; Ritchie, H. J. *J. Chromatogr.* **1987**, *387*, 65.
11. Jeřábek, K. *Anal. Chem.* **1985**, *57*, 1598.
12. Ogston, A. G. *Trans. Faraday Soc.* **1958**, *54*, 1754.
13. Crispin, T.; Halász, I. *J. Chromatogr.* **1982**, *239*, 351.
14. Jeřábek, K.; Setínek, K. *J. Polym. Sci. Part A Polym. Chem..* **1990**, *28*, 1387.
15. Gates, B. B.; Rodriguez, W. *J. Catal..* **1973**, *31*, 27.
16. Jeřábek, K.; Shea, K. J.; Sasaki, D. Y.; Stoddard, G. J. *J. Polym. Sci. Part A Polym. Chem..* **1992**, *30*, 605.
17. Shea, K. J.; Sasaki, D. Y.; Stoddard, G. J. *Macromolecules*, **1989**, *22*, 1722.
18. Biffis, A.; Corain, B.; Zecca, M.; Corvaja, C.; Jeřábek, K *J. Am. Chem. Soc.* **1995**, *117*, 1603.
19. Hwang, J. S.; Mason, R. P.; Hwang, L. P.;Freed, J. H. *J. Phys. Chem.* **1975**, *79*, 489.
20. Jeřábek, K.; Hanková L.; Revillon A. *Ind. Eng. Chem. Res.* **1995**, *34*, 2598.

Chapter 13

Characteristics of Modern Media for Aqueous Size Exclusion Chromatography

Lars Hagel

Pharmacia Biotech AB, S–75182 Uppsala, Sweden

Downloaded by UNIV MASSACHUSETTS AMHERST on October 8, 2012 | http://pubs.acs.org
Publication Date: May 30, 1996 | doi: 10.1021/bk-1996-0635.ch013

Important characteristics of media for size exclusion chromatography include particle size, pore volume, sorptive properties and matrix rigidity. However, the single most decisive parameter is the optimization of the selectivity to cope with the demands of high resolution separations. Whereas traditionally media are manufactured to encompass a broad separation range we now see a focus to a few key applications. These include a renewed interest in separation of smaller macromolecules, e.g. peptides and protein fragments and in dedicated separations such as monoclonal antibodies from growth media additives. The increase in selectivity may be obtained by selective grafting of polymers to reduce accessibility of pores to a small size range of solutes and in principle mimic the functionality of a single pore size support. The properties of such a medium designed for aqueous size exclusion chromatography, Superdex, is reviewed to elucidate the effect of important characteristics.

By definition, aqueous size exclusion chromatography is carried out using a porous support. The molecules are separated due to the varying degrees of steric exclusion from the pore volume as caused by different molecular sizes of the solutes. This will result in the molecules being eluted from the column in order of decreasing size. Furthermore, the separation will only take place over an elution volume corresponding to the pore volume. Thus, the effective separating volume in aqueous size exclusion is small as compared to adsorptive techniques (i.e. solutes will ideally only be eluted within one column volume). In preparative purifications this limitation is generally of little importance since the desired separation is achieved through employing a gel medium with a suitable selectivity. Also for analytical applications where one component is of major interest it is often possible to find a gel of matching selectivity. However, the analysis of broad molar mass distributions may demand a wide separation range to encompass the whole distribution and this may be obtained by

0097–6156/96/0635–0225$16.00/0

using a material of a large separation range or combination of several materials of different (but overlapping) separation ranges. It is also important to realize that chromatographic purification of peptides and proteins in most cases involves a combination of several techniques of complementary functional properties.

Many designations have been used for characterizing the separation of molecules according to size (*1-3*). Gel filtration and gel permeation have gained acceptance for describing the application in respectively aqueous and non-aqueous media, however, the general principle of employing porous media for separation of solutes according to molecular size is now called size exclusion chromatography (SEC).

Gel filtration, i.e. aqueous size exclusion chromatography has been utilized for more than thirty five years for separation of macromolecules according to size. The technique has proven to be an important complementary tool in purification schemes for proteins and peptides. This may mainly be attributed to gel filtration being a very gentle separation technique, thus preserving biological activity and yielding high recovery of sensitive proteins on gels consisting of natural polymers. Furthermore, the feature of separating reaction mixtures and solute aggregates , solely due to differences in solvated size of components has positioned aqueous size exclusion as a valuable tool for initial as well as final purifications.

Preparative gel filtration is useful as an initial step in the purification scheme for a quick clean up of crude samples to remove contaminants, reaction products or uncleaved protein, as an intermediate step for sample conditioning or partial purification or late in the purification process for final polishing or final product formulation.

During the last few years a trend towards using bench systems for small scale purification have been noticed. This is among other things due to the fact that the demand for material in subsequent steps (e.g. microanalysis, sequencing, PCR etc.) has been reduced but also that the interest in purifying very small sample volumes has increased, especially for studies of body fluids. The reliability and reproducibility of the performance of analytical systems have also made it possible to prepare sufficient amount of material through multiple cycle processing. However, the need for frequent column cleaning to ensure product integrity may cause multiple cycle small-scale fractionations to be an unfavorable strategy for purifying large amounts of sample for other purposes than laboratory or diagnostic use.

Development of media for size exclusion chromatography has been directed towards synthesis of gels with narrow pore size distributions to yield high resolving power and small particle sizes to yield efficient separations at high speed. However, since many parameters are interrelated, several factors must be considered when choosing a size exclusion column. The basic framework for understanding the theory behind the separation process in size exclusion has been established and this may be explored for optimization of size exclusion separations, though, as discussed below, there are still some fundamental issues, to be resolved.

Downloaded by UNIV MASSACHUSETTS AMHERST on October 8, 2012 | http://pubs.acs.org
Publication Date: May 30, 1996 | doi: 10.1021/bk-1996-0635.ch013

Downloaded by UNIV MASSACHUSETTS AMHERST on October 8, 2012 | http://pubs.acs.org
Publication Date: May 30, 1996 | doi: 10.1021/bk-1996-0635.ch013

Important Parameters for Size Exclusion Chromatography

Important inherent properties of materials for aqueous size exclusion are pore volume, selectivity and particle size which together with molecular characteristics such as molecular size and diffusivity and experimental parameters such as flow rate, column dimensions, sample volume and temperature will influence the separation result (i.e. resolvability, peak capacity, reproducibility and recovery). Different optimizations of the parameters are found for analytical and preparative separations. In some cases also non-size-exclusion effects are needed to take into consideration.

Matrix Characteristics. The selectivity of SEC, i.e. the ability to resolve molecules of similar size can, in the ideal case, not be regulated by adjusting the composition of the mobile phase (e.g. as for ion-exchange or reversed phase chromatography). Instead, it is the inherent physical characteristics of the matrix that will have a decisive influence on the separation in SEC.

Pore Volume. Since, in ideal SEC, no change in enthalpy takes place, the distribution coefficient will only depend upon the change in entropy as molecules diffuse from the extraparticle to the intraparticle space. The distribution coefficient is, macroscopically, a measure of the relative pore volume that is sterically accessible to the solute which yields the following expression for the retention (elution) volume, V_R, in SEC

$$V_R = V_o + K_D \cdot V_p \qquad (1)$$

where V_o is the void volume of the column and V_p is the pore volume of the bed and K_D is the distribution coefficient of the solute. The void volume, or dead volume, in SEC is equal to the interstitial volume occupied by liquid between the gel beads in the packed bed. From equation 1 it can be concluded that elution of solutes only takes place over the retention volume window given by $V_R=V_o$ (i.e. $K_D=0$) and $V_R=V_o+V_p$ (i.e. $K_D=1$) in ideal SEC. Thus, due to the limited separation volume the number of peaks that may be resolved by SEC is small as compared to ion exchange or reversed phase chromatography and a high pore volume is an important inherent parameter of a material for size exclusion chromatography.

Selectivity. The selectivity is a function of the pore size distribution of the gel medium. This means that the retention in SEC may not be adjusted by changing the composition of the mobile phase as long as this change does not influence solute size or pore dimensions. The relative retention may be expressed by dK_D/dR, the differential change in distribution coefficient , K_D, for a change in solute radius, R. Thus, the larger the absolute value of the selectivity, the further apart will the solutes be separated. The selectivity curve, i.e. a plot of the distribution coefficient versus solute size, (as opposed to the calibration curve where the retention volume or the distribution coefficient is the independent variable) will have a sigmoid shape with an approximately linear center region if K_D is plotted versus logR. The maximal selectivity of a SEC material is given by the slope of the linear part and has been calculated to be (ln10)/2 assuming spherical solutes separated on a single-pore-size support of cylindrical pore shape (*4*). This yields the following relationship for the selectivity

Downloaded by UNIV MASSACHUSETTS AMHERST on October 8, 2012 | http://pubs.acs.org
Publication Date: May 30, 1996 | doi: 10.1021/bk-1996-0635.ch013

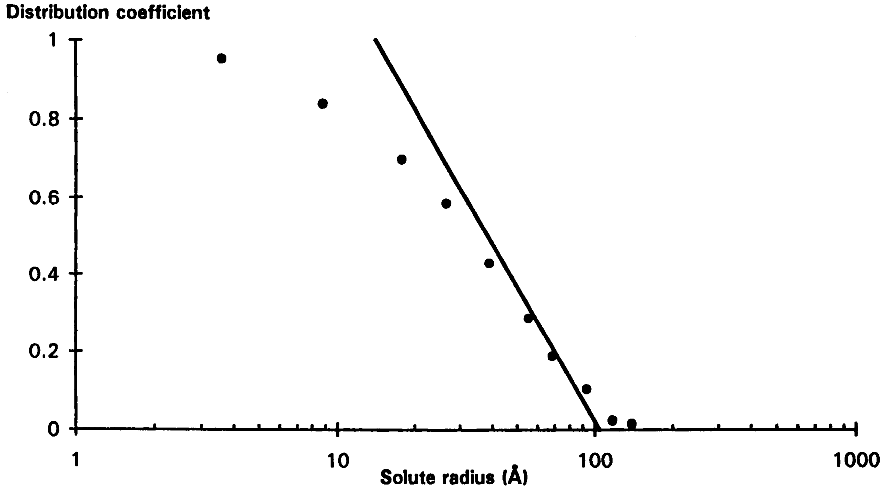

Figure 1. Selectivity curve of a standard size exclusion medium. Gel medium: Sephacryl S-300 (●). Column dimensions: 50x1.6 cm I.D. Sample: Dextran fractions (Pharmacosmos, Box 29, DK 4130, Viby, Denmark). Viscosity radius calculated according to Ref. 4 from $R_\eta = 0.271 \cdot M_r^{0.498}$ The line represents the theoretical selectivity of a hypothetical support of monomodal distribution of cylindrical pore size having a slope of -(ln10)/2 (*4*) .

$$-\frac{dK_D}{d\log R} \leq \frac{\ln 10}{2} \approx 1.15 \qquad (2)$$

In practice, a very high selective media may separate rougly a decade in molecular size (*4*). Figure 1 illustrates the selectivity curve of a typical size exclusion medium as compared to the theoretical limit. It may be noted that a high selectivity is accompanied by a small separation range (i.e. the range of molecular size the medium will separate). Therefore analysis of samples of broad molecular mass distributions are preferentially carried out on a wide pore size distribution medium or a combination of columns packed with materials of different but overlapping pore size distributions.

Particle Size. A small particle size will result in a low zone broadening of macromolecules, predominantly due to the small diffusion distances. The zone broadening of macromolecules may be related to the particle diameter, d_p, by the plate height, H, from the van Deemter equation (cf. equation 4) where axial dispersion (i.e. the B-term) may be ignored due to the low diffusivities at the eluent velocities commonly used in SEC of macromolecules and the relationship $H=L/(V_R/\sigma)^2$ which yields

$$w_b = d_p \cdot \frac{4 \cdot V_R}{\sqrt{L}} \cdot \sqrt{\frac{2\lambda}{d_p} + \frac{V_o}{V_R} \cdot \frac{\left(1 - \frac{V_o}{V_R}\right)}{30 \cdot D_s} \cdot u} \qquad (3)$$

where w_b is the base width of the peak (i.e. 4σ for a Gaussian peak), L is the bed height, λ is a geometrical factor of order unity, V_o/V_R is the ratio of zone velocity to mobile phase velocity, *u* is the eluent velocity, D_s is the diffusion coefficient of the solute in the pores of the matrix (which due to hindered diffusion may be as low as 5-20% of the free diffusion (*3*)). For small solutes the diffusion coefficient may be substantially large to reduce the effect from multiple path dispersion which necessitates the expansion of the first term to include this coupling and at low velocities axial dispersion may also contribute to zone broadening (cf. equation 4 and Figure 4). However, as seen from equation 3 the peak width of macromolecules is, especially at high eluent velocities, approximately proportional to the particle size which indicates the relative importance of using small particle sized media to get high resolution in SEC The increase in column back-pressure, the need to decrease the pore fraction to increase the mechanical stability by adding backbone matrix, the difficulty of packing media of very small particle size and the shear effects on elongated solutes at high interstitial velocities are some factors which cause the lower limit for particle size of SEC media to be between 2 µm and 5 µm (*5,6*). It may also, in this connection, be noticed that increased zone dispersion from coupling column in series will probably be more serious for media of small particle size than for media of large particle size.

Downloaded by UNIV MASSACHUSETTS AMHERST on October 8, 2012 | http://pubs.acs.org
Publication Date: May 30, 1996 | doi: 10.1021/bk-1996-0635.ch013

Downloaded by UNIV MASSACHUSETTS AMHERST on October 8, 2012 | http://pubs.acs.org
Publication Date: May 30, 1996 | doi: 10.1021/bk-1996-0635.ch013

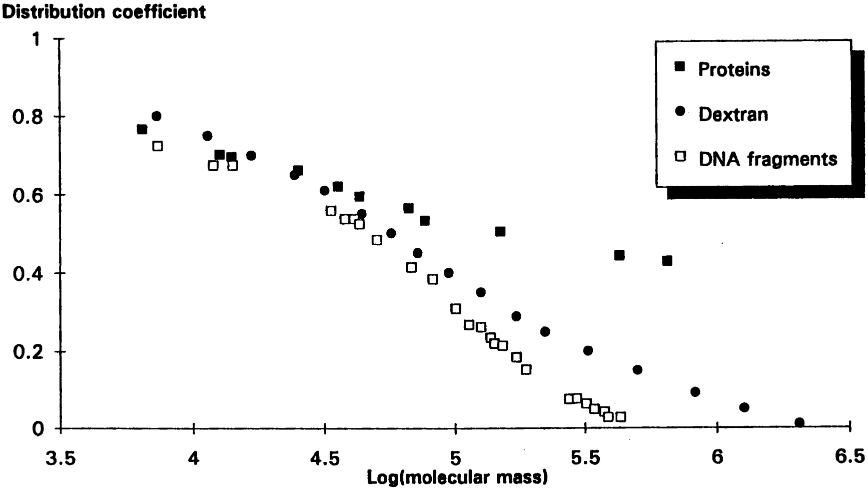

Figure 2. Distribution coefficient as function of molecular mass for solutes of different shape. Gel medium: Superose 6. Column dimensions: 30x1 cm I.D. Sample: (■) Globular proteins, representing compact spheroids; (●) Dextran fractions, representing flexible coils; ( ) DNA restriction fragments, representing rod-shaped molecules. Data for restriction fragments and proteins calculated from Ref. 8 by courtesy of Torgny Låås, Pharmacia.

Downloaded by UNIV MASSACHUSETTS AMHERST on October 8, 2012 | http://pubs.acs.org
Publication Date: May 30, 1996 | doi: 10.1021/bk-1996-0635.ch013

Solute Characteristics. The important properties of the solutes are molecular size which regulates the elution volume and the diffusion coefficient which will influence the zone broadening and thus the peak width.

Molecular Size. The relationship between the molecular size and the molecular weight is dependent upon the shape of the molecule. Thus, the radius of gyration of a molecule varies with molecular mass according to $R \propto M_r^{1/3}$ for a compact sphere, $R \propto M_r^{1/2}$ for a flexible coil, and $R \propto M_r$ for a rigid rod (*9*). This results in that the plots of distribution coefficient versus logarithm of molecular mass will differ substantially between solutes of different shape as illustrated by Figure 2. This leads to that the resolvability of e.g. DNA-fragments of intermediate length is larger than that of globular proteins of similar molecular masses. The Figure also demonstrates one of the shortcomings of using a calibration curve for evaluating solute size of unknown solutes in analytical SEC. Thus, unless the shape of the molecule is very close to that of the reference samples erroneous conclusions about the solute size will apparently be made. It has also been noted that the shape of solutes may vary as a function of molecular mass. Thus, the size of double stranded DNA of M_r less than ca. 13,000 has a rigid and globular shape, fragments of M_r ca. 70,000 should be regarded as rods and fragments with M_r larger than 700,000 forms random coils (*10*). The concept of universal calibration may be applicable to molecular shapes of flexible-coils and spheroids (*11*). However, this approach is not valid for all types of solutes, e.g. the elution of rod-shaped molecules differ from that predicted by universal calibration (*12*). This problem may be circumvented by employing the SEC column for separation of the solutes to be pure enough to allow an accurate size-determination of solutes in the effluent. Information about molecular mass or molecular shape may be done by sampling the effluent and a subsequent of-line size or mass determination or on-line by using mass-spectrometry, light scattering instruments, differential viscosity detectors etc. (*13-15*). The techniques mentioned yields complementary information, i.e. molecular mass, weight average molecular mass, radius of gyration, conformation, branching etc. and it is therefore advantageous to use them in series. Using on-line detectors also put lower requirements on the system, i.e. sorptive effects, flow rate variation and moderate column zone broadening will have no effect on the result.

Molecular Diffusivity. The molecular diffusivity is inversely proportional to the molecular radius and the solvent viscosity, and proportional to the temperature. Furthermore, the actual diffusion coefficient of solutes within the bead may, especially for large solutes, be only a fraction of the free diffusion. As seen from equation 3 (and equation 4) the diffusion coefficient will affect the zone broadening of the solute. However, the effect is rather small due to the large contribution from the A-term (cf. Figure 4) except at very low or very high velocities. Therefore, the zone broadening of solutes varies only slightly as can be seen from Figure 3. The negative effect of decreasing the molecular diffusivity seems to be partly compensated for by the decrease in retention volume of solutes of larger size (and thus low diffusion coefficient) except for very large solutes.

Running the separation at high temperature reduces the viscosity and thus yields an increase in diffusion coefficients of the solutes which may be utilized to increase the resolution or decrease the analysis time for macromolecules. Again, this

Downloaded by UNIV MASSACHUSETTS AMHERST on October 8, 2012 | http://pubs.acs.org
Publication Date: May 30, 1996 | doi: 10.1021/bk-1996-0635.ch013

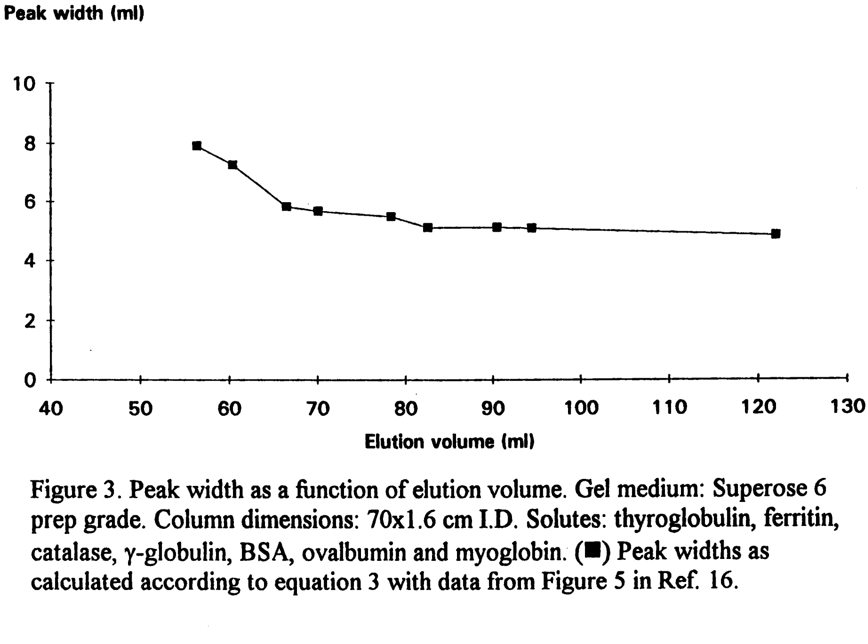

Figure 3. Peak width as a function of elution volume. Gel medium: Superose 6 prep grade. Column dimensions: 70x1.6 cm I.D. Solutes: thyroglobulin, ferritin, catalase, γ-globulin, BSA, ovalbumin and myoglobin. (■) Peak widths as calculated according to equation 3 with data from Figure 5 in Ref. 16.

Downloaded by UNIV MASSACHUSETTS AMHERST on October 8, 2012 | http://pubs.acs.org
Publication Date: May 30, 1996 | doi: 10.1021/bk-1996-0635.ch013

strategy may not be applied to SEC of low molecular weight solutes for which an increased diffusivity may result in increased zone broadening due to axial dispersion (cf. Figure 4a). On the other hand, when performing SEC at reduced temperatures, e.g. for the analysis of temperature sensitive solutes, the increased viscosity has to be taken into consideration when choosing the experimental conditions (i.e. the flow rate may need to be reduced to maintain the resolution). Thus, employing a matrix yielding a minimum of hindered diffusion (i.e. low tortuosity factors, large pore size) and a low retention time will be favorable to keep the influence from molecular diffusion as low as possible. However, the last two requirements are contradictory and accordingly an optimum in resolution is found at an intermediate retention volume corresponding to a distribution coefficient around 0.2 to 0.4 (*3*).

Experimental Parameters. The conditions that may be used to influence the separation result are the velocity of the mobile phase which will affect the peak width, the sample volume which under certain circumstances also will affect the peak width and finally the composition of the mobile phase to suppress solute-matrix interactions.

Flow Rate. The effect from the flow rate on zone broadening may be illustrated by the variation of the plate height according to the van Deemter equation as applied to SEC (*3,17,18*)

$$H \approx A + \frac{B}{u} + C \cdot u \approx 2 \cdot \lambda \cdot d_p + \frac{2\left[0.6 \cdot D_m + D_s\left(\frac{V_R}{V_o} - 1\right)\right]}{u} + \frac{\frac{V_o}{V_R}\left(1 - \frac{V_o}{V_R}\right) d_p^2}{30 \cdot D_s} \cdot u \tag{4}$$

The zone broadening is at low eluent velocities dominated by axial diffusion (the B-term) and at high eluent velocities mainly affected by the non-equilibrium term (the C-term), see Figure 4. At intermediate velocities a minimum plate height, which is proportional to the particle size of the medium is achieved (for well-packed columns this is close to 2 times the particle size).The position of the minimum is proportional to the ratio between solute diffusivity and particle size. Therefore, size exclusion of slowly diffusing solutes using particles of large size needs to be performed at low eluent velocity for optimal resolution (Figure 4b) whereas size exclusion of small solutes using particles of small size needs to be performed at high eluent velocities for low zone broadening (Figure 4a). The minimum is obtained at 4 to 6 times the quotient D_m/d_p (which corresponds to a nominal flow velocity, cm/h, of 5 to 7 times D_m/d_p, $cm^2/s/\mu m$).

As noted above, the A-term is not constant when solutes of high diffusivity are run (*17*). It may also be mentioned that a number of equations has been proposed for calculating zone broadening in liquid chromatography. However, a review of these showed that the van Deemter equation may be employed with confidence (*19*).

For media of large pore size and small particle size convective transport has been reported, even though the actual flow through the particle is negligible (*20*). In this case the van Deemter plot may be expected to yield an overestimate of the plate height at high eluent velocity.

Downloaded by UNIV MASSACHUSETTS AMHERST on October 8, 2012 | http://pubs.acs.org
Publication Date: May 30, 1996 | doi: 10.1021/bk-1996-0635.ch013

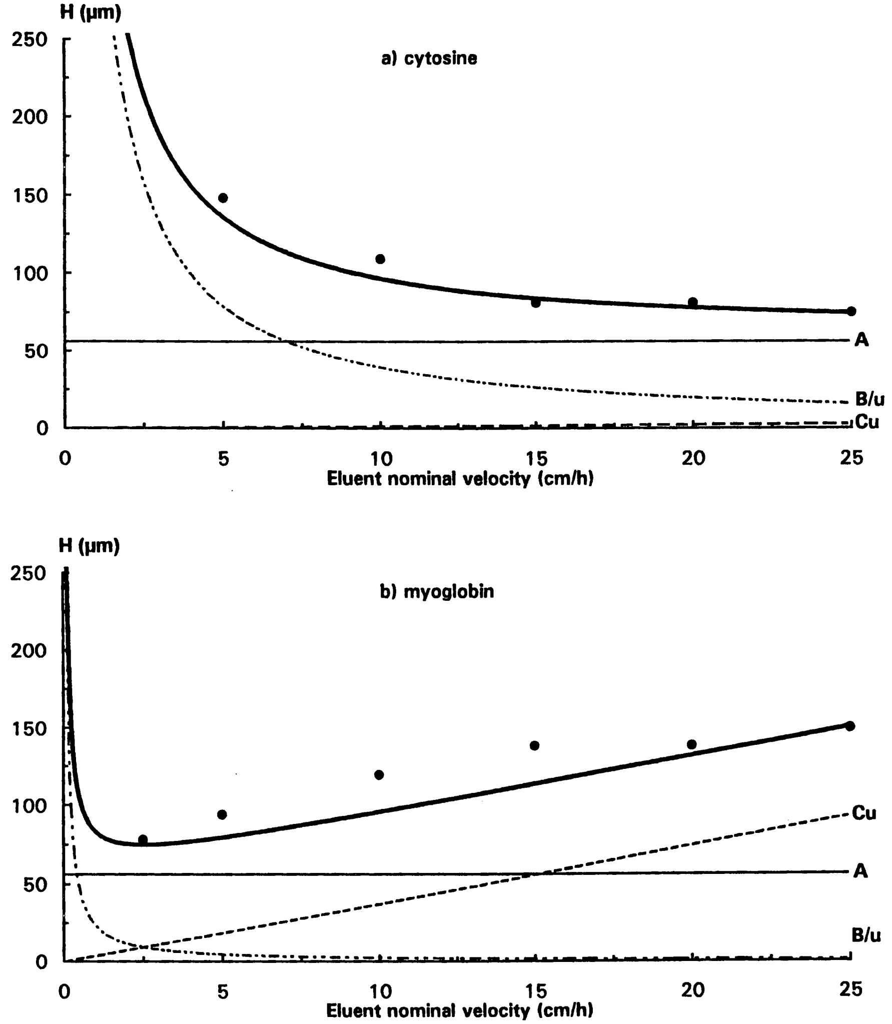

Figure 4. Influence of flow rate on zone broadening for large and small solutes. Gel medium: Superose 6 prep grade. Column dimensions: 70x1.6 cm I.D. Sample: a) cytosine; b) myoglobin. Dots represent experimental data and solid lines the theoretical contributions from the different terms in the van Deemter equation (equation 4). Reprinted from Ref. 3 with permission by VCH Publishers © (1989).

Sample Volume. The width of the injected sample plug will contribute to the peak width according to (*21*)

$$\frac{\sigma^2_{injector}}{\sigma^2_{peak}} = \frac{1}{1+\left(\dfrac{V_e}{V_{injector}}\right)^2 \cdot \dfrac{K_{injector}}{N}} \qquad (5)$$

where $K_{injector}$ is a constant for the injection device used (a value of 5 was found for an ordinary laboratory valve injector) and approaches 12 for a square wave plug injection (*21*). From equation 5 it is seen that the influence of the sample volume is reduced by keeping the injected volume, $V_{injector}$ low as compared to the elution volume and also, keeping the plate number, N, low. This, perhaps surprising result, is due to that a column having a high plate number yields narrow peak widths which are more affected by a small increase in injected volume than broad peaks from a column of low plate count (of course, the peak width will in most cases be smaller on a high plate number column except when the injected volume totally dominates the peak width, e.g. as in desalting). These guidelines are illustrated in Figure 5 showing the influence of sample volumes on zone broadening, expressed as reduced plate height H/d_p, for columns of various efficiencies and bed volumes. The conclusion drawn is that in analytical size exclusion, where the peak width is to be kept at a minimum to yield high resolution, the sample volume should generally not exceed 0.1% of the bed volume for columns having plate counts around 20,000. If the contribution from other parts of the system, e.g. connectors, tubings etc. are not insignificant then effects of the injected volume will first be noticed at higher volumes!

For preparative applications the maximum applicable volume will be a compromise between the cycle time (i.e. zone broadening due to non-equilibrium effects at high solvent velocity) and the number of cycles (i.e. zone broadening due to large sample volumes) in order to process a given volume within a given time (*22*). The effect of increasing the bed diameter to allow for application of larger sample volumes without sacrificing the resolution is also illustrated in Figure 5.

Non-size-exclusion Effects. Since the exposed surface of the solute, as well as of the gel matrix, may contain lipophilic, hydrophilic, and ionic groups, interactions between solutes and gel media are not uncommon. This may result in the solute being eluted earlier (e.g., as for ion-exclusion) or later (e.g., as for ionic or hydrophobic adsorption) than expected from the size of the solute. Fortunately, since the composition of the mobile phase may be chosen within wide limits the possibility to reduce or eliminate interaction phenomena in SEC is quite large.

From the many suggestions found in literature regarding suppression of solute-matrix interactions it may be concluded that it seems as though each solute-solvent-matrix system is unique which prevents a generally valid suggestion of mobile phase composition. As many solutes and matrix surfaces posses both ionic and hydrophobic

Downloaded by UNIV MASSACHUSETTS AMHERST on October 8, 2012 | http://pubs.acs.org
Publication Date: May 30, 1996 | doi: 10.1021/bk-1996-0635.ch013

Downloaded by UNIV MASSACHUSETTS AMHERST on October 8, 2012 | http://pubs.acs.org
Publication Date: May 30, 1996 | doi: 10.1021/bk-1996-0635.ch013

sites the optimum composition of the mobile phase will have to balance the different effects (viz. the influence of the electric double layer and Van der Waals forces) to a net zero effect. Solute-matrix interactions may be explained by applying the theory of potential barrier chromatography, as recently demonstrated for proteins of different hydrophobicity and surface charge (*23*). Hydrophobic solutes were preferentially chromatographed at a pH exceeding the isoelectric point and with a mobile phase containing 0.1 M sodium chloride to balance hydrophobic interaction and ion-exclusion effects. Solutes of intermediate hydrophobicity were chromatographed at higher ionic strength, 0.1 M sodium phosphate at a pH exceeding the pK_a of the cationic groups on the matrix to prevent ion-exchange interaction. Addition of an organic modifier will cause a decrease of Van der Waals interactions. However, this approach may not result in pure size exclusion but in a quasi equilibrium state where the net effects on the retention are zero. Thus, a recent work illustrated that even though the mobile phase (i.e. 0.1% TFA, 0.12 M phosphate and 10% methanol) was optimized to yield good relationship between size and elution volume of a large number of model peptides, the experimental conditions did not yield separation according to molecular volume of peptides from casein hydrolysate (*24*).

Since size exclusion is an entropy driven process, any large variation in retention due to temperature changes may be attributed to interaction phenomena, unless the conformation of the solute is extremely temperature sensitive.

Deviation of a solute from a straight line calibration curve is not necessarily an indication of solute-matrix interactions. Since the separation is based on solute size, solutes of varying shape but of same molecular weight will elute at different retention volumes, as illustrated in Figure 2. The influence of protein and peptide shape may be eliminated by running the separation under denaturing conditions (e.g. using 8M urea or 6M guanidine hydrochloride) which also will prevent reassociation of peptide fragments.

Separation Result. The separation capability of a medium may be quantified by the resolvability, i.e. the smallest difference in molecular size that the medium is able to completely separate, or the number of peaks that hypothetically may be resolved, i.e. the peak capacity.

Resolvability of SEC. The resolution in size exclusion chromatography, R_S, is given by (*3*)

$$R_s = \frac{2\left(V_{R_2} - V_{R_1}\right)}{w_{b_2} + w_{b_1}} = \frac{1}{4}\cdot\log\frac{R_2}{R_1}\cdot\left[\frac{b}{\dfrac{V_o}{V_p} + K_D}\right]\cdot\frac{\sqrt{L}}{\sqrt{H}} \qquad (6)$$

where b is the slope of the selectivity curve, K_D and H are respectively the average distribution coefficient and plate height, and L is the bed height (equation 6 may, by setting $(V_R\text{-}V_t)/V_t\text{=}k'$ be shown to be analogous with the resolution equation used in e.g. reversed phase chromatography). Thus, the resolution increases with increasing

Downloaded by UNIV MASSACHUSETTS AMHERST on October 8, 2012 | http://pubs.acs.org
Publication Date: May 30, 1996 | doi: 10.1021/bk-1996-0635.ch013

slope, pore volume and bed height and with decreasing void volume, distribution coefficient (though there is an optimum value of K_D as discussed above) and plate height. The plate height is in turn affected by solute diffusivity, particle size and solvent velocity as stated in equation 4. Utilizing gel media of high selectivity, large pore volume and long bed height may yield a resolution exceeding 1.5. This may be exploited to reduce the separation time by increasing the flow rate (or decreasing the column length). As an example, the increase in selectivity when going from a conventional gel filtration medium (e.g. Sepharose) to a medium of maximum selectivity (e.g. as indicated in Figure 1) may permit a doubling of the resolution or, in theory, reduce the separation time by a factor of four by increasing the flow rate (provided the third term in equation 4 is dominating) or decreasing the column length by this factor.

The maximum theoretical resolvability of SEC may be calculated from equations 4 and 6 and is illustrated for some different experimental conditions in Figure 6. It is shown that it would be possible to completely resolve (i.e. R_s=1.5) spherical solutes differing 30% in molecular mass and rod-shaped molecules differing 10% in molecular mass using a column having a plate count of 100,000 (*7*). If the difference in molecular mass is smaller than this, SEC is obviously not a suitable separation technique.

Peak Capacity. The experimental parameters that affect the resolution are; selectivity, particle size, pore volume, column length and eluent velocity, provided the column is efficiently packed. The interplay of some of these parameters is illustrated by the equation for peak capacity, i.e. the number of peaks the column can resolve, which may be regarded as a measure of the analytical capability of the column (*26*)

$$n_{R_s} = 1 + \frac{\frac{V_p}{V_t} \cdot \sqrt{N_{\max}}}{4 \cdot R_s} \qquad (7)$$

where n_{R_s} is the number of peaks resolved with the resolution factor R_s and N_{max} is the maximum plate count of the column. The equation is a modification of the equation given by Giddings and takes into account the fact that in size exclusion of macromolecules the peak width (cf. Figure 3) and not the plate count, as originally proposed, is roughly constant over the separation range (*27*). It may be noted that the simplification of Giddings equation sometimes used, i.e. $n_{1.0}=1+0.2 \cdot N^{1/2}$ yields unrealistically high values for peak capacities, even considering the lower resolution factor specified. A maximum peak capacity of size exclusion chromatography around 16 may be expected (*26*). This figure, albeit smaller than that for adsorptive techniques, is competitive compared with other size-separating techniques. For instance, the peak capacity of field flow fractionation was reported to be 15 at a resolution factor of unity, which corresponds to 10 at a resolution factor of 1.5 (*28*). The differences in peak capacity between traditional SEC columns and microparticulate media designed for analytical SEC is very small which is due to the fact that the latter columns are short and generally has low pore fraction. However, since the influence of the solvent velocity on the plate height is not as detrimental for particles

Downloaded by UNIV MASSACHUSETTS AMHERST on October 8, 2012 | http://pubs.acs.org
Publication Date: May 30, 1996 | doi: 10.1021/bk-1996-0635.ch013

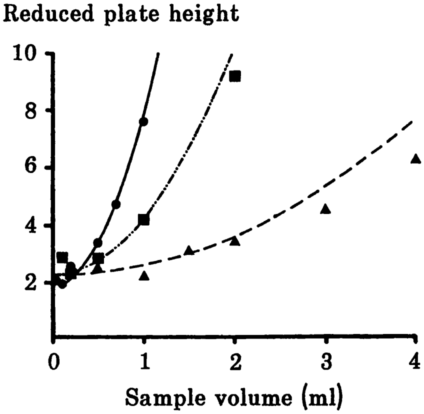

Figure 5. Influence of sample volume on zone broadening. Gel medium and column dimensions: (●) Superose 6, 50x1 cm I.D., N=20,000; (■) Superose 6 prep grade, 53x1 cm I.D., N=7,000; (▲) Superose 6 prep grade, 51x1.6 cm I.D., N=7,000. Sample: Cytidine. Reproduced with permission from Ref. 21 . © 1985 Elsevier.

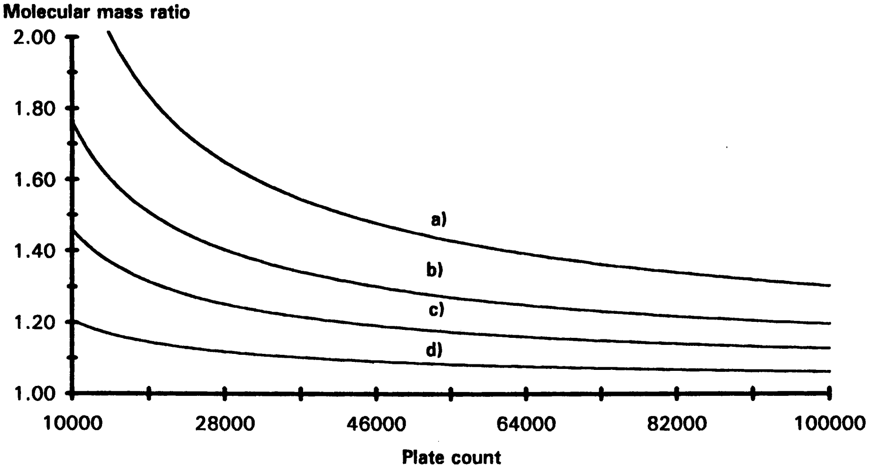

Figure 6. Influence of solute shape and matrix pore volume on the resolvability of SEC. Theoretical calculation of smallest molecular mass ratio of solutes that may be completely resolved, i.e. R_S=1.5, with size exclusion chromatography columns of various plate counts and permeabilities, V_p/V_0. Conditions: (a) spherical molecules, V_p/V_0=0.78; (b) spherical molecules, V_p/V_0=2.23; (c) random coil molecules, V_p/V_0=2.23; (d) rod shaped molecules, V_p/V_0=2.23. Reproduced with permission from Ref. 25 . © 1995 Academic Press.

Downloaded by UNIV MASSACHUSETTS AMHERST on October 8, 2012 | http://pubs.acs.org
Publication Date: May 30, 1996 | doi: 10.1021/bk-1996-0635.ch013

of smaller size as for traditional media fast analysis may be carried without too much loss in peak capacity as shown in Figure 7.

Evaluation of the Properties of Novel Media for Size Exclusion Chromatography

From the theoretical part it may be concluded that a high selectivity and a separation range being tailor made for the specific application, high efficiency to permit fast analysis and a large pore volume to allow large sample load are important characteristics of modern media for aqueous size exclusion chromatography.

The properties of a new family of media, designed for high resolution aqueous size exclusion chromatography of small and medium size biomolecules was evaluated with respect to theoretical attainable functional performance. The media, Superdex, is a composite material where dextran is covalently bound to the backbone of cross-linked agarose and the molecular mass and amount of dextran incorporated was adjusted to yield the desired selectivities (*29*). Data for this type of medium is given in Table I. The experimental evaluation was performed on FPLC system, and all materials used were from Pharmacia Biotech, Uppsala, Sweden unless otherwise stated.

Pore Volume and Pore Size. The pore volume of Superdex is reduced as compared to the base matrix (see Table I). The permeability, V_p/V_0, is typically 2.3 for the base matrix of Superdex prep grade and 1.8 for the base matrix of Superdex. The reduction in pore fraction is due to the matrix added in order to attain the desired selectivity (cf. Figure 9). Thus, it seems as though the manufacturer has prioritized selectivity over the pore volume. The pore fraction is still within reasonably high levels as compared with media of comparable selectivities, e.g. porous silica microspheres having a permeability, V_p/V_0, of 0.8 (*3*).

The apparent pore dimensions of the gel may be estimated by comparing the selectivity curve with that of a hypothetical media. In this case, the selectivity curve of a media having cylindrical pores of a uniform size of 60 Å radius was calculated (*4*). The procedure in Ref. 4 assumes that the viscosity radius of dextran may be used as a measure of the radius of an equivalent hard sphere which is supported by the co-elution of dextran and globular proteins of identical viscosity radius (*30,7,12*). The result is shown in Figure 8 together with experimental data for Superdex 75. The figure indicates, as expected from separation characteristics, that the functional pore dimension sensed by the molecules is very uniform. The slight deviation from the calculated selectivity curve, especially at very small solute size reflects the difficulty of finding a molecule for determination of the total liquid volume, a molecule which should not occupy any space itself! It may be noticed that we found that using glucose as a marker for total liquid volume an apparent selectivity curve which corresponds to a cylindrical pore radius of 64 Å is obtained, in good agreement with that roughly 4 Å of the radius will be occupied by glucose itself!

Selectivity. The selectivity is very close to the theoretical maximum for a hypothetical cylindrical pore shape support, i.e. (ln10)/2 (Ref. *4*). This is illustrated in Figure 9 which also shows the impact of the derivatisation of the base matrix for producing Superdex 200. The selectivity change is caused by covalently attaching

Downloaded by UNIV MASSACHUSETTS AMHERST on October 8, 2012 | http://pubs.acs.org
Publication Date: May 30, 1996 | doi: 10.1021/bk-1996-0635.ch013

Table I. Properties of Superdex

	Separation range (M_r, g/mol)	*Particle diameter (µm)*	V_p/V_o	*Plate counts (typical/meter)*	*Availability (column dimensions)*
Analytical media					
Superdex Peptide	100-7000	13-15	1.2	> 30000	30x1 cm 30x0.32 cm
Superdex 75	3000-70000	13-15	1.6	>30000	30x1 cm 30x0.32 cm
Superdex 200	10000-600000	13-15	1.7	>30000	30x1 cm 30x0.32 cm
Preparative media					
Superdex 30 prep grade	< 10000	34	1.8	15-20000	bulk 70x1.6 cm
Superdex 75 prep grade	3000-70000	34	2.1	15-20000	bulk 70x1.6 cm
Superdex 200 prep grade	10000-600000	34	2.2	15-20000	bulk 70x1.6 cm

Data as stated by the supplier, Pharmacia Biotech, Uppsala Sweden.

In Strategies in Size Exclusion Chromatography; Potschka, M., et al.;
ACS Symposium Series; American Chemical Society: Washington, DC, 1996.

Downloaded by UNIV MASSACHUSETTS AMHERST on October 8, 2012 | http://pubs.acs.org
Publication Date: May 30, 1996 | doi: 10.1021/bk-1996-0635.ch013

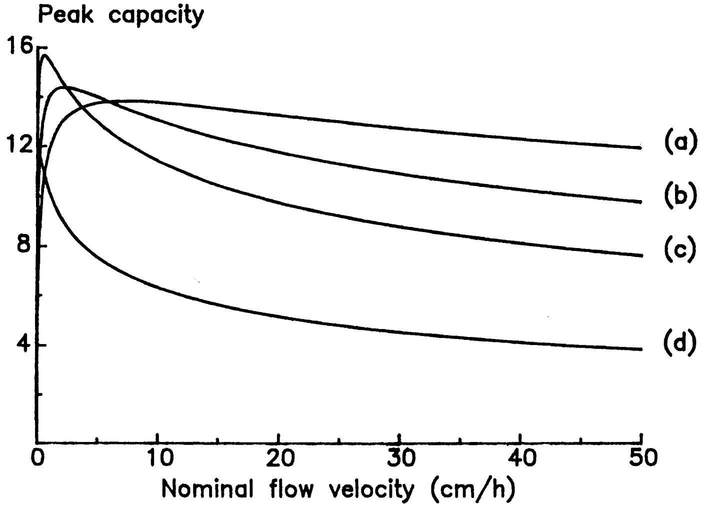

Figure 7. Peak capacity of size exclusion columns. Theoretical calculation of number of peaks completely resolved, i.e. R_s=1.5, by columns of various particle size, column length and permeability. Conditions: (a) d_p=4 μm, L=25 cm, V_p/V_0=0.78; (b) d_p=10 μm, L=30 cm, V_p/V_0=1.30; (c) d_p=60 μm, L=60 cm, V_p/V_0=2.20; (d) d_p=100 μm, L=100 cm, V_p/V_0=2.25. Reproduced with permission from Ref. 26 . © 1992 Elsevier.

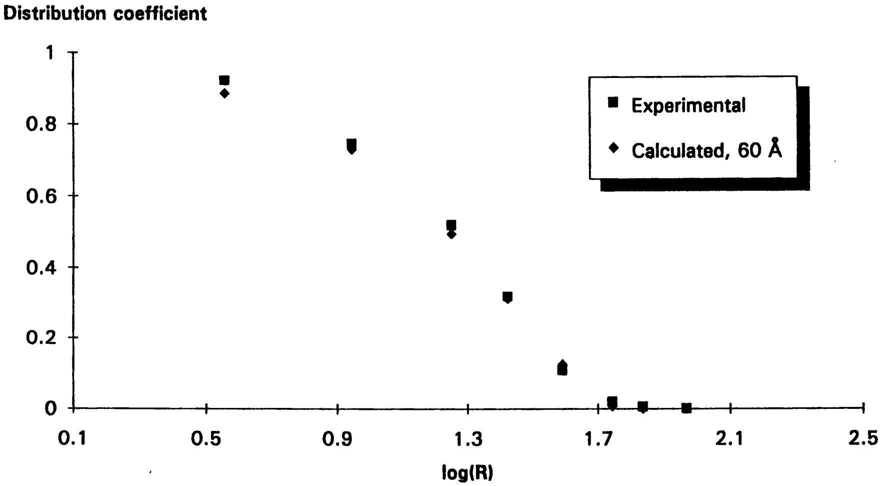

Figure 8. Selectivity curve of a high resolution medium as compared to a hypothetical single-pore size support. Gel medium: Superdex 75. Column dimensions: 30x1 cm I.D. Sample: (■) Dextran fractions (Pharmacosmos). (◆) K_D calculated for a hypothetical support having pores of 60 Å radius.

Downloaded by UNIV MASSACHUSETTS AMHERST on October 8, 2012 | http://pubs.acs.org
Publication Date: May 30, 1996 | doi: 10.1021/bk-1996-0635.ch013

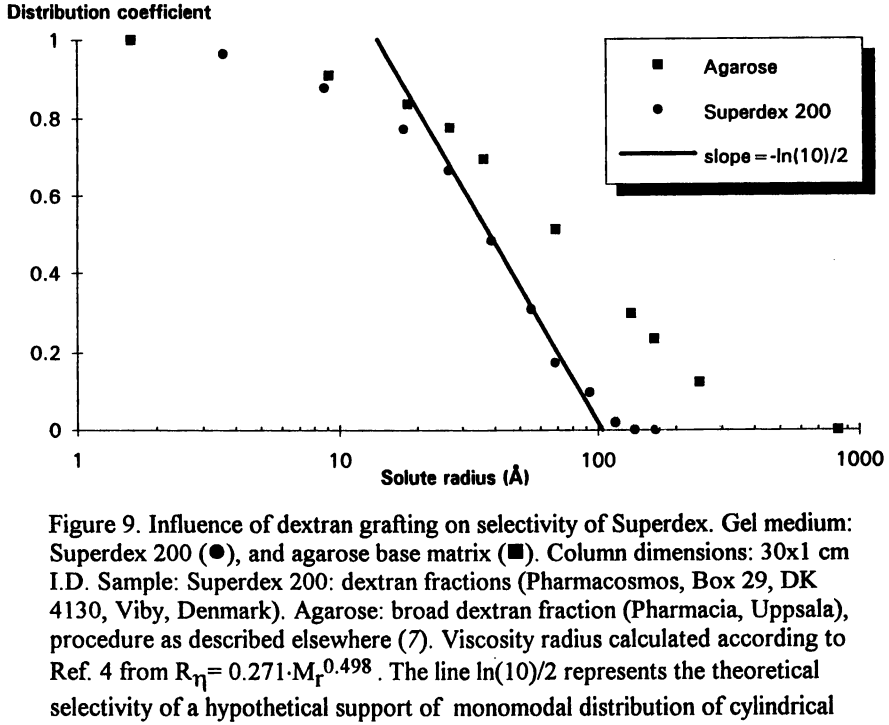

Figure 9. Influence of dextran grafting on selectivity of Superdex. Gel medium: Superdex 200 (●), and agarose base matrix (■). Column dimensions: 30x1 cm I.D. Sample: Superdex 200: dextran fractions (Pharmacosmos, Box 29, DK 4130, Viby, Denmark). Agarose: broad dextran fraction (Pharmacia, Uppsala), procedure as described elsewhere (*7*). Viscosity radius calculated according to Ref. 4 from $R_\eta = 0.271 \cdot M_r^{0.498}$. The line ln(10)/2 represents the theoretical selectivity of a hypothetical support of monomodal distribution of cylindrical pore size (*4*). Data for Superdex 200 used by courtesy of Torvald Andersson, Pharmacia.

Downloaded by UNIV MASSACHUSETTS AMHERST on October 8, 2012 | http://pubs.acs.org
Publication Date: May 30, 1996 | doi: 10.1021/bk-1996-0635.ch013

dextran to the agarose skeleton (*29*). This will reduce the conformational entropy of the solutes entering the porous network and thus decrease the distribution coefficient, and as seen from Figure 9 the effect is more pronounced for solutes of increasing molecular size. The selectivity of Superdex Peptide may be of special interest since this gel separates in the very low molecular weight range. The separation range of this gel is shown in Figure 10 illustrating that separation of oligopeptides differing only one amino acid in length may be obtained.

Particle Size. The particle size of Superdex varies between 13 µm and 34 µm (Table I) which probably is a compromise between highest attainable resolution, matrix rigidity and lowest possible matrix volume of the highly cross-linked agarose used as base matrix. The particle size of the bulk media is suitable for self-packed columns of larger dimensions (i.e. to accommodate larger sample volumes). For high speed analysis a particle size in the range of 3µm to 5µm would have been desirable, provided other characteristics could have been kept constant. However, a decrease in particle size is generally accompanied by a decrease in pore volume. For Superdex, the high selectivity and the comparatively large pore fraction may yield an excessive resolution that can be exploited to decrease the separation time, either by employing a shorter column or increasing the flow rate as exemplified in the theoretical section..

Molecular Size and Shape. The evaluation of molecular size from a calibrated column requires that the column is calibrated with proper reference substances and that solute-matrix interactions are absent. In many cases these conditions can be met and there are numerous examples given in literature where solute size has been successfully determined by SEC. However, with the development of on-line size detectors for SEC the possibility of using a high resolution column for separation and an on-line detector for characterization has rapidly been adopted. Particularly, the advancement in liquid interface of mass spectrometers leading to that the flow rates commonly used in liquid chromatography are now compatible with on-line mass spectrometry detection. One example was given by Nylander and co-workers who identified cleavage products of neuropeptides by electrospray ionization mass spectrometry connected to a high performance SEC column, Superdex Peptide, 3.2x300 mm, (*31*). They concluded that the extremely stable flow rate of the system used (SMART, Pharmacia Biotech, Uppsala, Sweden) was advantageous for the connection to the mass spectrometer (Finnigan MAT 95Q, Finnigan MAT, Bremen, Germany). A suspected interaction of amastatin and the gel matrix did not interfere with conclusions drawn since no assumption about column calibration was made. They pointed out the benefit of using high resolution SEC to achieve correct assignment of ions of similar mass-to-charge ratio that otherwise were treated as one component by the mass spectrometry software. The system was also applied for purification of β-amyloid peptide fragments which are extremely hydrophobic and could not be eluted from reversed phase chromatography (*31*).

Molecular Diffusivity. The influence of matrix properties on molecular diffusivity is yet not understood in detail, except that the degree of hindered diffusion increases as the size of the solute and the size of the openings in the size exclusion matrix approaches each other. However, since data for hindered diffusion presented

Downloaded by UNIV MASSACHUSETTS AMHERST on October 8, 2012 | http://pubs.acs.org
Publication Date: May 30, 1996 | doi: 10.1021/bk-1996-0635.ch013

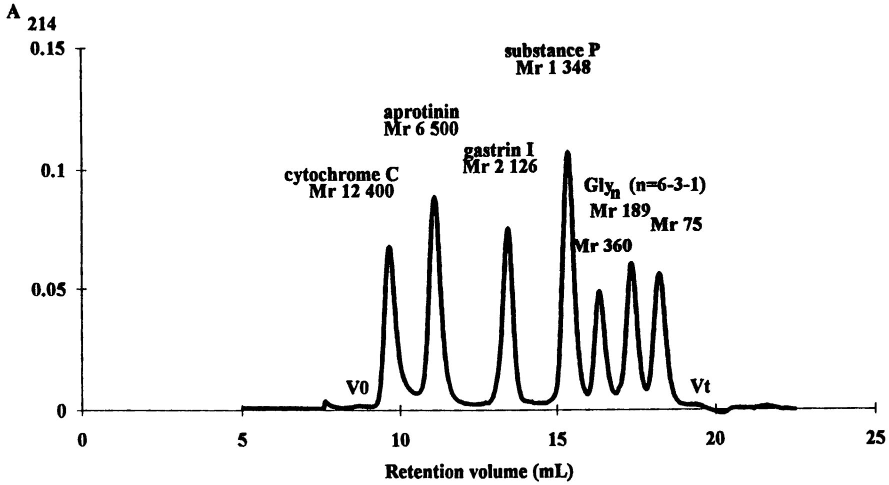

Figure 10. Separation of natural peptide standards on Superdex Peptide. Column dimensions: 30x1 cm I.D. Sample: Mixture of reference substances as indicated in the figure. Reproduced with permission from Ref. 42 (presented at ISPPP'94, Heidelberg, Germany, November 2-4, 1994). © 1995 Pharmacia Biotech AB.

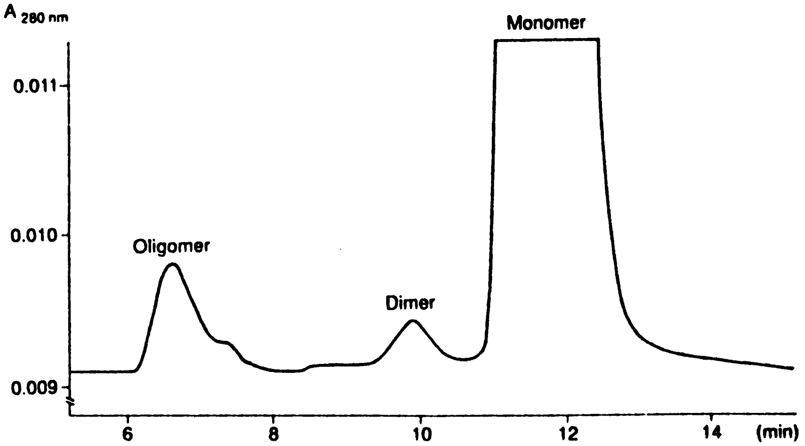

Figure 11. Analytical size-exclusion chromatography for determination of aggregates in preparations of recombinant human growth hormone (rhGH). Gel medium: Superdex 75. Column dimensions: 30x1 cm I.D. Sample: 50 μl rhGH. Reproduced by courtesy of B. Pavlu, Kabi-Pharmacia Peptide Hormones and H. Lundström, Pharmacia from Ref. 7 with permission. © 1993 Elsevier.

hitherto, are rather disparate and seems to be related to the solutes and matrices studied it may be concluded that gel structure probably has an impact on hindered diffusion (*32-39, 20*). Data reported indicates that differences between different matrices are of a factor 2 to 3.

A feature of small macromolecules such as peptides is their high diffusivity as compared to proteins. This permits rapid separations at higher eluent velocity and also that the zone broadening of molecules eluting near the void volume is not as excessive as noticed for proteins. This is shown in Figure 10 where the zone broadening of cytochrome C is of the same magnitude as for glycine.

Matrix Interaction. The growing interest in size exclusion of peptides have promoted gel manufacturers to also develop media suitable for this type of solutes. However, as discussed above, the variety of structural features of peptides and the fact that the relative surface area of the molecules is large as compared to that of proteins, interaction phenomena with other surfaces, matrices or solutes, may be expected to be more common with this class of substances. Therefore few gels possessing pure size exclusion behavior will probably be seen. Therefore, researchers will from time to time find it necessary to add modifiers to the mobile phase to mask interactions. Unfortunately, due to the different origins of the interactions, it is not likely that mobile phase conditions may successfully be transferred between gel systems of different chemical nature without adjustments. Chromatography of synthetic peptides of varying size, charge, and hydrophobicity may be used to monitor interactions at different conditions (*40*).

Resolvability. The resolvability of an optimal media for size exclusion chromatography should allow for a complete separation of globular proteins differing a factor of two in molecular mass (cf. Figure 6). This is exemplified in Figure 11 where the dimer of recombinant human growth hormone is completely separated from the monomer using Superdex 75. Furthermore, as noted, the separation was not affected by the addition of organic modifiers to the mobile phase, indicating that no solute-matrix interactions was present (Lundström, H. Pharmacia, personal communication, 1992).

An example of qualitative analysis of SEC was given by Soregan and coworkers who showed the different degree of aggregation of amyloid β peptides found in brain, a 42 residue β peptide, and in cerebrovasculum, a 40 residue β peptide (*41*). By selecting a gel where the aggregates were eluted in the void volume and the native form being eluted at an intermediate distribution coefficient a very favorable separation situation was created and this may have been used to further decrease the analysis time if necessary, see Figure 12. The column was calibrated and the apparent molecular mass of the second peak , i.e. 8-9 kDa, suggested that it represents a dimeric species in agreement with earlier results (*41*).

Peak Capacity. The peak capacity of an analytical SEC column should, preferentially, exceed 10. The separation of natural peptide and protein standards on Superdex Peptide is illustrative of the capability of modern media, from Figure 10 the peak capacity may be estimated to roughly 10 which may be expected to be the upper limit for a 13 µm media at 20 cm/h (cf. Figure 7). Also, the separation range, down

Downloaded by UNIV MASSACHUSETTS AMHERST on October 8, 2012 | http://pubs.acs.org
Publication Date: May 30, 1996 | doi: 10.1021/bk-1996-0635.ch013

Downloaded by UNIV MASSACHUSETTS AMHERST on October 8, 2012 | http://pubs.acs.org
Publication Date: May 30, 1996 | doi: 10.1021/bk-1996-0635.ch013

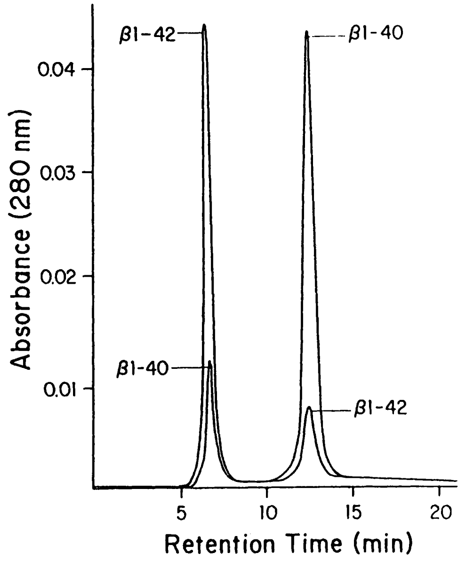

Figure 12. Determination of aggregation of amyloid β peptides from different sources by SEC. Gel medium: Superdex 75. Column dimensions: 30x1 cm I.D. Samples: β1-42, 42 residue β peptide found in brain and β1-40, 40 residue β peptide found in cerebrovasculum. Note that the chromatograms for the two runs are superimposed! Reproduced from Ref. 41 with permission. © 1994 The American Society for Biochemistry and Molecular Biology.

into the low molecular mass range makes this gel very suitable for separation of low molecular mass nucleotides, carbohydrates in addition to peptides and protein fragments for which suitable high performance SEC columns have been missing (*40*).

Conclusions

The performance of media for SEC is a compromise between speed (i.e. amount of data or substance per unit time) and resolution (i.e. quality of data or purity of product). Modern media address these issues through high selectivity, large pore volume and favorable efficiency, also extending the separation range to low molecular mass biomolecules, while yielding optimal values of peak capacities, e.g 10 to 13 peaks, and resolvability, e.g. separating protein monomer from dimer.

Acknowledgment

Sephacryl, Sepharose, Superose, Superdex, FPLC and SMART are trademarks owned by Pharmacia Biotech AB.

Literature Cited

1. Porath, J.; Flodin, P. *Nature*, **1959**, *183*, 1657.
2. Moore, J. C. *J. Polym. Sci.*, Part A, **1964**, *2*, 835.
3. Hagel, L. In *Protein Purification, Principles, High Resolution Methods and Applications;* Janson, J.-C.;Rydén, L. Eds.; VCH Publishers Inc., New York, 1989, Chapter 3, pp 63-106.
4. Hagel, L. In *Aqueous Size-Exclusion Chromatography;* Dubin, P., Ed.; J. Chromatogr. Libr.; Elsevier: Amsterdam, 1988, Vol 40, pp 119-155.
5. Verzele, M.; Dewaele, C.; Duquet, D. *J. Chromatogr.*, **1987**, *391*, 111.
6. Barth, H.G.; Carlin F. J. *J. Liq. Chromatogr.*, **1984**, *7*, 1717.
7. Hagel, L. *J. Chromatogr.*, **1993**,*684*,19-25.
8. Ellegren, H.; Lååʂ, T. *J. Chromatogr.*, **1989**, *467*, 217.
9. Yau, W. W.; Bly, D. D. In *Size Exclusion Chromatography* (GPC); Provder T., Ed.; ACS Symposium Series, American Chemical Society: Washington, D.C., 1980, pp 197-206.
10. Kasai, K.-i., *J. Chromatogr.*, **1993**, *618*, 203.
11. Benoit, H.; Grubisic, Z.; Rempp, P.; Decker, D.; Zilliox, J. G. *J. Chim. Phys.*, **1966**, *63*, 1507.
12. Dubin, P. L.; Principi, J. M. *Macromolecules*, **1989**, *22*, 1891.
13. Yau, W. W. *Chemtracts-Macromolecular Chemistry*, **1990**, *1*, 1.
14. Jackson, C.; Nilsson, L. M.; Wyatt, P. J. *J. Appl. Polym. Sci.*, **1989**, *43*,99.
15. Mori, S. *J. Chromatogr.*, **1993**, *637*, 129.
16. Hagel, L.; Andersson, T. *J. Chromatogr.*, **1984**, *285*, 295.
17. Giddings, J. C.; Mallik, K. L. *Anal. Chem.*, **1966,** *38*, 997 .
18. Dawkins, J. V. In *Comprehensive Polymer Science*, Booth, C.; Price, C., Eds; , Polymer Characterisation; Pergamon Press: Oxford, 1989, Vol. 1; pp 231-258.
19. Katz, E.; Ogan, K. L.; Scott, R. P. W. *J. Chromatogr.*, **1983**, *270*, 51.
20. Potschka, M. *J. Chromatogr.*, **1993**, *648*, 41.
21. Hagel, L. *J. Chromatogr.*, **1985,** *324*, 422.
22. Hagel, L.; Lundström, H.; Andersson, T.; Lindblom, H. *J. Chromatogr.* **1989,** *476*, 329.
23. Golovchenko, N. P.; Kataeva, I. A.; Akimenko, V. K. *J. Chromatogr.* **1992,** *591*, 121.
24. Lemieux, L.; Piot, J.-M.; Guillochon, D.; Amiot, J. *Chromatographia*, **1991,** 32, 499.
25. Hagel, L. In *Size exclusion* in Encyclopedia of Analytical Science, Academic Press Ltd., London, **1995**, Vol. 5; 2620.
26. Hagel, L. *J. Chromatogr.*, **1992,** *591*, 47-54.
27. Giddings, J. C. *Anal. Chem.*, **1967,** *39*, 1027.
28. Litzén, A.; Walter, J. K.; Krischollek, H.; Wahlund, K.-G. *Anal. Biochem.*, **1993,** *212*, 469 .
29. Kågedal, L.; Engström, B.; Ellegren, H.; Lieber, A.-K.; Lundström, H.; Sköld A.-L.; Schenning, M. *J. Chromatogr.*, **1991,** *537*, 17-32.
30. Frigon, R. P.; Leypoldt, J. K; Uyejl, S.; Hendersson, L. W. *Anal. Chem.*, **1983,** *55*, 1349.

Downloaded by UNIV MASSACHUSETTS AMHERST on October 8, 2012 | http://pubs.acs.org
Publication Date: May 30, 1996 | doi: 10.1021/bk-1996-0635.ch013

31. Nylander, I.; Tan-No, K.; Winter, A.; Silberring, J. *Life Sciences*, **1995**, *57*, 123.
32. van Kreveld, M. E.; van den Hoed, N. *J. Chromatogr.*, **1978**, *149*, 71.
33. Knox, J. H.; McLennan, F. *J. Chromatogr.*, **1979**, *185*, 289.
34. Leypoldt, J. K.; Frigon, R. P.; Henderson, L. W. *J. Appl. Polym. Sci.*, **1984**, *29*, 3533.
35. Dawkins, J. V.; Yeadon, G. J. Chromatogr., **1981**, *206*, 215.
36. Stadalius, M. A.; Ghrist, B. F. D.; Snyder, L. R. *J. Chromatogr.*, **1987**, *387*, 21.
37. Muhr, A. H.; Blanshard, J. M. V. *Polymer*, **1982**, *23*, 1012.
38. Key, P. Y.; Sellen, D. B. *J. Polym. Sci.: Polym. Phys. Ed.*, **1982**, *20*, 659.
39. Moussaoui, M.; Benlyas, M.; Wahl, P. *J. Chromatogr.*, **1991**, *558*, 71.
40. Mant, C. T.; Hodges, R. S. *J. Liq. Chromatogr.*, **1989**, *12*, 139.
41. Soregan, B.; Kosmoski J.; Glabe, C. *J. Biol. Chem.* **1994**, *269*, 28551.
42. Hedlund, H.; Winter, A. *Superdex Peptide, a new size exclusion medium tailored especially for peptide separations*, Mini Poster Code No. 18-1060-84, 1995, Pharmacia Biotech AB, Uppsala, Sweden.

Downloaded by UNIV MASSACHUSETTS AMHERST on October 8, 2012 | http://pubs.acs.org
Publication Date: May 30, 1996 | doi: 10.1021/bk-1996-0635.ch013

Chapter 14

Review of Critical Conditions of Adsorption and Limiting Conditions of Solubility in the Liquid Chromatography of Macromolecules

D. Hunkeler[1], M. Janco[2], and D. Berek[2]

**[1]Department of Chemical Engineering, Vanderbilt University,
Nashville, TN 37235
[2]Polymer Institute, Slovak Academy of Sciences,
84 236 Bratislava, Slovakia**

The development of critical conditions of adsorption and limiting conditions of solubility of macromolecules are reviewed. These two related methodologies, which both involve the combination of entropic and enthalpic polymer-sorbent-mobile phase interactions, are contrasted. The unique separation mechanisms and area of applicability are also discussed. A summary of the systems for which critical conditions and limiting conditions have been observed is presented along with examples of some historical and key results. The limitations of these methodologies is also discussed. This brief review chapter concludes with a list of some unresolved problems and some possible future research directions.

This chapter presents an introduction and concise review of two similar liquid chromatographic techniques which combine interactive and size exclusion separations of macromolecules. Critical conditions of adsorption (LCCC), as so named by Belenkii in his pioneering works in this area [1,2], involve the combination of exclusion (SEC) and adsorption (LAC) mechanisms. By appropriately balancing the adsorption of macromolecules on the column packing and their exclusion from the packing pores the critical conditions are reached at which the retention volume is independent of the molar mass of solutes, i.e. macromolecules of different molar masses elute at the same retention volume roughly equal to the volume of eluent within the column.

The extent of adsorption of macromolecules can be controlled by the composition of appropriate mixed mobile phases and alternatively by temperature or even pressure within the liquid chromatographic system. For critical conditions of adsorption the interactions between the polymer chain with the mobile and stationary phases control the elution. Therefore, the type of adsorbent utilized and its surface characteristics have significant effects on the separation characteristics. As we shall discuss, this permits the separation of macromolecules according to non-steric properties. The method has so far been limited to molar masses of approximately 100,000 daltons.

0097–6156/96/0635–0250$15.00/0

Hunkeler, Macko and Berek [3] attempted to modify the critical condition approach and sought a binary mobile phase where small changes in the composition had a significant effect on the thermodynamic quality of the solvent. Initially, the toluene-methanol system was investigated since the Mark-Houwink exponent is very sensitive to the level of methanol for polystyrene-toluene. The aim of the limiting condition work was to attempt to extend the molecular weight range where retention was independent of the size of macromolecules, particularly to high polymers so that the method could be applied to commercially relevant systems. The limiting condition approach of Hunkeler, Macko, Berek and later Janco [4,5] involved the exclusion of a polymer in a mobile phase which was indeed a non-solvent for the polymer probe. To accomplish this the polymer needed to be injected in a thermodynamically good solvent. For example, polystyrene was injected in toluene for the methanol-toluene system. The resulting mechanism, which will be detailed later in this chapter, is the combination of size exclusion, precipitation and possibly also liquid adsorption chromatography, with the result that the polymer elutes just on the 'limit' of its solubility. These so named limiting conditions of solubility are not as sensitive to the mobile phase composition as they are for critical conditions of adsorption. They have, however, been identified for a variety of macromolecules for molar masses up to several hundred thousand daltons. For limiting conditions, the interaction between the polymer chain and molecules of mobile phase influences the retention of the solute. However, the chemical nature of the column packing surface does not seem to play an important role in the mechanism.

It needs to be mentioned that the liquid chromatography under limiting conditions of solubility is a fairly recent development. Therefore, this review, while comprehensive, is somewhat limited in scope. Furthermore, extensive reviews on critical conditions are under preparation [6] and this chapter is not intended to duplicate such efforts. Rather, it is presented as an introduction to provoke some further basic and applied research in the combination of size exclusion and interactive mechanisms of chromatography. Both the critical and limiting conditions are potentially very powerful tools. If either method is to proceed significantly it will require the cooperation of synthesis and application chemists with those involved in the analytical methods development. The prospects for such techniques could be enormous since they basically involve the application of an inexpensive, and isocratic, liquid chromatography methodology to characterizations which would normally be limited to much more elaborate equipment. Alternatively, they have the potential to provide data that cannot be obtained by conventional methods, at all. One of the ultimate goals of either of these methods is the application to various types of polymer blends or copolymers. The evaluation of such potential is one of the likely directions for further research in the immediate future.

Discussion

Liquid Chromatography of Macromolecules under Critical Conditions of Adsorption. Belenkii and Gankina [1,2] first observed critical conditions by varying the eluent composition in a mixture of three solvents. Their experiments involved the size exclusion chromatography of polystyrene on silica gel in a thin layer chromatography arrangement. Through small adjustments to the eluent composition, a mobile phase was identified where the retention volume of a polymer was independent of its molar mass. Indeed, the polymeric retention volumes were as high as observed for inert low molecular weight substances. Belenkii and Gankina called these conditions 'critical' and postulated that under such an arrangement the macromolecules were 'invisible' to the gel. In this way the gel seemed to be totally permeable, independent of its pore size. Later, Tennikov found a similar effect in a column liquid chromatography arrangement [7] and noted that the critical conditions were highly temperature sensitive. Nefedov and Zhmakina have added that the critical composition of the eluent, for a given polymer and column packing, may also depend on the pressure within the system [8]. By comparison, Hunkeler, Macko and Berek [4] showed that limiting conditions were unaffected by large changes in the operating pressure of a liquid chromatograph.

Belenkii and Gankina [1,2] proposed that at the critical eluent composition the total free energy of the process which takes places around the gel is zero due to a balancing of entropic (exclusion) and energetic (adsorption) effects. This is somewhat unexpected since both the entropic and enthalpic terms change with the molecular weight of the polymer in a different manner, as is illustrated by the schematic in Figure 1. To achieve a molar mass independent elution therefore requires the two effects to have an identical molecular weight dependence. This would certainly not be expected based on a priori knowledge, however, the elucidation of critical conditions is well documented in several polymer-binary eluent-stationary phase systems (Table I). This includes the separation of linear and cyclic oligomers and polymers with molar masses up to 100,000 daltons. The upper molecular weight limit may well be caused by the rapid increase in the extent of adsorption with chain length.

Applications of Critical Conditions of Adsorption. Liquid chromatography under critical conditions of adsorption have been used for determination of functionality type distribution of oligomers [9], for separation of oligomers [10] and polymers [11] according to their topology, for separation of polymer blends [12] and our latest results indicate that LCCC can be used for polymer separation according to their tacticity [13]. Critical conditions are attractive for the chromatography of copolymers. If the stationary phase does not 'see' one part of the copolymer molecule the second 'visible' portion can be separated as if it were in isolation and its molar mass (M) and molar mass distribution (MWD) can be determined [14-17]. Skvortsov and Gorbunov [18] have noted that it is necessary for the 'invisible' portion of the chain to be a free end. This statement has not been disproved experimentally and thus far critical conditions have been limited to the characterization of the central block of triblock copolymers. It is generally believed that the critical condition concept cannot be used for the central block of a triblock copolymer or for random copolymers, although further investigations are proceeding.

Liquid Chromatography of Macromolecules under Limiting Conditions of Solubility. The so-named 'limiting conditions of solubility' are accomplished by employing an eluent which is a weak non-solvent, for the polymer probe, while the sample is dissolved in a thermodynamically good solvent. The mobile phases so far employed have been binary or ternary mixtures which, at the temperatures used for the measurement, consist of a thermodynamically good solvent and a non-solvent. In this case, homopolymers with different molecular weights elute from the chromatographic column at the same retention volume which is roughly equal to the volume of liquid in column. That is, under limiting conditions of solubility there is no separation according to molar mass, as is also the case for critical conditions of adsorption. This permits the method to be applied to separations based on other properties of the given polymer, as will be discussed later.

The following mechanism is believed to cause the limiting condition phenomena: at low levels of non-solvent, such as methanol in toluene or water in tetrahydrofuran for the polystyrene or polymethylmethacrylate systems, the calibration curves shift slightly to lower retention volumes due to the suppression of adsorption and a reduced effective pore size of the column packing. The accumulation of non-solvent in the sorbent pores may lead partitioning effects which reduce the retention volume in the pores of the column packing [19]. At higher quantities of non-solvent, in the vicinity of the theta-composition (e.g. 76.9 vol% of toluene for polystyrene in toluene-methanol at 25 °C [20], or 35.7 vol% of toluene for polymethylmethacrylate in toluene-methanol at 26.2 °C [21]) the thermodynamic quality of the solvent is strongly reduced. Mixtures containing more methanol are non-solvents for polystyrenes. If such a mixture is used as an SEC eluent and the injected polymer is dissolved in a good

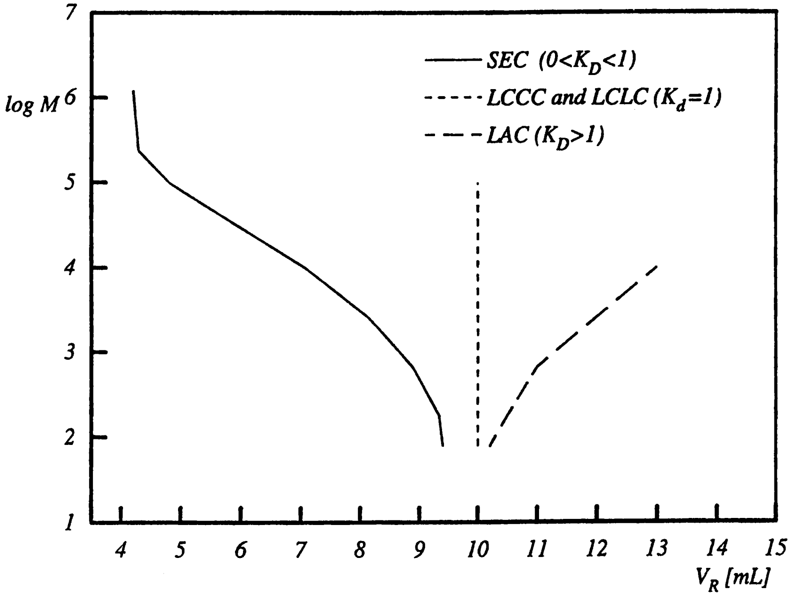

Figure 1: Schematic of calibration curves obtained from size exclusion chromatography (SEC), liquid adsorption chromatography (LAC), liquid chromatography under critical conditions of adsorption (LCCC) and liquid chromatography under limiting conditions of solubility (LCLC).

solvent (e.g. toluene), the macromolecules move together with the zone of their initial solvent. If macromolecules move faster due to exclusion processes they encounter the non-solvent and precipitate. They then redissolve as the injection zone (good solvent) reaches the precipitated polymer. This 'microgradient' process of precipitation-redissolution occurs many times throughout the column with the polymer eluting just in the front part of the solvent zone (Figure 2). As a consequence, the macromolecules move with a velocity similar to the velocity of the solvent zone and elute at the 'limit' of their solubility, hence the nomenclature limiting conditions. The reversibility of the polymer precipitation in limiting conditions is an essential component in the separation mechanism, as will be discussed later in this review. Because the polymer elutes very close to the solvent peak, mass specific detectors such as those based on evaporative light scattering, are preferable to DRI detectors in the operation of LCLC. Table II lists the limiting conditions which have been reported to date for various polymer-eluent combinations.

The primary differences between 'Limiting Conditions of Solubility' and 'Critical Conditions of Adsorption' are summarized in Table III.

Applications of Limiting Conditions of Solubility. A limiting condition based method for the characterization of the molecular weight distribution (MWD) of one component of a binary polymer blend has been developed where both polymers co-elute. In this technique a polymer mixture is dissolved in a good solvent for both constituents and is injected into an eluent which is a weak non-solvent for one component of the blend while it is a solvent for the other component. A typical

TABLE I: Summary of Critical Conditions which have been Identified for Polymer-Stationary Phase-Mobile Phase Combinations

Polymer	Stationary Phase	Mobile Phase (vol %/vol %)	Investigator [Reference]
Polystyrene	Unmodified Silica Gel 10 nm Pore Size 5-10 μm Particle Size	Cyclohexane/ Benzene/Actone (40/16/2)*	Belenkii, Gankina [1,2]
Polystyrene	Unmodified Silica Gel 10 nm Pore Size 63-90 μm Particle Size	Chloroform/Tetrachloromethane (5.5/94.5)	Tennikov, Nefedov, Lazareva, Frenkel [7]
Polystyrene	Macroporous Glass 25-110 nm Pore Size 25-32 μm Particle Size	Chloroform/Tetrachloromethane (4.5/95.5)	Nefedov, Zhmakina [8]
Oligo(1,3,6-trioxanes)	C_{18} Modified Silica Gel	Acetonitrile/Water (49.5/50.5)	Schulz, Much, Kruger, Wehrsted [11]
Polymethylmethacrylate	Unmodified Silica Gel Nucleosil 10 nm Pore Size	Methylethylketone/ Cyclohexane (73/27)	Pasch, Augenstein [12,15]
Polymethylmethacrylate	Unmodified Silica Gel Lichrosphere 30 + 100 nm Pore Size	Methylethylketone/ Cyclohexane (70/30)	Pasch, Brinkman, Gallot [12,14,15]
Syndiotactic Polymethylmethacrylate	Unmodified Silica Gel 12 nm Pore Size	Tetrahydrofurane/n-Hexane (83.2/16.8)	Berek, Janco, Hatada [13]
Polydecylmethacrylate	C_{18} Modified Silica Gel 30 + 100 nm Pore Size	Chloroform/Ethanol (61/39)	Pasch, Augenstein, Trathnigg [16]
Polystyrene	C_{18} Modified Silica Gel 30 + 100 nm Pore Size	Tetrahydrofurane/ Acetonitrile (49/51)	Pasch, Gallot, Trathnigg [17]
Polybutadiene Oligomers	Unmodified Silica Gel 100 Å Pore Size	Hexane/Toluene (85/15)	Gorshkov, Evreinov, Entelis [24,25]
Polybutadiene Oligomers	Unmodified Silica Gel 100 Å Pore Size	Hexane/Dichloromethane (76/24)	Gorshkov, Evreinov, Entelis [24,25]

Table I. *Continued*

Polymer	**Stationary Phase**	**Mobile Phase (vol %/vol %)**	**Investigator [Reference]**
Polybutadiene Oligomers	Unmodified Silica Gel 100 Å Pore Size	Heptane/Methylethyl-ketone (99.5/0.5)	Gorshkov, Evreinov, Entelis [24,25]
Polysulfone Oligomers	Unmodified Silica Gel 60 Å Pore Size	Chloroform/Tetra-chloromethane (53/47)	Guryanova, Pavlov [18]
Polycarbonate Oligomers	Unmodified Silica Gel 60 Å Pore Size	Chloroform/Tetra-chloromethane (30/70)	Guryanova, Pavlov [26]
Polybutylene-terepthalate Oligomers	Unmodified Silica Gel 60 Å Pore Size	Tetrahydrofuran/ Heptane (80/20)	Guryanova, Pavlov [26]
Polypropylene-glycol	Unmodified Silica Gel 100 Å Pore Size	Methylethylketone/ Ethylacetate (5/95)	Gorshkov, Evreinov, Entelis [27]
Polyethyleneglycol	Unmodified Silica Gel	Methylethylketone/ Chloroform (35/65)	Filatova, Gorshkov [28]
Polyethyleneglycol	Unmodified Silica Gel	Methylethylketone/ Hexane (92/8)	Filatova, Gorshkov [28]
Polyethyleneglycol	Unmodified Silica Gel	Tetrahydrofuran/ Ethylacetate (7/93)	Filatova, Gorshkov [28]
Polyethyleneglycol	Unmodified Silica Gel	Methylethylketone/ Ethylacetate (27/73)	Filatova, Gorshkov [28]
Polydiethylene-glycol adipate	Unmodified Silica Gel 100 Å Pore Size	Hexane/ Methylethylketone (8/92)	Gorshkov, Evreinov, Entelis [29]
Polymethyl-methacrylate	Unmodified Silica Gel 300 Å Pore Size	Dichloromethane/ Acetonitrile (41.5/58.5)	Zimina, Kever, Melenevskaya, Fell [30]
Polybutyl-methacrylate	Unmodified Silica Gel 300 Å Pore Size	Dichloromethane/ Acetonitrile (90.7/9.3)	Zimina, Kever, Melenevskaya, Egonnik [31]
Oligocarbonates	Unmodified Silica Gel 600 Å Pore Size	Chloroform/ Tetrachloromethane (17/83)	Gorshov, Prudskova, Guryanova [32]

*** volume ratio**

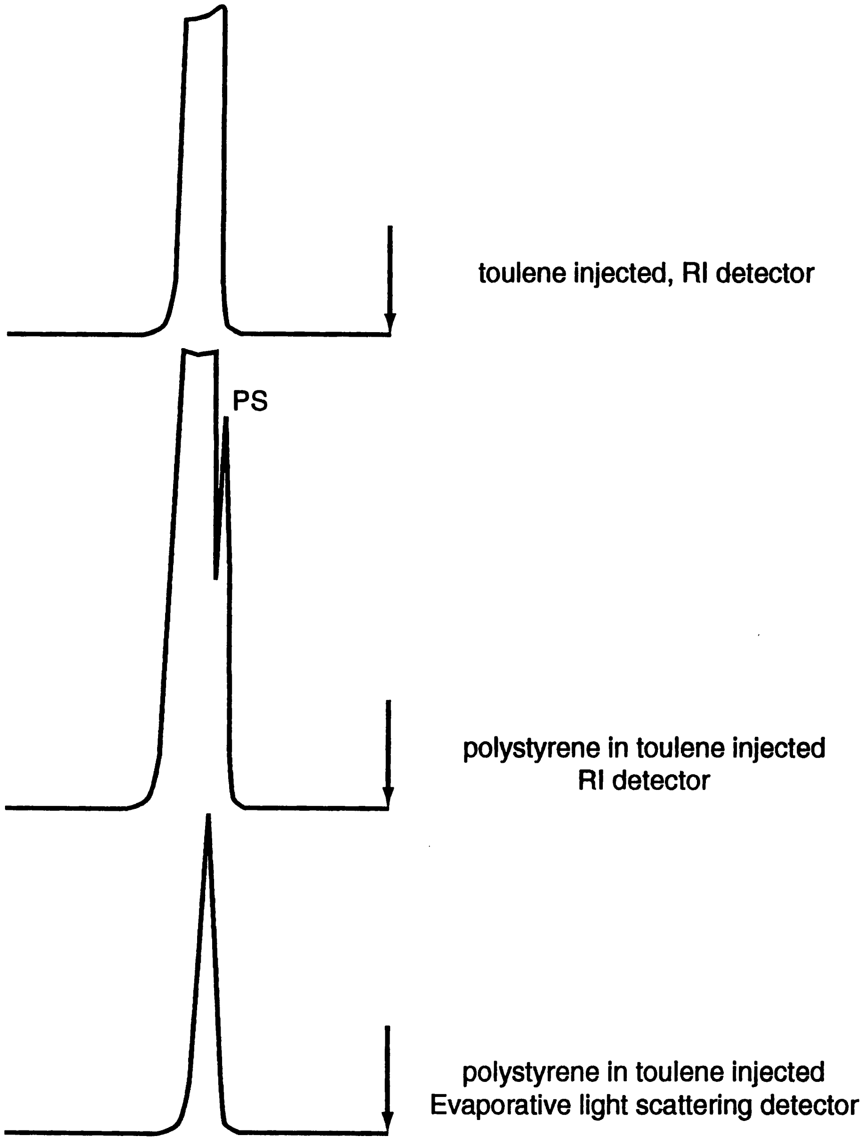

Figure 2: The elution of the polymer and solvent in a limiting condition experiment using differential refractive index (RI) and evaporative light scattering detectors

(Reproduced from reference 4. Copyright 1993 American Chemical Society.)

TABLE II: Summary of Limiting Conditions which have been Identified for Polymer-Stationary Phase-Mobile Phase Combinations

Polymer	Stationary Phase	Mobile Phase (w %/w %)	Investigator [Reference]
Polystyrene	Unmodified Silica Gel 10 μm Particles 800 Å Pore Size	Toluene/Methanol (68/32)*	Hunkeler, Macko, Berek [3,4]
Polystyrene	Unmodified Silica Gel 10 μm Particles 1000 Å Pore Size	Toluene/Methanol 50/50	Hunkeler, Janco, Guryanova, Berek [5]
Polystyrene	Unmodified Silica Gel 10 μm Particles 1000 Å Pore Size	THF/Water (64/36)	Hunkeler, Janco, Guryanova, Berek [5]
Polystyrene	Unmodified Silica Gel 10 μm Particles 1000 Å Pore Size	THF/n-Hexane (50/50)	Hunkeler, Janco, Berek [23]
Polymethyl-methacrylate	Unmodified Silica Gel 10 μm Particles 800 Å Pore Size	Toluene/Methanol (27/73)*	Hunkeler, Macko, Berek [3,4]
Polymethyl-methacrylate	Unmodified Silica Gel 10 μm Particles 1000 Å Pore Size	Toluene/Methanol (20/80)	Hunkeler, Janco, Guryanova, Berek [5]
Polymethyl-methacrylate	Unmodified Silica Gel 10 μm Particles 1000 Å Pore Size	THF/Water (64/36)	Hunkeler, Janco, Guryanova, Berek [5]
Polymethyl-methacrylate	Unmodified Silica Gel 10 μm Particles 1000 Å Pore Size	THF/n-Hexane (82/18)	Hunkeler, Janco, Berek [23]
Polyvinylacetate	Unmodified Silica Gel 10 μm Particles 1000 Å Pore Size	THF/Water (64/36)	Hunkeler, Janco, Berek [23]
Polyvinylacetate	Unmodified Silica Gel 10 μm Particles 1000 Å Pore Size	THF/n-Hexane (80/20)	Hunkeler, Janco, Berek [23]
Syndiotactic Polymethyl-methacrylate	Unmodified Silica Gel 10 μm Particles 500 Å Pore Size	THF/n-Hexane (75/25)	Berek, Janco, Kitayama, Hatada [22]
Syndiotactic Polymethyl methacrylate	Unmodified Silica Gel 10 μm Particles 1000 Å Pore Size	THF/n-Hexane (82/18)	Berek, Janco, Kitayama, Hatada [22]

* vol %/vol %

Table III: Comparison of the Limiting Conditions of Solubility and Critical Conditions of Adsorption

Liquid Chromatography under "Limiting Conditions" of Solubility (LCLC)	Liquid Chromatography under "Critical Conditions" of Adsorption (LCCC)
Eluent is a liquid (usually a mixture of liquids) which is a nonsolvent for the analysed sample.	Eluent is a liquid (usually a mixture of liquids) in which specific adsorption effects have a place. It can be a mixture of a solvent and nonsolvent for the sample, but in any case the resulting mixture is a solvent for the analyzed sample.
The sample is disolved and injected into the chromatographic column in a pure solvent.	The eluent is disolved as a sample in the mobile phase.
The hydrodynamic volume of the polymer coil is changed.	In the optimum case, the hydrodynamic volume of the polymer coil is not changed.
The result is achieved through a 'microgradient' precipitation-redissolution process occurring throughout the column.	The result is achieved through a combination of exclusion and adsorption mechanisms.

TABLE IV: Characterization of a Blend of Polystyrene and Polymethylmethacrylate under SEC and Limiting Conditions

Separation Mechanism	Stationary and Mobile Phases	Polymer System	Mn ($x10^{-3}$)	Mw ($x10^{-3}$)	Mw/Mn
SEC	PL-Gel/ THF	Polystyrene	348	432	1.24
SEC	SI-1000/ THF	Polystyrene	345	429	1.24
SEC	SI-1000/ THF: Hexane 82:18 vol%	Polystyrene	346	424	1.23
SEC	SI-1000/ THF	Polystyrene + PMMA	251	391	1.55
LCLC	SI-1000 THF: Hexane 82:18 vol%	Polystyrene + PMMA	368	453	1.23

example is the separation of polystyrene (PS) from polymethylmethacrylate (PMMA) over bare silica gel using THF/n-hexane as the mobile phase (Figure 3). In this case, the PS elutes under a size exclusion mechanism with its MWD correctly estimated. The second polymer (PMMA) elutes at its limiting condition. Its molecular weight distribution can also be determined, if desired, with the addition of a second step, i.e. conventional SEC separation. This is demonstrated in Table IV. The first two rows of Table IV show the number and weight average molecular weights for a polystyrene characterized on two different columns using THF as an eluent. The third row demonstrates that the characterization of the same polystyrene can be carried out using a binary eluent over the silica gel sorbent without losing any accuracy in the molecular weight estimation. The fourth row illustrates the drastic overprediction of the molecular weight averages for PS due to the influence of the PMMA when the measurement is made in the SEC mode. By comparison, the elution of the PMMA does not influence the quantification of the polystyrene peak when the separation is carried out under its limiting condition of solubility, as is shown in the fifth row data of Table IV. The characterization of polymer blends has also been accomplished using LCLC with THF/water and toluene/methanol as mobile phases. These provided limiting conditions for PS while either PMMA or polyvinylacetate eluted in the SEC mode.

Berek et al. have shown that under limiting conditions of solubility the tacticity of macromolecules can also be estimated [13].

Future Research Directions in LCCC and LCLC. Before critical or limiting conditions can be applied to important unresolved issues in polymer characterization, such as the simultaneous estimation of the composition and molar mass distribution of copolymers, significant research is required on the further elucidation of the separation mechanism, as well as the generalization of these phenomena. Therefore, while it would be advantageous to examine different combinations of stationary phases, mobile phases and macromolecules, particularly if such studies were carried out systematically, more sophisticated investigations are also warranted. For example, it would be beneficial to generalize the macromolecular, sorbent and mobile phase requirements for attaining either critical or limiting conditions. This might include the correlation of polymer, sorbent and solvent parameters with the occurrence of critical or limiting

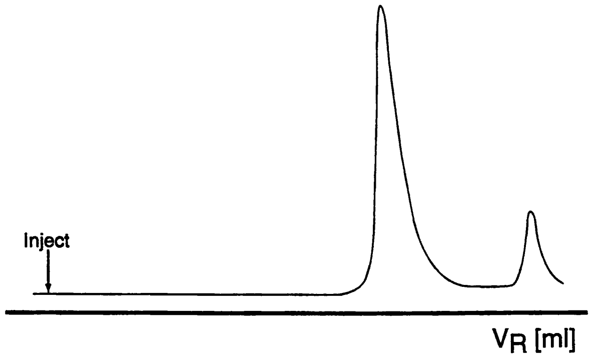

Figure 3: Characterization of a blend of polystyrene and polymethylmethacrylate under limiting conditions of solubility (THF/n-hexane, 82:18 vol%). A bare silica gel column with a 100 nm pore size was utilized for the experiments. The peak at lower retention volumes is the polystyrene which is eluted in the SEC mode. The PMMA peak elutes under limiting conditions and its molecular weight distribution is not resolved.

conditions. In particular, sorbent properties such as the pore size, pore volume, chemical nature of the surface as well as the preferential sorption of liquids on sorbents could be investigated. Macromolecular characteristics such as their size in good, poor and theta solvents, the preferential solvation of chains, as well as the polymer solubility in various eluents should be quantified on well defined uniform molecular weight standards. Mobile phase parameters could include the elution strength of the solvent. Additionally, the effect of temperature on limiting conditions remains to be elucidated. Another area of research could be the effect of the polymer concentration and sample volume injected into the chromatographic column on the elution of solute in LCLC.

Critical and limiting conditions may also be evaluated as potential tools to quantify the branching distribution, to evaluate mixtures of linear and cyclic macromolecules, and to distinguish polymer tacticity. Additionally, the application of either method for the high temperature characterization of polyolefins has not yet been established.

Literature Cited

1. Belenkii, B.G., Gankina, E.S., Tennikov, M.B., Vilenchik, L.Z., Dokl. Akad. Nauk SSSR, **1976**, *231*,1147 and J. Chromatogr., **1978**, *147*,99.
2. Belenkii, B.G., Gankina, E.S., *J. Chromatogr.*, **1977**, *141*,13.
3. Hunkeler, D. Macko, T. Berek, D., *Polymeric Materials Science and Engineering*, **1991**, *65*,101.
4. Hunkeler, D. Macko, T. Berek, D., in *Chromatography of Polymers: Characterization by SEC and FFF*, C7, Provder, T. Ed., ACS Books, Washington, DC, 1993.
5. Hunkeler, D., Janco, M., Guryanova, V.V., Berek, D., in Chromatographic Characterization of Polymers, Provder, T., Barth, H., Urban, M., Eds., ACS Books, Washington, DC, 1995.
6. Pasch, H. in preparation; Janco, M., Berek, D., in preparation.
7. Tennikov, M.B., Nefedov, P., Lazareva, M., Frenkel, S.Ja.,*Vysokomol. soedin.*, **1977**, *A19*,657.
8. Nefedov, P.P., Zhmakina, T.P., *Vysokomol. soedin.*, **1981**, *A23*,276.
9. Entelis, S.G., Evreinov, V.V., Gorshkov, A.V., *Adv.Polym.Sci.*, **1987**, 76,129.
10. Gorshkov, A.V., Evreinov, V.V., Entelis, S.G., *Dokl.Akad.Nauk SSSR*, **1983**, *272*, 632.
11. Schulz, G., Much, H., Kruger, H., Wehrsted, G., *J.Liq.Chromatogr.*, **1990**, *13*, 1745.
12. Pasch, H., *Polymer*, **1993**, *34*,4095.
13. Berek, D., Janco, M., Hatada, K., in preparation.
14. Pasch, H., Brinkmann, C., Gallot, Y., *Polymer*, **1993**, *34*,4100.
15. Pasch, H., Augenstien, M., *Makromol. Chem.*, **1993**, *194*,2533.
16. Pasch, H., Augenstien, M., Trathnigg, B., *Makromol. Chem.Phys.*, **1994**, *195*,743.
17. Pasch, H., Gallot, Y., Trathnigg, B., *Polymer*, **1993**, *34*,4986.
18. ,Gorbunov, A.A., Skvortsov, A.M., *Vysokomol. Soedin.*, **1988**, *A30*,895.
19. Spychaj, T., Berek, D., *Polymer*, **1979**, *20*,1108.
20. Rossi, C., Bianchi. U., Bianchi, E., *Makromol. Chem.*, **1960**, *41*,31.
21. Chinai, S.N., Valles, R.J., *J.Polym.Sci.*, **1959**, *39*, 363.
22. Berek, D., Janco, M., Kitayama, T., Hatada, K., *Polym. Bull.*, **1994**, *32*, 629.
23. Hunkeler, D. Janco, M., Berek, D., Symposium on Size Exclusion Chromatography, Analytical Division, ACS Meeting, San Diego, CA, April 2-7, 1995.
24. Gorshkov, A.V., Evreinov, V.V., Entelis, S.G., *Zh.fiz.khim.*, **1985**, *59*, 1475.
25. Gorshkov, A.V., Evreinov, V.V., Entelis, S.G., *Zh.fiz.khim.*, **1985**, *59*, 2847.
26. Guryanova, V.V. Pavlov, A.V., *J.Chromatogr.*, **1986**, *365*,197.
27. Gorshkov, A.V., Evreinov, V.V., Entelis, S.G., *Zh.fiz.khim.*, **1988**, *62*, 490.

28. Filatova, N.N., Gorshkov, A.V., *Vysokomol. soedin.*, **1980**, *A30*,953.
29. Gorshkov, A.V., Evreinov, V.V., Entelis, S.G., *Zh.fiz.khim.*, **1985**, *59*, 958.
30. Zimina, T.M., Kever, J.J., Melenevskaya, E.Yu., Fell, A.F., *J.Chromatogr.*, **1992**, *593*,233.
31. Zimina, T.M., Kever, J.J., Melenevskaya, E.Yu., Egonnik, V.N., Belenkii, B.G., *Vysokomol. soedin.*, **1991**, *A33*, 1349.
32. Gorshkov, A.V., Prudskova, T.N., Guryanova, V.V., Eveinov, V.V., *Polymer Bulletin*, **1986**, *15*, 465.

Downloaded by UNIV MASSACHUSETTS AMHERST on October 8, 2012 | http://pubs.acs.org
Publication Date: May 30, 1996 | doi: 10.1021/bk-1996-0635.ch015

Chapter 15

Compositional Heterogeneity of Poly(vinyl alcohol): Characterization by Liquid Chromatography Techniques

**Elizabeth Meehan[1], Simon P. Reid[1,2], Frank P. Warner[1],
Michael Patterson[2], and John V. Dawkins[2,3]**

**[1]Polymer Laboratories Limited, Essex Road, Church Stretton,
Shropshire SY6 6AX, United Kingdom**
**[2]Department of Chemistry, Loughborough University of Technology,
Loughborough, Leicestershire LE11 3TU, United Kingdom**

Samples of partially hydrolysed poly(vinyl alcohol) PVOH may contain several heterogeneities requiring the development of chromatographic techniques for characterization. Size exclusion separations have been carried out using a number of aqueous eluents, incorporating electrolyte, or electrolyte/organic modifier, or surfactant. The most favourable molecular size separation was obtained using 0.25% w/v sodium lauryl sulfate as eluent. Compositional distributions for water-based polymers can be assessed using high-performance liquid chromatography employing a reversed-phase column. For PVOH, gradient elution with water/tetrahydrofuran with a wide pore polystyrene-based packing produced separations dependent on degree of hydrolysis and sequence length distribution. The elution results were verified with a column packed with non-porous beads. Partially hydrolysed PVOH samples appeared to have a broad distribution of composition.

Size exclusion chromatography (SEC) is well established as a technique for determining the molar mass distribution (MMD) of homopolymers. Heterogeneous copolymers contain distributions in both molar mass M and copolymer composition. Copolymer characterization based on SEC is often performed with on-line selective concentration detectors (1,2). For heterogeneous copolymers this SEC-based method is only capable of producing average composition data across a chromatogram, because copolymer chains having the same molecular size in solution will have variations in molar mass and composition (3,4).

Off-line light scattering has been developed to determine data for M and compositional heterogeneity for copolymers (5-8). The parameters used to quantify the compositional heterogeneity of a copolymer sample, as determined from light scattering data, represent the effect of M on compositional heterogeneity, and overall compositional drift. Therefore, addition of on-line low-angle laser light scattering detection to an SEC system with dual concentration detection can permit for some types of copolymers the calculation of compositional heterogeneity at each elution volume together with overall heterogeneity parameters (9,10).

[3]Corresponding author

0097–6156/96/0635–0262$15.00/0

When copolymers contain composition heterogeneities, some type of cross-fractionation procedure, involving separating by composition fractions previously separated by size (or vice versa), can be attempted, but the experimental work involving transfers between techniques is quite time-consuming. In orthogonal chromatography, on-line transfer can be automated and Balke et al (11-14) demonstrated copolymer separations with two chromatographic systems in which copolymer is separated first by SEC and second by non-exclusion mechanisms. This procedure which may be termed coupled column chromatography (CCC) has been investigated further in order to demonstrate how non-exclusion separations dependent on copolymer composition in the second column can be influenced by choice of polymer-based stationary phase and by the liquid components in the mobile phase (15,16).

A major aim of our continuing program on chromatographic techniques is to develop a methodology for separations of water-based copolymers according to composition with a polymer-based stationary phase. Such an objective would suggest studies of high performance liquid chromatography (HPLC) with aqueous eluents for more polar polymers with for example a crosslinked polystyrene-based packing, indicating a reversed-phase separation. A range of partially hydrolysed samples of poly(vinyl alcohol) (PVOH) which is normally produced by hydrolysis of poly(vinyl acetate) (PVAC) with an acid or a base catalyst was chosen for these investigations. Products with levels of hydrolysis above 70% are water soluble and have many useful applications (17). Characterization of partially hydrolysed PVOH may be regarded as a copolymer problem with heterogeneities in molecular weight M and composition (VOH content). An important extension of this work in the longer term is to perform an orthogonal, or two dimensional, experiment by coupling SEC with HPLC for partially hydrolysed PVOH, but as yet it is unclear whether CCC should operate by SEC-HPLC or HPLC-SEC.

Aqueous SEC because of the nature of the analytical columns available and the polymer systems under investigation demands modification of the aqueous eluent in order to minimise secondary interaction effects whilst ensuring full dissolution of the sample (18). Aqueous SEC studies on PVOH have been reported (19), but it is apparent that the variation in properties associated with degree of hydrolysis render the interpretation of data difficult. If partially hydrolysed PVOH is to be characterized by aqueous SEC, the eluent employed needs to be such that there is no secondary effect on the size of the polymer in solution or on the retention mechanism on the column.

HPLC methods for PVOH can be developed from observations on adsorption of PVOH onto polystyrene latex for which adsorption has been shown to increase with a decrease in the solvency of the medium, water being a better solvent as the degree of hydrolysis increases (20). This suggests that HPLC by a reversed-phase mechanism on columns packed with polystyrene beads may lead to a separation of PVOH based on VAC content. Gradient elution, where the solvent composition is gradually changed, will facilitate separation of multicomponent samples by HPLC.

The aim in this paper is to report independent studies of separations of PVOH by SEC and HPLC. The work on SEC is directed towards the effect of changing the constitution of the mobile phase on the elution characteristics of partially hydrolysed PVOH. For HPLC a separation method suitable for the analysis of PVOH covering a wide range of VAC content is required. Results from these independent studies will permit consideration in the future on how to couple the two chromatographic systems.

Experimental

A range of PVOH samples was derived from a single source of PVAC by alcoholysis in a methanol/methyl acetate medium using an alkaline catalyst to produce blocky polymer and an acid catalyst to produce random polymer (17). The average degree of hydrolysis was determined by a titration method (17) and the blockiness factor was determined by ^{13}C-NMR spectroscopy (21).

Downloaded by UNIV MASSACHUSETTS AMHERST on October 8, 2012 | http://pubs.acs.org
Publication Date: May 30, 1996 | doi: 10.1021/bk-1996-0635.ch015

Sample solutions for chromatography were prepared by stirring an accurately weighed sample of polymer in eluent (SEC) or water (HPLC) and heating to 90°C for dissolution.

SEC analysis was carried out using a system comprising a model 64 pump, a model 98 refractive index detector (both Knauer, Germany) and a model 7125 injection valve (Rheodyne, USA). The first columns used (two in series) were polymeric based, with a particle size of 8μm and an exclusion limit based on poly(ethylene oxide) of 200,000 (PL aquagel-OH 40, 300 x 7.5 mm, Polymer Laboratories, UK). Further analysis used the same type of packing but with a higher exclusion limit of 1,000,000 (PL aquagel-OH 50, 300 x 7.5 mm). An eluent flow rate of 1.0mL/min was used and samples were analyzed in various eluent systems with an injection volume of 200μL and sample concentration of 0.5% w/v. The eluent modifiers $NaNO_3$, methanol, sodium lauryl sulfate (Fisons, UK) required no further treatment and were used as supplied.

HPLC analysis was carried out using a gradient system comprising two model 64 pumps controlled by a model 50 HPLC programmer, a dynamic mixing chamber (Knauer, Germany), a model 7125 injection valve (Rheodyne, USA), and a model PL-EMD 950 evaporative mass detector (Polymer Laboratories, UK). The column used was a polymeric-based reversed-phase packing of polystyrene/divinylbenzene (PS/DVB) with a particle size of 8μm and a pore size designation of 4000Å (PLRP-S 4000Å 8μm 50 x 4.6mm, Polymer Laboratories, UK). Further studies employed an experimental column of the same dimensions packed with non-porous PS/DVB particles of the same diameter. An eluent flow rate of 1.0mL/min was used throughout and samples were analyzed at room temperature using a linear gradient of water and tetrahydrofuran (THF) with an injection volume of 50-1000μL and sample concentrations of 0.2-0.5% w/v. HPLC grade water (Rathburn, UK) and HPLC grade THF (Fisons, UK) were used throughout. The mass detector was operated at an evaporation temperature of 90-100°C using compressed air as nebulizer gas at a flow rate of 12-14L/min.

Results and Discussion

Poly(vinyl alcohol). The two series of model PVOH polymers were derived by hydrolysis from a single source of PVAC, with blocky or random architectures dependent on the method of hydrolysis (17). In ^{13}C-NMR studies of PVOH when the methylene carbon is considered, the spectrum contains three peaks corresponding to the three possible chain sequences which can be used to calculate relative sequence lengths (21). Typically, alkaline hydrolysed samples with a degree of hydrolysis of 70% had a blockiness factor, n, of 0.4, which increased to 0.43 for a degree of hydrolysis of 80%. These results may be compared with acid hydrolysed samples with degrees of hydrolysis between 72 and 76%, having a value of n of 0.83. As values for n increase, the blockiness of the polymer decreases, (a perfectly random polymer would exhibit a value of n=1). These results confirmed that the alkaline hydrolysed samples were blocky and also the blockiness decreased with increasing degree of hydrolysis.

Size Exclusion Chromatography. As the PVOH samples were all produced from a single source of PVAC, it was expected that the molecular size in solution of all the hydrolysed polymers would be similar, that is the SEC chromatograms would exhibit similar profiles. The first SEC eluent used was 0.05M $NaNO_3$ which had been reported in the literature as being suitable for a relatively high degree of hydrolysis PVOH (88% or greater) (22). Initial experiments were performed with alkaline hydrolysed PVOH covering the hydrolysis range 77.7% to 100. A general trend was observed, that as the degree of hydrolysis decreased the detector response decreased and the peak retention time increased. This type of behaviour could be caused by either adsorption of the polymer onto the column packing material or a decrease in molecular size or a change in polymer refractive index as the VAC content of a sample increased. In order to

Downloaded by UNIV MASSACHUSETTS AMHERST on October 8, 2012 | http://pubs.acs.org
Publication Date: May 30, 1996 | doi: 10.1021/bk-1996-0635.ch015

Downloaded by UNIV MASSACHUSETTS AMHERST on October 8, 2012 | http://pubs.acs.org
Publication Date: May 30, 1996 | doi: 10.1021/bk-1996-0635.ch015

investigate this further the eluent was modified to include a higher salt concentration (0.2M) and 20% by volume methanol. Previous studies (23) have indicated that the addition of this organic modifier is sufficient to suppress hydrophobic interactions for synthetic polymers. With this eluent modification chromatograms with improved consistency were obtained, presumably as a result of suppressed interaction or improved solubility, but there was still a gradual decrease in detector response as the degree of hydrolysis decreased.

It has been suggested (24,25) that in aqueous solution sodium lauryl sulfate (SLS) binds readily with PVOH thus inhibiting intermolecular interactions resulting in dissociation of multimers which will reduce molecular size. If this were the case, then an eluent based on SLS may be useful since it will present the polymer molecules in an expanded form irrespective of degree of hydrolysis, and thus yield a separation based on true size in solution. However, SLS must be used at a level below its critical micelle concentration in order to avoid induced micellization. Initial SEC chromatograms for alkaline hydrolysed PVOH samples indicated similar elution patterns for all degrees of hydrolysis above 70%, but chromatograms for the PL aquagel-OH 40 columns exhibited peaks showing excluded chains. When the pore size was increased for the PL aquagel-OH 50 columns and the same eluent employed, all samples eluted with very similar profiles, see Figures 1 and 2, which suggested that a true size exclusion separation mechanism was taking place in the absence of secondary interaction effects.

Determination of MMD from the chromatograms in Figures 1 and 2 must be determined carefully. Procedures based on molar mass calibrations should be attempted cautiously in view of the results on composition heterogeneity (see next section). Furthermore, application of a universal calibration approach may have to assess whether a blocky versus random chain architecture of VAC units may influence the dependence of chain size on M. Also it is possible that partially hydrolysed PVOH may contain long-chain branching dependent on the conditions of polymerization of VAC. A full characterization of some partially hydrolysed PVOH samples would therefore require an extensive programme of experiments to determine distributions in M, composition, sequence length and branching.

High Performance Liquid Chromatography. Samples of PVOH were analysed using a PLRP-S 4000Å 8μm 50 x 4.6mm column with gradient elution from 99% water/1% THF to 30% water/70% THF in 8 min. Typical HPLC chromatograms obtained for alkaline hydrolysed samples of different degrees of hydrolysis are shown in Figure 3. Fully hydrolysed PVOH always exhibited a relatively sharp early eluting peak, indicating limited interaction with the packing material. For samples of partially hydrolysed PVOH, broader and later eluting peaks were observed indicating stronger interactions at higher levels of VAC.

Typical chromatograms for acid hydrolysed samples, shown in Figure 4, exhibited a similar trend to those for the alkaline samples. At lower degrees of hydrolysis, the increased VAC content enhanced interactions with the PS/DVB packing material at the start of the gradient (99% water/1% THF). Thus, a higher concentration of THF is required to release the samples resulting in increased elution time. A strong correlation was observed between elution time and degree of hydrolysis for both acid and alkaline hydrolysed samples. In general, the samples of alkaline hydrolysed (blocky) PVOH eluted later than the acid hydrolysed (random) samples for the same degree of hydrolysis. A more blocky distribution of acetate groups, that is a longer sequence length, presents a larger segment for column adsorption and requires correspondingly higher THF content to elute the sample. This difference is not observed at high degrees of hydrolysis, greater than 90%, where the sequence lengths in random and blocky samples are similar.

As with the SEC experiments, it was desirable to ensure that the HPLC separations operated by a single mechanism. An HPLC column with very wide pores (designation 4000Å) was selected following consideration of the molecular size

Downloaded by UNIV MASSACHUSETTS AMHERST on October 8, 2012 | http://pubs.acs.org
Publication Date: May 30, 1996 | doi: 10.1021/bk-1996-0635.ch015

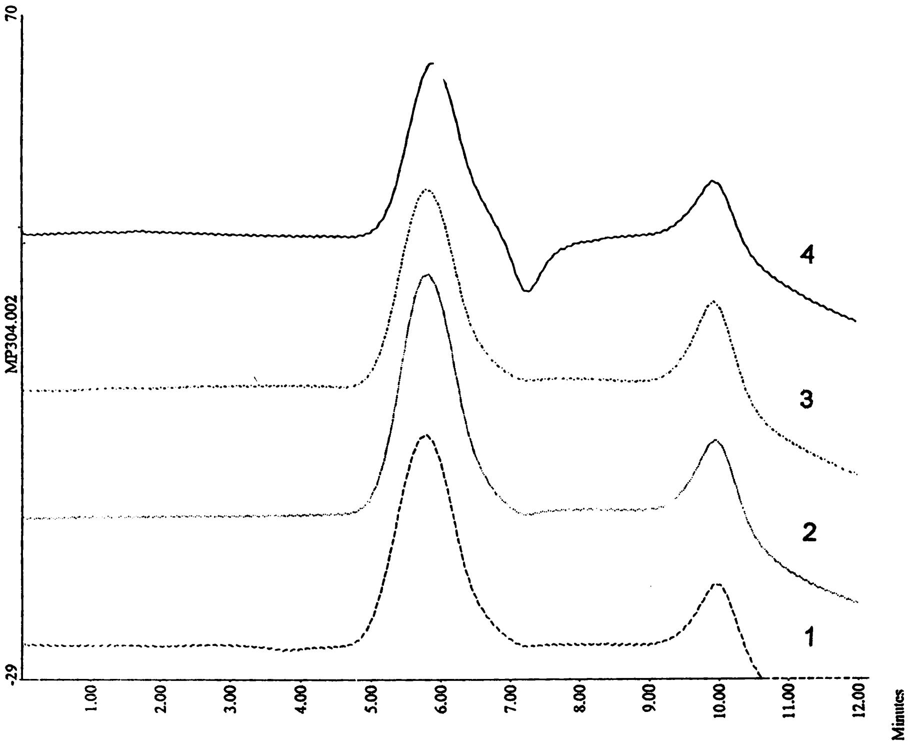

Figure 1. Effect of degree of hydrolysis on SEC chromatograms for alkaline hydrolysed (blocky) PVOH. Columns: 2 x PL aquagel-OH 50, 8μ, 300x7.5mm, eluent: 0.25% sodium lauryl sulfate. 1. 73.7%, 2. 83.6%, 3. 89.8%, 4. 100%.

Downloaded by UNIV MASSACHUSETTS AMHERST on October 8, 2012 | http://pubs.acs.org
Publication Date: May 30, 1996 | doi: 10.1021/bk-1996-0635.ch015

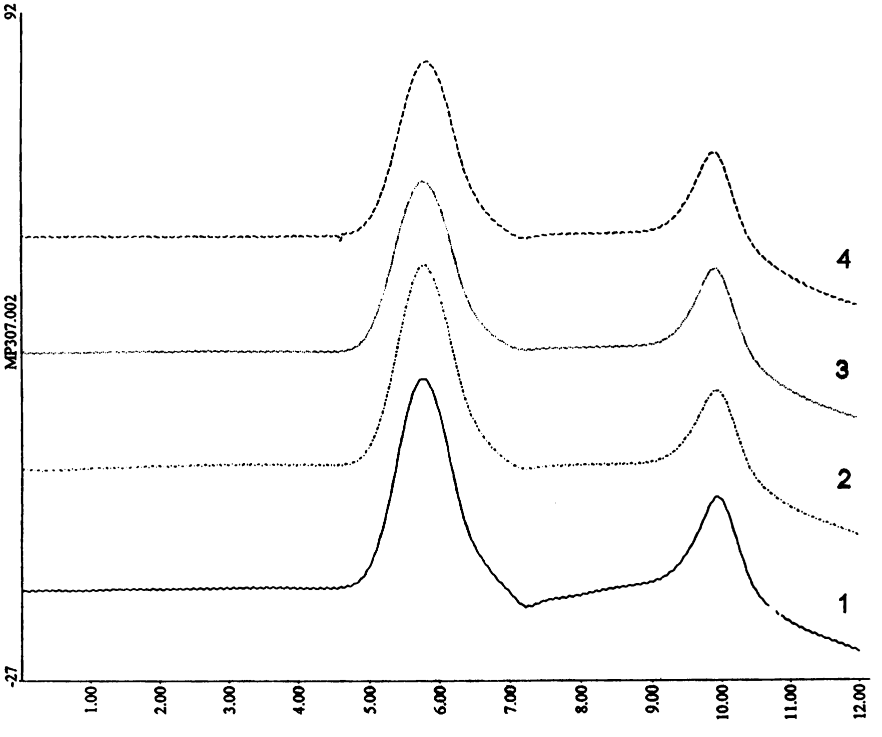

Figure 2. Effect of degree of hydrolysis on SEC chromatograms for acid hydrolysed (random) PVOH. Columns: 2 x PL aquagel-OH 50, 8μ, 300x7.5mm, eluent: 0.25% sodium lauryl sulfate. 1. 75.6%, 2. 84.6%, 3. 93.9%, 4. 97.2%.

Downloaded by UNIV MASSACHUSETTS AMHERST on October 8, 2012 | http://pubs.acs.org
Publication Date: May 30, 1996 | doi: 10.1021/bk-1996-0635.ch015

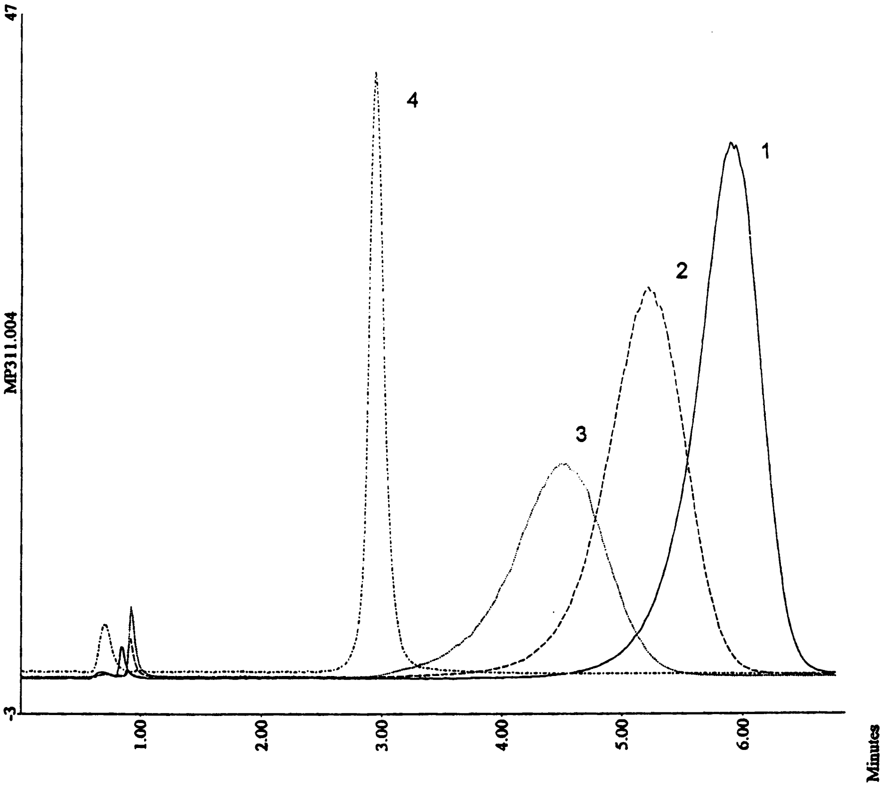

Figure 3. Effect of degree of hydrolysis on HPLC chromatograms for alkaline hydrolysed (blocky) PVOH. Column: PLRP-S, 4000Å, 8μ, 50x4.6mm, eluent A: 99% water / 1% THF, eluent B: 100% THF, gradient: 1 to 70% eluent B in 5 minutes. 1. 73.7%, 2. 83.6%, 3. 89.8%, 4. 100%.

Downloaded by UNIV MASSACHUSETTS AMHERST on October 8, 2012 | http://pubs.acs.org
Publication Date: May 30, 1996 | doi: 10.1021/bk-1996-0635.ch015

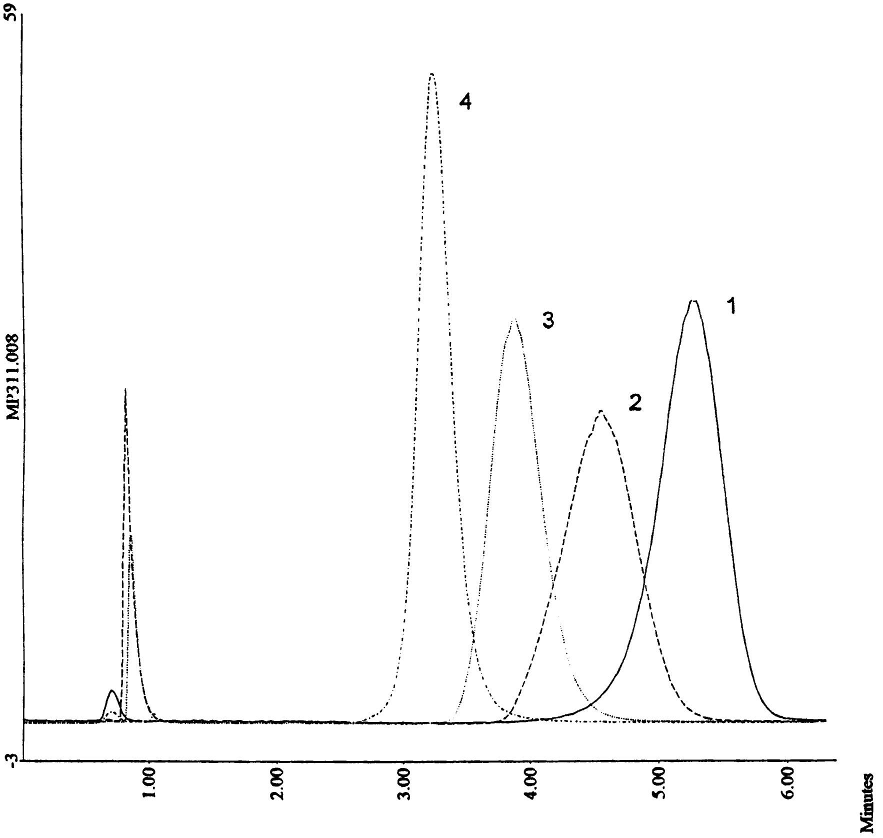

Figure 4. Effect of degree of hydrolysis on HPLC chromatograms for acid hydrolysed (random) PVOH. Column: PLRP-S, 4000Å, 8µ, 50x4.6mm, eluent A: 99% water / 1 % THF, eluent B: 100% THF, gradient: 1 to 70% eluent B in 5 minutes. 1. 75.6%, 2. 84.6%, 3. 93.9%, 4. 97.2%.

information obtained by SEC. This wide-pore packing should not permit any separation based on a size exclusion mechanism although the possibility could not be overlooked. In order to investigate this further, an experimental column was packed with non-porous PS/DVB beads and the gradient elution analysis was repeated. Although retention times were shorter overall, due to the lower surface area for interaction compared to the porous beads, the trends in Figures 5 and 6 for the non-porous beads were similar to those reported for the wide-pore packing. All these results confirm that HPLC separations of partially hydrolysed PVOH are dependent on VAC content and sequence length distribution.

Downloaded by UNIV MASSACHUSETTS AMHERST on October 8, 2012 | http://pubs.acs.org
Publication Date: May 30, 1996 | doi: 10.1021/bk-1996-0635.ch015

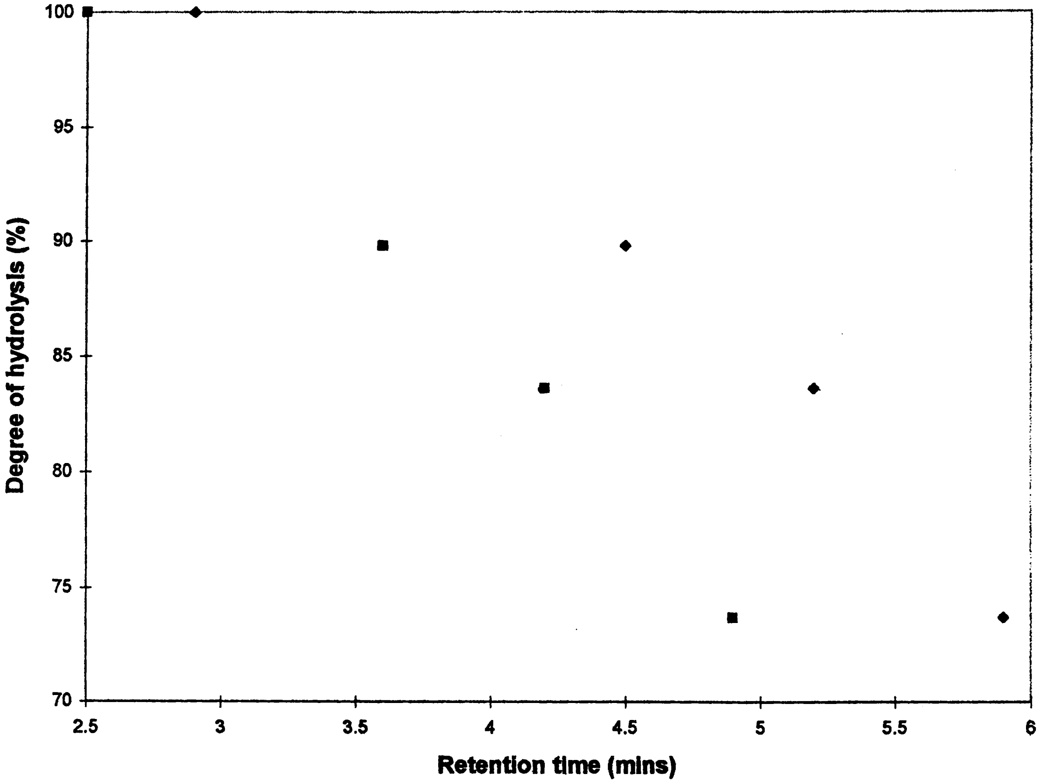

Figure 5. Retention time as a function of degree of hydrolysis for alkaline hydrolysed PVOH. (◆) Column: PLRP-S, 4000Å, 8μ, 50x4.6mm; (■) Column: PS/DVB, non-porous, 8μ, 50x4.6mm; eluent A: 99% water / 1% THF, eluent B: 100% THF, gradient: 1 to 70% eluent B in 5 minutes.

Downloaded by UNIV MASSACHUSETTS AMHERST on October 8, 2012 | http://pubs.acs.org
Publication Date: May 30, 1996 | doi: 10.1021/bk-1996-0635.ch015

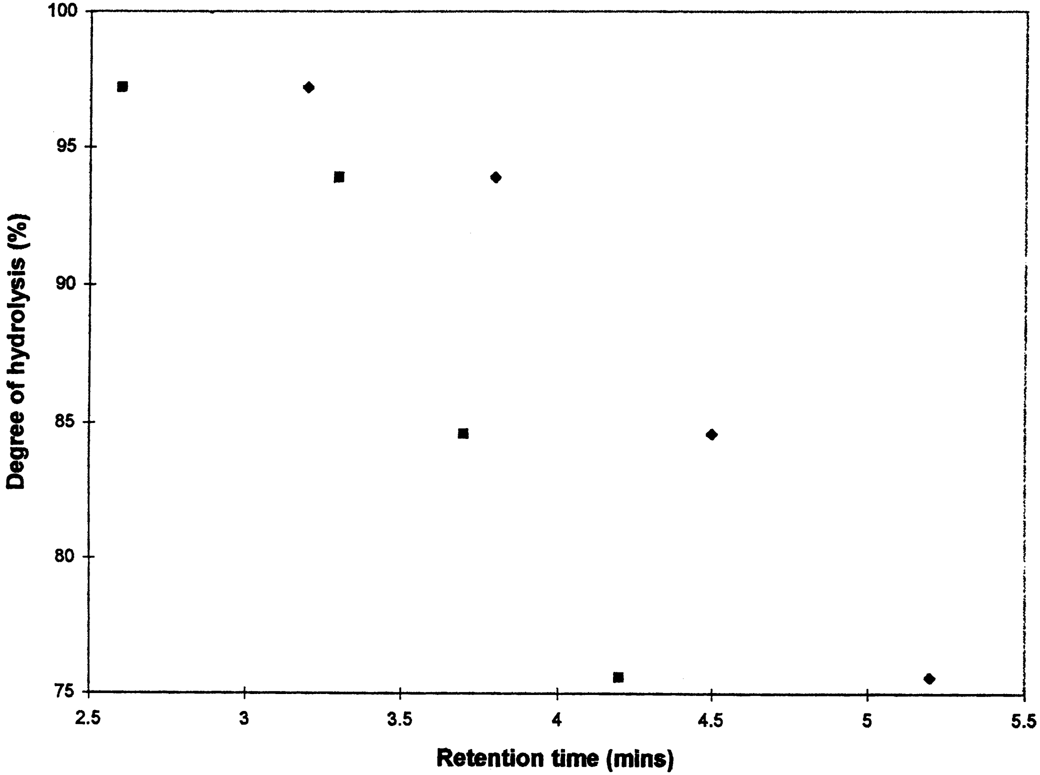

Figure 6. Retention time as a function of degree of hydrolysis for acid hydrolysed PVOH. (◆) Column: PLRP-S, 4000Å, 8μ, 50x4.6mm; (■) Column: non-porous PS/DVB, 8μ, 50x4.6mm; eluent A: 99% water / 1% THF, eluent B: 100% THF, gradient: 1 to 70% eluent B in 5 minutes.

The PVOH samples studied were prepared by alcoholysis of PVAC in the presence of methanol/methyl acetate. However, it has been shown (26), that PVOH obtained by alcoholysis in the presence of methyl acetate exhibits a relatively wide distribution of degree of hydrolysis. This may explain the broad HPLC chromatograms observed for partially hydrolysed polymers in Figures 3 and 4, whereas, in the case of the fully hydrolysed sample, where no such compositional variation exists, the chromatogram was much narrower.

Conclusion

SEC analysis of PVOH covering a wide range of degrees of hydrolysis has proved to be difficult, but it has been found that 0.25% sodium lauryl sulfate as an aqueous SEC eluent results in chromatograms which appear to be consistent with a size exclusion mechanism. An HPLC method using gradient elution with water/THF has been developed for the separation of PVOH polymers based on degree of hydrolysis. These elution results were verified with a column packed with non-porous beads. The peaks observed for partially hydrolysed PVOH samples are relatively broad indicating a distribution of composition. Current work is directed to studies of CCC in order to determine the order of separation techniques.

Acknowledgments

The authors wish to express their thanks to the Engineering and Physical Sciences Research Council, European Vinyls Corporation (UK) Ltd, ICI Chemicals and Polymers Ltd and Harlow Chemical Company Ltd for their support, and to A.J. Handley, A. Nevin, S. Ormondroyd and P.L. Shaw for helpful discussions.

Literature Cited

1. Runyon, J R; Barnes, D E; Rudd, J F; Tung, L H *J Appl Polym Sci* 1969, 13, 2359.
2. Quivoron, C In *Steric Exclusion Liquid Chromatography of Polymers* Janca, J, Ed; Marcel Dekker; New York, 1984; pp 213-280.
3. Hamielec, A *Pure Appl Chem* 1982, 54, 293.
4. Burgess, F J; Cunliffe, A V; Dawkins, J V; Richards, D H *Polymer* 1977, 18, 733.
5. Bushuk, W; Benoit, H *Can J Chem* 1956, 36, 1616.
6. Krause, S *J Phys Chem* 1961, 65, 1618.
7. Leng, M; Benoit, H *J Polym Sci* 1962, 57, 263.
8. Benoit, H; Froelich, D In *Light Scattering from Polymer Solutions* Huglin, M B Ed: Academic Press: London, 1972; p 467.
9. Dumelow, T PhD Thesis, Loughborough University of Technology, UK, 1984.
10. Dumelow, T; Holding S R; Maisey L J; Dawkins, J V *Polymer* 1986, 27, 1170.
11. Balke, S T; Patel, R D In *Size Exclusion Chromatography (GPC)* Provder, T Ed; *ACS Symposium Series* 138; Washington, 1980; pp 149-152.
12. Balke, S T; Patel, R D *J Polym Sci Part B* 1980, 18, 453.
13. Balke, S T; Patel, R D In *Polymer Characterization - Spectroscopic, Chromatographic and Physical Instrumental Methods* Craven, C Ed; *Am Chem Soc* Advances Chemistry Series 203; Washington, 1983, pp 281-310.
14. Balke, S T; In *Detection and Data Analysis in Size Exclusion Chromatography* Provder T Ed; *ACS Symposium Series* 352; Washington, 1987, pp 59-77.
15. Montenegro, A M C, PhD Thesis, Loughborough University of Technology, UK, 1986.

Downloaded by UNIV MASSACHUSETTS AMHERST on October 8, 2012 | http://pubs.acs.org
Publication Date: May 30, 1996 | doi: 10.1021/bk-1996-0635.ch015

16. Dawkins, J V; Montenegro, A M C *Brit Polym J* 1989, 21, 1.
17. Finch, C A; Ed. *Poly(vinyl alcohol), Properties and Applications*, Wiley:London, 1973.
18. Barth, H G *J Chromatogr Sci* 1980, 18, 430.
19. Meehan, E; O'Donohue, S; Williams, A G; Dawkins, J V *J Appl Polym Sci:Appl Polym Symp* 1992, 51, 151.
20. Barker, M C; Garvey, M J; *J Colloid Interface Sci* 1980, 74, 331.
21. Moritani, T; Fujiwara, Y; *Macromolecules* 1977, 10, 532 .
22. Nagy, D J *J Polym Sci, Part B:Lett* 1986, 24, 87.
23. Warner, F P; Meehan, E; Oakley, S; Boden, G; Presented at the International GPC Symposium, San Francisco, USA, October 1991.
24. Aladjoff, I; Nilsson, H; Silvegren, C; Tornell, B *Acta Chem Scand* 1982, A36, 259.
25. Aladjoff, I; Nilsson, H; Silvegren, C; Tornell, B *Acta Chem Scand* 1982, A36, 267.
26. Noro, K *Brit Polym J* 1970, 2, 128.

Downloaded by UNIV MASSACHUSETTS AMHERST on October 8, 2012 | http://pubs.acs.org
Publication Date: May 30, 1996 | doi: 10.1021/bk-1996-0635.ch015

Chapter 16

Nonstandard Methods Based on Size Exclusion Chromatography Principles

"Critical" Chromatography, High-Performance Membrane Chromatography, Thin-Layer Chromatography, and Microbore Size Exclusion Chromatography

B. G. Belenkii, E. S. Gankina, G. E. Kasalainen, and M. B. Tennikov

**Institute for Analytical Instrumentation of Russian Academy of Sciences,
26 Rijsky pr., 198103 Saint Petersburg, Russia**

For a long time chromatographic fractionation has been considered the most appropriate method for collection of narrow macromolecular fractions according to molecular weight (MW) and chemical structure. Very polydisperse polymers, consisting of macromolecules heterogeneous with respect to mass chemical structure require a high resolution method for high quality fractionation. For syntethic polymers a liquid chromatography is such a method (*1,2*), while for biopolymers gel electrophoresis or capillary electrophoresis in uncross-linked polymer solutions are the most suitable.

The investigators have been trying to develop the theoretical concepts of chromatography of polymers which permit to determine the correlation of chromatographic parameters such as the retention volume, peak dispersion with polymer polydispersity parameters including molecular weight distribution (MWD), the chemical structure, the compositional and functional group inhomogeneity. Development of conceptions of SEC such as the universal Benoit calibration, the modern theory of polymer adsorption chromatography on porous sorbents ("critical" chromatography) result in new possibilities for precise polymer fractionation.

The technical development of macromolecular chromatography has proceeded in following directions: two-dimensional fractionations according to several types of polydispersities; combination of chromatography with other fractionation methods (high- speed sedimentation, mass spectrometry); utilization of highly-informative chromatographic detectors such as Fourier transform infrared (FTIR), low angle laser light scattering (LALLS), and multiangle laser light scattering (MALLS); preperation of SEC-column with linear weight range calibration dependencies, a micro-SEC-chromatography (*3,4*). The combination of SEC with MALLS-detector permits to solve the absolute MWD-determination problem (*5*). The matrix association light desorption

0097–6156/96/0635–0274$23.25/0

ionization method (MALDI) permits us to directly determine all types of macromolecules from macromolecular population - polymers (*6*). So MALDI may solve the problem of the absolute determination of composition heterogeneity of copolymers and functionality of oligomers, which are now solved by "critical" chromatography, although the latter is limited by oligomers and polymers with MW < 10^5 Da.

Simultaneously two other analytical problems connected with the MWD of polymers have been solved:

1. MWD-determination of giant-macromolecules (by increase of MW-sieving of SEC (*7*), employment of correlation laser spectroscopy (*8*), hydrodynamic chromatography (*9*), and field-flow fractionation (*1*)).
2. Development of an express semi-quantitative inexpensive, yet highly informative method for determination of polymer polydispersity and purity using the thin-layer chromatography (TLC) has been developed (*1,10*).

The success of high-performance analytical separation of biopolymers by gel electrophoresis is well known. This includes the complete separation of polypeptides of a mammalian cell lysate (MW > 12,000 Da) by 2-D gel-electrophoresis (*11*), the separation of hemoglobins differing by one methylene-group at MW ~ 66,000 Da (*12*), and the separation of more than 700 oligo- and polynucleotides by HPCE. For synthetic polymers, for example, the complete separation of the polysterines of MW ~ 50 kDa with one, two, and without, carboxylic end groups by adsorption TLC is also possible (*1*).

The preparative fractionation of polymers is much less successful, although the demand for this is great. The higher the cost of polymers, the more important their separation according to chemical composition and MW. For successful preparative fractionation one has to solve a difficult problem of increasing the scale of the fractionation without losses in resolution. There are several ways of solving this problem:

1. To move to fractionations with greater capacity and selectivity. For example, the use of adsorption chromatography instead of size exclusion chromatography can be considered.
2. To organize the separation process according to the definite parts of a polymer, while other groups are excluded from the separation, for example, by transferring them to "chromatographically invisible" ones using chromatography under "critical" conditions.
3. To develop new hybrid high-performance separation methods. For example, high-performance membrane chromatography (HPMC) has been developed by combining HPLC, with its high selectivity and efficiency, and Membrane Technology (MemTech), a cheap method with unlimited possibilities with respect to scaling up.

This article presents a review of nonstandard SEC-methods for polymer analysis. These include micro-SEC and methods, which are based not only

Table I. Advantages of Microcolumn SEC

N	*Effect*	*Applications*
1.	Decrease in the eluent consumption	Analysis of MWD of polyamides using perfluorated alcohols and acids
2.	Decrease in the mass of polymeric analyte	Determination of MW and MWD of biopolymers and synthetic polymers (investigation of new polymers)
3.	High performance columns with high quality sorbent packing (a decrease in the effect of low diffusion coefficients for polymers and decrease in spreading caused by flow rate profile	Analysis of the MWD of oligomers Precise analysis of polymer MWD Analysis of low- molecular-weight additives to polymers
4.	The use of exotic eluents, precise sorbents and calibration standards	Physico-chemical investigations of new polymer solutions
5.	Decrease in adsorption of polar polymers and proteins on the column walls and on the sorbent resulting from an increase in the ratio of the solute to sorbent masses	Trace analysis Precise analysis of high-molecular-weight polymer fractions
6.	High-speed separation	Monitoring of polymerization and depolymerization Use in the second (isocratic) cascade of two-dimensional chromatography of macromolecules

SOURCE: Adapted from ref. 4.

on the SEC-fractionation effect (genuine SEC), but also on the interaction of the analyte with the pore surface , such as the interactive (adsorption) chromatography of polymers and oligomers ("critical" chromatography), thin-layer chromatography, and high-performance membrane chromatography.

The authors of the present article have made the pioneering studies in these directions and take part in developing the above-listed chromatographic methods and their practical applications.

Micro-SEC chromatography of polymers

The primary advantage of micro-LC is a decrease in the eluent, sorbent, and sample requirements (*13-16*). In fact, special sorbents for size-exclusion chromatography (SEC) are expensive. Further, highly toxic solvents (perfluorinated alcohols or acids) are often used for polymer analysis, and protein molecular weight determinations are difficult because large sample masses are not available.

Therefore, the construction of a chromatograph for microcolumn size-exclusion chromatography (MSEC) of polymers (micro- gel- chromatograph) is of considerable interest. A number of papers are dedicated to MSEC (*17 -24*). A flexible fused silica column for MSEC of oligomers was described first by D. Ishii and T. Takeuchi and by T. Takeuchi et al (*25,26*). Similar columns with inner diameters, dc, of 28 and 50 micrometers and lengths up to 90 cm (N = 90,000 plates) have also been used for MSEC of proteins (*27*). These advantages of MSEC are summarized in Table I . As is evident, there is a uniqal field of application of MSEC to polymer MWD-analysis in which MSEC exhibits decisive advantages over SEC with conventional columns.

However, the construction of a microcolumn gel chromatograph is very complex endeavor because a highly sensitive refractometric detector with a cell volume less than 0.1 μL should be used, and high reproducibility (0.1-0.3 %) of retention time for polymers with a distribution coefficient , kd , less than or equal to one should be ensured. There are some difficulties with high performance column preparations , calibration and information processing for MSEC. In papers (*3,4*) the main problems of MSEC were considered:
1. The achievement of retention volume reproducibility similar to that of gel chromatograph with conventional columns (*dc* = 4-6 mm).
2. The design of a refractometric detector with a cell corresponding to a column diameter < 0.5 mm.

The optimization of micro-LC has been described in the literature in great detail (*13-16,28*). However, the optimization of a syringe pump (only possible pump for micro-LC) is a relatively new problem and has not been considered sufficiently (*3*). The eluent delivery system works not only under conditions of constant elution rate, but also under transitional conditions related to pressure changes in the pump chamber (ΔP which modifies the eluent volume when the pump is switched on and when troubles arise according to the compressibility factor β of the eluent). Moreover, the large pump chamber volume increases the time of the transitional process needed for stabilization of the eluent flow rate. These problems have been considered in (*29*).

On the other hand, a large pump chamber and a small chromatographic column form a thermometer with great sensitivity to temperature changes, ΔT. This reaction is determined by thermal expansion, according to thermal expansion coefficient of the liquid, α.

We can also define the requirements for the hydraulic system of the chromatograph with a syringe pump. The pressure, P, built up in the syringe chamber and the flow rate, Q, of the eluent in the column are connected by:

$$Q = P/K \qquad (1)$$

where K is hydraulic resistance of column. The transition time, τ, (to a new chromatographic regime after changing pressure) is:

$$\tau = V_P \beta K \qquad (2)$$

where V_P is the pump chamber volume, β is the compressibility factor of the eluent. The liquid volume V in the pump with fluctuations in temperature (ΔT) and pressure (ΔP) is related to the volume of liquid, V_o, at the initial temperature as:

$$V = V_o(1 + \alpha\Delta T) \qquad (3)$$

and at the initial pressure:

$$V = V_o(1 - \beta\Delta P) \qquad (4)$$

Hence, we have

$$\Delta T = -(\beta/\alpha)\Delta P \qquad (5)$$

Since the related deviation in the retention time, $\Delta t_R/t_R$, depends on pressure variations $\Delta P/P$ as follows:

$$\Delta t_R/t_R = \Delta P/P \qquad (6)$$

we can obtain the desired dependence for ΔT:

$$\Delta T = -P_{\infty}(\beta/\alpha)\,\delta \qquad (7)$$

where P_{∞} is the static pressure, and δ is the predetermined value of $\Delta t_R/t_R$.

The instability of eluent velocity is the main problem that should be solved in the construction of a micro-gel chromatograph. The experimental dependence of the stabilization time τ (which is proportional to the logarithm of the disturbing factor amplitude ,e.g. ΔP, ΔT or ΔK) on the volume V_P of the eluent delivery system is shown in Figure 1. It is clear that when $V_P < 1$ mL then at $\Delta P = 1$ MPa we have $\tau = 2$ min. In a real experiment when $\Delta P \cong 0.1$ MPa, a pump with $V_P \cong 1$mL ensures good reproducibility of t_R ($\cong 0.1\%$).

Hence, the usage of microcolumns (dc < 1 mm) requires the volume of the eluent delivery system be minimized ($V_P < 1$ mL) and the system must be thermostatted at an amplitude $\Delta T < -P_{\infty}(\alpha/\beta)\delta$.

The other complicated problem of MSEC is the detection of the polymer solution - effluent from MSEC-column with an inner diameter < 0.5 mm. For precise polymer MWD determination it is necessary to use a detector with a minimal detectable refraction, Δn, of 3×10^{-8} refractive index units, a detector cell volume of 0.1 mL, and a relative stability $d(\Delta n)/\Delta n) < 0.5\%$. Exactly such a detector was designed for micro-gel-chromatograph on the basis of a polarizing interferometer with laser light source. The usage for MSEC of the goniometric (hollow prism) and Fresnel refractometers is impossible because, for refractometers of these types, the cell has an unfavorable volume-to-surface ratio. As a result the effect of surface cell contamination on the detector signal increases with a decrease in cell volume. As distinguished from the above detectors where the optical refraction effect takes place in a thin (approximately one light wavelength, λ) liquid layer near the wall where the liquid composition can differ from that in the bulk, in the interferometric detector the optical effect is determined by the bulk solution. Moreover, a goniometric cell contains poorly swept zones.

A polarizing interferometer with birefringent light beam splitting which has considerable advantages as compared both to the interferometers operating in the visible light range and to other types of refractometers. The design of these refractometers is shown schematically in Figure 2. The high long-term stability (low drift) and low noise level (Figure 3) are due to a system of angular mirrors mounted on a glass ceramic monoblock and one planar-parallel calcite plate (10). The polarized light beams with equal intensities pass through a half-wave plate (11), the sample and reference cells (12), and then are superimposed into one beam with the aid of the same calcite plate. A $\lambda/4$ compensating plate (13) is mounted directly on the mono-

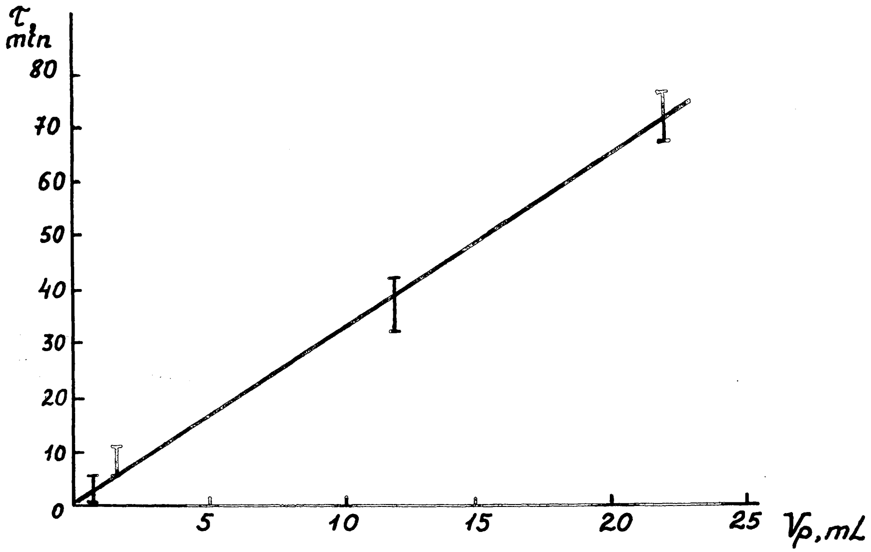

Figure 1. Stabilization time τ vs volume Vp of the eluent delivery system. Conditions: 300 mm x 0.5 mm i.d. column, 6 mL/min - elution rate, ΔP = 3.0 MPa, after a rapid pressure change of + 1.0 MPa. (Adapted from ref. 4)

In Strategies in Size Exclusion Chromatography; Potschka, M., et al.;
ACS Symposium Series; American Chemical Society: Washington, DC, 1996.

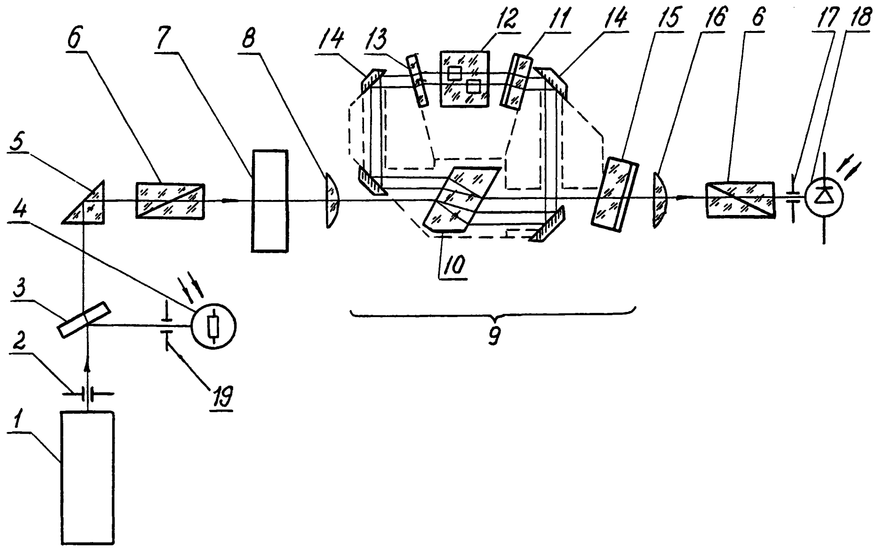

Figure 2. Diagram of the laser refractometric detector optics .
(1) - Helium-neon laser, (2, 17and 19) - diaphragms, (3)- glass plate, (4) - photoresistance detector, (5) - right angle prism, (6) - polarizers, (7) -electrooptical modulator based on a DKDR-crystal, (8 , 16) - lenses, (9) - monoblock of the polarizing interferomemter,(10) - planar-parallel calcite plate, (11) - half-wave plate, (12) - optical cells, (13) - protective glass window , (14) - mirrors , (15) - quarter-wave compensator, (18) - photodiode.
(Adapted from ref. 4)

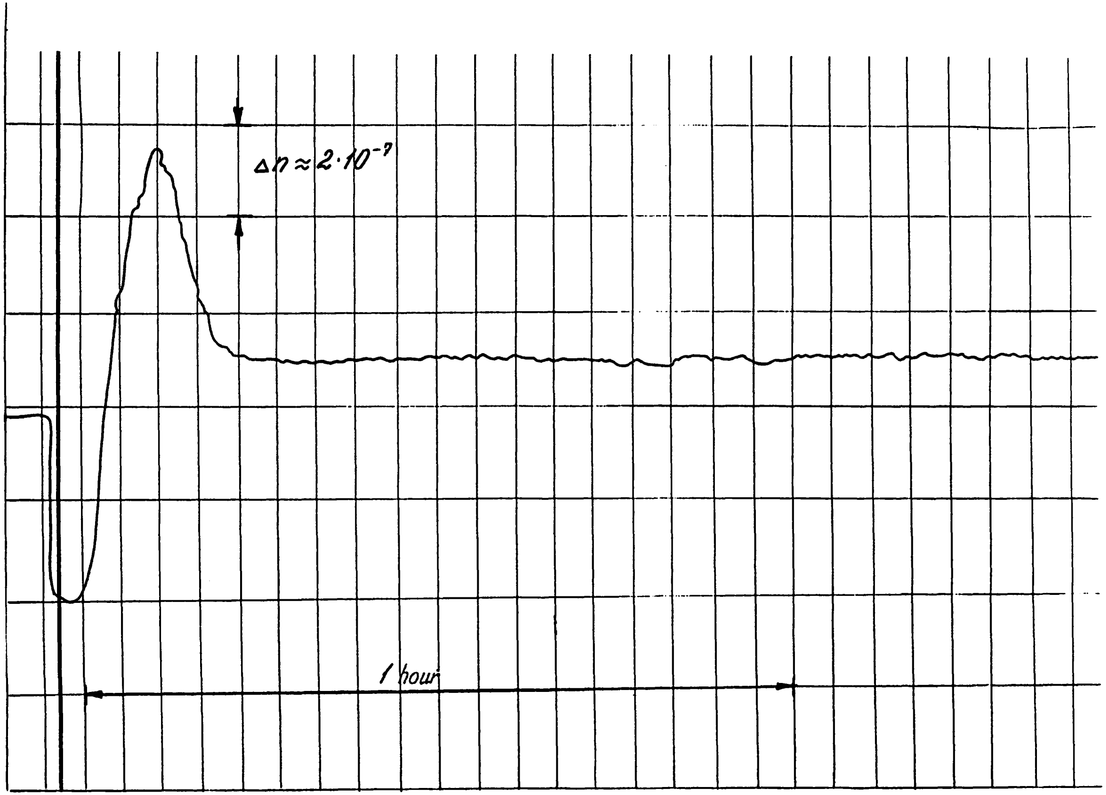

Figure 3. Recording the output signal of a laser refractometric detector from the moment that the instrument is switched on. (Adapted from ref. 4)

block. The superimposition of two orthogonally polarized light beams with the same intensities leads to the formation of an elliptically polarized light beam.

The change in $n(\Delta n)$ can be determined from the state of polarization of the light beam. If, before superimposition, each light beam passes through a differential planar-parallel cuvette with cell length l, then the change in analyze phase difference, $\Delta\theta$, of the components of elliptically polarized light is related to Δn of the contents of the two cuvettes by the equation (*29,30*):

$$\Delta\theta = (2\pi l / \lambda)\Delta n \tag{8}$$

The design of this refractometer is not only compact but also ensures high detector stability because neither the change in beam propagation direction, nor that in position of the mirror system as a whole, nor the effect of thermal strains, leads to a change in the difference between the interfering light beams.

The measurement of phase difference ($\Delta\theta$) is carried out as the measurement of the angle ϕ between the polarization plane of linearly polarized light and the axis of the quarter wavelength plate axis (*30,31*) is:

$$\phi = \theta / 2 \tag{9}$$

The sample and reference detector cells are direct-flow cells and are shaped as rectangular channels 0.5 mm x 0.5 mm. The geometric length of the beam path in the cell is 0.5 mm, and V_d corresponding to the height of the passing light beam (0.3 mm) is about 75 nL.

The temperature control of the sample and reference cells of the refractometer is particularly critical. Permissible temperature fluctuations (ΔT) are 10 °C or less. This problem is solved by placing both cells and the column in a single copper block heat exchanger, the temperature of which is maintained by a jacket thermostatted to within +0.05 °C with an external ultrathermostat. In an instrument of this construction the temperature difference in cells as determined from heat calculation and as indicated by signal fluctuations in the base line drift does not exceed 10^{-5} to 10^{-4} °C. The limiting factors for the detector signal-to-noise ratio under these conditions are moisture concentration in solvent, optical noise, and temperature instability.

This design ensures the desired detector parameters: minimal detectable Δn is $3{*}10^{-8}$ of refractive index units, detector volume (V_d) is 0.1 µL, and relative stability, $d(\Delta n)/\Delta n$, is 0.5 %. However, there are characteristics which make it possible to use this detector design for columns with

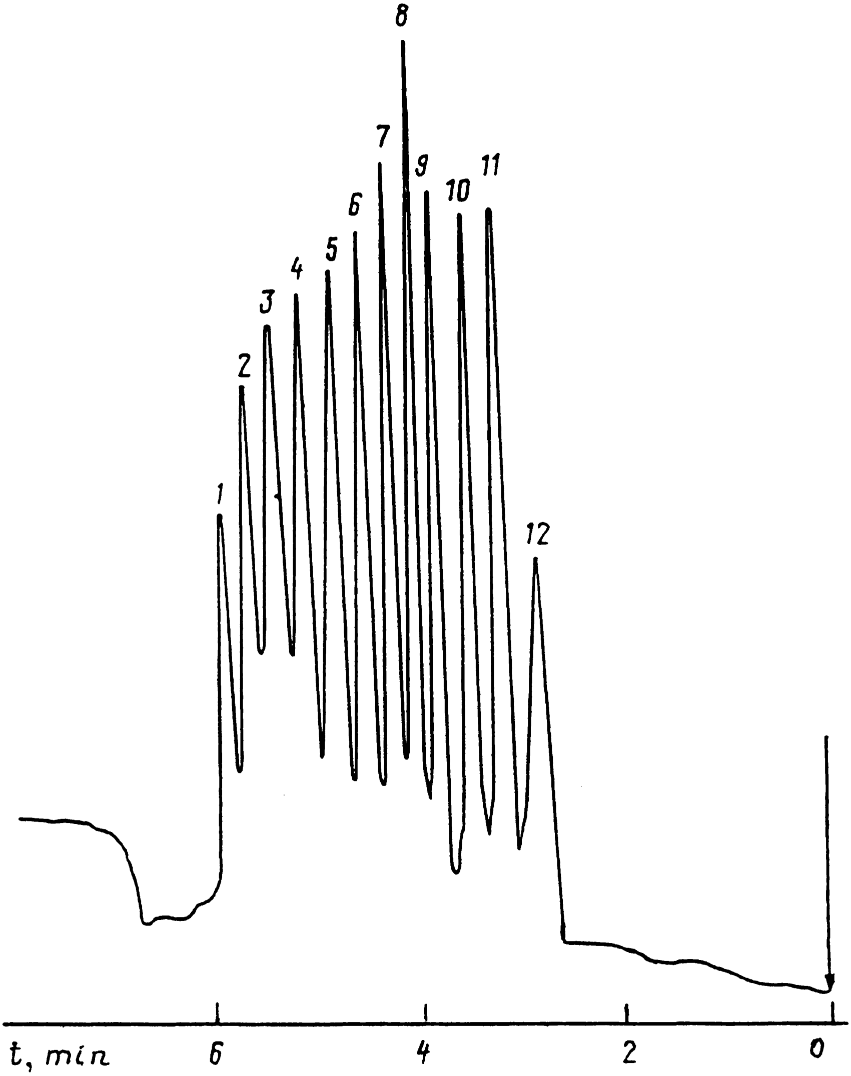

Figure 4. MSEC of PS standards on a Teflon 350-mm x 0.5 -mm i.d. microcolumn (N = 20,000 plates) .

Conditions: mixture of microspherical Nucleosil silica gels, *dp* = 5 μm, with a linear molecular weight calibration dependence; ethyl methyl ketone eluent, 7.6 μL/min elution rate; 0.1 mg/mL PS standards concentration; sample volume V_S = 0.06 μL;

MW : (1) $3 \cdot 10^6$ Da, (2) $8.3 \cdot 10^5$, (3) $4.02 \cdot 10^5$, (4) $1.96 \cdot 10^5$, (5) $9.72 \cdot 10^4$, (6) $5.5 \cdot 10^4$, (7) $2.6 \cdot 10^4$, (8) $1.3 \cdot 10^4$, (9) $5 \cdot 10^3$, (10) $2.025 \cdot 10^3$, (11) $4.8 \cdot 10^2$, (12) 78 (benzene).

(Adapted from ref. 4)

inner diameters dc = 0.2 mm. The threshold sensitivity of such detector with respect to the substance mass will be approximately 1 pg.

The modern concepts of a chromarograph for MSEC considered above, form the basis for the development of a microcolumn gel chromatograph with a refractometric (interference - polarizing) detector. Teflon columns (*dc* = 0.5 mm) were used because the fused-quartz columns of such diameter lose flexibility and become brittle. Moreover, when the Teflon column is pac-ked at the pressure that exceeds the operating pressure, the sorbent in the column is compressed (radial compression) thus increasing the column efficiency (up to *N* = 15,000 - 20,000 plates for a length of 350 mm).

The volume of the thermostatted eluent injection system of this chromatograph (*Vp* = 1.5 mL) ensures determinations of the number average and weight average molecular weights, Mn and Mw, with reproducibilities of about 2-4 % (*4*). These data correspond to those of the MWD- analysis on modern high-performance gel chromatographs with conventional columns.

This microcolumn chromatograph is fitted with a corrosion-resistant hydraulic system made of titanium - zirconium alloy. Therefore, it may be used with any eluents including corrosion-active ones with a solvent consumption of about 50 µL (1 drop) for one analysis. The chromatograph utilizes a computer system for data processing (*24*).

Examples of analysis carried out with this micro-gel chromatograph are shown in Figures 4 - 8 . Figure 4 shows the chromatogram of polystyrene standards. Figure 5 demonstrates a calibration curve for retention volume V_R vs. *log (MW)* for this column. This curve was obtained by using different polystyrene standards (PS). Figure 6 demonstrates MSEC of proteins. This makes it possible to determine their MW with relatively high precision (to within 2 %) in the analysis of a 50-ng protein preparation (*32*). The application of MSEC to the analysis of the MWD of polar polymers (polyesters and polyamides) is of particular interest because in this case highly toxic perfluorinated acids or alcohols should be used as eluents. Figures 7, 8 show exclusion chromatograms of polyethylene terephthalate and polyamide fibers obtained with the micro-gel chromatograph using 50 ng of analyte and one drop (approximately 50 mL) of solvent. These samples were used as material evidence from a crime scene. The investigation was conducted to establish identities of the fibers and to compare them to fibers from suspected people. The unique characteristics of the MWD of each lot of polymers obtained in a certain polymer reactor made it possible to use the MWD as polymer "fingerprint".

In further developments of this micro-gel chromatograph we anticipate replacing the Teflon columns with flexible fused-silica capillaries (*dc* = 0.2 mm). Moreover, as a result of sorbent particle diameter reduction it is possible to decrease the column length and analysis time. By reducing the

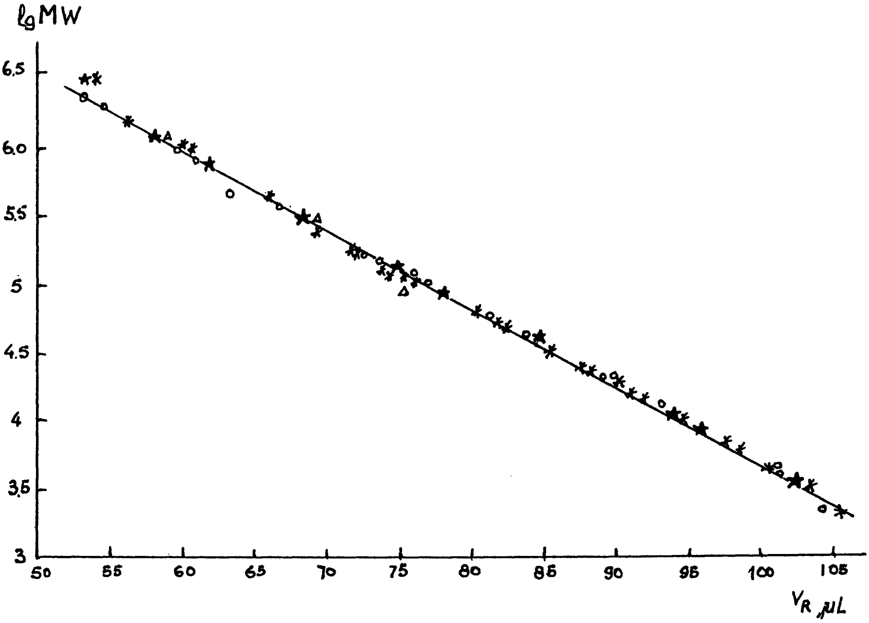

Figure 5. Calibration dependence of V_R on *lg MW* for PS standards obtained on a column 730 mm x 0.5 mm i.d. (N = 35,000 plates) packed with a mixture of Nucleosil silicagels with a linear molecular weight calibration dependence .

Conditions: ethyl methyl ketone eluent; 3 μL/min flow rate; PS standards were from the Institute of Macromolecular Compounds, Academy of Sciences of the USSR (*), Waters Associates (0), Altex (Δ), and Polymer Laboratories (★).

The MW of PS lots were: (1) 3,000 K (Δ, N 902-64), (2) 2,950 K (★, N 20145-1) , (3) 2,300 K (o, N 61970), (4) 1,987 K (o, N 61970), 5) 1,130 K (★, N 20141-1), (6) 1,000 K (Δ, N 902-63), (7) 830 K (o, N 25167), (8) 655K (o, N 25167), (9) 675 K (★, N 29140-1), (10) 451 K (o, N 25166), (11) 402 K (o, N 25166), (12) 370 K (★, N 20138-1), (13) 300K (Δ, N 902-62), (14) 196K(o, N 41984), (15) 171 K (o, N 41984), (16) 120 K (★, N 20135-7), (17) 100 K (Δ, N 902-61), (18) 11 K (o, 41955), (19) 97.2 K (o, N 41995), (20) 68 K (★, N 20134-1), (21) 50 K (o, N 25170), (22) 34.5 K (o, N 25170), (23) 34.5 K (o, N 902-60), (24) 34.5 K (★, N 20132-2), (25) 20.5 K(o, N 25168), (26) 19.75 K (o, N 25168), (27) 9.8 K (o, N 25171), (28) 10 K (o, N 25171), (29) 9.4 K (★, N 20129-1), (30) 7.6 K (★, N 20128-1), (31) 4.8 K (o, N 25169), (32) 3.55 K (o, N 25169), (33) 3.1 K (★, N 20126), (34) 2.0125 K (o, N 61971).

(Adapted from ref. 4)

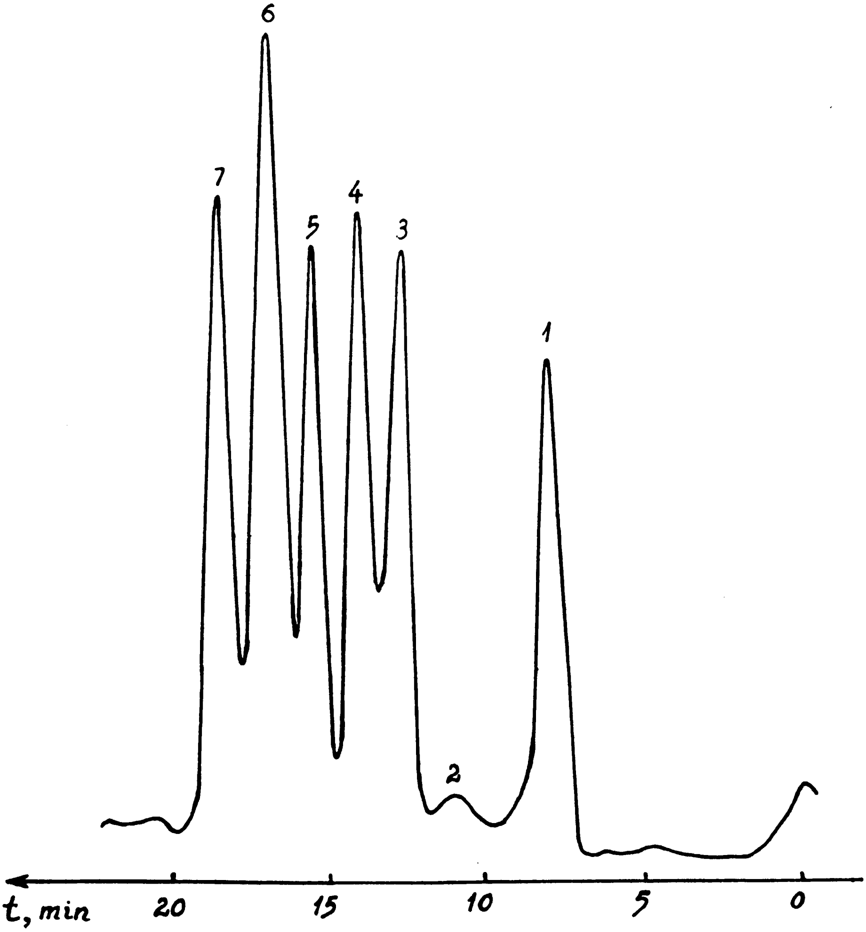

Figure 6. MSEC of proteins on a 300-mm x 0.5 -mm i.d. column (N = 10,000 plates).

Conditions: TSK - 3,000 SW sorbent, *dp* = 10 µm, additionally treated with glycidyl - propyltrimethxysilan; pH = 6.8 , phosphate buffer , 0.2 M NaCl eluent. Peak identifications: (1) Thyroglobuline (MW = $6*10^5$ Da), (2) BSA-dimer ($1.3*10^5$ Da, MW = 1.36 $*10^4$ Da), (3) BSA (MW= $6.5*10^4$ Da), (4) ovalbumin (MW = $4.5*10^4$ Da), (5) carboanhydrase (2.9*10 Da), (6) cytochrom C ($1.25*10^4$ Da), (7) glycine.
(Adapted from ref. 4)

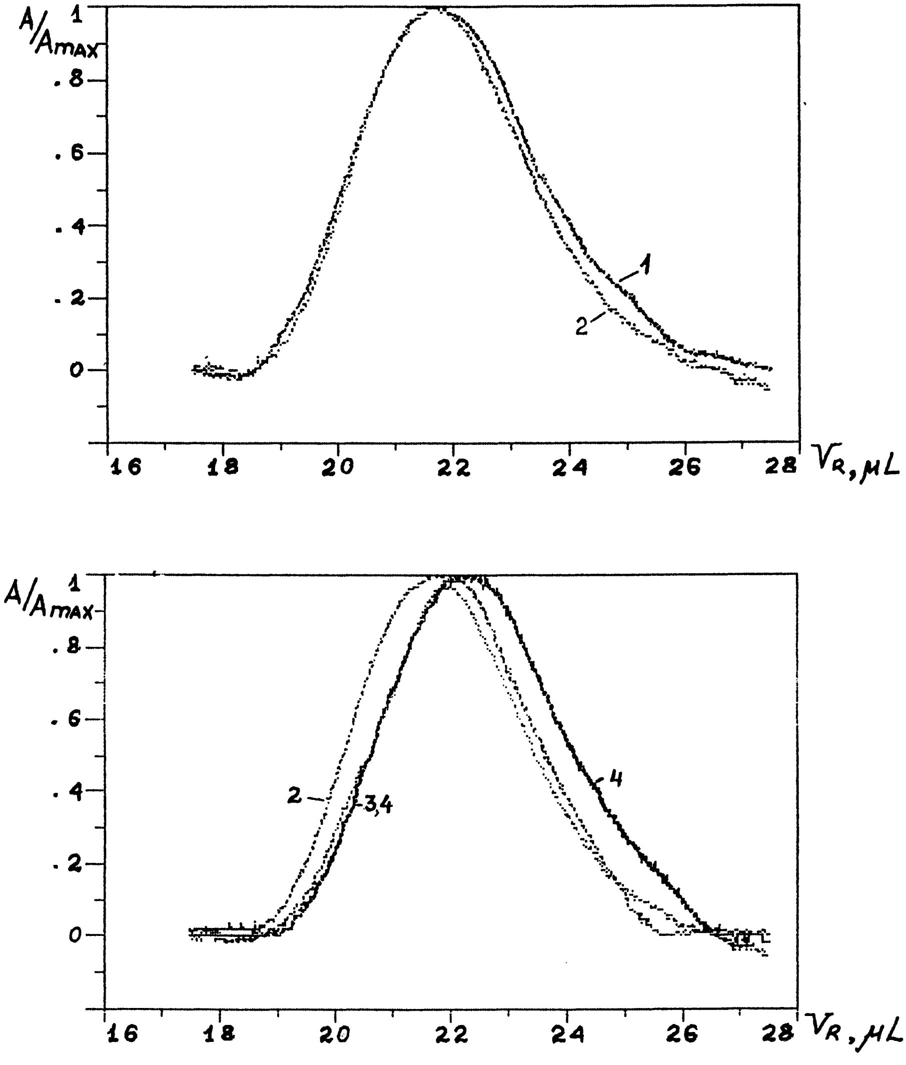

Figure 7. MSEC of polyamide fibers in hexafluoroisopropanol with sodium trifluoroacetate.

Conditions: 350-mm x 0.5-mm i.d. column; mixture of 5-μm Nucleosil silica gels; 2.5 μL/min elution rate. Peak identifications: (1) sample from the place of the crime (a rope from corpse that has been lying in water for six months), (2) sample found in the possession of the suspected person, (3, 4) sample from a collection.

(Adapted from ref. 4)

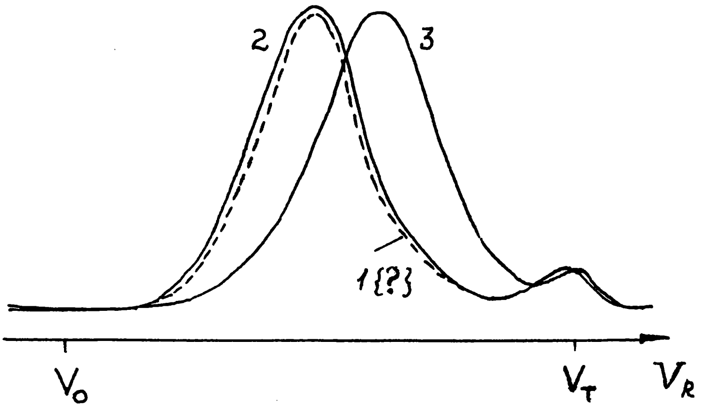

Figure 8. MSEC of polyethylene terephthalate fibers in trifluoroacetic acid.

Conditions: 350-mm x 0.5-mm i.d. column; 5-μm particles; 3 μL/min elution rate. Peak identifications: (1) fiber from a shirt (7μg) found at the place of the crime. (2 and 3) samples identificated with fiber 1. (Adapted from ref. 4)

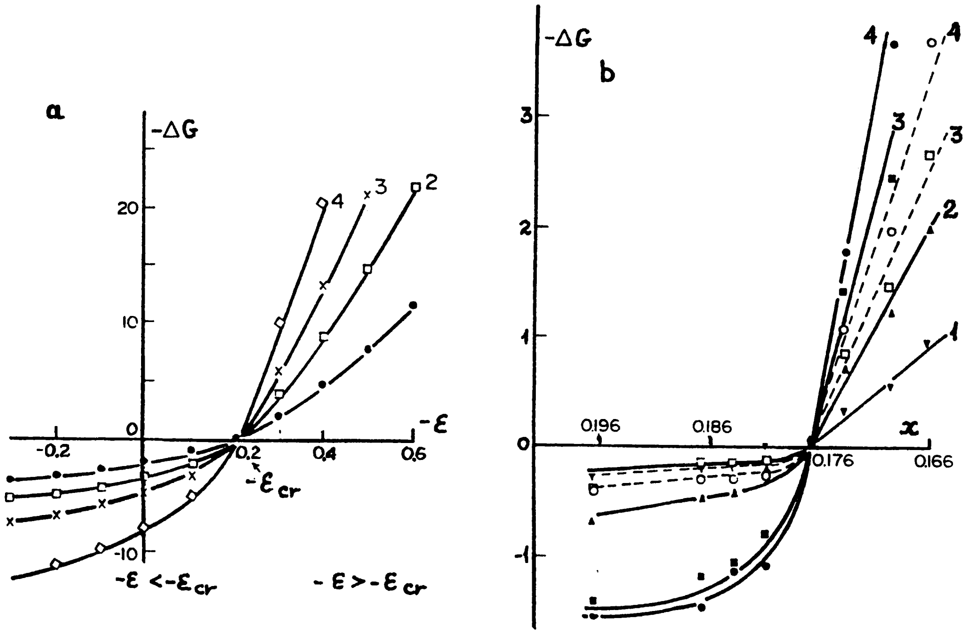

Figure 9. Value of $-\Delta G$ of the macromolecule when it enters the pore: (a) vs $-\varepsilon$ for model chains in a slit with a width of 5 with N = 40 (1), 80 (2), 120 (3), 200 (4); (b) vs volume fraction of acetone (x) in pores of KSK silica gel with D ≡100 A(1-4) and silochrome S-80 with D ≡500 A (3',4') for PS with MW*10^{-4} : 1.98 (1), 5.1 (2), 11.1 (3, 3'), 17.3 (4,4'). (Reproduced with permission from reference 38. Copyright 1978 Elsevier Science, Ltd.)

pressure it is also possible to considerably increase the column efficiency, which is particularly important in oligomer analysis.

"Critical" chromatography of polymers

The development of polymer chromatography was accompanied by establishment of universal dependencies of retention volumes V_R on macromolecule gyration radius, $R \sim \eta M$, where η is the intrinsic viscosity, M - molecular weight of polymer, and pore size (halfwidth -pore radius, d): for single sorbent (d = const) - the Benoit experimental dependence $V_R(R)$ (*33*) and for different sorbents - theoretical dependence established by Casassa (*34*) and confirmed by many experimentators $V_R(g)$, where $g = R/d$.

The establishment of the single mechanism of exclusion and adsorption chromatography of macromolecules is an outstanding achievement of polymer chromatography (*2,35-39*). The main features of unified mechanism of size-exclusion and adsorption chromatography of macromolecules on porous adsorbents are:

1. A behavior of macromolecules in adsorption (interaction) chromatography on the porous adsorbent depends on the value of interaction energy with the pore surface.
2. The critical value, $-\varepsilon = -\varepsilon_{cr}$, at which the Gibbs energy of adsorption $-\Delta G = 0$ and can be observed experimentally (first by B. Belenkii at al (*35*)).
3. The ratio of ε to ε_{cr} determines the mutual influences of size-exclusion and adsorption interaction of macromolecules with porous adsorbent.

In Figure 9 the dependencies of $-\Delta G$ vs $-\varepsilon$ for the chromatography of model chains in a slit are plotted for various volume fractions of acetone. A porous sorbent was used. When $-\varepsilon < -\varepsilon_{cr}$ a SEC mechanism operates. SE -effects are controlled by adsorption: the greater $-\varepsilon$ the less the SE-effect. At $\varepsilon = -\varepsilon_{cr}$ the SE-effect and adsorption effect are mutually compensated ($-\Delta G = 0$) and the macromolecules of all masses have the same distribution coefficient $Kd = 1$. This is "critical" chromatography at which the macromolecules are "chromatographically invisible" and all elute at the same rate. When $-\varepsilon > -\varepsilon_{cr}$ one operates under adsorption chromatography.

The single mechanism of exclusion and adsorption chromatography permits to propose the universal one-parametric dependence (*36*):

$$Q = (K - Ksec)/(1 - Ksec) = \pi/2\, \Gamma^{-1} \{ 1 - Y(\Gamma) \} \qquad (10)$$

where

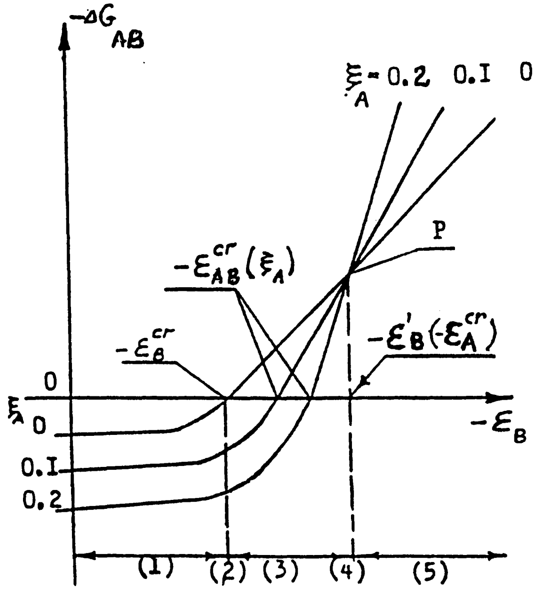

Figure 10. The "critical" chromatography of block-copolymer "AB": Gibbs energy of AB adsorption ($-\Delta G_{AB}$) vs energy of interaction of a segment of block B with the adsorbent surface ($-\varepsilon_B$). (1) SEC of AB, (2) "critical" on B, (3) "pre-critical" on A, (4) "critical" on A, (5) "near-critical" on A. (Adapted from ref. 40)

$$Y(\Gamma) = exp\,(\Gamma^2)\,\{1 - erf\,(\Gamma)\} \tag{11}$$

Here $\Gamma = -R/H$, where H is a dimensionless adsorption correlation length, $erf\,(\Gamma)$ is a probability integral. The dependence $Q(\Gamma)$ is correct for precritical (from genuine SEC to "critical" chromatography at $-\varepsilon = -\varepsilon_{cr}$), "critical" and adsorption chromatography ($-\varepsilon > -\varepsilon_{cr}$). The adsorption correlation length, H, determines a "near-wall" layer thickness of macromolecule. In adsorption area H is positive and decreases with incresing $(-\varepsilon)$. Under critical conditions H is infinitely large. In the precritical area H is negative and decreases with decreasing $(-\varepsilon)$. In SEC area $(-\varepsilon$ is infinitely large, H is infinitesimal) the $Q(\Gamma)$ transforms to Casassa dependence.

In the case of heteropolymers under "critical" conditions one part of macromolecule (the main chain of oligomer or one block of a block-copolymer) becomes chromatographically "invisible" (when -ΔG of the heteropolymer does not depend on the MW of one of its parts). The "critical" conditions permit us to characterize the functionalities of oligomers, their MWD, the MWD of any block and, therefore, the composition inhomogeneity of block-copolymers.

Let us consider this phenomenon taking "AB" block-copolymer as an example (*40*). Figure 10 shows the dependence of Gibbs energy $(-\Delta G)$ of a block-copolymer on the energy of interaction between macromolecular segments and the adsorbent surface $-\varepsilon_B$ (under conditions when M_B = const). This dependence is based on fact that the Gibbs energy of adsorption of block-copolymer AB $(-\Delta G_{AB})$ is sum of Gibbs adsorption energies of block A $(-\Delta G_A)$ and block B $(-\Delta G_B)$:

$$(-\Delta G_{AB}) = (-\Delta G_A) + (-\Delta G_B) \tag{12}$$

One can see that the character of this dependence modifies passing through five zones of $-\varepsilon_B$ thus ensuring the following chromatographic modes:

1. SEC of block-copolymers $(-\varepsilon_{AB} < -\varepsilon_{ABcr})$;
2. "critical" chromatography for the block B $(-\varepsilon_B = -\varepsilon_{Bcr}, -\varepsilon_A < -\varepsilon_{Acr})$;
3. "pre-critical" chromatography for the block A $(-\varepsilon_B > -\varepsilon_{Bcr}, -\varepsilon_A < -\varepsilon_{Acr})$;
4. "critical" chromatography for the block A $(-\varepsilon'_B = -\varepsilon_B > -\varepsilon_{Bcr}, -\varepsilon_A = -\varepsilon_{Acr})$;
5. "near-critical" chromatography for the block A $(-\varepsilon_B > -\varepsilon_{Bcr}, -\varepsilon_A > -\varepsilon_{Acr})$.

The MWD and composition inhomogeneity of block-copolymers can be determined by mode (2), corresponding to the "critical" hromatography for a more "sticky" block B and SEC for block A. Inthis case the block B is chromatographically "invisible". That permits us to determine precisely the

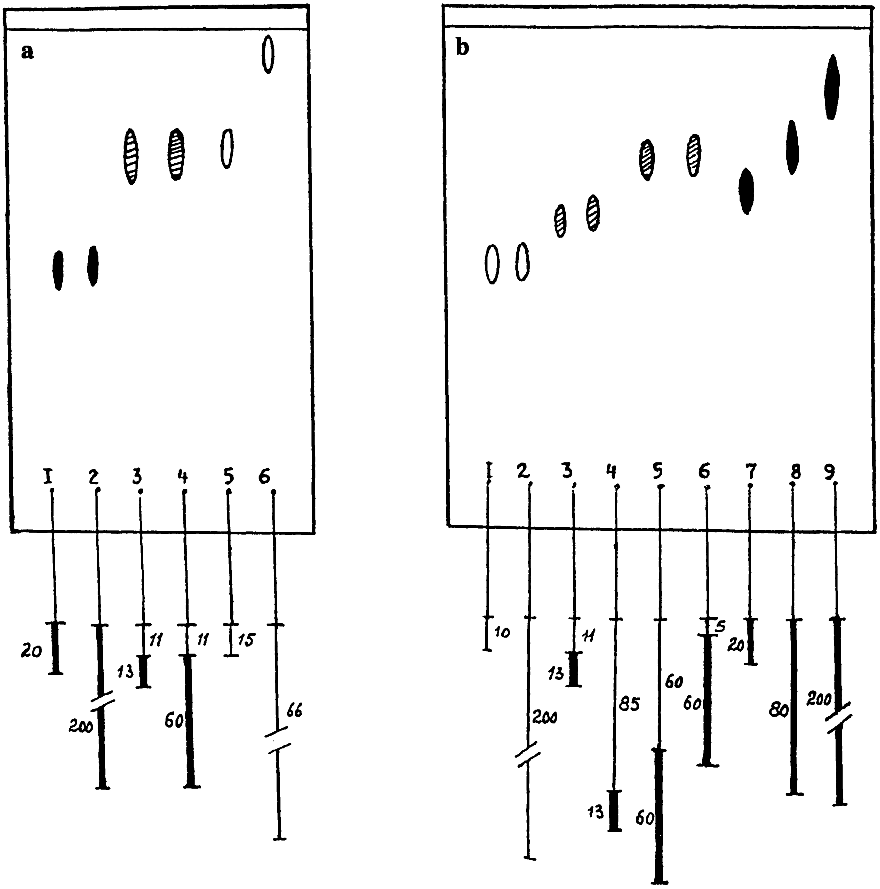
a
1
2
3
4
5
6
20
200
13
11
11
60
15
66
b
1
2
3
4
5
6
7
8
9
10
200
13
11
85
13
60
60
60
5
20
80
200

Figure 11. The determination of the MWD for one of the block (A,B) of block-copolymer AB by SEC in critical conditions for more stcky block : (a) $-\varepsilon_{Bcr} > -\varepsilon_{Acr}$: "critical" on B, $-\Delta G_B = 0$, SEC of A, $-\Delta G_A = -T\Delta S$; MWD of A (in system "cyclohexan-toluene-MEK" 9:1:2.3) ; (b) $-\varepsilon_{A\,cr} > -\varepsilon_{B\,cr}$: "critical" on A, $-\Delta G_A = 0$, SEC of B, $-\Delta G_B = -T\Delta S$; MWD of B (in system "cyclohexan-toluene-MEK-Pyr" 9:0.4:0.4:4). Samples: 0, —— PS; ●, ▬ Pt-BMA; ⊜ - AB.
(Adapted from ref. 40)

MWD of block A with the aid of SEC. It is always possible to change the chromatographic system in such a way that block B becomes more "sticky". Then using the mode of chromatography which is "critical" to the more "sticky" block (now the block A) one can determine the MWD of block B by SEC, as is shown in Figure 11. In this figure the thin-layer chromatograms of P-tret-BMA-PS block-copolymers are presented. The length of solid and thin lines corresponds to the MW of P-tret-BMA and PS-blocks.

The preparative fractionation of block-copolymers according to the MW of blocks can be carried out by chromatography in regime (2) as well as in regime (4). At the same time, regime (4) corresponding to a definite MW of "sticky" block does not make it possible to distinguish this block-copolymer according to the block A length. This regime can be applied, for example, for fractionation of block-copolymer with a fixed length of block B and any length of the block A according to the number of functional groups. Figure 12 shows the heteropolymer types which can be separated according to the MW of theirs parts or functional groups number of oligomers by chromatography under "critical" conditions (*41*). The optimal conditions of this preparative fractionation will be shown further. Interesting examples of critical chromatography applications to two-dimensional separation of oligomers (according to MW, functionality, block size of block-copolymers) are shown in articles (*42*, *43*).

TLC of polymers and oligomers

The possibilities of adsorption (interactive) macromolecular chromatography are remarkably great for fine polymer fractionation and their polydispersity analysis according to chemical structure and MW, and the determination of high-MW and low-MW admixtures in polymers. At the same time the adsorption chromatography is difficult to realize in the column mode (HPLC) because adsorption activity conditioning for hydrophilic sorbents (silica gel) in chromatographic columns is difficult. Hence, in HPLC adsorption is mainly realized, not in normal-phase chromatography with silica gel sor bent, but rather in reverse-phase chromatography where, because of sorbent hydrophobicity, the achievement of column sorbtion characteristics is easier. There is one factor which limits the employment of a universal polymer analysis method: gradient adsorption chromatography. Hence, it is necessary to use the columns optimized with respect of length. This has led to the development of high-performance membrane chromatography (HPMC) of polymers (see next Part of the present paper).

The solution to the problem was found in the employment of a thin-layer variant of adsorption polymer chromatography proposed by X. Inagaki (*44*), B. Belenkii and E. Gankina (*45*) for the analysis of copolymer polydispersity. Examples of TLC applications for polymer analysis have been des-

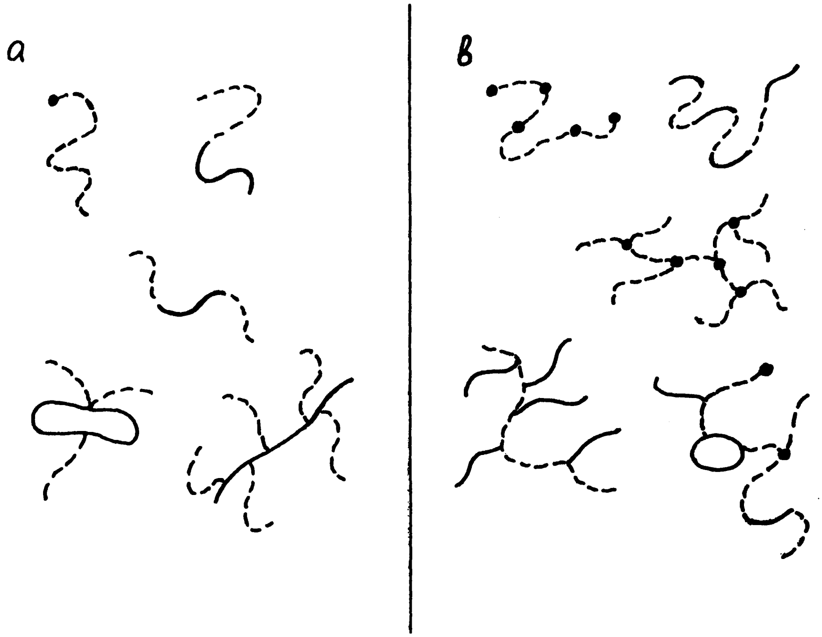

Figure 12. Types of macromolecules for which the "invisibles" method is precise : (a) for any pores, (b) only on adsorbents with narrow pores; (-----) "invisible" components under critical conditions.

cribed in (*2,10*). TLC is an old method for chromatographic analysis, which has been intensively developed over the past few years. As was stated by K. Unger: " At present there is renaissance of the more than 30-years-old microanalytical method of TLC". Growth in the interest in TLC over the past few years is the result of improved instrumentation and automation which have raised the precision of TLC and created new technical possibilities:

1. new separation techniques: gradient and forced flow systems;
2. microprocessor - controlled coupling procedures with spectrometric methods: TLC-UV-VIS, TLC-FTIR, TLC-Raman, TLC-NMR, TLC-MS;
3. "on-line" combination of LC-methods: TLC-HPLC, TLC-SAC.

New possibilities for classic TLC, as compared with the modern mode of TLC - HPTLC (high-performance TLC), are shown in Table II. HPTLC opens new possibilities for polymer TLC-analysis. The distinguishing features of polymer HPTLC are the following:

1. The TLC of polymers is the most simple and effective mode of realizing adsorption (interactive) chromatography of macromolecules . Special TLC-plates without binder (*46*) permit one to realize the true interaction between the polymer and the sorbent inner surface and to use, for detection, any reagent including corrosive ones. For example, the sulfuric acid with potassium permanganate is a universal reagent for polymer detection.
2. The possibility of using the adsorption mode of chromatography with cheap thin-layer plates, conditioning or thermostatting.
3. The realization of gradient conditions by using polyzonal TLC with a frontal separation multicomponent eluent according to the plate length and also other methods based on the eluent composition programming.
4. The realization of two-dimensional chromatography by consecutive immersion of TLC-plate into two eluents (with turning the plate by 90 °C and intermediate drying).
5. The possibility for simultaneous chromatography of several (~10) polymer samples. This essentially facilitates and simplifies the comparison of their chromatographic behavior with that of standards and significantly increases analysis productivity.
6. The possibility of exposing all components of the sample since the whole TLC-plate, from the start (*R_f = 0*) to eluent moving boundary (*R_f = 1*), is available for detection and observation. The main features of polymer TLC are shown in more detail in the Table III.

At the same time, TLC is not as good as HPLC with respect to a number of parameters :

1. difficulty of quantitative analysis (HPLC is an "on line" method, TLC is an "off line" method);
2. difficulty of fraction collection;
3. imprecision of *R_f*- determination (unsufficient precision is compensated

Table II. Thin - Layer Chromatography

Classical mode (TLC)

1. Very cheap universal semiquantitative analytical method.
2. Identification by reference samples.
3. Manual procedure with use of precoated layers, simple equipment, pre- and post-chromatographic microchemical detection methods.

Modern mode (HPTLC)

1. A precision quantitative method for parallel analysis many simple mixtures (the hardware cost is about the same as for HPLC).
2. Relatively low analytical cost - up to 10 samples can be separated on one TLC-plate with the aid of a few milliliters of mobile phase.
3. The high selectivity of HPTLC is the result of chromatographic separation, detection, and identification by microchemical and "on-line" spectrometric methods.
4. Instrumentation and automation of sample application and development as a method of error reducing and analysis acceleration (70 times faster than HPLC of one sample).

Table III. Main Features of Polymer TLC

1. The possibility of obtaining independent separation of macromolecules according to only type of polydispersity.

2. Unified mechanizm of size-exclusion TLC (SETLC) and adsorption TLC (ATLC) of polymers.

3. The slow kinetics of adsorption - desorption and low diffusion coefficient of macromolecules demand of special size of TLC- plates: Lopt = 5 cm, dopt = 5 mm.

4. The slow dissolution of polymers at the starting zones in TLC leads to tailing spots on the plate. A Decrease of dp and increase of starting zones distance suppresses the tailing.

5. The viscosity effect in SETLC leads to the deformation and rupture of the polymer zones. This effect may be used for determination of intrinsic viscosity [h]. The mechanism of this phenomenon is similar to that of destruction of oil and water boundaries at water encroachment of oil bore holes.

6. TLC polymers methods are based on the types and values of interaction energies of macromolecules with the surface of pores and the solvent: SETLC - ATLC (including CrTLC) and dissolution - precipitation TLC (PTLC).

Table IV. HPLC and TLC (HPTLC) (Possibilities)

N	*Description*	*HPLC*	*TLC, HPTLC*
1.	Throughput (number of samples per unit time)	1	10 (HPTLC)
2.	Requirements to cleanliness of samples and purity of solvent	high	low
3.	Detection:		
	Versatility	medium	high
	Sensitivity	high	less than HPLC
	Masking effect (solvent influence)	medium	low
4.	Cost of:		
	Equipment	high	TLC - low HPTLC - high
	Solvent	high	low
	Labour (scientist qualification)	medium	high
5.	Automation possibility	good	medium
6.	Number of components in sample	large	medium large (AMD)
7.	Development versatility	high (SEC,RP,IE)	medium (Ads.)
8.	Possibility of two-dimensional chromatography	poor	good
9.	Prestigiousness of technique	high	medium

In Strategies in Size Exclusion Chromatography; Potschka, M., et al.;
ACS Symposium Series; American Chemical Society: Washington, DC, 1996.

in TLC by parallel chromatography of samples, including polymer standards);

4. complexity, and sometimes impossibility, of using several detectors "on line" for absolute determination of MW (for example, MALLS- detector);
5. complexity of realization of TLC in the SEC-regime (SETLC). For this the preliminary filling of sorbent pores by solvents is required and this unfortunately stops the capillary force action, causing eluent to move along the plate. In the dry plates polymers with $K_d < 1$ move with the eluent front, but in filling sorbent pores the eluent front velocity decreases by $(1+V_p/V_0)$. As the result, R_f of the such polymer is corresponded to SEC with $K_d = 1$.

For the realization of SETLC the following methods have been used (*10*):

1. Preliminary moistening of the plate with solvent.
2. Exposure of the plate to saturated eluent vapors.
3. Employment of over-pressured layer chromatography - OPLC (method similar in realization to HPLC).

These methods (excluding OPLC) exhibit unsatisfactory reproducibility and fractionation selectivity. The latter is the result of the polymer spots distribution by SEC on the less than half of a plate (from $R_f > 0.5$ to $R_f = 1$). This is a too short distance for SEC on the plate length of 10 cm. The comparison of TLC and HPLC is shown in the Table IV.

Therefore, the polymer TLC is inexpensive, convenient, high-informative, owing to the possibilities of the adsorption ("critical") chromatography method of polymer analysis. This method is remarkable by its high productivity, ease of realization of the two-dimensional chromatography and the possibility of comparing the samples with standards. At the same time TLC of polymers is a predominantly qualitative method for determination of purity, inhomogeneity (polydispersity according to MW and chemical composition for copolymers, functionality and MWD for oligomers).

For practical applications of polymer TLC it is necessary to have polymer standards. The latter is now simplified by employment of SEC- MALLS and MALDI -methods permitting preparation of standards of homopolymers, copolymers, and oligomers naturally in laboratories. At the same time, the TLC of polymers is a convenient method for teaching students the concepts of polymer polydispersity.

Figures 13-19 show examples of TLC application to polymer analysis: for the determination of MWD of homopolymers, copolymers and oligomers, the compositional inhomogeneity of random and block-copolymers, the functionality of oligomers, and the purity of copolymers. Figure 13 shows the separation of PS according to MW from oligomers to high polymers. In Figure 14 the changing modes of PS TLC - from the adsorption one to size-exclusion at changing eluent composition are shown: (a) and (b) - adsorption TLC; (c) - "critical" TLC (the independence of R_f from PS MW); (d), (e)

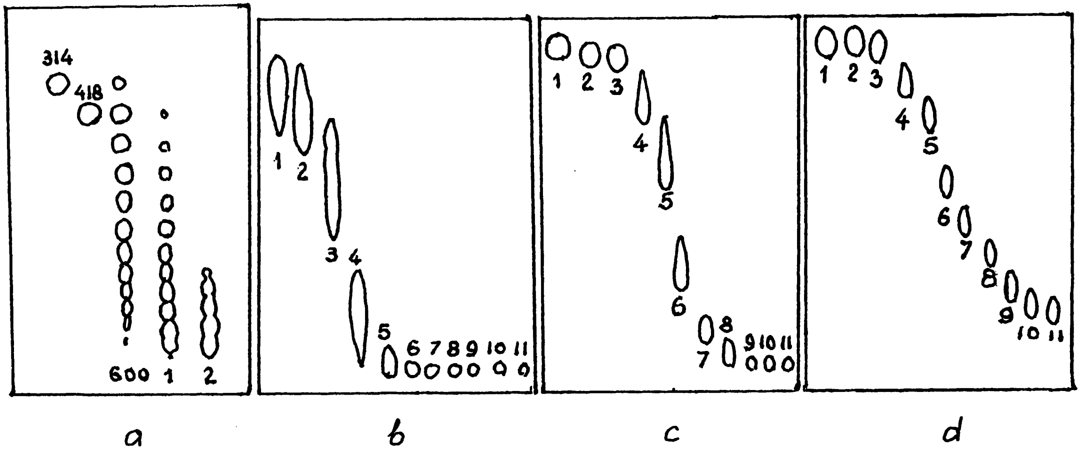

Figure 13. TLC of PS samples with narrow dispersity (MW/Mn 1.2) in systems cyclohexane-benzene-acetone (a) 14:3:0; (b) 13:3:0.1; (c) 12:4:0.4; (d) 12:4:0.7. PS samples: 314-PS-trimer and 418-tetramer, 600-PS with Mn = 600, 1 (Mn = 900), 2 (Mn= $2.3*10^3$), 3 (MW =$5*10^3$, Mn = $4.5*10^3$), 4 (MW =$10.3*10^3$, Mn = $9.7*10^3$), 5 (MW = $1.985*10^4$, Mn = $1.965*10^4$), 6 (MW = $5.1*10^4$, Mn = $4.9*10^4$), 7 (MW = $9.82*10^3$, Mn = $9.62*10^4$), 8 (MW = $1.73*10^5$, Mn =$1.64*10^5$), 9 (MW =$4.11*10^5$, Mn=$3.92*10^5$), 10 (MW =$8.67*10^5$, Mn =$7.73*10^5$), 11 (MW=$2.145*10^6$, Mn = $1.78*10^6$).
(Adapted from ref. 10)

In Strategies in Size Exclusion Chromatography; Potschka, M., et al.;
ACS Symposium Series; American Chemical Society: Washington, DC, 1996.

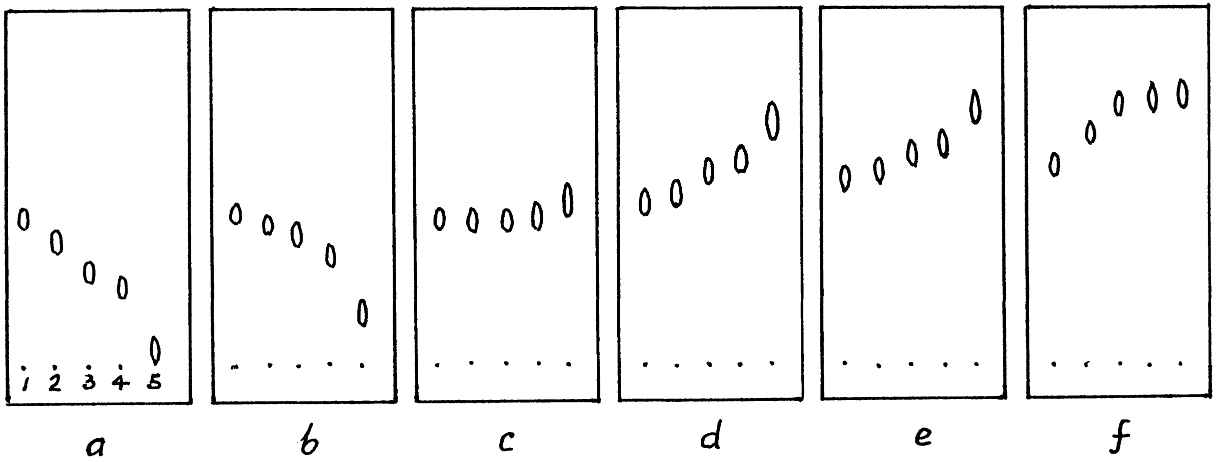

Figure 14. TLC of PS 5-9 (left to right) (see Figure 13) on KSK silica gel in a cyclohexane-benzene-acetone system (40 : 16: γ) where γ is 1.5 (a), 1.8 (b), 2 (c), 2.2 (d), 2.5 (e), 2.8 (f) with preliminary plate saturation for 2 hr.
(Adapted from ref. 10)

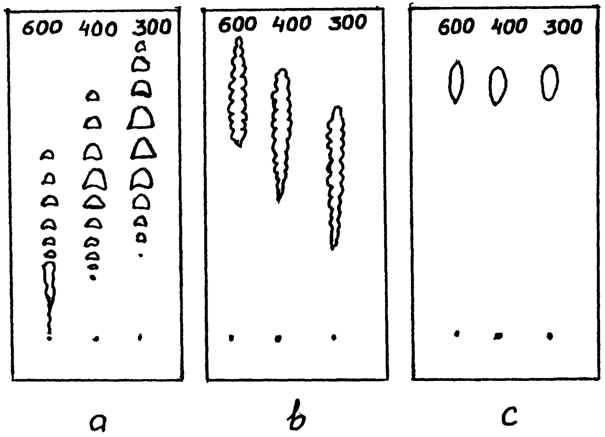

Figure 15. TLC of oligomers : (a) TLC of polyoxyethylene with Mn = 300, 400 and 600 on KSK silica gel in pyridine-water (0.1: 10); (b) the same on aluminium oxide in chloroform-ethanol (10:1); (c) the same on KSK silica gel in chloroform-pyridine (5:7).
(Adapted from ref. 10)

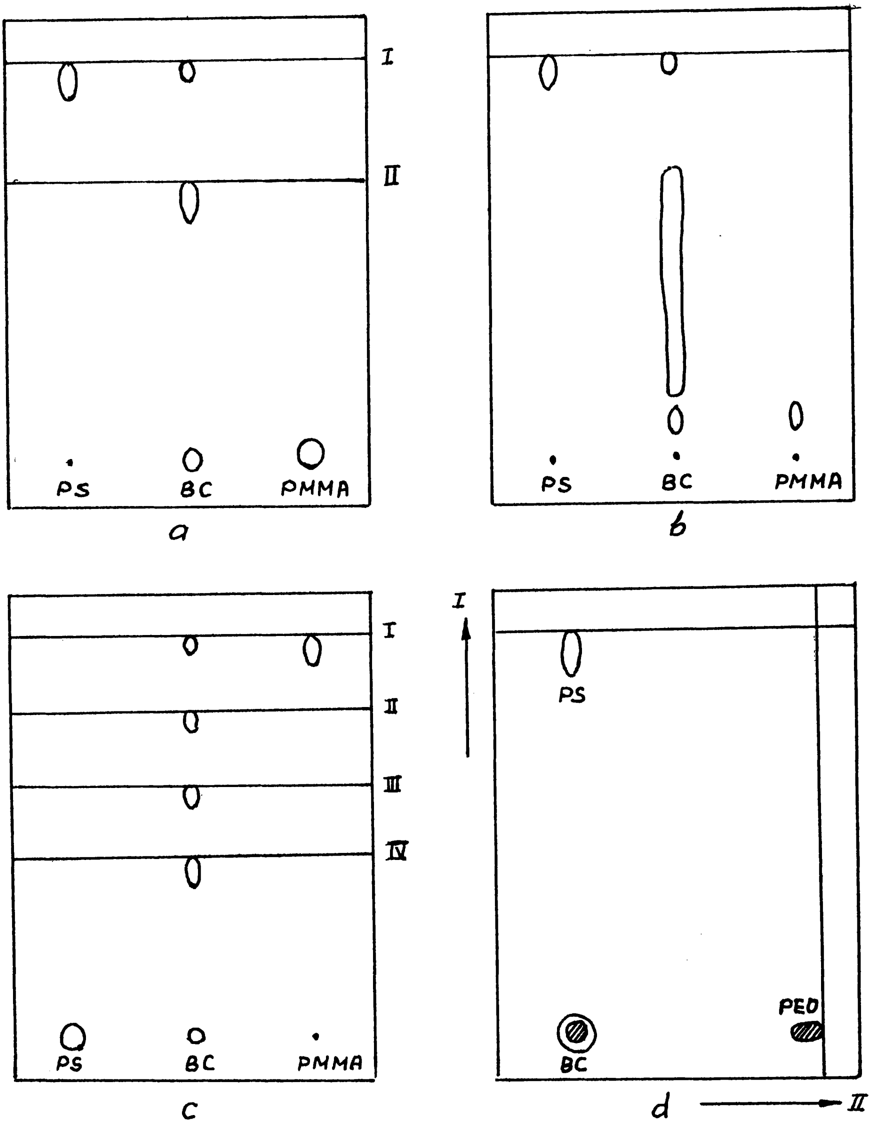

Figure 16. TLC of block-copolymers: (a) Step wise TLC of PS-PMMA BC (eluent fronts are for (I) benzene, (II) chloroform- MEK (6:3)); (b) Gradient TLC of PS-PMMA BC (chloroform-MEK (6:1) with the addition of 6 ml MEK for 12 min); (c) Multistage stepwise TLC of PS-PMMA BC:(I) acetone with 50% methanol, (II) 40%, (III) 30% , (IV) 20%); (d) Two-dimensional TLC of PS-PEO BC in benzene (direction I) and pyridine-water (3:9) (direction II); MW: PS - 1.11•10^5 Da, PMMA - 4.0•10^4 , PEO - 1•10^5 . (Adapted from ref. 10)

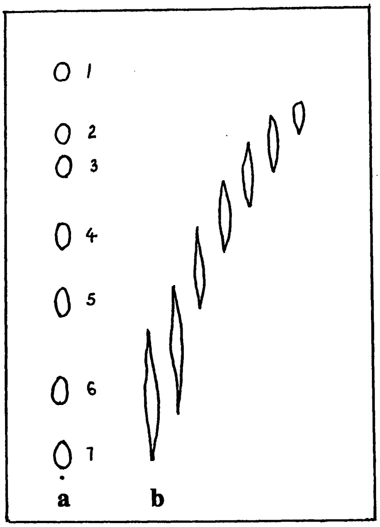

Figure 17. Gradient adsorption TLC of random copolymers : (a) Styrene/acrylonitrile (54), (b) vinyl chloride/vinyl acetate (56).
Eluents: (a) from methylenechlorid - CCl_4 (5:1) to acetonitril (3); (b) from dichloromethane - CCl_4 (3:3) to dichloromethane-MEK (5:2);
(a) 1-7 samples with 4.5, 12.2, 18.7, 25.4, 31, 37.4, 49.7 % of acrylonitrile; (b) 1-7 (from left to right) samples with 28, 24, 25, 10, 10, 7.5, 6 and 0% of vinyl acetate.
(Adapted from ref. 10)

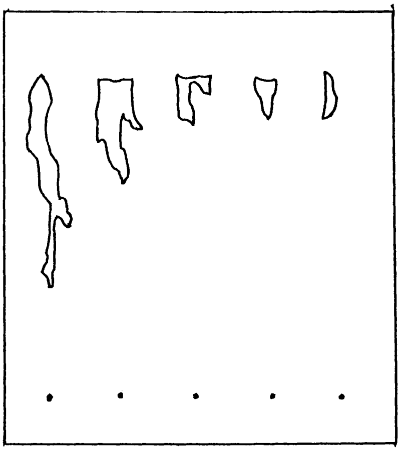

Figure 18. TLC of PS with MW =$2 \cdot 10^5$ in toluene. The amount of sample (from left to right): 30, 20, 15, 10, 5, and 0.25 µg .
(Adapted from ref. 10)

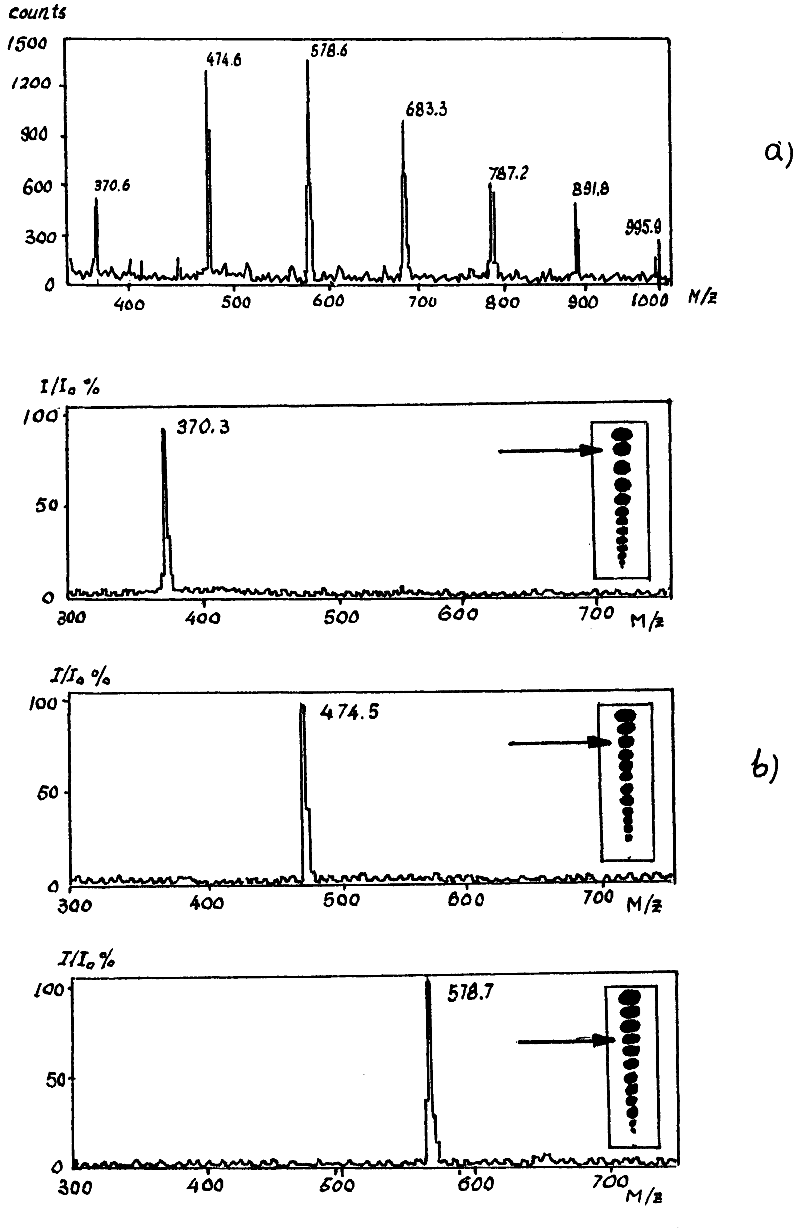

Figure 19. TLC and mass spectrometry with ionization by ^{252}Cf Fission fragments in the investigationof the molecular weight distribution of oligomers. (a) mass spectrum of positive ions from PS with *Mp* =480 at an accelerating voltage of + 20 kV; (b) mass spectra of oligomerhomologs (shown by arrow on the chromatogram) of PS with *Mp* = 580 at an accelerating voltage of + 25 kV.
(Adapted from ref. 48)

Table V. Applications of Polymer TLC Analysis

Homopolymers

1. Determination of MWD and M
2. Microstructure analysis
2.1. Stereoregularity
2.2. Geometric isomers (cis - trans, "head to head" ets)
2.3. Isotops composition
2.4. Functional group contents
2.5. Branching

Copolymers

1. Statistic copolymers (compositional inhomogeneity)
2. Block-copolymers
2.1. Identification (diagnostics) and determination of purity
2.2. Compositional inhomogeneity
2.3. Combination with hydrolysis and ozonolysis
3. Graft-copolymers (combination with hydrolysis)

Olygomers

1. Determination of distribution according to types of functionality
2. Determination of MWD (including determination for each type of functionality)
3. Absolute determination of MWD by combination with NMR and MS (MALDI TOF MS)

Viscosity effect investigation

1. Boundary stability of polymer solution zones (in correlation with the problem of water encroachment of oil bore holes)
2. Determination of intrinsic viscosity [η]

and (f) - SETLC. Figure 15 shows TLC of oligomers. There are three variants of polyoxyethylene chromatograms with OH-end groups: with positive *Rf*-dependenceon MW (a), negative *Rf*-dependence on MW (b), and without *Rf*-dependence on MW (c). The last figure demonstrates "invisible" (from MW) TLC of polymers. The "invisible" TLC permits one to determine the functionality of oligomers and the MWD of each functional groop. One of the main applications of polymer TLC is in the diagnosis of block-copolymers (BC), i.e. obtaining the answer to the question: whether a sample is a mixture of homopolymers or BC, and determining BC-purity (existence or absence of homopolymers corresponding to BC-blocks). Figure 16 shows examples of similar TLC-diagnosis by one-dimensional and two-dimensional TLC by means of comparison of *Rf* for polymer impurities and polymer standards. It is necessary to note the excellent possibility of copolymer fractionation according to their chemical composition (for the determination of random copolymer inhomogeneity), as shown in Figure 17. SETLC is a convenient method for the investigation of spot form and polymer solution boundary stability (the chromatographic spot) as function of polymer solution concentration and intrinsic viscosity *(η)* of the polymer (Figure 18). This phenomenon has a direct relationship to the investigation of oil extraction with water encroachment of bore holes. TLC permits one to make an experimental model of this process with the goal of selecting the optimal type of polymer and its concentration for water-polymer encroachment of boreholes. A very interesting example of the absolute determination of oligomer MW by combination of TLC and mass-spectroscopy is demonstrated in Figure 19. The complete applications of polymer TLC analysis is shown in Table V.

High-performance membrane chromatography of polymers

Liquid chromatography and membrane technology are the main methods for the isolation and purification of polymers and biopolymers. Membrane technologies are distinguished by high productivity, ease of scale-up, and low operating costs. They operate at low pressure but are characterized by low separating capacity (number of resolved peaks). On the other hand, modern HPLC displays high efficiency and selectivity. However, applications of high pressure in HPLC (up to 50.0 MPa) requires expensive instrumentation and makes scale-up difficult since gun technology should be used in the manufacture of preparative HPLC-columns. Nevertheless, membrane technology and HPLC do not compete for use in the different stages of biopolymer isolation and purification.

It is of considerable interest to increase the separation capacity of membrane technology to the HPLC level. This would enable us to unite in a

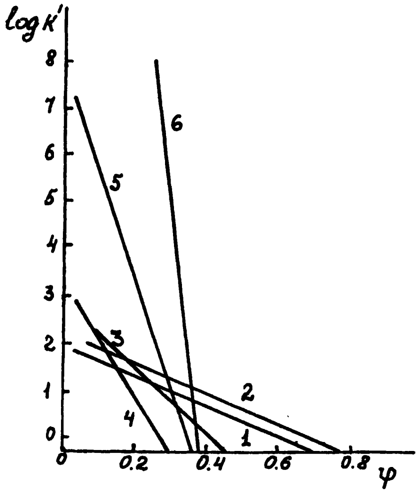

Figure 20. *Log k'* **as function of displacer concentration ϕ at RP-chromatography. (1) benzene (M= 78 Da, S= 2.87, Log kw =1.85) , (2) toluene 92, 3.12, 2.21), (3) (Tyr)3 (500, 6.8, 2.97), (4) Leu-enkephaline (600, 11.3, 3.18), (5) Insuline (6000, 22.7, 7.87), (6) BSA (69000, 64.7, 24.5).** (Reproduced with permission from reference 53. Copyright 1993 Elsevier Science, Ltd.)

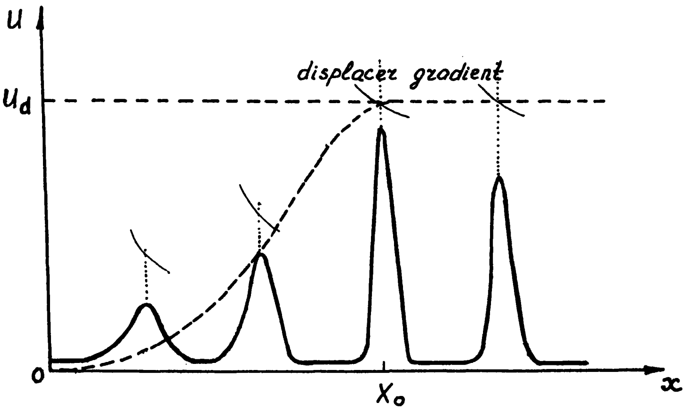

Figure 21. The changes of elution rate and chromatographic peak shape on column length.

(Reproduced with permission from reference 53. Copyright 1993 Elsevier Science, Ltd.)

single "hyphenated" method with the advantages of HPLC: high selectivity and efficiency and those of membrane technology: operation at low pressure and ease of scale-up. This problem was solved for proteins by the optimization of gradient chromatography (with eluent composition programming) according to the column length. On this basis, a new separation method was developed : high performance membrane chromatography, HPMC (*49-55*).

The principal feature of the adsorption of macromolecules is the extremely strong dependence of the adsorption coefficient (distribution coefficient - *Kd*) on the displacer concentration (Figure 20). As a result of this feature the transition from strong adsorption ($Kd > 100$) to full desorption ($Kd = 1$) occurs at a slightly varying the displacer concentration ϕ. If the change in the displacer concentration occurs according to a certain, for example linear law, similar change take place for some delay at any point in chromatographic column, and the spreading of the displacer front concentration is ignored. As ϕ increases to ϕ_{cr} the protein zone begins to move through the sorbent layer. The motion rate of this zone increases with increasing distance x (Figure 21). It has been shown (*53*) that at point $x = X_o$ the protein zone rate becomes approximately equal to the displacer rate and the zone moves at a constant velocity under gradient compression conditions. For linear gradient:

$$\phi = \phi_o + B\,t \tag{13}$$

the critical distance may be determined for a protein from the following simple equation:

$$X_o = \lambda\, u/(B\, S \varkappa) \tag{14}$$

where S (the adsorption coefficient) is the slope of $\log k'(t)$ dependence :

$$\log k'(t) = \log kw - S\,\phi\,(t) \tag{15}$$

where kw is k' at $\phi = 0$, $k' = kd\,(Vp/Vo)$. Vp and Vo are pore volume and interparticle volume of sorbent layer, $Vp/Vo = \varkappa$. Coefficient B in equation 13 is the gradient steepness , and λ is the approximation coefficient (at $\lambda = 1$ $u = 0.95\,u_d$).

It has also been shown (*53*) that performing the separation at a column length $L = X_o$ results in the minimum band broadening. At distances $x \ll X_o$, extremely large band broadening is observed due to high instantaneous capacity factor k' of a protein and the resulting hindered sorption-desorption kinetics. This considerable protein zone spreading reduces sharply at a distances $L < Xo$ due to gradient contraction and to diminishing k'. On the other hand, at the distance $x > Xo$ gradient contraction becomes weaker with the displacer gradient front spreading. At the point $x = Xo$ the protein zone is the narrowest because at $Kd = 1$ the volume spreading is minimal. It is necessary to stop the protein fractionation process at this step. For this purpose it is necessary to limit the sorbent layer thickness to $L = Xo$. In equation 14, the limit, Xo, is a few millimeters for protein (S is large). However, this signifies that one can pass from columns with sorbent to sorbing membranes, and thus, HPMC came into existence. Equation 14 also shows that the decrease in the elution rate (u) permit us to decrease the membrane thickness ($h = Xo$).

It is important that our sorbing membranes should be a perfusion system, which is characterized an extremely high inner diffusion coefficient (by three orders of magnitude higher then in ordinary sorbents (*54*)). This permits one to work with a membrane with $h < Xo$ without any risk of zone spreading at high elution rates. There also are another aspects of Xo and h correction. In the simple case, when $Xo < h$, the protein retention time t_R is determined by the sum of the time of generation of critical displacer concentration, $t_G(\phi_{cr})$, the dead time in the chromatograph's connections, td, and the motion time of ϕ_{cr} (together with the protein zone) on the membrane $tc = h/u_d$, where u_d is the displacer velocity defined as $u_d = u\,(1 + Vp/Vo)$:

$$Xo < L\!: t_R = t_G(\phi cr) + L/u_d + td. \qquad (16)$$

In the case when $Xo > h$ the dependence of t_R is more complicated:

$$Xo > L\!: t_R = t_G(\phi cr) + t\,(SB, ko, L) + td \qquad (17)$$

In the preceding case t_R is simply determined by $\Delta t_G(\phi_{cr})$, the displacer velocity, membrane thickness (column length), and td. In the case $Xo > h$ an important role is also played by S and ko, where ko is k' at $\phi = 0$ (equation 17). Therefore in the former case the difference of protein retention times, Δt_R, is simply determined by $\Delta t_G(\phi_{cr})$ (equation 17). But in the latter case it is also determined by S, ko and L/h.

$$Xo < L\!: \Delta t_{R\,1,2} = \Delta t_G(\phi_{cr})_{1,2} \qquad (18)$$

$$Xo > L\!: \Delta t_{R\,1,2} = \Delta t_G + \Delta t(S,B,ko,L)_{1,2} \qquad (19)$$

Hence, the proteins distinguished by ϕ_{cr} are separated in the former case but can mix in the latter case because of the influence of S, ko, and h on t_R in the direction opposite to that on ϕ_{cr}. The application of thin membranes results into the decrease of longitudinal spreading in an isocratic elution regime. Hence, the step wise regime of gradient elution is especially favorable for the HPMC of proteins. The strong step wise displacer gradient (high B in equation 14) results in decrease of Xo (decrease of the optimal membrane thickness).

HPMC is a hybrid method which combines the advantages of HPLC and Membrane Technology and excludes their limitations (Table VI). The transition from a column packed with granular sorbent to porous membranes leads to the following additional effects:

1. A decrease in the dead volume of the sorbent layer and , hence, in the separation time.
2. A decrease in spreading due to perfusion effect (flow through the inner pores) which is characterized by convective internal diffusion with the diffusion coefficient being 10^3 - 10^4 times that in ordinary HPLC. The other manifestation of perfusion effects is the independence of zone dispersion on mobile phase flow rate or even a decrease in dispersion with increasing flow rate.
3. The small contribution of the exclusion effect on perfusion porous membranes because thin membranes have small Vp. Therefore, a system of chromatographic "invisibility" can exist not only at $-\varepsilon = -\varepsilon_{cr}$, but also at $-\varepsilon < -\varepsilon_{cr}$. This extends the possibility of the design of systems for "invisible" chromatography when "critical" conditions are applied at HPMC.
4. A considerable decrease in the cost of the membrane cartridge as compared to that of a HPLC column packed with a microgranular adsorbent.

Several scientific teams (*49-55*) have pioneered the practical development of HPMC of proteins in ion-exchange, hydrophobic-interaction, reversed-phase and affinity modes of chromatography and have described porous membranes for HPMC prepared from regenerated cellulose (*52*) and from hydrolyzed polyglicidyl methacrylate (PGMA) - ethylene dimethacrylate (EDMA) copolymer (*49-51*, *53-55*). Both materials suffer from short comings. Membranes from regenerated cellulose swell strongly, and the degree of swelling changes with mobile phase composition. On the other hand, PGMA-EDMA membranes are fragile and can cause non-specific hydrophobic adsorption of proteins due to EDMA hydrophobicity. These defects are eliminated for PGMA-EDMA membranes on to which hydrophilic PGMA oligomers are grafted. The functional groups (adsorption cites) may be subsequently introduced into this flexible oligomer chain located into the pore (Figure 22). Since residual oxirane groups of PGMA are hydrolyzed

Table VI. HPMC is hibrid method of HPLC and Membrane Technology

	HPLC	*Membrane technology*	*HPMC*
1. Merits	High selectivity High efficiency	Low pressure operation - low cost Easy scaling High productivity	High selectivity High efficiency Low pressure operation - low cost Easy scaling High productivity
2. Limitation	High pressure operation - high cost Difficult scaling Low productivity	Low selectivity Low efficiency	NONE

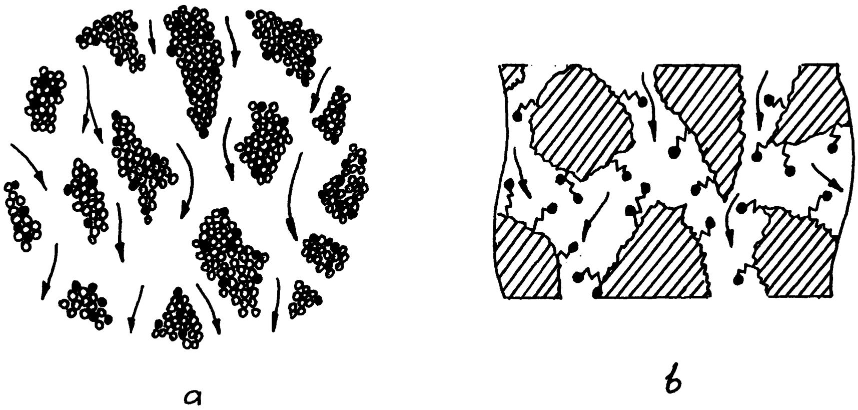

Figure 22. Structure of the perfusion sorbent (a) and PGMA-EDMA -G grafted membrane (b). Filled circles are functional groups (adsorption cites) .

(converted to diols), the surface of PGMA-EDMA-G (onto which PGMA is grafted) membranes becomes adsorptionally inert to proteins and all non-specific interactions are eliminated. This grafting also increases the mechanical strength of membranes. Figure 23 shows the increase in HPMC efficiency when PGMA is grafted onto PGMA-EDMA membranes (the narrowing chromatographic zones at multistage HPMC). Examples of protein separation on the PGMA-EDMA-G membranes are shown below (Figures 24-27).

Sorbing membranes, in addition to their application in HPMC, may be an effective matrix for heterophase sorption - catalytic processes in which ligands immobilized on the matrix interact with biopolymers. Table VII shows the state of the art and the future of HPMC. We can make certain explanations of this table. HPMC may be used for fractionating flexible chain polymers in the application of adsorption chromatography:

$$-\varepsilon > -\varepsilon_{cr} \; (-\Delta G > 0) \tag{20}$$

for heteropolymers and "critical" chromatography for heteropolymers. For example, for a block copolymer "AB":

$$-\varepsilon_A = -\varepsilon_{A\,cr}, \; -\varepsilon_B < -\varepsilon_{B\,cr} \; (-\Delta G_A = 0, \; -\Delta G_B < 0) \tag{21}$$

and

$$-\varepsilon_A > -\varepsilon_{Acr}, \; -\varepsilon_B = -\varepsilon_{Bcr} \; (-\Delta G_A > 0, \; -\Delta G_B = 0) \tag{22}$$

These regimes correspond to critical-exclusion and adsorption- critical chromatography.

If the eluent is changed in such a way that both blocks alternatively respond to conditions (21) and (22), the MWD of each block, and consequently the composition inhomogeneity of block-copolymer, can be determined successfully. However, since the conditions (21) and (22) are unique, their choice is a complex problem. HPMC is a different matter. Here the size-exclusion regime of chromatography is practically absent because of the small volume of pores in thin membranes. As a result, the determination of MWD of any blocks can be made only by adsorption chromatography with exclusion or "critical" chromatography of other block-copolymer:

$$-\varepsilon_A > -\varepsilon_{Acr}, \; -\varepsilon_B \leqslant -\varepsilon_{Bcr} \; (-\Delta G_{AB} > 0) \tag{23}$$

In this regime the choice of eluent composition is much simpler. The

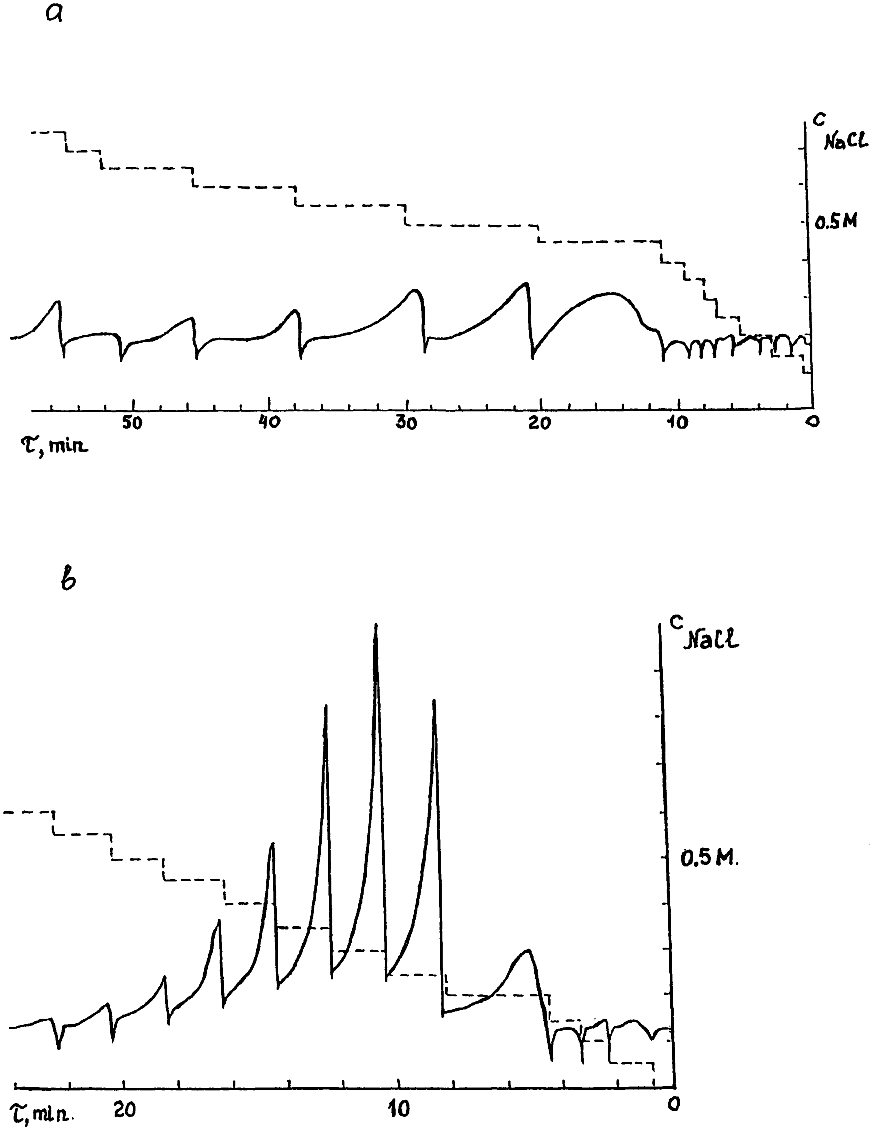

Figure 23. Fractionation of crude ferritin on DEAE - PGMA - EDMA membranes with step wise gradient elution.
(a) nongrafted membrane, (b) grafted one with PGMA.

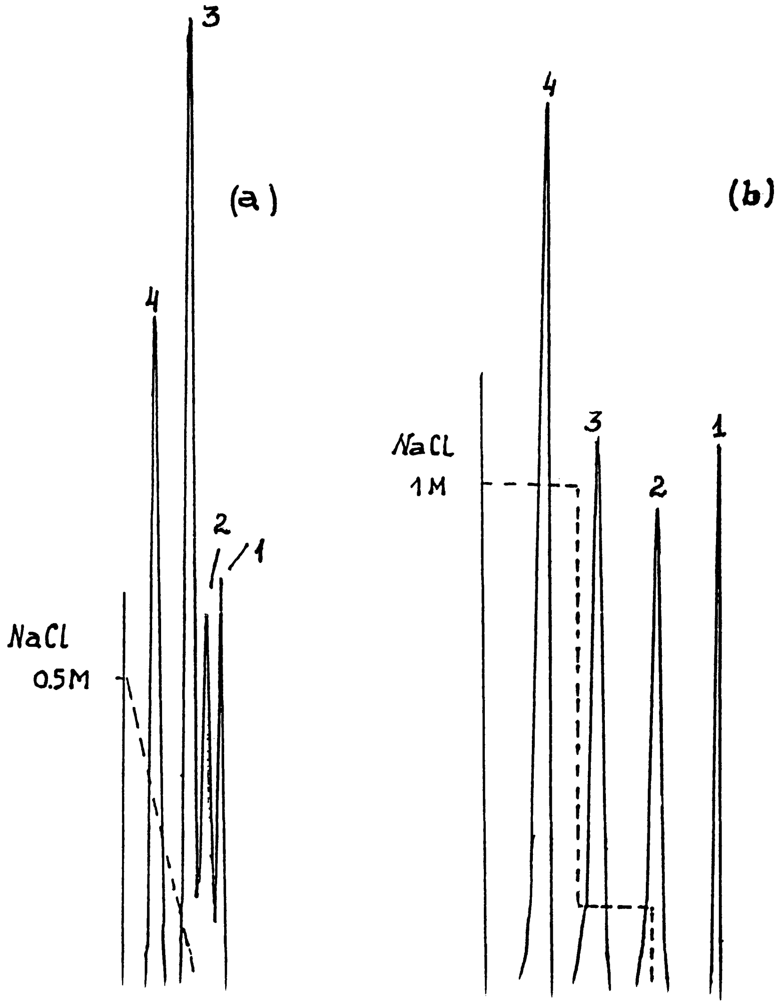

Figure 24. HPMC of proteins on the PGMA-EDMA grafted membranes: (a) on a sulfo-PGMA-EDMA-G-membrane (diameter - 25 mm and thickness- 1 mm), flow rate 2 mL/min , two-step linear gradient (0 - 0.5M NaCl in 0.02M Na_2HPO_4, pH =7.0)- 5 min; peaks: (1) ribonuclease , (2) α-chymotrypsinogen, (3) cytochrome C, (4) lysozyme;
(b) on a DEAE-PGMA-EDMA-G-membrane 15 x 1 mm, flow rate-4mL/min, step wise gradient (0 - 1M NaCl in 0.01M Tris, pH =7.6); peaks: (1) lactalbumin, (2) ovalbumin, (3) soya trypsin inhibitor, (4) ferritin.

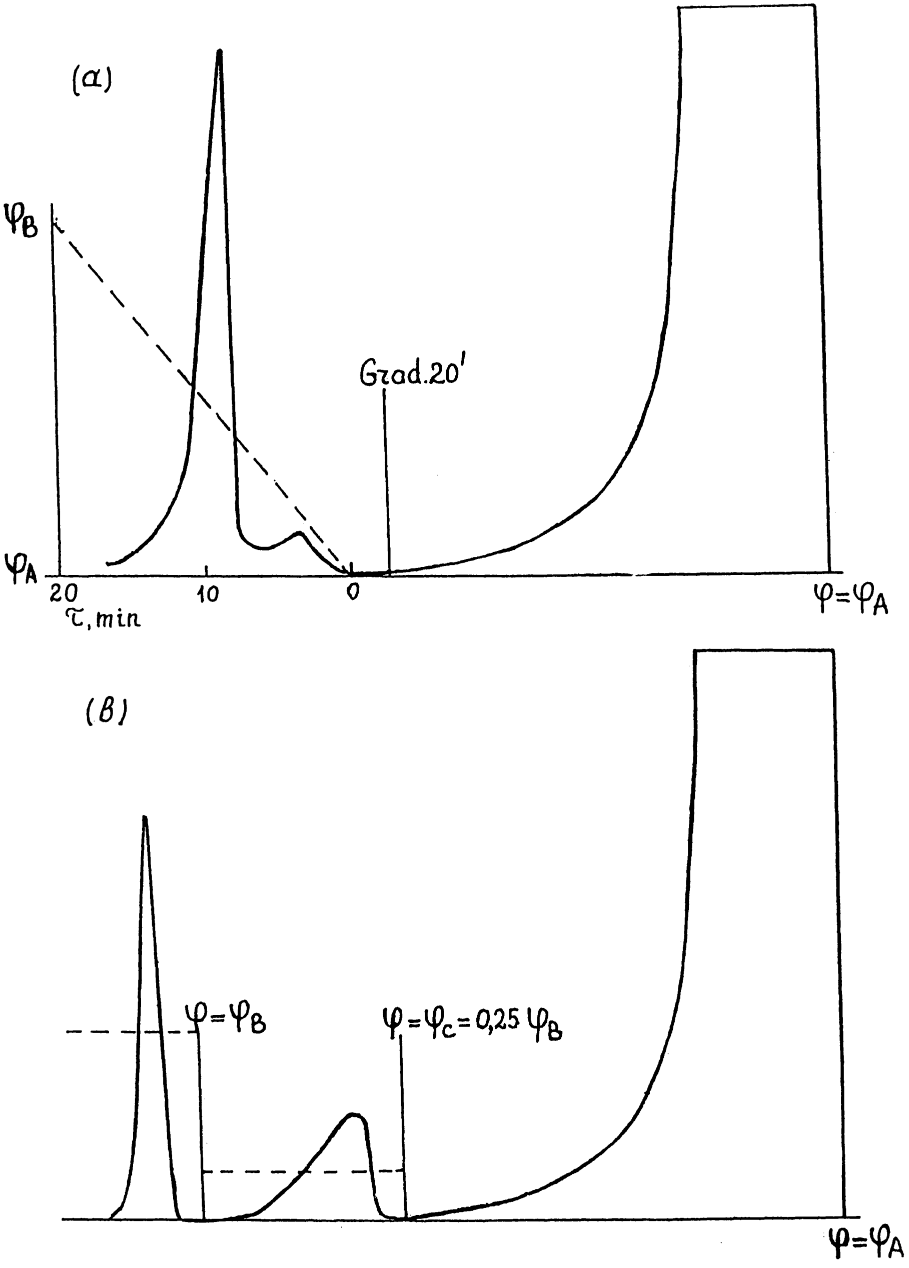

Figure 25. The simple preparation of lysozime from white of egg by HPMC on sulfo-PGMA-EDMA-membrane.
(a) gradient of NaCl in 0.02M phosphate buffer, pH = 7.0;
(b) two-step elution by the same buffer.

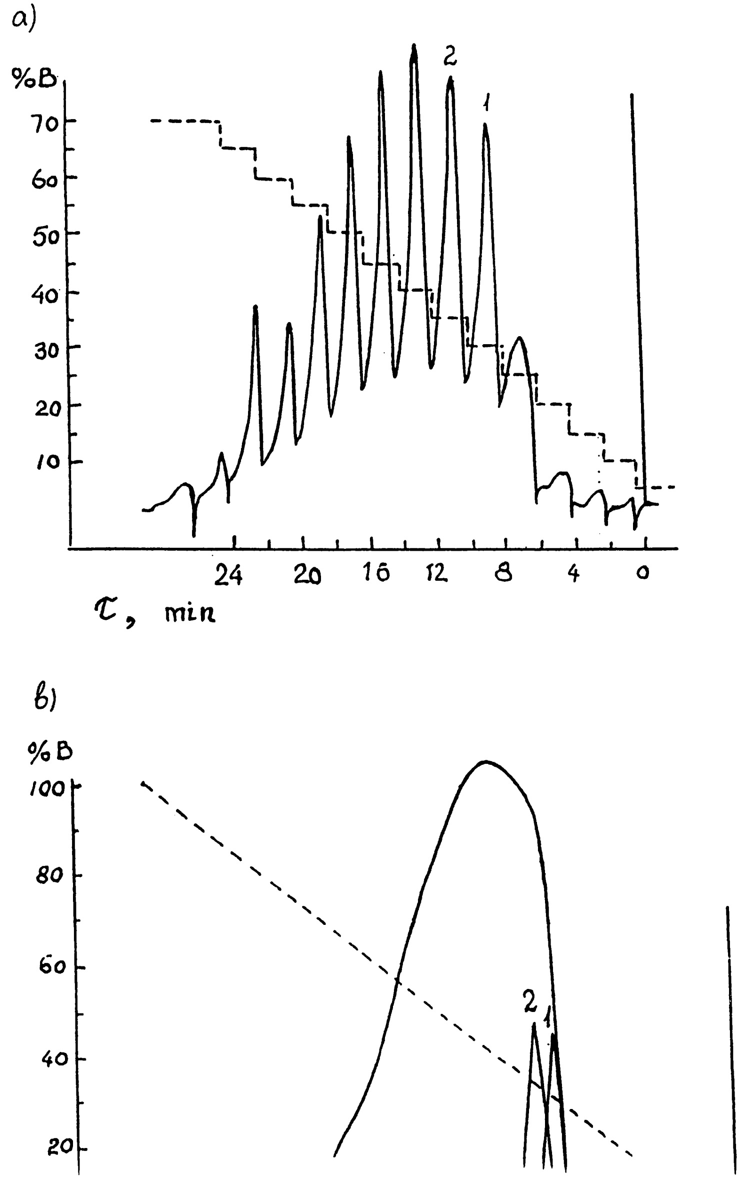

Figure 26. HPMC fractionation of crude ferritin on PGMA-EDMA-DEAE-grafted membrane 15 x 1 mm:
conditions: buffer A - 0.01M Tris, pH =7.6, buffer B - 1M NaCl in A, gradient from A to B ; flow rate- 2 mL/min;
(a) multistage stepwise gradient (by 0.05 M NaCl in 2 min); (b) linear gradient elution (20 min) and rechromatograms of fractions 1,2 (a). (Reproduced with permission from reference 55. Copyright 1995 Eaton Publishing Co.)

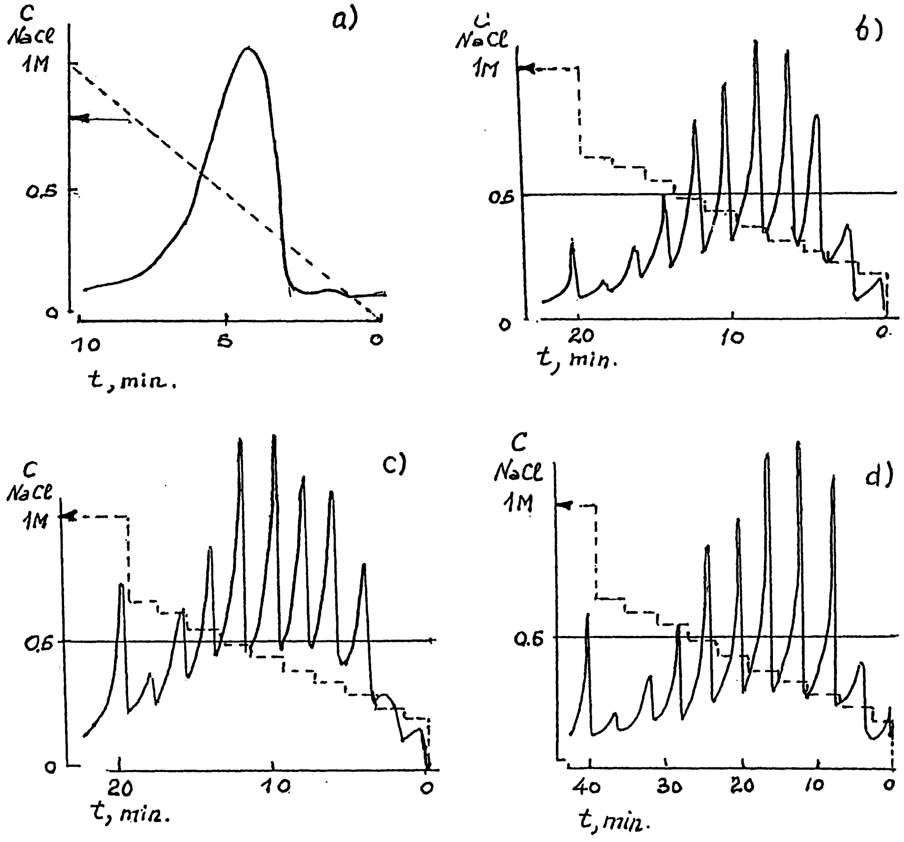

Figure 27. Fractionation of crude ferrtin by ion-exchange HPMC with multistage stepwise gradient elution on the PGMA-EDMA-DEAE-G-membrane . Conditions: buffer A- 0.01M Tris-HCl, pH =7.6, buffer B - 1.0 M NaCl in A, gradient - from A to B;
(a) linear gradient, time- 10min; (b) multistage stepwise gradient : by 0.05 M NaCl in 2 min, flow rate - 2mL/min; (c) gradient is identical to (b), flow rate- 1 mL/min; (d) gradient: by 0.05 M NaCl in 4 min, flow rate - 2 mL/min.
(Reproduced with permission from reference 55. Copyright 1995 Eaton Publishing Co.)

Table VII. HPMC Development
(State of the Art and Future)

Membrane structure and the main aspects of its applications

---

1. Membrane performance improvement (selectivity, efficiency and productivity) by improving its perfusion properties, adsorption-desorption kinetics and the adsorption centers topology of membranes.

2. Development of chromatographic aspects of HPMC to provide better performance than HPLC-columns.

3. Development of membrane technological aspects of HPMC (productivity much more than for preparative HPLC), combination HPMC with other kinds of membrane technology for industrial high-performance membrane processes of protein separation and purification.

Other applications

---

4. To planar analytical techniques:
   TLC, selective electroblotting, electrodesorption from the hydrophobic membranes will have a very high separating capacity for proteins. In practice this process may be carried out in a flat channel flow cells under electrical field flow fractionation conditions.

5. For solid phase reactions of macromolecules:
   enzyme-reactor, binding (HPMC), matrix synthesis of DNA.

Theory

---

6. Analytical studies and modeling of the movement and spreading of chromatographic zones during HPMC. Investigation of the flow rate effect.

□

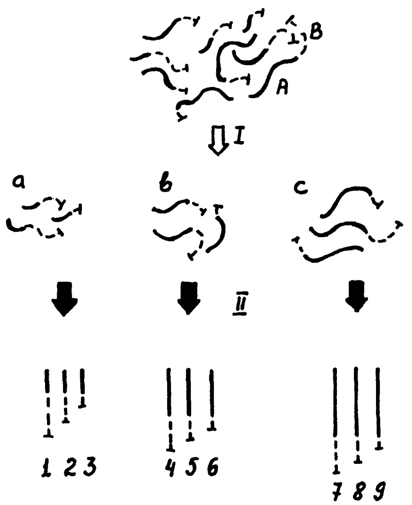
B
A
I
a
b
c
II
1 2 3
4 5 6
7 8 9

Figure 28. Two-direction fractionation of AB-block copolymer by HPMC (scheme); the white arrow - I direction (according to M_A): $-\varepsilon_A > -\varepsilon_{A\,cr}$, $-\varepsilon_B < -\varepsilon_{B\,cr}$; the black arrow - II direction (according to M_B): $-\varepsilon_A < -\varepsilon_{Acr}$, $-\varepsilon_B > -\varepsilon_{B\,cr}$.

The labels a, b, c and numbers 1–9 indicate differences in molecular structure.

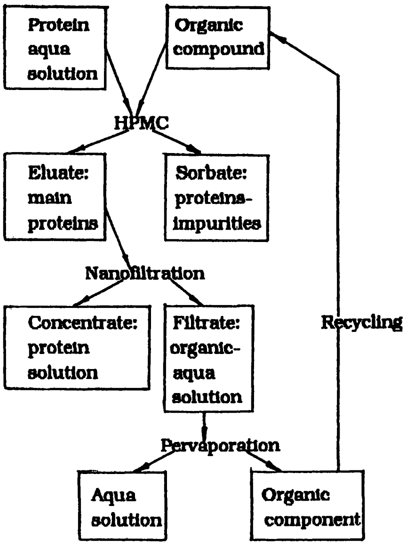
Protein aqua solution
Organic compound
HPMC
Eluate: main proteins
Sorbate: proteins-impurities
Nanofiltration
Concentrate: protein solution
Filtrate: organic-aqua solution
Recycling
Pervaporation
Aqua solution
Organic component

Figure 29. Protein purification using only Membrane techniques.

scheme for two-direction separation of block-copolymer by HPMC is shown in Figure 28. After fractionation in the first direction (white arrow) block-copolymer macromolecules are separated according to M_A by adsorption chromatography. The fractions (ultra narrow to M_A and widely disperse to M_B) are separated in the second direction (black arrows) by adsorption HPMC for block B (exclusion or "critical" conditions of HPMC for block A).

The very important and interesting prospect of the development of HPMC is a complete membrane process of protein purification. The modern methods of protein separation are based on liquid chromatography (HPLC) in which both the main (target) protein and protein impurities are absorbed. These processes are accompanied by partial protein denaturation. It is advisable to adsorb only protein impurities and to permit passing the main protein solution through a membrane without sorption (and denaturation), to concentrate the target protein by nanofiltration and to return the organic component of solution filtrate to the technological process by pervaporation (Figure 29).

Conclusions

Nonstandard methods based on SEC principles intrinsically enlarge polymer and biopolymer chromatography capabilities in analytical and preparative scales. The expansion of SEC capabilities is connected with miniaturization of the method by first working out a capillary variant of SEC. Analytical applications of macromolecule interaction with pore surface has also led to the discovery of the "critical" chromatography of macromolecules. This method permits one to chromatographically investigate (to determine the number and MWD) different parts of macromolecules of heteropolymers (copolymers, functional oligomers). The development of polymer TLC has made possible an inexpensive universal method for diagnosis and quantitative determination of practically all types of polymer polydispersities, and the determination of polymer purity. At present, TLC is a semi-quantitative method but it has good perspectives for its transformation to a fully quantitative method. TLC also permits one to investigate the polymer zone boundary broadening. This effect has direct relation to intensification of oil extraction by water encroachment of bore-holes (i.e. by pumping the polymer solution at the periphery of the bore-hole). TLC of polymers is also an excellent teaching tool - to illustrate polymer polydispersity.

Finally, the polymer preparative liquid chromatography variant, HPMC, is a superoptimized method for the preparative fractionation of macromolecules. HPMC has excellent perspectives for superseding classical chromatographic processes for obtaining high purity polymers (biopolymers) by using a combination of purely membrane processes: HPMC, nanofiltration and pervaporation.

The aforementioned investigations, which had initially analytical goals, have led to the excellent theoretical results: the development of the adsorption polymer theory, working out theoretical foundations of TLC and capillary liquid chromatography, the discovery of new variants of polymer chromatography: "critical" chromatography of macromolecules and HPMC - the optimized hybrid technology, synthesized HPLC and membrane process possibilities. All of these investigations have made valuable contributions to polymer science and polymer separation technology development.

Literature Cited

1. Yan, W.W.; Kirkland, J.J.; Bly, D.D. *Modern size - exclusion chromatography ;* J. Wiley and Sons: N.Y., NY, 1979; p 485.
2. Belenkii, B.G.; Vilenchik, L.Z. *Modern liquid chromatography of macromolecules;* Elsevier: Amsterdam, 1983; p 436.
3. Alexandrov, M.L.; Belenkii, B.G.; Gotlib, V.A.; Kever, J.E. *J. Microcolumn Sep.* **1992,** *vol 4*, p 379.
4. Belenkii, B.G.; Gotlib, V.A.; Kever, J.E. *Naychnoe priborostroenie* , USSR. **1991,** *vol 1, N 1*, p 9.
5. Wayatt P.J. *J. Liquid Chromatogr.* **1991,** *vol 14*, p 2351.
6. Harold Pasch. *Proceedings of 7 th Int. Symp. on polymer analysis and characterization;* Les Dablerets, Switzerland, May 1994, p 14.
7. Chubarova, E.V.; Nesterov , V. V. *J. Liquid Chromatogr.* **1990,** *vol 13* , p 1825.
8. Vilenchik , L. Z. ; Belenkii, B. G. ; Nesterov, V. V. ; Chubarova , E. V.; Noskin, V.A.; Ivanova, M.A.; Piskareva, I.P. *Dokl. Acad. Nayk.*, USSR . **1987,** *vol 295*, p 119.
9. Tijssen, R.; Bos, J.; Vankreveld , M.E. *Anal. Chem.* **1986,** *vol 58*, p 3036.
10. Gankina , E. S. ; Belenkii , B. G. *In Handbook of chromatography;* Sherma, J. and Fried, B., Eds.; Marcel Dekker: N.Y., NY, 1991, p. 1047.
11. Colbert, R. A.; Amatruda, J. M.; and Young, D.S. *Clin. Chem.* **1984,** *vol 30*, p 2053.
12. Rigetty, P.G. *J. Chromatogr.* **1990,** *vol 516*, p 3.
13. *Microcolumn high-performance liquid chromatography;* Kusera, P., Ed.; Elsevier: Amsterdam , 1984.
14. *Microcolumn separations : columns , instrumentations and ancillary techniques*, Novotny, M.V.; and Ishii, D., Eds.; Elsevier: Amsterdam , 1985.
15. *Small bore liquid chromatography columns; their properties and uses;* Scott, R.P.W., Ed.; Wiley: N.Y. , NY, 1984.

16. Belenkii, B.G.; Gankina, E.S.; Malt'sev, V.G. *Capillary liquid chromatography;* Consultants Bureau: N.Y., A Division of Plenum: N.Y., London, 1987.

17. Jinno, K.; and Nishibara ,M. *Anal. Lett.* **1980,** *vol 13,* p 673.

18. Kever, J.J.; Gankina ,E.S.; Belenkii ,B.G. *Visocomol. Soedin.,* USSR. **1981,** *vol A-23,* p 234.

19. Kever, J. J.; Belenkii, B. G.; Gankina, E. S.; Vilenchik, L. Z.; Kurenbin, O.I.; and Zhmakina, T.P. *J. Chromatogr.* **1981,** *vol 207,* p 145.

20. Kever, J. J.; Belenkii, B. G.; Gankina, E. S.; Vilenchik, L. Z.; Kurenbin, O.I.; and Zhmakina, T.P. *J. High Resolut. Chromatogr. Chromatogr. Commun.* **1981,** *vol 4,* p 425.

21. Alexandrov, M. L.; Belenkii, B. G.; Gankina, E. S.; Gotlib, V. A.; Kever, J.J.; Komarov, N.N.; Pavlenko, V.A. *J. High Resolut. Chromatogr. Chromatogr. Commun.* **1983,** *vol 6,* p 629.

22. Kever, J. J.; Belenkii, B. G.; Gankina, E. S.; Vilenchik, L. Z.; Kurenbin, O.I.; Zhmakina, T.P. *Visokomol. Soedin.,* USSR. **1982,** *vol B-24,* p 403.

23. Vilenchik, L. Z.; Kurenbin, O. I.; Zhmakina, T. P.; Belenkii, B. G. *Visokomol. Soedin.,* USSR. **1980,** *vol A-22,* p 2801.

24. Vilenchik, L. Z.; Kurenbin, O. I.; Zhmakina, T.P.; Nesterov, V.V.; Chubarova, E.Y.; and Belenkii, B. G. *Visokomol. Soedin.,* USSR. **1980,** *vol A-22,* p 2804.

25. Ishii ,D.; Takeuchi ,T. *J. Chromatogr.* **1983,** *vol 255,* p 349.

26. Takeuchi ,T.; Ishii, D.; and Mori, S.J. *Chromatographia.* **1983,** *vol 257,* p 327.

27. Kennedy, R.T.; and Jorgenson, J.W. *J. Microcolumn Sep.* **1990,** *vol 2,* p 120.

28. Belenkii, B.G. *J. Chromatogr.* **1988,** *vol 434,* p 337.

29. Belenkii, B.G.; Bello, M.C.; Kever, J.J.; Koroleva E.M. *In Sintez, Structura i Svoystva polimerov;* Koton, M.M. ,Ed.; Nayka: Leningrad, USSR, 1989: p 253.

30. Francon, M.; Mallick, S. *Polarization interferometry application in microscope and macroscopy;* N.Y., 1971.

31. Azzam, R. M.; and Boshara, N. M. *Ellipsometry and polarized light;* Amsterdam, Oxford, N.Y. 1977.

32. Kever ,E.E.; Zimina, T.M.; and Belenkii, B.G. *Bioorganicheskaya Chim,* USSR. **1989,** *vol 15,* p 1019.

33. Grubisic, Z.; Rempp, P.; Benoit, H. *J. Polym. Sci. B.* **1967,** *vol 5,* p. 753.

34. Casassa, E.F. *J. Polym. Sci. B.* **1967,** *vol 5,* p. 773.

35. Belenkii, B.G.; Gankina, E.S.; Tennikov, M.B.; Vilenchik, L.Z. *Dokl. Akad. Nauk,* USSR. **1976,** *vol 231,* p 1147.

36. Gorbunov, A.A.; Skvortzov, A.M. *Doklady Akad. Nayk.* **1987,** *vol 294,* p 396.

37. Tennikov, M.B.; Nefedov, P.P.; Lazareva, M.A.; Frenkel, S.Yu. *Vysokomol. Soedin.* USSR . **1977,** *vol A-19,* p 657.

38. Belenkii, B.G.; Gankina, E.S.; Tennikov, M.B.; Vilenchik, L.Z. *J. of Chromatogr.* **1978,** *vol 147,* p 99.

39. Belenkii, B.G. *Pure and Appl. Chem.* **1979,** *vol 51,* p 1519.

40. Belenkii, B. G. ; Gankina , E. S. ; Zgonnik , V. N. ; Malachova, I. I.; Melenevskaya, E.D. *Vysokomol. Soedin.,* USSR. **1991,** *vol A-33,* p 2487.

41. Gorbunov, A. A. ; Skvortzov, A. M. *Vysokomol. Soedin.* , USSR. **1988,** *vol A-30,* p 895.

42. Pasch, H.; Much, H.; Schulz, G.; Gorshkov, A.V. *LC-GC International.* **1992,** *vol 5,* p. 38.

43. Entelis, S. E.; Evreinov, V.V.; Kuzaev, A.I. *Reaksionnosposobnie oligomeri*; Khimia: Moscow, Russia, 1995; 304 p.

44. Inagaki, H.; Matsuda, H.; and Kamiyama, F. *Macromolecules,* **1968,** *vol 1,* p 520.

45. Belenkii, B.G.; Gankina, E.S.; and Turkova , L.D. *Lektsii II shkoly po metodam ochistki i otsenki chistoty monomerov, polymerov;* Chernogolovka, USSR, 1968; p 216.

46. Belenkii , B. G. ; Gankina , E. S. ; Litvinova , L. S.; Efimova , I. I. ; Vaskovskii, V. E.; Chotimchenko , S. V.; Kikarev, V. V. *Bioorganicheskaya Chim.,* USSR. **1984,** *vol 10,* p 244.

47. Litvinova, L.S.; Gankina, E.S.; Kurenbin, O.I.; Belenkii, B.G. *Visocomol. Soedin.,* USSR. **1990,** *vol A-32,* p 535.

48. Belenkii , B.G. ; Bondarenko , P.V. ; Gankina , E.S. ; Zubarev, R. A.; Knysh, A.N.; and Koltsova, O. *Vysokomol. Soedin.,* USSR. **1991,** *vol A-33,* p 2020.

49. Tennikova ,T.B.; Belenkii, B.G.; Svec, F. J. *Liquid Chromatogr.* **1990,** *vol 13,* p 63.

50. Tennikova, T.B.; Bleha, M.; Svec ,F.; Almazova, T.V.; Belenkii, B.G. *J. Chromatogr.* **1991,** *vol 555,* p 97.

51. Josic , Dj.; Rensch, J.; Loster, K.; Baum, O.; Reuter, W. *J. Chromatogr.* **1992,** vol 590, p 173.

52. Gerstner, J.A.; Hamilton,R.; Kramer, S.M. *J. Chromatogr.* **1992,** *vol 596,* p 173.

53. Belenkii, B. G. ; Podkladenko, A. M. ; Kurenbin, O. I. ; Malt'sev, V.G.; Nasledov, D.G.; Trushin, S.A. *J. Chromatogr.* **1993,** vol 645, p 1.

54. Tennikova, T.V.; Svec, F. *J. Chromatogr.* **1993,** *vol 646,* p 279.

55. Belenkii, B.G.; Malt'sev, V.G. *Biotechniques* **1995,** *vol 18(2),* p 288.

Downloaded by UNIV MASSACHUSETTS AMHERST on October 8, 2012 | http://pubs.acs.org
Publication Date: May 30, 1996 | doi: 10.1021/bk-1996-0635.ch017

Chapter 17

Method for Studying Micelle Formation Using Size Exclusion Chromatography, Light Scattering, and UV Spectroscopy

L. Z. Vilenchik[1], Shikha Barman[2], and C. P. Pathak[2]

**[1]PerSeptive Biosystems, 500 Old Connecticut Path,
Framingham, MA 01701
[2]Focal Interventional Therapeutics, 4 Maguire Road,
Lexington, MA 02173**

A method for the direct observation and measurement of micelles has been developed. At higher solution concentrations, multi-angle laser light scattering in batch mode was used, and at lower concentrations, Size Exclusion Chromatography with dual detection (Light Scattering and Refractive Index) was employed. Micelle formation for PEG and a copolymer of PEG with lactate and acrylate groups (8KLX) were observed using this method. The critical concentrations for the micelle formation were determined for the PEG and 8KLX macromolecules. Confirmation of the results was obtained using an independent spectrophotometric method.

The phenomena of macromolecular association, complexation and micelle formation occupy a very important place in polymer and biopolymer chemistry. All of these phenomena are strongly dependent upon the concentration of the macromolecules in solution. The size and number of the macromolecular aggregates in solution increase with increasing concentration.

Size Exclusion Chromatography (SEC) /1/ is one of the most reliable methods for the determination of molecular weight and size of macromolecules in solution. In principle, this method may be used for the corresponding characterization of macromolecular aggregates. However, aggregation normally occurs at concentration levels higher than those used in SEC. Common SEC solute concentrations range from 1% to 5%, and after passing through the chromatographic system, are diluted by a factor of 30-50. As a result, when the solutions reach the detector cell, their concentration is less 0.1%. Frequently, such concentration levels are not enough for aggregate formation, and direct determination of molecular weights and sizes of these macromolecular aggregates becomes impossible.

The use of SEC with two detectors on line (multi-angle light scattering, LS, and refractive index, RI) affords a new opportunity to observe these aggregates directly in

0097–6156/96/0635–0328$15.00/0

Downloaded by UNIV MASSACHUSETTS AMHERST on October 8, 2012 | http://pubs.acs.org
Publication Date: May 30, 1996 | doi: 10.1021/bk-1996-0635.ch017

solution. This method which allows for the determination of the molecular weight and size of these aggregates is described in the following scheme.

SCHEME OF SEC WITH LS AND RI DETECTORS ON LINE

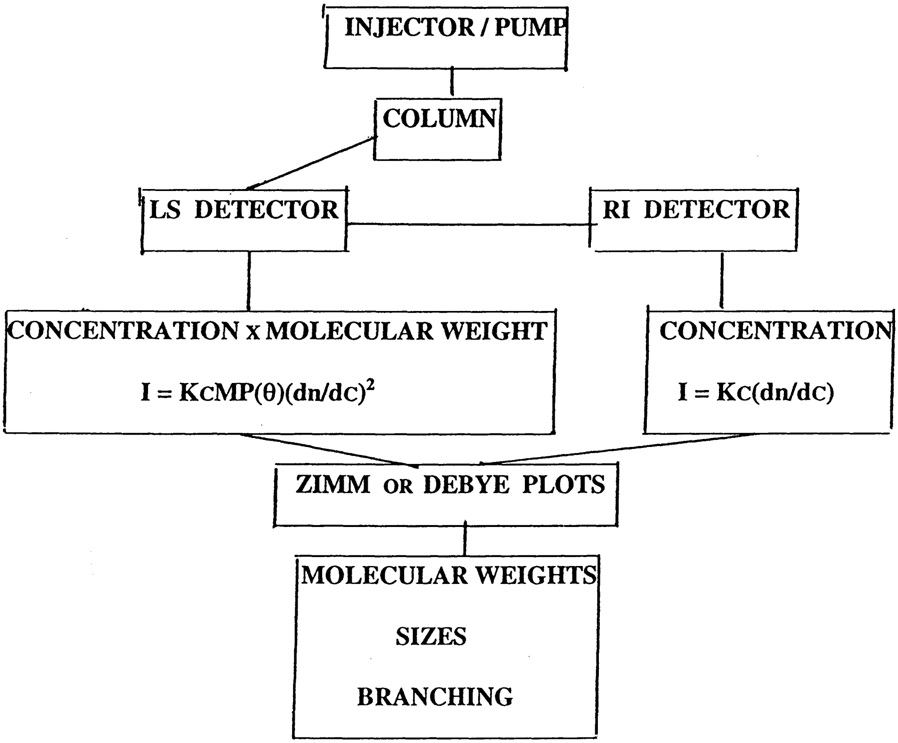
INJECTOR / PUMP
COLUMN
LS DETECTOR
RI DETECTOR
CONCENTRATION x MOLECULAR WEIGHT
I = KcMP(θ)(dn/dc)²
CONCENTRATION
I = Kc(dn/dc)
ZIMM OR DEBYE PLOTS
MOLECULAR WEIGHTS
SIZES
BRANCHING

The LS detector gives a signal proportional to the product of the molecular weight and the concentration /2,3/ (Eq. 1)

$$I_{LS} = K_{LS}M_{W}c(dn/dc)^2 P(\theta) - 2A_2cM_W{}^2 P^2(\theta) \qquad (1)$$

where Mw is weight average molecular weight, c is the solute concentration, dn/dc is the refractive index increment, A2 is the second virial coefficient, P(θ) is angle dependable form factor, θ is a light scattering angle.

The RI detector gives a signal proportional to the concentration of the macromolecular solution and the refractive index increment (dn/dc) /4, 5/

$$I_{RI} = K_{RI}c(dn/dc) \qquad (2)$$

Here, K_{LS} and K_{RI} are coefficients of proportionality detected using the procedures and software available from Wyatt Technology, Inc.

Using both of the signals (LS and RI) for a few concentrations allows to calculate molecular weight by means of Zimm or Debye plots. In two detector SEC each point of the LS and RI chromatograms gives us the signals that correspond to only one concentration. It is not even necessary to perform a chromatographic separation. If we inject a solution inside the chromatographic system without a chromatographic column, we will not get any separation of macromolecules according to their size. Instead, we will get only broadening of the injected solution. However, the pair of the corresponding LS and RI chromatograms is enough to calculate weight average molecular weight of macromolecular compounds.

To obtain the molecular weight distribution (MWD) of a polymer using classical light scattering, we have to perform preliminary fractionation of the polymer into at least 10 narrow fractions, and then prepare 5-6 different concentrations of each fraction. The advantage of standard SEC/LS over classical light scattering is the determination of average molecular weights (AMW) and MWD of polymers using only one chromatographic run with one concentration of the polymer solution. The SEC/LS method without a chromatographic column cannot give a MWD but allows for the quick determination of the AMW. The method is more rapid and operates at solute concentrations significantly higher than standard SEC/LS analysis. The AMW values obtained using this method agree with those obtained from standard SEC/LS. The reliability of this new method has been demonstrated by comparison with standard SEC/LS data for the same polymer solutions (Figs.1-4, Table 1).

Experimental.

Hewlett Packard liquid chromatographic system 1050, Toso Haas column G 2000 Sw_{xl}, 6mm ID x 4 cm, RI Hewlett Packard detector, multi-angle light scattering photometer DAWN DSP from Wyatt Technology Inc. /6/ , and U-3000 Hitachi spectrophotometer were used in these experiments. Deionized water was used as a solvent. Polymer samples that were investigated were polyethylene glycol (PEG) from Union Carbide, copolymers of the PEG with lactate and acrylate groups (8KLX) synthesized in house, and ficols samples (that have globular shape of molecules) with different molecular weight. The two groups of macromolecules were chosen to show the applicability of the two detector SEC without chromatographic column to determine average molecular weights to both flexible-chain and globular macromolecular samples with different polydispersity.

Downloaded by UNIV MASSACHUSETTS AMHERST on October 8, 2012 | http://pubs.acs.org
Publication Date: May 30, 1996 | doi: 10.1021/bk-1996-0635.ch017

All solutions were filtered through 0.02 m filters Anotop-25 from Altech just prior to chromatographic runs or LS measurements in batch mode. Temperature was ambient.The chromatographic experiments were repeated 3 times to check the reproducibility of the data. Each LS measurement in batch mode was repeated 10 times, and the data were averaged both with and without Wyatt Technology software. The standard deviations for Mw and size of macromolecules and their aggregates were less than 10 %. All the experiments were repeated at least once with freshly prepared and filtered solutions and gave data within the above mentioned experimental limits.

Downloaded by UNIV MASSACHUSETTS AMHERST on October 8, 2012 | http://pubs.acs.org
Publication Date: May 30, 1996 | doi: 10.1021/bk-1996-0635.ch017

Results and discussion.

1. Comparison SEC/LS data with and without a chromatographic column

The Figure 1 shows a typical chromatogram for the PEG-8000 sample using the chromatographic column G2000 SW xl. The narrow unimodal peak indicates that there is no aggregation at this low concentration level (0.7% at the injection and 0.08% in the detector cell).

The Figure 2 shows an example of the RI and LS chromatograms for a polydisperse trimodal ficol sample with Mw=139000. Because the LS detector is more sensitive to higher molecular weight compounds, it is possible to observe a small amount of small size but high density and high molecular weight macromolecules which are not detected by the RI detector (see for example the third peak in Figure 2).

If we use only a guard column for the analysis, broadening of the chromatographic zone significantly decreases and the polymer concentration inside the zone increases relative to cases where the SEC column is also used. However, for PEG-8000 we still observe a unimodal peak if the injected concentration is close to 0.1%. The Figure 3 shows the corresponding LS and RI chromatograms.

Chromatograms using only the guard column for the trimodal ficol sample (Mw=139000) are shown in Figure 4. In this case we see only one mode with an average molecular weight within experimental error of the AMW determined when the SEC column was used in the analysis. (Compare with Figure 2.)

Table 1 provides weight average molecular weights for different PEG and ficol samples that were obtained by means of applied to chromatographic runs with and without the G 2000 SWxl column software ".Astra"/6/

Downloaded by UNIV MASSACHUSETTS AMHERST on October 8, 2012 | http://pubs.acs.org
Publication Date: May 30, 1996 | doi: 10.1021/bk-1996-0635.ch017

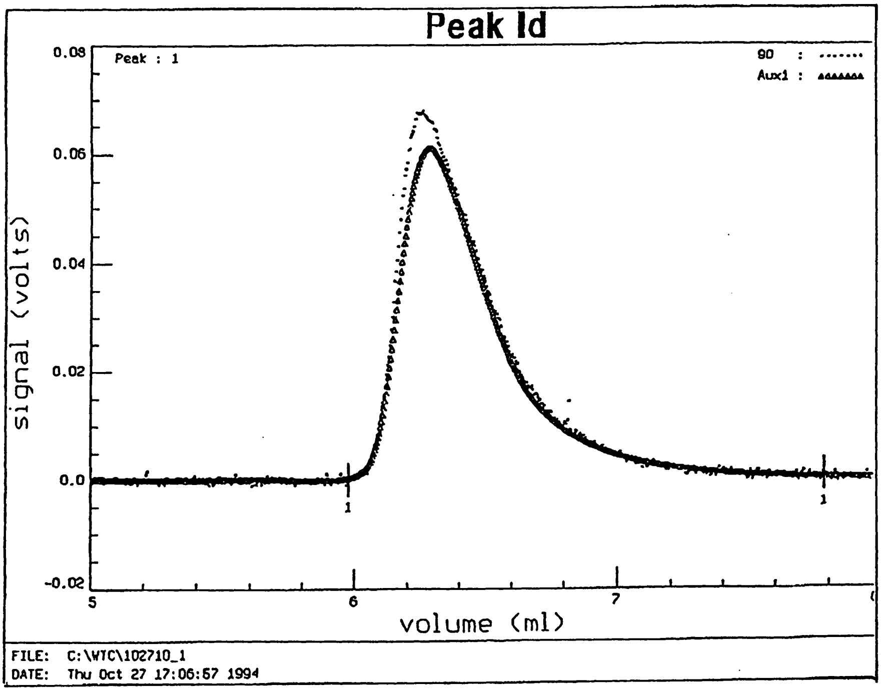

Figure 1.
LS and RI chromatograms of PEG 8000 in water with using chromatographic column G 2000 SW xl. Flow rate is 1 ml/min. Injection volume is 50 µl. Solute concentration is 7 mg/ml. The concentration at peak maximum is 0.8 mg/ml., dn/dc=0.134. Molecular weights according to "ASTRA" software are following: Mw=7900, Mn=7800, Mz=8100, Mw/Mn=1.01, Mz/Mn=1.04.

Downloaded by UNIV MASSACHUSETTS AMHERST on October 8, 2012 | http://pubs.acs.org
Publication Date: May 30, 1996 | doi: 10.1021/bk-1996-0635.ch017

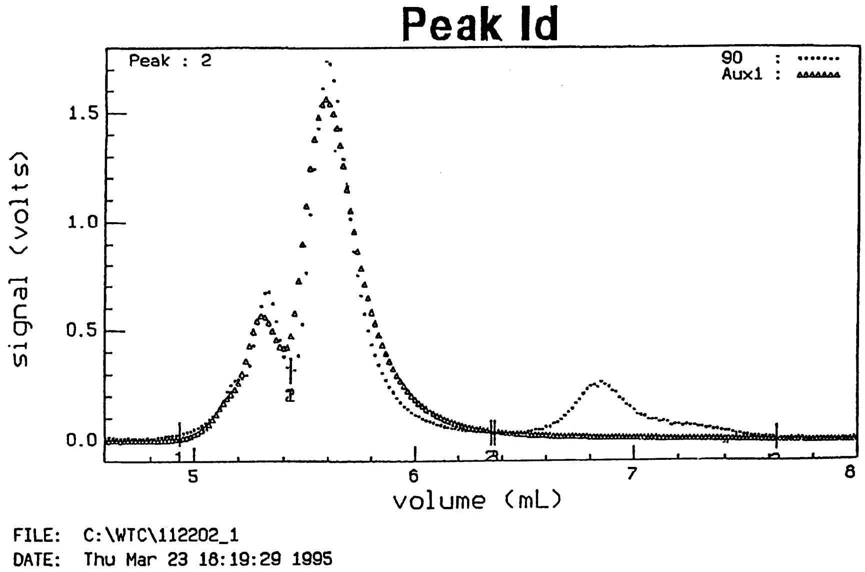

Figure 2.

LS and RI cromatograms of a polydisperse Ficol sample A_4 in water with using chromatographic column G 2000 SW xl. Flow rate is 1 ml/min. Injection volume is 50 µl. Solute concentration is 7 mg/ml., dn/dc=0.159. Average molecular weights for whole sample according to "ASTRA" software are following: Mw=139000, Mn=123000, Mz=214000, Mw/Mn=1.13, Mz/Mn=1.74. Contain of the first peak in the sample is 20%, Mw=151000. Contain of the second peak is 77%, Mw=123000. Contain of the third peak is 3%, Mw=552000.

Downloaded by UNIV MASSACHUSETTS AMHERST on October 8, 2012 | http://pubs.acs.org
Publication Date: May 30, 1996 | doi: 10.1021/bk-1996-0635.ch017

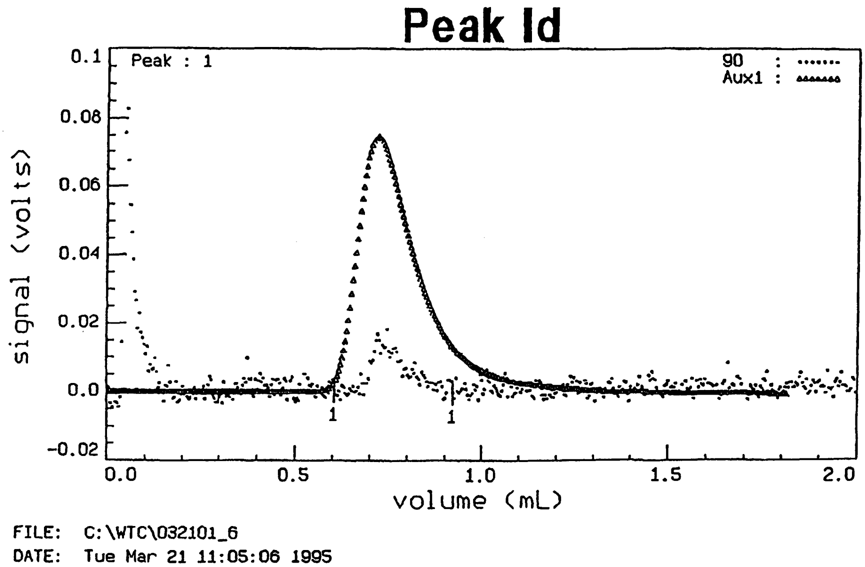

Figure 3.
LS and RI chromatograms of PEG 8000 in water with using guard column SW xl. Flow rate is 0.5 ml/min. Injection volume is 25 µl. Solute concentration is 1.25 mg/ml. The concentration at peak maximum is 0.2 mg/ml., dn/dc=0.134. Molecular weights according to "ASTRA" software are following: Mw=8700, Mn=7000, Mz=11300, Mw/Mn=1.25, Mz/Mn=1.61.

Downloaded by UNIV MASSACHUSETTS AMHERST on October 8, 2012 | http://pubs.acs.org
Publication Date: May 30, 1996 | doi: 10.1021/bk-1996-0635.ch017

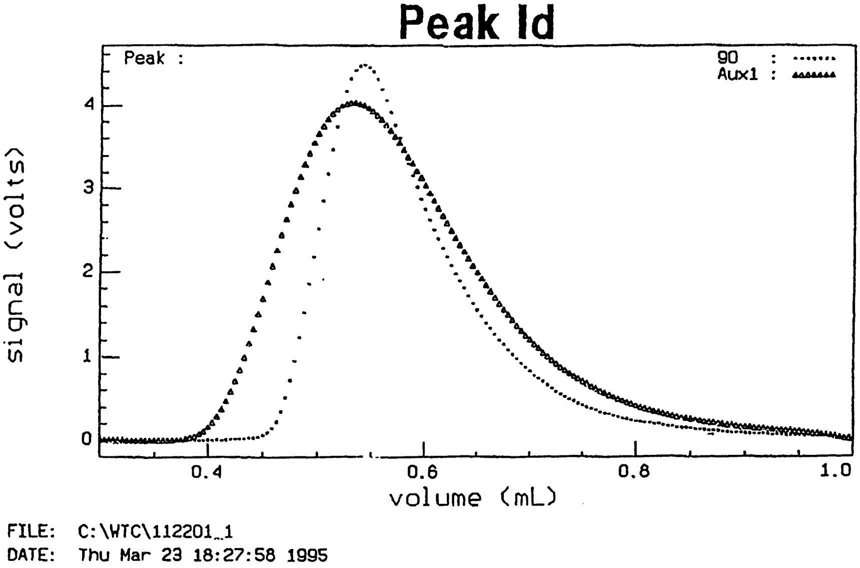

Figure 4.
LS and RI chromatograms of Ficol A_4 in water with using guard column SW xl. Flow rate is 0.5 ml/min. Injection volume is 50 µl. Solute concentration is 7 mg/ml., dn/dc=0.159. Molecular weights according to "ASTRA" software are following: Mw=143000, Mn=103000, Mz=164000, Mw/Mn=1.40, Mz/Mn=1.60.

Table 1.
Weight average molecular weights for different PEG and ficol samples obtained with and without a chromatographic column

Sample name	Mw using a chromatographic column	Mw without using a chromatographic column
PEG-3350	3500	3800
PEG-8000	8000	8300
PEG-10000	10000	9700
Ficol AS	20000	22000
Ficol A7	28000	32000
Ficol R2	51000	48000
Ficol A6	68000	63000
Ficol A5	84000	92000
Ficol R20	97000	108000
Ficol A4	139000	143000

The Table 1 shows that the difference between the two groups of data is on average less than 10% which is within the experimental error. Therefore, we can conclude that the dual detector chromatography method without using a chromatographic column provides reliable values for weight average molecular weights.

2. Study of micelle formation under chromatographic conditions.

Micelle formation was observed in chromatographic and batch modes for PEG-8000 and its copolymers, 8KLX, containing different numbers of lactate and acrylate groups. The hydrophobic portion of the copolymers 8KLX (lactate groups) forms the kernel of the micelles with the hydrophilic portion forming around the kernel. as a result, micelle formation is observed in the solution. The phenomenon is dependent on the solute concentration: at higher concentrations the micelles are formed in greater numbers and with larger size. Since our primary goal is not the investigation of the micelle formation phenomenon, we would like to encourage others to evaluate this new method as a means of study micelle formation and aggregation in solutions. We will not discuss any publications in the area but would like to emphasize that the water used to prepare the polymer solutions and the solutions themselves were carefully filtered through a 0.02 μ filter. No particulate impurities with size greater than 0.02 μ were present in the solutions before chromatographic runs or LS measurements performed in batch mode. Micelle formation at high solute concentrations unattainable in a standard chromatographic system was observed when

Downloaded by UNIV MASSACHUSETTS AMHERST on October 8, 2012 | http://pubs.acs.org
Publication Date: May 30, 1996 | doi: 10.1021/bk-1996-0635.ch017

Downloaded by UNIV MASSACHUSETTS AMHERST on October 8, 2012 | http://pubs.acs.org
Publication Date: May 30, 1996 | doi: 10.1021/bk-1996-0635.ch017

chromatography was performed using only a guard column. The guard column was employed provide a pressure drop inside the chromatographic system and to separate the LS detector response for the injection from the real light scattering signal. The use of the guard column allows also to obtain a separation of the macromolecules from larger aggregates if these aggregates are present in solution.

Figure 5 shows RI and LS chromatograms for a PEG-8000 sample exhibiting a solute concentration of 2.7 mg/ml at the peak maxima. Comparison of the LS chromatograms in Figure 5 and Figure 3 (where the solute concentration is 10 times lower) indicates the presence of an additional peak in high molecular weight area corresponding to PEG aggregates.

8KLX samples form aggregates more readily than PEG due to the hydrophobic-hydrophilic nature of the sample, and form micelles at lower solute concentration levels. Figure 6 demonstrates this phenomenon for a chromatographic run using only guard column. In this case the concentration of the injected solution was the same as for PEG in Figure 1, but the LS photometer clearly detects the micelle peak.

If we increase the polymer concentration in the solution, the micelles will be present in greater number. In addition, the average molecular weight of the micelles observed in the second peak increase from 8500 dalton to 9200 dalton (Figure 7).

The accuracy for the measurement of the micelle molecular weight in the first peak is not high due to the small response of the RI detector at very small micelle concentrations. The average molecular weights for the whole samples being investigated are much more accurate. These values are collected in the Table2.

Table 2.
Average molecular weights for PEG-8000 and 8KLX at different solute concentrations

Solute concentration %	PEG-8000 Mw	8KLX Mw
0.1	8000	8500
0.2	8000	11000
0.3	8000	12000
0.5	8000	15000
0.6	12000	19000

Downloaded by UNIV MASSACHUSETTS AMHERST on October 8, 2012 | http://pubs.acs.org
Publication Date: May 30, 1996 | doi: 10.1021/bk-1996-0635.ch017

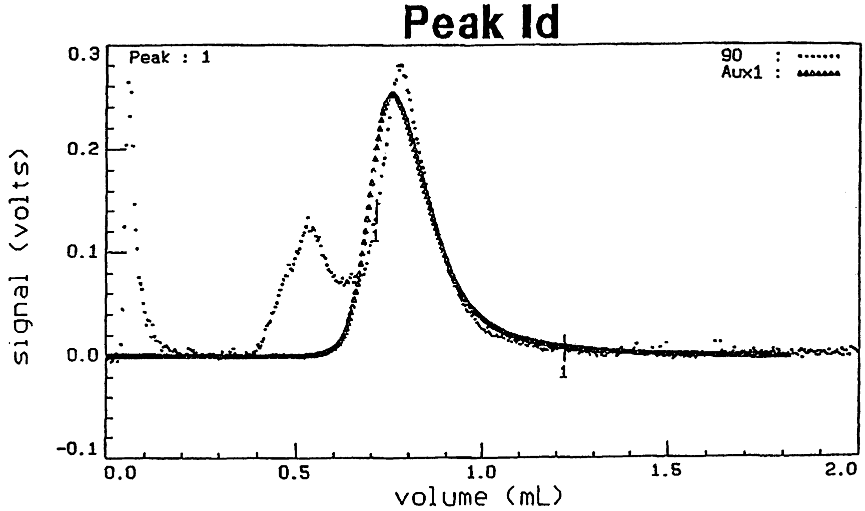

FILE: C:\WTC\112201_8
DATE: Thu Mar 23 17:35:39 1995

Figure 5.
LS and RI chromatograms of PEG 8000 in water with using guard column SW xl. Flow rate is 0.5 ml/min. Injection volume is 50 µl. Solute concentration is ~ 10 mg/ml. The concentration at peak maximum is 2.7 mg/ml., dn/dc=0.134., Molecular weights according to "ASTRA" software are following: Mw=8300, Mn=8000, Mz=8600, Mw/Mn=1.04, Mz/Mn=1.08.

Downloaded by UNIV MASSACHUSETTS AMHERST on October 8, 2012 | http://pubs.acs.org
Publication Date: May 30, 1996 | doi: 10.1021/bk-1996-0635.ch017

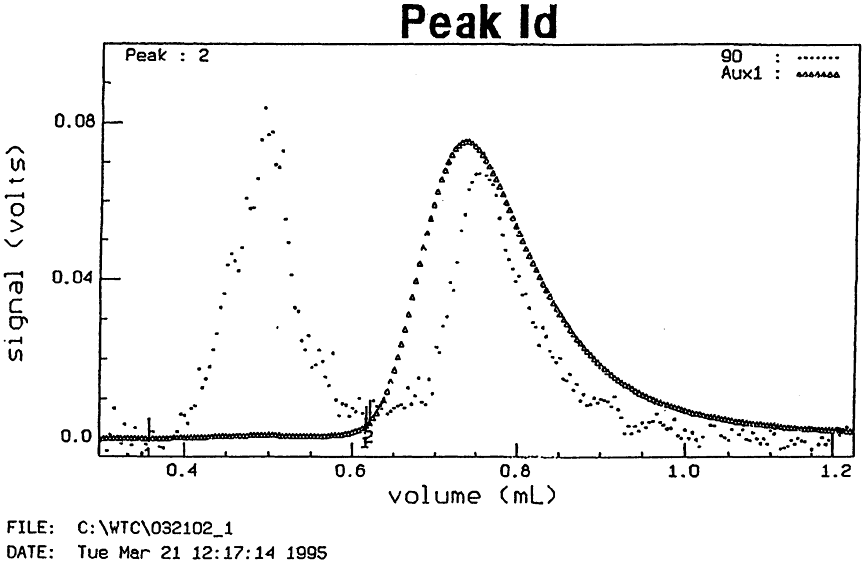

Figure 6.
LS and RI chromatograms of PEG 8000 copolymer with lactate and acrylate groups in water with using guard column SW xl. Flow rate is 0.5 ml/min. Injection volume is 25 µl. Injected solute concentration is 5 mg/ml. The concentration at main (second) peak maximum is 0.6 mg/ml, contain in the sample 99%. The concentration at micelle (first) peak maximum is 0.0014 mg/ml., contain inthc samplc 1%. dn/dc=0.134. Average molecular weights according to "ASTRA" software are following: Mw=17000, Mn=6800, Mz=576000, Mw/Mn=2.53, Mz/Mn=84.4. For the micelle peak Mw=966000, for the second peak Mw=8800.

Downloaded by UNIV MASSACHUSETTS AMHERST on October 8, 2012 | http://pubs.acs.org
Publication Date: May 30, 1996 | doi: 10.1021/bk-1996-0635.ch017

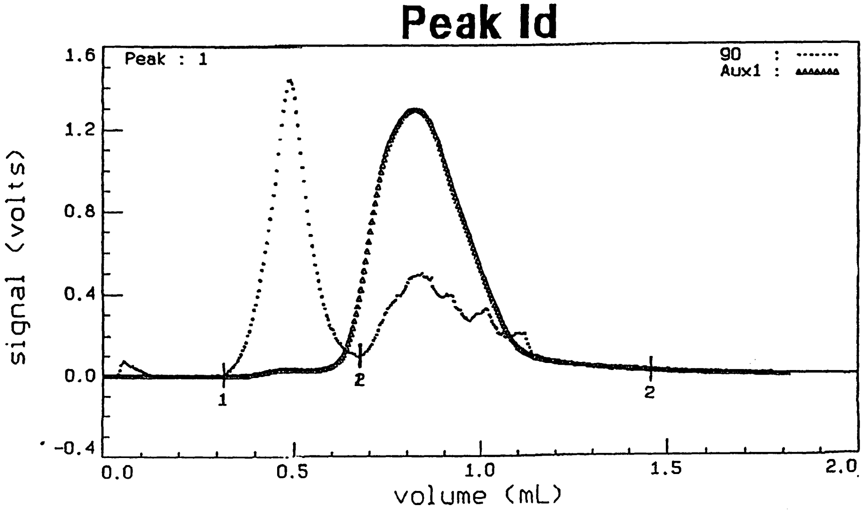

FILE: C:\WTC\03150511
DATE: Thu Mar 23 17:58:38 1995

Figure 7.

LS and RI chromatograms of PEG 8000 copolymer with lactate and acrylate groups in water with using guard column SW xl. Flow rate is 0.5 ml/min. Injection volume is 15 µl. Injected solute concentration is 100 mg/ml. The concentration at main (second) peak maximum is 5.8 mg/ml, contain in the sample 95.6%. The concentration at micelle (first) peak maximum is 0.118 mg/ml., contain in the sample 4.4%. dn/dc=0.134. Average molecular weights according to "ASTRA" software are following: Mw=24000, Mn=9200, Mz=734000, Mw/Mn=2.56, Mz/Mn=79.4. For the micelle peak Mw=294000, for the second peak Mw=9200.

Downloaded by UNIV MASSACHUSETTS AMHERST on October 8, 2012 | http://pubs.acs.org
Publication Date: May 30, 1996 | doi: 10.1021/bk-1996-0635.ch017

From these data it is possible to say that aggregation of the PEG-8000 start when the concentration of the solution is higher 0.5%. The micelle formation for the 8KLX starts at a much lower concentration, around 0.2%. This means the concentrations of 0.5% and 0.2% may be considered the critical points for micelle formation for the PEG and 8KLX correspondingly. Figure 8 illustrates the data.

3. Study micelle formation using multi-angle LS photometer in batch mode.

Our chromatographic studies of micelle formation was limited by the maximum solute concentration level. Since maximum signal for Hewlett Packard RI detector cannot exceed 2.2 volts, the corresponding maximum solute concentration at the peak maximum is around 6 mg/ml. Therefore, the chromatographic method can not be used to study micelle formation at concentrations higher than this level. To conduct an investigation of micelle formation at higher concentration levels, we used a multi-angle LS photometer in batch mode. For this case the theoretically-derived form factor $P(\theta)$ in Eq. 1 is related to the mean square radius of gyration $<s^2>^{1/2}$ when $\mu^2<s^2> <<1$

$$P(\theta)=1-2\mu^2<s^2>/3!+... \quad (3)$$

where $\mu=(4\pi/\lambda)\sin(\theta/2)$ and λ is the wavelength of incident radiation.

So, by use of the LS photometer, it is possible to determine an average size of macromolecules and their aggregates in the solution at concentrations significantly higher than those attainable under the chromatographic conditions. The data are shown in the Table 3 and Figures 9 and 10. Since the LS photometer used (DAWN DSP) was not able to observe macromolecules of size less than 5 nm, we calculated sizes for the PEG and 8KLX molecules below the limit. In these cases, the sizes can be calculated according to the Flory-Fox equation

$$[\eta]=\Phi<s^2>^{3/2}/M) \quad (4)$$

with the corresponding values of Mark-Houwink constants K and a

$$[\eta]=KM^a \quad (5)$$

where $[\eta]$ is the intrinsic viscosity, M is the molecular weight, and Φ is the Flory constant.

4. Spectroscopic study of micelle formation.

The aggregation characteristics of the 8KLX macromolecules were studied by using a dye solubilization technique. 1,6 diphenyl 1,3,5 hexatriene (DPH, Aldrich, 99.99% purity) was chosen as a molecular probe. Macromolecular solutions were prepared in screw-capped vials in deionized water at concentrations ranging from 0.01% - 10% (w/v). 10 ml of 0.005 mM solution of the dye in methanol was added to each vial and equilibrated for at least an hour. The UV-Vis spectra of these solutions were obtained between 200-500 nm. The absorbance of DPH at 356 nm was plotted with respect to

Downloaded by UNIV MASSACHUSETTS AMHERST on October 8, 2012 | http://pubs.acs.org
Publication Date: May 30, 1996 | doi: 10.1021/bk-1996-0635.ch017

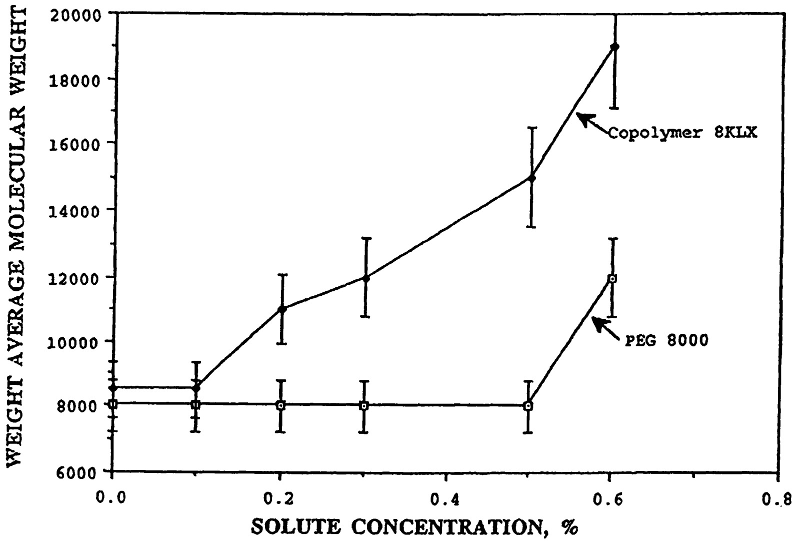

FIGURE 8
AVERAGE MOLECULAR WEIGHT OF POLYMER SOLUTION AS A FUNCTION OF SOLUTE CONCENTRATION

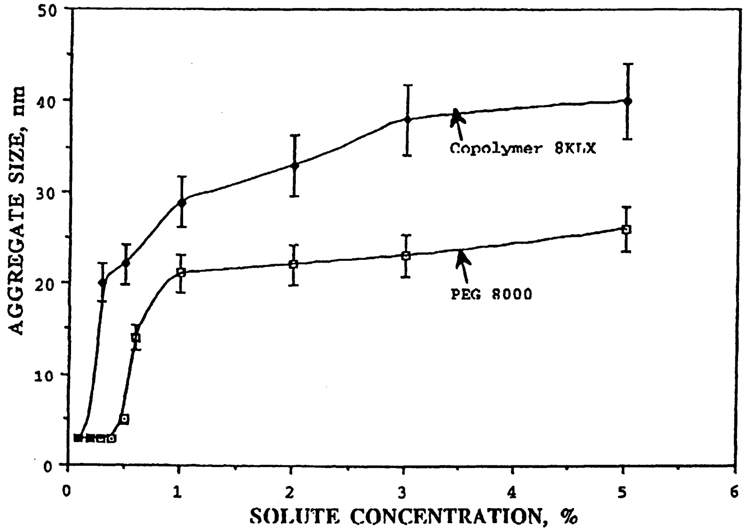

FIGURE 9
AVERAGE SIZE OF MACROMOLECULES AND THEIR AGGREGATES IN THE SOLUTION AS A FUNCTION OF CONCENTRATION

Downloaded by UNIV MASSACHUSETTS AMHERST on October 8, 2012 | http://pubs.acs.org
Publication Date: May 30, 1996 | doi: 10.1021/bk-1996-0635.ch017

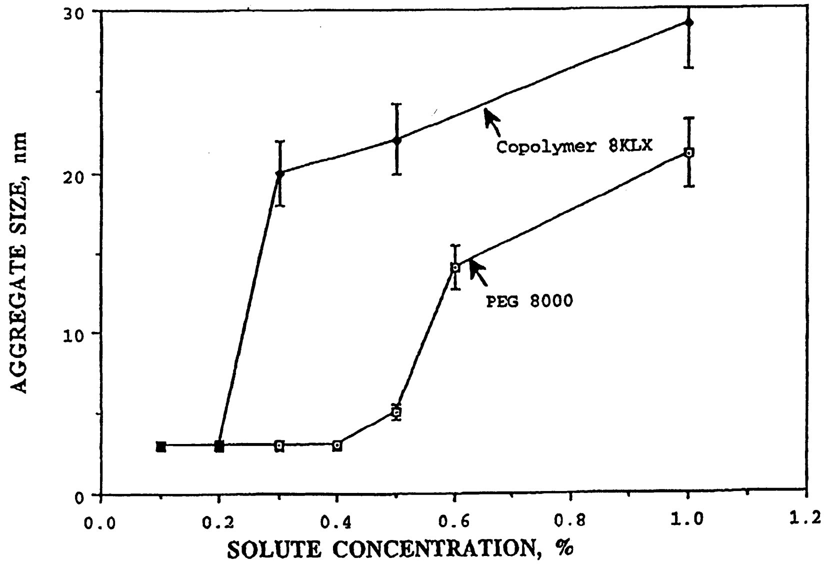

FIGURE 10
AVERAGE SIZE OF MACROMOLECULES
AND THEIR AGGREGATES IN THE SOLUTION
AS A FUNCTION OF CONCENTRATION BELOW 1%

Downloaded by UNIV MASSACHUSETTS AMHERST on October 8, 2012 | http://pubs.acs.org
Publication Date: May 30, 1996 | doi: 10.1021/bk-1996-0635.ch017

Table 3.
Average sizes of macromolecular species present in solutions of PEG-8000 and its copolymer 8KLX

Solute concentration, %	Average size for PEG molecules and their aggregates, nm	Average size for 8KLX and their micelles, nm
0.1	3*	3*
0.2	3*	18
0.4	3*	-
0.5	5	25
0.6	14	-
1.0	21	33
2.0	22	33
3.0	23	37
5.0	26	39

* Calculated from Eq. 4.

Downloaded by UNIV MASSACHUSETTS AMHERST on October 8, 2012 | http://pubs.acs.org
Publication Date: May 30, 1996 | doi: 10.1021/bk-1996-0635.ch017

logarithm of concentration. The critical concentration for micelle formation, cmc, was determined from the inflection of the absorbance vs. log concentration curve /7/.

At low concentrations, macromolecules of 8KLX samples do not associate in aqueous solution, DPH was not solubilized in hydrophobic environment and therefore, the UV-Vis intensities due to DPH are very low.

At higher concentrations, exceeding the cmc, the macromolecules formed micelles and DPH was solubilized in the hydrophobic micelle environment, and is observable by measurement of its characteristic absorbance at 356 nm.

A comparison of the spectroscopic data (Fig. 11) and the data from LS batch method or the chromatographic method (Fig. 8-10) gives a good correlation for the critical micelle concentrations obtained from the methods.

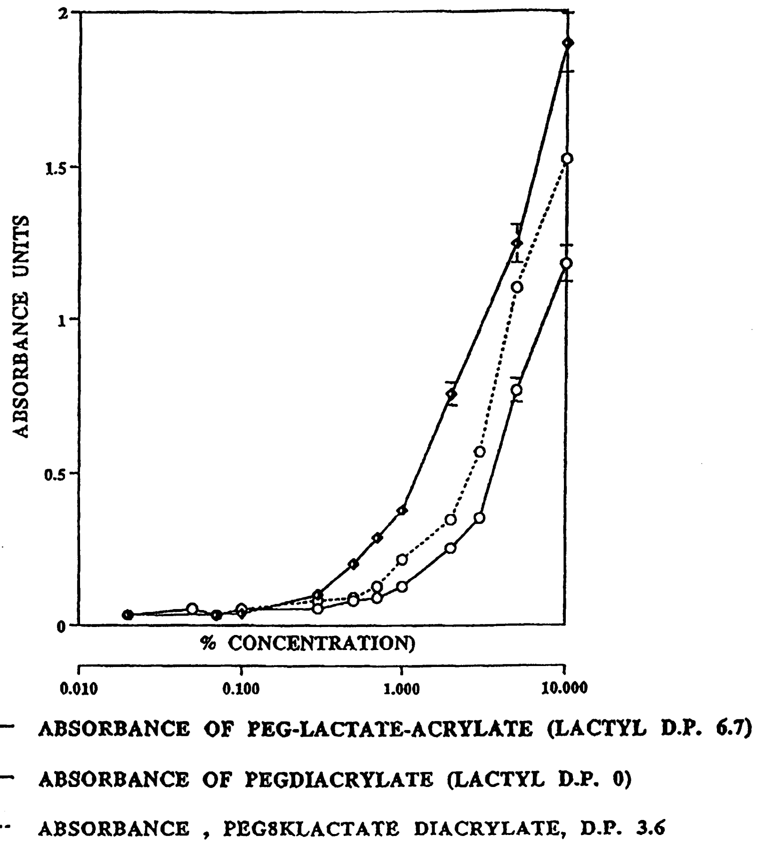

FIGURE 11

DETERMINATION OF CRITICAL MICELLAR CONCENTRATION OF PEG DIACRYLATE AND PEG-LACTATE-ACRYLATE (D.P. 6.7, 3.6)

Conclusion

The data obtained show that using a multi-angle LS photometer in batch mode and in the chromatographic mode without a chromatographic column with an additional RI detector in line, it is possible to determine weight average molecular weights and sizes of macromolecular species and study the phenomenon of micelle formation over a wide range of solute concentrations.

Literature Cited

1. Moore, J. C. *J. Polym. Sci. Part A* **1964,** , *835,* 2.
2. Debye, P. *Appl. Phys.* **1944,** *15,* 338.
3. Zimm, B. *J. Chem. Phys.* **1948,** *16,* 1093.
4. Jones, A. G. *Analytical Chemistry. Some new techniques;* L.; 1959; p.196.
5. Belenkii, B. G.; Vilenchik, L. Z. *Modern Liquid Chromatography of Macromolecules;* J. Chromatogr. Library-vol. 25; Elsevier; Amsterdam, 1983; p. 199.
6. Wyatt, P. *Analytical Chimia Acta* **1993,** *272,* 1.
7. Alexandris, P.; Holzwarth, J. F.; Hatton, A.T. *Macromolecules* **1994,** *27,*2414.

Downloaded by UNIV MASSACHUSETTS AMHERST on October 8, 2012 | http://pubs.acs.org
Publication Date: May 30, 1996 | doi: 10.1021/bk-1996-0635.ch017

Downloaded by UNIV MASSACHUSETTS AMHERST on October 10, 2012 | http://pubs.acs.org
Publication Date: May 30, 1996 | doi: 10.1021/bk-1996-0635.ch018

Chapter 18

Comparison of Secondary Effects in Aqueous Size Exclusion Chromatography Between Sodium Poly(styrenesulfonate) Compounds of Different Sulfonations

Preliminary Study

Sadao Mori and Toshitaka Oosaki

Department of Industrial Chemistry, Faculty of Engineering, Mie University, Tsu, Mie 514, Japan

Hydrophobic interactions of sodium poly(styrenesulfonate) compounds (NaPSS) of different sulfonation were investigated. One was commercially available and was considered to be less than 85% degree of sulfonation. The other was prepared in our laboratory from sodium styrenesulfonate monomer and was considered to be 100% sulfonation. Column was Shodex PROTEIN KW-804 packed with glycerylpropylgroup bonded silica gel. Mobile phase was sodium phosphate buffer at pH 7.0 at different ionic strengths. Calibration plots for these two types of NaPSS pullulan showed that retention volumes of NaPSS increased with increasing the ionic strength, but the extent was different between two types of NaPSS. Hydrophobicity of low sulfonated NaPSS was originated from both unreacted phenylgroups and the backbone C-C linkage. Highly sulfonated NaPSS still exhibited some hydrophobicity which may be originated from the backbone C-C linkage.

Aqueous size exclusion chromatography (ASEC) is the technique that permits the separation and the measurement of molecular weight (MW) averages of water-soluble polymers which include ionic or nonionic synthetic polymers and proteins. However, since both the stationary phase and the polyer solute in ASEC of ionic polymers possess numerous polar groups, mutual interactions between them will lead to non-ideal SEC. These mutual interactions are divided into two secondary effects: ion exclusion and hydrophobic interactions.

In the previous paper (*1*), elution behavior of sodium poly(styrenesulfonate)(NaPSS) compounds compared with nonionic linear polysaccharide (pullulan) on several types of ASEC columns was reported at varing ionic strengths of the mobile phase. The divergence of the hydrodynamic volume calibration curves of NaPSS from that of the pullulan was observed and the calibration curves of NaPSS changed with changing the ionic strength. These phenomena were ascribed to the combination of three separation effects: size exclusion, ion

0097–6156/96/0635–0347$15.00/0

exclusion, and hydrophobic interactions. There are a number of similar studies concerning the secondary effects in ASEC of sodium poly(styrenesulfonate) compounds (*2-6*).

NaPSS samples used in the previous study were purchased from the commercial source and were prepared from polystyrene samples of narrow MW distributions by sulfonation. Therefore, the degree of sulfonation of the NaPSS samples used in the work was supposed to be less than 85% and the unreacted phenyl groups may be considered to be the main sites of hydrophobic interactions.

In the present work, the preparation of NaPSS of 100% degree of sulfonation has been attempted and the elution behavior of both commercial NaPSS samples (designated as low sulfonated NaPSS) and NaPSS samples prepared in our laboratory (designated as highly sulfonated NaPSS) has been compared. This is the preliminary report on this matter. The detailed study on this subject will be published elsewhere.

Experimental

Preparation of NaPSS of 100% degree of sulfonation. Sodium styrene sulfonate (monomer)(reagent grade, Tokyo Kasei, Japan) was purified by recrystalization two times with the water-acetone system. 5.3 g of the monomer, 0.3 g of sodium sulfite, and 0.14 g of potassium peroxydisulfate (these two reagent were used as polymerization initiators) were dissolved in 15 mL of degassed distilled water and the solution was reacted for 1 h at 45 °C under reduced pressure. The reaction solution was then poured into excess acetone with stirring. The precipitated material was dissolved in water and the solution was poured into excess acetone. This process was repeated two times and then the obtained precipitate was dried at room temperatures under vacuum.

The polymer sample was then fractionated into eight fractions by fractional precipitation, dissolving the polymer sample in 4 N sodium iodide solution in the concentration of 1% and kepting the solution at 20 °C, followed by dropping 9.1 N sodium iodide solution into the polymer solution. Precipitated material was filtered and each fraction was purified by dissolution of the filterated fraction into water, followed by reprecipitation of the material into acetone.

ASEC. Measurements were performed on a Jasco high-performance liquid chromatograph Model TRIROTAR-V (Jasco, Tokyo, Japan) with a refractive index detector Model SE-11 (Showa Denko, Tokyo, Japan). A column was Shodex PROTEIN KW-804 (300-mm x 8-mm id.d) packed with glycerylpropyl group-bonded silica gel (a glycophase-bonded support). Pullulan standards which are nonionic linear polysaccharides were purchased from Showa Denko and NaPSS standards were from Pressure Chemical (Pittsburgh, PA).

The mobile phase was made up from sodium monohydrogen phosphate, Na_2HPO_4, and sodium dihydrogen phosphate, NaH_2PO_4, to the disired ionic strength at pH 7.0. Ionic strength was changed from 0.005M to 0.3M. The flow rate was 1.0 mL/min. The sample were dissolved in the solvent used as the mobile phase in the concentration of 0.05% and injection volume of these sample solutions was 0.1 mL.

Downloaded by UNIV MASSACHUSETTS AMHERST on October 10, 2012 | http://pubs.acs.org
Publication Date: May 30, 1996 | doi: 10.1021/bk-1996-0635.ch018

Downloaded by UNIV MASSACHUSETTS AMHERST on October 10, 2012 | http://pubs.acs.org
Publication Date: May 30, 1996 | doi: 10.1021/bk-1996-0635.ch018

Results

Calibration plots for low sulfonated NaPSS, highly sulfonated NaPSS and pullulan standards are shown in Figure 1 at various ionic strengths. The effect of the ionic strength on retention volume for pullulan was almost negligible. In contrast to pullulan, the significant difference in retention volume for NaPSS with ionic strength was observed. The intersitial volume was estimated to be at 6.0 mL with low sulfonated NaPSS having MW 10^6.

Retention volume of both types of NaPSS increased with increasing the ionic strength. At lower ionic strengths (0.005 M and 0.01 M), both types of NaPSS eluted from the column earlier than pullulan and they possessed the almost similar calibration plots at each ionic strength. At higher ionic strengths (0.2 M and 0.3 M), they

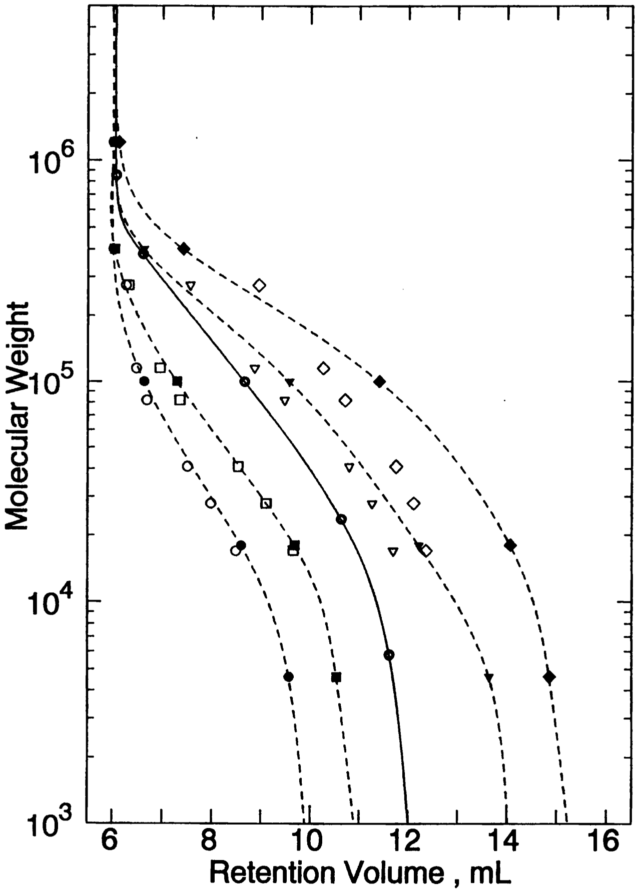

Figure 1. Calibration plots for pullulan (⊙), low sulfonated NaPSS (filled marks), and highly sulfonated NaPSS (open marks). A solid line is a pullulan calibration curve and broken lines are calibration curves for low sulfonated NaPSS. Ionic strength; ● ○ , 0.005 M; ■ □ , 0.01 M; ▼ ▽ ,0.2 M; ◆ ◇ , 0.3 M.

eluted later than pullulan and highly sulfonated NaPSS eluted earlier than low sulfonated NaPSS having the similar MW. This difference in retention volume became larger with increasing the ionic strength.

Discussion

Shodex PROTEIN KW-804 column still has some amount of unreacted silanol groups on the surface of packings. Early elution of NaPSS relative to pullulan on the column is governed by the ion exclusion effect as reported in the previous paper. The extent of the electro static interactions between NaPSS and the packings was almost the same, implying that the electrorepulsive force of low sulfonated NaPSS is similar to that of highly sulfonated NaPSS.

Glycerylpropyl(1,2-dihydroxy-3-propoxypropyl) groups which are bonded on the surface of the packings are hydrophilic and therefore, hydrophobic interactions between the support and NaPSS solutes are supposed to be small. However, as reported in the previous paper, late elution of NaPSS relative to pullulan is governed by hydrophobic interactions between NaPSS and the packings. The extent of the hydrophobic interactions of low sulfonated NaPSS is larger than highly sulfonated NaPSS, implying that the hydrophobic interactions of low sulfonated NaPSS are governed by both unreacted phenyl groups and the backbone C-C linkage of propoxypropyl groups on the packings. Hydrophobic parts of highly sulfonated NaPSS are only the backbone C-C linkage, therefore, hydrophobic interactions of highly sulfonated NaPSS are smaller, resulting early elution than low sulfonated NaPSS.

In conclusion, hydrophobicity of low sulfonated NaPSS is originated from both unreacted phenyl groups and the backbone C-C linkage. Highly sulfonated NaPSS still exibits some hydrophobicity in the ASEC system examined in this work and the main site of the hydrophobicity is originated from the backbone C-C linkage. Low sulfonated NaPSS is supposed to have unreacted ohenyl groups (Dubin,P., Indiana University Purdue University Indianapolis, personal communication, 1994).

Literature Cited

(1) Mori, S. *Anal. Chem.* 1989, *61*, pp 530-534.
(2) Spatorico, A. L. Beyer, G. L. *J. Appl. Polym. Sci.* 1975, *19*, pp 2933-2945.
(3) Rochas, C.; Domard, A.; Rinaudo, M. *Eur. Polym. J.* 1980, *16*, pp 135-140.
(4) Callec, G.; Anderson, A. W.; Tsao, G. T.; Rollings, J. E. *J. Polym. Sci. Polym. Chem. Ed.* 1984, *22*, pp 287-293.
(5) Dubin, P. L.; Tecklenburg, M. M. *Anal. Chem.* 1985, *57*, pp 275-279.
(6) Soria, V.; Campos, A.; Garcia, R.; Parets, M. J. *J. Liq. Chromatogr.* 1990, *13*, pp 1785-1808.

Downloaded by UNIV MASSACHUSETTS AMHERST on October 10, 2012 | http://pubs.acs.org
Publication Date: May 30, 1996 | doi: 10.1021/bk-1996-0635.ch018

Chapter 19

Molecular Characteristics of Glucans: High-Amylose Cornstarch

A. Huber[1] and W. Praznik[2]

[1]Institut für Physikalische Chemie, Heinrichstrasse 28,
A–8010 Graz, Austria
[2]Interuniversitäres Forschungszentrum für Agrarbiotechnologie,
Konrad-Lorenzstrasse 20, A–3430 Tulln, Austria

Macroscopic properties of starch are determined by molecular characteristics such as molecular weight distribution, branching characteristics, glucan coil packing density and coil dimensions. For determination of these characteristics, glucan fractions of high-amylose corn starch have been prepared by selective precipitation. A fraction of 70% mass was fractionated by n-butanol precipitation and is expected to consist of non-branched (nb) and long-chain branched (lcb) glucans. A second fraction of 30% mass was precipitated by an excess of methanol from the prior n-butanol complexation and is expected to consist of short-chain branched (scb) glucans. For analytical purposes the glucans were dissolved in DMSO to get true solutions. These samples were separated on a SEC-system with an aqueous eluent, a procedure which includes an in-line switching of glucan-solvent from DMSO to water. Dual in-line detection of mass and scattering intensity yielded basic data to achieve distributions of sphere-equivalent glucan-coil dimension (R_eD) and of absolute molecular weights as well in terms of mass (MWD_m) as of number (MWD_n) of constituting components. Additional application of enzymatically catalyzed hydrolization of branching linkages yielded the constituting glucan chain distribution and information about chain lengths of branches.

Glucans from green plants represent the major renewable feedstock for industrial utilization and thus, deserve general attention as much as they are of considerably and increasing econcomic interest (1,2). Although available in huge amounts, these materials are hard to handle, because of their highly fluctuating qualities given by the dependence of material properties on a wide variety of molecular parameters (3,4) which in turn are controlled by environmental conditions: mutual dependence of internal composition, dimensions and structure/ conformation, of macroscopic

0097–6156/96/0635–0351$15.00/0

arrangement of constituting components and of functionalities far away from thermodynamic equilibrium. Like the properties of any components within such complex systems, glucans are affected by these circumstances and mirror the history of influences in their macroscopic and molecular characteristics. Molecular characteristics can be written as one edge of a triangle of mutual dependences of

$$\begin{tikzcd}
\text{structure/arrangement of constituting components} \arrow[d, <->] \arrow[dr, <->] & \\
\text{functionality} \arrow[r, <->] & \text{sensitivity towards/ transformation on external influences}
\end{tikzcd}$$

and determination of these characteristics is one piece in the puzzle to improve understanding of complex systems in general, and of polymer-characteristics, specifically.

Historically, starch is supposed to consist of two fractions, namely amylose (non-branched) and amylopectin (branched), but purification of these fractions, particularely of amylose, is more or less impossible without generating artefacts (5). Additionally, this traditional classification refers to ideal situations and better should be replaced by distinguishing between non-branched (nb) long-chain-branched (lcb) and short-chain-branched (scb) glucans (6). Within this concept non-branched glucans are supposed to be the initially synthesized oligomers/polymers, whereas branching occurs as a secondary step. Kind and extent of branching thereby mainly is determined by the need for specific polymer-characteristics within the producing organism to keep up or to enable certain system-functionalities. Consequently, the molecular characteristics of starch-glucans strongly depend on the history of their creation, in particluar on the activities of plant-specific enzyme-systems, but additionally on global influences and limiting conditions for the glucan-producing plant-cells (7). Investigation of molecular characteristics of starch glucans therefore includes investigation of system properties and any result will mirror system properties.

Materials and Methods

Sample. High amylose corn starch was provided by Cerestar R&D/Belgium as dry white powder. The sample was dissolved in 90% aqueous DMSO with a concentration of 1% (wt./v). Dissolution was completed by stirring over night at 70°C. A clear solution was obtained either immediately or after centrifugation (3000 rpm, 15 min). Analysis of non-dissolved residues proved them to be non-starch materials. DMSO dissolved starch samples can be stored for several weeks without significant aging-effects such as degradation, aggregation or retrogradation (8). For analysis in terms of molecular weight distribution (MWD) and branching characteristics (nb, lcb, scb), the initially purified glucans from high amylose corn starch were fractionated according to their different ability to form precipitation complexes with n-butanol and methanol, respectively. The consecutive steps for characterization of these glucan fractions are listed in Table I.

Enzymatically Catalyzed Debranching. For specific debranching the 90% aqueous DMSO dissolved glucans were diluted with 2 volumes of aqueous buffer and then mixed with pullulanase (EC 3.2.1.41), an $\alpha(1\rightarrow6)$-glycosidic linkage hydrolizing enzyme (Hayashibara; 0.3 IU mg^{-1} carbohydrates). Hydrolysis was performed at 37°C for 48 h in total, with additional pullulanase incubation after 24 h to ensure complete debranching (8).

SEC-DRI/LALLS. For the SEC-DRI/LALLS-experiments (9) an interferometric differential refractometer at a wavelength of DRI($\lambda_{630\ nm}$) (Wyatt Technology, Optilab 903) and a low angle laser light scattering (LALLS) instrument (TSP, KMX-6) were utilized. Size-exclusion chromatography of the glucans was performed utilizing a set of TSK columns, G6000 PW, G5000 PW and G3000 PW, each with l=600 mm, ID=7mm, (ToyoSoda). Eluent for SEC was 0.05 M NaCl$_{aqu}$ at a flow rate of 0.8 mL min^{-1}.

Table I. Applied Techniques for Characterization of Starch Glucans

Technique	**Sample** / Activity / achieved Characteristics	
purification	glucans of high-amylose **corn-starch**	
dissolution	in 90% aqueous DMSO	
fractionation	n-butanol-precipitate: **nb/lcb-glucans**	n-butanol-supernatant
		methanol-precipitate: **scb-glucans**
dissolution	90% aqueous DMSO	90% aqueous DMSO
SEC-DRI/LALLS-analysis, aqueous eluent	absolute MWD	absolute MWD
enzymatically catalyzed de-branching	pullulanase-catalysis: **debranched nb/lcb-glucans**	pullulanase-catalysis: **debranched scb-glucans**
SEC-DRI/LALLS-analysis, aqueous eluent	absolute MWD, branching charact.	absolute MWD, branching charact.
absolute MWD from SEC-DRI/LALLS & Universal Calibration	**initial & debranched nb/lcb-glucans:** coil dimensions, coil packing density	**initial & debranched scb-glucans:** coil dimensions, coil packing density

Results and Discussion

Aqueous SEC of DMSO-dissolved High-Amylose Corn-Starch Glucans. Dissolution of starch glucans needs breaking of H-bondings. Aqueous K OH as well as DMSO are so-called H-bond breakers and yield true glucan solutions. For chromatographic analyses advantages of DMSO compared to aqueous K OH are obvious: quartz-cells (e.g. in light scattering instruments) do not withstand alkaline pH; no neutralization is required and therefore no change/increase of ionic strength has to be considered; no accompanying substances such as proteins and/or lipids will be dissolved by DMSO and therefore, dissolving starch glucans in DMSO is also a purification step. This fact has to be considered for consecutive analytical activities. DMSO provides long-time stable glucan-solutions and destroys supramolecular structures which, at certain states of investigation, even might be of interest.

If DMSO-dissolved starch glucans are applied to an aqueous SEC-system, simultaneously with separation, an internal switching of glucan-solvent from DMSO to water is included because initial solvent DMSO will be shifted to/beyond the total permeation volume ofthe utilized SEC-system. As a minor dissadvantage from the pratical point of view, the SEC-system needs approximately one additional column-volume of eluent for regeneration of equlibrium conditions before application of the next sample.

Sample Concentration. For traditional calibrated SEC there is no primary need to know precise sample concentration. But of course there exists some kind of secondary interest in sample concentration to check the recovery and to assure that no specific fraction remains attached on the SEC-matrix or on in-line filters. This situation changes for detector based analysis where sample concentration becomes just one of the parameters needed to compute polymer characteristics such as molecular weight. Then the accuracy of sample concentration determines the accuracy of computed molecular weights. To increase this accuracy means to be sure about the mass of sample, that actually passes the detector cell. On-line mass detection by means of an interferometric refractometer which, once calibrated, either enables determination of specific refractive index increment or sample concentration yields this as 'true' as possible mass-information.

As additional advantages of on-line determination of sample concentration there is no need for prior (mass consuming) determination of moist content and, taking advantage of the SEC-separation mechanism, oligomer/polymer-concentrations of interest can be determined separated and separately from accompanying low-molecular components such as salts.

Molecular Weight of Polymers and Light Scattering. Static light scattering is an established technique to determine molecular weight of dissolved polymers. From the practical point of view there are two possibilities to achieve this information: either by detection of angular dependence of scattering intensity and extrapolation to zero-angle (MALLS-technique: multi-angle laser light scattering), or by experimental determination of scattering intensity at a sub-critically low scattering angle (below approx. 7°: LALLS-technique: low angle laser light scattering). An advantage of a MALLS-technique is that, in addition to molecular weight, information about particle-dimension in terms of the radius of gyration and about particle-shape from the particle scattering function (P_Θ) can be achieved. On the other hand, LALLS-instruments with a fixed low scattering angle provide instrument construction (geometry, optical pathways) to gather scattered intensity from the total spatial-segment of the scattering angle, which results in a significantly increased detection-sensitivity.

If a scattering instrument is connected as detector to a SEC-system, there are some additional considerations: in more or typically the eluted particles are not large enough to yield a particle scattering function different from P_Θ=1.0 and thus, usually no shape-information can be achieved; nevertheless, the radius of gyration for the eluted components can be determined. However, particle dimensions are also provided by SEC which separates components according to their size. Both, radius of gyration and chromatograpghic retention radius are complicated functions of molecular weight whereas scattering intensity at low scattering angles is directly correlated with molecular weight. For the investigated glucans of high-amylose cornstarch the parameter of primary interest is the molecular weight, and thus, a LALLS-detector with spatial detection of scattering intensity at 5° was connected to the SEC-DRI/LALLS experimental setup to get the scattering data from experiment and not from extrapolation.

Dissolution and Preparative Fractionation. According to the initial step in Table I, the purified high-amylose corn starch was dissolved in 90% aqueous DMSO and fractionated by precipitating a nb/lcb-glucan-fraction with n-butanol and a scb-glucan-fraction with excess of methanol from the remaining supernatant. This procedure refers to the ability of glucan-helices to form precipitation-complexes with more or less apolar agents (e.g. methanol, n-butanol) in aqueous media. It is well known that this complexation-potential increases with increasing lengths of the helices and thus, non-branched as well as long-chain-branched glucans are expected to form precipitation-complexes with n-butanol. Branching breaks helical structures and dissables the formation of precipitation complexes.

Application of this preparative fractionation procedure to the high-amylose corn starch yielded a composition of 70% n-butanol precipitate, expected to be nb/lcb-glucans, and 30% of methanol precipitate, expected to be scb-glucans.

Absolute Molecular Weights: Mass and Number Distribution. The initial result that is obtained from SEC-DRI/LALLS-experiments is a mass modulated molecular weight distribution: MWD_m. This includes the mass contribution of all i constituting components with weight average molecular weight $M_{w,i}$ and is computed from light-scattering (Rayleigh factor: R_Θ)- and mass (c)-data plus some additional constants (e.g.: Θ: scattering angle, K: optical constant, P_Θ: particle scattering function, A_2: second virial coefficient)

$$MWD_m = \frac{K \, . \, c_i}{R_{\Theta,i}} = \frac{1}{P_{\Theta,i}} \, . \, \frac{1}{M_{w,i}} + 2A_2.c_i$$

The initial glucan-mixture and the two glucan fractions were dissolved in 90% aqueous DMSO and analyzed by means of SEC-DRI/LALLS to get their MWD_m.

The resulting molecular weight distributions are shown in Figure 1. Both, the total corn glucan mixture and the two fractions cover the same range of molecular weight from 10.10^3 - 30.10^6 g M^{-1}. The initial mixture contains components in the highest molecular domain which couldn't be recovered in any of the two fractions. There is no final answer why these components disappear, but most probably these are aggregates which are destroyed. However, mass distributions of the two fractions differ slightly and their values for the weight average molecular weight are Mw=515000 g M^{-1} for the n-butanol precipitate and 497000 g M^{-1} for the methanol precipitate.

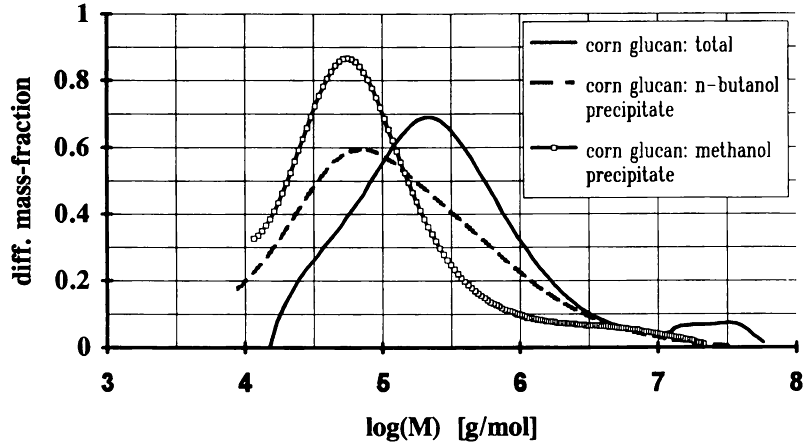

Figure 1. Mass modulated molecular weight distribution MWD_m of high-amylose corn starch glucans and of glucans from n-butanol- and methanol-precipitation.

Because dual-detection in SEC-DRI/LALLS-experiments does not requiare external calibration to obtain molecular weights of investigated polymers, it is often called an absolute technique. Often MWD_m is the kind of molecular weight distribution that is needed, but if e.g. branching characteristics are to be estimated/determined, one also needs the number modulated molecular weight distribution: MWD_n. Conversion of MWD_m into MWD_n is achieved as the ratio of mass-fraction (fr_m) and molecular weight (M) for each of the i components of MWD_m (10):

$$MWD_n = \frac{fr_{m_i}}{M_i}$$

Conversion of molecular weight distribution (MWD_m, MWD_n) into degree of polymerisation distribution (dpD_m, dpD_n) for the glucans of high amylose corn starch is computed as the ratio of molecular weight M and molecular weight of a glucose-monomer (M_0) for each of the i components.

$$dpD = \frac{M_i}{M_0} = \frac{M_i}{162}$$

Coil Conformation and Dimensions of High-Amylose Corn-Starch Glucans. A universal calibration function was established with well defined and commercially abvailable dextran standards (Pharmacosmos dextran standard kit). Comparing absolute calibration functions (log(M) versus V_{ret}) from SEC-DRI/LALLS with universal calibration function (log(M.[η]) versus V_{ret}) yields intrinsic viscosity versus M and thus the Staudinger/Mark/Houwink exponent SMH_a as a function of M for both glucan fractions (Figures 2a, 2b, Table II). SMH_a is an indicator of polymer-coil conformation.

The obtianed values for the glucan coil conformation indicator SMH_a for the mass main-fractions classify the n-butanol precipitate as loosely packed coils, whereas the methanol precipitated glucans seem to be quite compact coils (Table II). This fits very well with the expected branching characteristics of the two fractions: nb/lcb-glucans are known to form less compact coils than scb-glucans. Additionally, both fractions contain a minor number of components of the other fraction, a fact, that can be explained by equilibria of precipitation-fractionation.

With data for SMH_a and adjusted values for the constant K (keeping intrinsic viscosity above 1.0 mL g^{-1} and specific volume above 0.7 cm^3 g^{-1}, an empirical limit for globular proteins) distributions of sphere-equivalent polymer coil volumes (V_eD), sphere-equivalent glucan coil radii (R_eD) (Figure 3) and glucan coil packing density (ρ_eD) (Figure 4) were computed.

$$V_e = \frac{K\ M^{a+1}}{2.5\ N_A}$$

$$R_e = \left(\frac{3}{4\pi} \cdot \frac{K\ M^{a+1}}{2.5\ N_A}\right)^{\frac{1}{3}}$$

$$\rho_e = \frac{M}{N_A} \cdot \frac{1}{V_e}$$

For both glucan fractions the coil dimensions in terms of radii (R_e) of occupied sphere-equivalent volume range between 2 nm and approx. 60 nm, with a maximum close to 3 nm for the methanol precipitate and close to 6 nm for the n-butanol precipitate (Figure 3). Again, these results support the assumption, that n-butanol precipitated glucans are a mixture of nb/lcb-glucans which occupy more volume at a given degree of polymerization than methanol precipitated scb-glucans which pack much more compact. Coil-packing densities shows up with 5-6 times higher packing densities for the methanol precipitated glucans compared to the n-butanol precipitate (Figure 4).

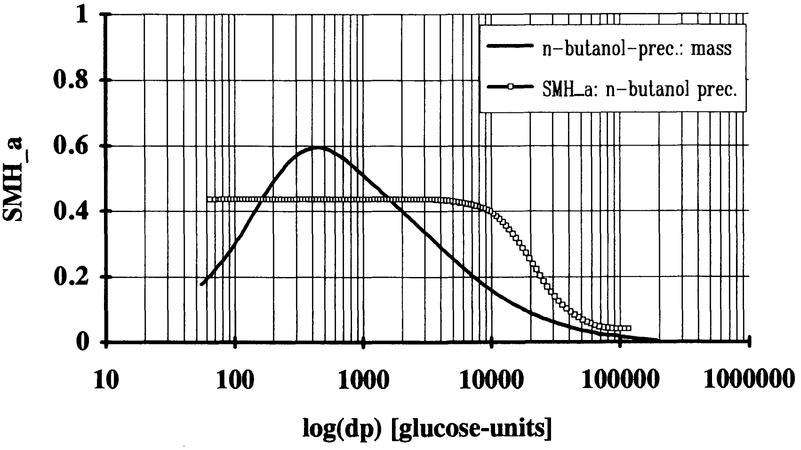

Figure 2a. dpD_m for n-butanol-precipitate of high-amylose corn starch and corresponding coil-conformation indicator SMH_a.

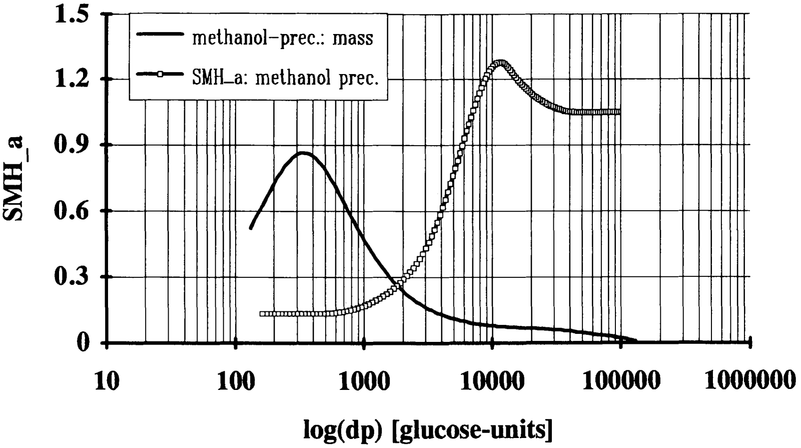

Figure 2b. dpD_m for methanol-precipitate of high-amylose corn starch and corresponding coil-conformation indicator SMH_a.

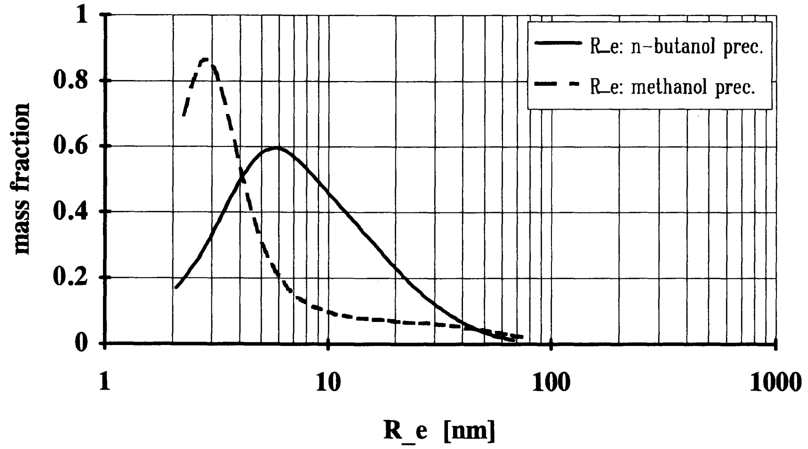

Figure 3. Mass distribution of glucan coil dimensions for high-amylose corn starch glucans: sphere equivalent radii distribution (R_eD).

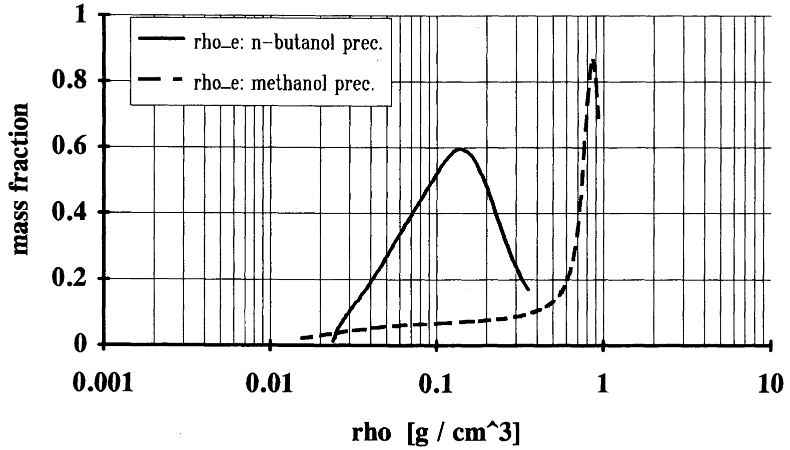

Figure 4. Mass distribution of glucan coil packing density (ρ_eD) for n-butanol and methanol precipitate of high-amylose corn starch glucans.

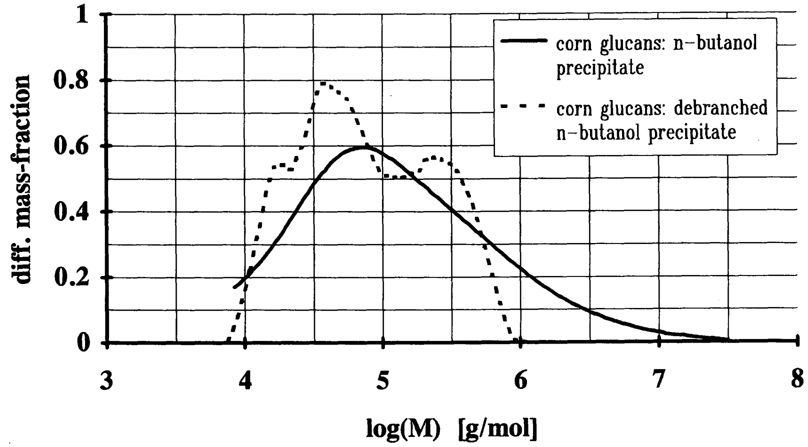

Figure 5a. MWD$_m$ for n-butanol precipitate of high-amylose corn starch before and after pullulanase-catalyzed complete debranching.

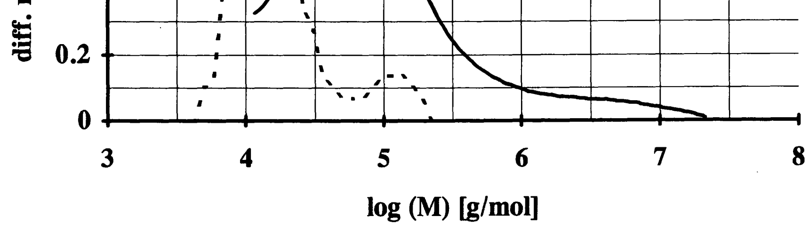

Figure 5b. MWD$_m$ for methanol precipitate of high-amylose corn starch before and after pullulanase-catalyzed complete debranching.

Enzymatically Supported Branching Analysis. To gain more detailed information about the branching characteristics, both glucan-fractions were modified by means of the catalytic action of pullulanase. This enzyme specifically hydrolizes $\alpha(1\rightarrow6)$-glycosidic linkages, the branching linkage in starch glucans and yieldes the constituting glucan-chain distributions.

Figures 5a and 5b show the resulting absolute molecular weight distributions MWD$_m$ before and after pullulanase-debranching action. Both, the n-butanol precipitated glucans and the methanol-precipitated ones became significantely modified. High molecular weight glucans obviously are branched because they vanish in both fractions. The resulting fragments for the methanol-precipitated glucans shift to lower molecular weights than those from the n-butanol precipitation, a fact, which again supports the expected branching characteristics.

Table II. Characteristics of Glucans from High-Amylose Corn Starch

Parameter	n-butanol precipitate **nb/lcb glucans**		methanol precipitate **scb glucans**	
starch composition	70 %		30 %	
	initial	debranched	initial	debranched
Mw [g M^{-1}]	515 000	191 000	497 000	29 000
dpw [glucose-units]	3 180	1 180	3 070	180
number of particles	100 %	184 %	100 %	> 2000 %
coil conformation				
SMH_a	0.437		0.132	
K	0.14		0.70	
sphere equivalent coil dimensions				
R_e range [nm]	2 .. 80		2 .. 80	
R_e(Max) [nm]	6		3	
packing density of equivlane sphere				
ρ_e range [g cm^{-3}]	0.02 .. 0.3		0.02 .. 0.9	
ρ_e(Max) [g cm^{-3}]	0.15		0.85	
dp of branches				
range [dp]	65 .. 2000		20 .. 160	
dp(Max_1) [dp]	90		65	
dp(Max_2) [dp]	200			

As branching characteristics are correlated with the number of particles rather than with the mass, the constituting glucan-dp-distributions are converted from mass- to number distribution (Figures 6a, 6b) and, finally, SEC-DRI/LALLS-analysis-results before and after hydrolysis of branching linkages are plotted to extract detailed information on the branch-dps and branch-dp-distribution (Figures 7a, 7b).

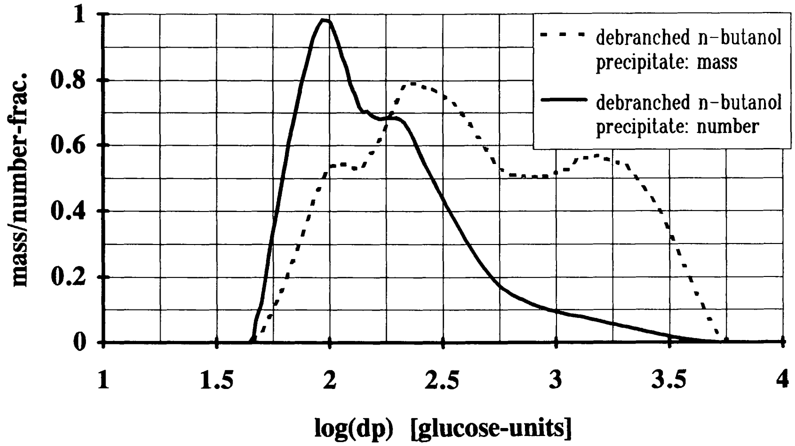

Figure 6a. Degree of polymerization distribution for pullulanase-debranched n-butanol precipitate of high-amylose corn starch: distribution of mass fractions dpD_m and of number fractions dpD_n.

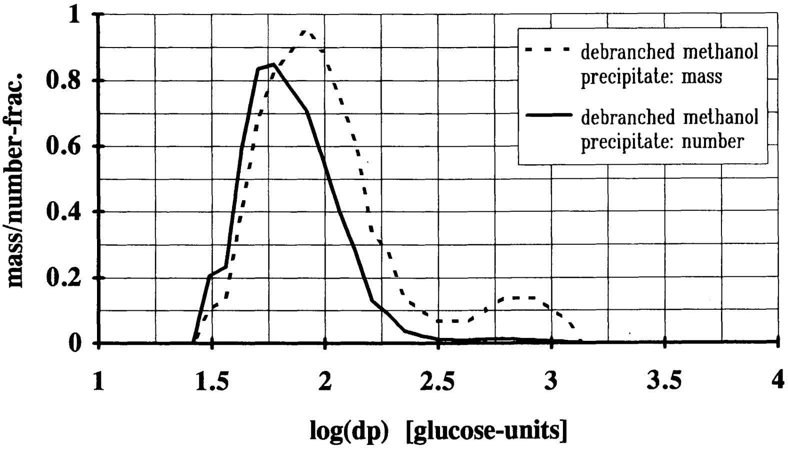

Figure 6b. Degree of polymerization distribution for pullulanase-debranched methanol precipitate of high-amylose corn starch: distribution of mass fractions dpD_m and of number fractions dpD_n.

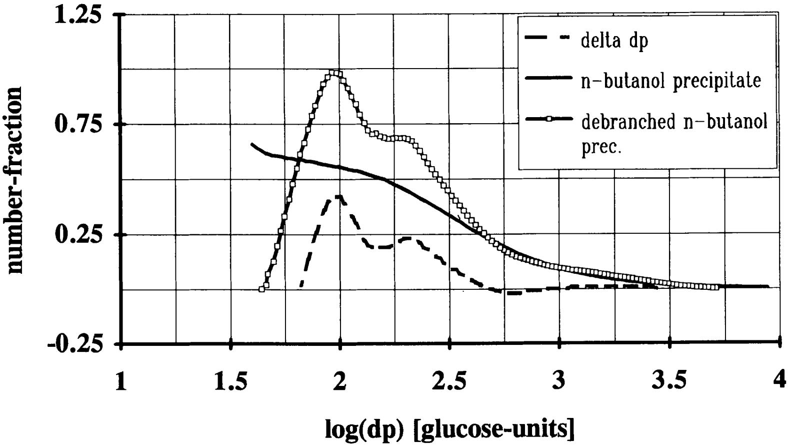

Figure 7a. dpD$_n$ of n-butanol precipitate before and after hydrolysis of branching linkages. Degradation/accumulation domains (delta dp) due to debranching action.

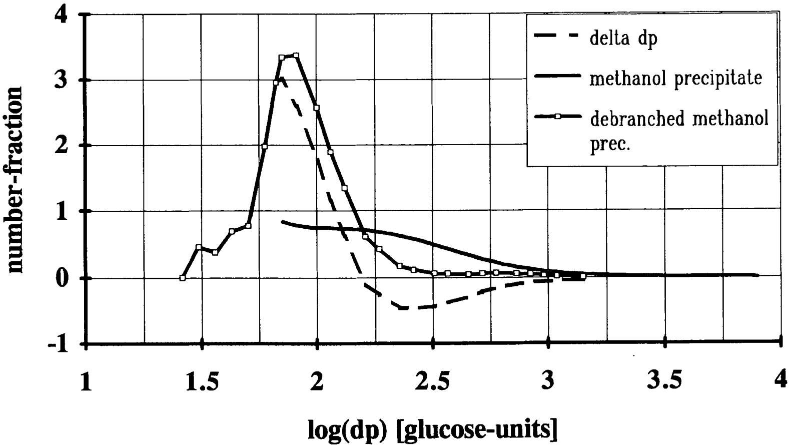

Figure 7b. dpD$_n$ of methanol precipitate before and after hydrolysis of branching linkages. Degradation/accumulation domains (delta dp) due to debranching action.

For the n-butanol precipitate (Figure 7a) the debranching action yields an increase of approx. 80% in the particle number mainly from hydrolysis of a minor number of high-molecular glucans. After debranching action glucan-chain-lengths in the range between dp=60 to dp=450 with two maxima at dp=90 and dp=220 was identified. A third, but very tiny glucan-chain population is located around dp≈2000 (Table II).

Hydrolysis of branching linkages for the methanol precipitate of high-amylose corn starch yielded a quite different result compared to the glucans of n-butanol precipitation (Figure 7b). Particle number increased dramatically for more than 2000%, and virtually all glucan molecules were affected by the enzymatic action. As a result, a constituting glucan dp-distribution ranging between dp=20 and dp=160 with a maximum at dp=65 was found (Table II).

In summary, we have employed fractionation techniques, dissolution in DMSO, separation of glucan-fractions by means of SEC in an aqueous eluent, enzymatically catalyzed modification of glucan fractions. Based on extended interpretation of experimental data, the attributed 'high-amylose'-status of the high-amylose corn starch could be rationalized and linked to molecular characteristics. The main mass fraction of these glucans (70%) formed precipitation-complexes with n-butanol, it has a coil conformation indicator for loose packed polymer coils and yielded branches with dps close to 100 and above which have to be assigned as long-chain branches. The second fraction with 30% mass, precipitated with excess of methanol from the supernatant of the n-butanol complexation, was identified as short-chain branched glucan-type.

Acknowledgements. This work was supported by the Austrian Fonds zur Förderung wissenschaftlicher Forschung (FWF) project P 9059 CHE. Special thanks to Cerestar, Vilvoorde/Belgium, for providing the high-amylose corn starch.

Literature Cited

1. Starr, C.; Searl, M.F.; Alpert, S., *Science*, **1992**, 256, 981.
2. Kauppi, P.E.; Mielikäinen, K; Kuusela, K., *Science*, **1992**, 256, 70.
3. *Polysaccharide*; Burchard, W., Ed.; Springer Verlag: Berlin Heidelberg, Germany, 1985.
4. *Polysaccharides - Topics in Structure and Morphology*; Atkins, E.D.T., Ed.; Topics in Molecular and Structural Biology, Vol. 8; VCH: Weinheim, Germany 1985.
5. Pfannemüller, B. In *Polysaccharide*; Burchard, W., Ed.; Springer Verlag, Berlin Heidelberg, Germany, 1985, 25-42.

6. *Polymeranalytik I*; Hoffmann, M.; Krömer, H.; Kuhn R., Eds.; Georg Thieme Verlag, Stuttgart, Germany, 1977.
7. Praznik, W.; Rammesmayer, G.; Spies, T.; Huber, A., *Cabohydr.Res.*, **1992**, 227, 171.
8. Praznik, W.; Huber, A.; Watzinger, S.; Beck, R.H.F., *Starch/Stärke*, **1994**, 3, 88.
9. Huber, A. In *Analysis of Polymers*; Kulicke, W.-M., Ed.; Macromolecular Symposia, Vol. 61; Hüthig & Wepf Verlag: Basel Heidelberg New York, 1992, 248-270.
10. Shortt, D.W., *J.Liqu.Chromatogr.*, **1993**, 16, 3371.

Downloaded by UNIV MASSACHUSETTS AMHERST on October 10, 2012 | http://pubs.acs.org
Publication Date: May 30, 1996 | doi: 10.1021/bk-1996-0635.ch020

Chapter 20

Size Exclusion Chromatography of Polysaccharides in Dimethylacetamide–Lithium Chloride

André M. Striegel[1] and Judy D. Timpa[2]†

[1]**Chemistry Department, University of New Orleans,**
New Orleans, LA 70148
[2]**Agricultural Research Service, U.S. Department of Agriculture,**
Southern Regional Center, P.O. Box 19687, New Orleans, LA 70179

Size exclusion chromatography has long been the method of choice for characterization of polymers and polysaccharides. A chief impediment to this process has been the lack of suitable solvents for the polysaccharides with more intricate secondary valence bond networks, such as cellulose, chitin, and starch. To this effect the solvent *N,N*-dimethyl acetamide with lithium chloride (DMAc/LiCl) has been utilized. With it we can accomplish dissolution of a wide variety of polysaccharides without the need for prior derivatization or extraction. The homogenization of solvent and chromatographic mobile phase greatly simplifies experimental conditions and variables. Here we address the choice of this solvent system and present results of universal calibration and light scattering studies of cellulose and pullulans dissolved in DMAc/LiCl.

Although the importance of polysaccharides in a variety of fields has been widely recognized for a number of years, no single common theory has emerged to explain the remarkable diversity and complexity of these molecules (*1*). This has led to the conclusion that even for biological systems no single unifying function seems to exist (*2*). Optimizing functions and understanding the roles of polysaccharides are directly dependent upon knowledge of the composition, structure, and molecular weight distribution (MWD), and the extent to which these properties affect the molecules' behavior. Physical properties of the polysaccharides will be dictated by molecular structure. As such, when comparing branched and linear polysaccharides of equal molecular weight, the branched molecule, being more compact, will have a smaller radius of gyration, its hydrodynamic volume will be smaller, and its solution viscosity lower than those of the linear polymer.

The technique of size exclusion chromatography, or SEC (also termed gel permeation chromatography, or GPC), allows the determination of molecular weight averages and, more importantly, molecular weight distributions. With it the calculation

---

†Deceased

This chapter not subject to U.S. copyright
Published 1996 American Chemical Society

Downloaded by UNIV MASSACHUSETTS AMHERST on October 10, 2012 | http://pubs.acs.org
Publication Date: May 30, 1996 | doi: 10.1021/bk-1996-0635.ch020

of a number of other characteristic solution properties is also possible. Of particular importance when performing studies of this type is the homogenization of experimental conditions, i.e. solvent, mobile phase, temperature, flow rate, method(s) of detection, adequate linear standards for performing branching calculations, proper calibration techniques, etc. The first of these conditions, the choice of solvent, has caused considerable difficulty when studying polymers, as techniques for polymer characterization usually depend on dissolution of the polymer (*3*). Polysaccharides such as cellulose, starch, and chitin, among many, are extremely difficult to dissolve. For cellulose, metal complex solutions, which often degrade the molecule through oxidation, are unstable, and many are colored. An alternative approach that has been extensively used with cellulose is to convert to a derivative soluble in an organic solvent which can then be conveniently characterized. The methods for obtaining solutions of cellulose involving derivatization can lead to hydrolytic and/or oxidative changes. In addition to the steps required for preparation of the derivative with strict attention to avoid degradation, a narrow range in degree of substitution is required to achieve dissolution. Agents such as sodium hydroxide or other alkaline solvents capable of selectively removing the non-cellulosic components seldom leave the cellulose unchanged; the remaining insoluble cellulose may be degraded, altered in crystallinity, and/or not absolutely pure (*4*). To characterize a cellulose polymer that is truly representative of the fiber matrix has proven to be a challenge. An even greater challenge is to find a means of characterizing not only the cellulose polymer, but also other polymers and polysaccharides that may co-exist in cotton fibers or plants at different stages of development, or in biological samples.

Previous studies by our group have demonstrated that *N,N*-dimethyl acetamide with lithium chloride (DMAc/LiCl) has the capability of dissolving a wide variety of representative polysaccharides differing in molecular weight, branching, linkage, and anomeric configuration, without the need for prior extraction, derivatization, or fractionation (*5,6*). We have determined DMAc/LiCl to be a thermodinamically good solvent that will break the secondary valence links of the molecule and buttress the macromolecular backbone. An additional advantage is that the solvent and the chromatographic mobile phase are thus identical. In this paper we will address our choice of this particular solvent, and give examples of results.

Previously we have utilized SEC with dual detection: A concentration detector (refractive index or RI) preceded by a differential viscometer (DV). Use of these has permitted the application of the concept of universal calibration. Recently we have incorporated a multi-angle laser light scattering (LS) detector into our experimental set-up. With it absolute macromolecular characterization of molecules with radii of gyration (Rg) between approximately 10 nm and 50 nm is possible. In terms of molecular weight this translates approximately from 1,000 Da to over 1,000,000 Da for random coils, higher for spherical molecules and lower for rigid rods. Here we use the techniques of universal calibration and light scattering to characterize the solution properties of cellulose and pullulans dissolved in DMAc/LiCl. Average molecular weights and molecular weight distributions will be presented, and we will show differences in the detection ability of LS versus RI or DV.

Experimental

Materials. Samples included cellulose 5 (J. T. Baker Chemical Co., Phillipsburg, NJ, cat. no. 1528-1) and pullulan 1 (Pfanstiehl, Waukegan, IL, cat. no. 12474). Polystyrene standards were from Toyo Soda Manufacturing (Tokyo, Japan), types F-288, F-20, F-80, F-10, F-128, F-4, F-40, F-2, A-5000, F-1, with nominal molecular weights (Da) of 2.89 $\times 10^6$, 1.9 $\times 10^5$, 7.1 $\times 10^5$, 1.02 $\times 10^5$, 1.26 $\times 10^6$, 4.39 $\times 10^4$, 3.55 $\times 10^5$, 1.96 $\times 10^4$, 6.2 $\times 10^3$, 1.03 $\times 10^4$, respectively. The solvent was *N,N*-dimethylacetamide (Burdick & Jackson, Muskegon, IL), dried with molecular sieves (Baker, activated type 3A). Lithium chloride (Baker) was oven-dried and stored in a desiccator.

Sample Preparation. Sample preparation was performed following a simplified version of the protocol used with cotton (*7*). 30 mg of polysaccharide was added to 5 mL DMAc in 10 mL ReactaVials with a conical magnetic stirrer in a heating block. The temperature was raised to 150°C and maintained with stirring for 1 hour. The mixture was allowed to cool to 100°C and 0.250 g dried LiCl was added. The vials were shaken by hand and returned to the heating block, where the mixture was maintained with stirring at 100°C for 1 hour. The temperature of the block was lowered to 50°C and samples were stirred at this temperature overnight. The solutions were quantitatively transferred to 50 mL volumetric flasks and diluted to volume with DMAc. They were then filtered through a solvent-resistant Teflon disposable filter. An extraction apparatus was employed with 10 cm^3 glass syringes fitted onto filters with 4 mL glass vials held in the small volumetric holder. The final concentration of each polysaccharide was 0.6 mg/mL in DMAc/0.5% LiCl. This concentration of LiCl was chosen based on the Ekmanis procedure for cotton dissolution (*7,8*). This procedure presents two main advantages: First, the concentration of salt is substantially lower than in other methods of cellulose dilution in DMAc/LiCl, which involve pre-swelling the cellulose in water, followed by solvent exchange to DMAc. Second, as there is no solvent exchange in this method, it is essentially a "one pot" procedure and therefore attractive for handling large numbers of samples.

Chromatography. The mobile-phase/solvent for GPC was DMAc/0.5% LiCl prepared by raising the temperature of 1 L of DMAc to 100°C and then adding 5 g of dried LiCl. The salt was stirred until it dissolved, and the solvent was filtered through a Teflon filter with a glass filter apparatus. Filtered samples were analyzed on a GPC system consisting of an automated sampler (Waters WISP, Milford, MA) with an HPLC pump (Waters Model 590), pulse dampener (Viscotek, Houston, TX), multi-angle light scattering detector (Wyatt miniDAWN, Santa Barbara, CA), viscometer detector (Viscotek Model 100), and refractive index detector (Waters Model 410), at a flow rate of 1.0 mL/min. The detectors were connected in series, with the refractive index detector last due to back-pressure considerations. The columns configuration consisted of three 10μ Mixed-B columns (Burdick & Jackson/Polymer Laboratories, Amherst, MA) preceded by a guard column (Burdick & Jackson/Polymer Laboratories). The system was operated at 80°C, with temperature

Downloaded by UNIV MASSACHUSETTS AMHERST on October 10, 2012 | http://pubs.acs.org
Publication Date: May 30, 1996 | doi: 10.1021/bk-1996-0635.ch020

controlled by a column heater (Waters column temperature system). Injection volumes were 100 μL with a run time of 34 min per sample. Data acquisition and calculations were performed using the software packages TriSEC GPC (Viscotek, Version 2.70), ASTRette (Wyatt, Version 3.04), ASTRA (Wyatt, Version 4.0), and EASI (Wyatt, Version 6.0).

Universal Calibration. The concept of universal calibration, proposed by Flory in the 1950s and confirmed experimentally by Benoit *et al.* in the 1960s, allows calculation of MW values without the need for standards with the identical chemical structure of the analyte (*9, 10*). It does so by taking into account not only the MW of the molecule but also it's intrinsic viscosity. As such, the log of the product of the molecular weight and the intrinsic viscosity, termed the hydrodynamic volume, may be plotted versus the retention time to obtain a linear calibration curve. Benoit *et al.* showed that molecules with a variety of conformations (i.e., linear, star shaped, comb shaped, ladder shaped, etc.) and molecular weights fall on this curve. Universal calibration was determined with polystyrene standards dissolved directly in DMAc/0.5% LiCl. The universal calibration curve (Figure 1) was linear as a logarithmic function of the product of the intrinsic viscosity times molecular weight versus retention volume using a third-order fit. Data were obtained from two dissolutions per sample with two GPC runs per dissolution.

Light Scattering. For a comprehensive review of the theory and applications of light scattering for absolute macromolecular characterization, the reader is referred to the article by Wyatt (*11*). In our experimental set-up, the miniDAWN system consists of a 20 mW semiconductor laser operating at 690 nm. Photodiode detectors are placed at 45°, 90°, and 135°. The calibration constants for the three GPC detectors are: RI: 2.467×10^{-6}; DV: 1.000×10^{-4}; LS: 7.582×10^{-6}. The LS/RI delay was 0.433 mL. Refractive indices were as follows: DMAc/0.5% LiCl: 1.438; cell: 1.519; dn/dc: 0.163.

Results and Discussion

The DMAc/LiCl Solvent System. Considerable effort has been devoted to finding practical direct solvents for cellulose. A relatively new solvent system is DMAc/LiCl. Our group has utilized it to dissolve cellulose, chitin, amylose, amylopectin, arabinogalactan, and dextrans, among others. The molecular weight distributions of the cellulose and pullulan samples dissolved in DMAc/LiCl may be seen in Figure 2. Although a universally accepted mechanism of dissolution of cellulose in DMAc/LiCl has not been arrived at, some facts are known. Nuclear magnetic resonance (NMR) studies show that the solvent does not react with cellulose, and that a true solution is formed. There is likewise no degradation of the polymer by the solvent, in contrast to other solvents which rapidly degrade the macromolecular backbone. Common to all dissolution mechanisms are the complexation of Li^+ with the carbonyl oxygen of the DMAc, and disruption of the extensive hydrogen bond web present in cellulose

Downloaded by UNIV MASSACHUSETTS AMHERST on October 10, 2012 | http://pubs.acs.org
Publication Date: May 30, 1996 | doi: 10.1021/bk-1996-0635.ch020

Downloaded by UNIV MASSACHUSETTS AMHERST on October 10, 2012 | http://pubs.acs.org
Publication Date: May 30, 1996 | doi: 10.1021/bk-1996-0635.ch020

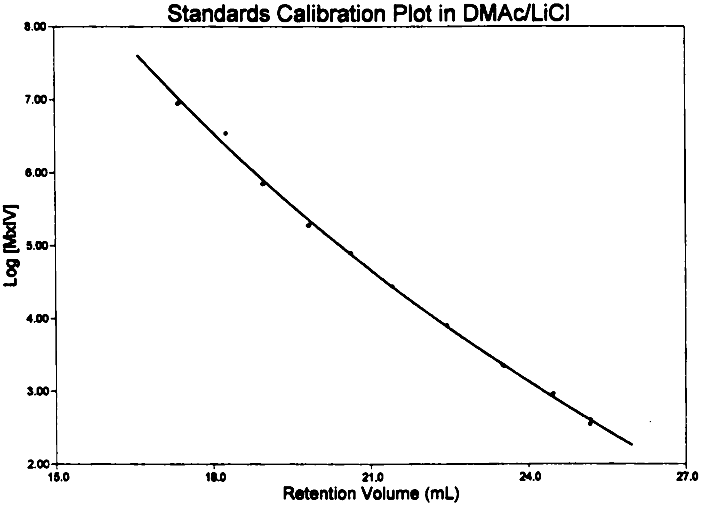

Figure 1.
SEC calibration plot of polystyrene standards in DMAc/0.5% LiCl.

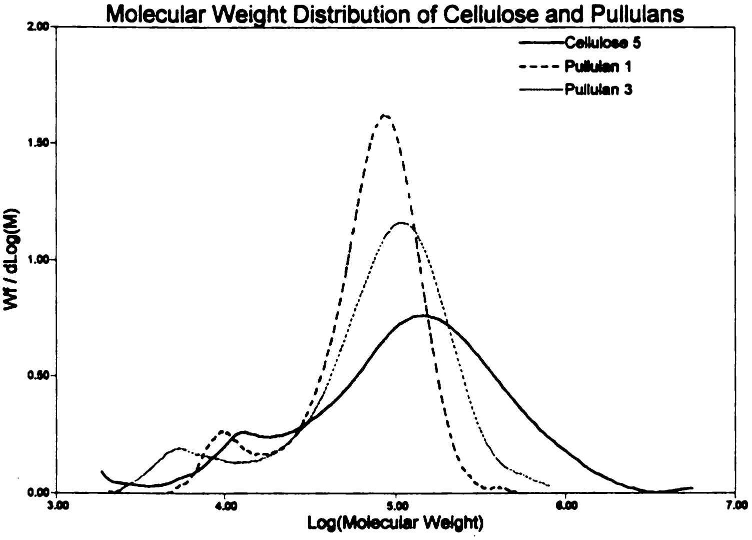

Figure 2.
Molecular weight distribution (MWD) of cellulose 5, pullulan 1, and pullulan 3.

Downloaded by UNIV MASSACHUSETTS AMHERST on October 10, 2012 | http://pubs.acs.org
Publication Date: May 30, 1996 | doi: 10.1021/bk-1996-0635.ch020

by H-bonding of the Cl^- with the cellulosic hydroxyl groups. These results have been corroborated by NMR and titration experiments (*4*).

DMAc, a polar aprotic solvent, is and ideal choice to dissolve an ionic compound such as LiCl. It solvates the cation extremely well but, because of its inability to form H-bonds, does not solvate the anion to any appreciable extent. The anion in this solvent is unencumbered by a layer of solvent molecules and therefore poorly stabilized by solvation. Such a "naked" anion will be highly active as a nucleophile. Cl^-, being smaller and therefore less polarizable (than Br^-), is less nucleophilic. It will be less tightly bound to the solvent and can thus break the inter- and intra-molecular hydrogen bonds of cellulose, helping effect dissolution. Use of both DMAc and LiCl to bring about dissolution seems exclusive. In other words, other solvents such as dimethyl sulfoxide (DMSO), dimethyl formamide (DMF), formamide, ethanolamine, etc., seem ineffective (with the exception of 1-methyl-2-pyrrolidenone, the cyclic analog of DMAc). Likewise ineffective is the use of other alkali metals or other halogens *in lieu* of either Li, Cl, or both (*12*).

Use of DMAc/LiCl in the analysis of widely varying polysaccharides presents a number of advantages. It provides a common solvent system in which to dissolve the polysaccharides, and as such any solvent effects which may result become negligible during comparisons. The solvent may also be used as the chromatographic mobile phase for SEC with multiple detectors. Solvent exchange from the solvent to the mobile phase is not necessary, and concerns about partition coefficients, etc. are eliminated. Alteration of the solvent by the polymer, which may affect light scattering results, is non-existent, as shown by NMR experiments. SEC with DMAc/LiCl as the solvent/mobile phase was utilized by our group to monitor cell-wall polymers during cotton fiber development, and to quantify the effects of extrusion processing on starches from corn and wheat (*13, 14, 15*). We have performed studies in our laboratory of polysaccharides dissolved in this solvent. Based on viscosity values and values of the Mark-Houwink constant *a*, the decrease of which could be directly related to the increase in branching in a series of dextrans, DMAc/LiCl may be considered a thermodynamically favorable ("good") solvent, i.e. one that effectively dissolves associated segments found within a coil, thus lowering the coil density and increasing the viscosity.

Universal Calibration and Light Scattering. For the purposes of contrasting universal calibration with light scattering we will describe the work done with cellulose and pullulan. These are both linear glucans. The former consists of β-(1→4) linkages, and the latter of α-(1→6) linkages. As mentioned earlier, when performing branching calculations, it is important that the linear standard used cover the range of the MWD of the analytes. For this reason we used cellulose 5 as a linear standard. It's calculated weight-average molecular weight, $\bar{M}_w = 3.3 \times 10^5$, agrees well with previously reported values of 3.2×10^5 (*16*), and cellulose is well known for its linearity. As may be seen in Figure 2, the MWD of the cellulose extends beyond the range of that of the pullulans. Results of the universal calibration branching studies of these and other polysaccharides, performed in our laboratory, established the lack

Downloaded by UNIV MASSACHUSETTS AMHERST on October 10, 2012 | http://pubs.acs.org
Publication Date: May 30, 1996 | doi: 10.1021/bk-1996-0635.ch020

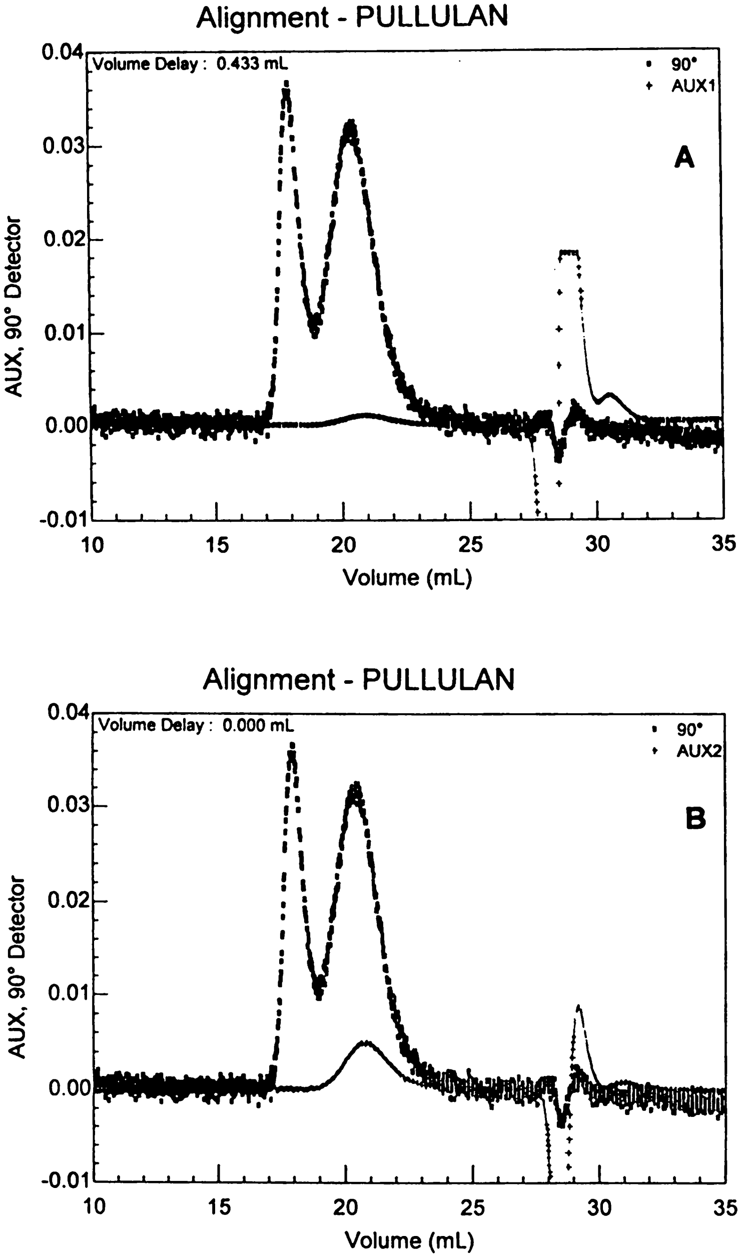

Figure 3.

Pullulan 1: (A) Alignment of 90° light scattering (LS) trace with RI detector trace (AUX1). (B) Alignment of 90° LS trace with DV detector trace (AUX2).

Downloaded by UNIV MASSACHUSETTS AMHERST on October 10, 2012 | http://pubs.acs.org
Publication Date: May 30, 1996 | doi: 10.1021/bk-1996-0635.ch020

of branching of pullulan calculated as branching number (Bn) and branching frequency (λ), and as reflected in the parameters *a*, Rg, and [η] (*5,6*). In universal calibration the radius of gyration may be calculated at every SEC slice by using Flory-Fox and Ptitsyn-Eisner theory, whereby

$$Rg = (1/6^{1/2})\{[\eta]M/\Phi_0/(1-2.63\varepsilon+2.86\varepsilon^2)\}^{1/3} \qquad (1)$$

where Φ_0 is the Flory universal constant, equal to 2.86×10^{21}, and $\varepsilon = (2a-1)/3$, with *a* being the Mark-Houwink exponent constant (*17*). Branching calculations performed with LS data and using cellulose 5 as a linear standard confirm the lack of branching in the pullulans, yielding straight lines which virtually overlap the baseline for both the branching frequency vs. molecular weight and branching number vs. molecular weight plots. In LS the radius of gyration is derived from the slope of the familiar Debye plot (the plot's intercept yields $\bar{M}_w$).

Table I shows the calculated $\bar{M}_w$, $\bar{M}_n$, and Rg_w of the cellulose and pullulans, utilizing universal calibration with polystyrene standards and light scattering. $\bar{M}_w$ values are in close agreement with those supplied by the manufacturer or previously published in the literature. Universal calibration and light scattering $\bar{M}_n$ and Rg_w values, which are in close agreement with each other, are not available from the manufacturer. It can be observed in the lower traces of Figures 3A and 3B that both the refractive index and the viscometer detectors observed a single peak for pullulan 1.

Table I. MW averages and radius of gyration of cellulose and pullulans using universal calibration and light scattering

Sample ID	Supplied	Universal Calibration			Light Scattering		
	$\bar{M}_w$	$\bar{M}_w$	Mn	Rg_w	$\bar{M}_w$	$\bar{M}_n$	Rg_w
Cellulose 5	3.2×10^{5a}	3.3×10^5	4.2×10^4	16.2	3.2×10^5	2.8×10^4	14.5
Pullulan 1	1.0×10^5	1.1×10^5	3.5×10^4	12.3	1.2×10^5	6.9×10^4	18.7
Pullulan 3	3.0×10^5	3.1×10^5	3.4×10^4	14.5	2.8×10^5	5.0×10^4	20.7

[a] Value from (*16*).

The Debye plot for pullulan 1 is shown in Figure 4. The $\bar{M}_w$, taken at the maximum of the second peak, is in close agreement with both the supplied value and with that determined using universal calibration. The values for pullulan 1 and 3 are compared in Table I.

As can be seen in the upper trace in Figures 3A and 3B, corresponding to the signal from the 90° LS photodiode detector, two large peaks may be observed. These are evident in the output from all three angles being monitored (Figure 5). The large peak at lower elution volume is not observed with either the RI or the viscometer detectors (Figures 3A,B and 5). This peak at lower elution volume is most probably

Downloaded by UNIV MASSACHUSETTS AMHERST on October 10, 2012 | http://pubs.acs.org
Publication Date: May 30, 1996 | doi: 10.1021/bk-1996-0635.ch020

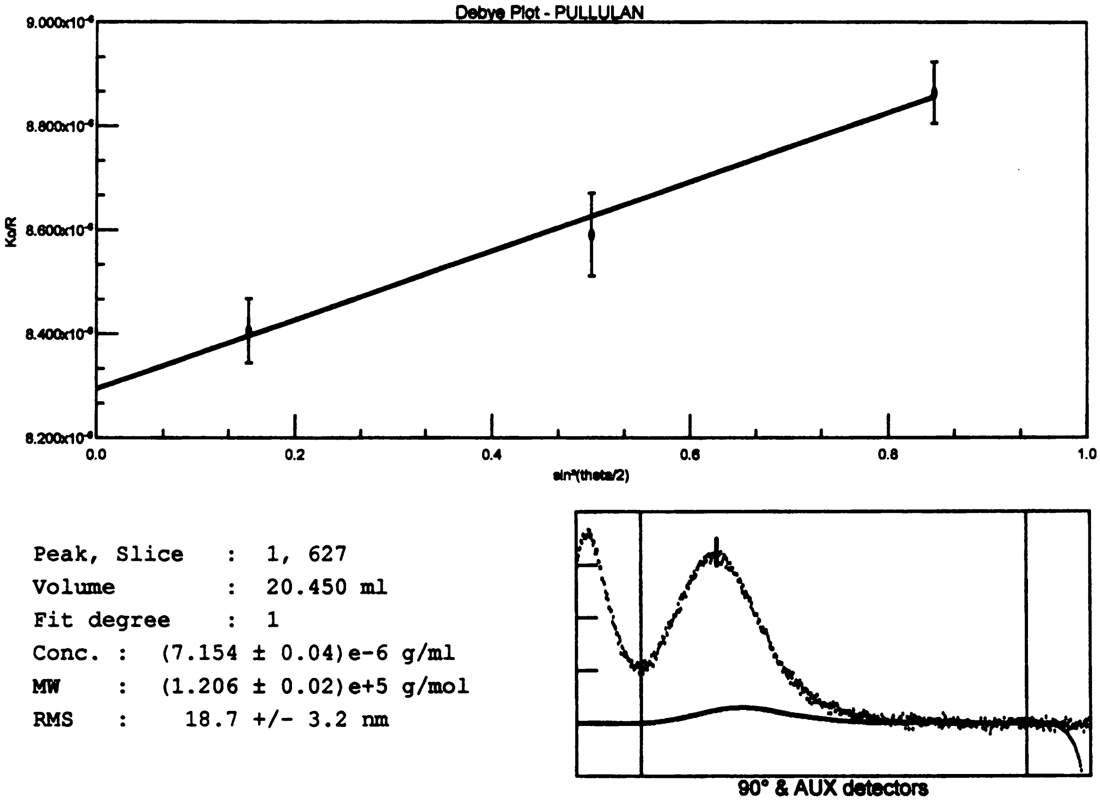

```
Peak, Slice   :  1, 627
Volume        :  20.450 ml
Fit degree    :  1
Conc. :  (7.154 ± 0.04)e-6 g/ml
MW    :  (1.206 ± 0.02)e+5 g/mol
RMS   :    18.7 +/- 3.2 nm
```

Figure 4. Debye plot for pullulan 1.

Downloaded by UNIV MASSACHUSETTS AMHERST on October 10, 2012 | http://pubs.acs.org
Publication Date: May 30, 1996 | doi: 10.1021/bk-1996-0635.ch020

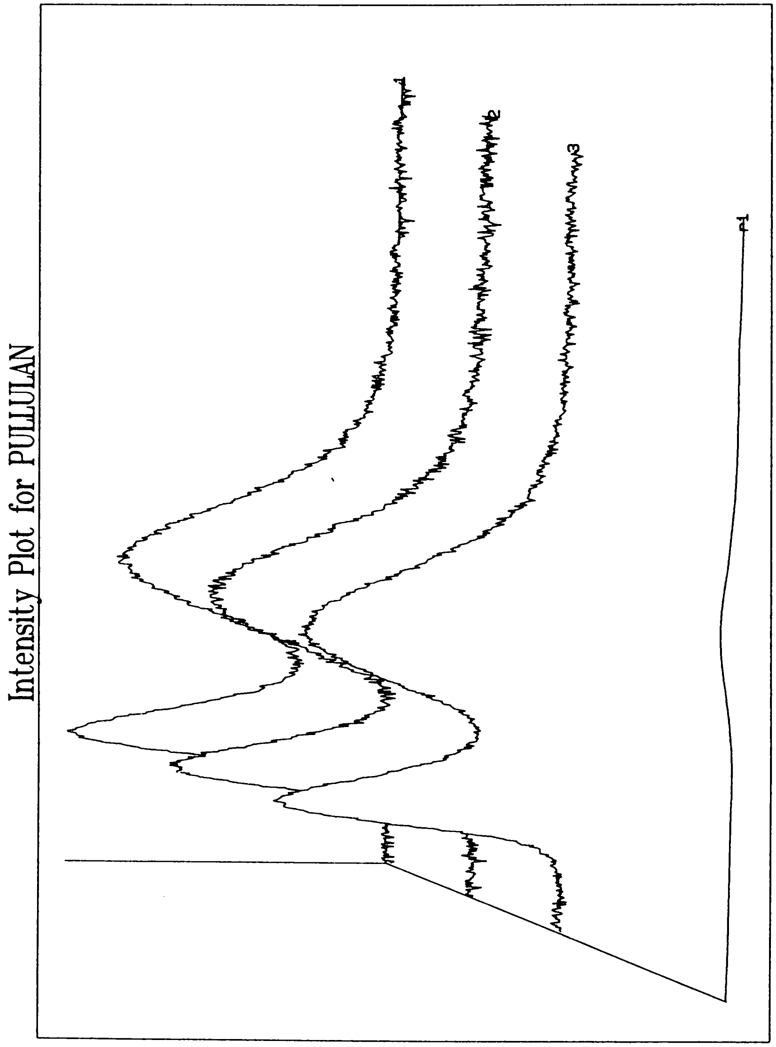

Figure 5. **Intensity plot for pullulan 1: 1 = 45° light scattering (LS) detector; 2 = 90° LS detector; 3 = 135° LS detector; ri = refractive index detector.**

Downloaded by UNIV MASSACHUSETTS AMHERST on October 10, 2012 | http://pubs.acs.org
Publication Date: May 30, 1996 | doi: 10.1021/bk-1996-0635.ch020

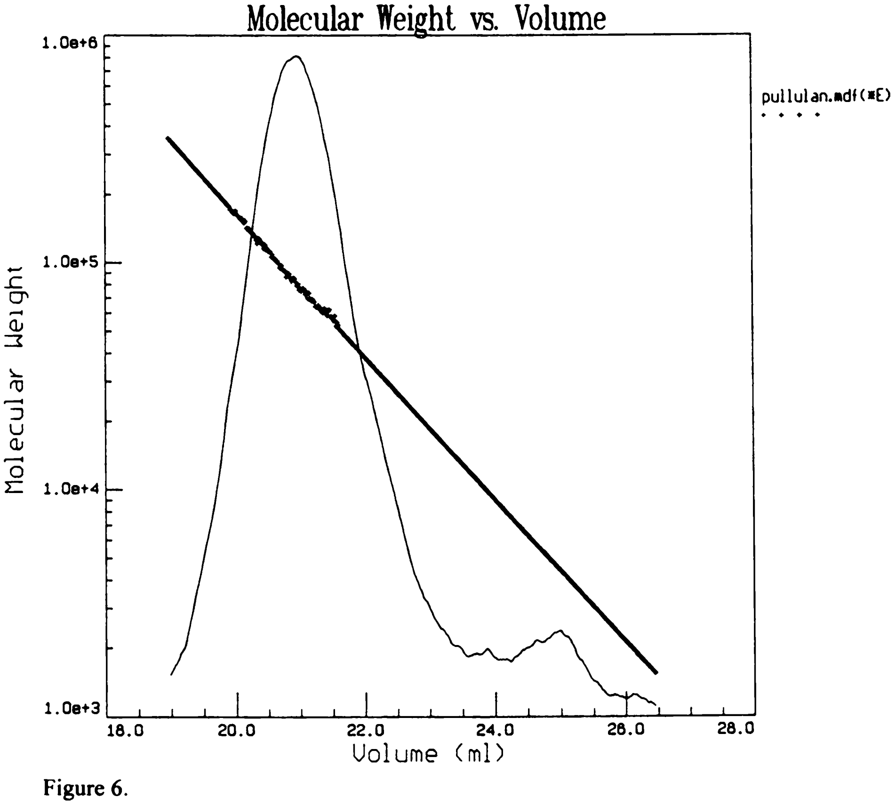

Figure 6.

Molecular weight vs. volume plot for pullulan 1. Universal calibration (—) and light scattering (+++).

an indication of solution aggregates, and was not included in the calculation of the average MW by LS. It was observed with pullulan 3 as well. Solution aggregates have also been observed by other groups for dextrans dissolved in aqueous solution; their existence is still not well understood (*18*). As the higher molecular aggregate peak is not seen by either the RI or DV detectors, utilizing these pullulans as calibration standards would have resulted in incorrect molecular weight determinations for samples analyzed by SEC with RI and/or DV detection alone.

The polydispersity of the sample is exemplified in the lack of alignment of the LS and RI, or LS and DV, maxima (of the peak at higher elution volume). This lack of alignment is due to the LS signal being proportional to the product of concentration and molecular weight, whereas the RI and DV signals are proportional only to concentration. This also explains why LS is more sensitive to aggregates, as its detector signal will be higher for the higher molecular weight fraction (*18*). Figure 6 shows the molecular weight vs. volume plot for pullulan 1 obtained with universal calibration contrasted to that obtained with light scattering. The light scattering trace has been extrapolated at the highest and lowest extremes to reduce the inherent noise.

Conclusions

We have utilized SEC for the analysis of polysaccharides dissolved in DMAc/LiCl. Use of this solvent system permits a wide variety of polysaccharides differing in extent of branching, linkage, and anomeric configuration to be dissolved in a common solvent. The solvent may also be utilized as the mobile phase, thus eliminating another experimental variable and facilitating procedures. Dissolution of the polysaccharides in DMAc/LiCl does not affect the solvent, as results for cellulose indicate a true solution in formed.

Results from both universal calibration and multi-angle laser light scattering gave weight-average molecular weights comparable to those supplied by the manufacturer, and number-average molecular weights and radii of gyration comparable to each other. The branching in pullulan was determined to be essentially non-existent by both methods of analysis. A linear cellulose standard, whose MWD spans the range of that of the pullulans, was used for the branching calculations. The light scattering detector did supply evidence of pullulan aggregates in solution, as exemplified by an additional peak at lower elution volume (higher molecular weight) than the only peak observed with the RI and DV detectors. As similar results have been observed by other groups with dextrans dissolved in aqueous solution, caution should be exercised when using polysaccharides as calibration standards in SEC with RI and/or DV detection alone. Potential difficulties may be avoided by either the use of well-characterized, narrow MWD standards (such as polystyrenes), or of a light scattering detector. The LS detector provides an additional means of observing the polydispersity of the samples, by comparing the maxima of the LS and RI and/or DV traces of the common peak.

Downloaded by UNIV MASSACHUSETTS AMHERST on October 10, 2012 | http://pubs.acs.org
Publication Date: May 30, 1996 | doi: 10.1021/bk-1996-0635.ch020

Safety Considerations and Notes

N,N-dimethyl acetamide is an exceptional contact hazard that may be harmful if inhaled or absorbed through the skin and may be fatal to embryonic life in pregnant females (Baker Chemical Co., N,N-dimethylacetamide, Material Safety Data Sheet, 1985, D5784-01; pp.1-4.

Names of companies or products are given solely for the purpose of providing specific information. Their mention does not imply recommendation or endorsement by the United States Department of Agriculture over others not mentioned.

Downloaded by UNIV MASSACHUSETTS AMHERST on October 10, 2012 | http://pubs.acs.org
Publication Date: May 30, 1996 | doi: 10.1021/bk-1996-0635.ch020

Acknowledgments

We thank Dr. Richard Cole (University of New Orleans) for his advice and partial sponsorship of this work under USDA, ARS Cooperative Agreement 58-6435-2-110. We also thank Dr. Barbara Triplett (SRRC) for helpful discussions.

Literature Cited

1. Varki, A. *Glycobiology* **1993,** *3,* 97-130.
2. Dwek, R. A. *Biochem. Soc. Trans.* **1995,** *23,* 1-25.
3. Timpa, J. D. *Trends Polym. Sci.* **1993,** *4,* 105-110.
4. Dawsey, T. R.; McCormick, C. L. *JMS-Rev. Macromol. Chem. Phys.* **1990,** *C30,* 405-440.
5. Striegel, A. M.; Timpa, J. D. *Carbohydr. Res.* **1995,** *267,* 271-290.
6. Striegel, A. M.; Timpa, J. D. *Int. J. Polym. Anal. Charac.* (in press).
7. Timpa, J. D. *J. Agric. Food Chem.* **1991,** *39,* 270-275.
8. Ekmanis, J. L. paper presented at The Pittsburgh Conference and Exposition, **1987,** Atlantic City, NJ, Abstract 783.
9. Grubisic, A; Rempp, P.; Benoit, H. A. *Polym. Lett.* **1967,** *5,* 753-759.
10. Flory, P. J. *Principles of Polymer Chemistry;* Cornell University Press: Ithaca, N.Y., 1953.
11. Wyatt, P. J. *Anal. Chim. Acta* **1993,** *272,* 1-40.
12. Turbak, A. F.; El-Kafrawy, A.; Snyder, Jr., F. W.; Auerbach, A. B. U.S. Patent 4,352,770, **1982.**
13. Wasserman, B. P.; Timpa, J. D. *Starch/Starke* **1991,** *43,* 389-392.
14. Politz, M. A.; Timpa, J. D.; White, A. R.; Wasserman, B. P. *Carbohydr. Polym.* **1994,** *24,* 91-99.
15. Politz, M. A.; Timpa, J. D.; Wasserman, B. P. *Cereal Chem.* **1994,** *71,* 532-536.
16. McCormick, C. L.; Callais, P. A.; Hutchinson, B. H. *Macromol.* **1985,** *18,* 2394-2401.
17. Yau, W. W. *Chemtrends: Macromol. Chem.* **1990,** *1,* 1-36.
18. Navarro, G. A. paper presented at 4th Simposio Latinoamericano de Polímeros, **October 1994;** Gramado, Brazil.

Chapter 21

Renaissance in Ultracentrifugal Sedimentation Equilibrium Calibrations of Size Exclusion Chromatographic Elution Profiles

Juraj Mlynár and Simo Sarkanen

Department of Forest Products, University of Minnesota,
2004 Folwell Avenue, St. Paul, MN 55108

Of the three traditional techniques that have been most reliable in their application to polymers for determining molecular weight averages, only ultracentrifugal sedimentation equilibrium analyses can provide information directly about the polydispersity of a solute. Thus, when used in conjunction with size exclusion chromatography, analytical ultracentrifugation is uniquely suited to examining how polydispersity varies with the hydrodynamic volume of the species that constitute a polymeric sample. Almost impeccable fidelity has now been attained in fitting, to empirical sedimentation equilibrium data, sums of exponential terms that formally reflect the distributions of ideal macromolecular solute components in the centrifugal field. Although the component molecular weights and corresponding concentrations in each case represent principally the values of adjustable parameters that satisfy the curve fit, the ensuing z-average molecular weights have become, perhaps for the first time, quite reliable; even the weight-average molecular weights exhibit appreciable sensitivity to the degree of refinement ultimately achieved. The approach has been successfully applied to the characterization of lignin derivatives, which are complicated mixtures of macromolecular complexes and individual components; fortunately these species are not usually interconverted rapidly under the ultracentrifugal conditions employed. Not surprisingly, such fitting of exponential terms to sedimentation equilibrium data is even more straightforward for paucidisperse polystyrene fractions.

The classical Beckman model E analytical ultracentrifuge was designed in the 1950's and subsequently improved through modifications related to the photoelectric scanning system implemented during the 1960's (*1-4*). As a means for absolute molecular weight determinations, analytical ultracentrifugation gradually lost ground during the 1970's to alternative methods such as light-scattering and viscosimetric measurements which were

0097–6156/96/0635–0379$15.50/0

quicker and easier to use. Concomitantly the Beckman model E ultracentrifuge was steadily becoming more expensive to maintain, and in the early 1980's production of the instrument was discontinued altogether.

This lamentable state of affairs meant that the majority of investigators were restricted to light scattering and viscosimetric measurements as the most reliable means for determining molecular weights. Yet appropriate analyses of ultracentrifugal sedimentation equilibrium data facilitate calculation of both the weight-average and z-average molecular weight ($\overline{M}_w$ and $\overline{M}_z$) for a polymer sample. Accordingly, redistribution of macromolecular solute species in the centrifugal field affords information about the polydispersity of a (paucidisperse) solute without the need for further chromatographic fractionation. Thus analytical ultracentrifugation offers unique advantages in characterizing the molecular weight distributions of polymeric components that cannot be conveniently separated into members of a single homologous series.

From such a perspective, lignin derivatives are especially worthy candidates for ultracentrifugal sedimentation equilibrium analysis: their colligative behavior is strongly influenced by pronounced noncovalent interactions between the individual molecular species; the resulting macromolecular complexes are usually assembled and dismantled relatively slowly with respect to the time required to attain sedimentation equilibrium, but the populations of these entities are nevertheless profoundly affected by solution composition and prior incubation conditions to which the sample has been exposed (*5-11*).

Lignins. As cell wall components in all vascular plants and woody tissues, lignins represent the second most abundant group of naturally occurring polymers. They exhibit significant variations in structure with plant species, type of cell, and morphological region of the cell wall in which they are present (*12-14*). The final step in lignin biosynthesis involves the enzyme-catalyzed dehydrogenative polymerization of three monolignols, *viz.* *p*-hydroxycinnamyl (*p*-coumaryl) alcohol, 4-hydroxy-3-methoxycinnamyl (coniferyl) alcohol, and 4-hydroxy-3,5-dimethoxycinnamyl (sinapyl) alcohol. The consequent macromolecules may embody as many as 10 different linkages between the monomer residues, but approximately half of these are of the same β-*O*-4 alkyl aryl ether type (*15*). In gymnosperms (softwoods), the primary lignin precursors are the coniferyl and *p*-coumaryl alcohols, while in angiosperm dicotyledons (hardwoods) sinapyl alcohol is also prominently incorporated into the biopolymer. On the other hand, the lignins of grasses and cereals, in addition to units derived from the three primary monolignol precursors, contain some covalently bound *p*-coumaric and ferulic acids.

In hardwoods and softwoods, lignins comprise between 25 and 30% w/w, respectively, of the woody tissue. Since the majority of the interunit linkages in these macromolecules are much more stable than those in most other biopolymers, lignins cannot be isolated from plant or wood cell walls without substantial degradation. The resulting lignin derivatives thus may vary widely in the extent to which they have been modified with respect to the structures present in the native biopolymer (*15*, *16*).

Size-Exclusion Chromatography of Lignin Preparations. Size-exclusion chromatographic analyses of lignin preparations without corresponding absolute molecular weight calibrations can yield quite misleading results. Thus the body of an apparently normal elution profile may well harbor a local region where the molecular weights of the solute components emerging from the column actually increase with retention volume (*17*). Indeed the identity of the mobile phase often has a profound effect upon the size-exclusion chromatographic elution profiles of lignin derivatives. For example, the elution profiles generated from poly(styrene-divinylbenzene) columns in DMF or DMSO extend multimodally to very high apparent molecular weights, whether or not the hydroxyl groups on the lignin derivative components have been acetylated (*5*, *18*); significant populations of associated macromolecular complexes therefore appear to be present under such conditions. On the other hand, the profiles of the same lignin samples in THF, and DMF containing 0.10 *M* LiCl or LiBr, are displaced to higher elution volumes (*5*, *18*) but absolute molecular weight determinations have not been carried out to establish whether this tendency arises from dissociation of the macromolecular lignin complexes or enhancement of reversible adsorption to the column packing material. Whatever the case, the elution volumes for polystyrene fractions from poly(styrene-divinylbenzene) columns increase markedly with mobile phase polarity (*18*), so that the variations in elution behavior of lignin derivatives have more than one underlying cause.

Ultracentrifugal Sedimentation Equilibrium Analysis. The Beckman Optima XL-A analytical ultracentrifuge can thus fulfill a uniquely important function in elucidating the actual molecular weight distributions of lignin derivatives and other polymers unambiguously. At equilibrium in the solution columns of the cell assemblies within the rotor, the concentration c_r of each solute species varies ideally with radial distance r from the center of rotation according to

$$c_r = c_m \exp\{M[(1-\bar{\upsilon}_2\rho)\omega^2/2RT](r^2 - r_m^2)\} \tag{1}$$

where c_m and r_m respectively are the solute concentration and radial distance corresponding to the meniscus, M and $\bar{\upsilon}_2$ respectively are the molecular weight and partial specific volume of the solute, ρ is the density of the solvent, ω is the angular velocity, R is the gas constant and T is the absolute temperature. Since the extent to which c_r varies exponentially with r^2 depends on M, a polydisperse sample will experience the redistribution of solute components with different molecular weights during the attainment of sedimentation equilibrium in the ultracentrifugal field. Consequently the local molecular weight averages of the solute will increase monotonically with r in the solution column within the rotor. In sector-shaped cells, the weight- and z-average molecular weights ($\overline{M}_w$ and $\overline{M}_z$, respectively) may be calculated (*19*) from

$$\overline{M}_w = \frac{RT\int_m^b \left(\frac{dc}{dr}\right)dr}{(1-\bar{\upsilon}_2\rho)\omega^2\int_m^b cr\,dr} \tag{2}$$

$$\overline{M}_z = \frac{RT\int_m^b \left[\frac{1}{r}\left(\frac{d^2c}{dr^2}\right) - \frac{1}{r^2}\left(\frac{dc}{dr}\right)\right]dr}{(1-\bar{\upsilon}_2\rho)\omega^2\int_m^b \left(\frac{dc}{dr}\right)dr} \tag{3}$$

where c represents the total concentration of all solute species at radial distance r from the center of rotation when equilibrium has been attained, and the limits of integration are the meniscus and base of the solution column within the ultracentrifuge rotor.

Previously the point-by-point variation of weight-average molecular weight, $M_{w,r}$, with r in the ultracentrifuge cell has been evaluated by employing, from the overall sedimentation equilibrium curve, a "sliding" interval of (typically 13) consecutive ln c *versus* r^2 data points, at the middle of which the slope would be calculated through the Chebyshev polynomial fit of a quadratic function (*20*). Actually in this context an operational point average represented by M* has recently been deemed preferable as a means of determining the overall weight-average molecular weight, to which it is equal at the cell base. Nevertheless M* provides no advantage in obtaining the overall z-average molecular weight for the components in the ultracentrifuge cell; moreover the use of a "sliding" interval of consecutive data points for determining the point-by-point variation in the z-average molecular weight, $M_{z,r}$, with r has proven to be so sensitive to noise that reliability could only be approached through whole curve quadratic fitting (*20*).

The unique advantage of ultracentrifugal sedimentation equilibrium measurements lies in the fact that they can provide both weight-average and z-average molecular weights directly. However, if reliability in the values obtained for the overall z-average molecular weights is, in practice, going to necessitate whole curve fitting with suitable functions, then exponential terms should be used for the purpose: equations 2 and 3 have been derived from equation 1 without further assumptions of any kind. Indeed successful curve fitting of sedimentation equilibrium data has now been accomplished with functions representing sums of terms of the form expressed in equation 1. Using SigmaPlot 5.0 (Jandel Scientific, San Rafael, CA), unprecedented accuracy in characterizing the sedimentation equilibrium behavior of paucidisperse lignin derivative fractions has thus been achieved with a remarkably small number of appropriate exponential terms (*17*). The result has measurably improved the accuracy of $\overline{M}_w$ values, the calculation of which in the general case involves the first derivative of the sedimentation equilibrium curve, as shown in equation 2.

The presently reported work has established that fitting with sums of exponential terms is yet more far-reaching in its impact upon the values of $\overline{M}_z$ which, perhaps for the first time, may now embody a reasonable degree of reliability: their calculation requires not only the first but also the second derivative of the sedimentation equilibrium curve, as is evident from equation 3.

Moreover it should be obvious that, when sums of exponential terms are used for curve fitting, the somewhat cumbersome expressions in equations 2 and 3 can be avoided altogether. By integrating equation 1, the total concentration of each of the formal components (molecular weight M) can be readily determined, and hence $\overline{M}_w$ and $\overline{M}_z$ may be calculated directly from the weights of these species which are together equivalent to the curve experimentally observed at sedimentation equilibrium. Although not elaborated upon further here, values for $\overline{M}_n$ may concurrently be obtained by the same means without the inconvenience of having to estimate $M_{n,m}$, the number-average molecular weight at the meniscus of the sample solution column in the ultracentrifuge cell (*21*).

It may not be merely fortuitous that this analytical approach has been successfully implemented in response to problems expressly encountered with the size-exclusion chromatography of lignin derivatives: the molecular weight distributions of such preparations are notoriously difficult to determine. It is certainly not justifiable at present to consider the macromolecular complexes and individual components comprising a typical lignin derivative sample as members of a single homologous series.

Of course there is no reason to exclude common synthetic polymers from analyses by these means. Indeed it has been found that fitting appropriate exponential terms to sedimentation equilibrium data for paucidisperse standard polystyrene fractions is even more straightforward than for lignin derivatives. In the example described in the present report (*vide infra*), the value obtained for $\overline{M}_w$ is gratifyingly close to that claimed by the supplier.

Experimental Section

Kraft Lignin Derivatives. The most abundant lignin derivatives generally available are the industrial byproducts formed under the fairly severe conditions adopted in the kraft pulping process (typically at 170°C for ≥2 h in aqueous solution containing 45 gL^{-1} NaOH and 12 gL^{-1} Na_2S). These kraft lignins are thought to have suffered significant structural modifications compared with the native polymer (*16*).

The parent kraft lignin preparation employed in the presently reported work was isolated from black liquor produced from Jack pine (*Pinus banksiana*) by the Boise Cascade Corporation (International Falls, MN). After dilution (110 mL portions with 690 mL HPLC grade water), this black liquor was filtered through a VWR grade 617 paper (to remove residual fibrous material) and then, with vigorous stirring, acidified to pH 3.0 with aqueous 0.50 *M* H_2SO_4 (0.1 mL min^{-1}). The resulting solution containing suspended solids was centrifuged (3100 × g, 30 min.) and the precipitate was washed thoroughly three times by resuspending in water acidified (with dilute sulfuric acid on the first two occasions but thirdly with dilute hydrochloric acid) to pH 3.0 and centrifuging. Whenever centrifugation failed to precipitate all of the solid kraft lignin, the remaining suspension was basified to pH 8.5, whereupon the clear solution was rapidly reacidified to pH 3.0 and centrifuged. Finally all of the precipitated kraft lignin portions were suspended together in HPLC grade water (~500 mL) and the mixture was basified to pH 8.5 with aqueous 0.10 *M* NaOH. After centrifuging (3100 × g, 30 min.) to remove any colloidally suspended sulfur, the resulting solution was freeze-dried.

The purified Jack pine kraft lignin sample was then incubated at ambient temperature for 92.5 h in 1.0 *M* ionic strength aqueous 0.40 *M* NaOH (made up to 0.60 *M* NaCl) at 160 gL^{-1}, conditions that promote appreciable association between the individual molecular components (*10*). Upon ~25-fold dilution with water, the solution was acidified to pH 8.5 with aqueous hydrochloric acid and ultrafiltered (Amicon model 2000 teflon-coated 2 liter cell connected to a model RS12 teflon-coated reservoir) with a 500 nominal molecular weight cutoff membrane (Amicon YC05) using triply distilled (under N_2) high purity water (10 × volume of ultrafiltration cell). The resulting solution (pH 7.6, completely free of NaCl) was thereupon freeze-dried.

The associated kraft lignin sample (200 mg) was acetylated (freshly purified 1:1 v/v Ac_2O/pyridine, 20 mL, under N_2) at ambient temperature for 45 h. Pyridine (10 mL) and water (150 mL) were added to the resulting solution and, after vigorous stirring (30 min.) while cooling in ice, the acetylated lignin was extracted with (acid-free) chloroform. The pyridine was completely removed, by shaking with aqueous 2 *M* HCl, from the chloroform phase, which was then thoroughly washed with distilled water, dried (Na_2SO_4) and then the solvent was evaporated (30°C) under reduced pressure. The residue of acetylated kraft lignin was redissolved in (acid-free) chloroform and methylated with diazomethane (generated from *N*-methyl-*N*-nitroso-*p*-toluenesulfonamide) for 30 min. After shaking thoroughly with 5 consecutive volumes of aqueous 1.0 *M* H_2SO_4 and then triply distilled water, the chloroform solution was dried (Na_2SO_4) and the solvent evaporated (30°C) under reduced pressure to yield a preassociated acetylated methylated kraft lignin preparation.

Open Column Size-Exclusion Chromatography. Preparative and analytical size-exclusion chromatographic fractionations of the underivatized kraft lignin preparation through Sephadex G100 in aqueous carbonate-free 0.10 *M* NaOH were carried out respectively in 5.0 × 100 cm and 2.5 × 100 cm columns, to each outlet of which an ISCO V^4 detector was connected for monitoring the absorbance of the eluting species at 280 nm (where the ultraviolet spectrum of the sample exhibits a local maximum or shoulder) or at 320 nm. Gel batches were allowed to swell at room temperature for 3 days in eluant and then degassed (sonication under reduced pressure) prior to column packing. The column flow-rates were maintained between 6.1 and 6.5 mL $cm^{-2}h^{-1}$, an optimum range experimentally established for prolonging good column performance. Blue dextran and *p*-nitrophenol were adopted as void volume and low molecular weight markers, respectively.

The elution profiles themselves were digitized and transformed to plots of absorbance *versus* relative retention volume, V_R, which was operationally defined as $2(V-V_0)/(V_{pNP}-V_0)$, where V and V_{pNP} are the elution volumes of the sample and *p*-nitrophenol, respectively, and V_0 is the column void volume (taken as the beginning, rather than the maximum height, of the peak for blue dextran). The calculations were executed with a Fortran 77 program that was written to take account of both baseline drift and flow-rate fluctuations. The latter were monitored with precisely calibrated ~5 and ~15 mL siphons positioned as receivers for the outlets from the respective detector flowcells connected to the 2.5 and 5.0 cm diameter columns. Each sample was eluted through the column in the absence and presence of the standard blue dextran and *p*-nitrophenol markers to facilitate appropriate scaling of V_R.

The paucidisperse underivatized kraft lignin fractions secured for ultracentrifugal sedimentation equilibrium characterization were selected from the profile of the associated preparation (100 mg) upon elution through the 5.0 cm diameter column. Prior to the sedimentation equilibrium studies themselves, each fraction was re-eluted twice through the 2.5 cm diameter column, the peak segment extending above 70% of the maximum height being retained in both cases.

High Performance Size-Exclusion Chromatography. The molecular weight distribution of the acetylated methylated associated kraft lignin preparation in DMF was determined in terms of the corresponding elution profile from a 7.5 × 600 mm TSKgel G7000-H6 10^7 Å pore size poly(styrene-divinylbenzene) column fitted with 10 μ inlet and outlet frits. A 1.0 mL min^{-1} flow-rate was maintained by a Knauer model 64 pump, while the absorbance of the eluting species at 320 nm was monitored with a Knauer model 87 photometer equipped with a 10 mm pathlength flow cell. Under such conditions (where Lambert-Beer's law holds), 80% of 0.0034 mg (20 μL 0.17 gL^{-1} solution) sample loadings were recovered from the column.

From consecutive elution profiles for the acetylated methylated kraft lignin in DMF, the same paucidisperse fractions were manually collected in multiple series, the corresponding members of which were respectively combined with one another for subsequent ultracentrifugal sedimentation equilibrium studies. In order to minimize dissociation of the constituent macromolecular complexes, the solvent was removed (evaporation under reduced pressure at 30°C) immediately after isolating each fraction. Between the consecutive elutions of the acetylated methylated kraft lignin preparation, any remaining adsorbed species were cleaned from the column by injecting 20 μL aqueous 50% (v/v) DMF, water and purified dioxane in turn until no further ultraviolet-absorbing solute components were liberated from the column.

Analytical Ultracentrifugation. The paucidisperse underivatized and acetylated methylated kraft lignin fractions were diluted in aqueous carbonate-free 0.10 *M* NaOH and DMF, respectively, to concentrations ($8 - 9 \times 10^{-3}$ gL^{-1} or $4 - 5 \times 10^{-5}$ *M* with respect to the component monomer residues) for which the absorbance was 0.18 - 0.21 at wavelengths suitably chosen (so as not to engender excessive noise in the sedimentation equilibrium data) above and yet close to the ultraviolet cutoff of the reference solution or solvent (as the case may be). The resulting aqueous 0.10 *M* NaOH and DMF solutions were introduced (under N_2) into ultracentrifuge cells respectively assembled around charcoal-filled Epon and aluminum double-sector centerpieces; in the former, FC-43 (30 μL), a water-immiscible fluorocarbon, was included within each sample (but not reference) sector so that the base of the (420 μL) solution column could be precisely distinguished in the centrifugal field. The cell assemblies were inserted into a Beckman An-60 Ti rotor for characterization of the weight- and z-average molecular weights ($\overline{M}_w$ and $\overline{M}_z$) through sedimentation equilibrium at 20°C in the Beckman Optima XL-A analytical ultracentrifuge.

When equilibrium had been reached (so that there was no discernible change over a 24 h period), the sedimentation curves, representing absorbance at 280 and 320 nm *versus* radial distance (5.8 - 7.2 cm) from the center of rotation, were corrected for any conceivable optical imperfections in the cell assemblies by subtracting the corresponding data at a wavelength sufficiently long (600 nm) that the absorbance of the kraft lignin species is negligible (*cf.* ref. *6*). The area under each corrected sedimentation equilibrium curve was compared with that initially obtained at 1100 rpm in order to confirm that none of the solute species had escaped detection through sedimentation at the particular rotor speed to the base of the solution sector of the ultracentrifuge cell. Reliability in the values of $\overline{M}_w$ and $\overline{M}_z$ was established by consistency in the results obtained from two suitable wavelengths (280 and 320 nm) at each of two rotor speeds (appropriately selected from the range between 3800 and 57,000 rpm). While avoiding meniscus depletion conditions, these rotor speeds were, whenever possible, chosen so as to effect steep sedimentation equilibrium curves near the cell base without exceeding 1.8 absorbance units.

Analysis of Sedimentation Equilibrium Data. The partial specific volumes ($\bar{\upsilon}_2$) of the kraft lignin components (0.744 cm^3g^{-1}, taken to be independent of molecular weight) and the densities (ρ) of solution or solvent were measured at 20°C with a Paar 60/602 digital density meter.

Using SigmaPlot 5.0 (Jandel Scientific, San Rafael, CA), the sets of corrected sedimentation equilibrium data points for the underivatized and acetylated methylated paucidisperse kraft lignin fractions were curve fit to functions representing sums of terms of the form expressed in equation 1. In its curve fitting capacity, this commercial software employs the Levenberg-Marquardt algorithm based on a least squares procedure. Naturally the initial values assigned to the variable parameters could profoundly affect the speed of the curve fitting process, but in the absence of any prior information they

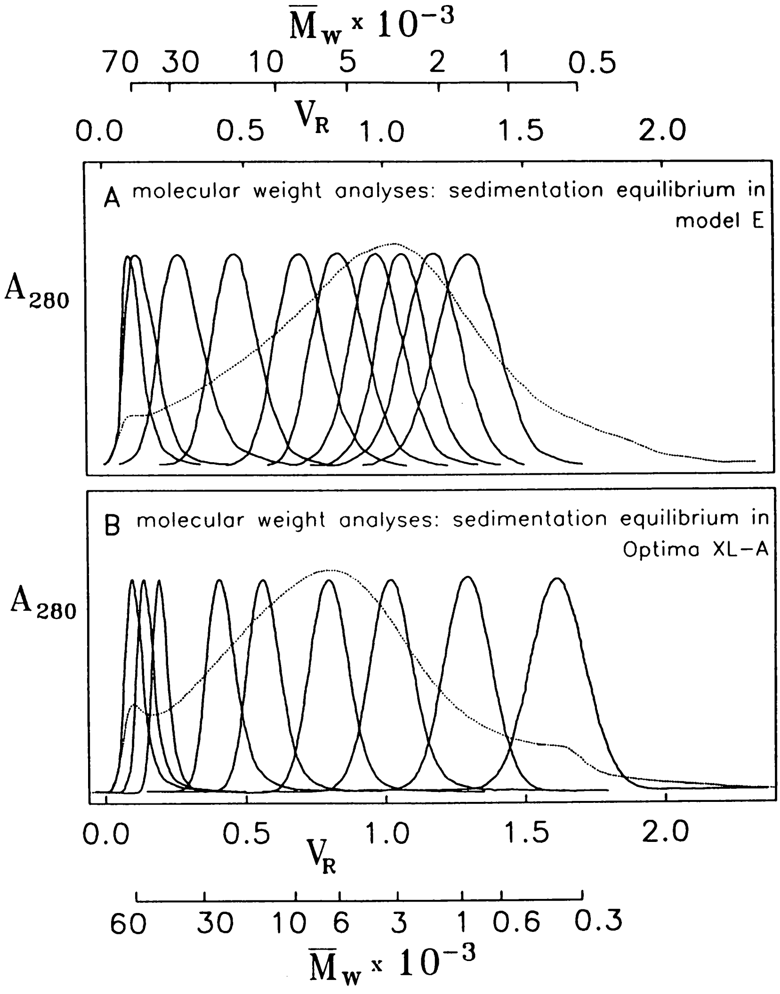

Figure 1. Kraft lignin samples from (A) Douglas fir (*7*) and (B) Jack pine (*17*) with paucidisperse fractions size exclusion chromatographically produced from respective parent preparations (*7*, *17*). Elution profiles (scaled to $V_{R,p\mathrm{NP}}$ = 2.0) in aqueous 0.10 *M* NaOH from Sephadex G100 monitored at 280 nm; weight-average molecular weights of paucidisperse fractions deduced from sedimentation equilibrium analyses in Beckman (A) model E (*7*) and (B) Optima XL-A (*17*) ultracentrifuges. (Adapted from refs. *7* and *17*.)

were all set at unity. Under such circumstances, one or even two series of preliminary iterations might be required to obtain initial values for the parameters that would then lead to satisfactory convergence. Otherwise the values realized at convergence did not depend upon those initially assigned.

In practice a stepsize had to be used which would allow the square root of the sum of squares of the residuals (the NORM) to reach a value ≤ 0.2 regardless of whether the tolerance, when set at a remote 10^{-7}, was satisfied by (the absolute value of) the change in the NORM from one iteration to the next. The most propitious stepsize was, of course, determined by the shape of the sedimentation equilibrium curve, but in this respect it was interesting that 10^n multiples ($-3 \leq$ integer $n \leq 3$) of any value, which proved effective in fitting the data for paucidisperse kraft lignin fractions, all engendered the same outcome.

Between 100 and 2000 (most commonly ~700) iterations were required for the curve fitting process to converge satisfactorily. No more than four individual terms of the form expressed in equation 1 were required for the fits of unprecedented accuracy that were achieved (*17*), and indeed two were usually quite sufficient for the vast majority of the paucidisperse underivatized kraft lignin fractions examined. The sums of the areas under the component exponential curves confirmed that the total mass of solute species detected at equilibrium did not differ by more than 1% from that initially present before sedimentation had begun (*vide supra*). As would be expected, the overall weight- and z-average molecular weights calculated directly from the individual values of molecular weight in the terms of the curve fitting expression were, to all intents and purposes, identical to those computed from equations 2 and 3, respectively.

Results and Discussion

The polymer sample adopted for the ultracentrifugal sedimentation equilibrium studies hereinafter described is none other than a representative of the most abundant industrial byproduct of converting wood chips chemically to cellulosic fibers for manufacturing paper. The molecular weight distribution of this Jack pine kraft lignin was investigated by eluting it through Sephadex G100 in carbonate-free aqueous 0.10 *M* NaOH. The resulting elution profile (*17*) depicted in Figure 1B may be usefully compared with that for a dissociated kraft lignin preparation previously isolated from Douglas fir (*Pseudotsuga menziesii* (Mirb.) Franco) which had been examined some 14 years earlier by means of the classical Beckman model E analytical ultracentrifuge (*7*) (Figure 1A). In both cases virtually identical chromatographic conditions were employed and the solute components were completely recovered from the respective columns. As far as the Jack pine kraft lignin is concerned (Figure 1B), the higher molecular weight species emerging from the column are predominantly associated macromolecular complexes, while those eluting later in the lower molecular weight region are primarily individual components (*8*, *10*). However, associated complexes contributed very little to the populations of higher molecular weight species in the (dissociated) Douglas fir kraft lignin preparation (*7*).

Nine fractions were chosen from the Jack pine kraft lignin profile and re-eluted twice through a smaller column of the same length (*17*) so that their individual profiles would conform quite closely to Gaussian shapes (*17*) (Figure 1B). These solutions were then adjusted to 8×10^{-3} gL^{-1} concentrations of the constituent kraft lignin species for subsequent ultracentrifugal sedimentation equilibrium analysis with the Beckman Optima

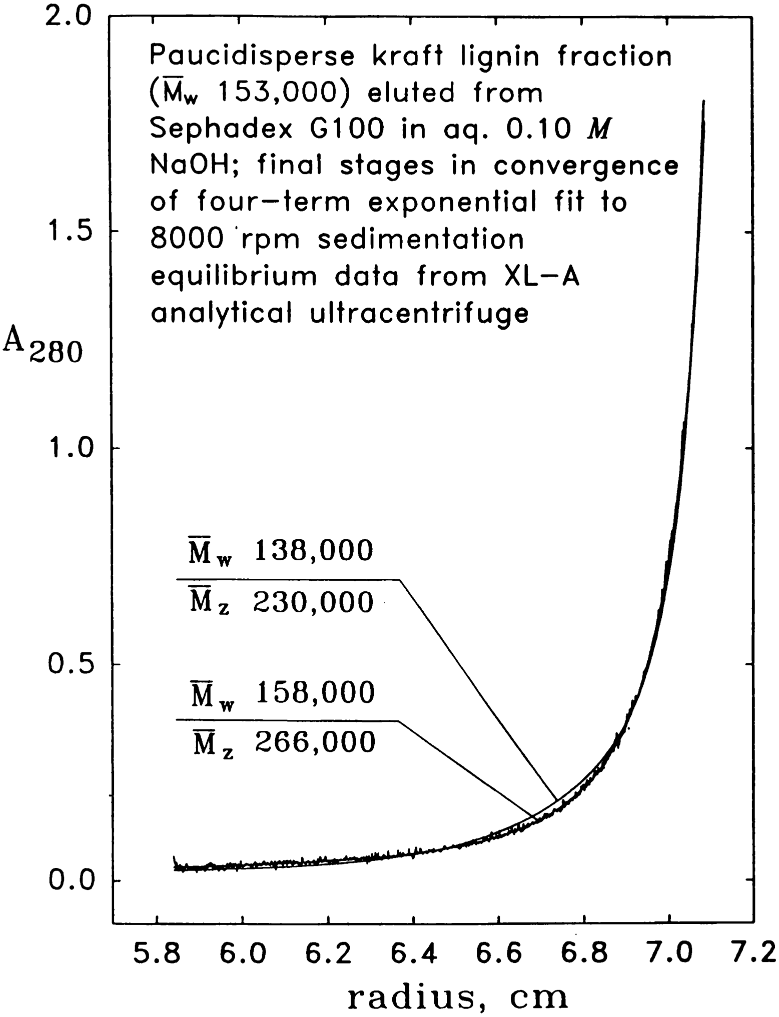

Figure 2. Final approach to successful sedimentation equilibrium analysis of Jack pine kraft lignin fraction with $\overline{M}_w = 153{,}000$ in aqueous 0.10 *M* NaOH. Concluding stages in convergence of four-term exponential fit to variation of relative solute concentration with radial distance from center of rotation at 8000 rpm in Beckman Optima XL-A ultracentrifuge. (Reproduced with permission from ref. *22*; copyright 1994 Waters Corporation.)

XL-A instrument. A very similar procedure had been used for securing paucidisperse fractions from the dissociated Douglas fir kraft lignin preparation (Figure 1A) that had been investigated earlier with the classical Beckman model E machine (*7*).

A representative sedimentation equilibrium curve for a paucidisperse Jack pine kraft lignin fraction scanned in the Beckman Optima XL-A analytical ultracentrifuge is illustrated in Figure 2 as a plot of A_{280} *versus* r (*22*); the data have been corrected for any possible optical imperfections in the corresponding cell assembly (see Experimental Section). Using SigmaPlot 5.0 (Jandel Scientific, San Rafael, CA), all such sets of corrected sedimentation equilibrium data were curve fit to sums of exponential terms with the same form as that expressed in equation 1 (*17*). In each instance only four individual terms were necessary for the unprecedented fidelity that was achieved by these exponential fits. The example depicted in Figure 2 is quite typical. A rotor speed was deemed suitable for sedimentation equilibrium analysis when, *inter alia*, the sum of the areas under the component exponential curves, which constituted the fit to the data, differed by less than 1% from the area encompassed by the corresponding plot (at wavelength λ nm) of A_λ *versus* r before sedimentation had begun. As would be expected, the weight-average molecular weights, $\overline{M}_w$, deduced directly from the individual values of M in the exponential terms (of the form expressed in equation 1) representing the curve fitting functions were identical to those computed using the formalism of equation 2.

On the other hand, the data for the paucidisperse Douglas fir kraft lignin fractions that had reached sedimentation equilibrium in the Beckman model E machine were analyzed through a very different procedure (*7*). As a prerequisite for obtaining reliable point-by-point molecular weight averages, the experimental ln c *versus* r data were first smoothed with orthogonal polynomials (*21*). Thereupon the point-by-point weight-average molecular weight, $M_{w,r}$, was calculated from the slope of ln c *versus* r^2 in the middle of a "sliding" interval (*cf.* ref. *20*) of 11 consecutive data points fitted with orthogonal least squares quadratic functions (*21*).

The weight-average molecular weights exhibit appreciable sensitivity to the fidelity of the curve fit to the sedimentation equilibrium data. The final stages in the convergence of the four-term exponential fit to the plot of A_{280} *versus* r at 8000 rpm for one of the high molecular weight ($\overline{M}_w$ = 153,000) paucidisperse Jack pine kraft lignin fractions in aqueous 0.10 *M* NaOH has been illustrated in Figure 2. Even though the penultimate curve-fit deviates only slightly from the (corrected) sedimentation equilibrium data points, the corresponding value computed for $\overline{M}_w$ is still too low by more than 12%.

When all sets of sedimentation equilibrium data for the paucidisperse fractions had been fitted with sums of the appropriate exponential terms, the overall calibration curve that unfolded for the Sephadex G100 elution profile of the Jack pine kraft lignin preparation in aqueous 0.10 *M* NaOH (Figure 3) was one of remarkable accuracy (*17*). The values of log $\overline{M}_w$ have been plotted against $V_{R,max}$, the relative retention volume at the peak of the profile for each paucidisperse fraction, but it should be borne in mind that this is only strictly valid for Schulz-Zimm distributions of solute species (*23*). As far as the parent Jack pine kraft lignin preparation is concerned, the calibration curve in Figure 3 is applicable only to $\overline{M}_w$ below 58,000: when a paucidisperse fraction has been selected from the region around the excluded limit of the gel, the elution volume at the peak of its profile increases appreciably upon re-elution owing to diffusion of the solute species during passage through the column.

In Figure 3, the accompanying plot of log $\overline{M}_z$ *versus* $V_{R,max}$ for the paucidisperse Jack

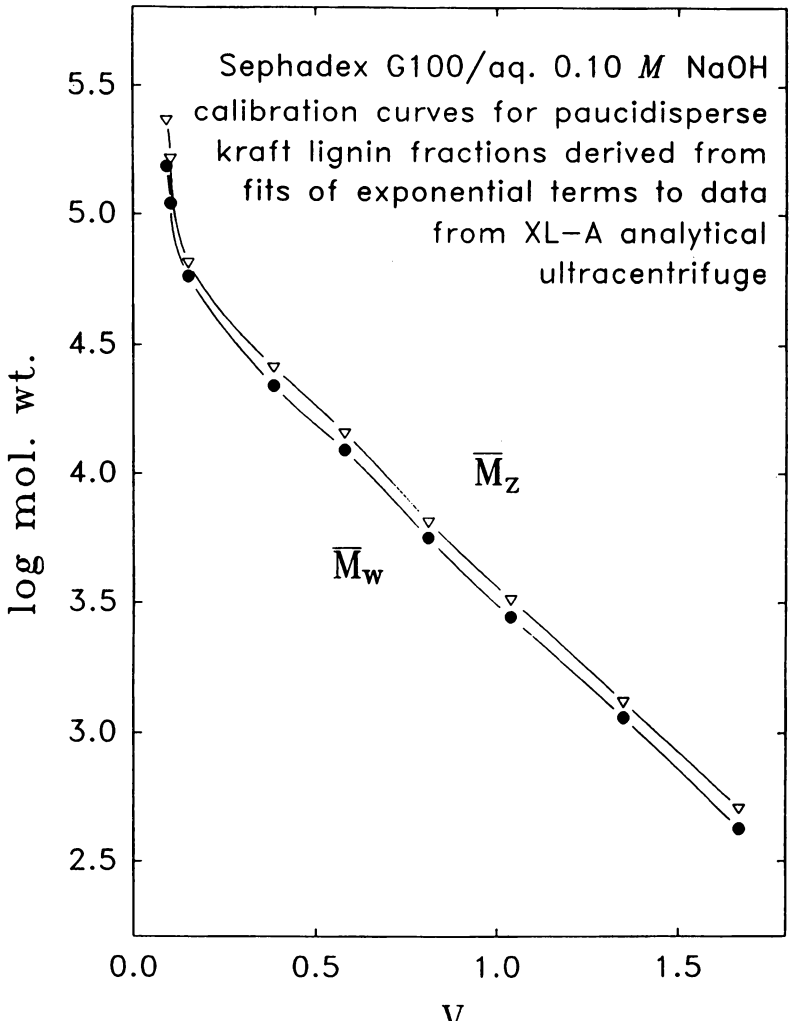

Figure 3. Primary (*17*) and secondary calibration curves for paucidisperse Jack pine kraft lignin fractions eluted through Sephadex G100 in aqueous 0.10 *M* NaOH (*17*). Semilogarithmic plots of weight- and z-average molecular weights *versus* relative retention volume deduced through fits of four exponential terms to sets of sedimentation equilibrium data from Beckman Optima XL-A ultracentrifuge for fractions in aqueous 0.10 *M* NaOH. (Adapted from ref. *22*.)

pine kraft lignin fractions forms a curve that is parallel to that of log $\overline{M}_w$. Throughout the range of elution volume for which $V_R \geq 0.15$, $\overline{M}_z/\overline{M}_w$ thus exhibits a constant value of 1.17 ± 0.03 for the paucidisperse Jack pine kraft lignin fractions; only within the region near the excluded limit does $\overline{M}_z/\overline{M}_w$ reach a value of 1.55. This is an important finding because it establishes that the polydispersity of kraft lignin species with a given hydrodynamic volume in aqueous alkaline solution does not increase with molecular weight.

There is a noteworthy corollary to the demonstrated invariance of $\overline{M}_z/\overline{M}_w$ in aqueous 0.10 *M* NaOH for the paucidisperse kraft lignin fractions secured from the range of elution volume removed from the excluded limit of the gel. A prerequisite for substantiating the result is that the $\overline{M}_z$ determinations themselves must be reliable. The computation of $\overline{M}_z$ requires both the first and second derivative of the sedimentation equilibrium curve (equation 3) and thus is more prone to error than the calculation of $\overline{M}_w$ where only the first derivative is involved (equation 2).

It is remarkable that the fidelity achieved by fits of only two exponential terms to the sedimentation equilibrium data for the paucidisperse kraft lignin fractions in aqueous 0.10 *M* NaOH was virtually indistinguishable from that attained with four terms. The formal molecular weights (M_1 and M_2) of the components described by the two exponential terms (that together respectively fit the sedimentation equilibrium curves) are compared in Figure 4 with the values of $\overline{M}_w$ for the kraft lignin fractions themselves. Clearly the scatter in M_1 and M_2 is far larger than that in $\overline{M}_w$, and thus the fluctuations of the formal component molecular weights appearing in the exponential terms of the curve-fitting expression are compensated by opposing variations in the corresponding weight concentrations.

The consequences of fitting orthogonal least squares functions to "sliding" intervals of consecutive sedimentation equilibrium data points (*21*) are readily evident in Figure 5. Here the primary calibration curve, which was compiled from a plot of log $\overline{M}_w$ *versus* $V_{R,max}$ for the paucidisperse Douglas fir kraft lignin fractions previously eluted through Sephadex G100 with aqueous 0.10 *M* NaOH (*7*), is clearly reasonably precise despite the inherent imperfections in the sedimentation equilibrium data furnished by the Beckman model E analytical ultracentrifuge employed for these older studies. In contrast the plot of log $\overline{M}_z$ *versus* $V_{R,max}$ is obviously subject to quite pronounced errors. The point-by-point z-average molecular weights, $M_{z,r}$, had been calculated as $M_{w,r}(1 + d \ln M_{w,r}/d \ln c)$ (*19*) in the middle of a "sliding" interval of 21 consecutive points representing $\ln M_{w,r}$ *versus* ln c fitted with orthogonal least squares linear to cubic functions (*21*). The overall $\overline{M}_z$ values are actually best summarized by ascribing to each Douglas fir kraft lignin fraction an average value for $\overline{M}_z/\overline{M}_w$ of 1.9 ± 0.3 that is effectively independent of molecular weight (*7*).

It is the standard deviation (± 16%), rather than the absolute magnitude, of $\overline{M}_z/\overline{M}_w$ that is relevant in this context. The earlier sedimentation equilibrium studies with the Beckman model E analytical ultracentrifuge were carried out at pH 9.5 even though the paucidisperse Douglas fir kraft lignin fractions had been originally secured from the size-exclusion chromatographic column in aqueous 0.10 *M* NaOH. (The conditions had been imposed as a precautionary measure to avoid the risk of damaging the aluminum ultracentrifuge rotor and cell housings within which the sample solutions were held.) Thus the cause of the large average value for $\overline{M}_z/\overline{M}_w$ (1.9) was the extensive association between the kraft lignin species that spontaneously occurs when the pH is reduced below

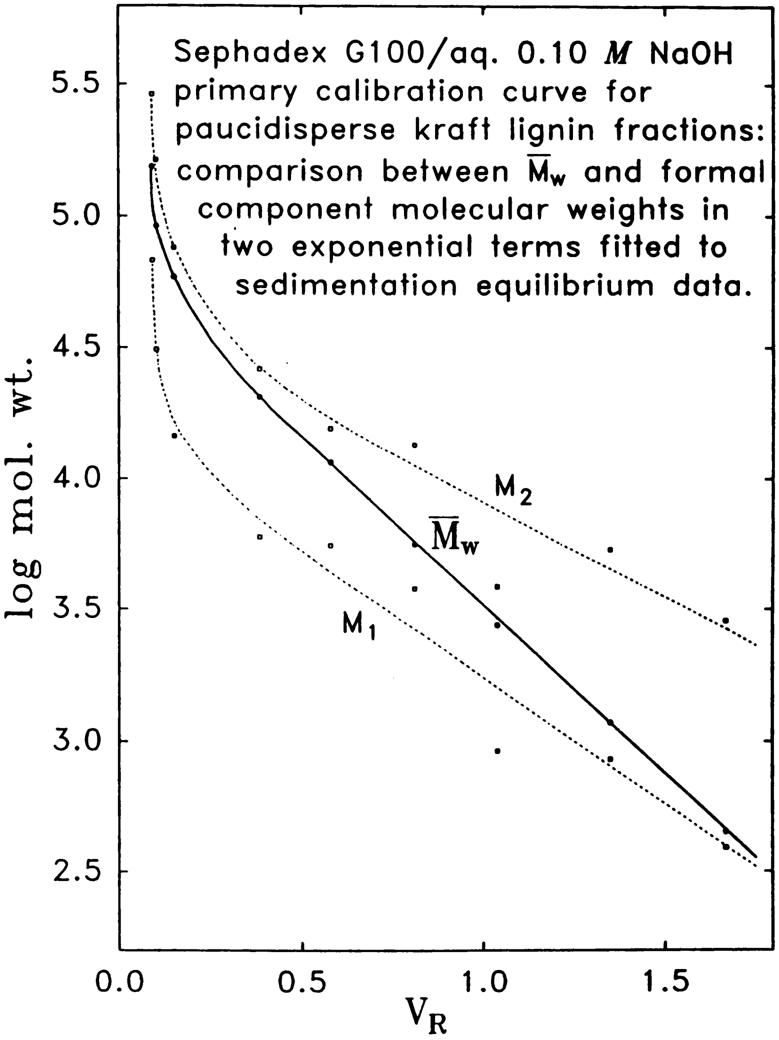

Figure 4. Comparison between weight-average molecular weight ($\overline{M}_w$) and the formal component molecular weights (M_1 and M_2) in two exponential terms fitted to the original sedimentation equilibrium data. Semilogarithmic plots *versus* relative retention volume of paucidisperse Jack pine kraft lignin fractions eluted through Sephadex G100 in aqueous 0.10 *M* NaOH.

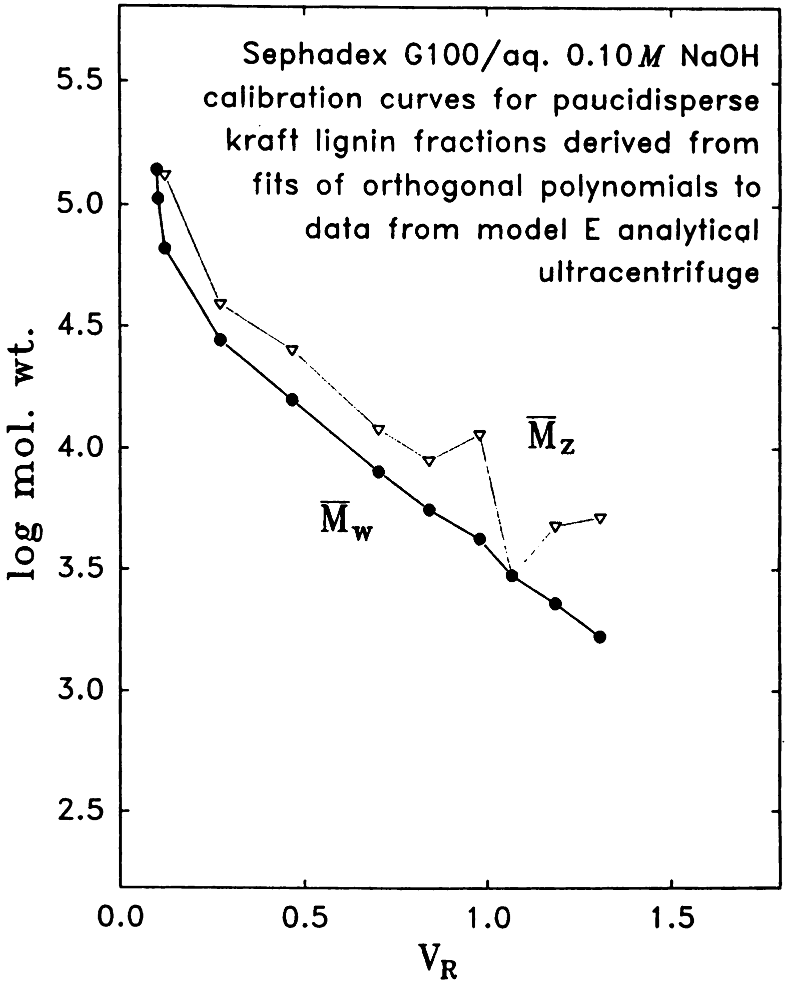

Figure 5. Primary and secondary calibration curves from data (*7*) for paucidisperse Douglas fir kraft lignin fractions eluted through Sephadex G100 in aqueous 0.10 *M* NaOH. Semilogarithmic plots of weight- and z-average molecular weights *versus* relative retention volume (rescaled to $V_{R,pNP} = 2.0$) deduced through fits of orthogonal least squares functions to "sliding" intervals of consecutive sedimentation equilibrium data points (*21*) from Beckman model E ultracentrifuge for fractions in aqueous solution at pH 9.5.

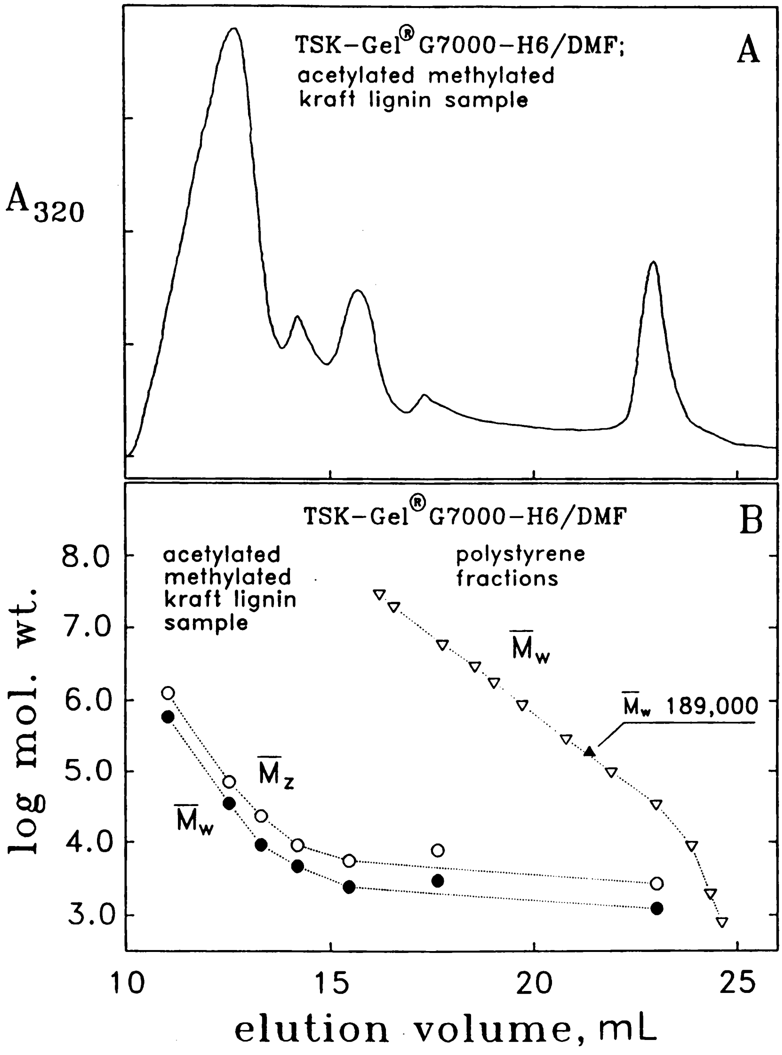

Figure 6. (A) Elution profile in DMF for acetylated methylated Jack pine kraft lignin derivative from TSKgel G7000-H6 column monitored at 320 nm (*17*); (B) corresponding semilogarithmic plots of weight-average (*17*) and z-average molecular weights (deduced from sedimentation equilibrium analyses) *versus* elution volume with primary polystyrene calibration curve (*17*) for same chromatographic system. (▲) $\overline{M}_w$ for polystyrene fraction examined in Beckman Optima XL-A ultracentrifuge. (Adapted from ref. *17*.)

11.5 (*24*). On the other hand, the standard deviation of $\overline{M}_z/\overline{M}_w$ for the paucidisperse Jack pine kraft lignin fractions examined through sedimentation equilibrium in the Beckman Optima XL-A instrument is only ± 2.6%.

A comparison of the primary and secondary molecular weight calibration curves in Figures 3 and 5 establishes that the marked difference between the errors in $\overline{M}_z/\overline{M}_w$ provided by the two studies arises predominantly from the values deduced for $\overline{M}_z$. Reliability for $\overline{M}_z$ presupposes almost impeccable fidelity in the curve fit to the sedimentation equilibrium data; this is far more difficult to achieve by fitting orthogonal least squares functions to "sliding" intervals of consecutive data points (*21*) than sums of appropriate exponential terms to the whole sedimentation equilibrium curve (Figure 2). However, success in fitting complete sedimentation equilibrium curves with sums of exponential terms requires a high degree of accuracy in the original experimental data from the ultracentrifuge.

Acetylation (Ac_2O/pyridine) and subsequent methylation (CH_2N_2) of the parent Jack pine kraft lignin yielded the derivative in which all hydroxyl groups had been acetylated and any carboxylic acid residues methylated. This acetylated methylated kraft lignin derivative was eluted in DMF through a (7.5 × 600 mm) TSKgel G7000-H6 10^7 Å pore size poly(styrene-divinylbenzene) column (*17*) (Figure 6A) from which 80% of the 0.0034 mg samples loaded were recovered when the flow rate was 1.0 mL min^{-1}. The result was comparable with that observed before with a PLgel 10^6 Å pore size poly(styrene-divinylbenzene) column (*11*), although the features previously discernible in the higher molecular weight region (*11*) have not been resolved within the corresponding 10 - 14 mL range of elution volume in Figure 6A.

Paucidisperse acetylated methylated kraft lignin fractions were selected from the TSKgel G7000-H6/DMF elution profile and the concentrations of the solute species were adjusted to 9×10^{-3} gL^{-1} for absolute molecular weight determinations by sedimentation equilibrium analyses using the Beckman Optima XL-A analytical ultracentrifuge (*17*). The sedimentation curves were again scanned at two wavelengths (280 and 320 nm) when equilibrium had been attained at more than one suitable rotor speed (chosen so as to ensure, *inter alia*, that the observable masses of solute species would be conserved). As before, the sedimentation equilibrium data were corrected for any possible optical imperfections in the cell assemblies (see Experimental Section).

With the SigmaPlot 5.0 software, sums of only four exponential terms of the form expressed in equation 1 again proved sufficient for the highly accurate curve fits to the sets of sedimentation equilibrium data gathered throughout the molecular weight range (600,000 - 1,000) encompassed by the paucidisperse acetylated methylated kraft lignin fractions in DMF (*17*). Furthermore the weight-average molecular weights, $\overline{M}_w$, deduced directly from the individual values of M in the exponential terms which constituted the curve-fitting function were, to all intents and purposes, identical to those calculated through the formalism of equation 2. It is worth mentioning that the fidelity achieved by fits of only two exponential terms was much worse than that attained with four to the sedimentation equilibrium curves for these paucidisperse acetylated methylated kraft lignin fractions in DMF, but three exponential terms provided enough adjustable parameters for the task.

The resulting molecular weight calibration curve for the profile describing the elution of the acetylated methylated kraft lignin derivative through the TSKgel G7000-H6 column in DMF is depicted in Figure 6B (*17*). The corresponding plot for standard polystyrenes in the same figure is based on molecular weight data provided by the suppliers (Polymer Laboratories, Inc., Polysciences, Inc., and the Pressure Chemical Co.) (*17*). The divergence of the two calibration curves from one another is striking. For instance, the acetylated methylated kraft lignin species emerging from the column at an elution volume around 15.0 mL possess molecular weights that are over 30,000 times smaller than those for the corresponding polystyrenes.

Such a drastic difference cannot be correlated with a compensating disparity between the intrinsic viscosities of the respective solute species; clearly the separation between the two calibration curves is beyond reconciliation through the application of universal calibration principles (*25*). It should be mentioned that, after evaporation of solvent from 0.10% solutions in DMF, the acetylated methylated kraft lignin entities visible through negative staining (with phosphotungstate) on a carbon-coated copper grid under the electron microscope exhibit apparent dimensions (~0.1 - 0.3 μ across) comparable to those of ~20 million molecular weight polystyrene components (*11*). It could be that the supramacromolecular kraft lignin complexes exhibiting, through their size-exclusion chromatographic behavior, such large apparent hydrodynamic volumes in DMF undergo, within the time taken to attain sedimentation equilibrium, substantial dissociation at the ~20-fold lower concentrations employed for analytical ultracentrifugation.

An important aspect of the molecular weight calibration curve for the elution profile of the acetylated methylated kraft lignin derivative in DMF is revealed by the $\overline{M}_z$ values for the fractions subjected to sedimentation equilibrium analysis (Figure 6B). The ratio $\overline{M}_z/\overline{M}_w$ (2.25 ± 0.25) is large but, within experimental error, does not vary systematically with $\overline{M}_w$. Indeed the magnitude of $\overline{M}_z/\overline{M}_w$ is reminiscent of the corresponding ratio for the underivatized Douglas fir kraft lignin fractions (*7*) examined in the Beckman model E ultracentrifuge at pH 9.5 (*vide supra*) after having originally been isolated size exclusion chromatographically in aqueous 0.10 *M* NaOH (Figure 5).

The acetylated methylated kraft lignin fractions ultimately analyzed with the Beckman Optima XL-A instrument represented accumulations of the respective solute species from multiple elutions of the parent preparation in DMF through the 10^7 Å pore size poly(styrene-divinylbenzene) column; the solvent was evaporated from each fraction between the successive size exclusion chromatographic steps. The following observation may be singularly relevant under these circumstances. Dissociation of a particular subset of the high molecular weight species in the acetylated methylated Jack pine kraft lignin preparation has been found to occur in DMF at concentrations two orders of magnitude greater, even, than those prevailing during ultracentrifugal sedimentation equilibrium analysis of the fractions (Mlynár and Sarkanen, unpublished observations). Moreover, the duration of the dissociative process was comparable to the time required for the acetylated methylated kraft lignin species to reach sedimentation equilibrium in the centrifugal field. Actually the onset of sedimentation in the ultracentrifuge was curiously preceded by a rather prolonged lag period; it seemed as though translational motion of the supramacromolecular kraft lignin complexes was initially impeded by long-range interactions of such compass as to fashion a quasi-gel structure throughout the body of the DMF solution!

Thus differences between the degrees of association for the acetylated methylated kraft lignin species during size exclusion chromatography and at equilibrium in the centrifugal field are probably responsible not only for the magnitude of $\overline{M}_z/\overline{M}_w$ but also for the large standard deviation among its experimentally determined values. The sets of ultracentrifugal sedimentation equilibrium data themselves are no less reliable than those secured for analyzing the paucidisperse underivatized Jack pine kraft lignin fractions in aqueous 0.10 *M* NaOH (Figure 3). Relatively small changes, however, in the solution histories of the acetylated methylated kraft lignin fractions in DMF can have very significant influences upon the degrees of association between the constituent species.

The relationship between log $\overline{M}_w$ and V_R for the elution of paucidisperse polystyrene fractions in DMF through the TSKgel G7000-H6 10^7 Å pore size poly(styrene-divinylbenzene) column (Figure 6B) appears to be quite accurate. This is gratifying because the plot is based upon molecular weight data furnished by the suppliers. One of the paucidisperse polystyrene fractions ($\bar{\upsilon}_2 = 0.917\ cm^3g^{-1}$ (*26*)) was chosen for confirmation of the values claimed for its molecular weight averages. The sedimentation curves for the 0.07 gL^{-1} sample in THF were scanned with the Beckman Optima XL-A analytical ultracentrifuge at two wavelengths (257 and 259 nm) when equilibrium had been reached at two rotor speeds (4800 and 5000 rpm) and, as before, the corresponding baseline, A_{600} *versus* r, was subtracted from the resulting sets of data. The fits of exponential terms (of the form expressed in equation 1) to the corrected sets of sedimentation equilibrium data for the polystyrene fraction were accomplished much more easily than with the paucidisperse kraft lignin fractions (whether derivatized or not): relatively few iterations (~110) of the Levenberg-Marquardt algorithm employed in the SigmaPlot 5.0 software were necessary for satisfactory convergence (Figure 7). Indeed the small standard deviation in the values for $\overline{M}_w$ (188,700 ± 1500) reflects the fidelity achieved in the fits of exponential terms to the four experimental sedimentation equilibrium curves.

On the other hand, the corresponding values for $\overline{M}_z$ exhibit considerably more scatter: the error in $\overline{M}_z/\overline{M}_w$ (1.38 ± 0.18) is 13%. This was caused by the relatively high level of noise appearing in the sedimentation equilibrium data at wavelengths close to the effective ultraviolet cutoff of the solvent (Figure 7). The impact of noise is much more pronounced on $\overline{M}_z$, the computation of which requires both the first and second derivative of the sedimentation equilibrium curve (equation 3).

Concluding Remark

The foregoing studies have persuasively illustrated the utility of ultracentrifugal sedimentation equilibrium measurements for interpreting size exclusion chromatographic elution profiles as molecular weight distributions for polymers. Fitting sums of exponential terms to sedimentation equilibrium curves represents a particularly convenient technique even for enigmatic and intractable polymer samples like lignin derivatives. However, no provision has been made here for determining virial coefficients so the average molecular weights obtained are apparent values corresponding to the finite solute concentrations employed (*cf.* ref. *20*). The most rigorous procedure for eliminating any effects arising from non-ideality would have required extrapolation of the apparent $\overline{M}_w$ and $\overline{M}_z$ from a series of different solute concentrations to zero. Be that as it may, such an exercise is very seldom attempted in a size exclusion chromatographic context, and anyway the component monomer residue concentrations ($\leq 5 \times 10^{-5}$ and 7×10^{-4} *M* for the lignin derivative and polystyrene, respectively) were so low that appreciable deviations from ideality would not be anticipated.

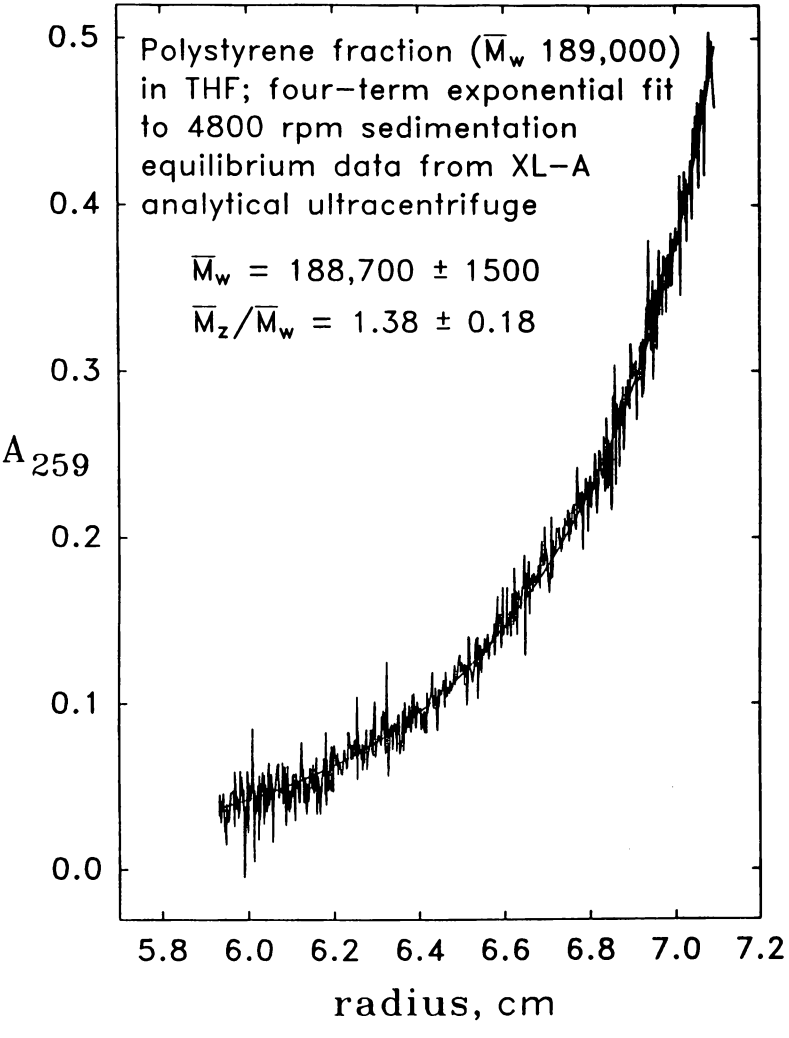

Figure 7. Sedimentation equilibrium analysis of polystyrene fraction in THF. Variation of relative solute concentration with radial distance from center of rotation monitored in Beckman Optima XL-A ultracentrifuge with curve fit to data points achieved by sum of exponential terms of the form expressed in equation 1.

Acknowledgments

Acknowledgment for support of this work is made to the Vincent Johnson Lignin Research Fund at the University of Minnesota, the Minnesota State Legislature through the recommendation of the Legislative Commission on Minnesota Resources, and the Minnesota Agricultural Experiment Station.

Paper No. 21,611 of the Scientific Journal Series of the Minnesota Agricultural Experiment Station, funded through Minnesota Agricultural Experiment Station Project No. 43-68, supported by Hatch Funds.

Literature Cited

1. Hanlon, S.; Lamers, K.; Lauterbach, G.; Johnson, R.; Schachman, H. K. *Arch. Biochem. Biophys.* **1962,** *99,* 157-174.
2. Schachman, H. K.; Gropper, L.; Hanlon, S.; Putney, F. *Arch. Biochem. Biophys.* **1962,** *99,* 175-190.
3. Lamers, K.; Putney, F.; Steinberg, I. Z.; Schachman, H. K. *Arch. Biochem. Biophys.* **1963,** *103,* 379-400.
4. Spragg, S. P.; Travers, S. *Anal. Biochem.* **1965,** *12,* 259-270.
5. Connors, W. J.; Sarkanen, S.; McCarthy, J. L. *Holzforschung* **1980,** *34,* 80-85.
6. Sarkanen, S.; Teller, D. C.; Hall, J.; McCarthy, J. L. *Macromolecules* **1981,** *14,* 426-434.
7. Sarkanen, S.; Teller, D. C.; Abramowski, E.; McCarthy, J. L. *Macromolecules* **1982,** *15,* 1098-1104.
8. Sarkanen, S.; Teller, D. C.; Stevens, C. R.; McCarthy, J. L. *Macromolecules* **1984,** *17,* 2588-2597.
9. Garver, T. M., Jr.; Sarkanen, S. *Holzforschung* **1986,** *40 (Suppl.),* 93-100.
10. Dutta, S.; Garver, T. M., Jr.; Sarkanen, S. *ACS Symp. Ser.* **1989,** *No. 397,* 155-176.
11. Dutta, S.; Sarkanen, S. *Mat. Res. Soc. Symp. Proc.* **1990,** *197,* 31-39.
12. Lewis, N. G.; Yamamoto, E. *Annu. Rev. Plant Physiol. Plant Mol. Biol.* **1990,** *41,* 455-496.
13. Saka, S.; Goring, D. A. I. In *Biosynthesis and Biodegradation of Wood Components*; Higuchi, T., Ed.; Academic Press: New York, 1985; pp 51-62.
14. Grisebach, H. In *The Biochemistry of Plants—A Comprehensive Treatise: Volume 7, Secondary Plant Products*; Conn, E. E., Ed.; Academic Press: New York, 1981; pp 457-478.
15. Adler, E. *Wood Sci. Technol.* **1977,** *11,* 169-218.
16. Gierer, J. *Holzforschung* **1982,** *36,* 43-51.
17. Himmel, M. E.; Mlynár, J.; Sarkanen, S. In *Handbook of Size Exclusion Chromatography*; Wu, C.-s., Ed.; Chromatographic Science Series 69; Marcel Dekker: New York, 1995; pp 353-379.
18. Chum, H. L.; Johnson, D. K.; Tucker, M. P.; Himmel M. E. *Holzforschung* **1987,** *41,* 97-108.
19. Adams, E. T., Jr. In *Characterization of Macromolecular Structure*; Publication 1573; Natl. Acad. Sci. U.S.A.: Washington, D.C., 1968; pp 84-142 (and references therein).

20. Harding, S. E.; Horton, J. C.; Morgan, P. J. In *Analytical Ultracentrifugation in Biochemistry and Polymer Science*; Harding, S. E., Rowe, A. J., Horton, J. C., Eds.; The Royal Society of Chemistry: Cambridge, 1992; pp 275-294.
21. Teller, D. C. *Methods Enzymol.* **1973,** *27,* 346-441 (and references therein).
22. Mlynár, J.; Sarkanen, S. In *International GPC Symposium Proceedings*; Waters Corporation: Milford, MA, 1994; pp 525-545.
23. Berger, H. L.; Schultz, A. R. *J. Polym. Sci. Part A* **1965,** *2,* 3643-3648.
24. Woerner, D. L.; McCarthy, J. L. *Macromolecules* **1988,** *21,* 2160-2166.
25. Cassassa, E. F. *Macromolecules* **1976,** *9,* 182-185.
26. Albright, D. A.; Williams, J. W. *J. Phys. Chem.* **1967**, *71,* 2780-2786.

Author Index

Barman, Shikha, 328
Belenkii, B. G., 274
Beneš, M. J., 190
Berek, D., 250
Busnel, Jean-Pierre, 52
Campos, A., 103
Chubarova, E. V., 127
Dawkins, John V., 262
Degoulet, Christophe, 52
Dubin, Paul L., 88
Ebeyer, Tony, 88
Figueruelo, J. E., 103
Gankina, E. S., 274
Garcia, R., 103
Ghazi, A., 36
Gómez, C., 103
Hagel, Lars, 225
Hoagland, David A., 173
Horák, D., 190
Hradil, J., 190
Huber, A., 351
Hunkeler, D., 250
Janco, M., 250
Jeřábek, Karel, 211
Kasalainen, G. E., 274
le Maire, M., 36
Meehan, Elizabeth, 262
Mlynár, Juraj, 379
Møller, J. V., 36
Mori, Sadao, 347
Müller, Axel H. E., 2
Nesterov, V. V., 127
Oosaki, Toshitaka, 347
Pathak, C. P., 328
Patterson, Michael, 262
Porcar, I., 103
Potschka, Martin, 67
Praznik, W., 351
Radke, Wolfgang, 2
Reed, Wayne F., 7
Reid, Simon P., 262
Rodrigues, Alirio E., 157
Romano, Vincent A., 88
Sarkanen, Simo, 379
Soria, V., 103
Striegel, André M., 366
Tassin, Jean-François, 52
Tennikov, M. B., 274
Timpa, Judy D., 366
Vilenchik, L. Z., 328
Warner, Frank P., 262

Affiliation Index

Academy of Sciences of the Czech Republic, 190,211
Agricultural Research Service, 366
Centre National de la Recherche Scientifique, 36
Focal Interventional Therapeutics, 328
Indiana University–Purdue University, 88
Institut für Physikalische Chemie, 351
Interuniversitäres Forschungszentrum für Agrarbiotechnologie, 351
Loughborough University of Technology, 262
Mie University, 347
PerSeptive Biosystems, 328
Pharmacia Biotech AB, 225
Polymer Laboratories Limited, 262
Russian Academy of Sciences, 127,274
Slovak Academy of Sciences, 250
Tulane University, 7
U.S. Department of Agriculture, 366

In Strategies in Size Exclusion Chromatography; Potschka, M., et al.;
ACS Symposium Series; American Chemical Society: Washington, DC, 1996.

Downloaded by 217.66.152.32 on October 8, 2012 | http://pubs.acs.org
Publication Date: May 30, 1996 | doi: 10.1021/bk-1996-0635.ix001

Downloaded by 217.66.152.32 on October 8, 2012 | http://pubs.acs.org
Publication Date: May 30, 1996 | doi: 10.1021/bk-1996-0635.ix001

Universidade do Porto, 157
Université Paris-Sud, 36
Université du Maine, 52
Universität Mainz, 2
Universitat de València, 103
University of Aarhus, 36
University of Massachusetts–Amherst, 173
University of Minnesota, 379
University of New Orleans, 366
Vanderbilt University, 250

Subject Index

A

Adsorption, critical conditions in LC, 250–260
Adsorption/desorption kinetics, intraparticle convection in chromatographic permeable packings, 164–165
Adsorptive protein retention, theories, 89
Agarose, packing for SEC, 201
Aluminum(III) oxides, packing for size exclusion chromatography, 206
Analysis
  column based, 36–187
  detector based, 2–31
  polymer composition, 250–323
Analytical ultracentrifugation, 385
Apparent weight-average molecular weight, 4–5
Aqueous size exclusion chromatography
  function, 347
  glucans, 354
  limitation, 225–226
  secondary effects between sodium poly(styrene sulfonate) compounds of different sulfonations, 225
Association equilibria, stationary phase in SEC with binary eluents, 113–114
Augmented diffusivity by convection, concept, 159–162
Average pore radius evaluation, stationary phase in SEC with binary eluents, 112

B

Binary eluents, modeling of stationary phase in SEC, 103–125
Biopolymers, separation methods, 274–275
Buoyant molecular mass, 39

C

Capillary electrophoresis, separation of biopolymers, 274
Cellulose
  packing for SEC, 201,203
  SEC in *N,N*-dimethylacetamide with lithium chloride, 366–378
Chain geometry, role in Monte Carlo simulation of SEC, 54–55,56*f*
Chromatographic permeable packings, intraparticle convection, 157–170
Chromatographic processes, performance using permeable particles, 163–164
Chromatographic radius, 53
Coil conformation, glucans, 357,358*f*,361*t*
Coil packing density, glucans, 357,359*f*
Coil radii, glucans, 357,359*f*
Coil volume, glucans, 357
Column surface charge density, 93
Composition, stationary phase in size exclusion chromatography with binary eluents, 119–122
Compositional heterogeneity of poly(vinyl alcohol) using liquid chromatography
  development of high-performance LC, 263
  experimental procedure, 263–264
  high-performance LC, 265,268–272
  poly(vinyl alcohol) structures, 264
  SEC, 264–265,266–267*f*
Confinement entropy, 183–186

Universidade do Porto, 157
Université Paris-Sud, 36
Université du Maine, 52
Universität Mainz, 2
Universitat de València, 103
University of Aarhus, 36
University of Massachusetts–Amherst, 173
University of Minnesota, 379
University of New Orleans, 366
Vanderbilt University, 250

Subject Index

A

Adsorption, critical conditions in LC, 250–260
Adsorption/desorption kinetics, intraparticle convection in chromatographic permeable packings, 164–165
Adsorptive protein retention, theories, 89
Agarose, packing for SEC, 201
Aluminum(III) oxides, packing for size exclusion chromatography, 206
Analysis
  column based, 36–187
  detector based, 2–31
  polymer composition, 250–323
Analytical ultracentrifugation, 385
Apparent weight-average molecular weight, 4–5
Aqueous size exclusion chromatography
  function, 347
  glucans, 354
  limitation, 225–226
  secondary effects between sodium poly(styrene sulfonate) compounds of different sulfonations, 225
Association equilibria, stationary phase in SEC with binary eluents, 113–114
Augmented diffusivity by convection, concept, 159–162
Average pore radius evaluation, stationary phase in SEC with binary eluents, 112

B

Binary eluents, modeling of stationary phase in SEC, 103–125
Biopolymers, separation methods, 274–275
Buoyant molecular mass, 39

C

Capillary electrophoresis, separation of biopolymers, 274
Cellulose
  packing for SEC, 201,203
  SEC in *N,N*-dimethylacetamide with lithium chloride, 366–378
Chain geometry, role in Monte Carlo simulation of SEC, 54–55,56*f*
Chromatographic permeable packings, intraparticle convection, 157–170
Chromatographic processes, performance using permeable particles, 163–164
Chromatographic radius, 53
Coil conformation, glucans, 357,358*f*,361*t*
Coil packing density, glucans, 357,359*f*
Coil radii, glucans, 357,359*f*
Coil volume, glucans, 357
Column surface charge density, 93
Composition, stationary phase in size exclusion chromatography with binary eluents, 119–122
Compositional heterogeneity of poly(vinyl alcohol) using liquid chromatography
  development of high-performance LC, 263
  experimental procedure, 263–264
  high-performance LC, 265,268–272
  poly(vinyl alcohol) structures, 264
  SEC, 264–265,266–267*f*
Confinement entropy, 183–186

Downloaded by 217.66.152.32 on October 8, 2012 | http://pubs.acs.org
Publication Date: May 30, 1996 | doi: 10.1021/bk-1996-0635.ix002

Copolymers
  molecular weight determination using gel permeation chromatography–light scattering, 2–6
  poly(ethylene glycol), micelle formation using SEC, light scattering, and UV spectroscopy, 328–346
Corn starch, high amylose, molecular characteristics, 351–364
Critical chain overlap concentration, 128
Critical chromatography of polymers
  AB block copolymer, 292–296
  main features of unified mechanism, 290*f*,291,293
Critical conditions of adsorption in liquid chromatography of macromolecules
  applications, 252
  calibration curves, 252,253*f*
  comparison to limiting conditions of solubility, 253,258*t*
  description, 250
  examples, 252,254–255*t*
  influencing factors, 250
  studies, 251–252
Critical size exclusion chromatography, use of multicomponent eluents, 103–104
Cross-sectional concentration, 178–179

D

Degradation index, 131
Degradation mechanism, macromolecules, 127–154
Detector-based analysis, studies, 2–31
Dextran, packing for SEC, 201,202*t*
N,N-Dimethylacetamide with lithium chloride, SEC of polysaccharides, 366–378
Dissolution, glucans, 355
Distribution coefficients, stationary phase in SEC with binary eluents, 122–125

E

Electron spin resonance–inverse steric exclusion chromatography, molecular accessibility of swollen gel resins, 219–221,222*f*
Electrophoretic velocity, 179
Electrostatic forces, soft body model of SEC, 69–71,72–74*f*
Electrostatic interactions
  between proteins and charged surfaces, importance, 88
  role in aqueous SEC between sodium poly(styrene sulfonate) compounds of different sulfonations, 350
Electrostatic models, protein retention in ion-exchange chromatography, 89
Elution chromatography, bovine serum albumin, 169
Elution rate, role in degradation of macromolecules in nonhomogeneous hydrodynamic fields, 131–133,144–146
Elution volume, 212–213
Entropy, 183
Enzymatically supported branching analysis, glucans, 360–364
Excluded volume model of SEC, retention, 68
Experimental pore radius evaluation, stationary phase in SEC with binary eluents, 112–113

F

Flexibility, role in Monte Carlo simulation of SEC, 57,61–65
Flexible chain solute, motion, 181–183
Flory–Huggins lattice theory, modeling of stationary phase in SEC with binary eluents, 103–125
Flow rate, role on media for aqueous size exclusion chromatography, 233–234
Flux, equations, 175
Fractionation
  glucans, 355
  polymers, 275
  requirements, 7
Fractogram, 145
Frictional coefficient, 37,39

Downloaded by 217.66.152.32 on October 8, 2012 | http://pubs.acs.org
Publication Date: May 30, 1996 | doi: 10.1021/bk-1996-0635.ix002

G

Gel chromatography for size and molecular mass characterization for proteins
  application to water-soluble globular proteins, 39–40
  calibration, 45–49
  fractal model, 49–50
  randomly coiled and elongated polymers, 41–45
  theory, 36–39
Gel electrophoresis
  comparison to SEC and hydrodynamic chromatography, 173–187
  separation of biopolymers, 274
Gel filtration, 226
Gel permeation chromatography–light scattering, molecular weight determination of copolymers, 2–6
Gel-phase accessibility, macroporous network polymers, 215,217–218
Gel-type resins, packing for size exclusion chromatography, 193
Gelation, 204
Gibbs free energy of retention, determination, 95
Glucans
  factors affecting properties, 351–352
  importance, 351
  kind and extent of branching, 352
  molecular characteristics, 351–364

H

Height equivalent to theoretical plate, relationship to superficial velocity, 167–168
Heterogeneous copolymers, characterization techniques, 262–263
High-amylose corn starch, molecular characteristics, 351–364
High-performance liquid chromatography, compositional heterogeneity of poly(vinyl alcohol), 262–272
High-performance membrane chromatography of polymers
  adsorption coefficient dependence on displacer concentration, 310*f*,311
  advantages, 309,313,314*t*
  applications, 313–320
  block copolymer separation, 315,322–323
  column length, 311–312
  complete membrane process of protein purification, 322*f*,323
  development, 315,321*t*
  eluent composition, 315,323
  stepwise gradient elution, 312–313
High-performance size exclusion chromatography, procedure, 384
Hydrodynamic chromatography, comparison to SEC and gel electrophoresis, 173–187
Hydrodynamic fields, nonhomogeneous, macromolecular behavior, 127–154
Hydrogen bond breaking, glucans, 354
Hydrophilic domains within polymer, inverse steric exclusion chromatographic characterization, 221–223
Hydrophobic interactions, role in aqueous SEC between sodium poly(styrene sulfonate) compounds of different sulfonations, 350

I

Intraparticle convection in chromatographic permeable packings
  applications, 170
  concept of augmented diffusivity by convection, 159–162
  elution chromatography of bovine serum albumin, 169
  frontal chromatography experiments, 168–169
  height equivalent to theoretical plate vs. superficial velocity, 167–168
  importance of adsorption–desorption kinetics, 164–165
  intraparticle velocity estimation, 165–166
  performance of chromatographic processes using permeable particles, 163–164

Downloaded by 217.66.152.32 on October 8, 2012 | http://pubs.acs.org
Publication Date: May 30, 1996 | doi: 10.1021/bk-1996-0635.ix002

Downloaded by 217.66.152.32 on October 8, 2012 | http://pubs.acs.org
Publication Date: May 30, 1996 | doi: 10.1021/bk-1996-0635.ix002

Intraparticle convection in chromatographic permeable packings—*Continued*
  protein separation by LC using permeable particles
    bed permeability, 166–167
    columns, 166
    efficiency of columns and height equivalent to theoretical plate, 167,168*f*,
Intraparticle velocity estimation, chromatographic permeable packings, 165–166
Intrinsic viscosity, 41
Inverse steric exclusion chromatography for morphology characterization
  combined electron spin resonance–inverse steric exclusion chromatography approach to molecular accessibility of swollen gel resins, 219–221,222*f*
  development, 211–212
  experimental procedure, 214
  gel-phase accessibility in macroporous network polymers, 215,217–218
  importance, 214–215
  ion-exchange catalysts, 215,216*f*,220*f*
  polymer carriers, 213–214
  pore definition, 213–214,216*f*
  simultaneous characterization of lipophilic and hydrophilic domains within one polymer, 221–223
  theory, 212–214
Ion-exchange catalysts, use in inverse steric exclusion chromatography for morphology characterization, 215,216*f*,220*f*

K

Kraft lignin derivatives, ultracentrifugal sedimentation equilibrium calibrations of SEC elution profiles, 379–398

L

Large pore permeable materials
  applications, 157,158*t*
  intraparticle convection, 159–170
Light scattering
  micelle formation, 328–346
  molecular weight determination of glucans, 354–355
  multiangle, *See* Multiangle light scattering–viscometric–refractometric detector coupling for polyelectrolyte characterization
Light scattering detector for copolymers, disadvantages, 3
Light scattering–gel permeation chromatography, molecular weight determination of copolymers, 2–6
Lignins
  precursors, 380
  SEC, 380–381
  ultracentrifugal sedimentation equilibrium analysis, 381–383
Limiting conditions of solubility in liquid chromatography of macromolecules
  applications, 253,258–259
  comparison to critical conditions of adsorption, 253,258*t*
  development, 250
  examples, 253,257*t*
  mechanism, 252–253,256*f*
Linear polymer chains, flexibility effect, 52–65
Lipophilic domains within polymer, inverse steric exclusion chromatographic characterization, 221–223
Liquid chromatography
  compositional heterogeneity of poly(vinyl alcohol), 262–272
  macromolecules
    critical conditions of adsorption, 250–260
    limiting conditions of solubility, 250–260
  protein separation, 166–168
Low-angle light scattering detectors, comparison to multiangle light scattering detectors, 17,20–21,22*f*

M

Macromolecular aggregates, importance of size and number, 328

Macromolecular chromatography, technical development, 274–275
Macromolecules
  critical conditions of adsorption in liquid chromatography, 250–260
  in nonhomogeneous hydrodynamic fields
    experimental procedure, 129,131
    importance, 127
    membrane experiments, 141–142,143*f*
    physical degradation model
      distortion of concentration homogeneity, 149
      pore size effect, 153
      mechanism, 149–152
      redistribution of polymer concentration, 148–149,153–154
    size exclusion chromatography
      degradation vs. thermodynamic quality of solvent, 135,137–141
      elution rate on degradation effect, 131–133
      retention on macromolecules on surface of solvent particles effect, 133–135,136*f*
      solvent effect, 130*f*,131
    thermal field flow fractionation
      elution rate effect, 144*f*,145–147
      process, 145
      quantitative evaluation of degree of degradation, 146*f*,147–148
  limiting conditions of solubility in LC, 250–260
  sizes, 53
Macroporous network polymers, gel-phase accessibility, 215,217–218
Macroporous resins, packing for size exclusion chromatography, 193–198
Mass-modulated molecular weight distribution, glucans, 355–356
Mass scaling laws, 7–8
Matrix interaction, characteristic of media for aqueous SEC, 245
Mean field approximation, soft body model of SEC, 71,75–77
Mean velocity, 174–175
Media for aqueous SEC
  experimental parameters
    flow rate, 233–234
    non-size-exclusion effects, 235
    sample volume, 235,238*f*
  matrix characteristics
    particle size, 229
    pore volume, 227
    selectivity, 227–229
  properties
    examples, 239,240*t*
    matrix interaction, 245
    molecular diffusivity, 243,245
    molecular shape and size, 243
    particle size, 243
    peak capacity, 245–246
    pore size, 239,241*f*
    pore volume, 239
    resolvability, 244*f*,245,246*f*
    selectivity, 239,242–243,244*f*
  reasons for interest, 226
  separation result
    peak capacity, 237,239,241*f*
    resolvability, 236–237,238*f*
  solute characteristics
    molecular diffusivity, 231–233
    molecular size, 230*f*,231
Membrane type, role in macromolecular behavior in nonhomogeneous hydrodynamic fields, 141–142,143*f*
Methanol
  adsorption isotherms, 118*f*,119
  adsorption models, 114–117,119
Micelle formation using SEC, light scattering, and UV spectroscopy
  chromatographic column effect, 331–336
  comparison to spectroscopic study, 334–346
  experimental description, 330–333
  guard column effect, 337,339*f*
  influencing factors, 336–337
  micelle formation using multiangle light scattering photometer in batch mode, 341–344
  polymer concentration effect, 337,340*f*,341,342*f*
  solute concentration effect, 337,338*f*

Downloaded by 217.66.152.32 on October 8, 2012 | http://pubs.acs.org
Publication Date: May 30, 1996 | doi: 10.1021/bk-1996-0635.ix002

Microcolumn size exclusion chromatography of polymers
  advantages, 276*t*,277
  column, 285
  optimization, 277–278
  polystyrene, 284–289
  problems, 279,280*f*
  refractometer design, 279,281–283,285
  requirements for hydraulic system, 278–279
  studies, 277
Modeling, stationary phase in SEC with binary eluents, 103–125
Molecular accessibility of swollen resins, electron spin resonance–inverse steric exclusion chromatography, 219–221,222*f*
Molecular characteristics of glucans
  aqueous SEC of dimethyl sulfoxide dissolved starch glucans, 354
  coil conformation, 357,358*f*,361*t*
  coil packing density, 357,359*f*
  coil radii, 357,359*f*
  coil volume, 357
  dissolution and preparative fractionation, 355
  enzymatically supported branching analysis, 360–364
  experimental procedure, 352–353
  H bond breaking using dimethyl sulfoxide dissolution, 354
  light scattering for molecular weight determination, 354–355
  mass-modulated molecular weight distribution, 355–356
  number-modulated molecular weight distribution, 356–357
  sample concentration, 354
  techniques, 352,353*t*
Molecular diffusivity, characteristic of media for aqueous SEC, 243,245
Molecular mass of proteins, characterization using gel chromatography, 36–50
Molecular shape and size, characteristic of media for aqueous SEC, 243
Molecular weight averages, determination using ultracentrifugal sedimentation equilibrium calibrations of size exclusion chromatographic elution profiles, 379–398
Molecular weights of copolymers determined using gel permeation chromatography–light scattering
  accuracy, 5–6
  comparison to gel permeation chromatography–viscometry, 6
  experimental procedure, 5
  theory, 3–5
Monte Carlo simulation of SEC
  comparison of simulation with theoretical results, 55–57,58*f*
  definition of sizes of macromolecule, 53
  experimental description, 53
  flexibility effect, 57,61–65
  partition coefficient calculation, 54
  pore geometry effect, 55,57,59–60*f*
  principle simulation, 54–55,56*f*
Morphology characterization, inverse steric exclusion chromatography, 211–223
Multiangle light scattering SEC
  advantages, 274
  applications, 274–275
Multiangle light scattering–viscometric–refractometric detector coupling for polyelectrolyte characterization
  advantages and disadvantages, 31
  applications, 31–32
  comparison of multiangle and low-angle light scattering detectors, 17,20–21,22*f*
  error analysis
    random errors, 30–31
    systematic errors, 25,27–30
  experimental description, 8,16–17
  instrumentation, 16
  light scattering
    calibration, 12–13
    minimum measurable mass, 14–15
    minimum measurable mean square radius of gyration, 13–14
    normalization of multiple photodetectors, 11–12
    principles, 10–11

Downloaded by 217.66.152.32 on October 8, 2012 | http://pubs.acs.org
Publication Date: May 30, 1996 | doi: 10.1021/bk-1996-0635.ix002

Multiangle light scattering–viscometric–refractometric detector coupling for polyelectrolyte characterization—*Continued*
  polyelectrolyte applications
    dimensions vs. ionic strength, 23,26,27*f*
    ionic strength effects on elution behavior, 21,22–23,24*f*
    liquidlike correlations under shear flow, 25,26*f*
  refractometer, 15–16
  typical data, 17,18*f*,19*t*
  viscometer, 8–10
Multicomponent eluents
  advantages, 103
  size exclusion chromatographic applications, 103
Multidetector approach for copolymers, disadvantages, 2

N

Net protein charge, role in protein retention in SEC, 88–102
Nonhomogeneous hydrodynamic fields, macromolecular behavior, 127–154
Nonstandard methods based on size exclusion principles
  critical chromatography, 290–296
  high-performance membrane chromatography, 309–323
  microcolumn SEC, 276–289,291
  thin-layer chromatography, 295–309
Number-average molecular weight, 4
Number-modulated molecular weight distribution, glucans, 356–357

O

Oligomers, thin-layer chromatography, 295–309
Open-column size exclusion chromatography, procedure, 384
Optical constant, 3

P

Packings, synthesis and characterization, 190–246
Packings for size exclusion chromatography
  based on inorganic materials
    aluminum(III) oxides, 206
    silica gel
      formation of porous structure, 203–204
      modifications, 205–206
      preparation, 203–204
    titanium(IV) oxides, 206
    zirconium(IV) oxides, 206
  based on natural organic polymers
    agarose, 201
    cellulose, 201,203
    dextran, 201,202*t*
  based on synthetic organic polymers
    control of bead size and bead size distribution, 200
    examples, 191,192*t*
    gel-type resins, 193
    macroporous resins
      mechanism of porous structure formation, 193–196
      nonsolvating diluent as porogen agent, 196,198*f*
      polymer as porogen agent, 196,198–199
      properties, 191
      solvating diluent as porogen agent, 196,197*f*
    post-cross-linked resins, 199
    preparation, 191
  properties, 206–207
  requirements, 190
Particle size, characteristic of media for aqueous SEC, 229,243
Partition coefficient
  calculation, 54
  definition, 37,76,212,214
Peak capacity, characteristic of media for aqueous SEC, 237,239,241,245–246
Permeable particles
  performance of chromatographic processes, 163–164
  protein separation using LC, 166–168

Downloaded by 217.66.152.32 on October 8, 2012 | http://pubs.acs.org
Publication Date: May 30, 1996 | doi: 10.1021/bk-1996-0635.ix002

Pointlike solute, motion, 180–181
Polydispersity, problem for macromolecular characterization, 7
Polyelectrolytes
  characterization using multiangle light scattering–viscometric–refractometric detector coupling, 7–32
  soft body theory of SEC, 67–86
Poly(ethylene glycol), micelle formation using SEC, light scattering, and UV spectroscopy, 328–346
Polymer(s)
  critical chromatography, 290–296
  high-performance membrane chromatography, 309–323
  microcolumn SEC, 277–289,291
  thin-layer chromatography, 295–309
  ultracentrifugal sedimentation equilibrium calibrations of size exclusion chromatographic elution profiles, 379–398
Polymer chains, linear, flexibility effect, 52–65
Polymer composition, analysis, 250–323
Polymer degradation, 127–128
Polymer separations, thermodynamic model, 173–187
Polysaccharides
  dissolution using *N*,*N*-dimethylacetamide with lithium chloride, 367
  factors affecting properties, 366
  importance, 366
  SEC in *N*,*N*-dimethylacetamide with lithium chloride, 366–378
Polystyrene
  modeling of stationary phase in size exclusion chromatography with binary eluents, 103–125
  sedimentation equilibrium analysis, 397,398*f*
Poly(vinyl alcohol), compositional heterogeneity using LC, 262–272
Pore geometry, role in Monte Carlo simulation of SEC, 55,57,59–60*f*
Pore size
  characteristic of media for aqueous size exclusion chromatography, 239,241*f*
Pore size—*Continued*
  role in macromolecular behavior in nonhomogeneous hydrodynamic fields, 142–143,153
Pore volume, characteristic of media for aqueous SEC, 227,239
Pore volume distribution, inverse steric exclusion chromatography, 211–223
POROS Q/M, protein separation by high-performance LC, 157–170
Post-cross-linked resins, packing for size exclusion chromatography, 199
Potential energy of sphere within cylinder, soft body model of size exclusion chromatography, 84–85
Potential–surface charge relationship, soft body model of SEC, 83–84
Protein(s)
  characterization of size and molecular mass using gel chromatography, 36–50
  separation using LC with permeable particles, 166–168
Protein charge, role in protein retention in SEC, 88–102
Protein retention in SEC
  application, 96,102
  chromatography of Superose 12, 94–95
  net protein charge effect, 96–102
  packing charge density effect, 96–102
  experimental description, 89–91,93
  Superose 12 surface charge density calculation, 92*f*,93
Pullulans, SEC in *N*,*N*-dimethylacetamide with lithium chloride, 366–378

Q

Q HYPER D, protein separation by high-performance LC, 157–170

R

Random errors, multiangle light scattering–viscometric–refractometric detector coupling for polyelectrolyte characterization, 30–31

Downloaded by 217.66.152.32 on October 8, 2012 | http://pubs.acs.org
Publication Date: May 30, 1996 | doi: 10.1021/bk-1996-0635.ix002

Downloaded by 217.66.152.32 on October 8, 2012 | http://pubs.acs.org
Publication Date: May 30, 1996 | doi: 10.1021/bk-1996-0635.ix002

Randomly coiled and elongated polymers, characterization of size and molecular mass using gel chromatography, 41–45
Refractometric–multiangle light scattering–viscometric coupling for polyelectrolyte characterization, *See* Multiangle light scattering–viscometric–refractometric detector coupling for polyelectrolyte characterization
Resolvability, characteristic of media for aqueous SEC, 236–238,244–246
Retention
  models for SEC, 67–68
  role in macromolecular behavior in nonhomogeneous hydrodynamic fields, 133–135–136*f*
Rotational correlation time of spin probe vs. that in free solution, 219

S

Sample volume, role on media for aqueous SEC, 235,238*f*
Secondary effects in aqueous size exclusion chromatography between sodium poly(styrene sulfonate) compounds of different sulfonations
  electrostatic interactions with packings, 350
  experimental description, 348
  hydrophobic interactions, 350
  ionic strength vs. retention volume, 349
Sedimentation equilibrium data, analytical procedure, 385,387
Selectivity, characteristic of media for aqueous SEC, 227–229,239,242–244
Separation of molecules according to size, designations, 226
Shape-memory pores, formation, 206–207
Signal of refractive index detector, 3–4
Silica gel, packing for SEC, 203–206
Size(s)
  definition for macromolecules, 53
  proteins, characterization using gel chromatography, 36–50
Size exclusion chromatography (SEC)
  aqueous, *See* Aqueous SEC
  comparison to gel electrophoresis and hydrodynamic chromatography, 173–187
  compositional heterogeneity of poly(vinyl alcohol), 262–272
  degradation vs. thermodynamic quality of solvent, 135,137–141
  determination
    molecular weight averages and distributions, 366–367
    size and molecular weight of macromolecules, 328
  development, 52
  elution rate on degradation effect, 131–133
  net protein charge and stationary-phase charge on protein retention effect, 88–102
  macromolecular behavior in nonhomogeneous hydrodynamic fields, 127–154
  micelle formation, 328–346
  modeling
    by Monte Carlo simulation, 52–65
    of stationary phase with binary eluents, 103–125
  modification for heterogeneous copolymer characterization, 262–263
  nonstandard methods, 274–323
  packings, 190–207
  polysaccharides in *N,N*-dimethylacetamide with lithium chloride
    experimental description, 366,368–369
    light scattering procedure, 369
    safety considerations, 378
    solvent system, 369–371
    universal calibration procedure, 369,370*f*
    universal calibration vs. light scattering, 371–377
  requirements, 7
  retention effect on macromolecules on surface of solvent particles, 133–135,136*f*
  soft body theory, 67–86
  solvent effect, 130*f*,131

Downloaded by 217.66.152.32 on October 8, 2012 | http://pubs.acs.org
Publication Date: May 30, 1996 | doi: 10.1021/bk-1996-0635.ix002

Size exclusion chromatography (SEC)—*Continued*
  solvent problems, 366
  stationary-phase modeling with binary eluents, 103–125
  use of multicomponent eluents, 103–104
  with light scattering and refractive index detectors, 328–330
Sodium poly(styrene sulfonate) compounds with different sulfonations, secondary effects in aqueous SEC, 347–350
Soft body model of size exclusion chromatography
  electrostatic forces, 69–74
  generality, 68
  mean field approximation, 71,75–77
  nonspherical solutes, 77–79
  potential energy of sphere within cylinder, 84–85
  restrictions, 68–69
  solution to integrals, 85–86
  surface charge–potential relationship, 83–84
  universal calibration, 79–82
Sol stage, 204
Solubility
  definition, 204
  limiting conditions in LC, 250–260
Solute(s), characteristics for aqueous size exclusion chromatography, 230–233
Solute distribution between chromatographic phases, stationary phase in SEC with binary eluents, 109–111
Solute potential, 175–176
Solution to integrals, soft body model of SEC, 85–86
Solvent
  problems in SEC, 366
  role in macromolecular behavior in nonhomogeneous hydrodynamic fields, 130*f*,131
Spectroscopic study, comparison to micelle formation using SEC, light scattering, and UV spectroscopy, 344–346
Starch, fractions, 352
Stationary-phase charge, role in protein retention in SEC, 88–102
Stationary-phase modeling in size exclusion chromatography with binary eluents
  association composition, 119–122
  association equilibria, 113–114
  average pore radius evaluation, 112
  distribution coefficients, 122–125
  experimental description, 103–107,109
  experimental pore radius evaluation, 112–113
  methanol adsorption isotherms, 118*f*,119
  methanol adsorption models, 114–117,119
  mobile and stationary phases of binary eluents, 107,108*f*
  solute distribution between chromatographic phases, 109–111
  stationary-phase composition, 119–122
  total pore volume evaluation, 111
Steric exclusion chromatography
  applications, 211
  inverse application, 211–212
Stoichiometric displacement models, protein retention in ion-exchange chromatography, 89
Stokes radius
  definition, 53
  viscosity based, *See* Viscosity-based Stokes radius
Superdex, characteristics for aqueous size exclusion chromatography, 225–246
Superficial velocity, relationship to height equivalent to theoretical plate, 167–168
Surface charge–potential relationship, soft body model of SEC, 83–84
Swollen polymer materials, inverse steric exclusion chromatography for morphology characterization, 211–223
Swollen resins, molecular accessibility, 219–221,222*f*
Syneresis, 204
Synthesis, packings, 190–246
Synthetic polymers, separation methods, 274–275
System peaks, formation, 104

Systematic errors, multiangle light scattering–viscometric–refractometric detector coupling for polyelectrolyte characterization, 25,27–30

T

Thermal field flow fractionation
  elution rate effect, 144*f*,145–147
  process, 145
  quantitative evaluation of degree of degradation, 146*f*,147–148
Thermodynamic model for polymer separations
  approach, 174
  comparison of methods, 173
  confinement entropy calculations
    chain models, 184
    failure of universal size parameter, 184–186
    matrix models, 183–184,185*f*
    trends discernible in elution behavior, 186
  constraints, 186–187
  gel electrophoresis
    connections to previous theory, 180
    modeling, 178–179
    molecular origin of separations, 178,182*f*
    motion
      flexible chain solute, 181–183
      pointlike solute, 180–181
  hydrodynamic chromatography, modeling, 177
  size exclusion chromatography
    assertion of equilibrium, 177
    modeling, 176
Thin-layer chromatography of polymers and oligomers
  advantages, 301
  applications, 295,297
  comparison to high-performance LC, 297,300*t*,301
  examples of applications, 301–309
  features of high-performance thin-layer chromatography, 297–299,301
  technical possibilities, 297,298*t*
Titanium(IV) oxides, packing for size exclusion chromatography, 206
Total pore volume evaluation, stationary phase in SEC with binary eluents, 112
Transport theory
  flux equations, 175
  mean solute velocity, 174–175
  solute potential expressions, 175–176
True molecular weight, 3
Two-dimensional separation according to molecular weight and chemical composition, 3

U

Ultracentrifugal sedimentation equilibrium calibrations of SEC elution profiles
  analytical theory, 381–383
  analytical ultracentrifugation procedure, 385
  development, 379–380
  high-performance chromatographic procedure, 384–385
  kraft lignin derivatives
    comparison of weight-average molecular weight and formal component molecular weights, 391,392*f*
    elution profile
      acetylated kraft lignin, 394*f*,395
      kraft lignin, 386*f*,387,389
    molecular weight calibration curves for acetylated kraft lignin, 394*f*,395–397
    preparation, 383–384
    primary and secondary calibration curves, 389–391,393*f*,395
    sedimentation equilibrium curve, 388*f*,389
  lignins, 380–381
  open-column chromatographic procedure, 384
  sedimentation equilibrium analysis of polystyrene fraction, 397,398*f*
  sedimentation equilibrium data analytical procedure, 385,387
Universal calibration
  importance, 52

Downloaded by 217.66.152.32 on October 8, 2012 | http://pubs.acs.org
Publication Date: May 30, 1996 | doi: 10.1021/bk-1996-0635.ix002

Universal calibration—*Continued*
  SEC, 79–82,369–377
  validity, 53
UV spectroscopy, micelle formation, 328–346

V

Vacant peak, 104
Viscometric–multiangle light scattering–refractometric detector coupling for polyelectrolyte characterization, *See* Multiangle light scattering–viscometric–refractometric detector coupling for polyelectrolyte characterization
Viscometric radius, 53
Viscosity-based Stokes radius
  calculation, 41
  characterization of size and molecular mass of proteins, 36–50
Viscosity radius, 79

W

Water-soluble globular proteins, characterization using gel chromatography, 39–40
Weight-average molecular weight, 4

Z

Zirconium oxides, packing for size exclusion chromatography, 206

Downloaded by 217.66.152.32 on October 8, 2012 | http://pubs.acs.org
Publication Date: May 30, 1996 | doi: 10.1021/bk-1996-0635.ix002